CHAPTER 1
EVOLUTION OF A SUCCESSFUL DESIGN

Thomas H. Brown, Jr., Ph.D., P.E.
Faculty Associate
Institute for Transportation Research and Education
North Carolina State University
Raleigh, North Carolina

1.1 EVOLUTION OF A DESIGN

Most likely you have, right at this moment, at least one machine design project in progress. Maybe you were the originator of the design, but I suspect you inherited this design from others. I further suspect that you have already identified elements of the design you feel could be improved. You might be under pressure from customer service or marketing to respond to some need for change. In responding successfully, either to your own observations for change or to those of others, the design will evolve. Recognizing that the evolutionary design process is decidedly complex, with a seemingly random sequence of steps, the primary purpose of *Standard Handbook of Machine Design* is to make the information you need as readily accessible and usable as possible.

As an example of how a design can evolve, and to provide perspective on how the information in this Handbook has traditionally been used, let me review for you a project I was given in my first job as a mechanical engineer. It involved the positioning of a microwave feed horn for a 30-ft-diameter antenna dish. The original design (not mine, by the way) called for a technician to climb up onto a platform, some 20 ft off the ground, near the backside of the feed horn. The technician had to loosen a half dozen bolts, rotate the feed horn manually, and then retighten the bolts. This design worked quite well until several systems were sold to a customer providing telecommunications along the Alaskan oil pipeline. Workers were not really safe going out in below 0°F weather, with snow and ice on everything. As a result of their concerns for safety, this customer asked that we provide remote positioning of the feed horn from the nearby control room.

The critical design requirement was that the positioning of the feed horn needed to be relatively precise. This meant that our design had to have as little backlash in the drive mechanism as possible. Being a young engineer, I was unaware of the wide variety of different drive systems, in particular their respective properties and capa-

bilities. I asked one of the older engineers for some direction. He suggested I use a worm drive since it cannot be back driven, and loaned me his copy of Joseph Shigley's book, *Mechanical Engineering Design.* He said that Shigley's book (a precursor to this Handbook) had been his primary source of information about worm drives, and a wealth of other machine design information. As it turned out, the resulting design worked as required. It not only pleased our Alaskan customer but became a standard on all antenna systems.

I did not get a promotion as a result of the success of this new design, nor did I receive a raise. However, I was proud, and, as you can surmise, still am. I credit this successful design evolution to the material on worm drives in Shigley's book. And there is more to this story. The worm drive gearbox we ultimately purchased contained a plastic drive element. This allowed the backlash to be greater than what could be tolerated in positioning accuracy and did not provide the necessary strength to break the feed horn loose from a covering of ice. The original manufacturer of the gearbox refused to change this drive element to metal for the units we would be buying. If we made the change ourselves, they said, the warranty would be voided. However, after absorbing the wealth of information on worm drives in Shigley's book, I felt confident that we could make this substitution without endangering the reliability of the unit. Also, because of Joseph Shigley's reputation in the mechanical engineering community and the extensive list of references he cited, I never felt the need to consult other sources.

Another aspect of this story is also important to note. In addition to the information on worm drives, I also used Shigley's book to find comprehensive design information on the many other machine elements in the new design: gear train geometry, chain drives, couplings, roller bearings, bolted joints, welds, lubrication, corrosion, and the necessary stress and deformation calculations I needed to make. All this information, and much more, was contained in the First Edition of the *Standard Handbook of Machine Design,* which Joseph Shigley coauthored with Charles Mischke. Now in its Third Edition, this Handbook includes the information machine design engineers have come to trust. We hope you will find this information invaluable as you constantly strive to improve your designs, whether by your own initiatives, or for other reasons.

1.2 USING THE HANDBOOK

Once the chapters for this Third Edition of the Handbook were determined, we decided that these chapters should be organized into nine sections, denoted Parts 1 through 9. Each section focuses on a distinct collection of related material. For example, Part 3, "Gearing," contains chapters on spur gears, helical gears, bevel and hypoid gears, worm gearing, and power screws. However, each chapter stands on its own, providing direct access to a specific area of interest or need.

This Handbook is a unique reference, capturing the breadth and depth of what is currently known about each of these design element topics. The nine sections are

Part 1. Machine Elements in Motion

Part 2. Machine Elements That Absorb and Store Energy

Part 3. Gearing

Part 4. Power Transmission

Part 5. Bearings and Lubrication

EVOLUTION OF A SUCCESSFUL DESIGN

Part 6. Fastening, Joining, and Connecting

Part 7. Load Capability Considerations

Part 8. Performance of Engineering Materials

Part 9. Classical Stress and Deformation Analysis

While there are many ways the nine sections could have been ordered, the order chosen for this Third Edition provides one sequence of steps to the evolutionary design process. For example, you might first consider the kinds of motions you need and how they might be accomplished. Part 1 might help you choose a classic mechanism or linkage, a cam, or maybe some arrangement of gears. Possibly your design needs to absorb or store energy, so the chapters included in Part 2 would provide the information you need. Depending on your design, Parts 3 and 4 cover virtually every type of gear set, drive type, coupling, and the common elements related to these devices. Part 5 covers how rotating elements might be supported, typically with either roller- or journal-type bearings. And if bearings are present, then lubrication and seals must be carefully considered.

Part 6 continues the design process to the consideration of how components will be assembled. Are there structural bolts, or just mechanical fasteners, or are parts to be welded? The coauthor of the chapter on welding is the well-known author of the preeminent book on welding, so this Handbook should provide all the information you need relative to this topic. The last chapter in this section presents the complex procedure necessary to maintain proper fits and tolerances, a full-time job in itself for some engineers. Everything an engineer needs to know about this area of manufacturing can be found in this Third Edition of the Handbook.

At some point, loads will be determined, both statically and dynamically; therefore, Part 7 contains the information you need to make decisions relative to the reliability of critical parts. Information on vibration, and just as important, its control, is provided in a chapter in this section. The selection of materials is covered in Part 8 and includes chapters on wear and corrosion. With regard to the problems of corrosion, one of the main components of a system I was responsible for failed due to excessive galvanic corrosion. The information contained in this Handbook helped me not make that mistake again.

The last section, Part 9, contains the classic information on stress and deformation calculations every mechanical engineer learns in school, but finds escapes exponentially if not used regularly. Here, four chapters provide every important calculation practicing engineers should need, and they are introduced in a manner that can be understood and used with confidence.

1.3 SOME OPPORTUNITIES TO DISCOVER

As mentioned earlier, this Third Edition of the *Standard Handbook of Machine Design* has been organized differently as compared to the two previous editions. In addition to grouping the chapters into nine sections, almost a dozen of the 50 chapters in the Second Edition, which contained a variety of information ancillary to the machine design process, have been removed. Therefore, the scope of this edition of the Handbook is focused on the more traditional machine design topics.

For those familiar with the previous editions, one chapter that was in the First Edition but not in the Second, "Pressure Cylinders," has been included in the Third. This additional chapter is located in Part 9, completing the information important

1.4 EVOLUTION OF A SUCCESSFUL DESIGN

relative to stress and deformation analysis. Also, one of the chapters in the two previous editions, "Sections and Shapes—Tabular Data," is now Appendix A.

Discovering opportunities to improve or evolve your designs successfully is one of the primary ways we expect you to use this Handbook. Each chapter has considerable design information and the format used is unique. What follows is a discussion of just some of the helpful information you will find in each chapter.

Part 1: *Machine Elements in Motion*

Chapter 2 in this section is undoubtedly one of the most distinctive chapters you will find anywhere. There is page after page of diagrams of every conceivable mechanism and machine device. There are snap-action mechanisms, linear actuators, fine adjustment devices, clamping and locating mechanisms, escapements and indexing mechanisms, oscillating mechanisms, ratchets and latches, reciprocating and reversing mechanisms, and couplings (see the commercial designs in Chap. 16) and connectors, including slider connectors.

There are devices that stop, pause, and hesitate motion, and devices that transport motion between machine elements. There are two pages of loading and unloading mechanisms, many that are commonly used for construction and earth-moving equipment, as well as bulk-handling railcars. You will find path generators, function generators, and even mechanical computing mechanisms, still finding a place in this electronic age. There are speed-changing mechanisms and multidegree mechanisms that form the basis of many robotic-type machines. I hope you enjoy as much as I do just flipping pages in this one-of-a-kind catalog of mechanical devices.

If a particular linkage catches your eye in Chap. 2, then the information contained in Chap. 3 takes you many steps further, providing all the geometry of motion diagrams, or kinematics, you will need. Details of the famous slider-crank and four-bar linkages are provided. The material in this chapter might seem intimidating graphically, but without it, the preciseness of the motion you most likely need will be difficult to achieve any other way.

If your machine requires a cam to achieve its design requirements, then Chap. 4 contains everything about this particular device. From simplified schematics to the complexity of cam trigonometry, everything a designer will need is here in these pages. There is even a computer program flowchart to help you develop a comprehensive analysis of your design, whether you use a programming code like FORTRAN or a personal computer spreadsheet.

The last chapter in this section, "Gear Trains," presents all the relative speed calculations for the two most common arrangements of gears: spur and planetary. Also, the speed calculations for differential gear trains are presented. Once these calculations are made, then the detailed specifications can be made using the information in Part 3.

Part 2: *Machine Elements That Absorb and Store Energy*

Personally, I have consulted Chap. 6, "Springs," as much as any other chapter in the Handbook. It contains information on every kind of spring, from the commonly used helical spring, with all its variations, to the unique Belleville spring washer. Elliptical and even torsion bar springs are covered. In fact, basically everything I know about springs is in this chapter, one of the longest in the Handbook.

Flywheels are an important machine element in devices such as automobile engines and punch presses. They act like an accumulator tank in an air compressor system, thus evening out the fluctuations in rotational motion. Careful sizing is necessary to make sure that just the right amount of inertia is provided. Too much can cause the system to be have too long a recovery period or too little inertia, causing the system to loose too much energy between loading cycles. For high-speed flywheels or machine elements like compressor blades, consideration of the inertial stresses developed can be important.

The late John Muir, in his book *How to Keep Your Volkswagen Alive,* said, "Brakes perform a negative function, applying negative acceleration to stop the car, remaining inert when not being used." Brakes may have a negative function; however, their design can be critical to a successful product. Chapter 8 covers all aspects of brakes and all aspects of what might be the opposite of brakes—clutches. Clutches are designed to transfer power evenly and gradually between two shafts rotating at different speeds, even when one shaft is at rest. There has been a great deal of ingenuity in the design of brakes and clutches, accounting for many patents and commercial products. Centrifugal, cone, and disk-type clutches and brakes are two such commercial success stories. Both brakes and clutches produce significant temperature gradients in service. The design considerations associated with temperature variations are covered in this important chapter, including information on selecting the right clutch or brake materials for your specific application.

Part 3: *Gearing*

One of the most fascinating sections in this Third Edition of the Handbook is Part 3, "Gearing." Most of us as mechanical engineers will never actually be involved in designing and manufacturing gear sets, even the simplest spur gear. However, it has always been comforting to know that this Handbook contained everything needed if we were ever put in the situation of having to design a set of gears. Chapter 9, "Spur Gears" is relatively short and straightforward, giving the impression that gears are not that complicated. Then, Chap. 10, "Helical Gears," makes the point, by the extent of the information provided, of just how complicated gear sets can be if they are to be done correctly. This is one of the longest chapters in the Handbook. Another equally long chapter, 11, covers "Bevel and Hypoid Gears." This has always been a special chapter, providing insight into one of the most magical machine elements in mechanical engineering. There are few vehicles on earth that do not have a differential, and every differential has either a bevel or hypoid gear set. All the geometry of motion is explained, with table after table and chart after chart of applicable formulas and performance data for all variations and design parameters.

I've already referred to the importance of the material in Chap. 12, "Worm Gearing," in my story about the remote positioning of an antenna feed horn project. As I said earlier, the information in this chapter was invaluable in helping me modify an existing design to satisfy the needs of a high-profile customer.

As I look back on the years I spent associated with large antenna systems, it seems as though every aspect of these systems had me searching the *Standard Handbook of Machine Design* for important information. Chapter 13, "Power Screws," was another of those chapters I became very familiar with, since the primary positioning of the antenna dish on the satellite was accomplished by heavy duty power screws driven by dc motors. This Handbook is where I obtained the information I needed.

Part 4: *Power Transmission*

This section contains four chapters directed at the requirements of transferring motion from one rotating axis to another, whether by the time-honored belt (Chap. 14) or chain (Chap. 15) configurations, or by the wide variety of couplings (Chap. 16) used to isolate and protect downstream machine elements. This seemed to be the best place to discuss the design of shafts (Chap. 17), from both a static and dynamic viewpoint. While new belt, chain, and coupling products are introduced every year, the basic design considerations remain the same. Speed ratio calculations; tension adjustment schemes; and materials, many of which are composite constructions, are universal to these machine elements. Serpentine-notched belts seek to combine the flexibility and low noise of traditional belt drives, while providing the positional accuracy to meet strict timing requirements such as in automotive applications. For large horsepower transfer, metal chain and sprocket drives, usually in multiple-strand configurations, seem the best approach—and what you need is provided in this Handbook.

Since lining up shafts exactly is difficult, if not impossible, the usual solution is a coupling between the shafts. This is another area of intense ingenuity and cleverness, with many of the successful products highlighted in this section. A complete discussion of universal joints and constant velocity joints is also included.

Part 5: *Bearings and Lubrication*

One of the great inventions of the twentieth century is the roller bearing—in particular, the tapered roller bearing. Roller bearings allow high speeds under relatively heavy loads not possible before their introduction. Every automobile on the road today has a plethora of roller-type bearings. Journal bearings, which were the primary bearing type before the roller bearing, are still an important mechanical design element. The main and rod bearings in an internal combustion engine are of the journal type. Chapter 19, "Journal Bearings," is one of the longest chapters in the Handbook, punctuating the amount of design information available. Its length also indicates the extent of the design considerations necessary for their successful use.

Bearings could not do their job without lubrication, and lubrication would be lost from most bearings without the proper seals. Traditional and nontraditional seal designs are presented in this section, including those operating in static conditions and those operating between rotating parts. Lubricants are another product in constant flux. This Third Edition presents the properties and uses of the more common and trusted oils, greases, and solid lubricants.

Part 6: *Fastening, Joining, and Connecting*

Chapter 22, "Bolted and Riveted Joints," covers the design of bolts and rivets used not only to hold parts together in an assembly but also as structural elements. Complex joints in tension and shear are presented, including the effect of gaskets in a structural joint. Calculations for the proper preload of a structural bolt are provided.

Chapters 23 and 24 cover every conceivable type of mechanical fastener. Chapter 23 presents design information for threaded fasteners while Chap. 24 presents design information for unthreaded fasteners.

If a connection must contain or keep out gases or liquids, then a gasket is usually

EVOLUTION OF A SUCCESSFUL DESIGN

specified. The types of gaskets typically available and their appropriate application criteria are provided in Chap. 25.

When disassembly is not required or when maximum strength is needed, then usually the only solution to connecting separate parts is a weld. All aspects of a welded connection are presented in Chap. 26. This chapter begins with the basic principles of the arc welding process, followed by the various commercial processes, including exhaustive information on the materials used in welding. This chapter also includes the information needed to design a welded joint to be as strong, or stronger, than the materials being welded together. Since failure of welded joints has had such a high impact on the safety of the public, many national codes and industry specifications have been established and must be met. These are covered in detail in Chap. 26.

As mentioned earlier, the ongoing effort in manufacturing to hold to a high standard of quality requires a thorough understanding of the factors in fits and tolerances. Chapter 27 presents the standards of fit universally accepted and the complications associated with a buildup of tolerances in an assembly.

Part 7: *Load Capability Considerations*

Chapter 28 covers static theories of failure, from the theories for ductile materials to brittle materials. Charts for determining stress concentration factors for various design geometries are provided. In contrast, Chap. 29 covers dynamic theories of failure, including the determination of endurance limits. For various design factors, such as surface roughness, size, loading, temperature, and a host of miscellaneous factors, the Marin equation is used to modify the endurance limit determined from experiment. Alternating and fluctuating loading are considered, including combined loading considerations.

Machine elements in compression must be analyzed to protect against buckling or sudden collapse. Chapter 30 covers all aspects of compression loading of beams and columns, from Euler's formulas to complex beam–column analysis.

Chapter 31 covers mechanical vibration, from the forced vibration of damped single-degree-of-freedom systems to multi-degree-of-freedom systems. Torsional vibration and vibration isolation are presented.

Part 8: *Performance of Engineering Materials*

This section contains four chapters focused on the decisions associated with the selection of materials for the critical parts in a design. Chapter 32 is a summary of the science of material behavior, including the procedures used to determine various material properties. It is one of the longer chapters in the Handbook. Chapter 33 focuses on the properties and engineering considerations of the most common material in machines—steel. Whatever manufacturing is process used, everything needed in designing with steel is provided.

Once in service, machine elements are subject to constant wear and the adverse effects of corrosion. Chapters 34 and 35, respectively, cover the important aspects of wear and corrosion. It would seem a shame to spend so much time on the other aspects of design only to be blindsided by these two factors. Corrosion, especially galvanic, is insidious and only careful selection of mating materials will avoid disaster. Chapter 35 contains a listing from "A" for *acetone* to "W" for *water* relative to their adverse reaction to other chemicals.

1.8 EVOLUTION OF A SUCCESSFUL DESIGN

Part 9: *Classical Stress and Deformation Analysis*

This last section in the Third Edition provides the mechanical design engineer with the fundamental formulas for stress (Chap. 36) and deflection of beams (Chap. 37). This section also includes the stress and deformation of special geometries, such as curved beams and rings (Chap. 38), and the stress and deformation of pressurized cylinders (Chap. 39), which are developed as a result of internal pressure or from the effects of a press or shrink fit.

Appendix

As indicated earlier, one of the chapters included in the First and Second Editions, "Sections and Shapes—Tabular Data," has been provided in this Third Edition as an Appendix. Here are found the properties of common cross-sectional areas used in various mechanical elements, particularly beams, and the properties of standard structural shapes, such as rectangular tubing, channels, angles, and variations on the I-beam.

1.4 FINAL THOUGHTS

The process of creating or improving a mechanical system is an adventure. Like all adventures, machine design has its complications and logistics. When we are successful meeting these difficult challenges, the pride and feeling of accomplishment are so exhilarating they might be compared to how Sir Edmund Hillary must have felt after his successful assault on Everest. Or how Sir Henry Royce, of the famous motorcar company Rolls-Royce, felt when he was knighted. While knighthood might not be one of our rewards for success, the recognition we receive is no less significant in our careers as design engineers—bringing admiration and respect from our peers and considerable personal satisfaction and enjoyment.

Adventures also have their heroes. In the field of machine design, no two individuals stand out more than Joseph Shigley and Charles Mischke. Their professional partnership has been synonymous with machine design for 20 years, and Joseph Shigley has been a household word in mechanical engineering for over 40 years. We hope the wealth of information contained in this Third Edition of the *Standard Handbook of Machine Design,* and the way in which it is presented, will provide the necessary resources for your design projects.

P · A · R · T · 1

MACHINE ELEMENTS IN MOTION

MACHINE ELEMENTS IN MOTION

CHAPTER 2
A THESAURUS OF MECHANISMS

L. E. Torfason
Professor of Mechanical Engineering
University of New Brunswick
Fredericton, New Brunswick, Canada

GLOSSARY OF SYMBOLS

R	Revolute pair or pin joint
P	Prismatic pair or sliding joint
C	Cylinder pair for joints that allow rotation and sliding along the cylinder axis
G	Spheric pair (globe) for ball joints
S_L	Screw pair with lead L
F	Planar pair (flat) for a joint that maintains two planes in contact

SUMMARY[†]

This chapter is intended to be used as an idea generator. Following the adage that a picture is worth 1000 words, this chapter was assembled with millions of "words" in figures and virtually none using the alphabet. I have taken the liberty of varying dimensions to better show the principle of operation. You should not scale the figures, but follow the regular synthesis procedure to determine the proper dimensions for the application in mind.

In this chapter a new notation is used for the kinematic representation of joints or pairs in a linkage.

[†] Readers will note a difference in the style and character of the figures in this chapter. When this manuscript was received, the illustrations, all conceived and executed by Professor Torfason, were seen to be original and unique. We asked for and received from the publishers special permission to reproduce them exactly as they were drawn—EDS.

COLLATERAL READING

L. J. Kamm, *Designing Cost-Efficient Mechanisms*, McGraw-Hill, New York, 1990.

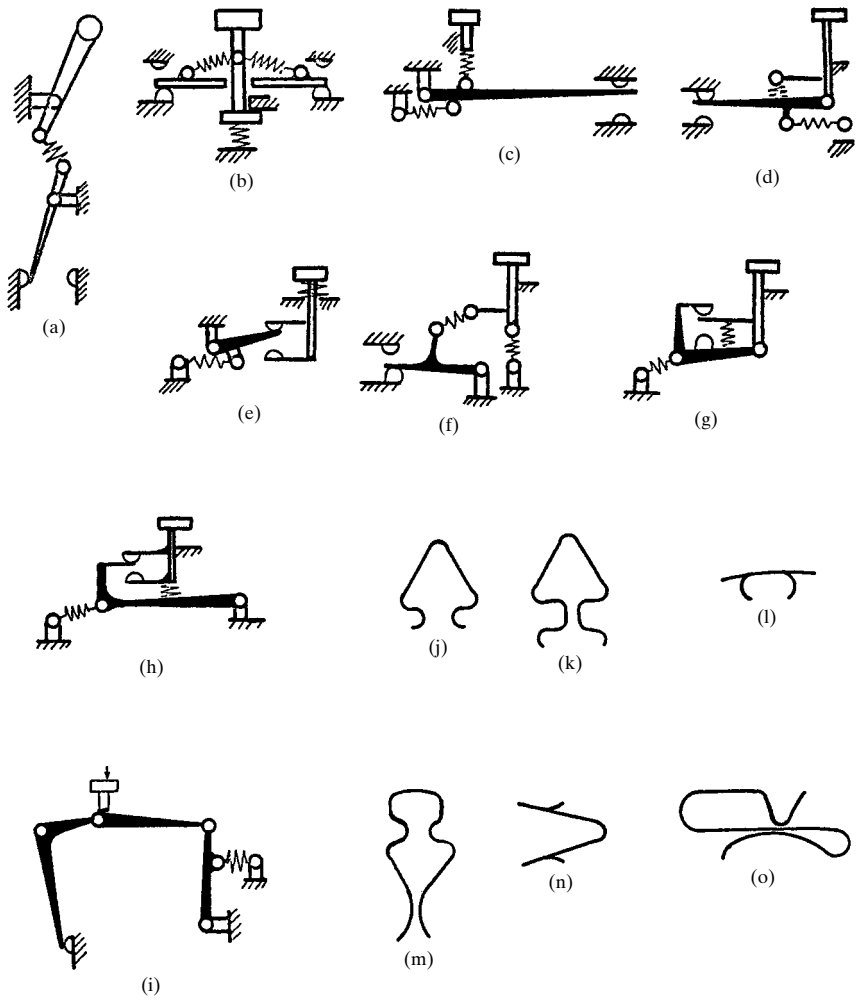

FIGURE 2.1 Snap-action mechanisms. These mechanisms are bistable elements in machines. They are used in switches to quickly make and break electric circuits and for fastening items. (*a*) Snap-action toggle switch; (*b*) to (*h*) seven variations of snap-action switches; (*i*) circuit breaker; (*j*) to (*o*), spring clips.

A THESAURUS OF MECHANISMS

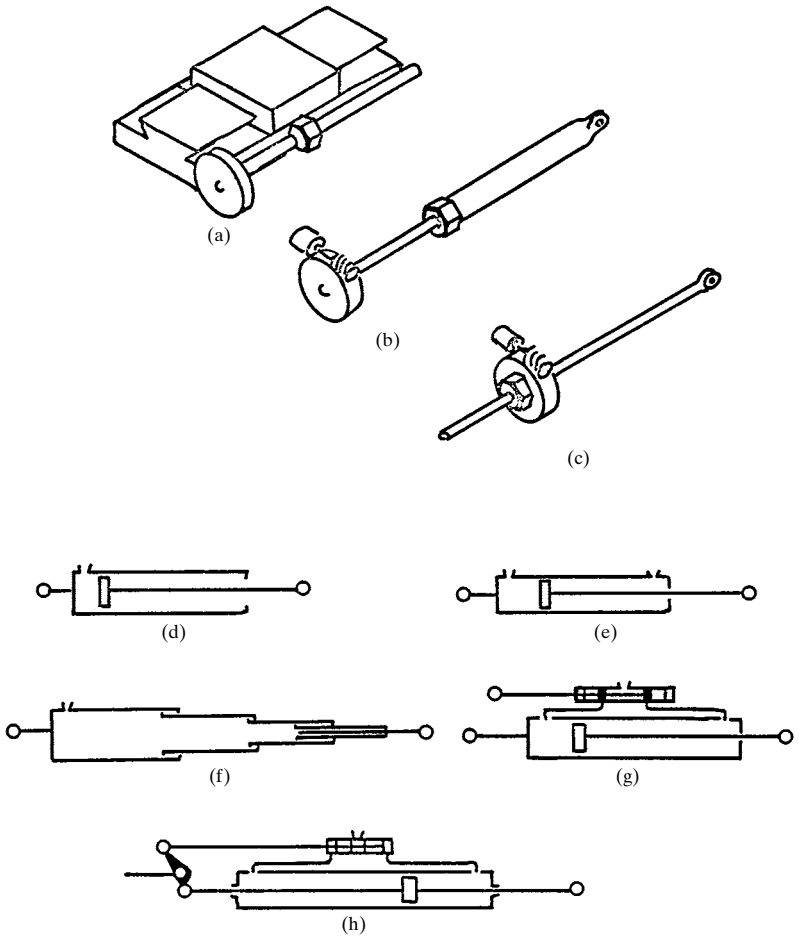

FIGURE 2.2 Linear actuators. These are devices that cause a straight-line displacement between two machine elements. (*a*) Lead screw; (*b*) worm gear with stationary nut; (*c*) worm gear with stationary screw; (*d*) single-acting hydraulic cylinder; (*e*) double-acting hydraulic cylinder; (*f*) telescoping hydraulic cylinder; (*g*) hydraulic cylinder with positional feedback; (*h*) hydraulic cylinder with floating link feedback.

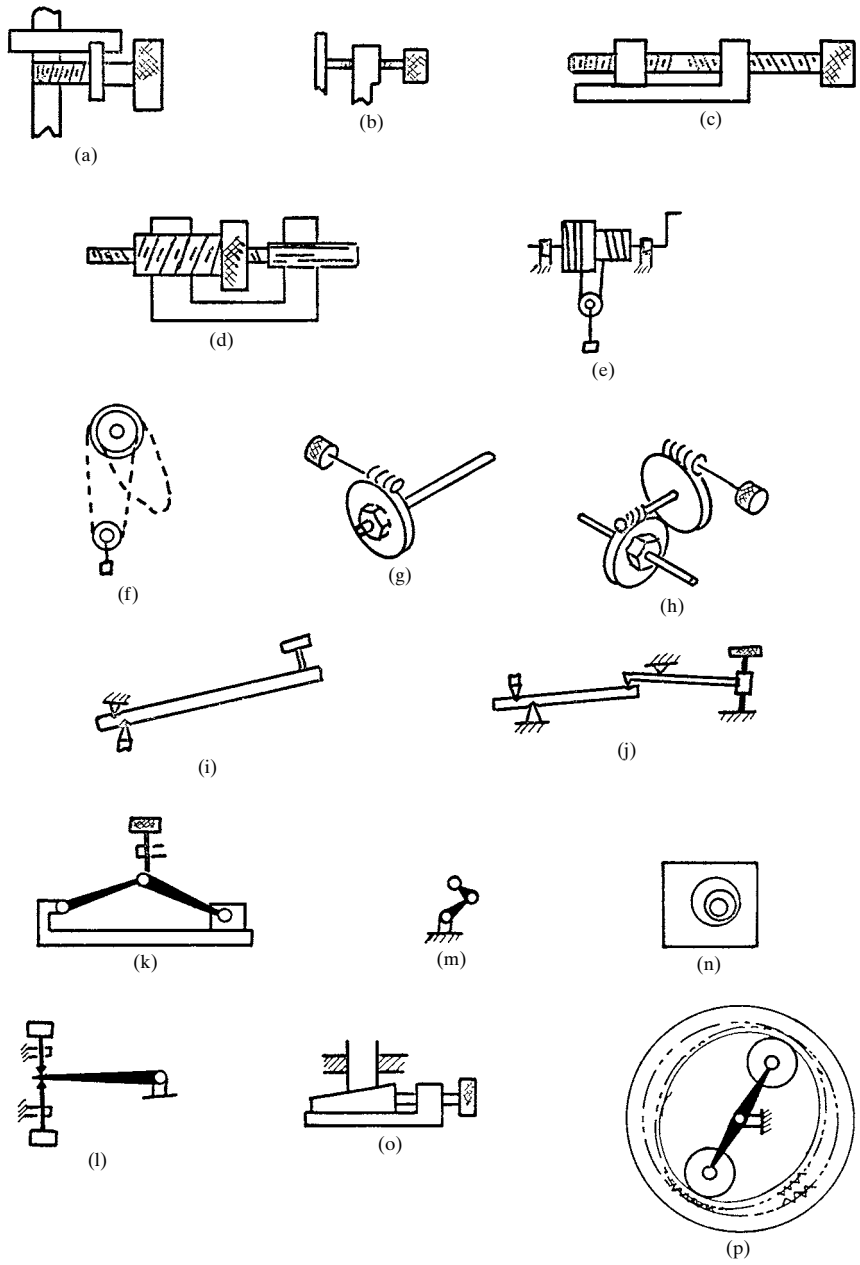

FIGURE 2.3 Fine adjustments I. Fine adjustments for stationary mechanisms are mechanisms that make a small change in the position of a mechanical member. (*a*), (*b*) Screw adjustments; (*c*), (*d*) differential screws; (*e*) Chinese windlass; (*f*) differential hoist; (*g*) worm gear and screw; (*h*) worm gears in series; (*i*) lever; (*j*) levers in series; (*k*) toggle mechanism; (*l*) screws to adjust angular position; (*m*), (*n*) eccentric cranks; (*o*) wedges; (*p*) harmonic drive.

A THESAURUS OF MECHANISMS

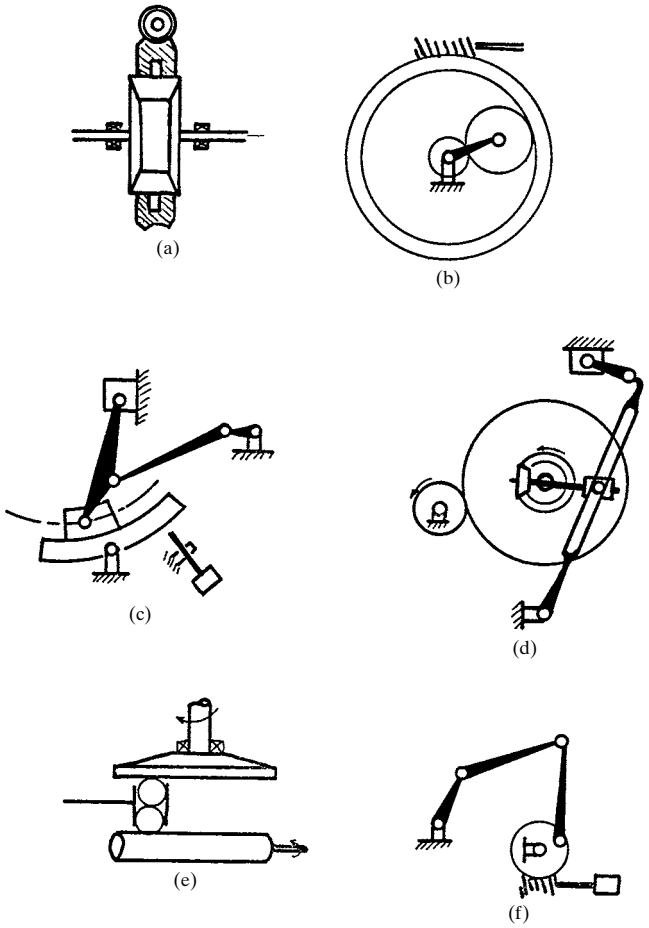

FIGURE 2.4 Fine adjustments II. Fine adjustments for moving mechanisms are adjusting devices which control the motion of linkages such as stroke, etc., while the mechanism is in motion. (*a*), (*b*) Differential gear adjustment; (*c*) adjustable-stroke engine; (*d*) adjustable stroke of shaper mechanism; (*e*) ball and disk speed changer; (*f*) adjusting fixed center of linkage for changing motion properties.

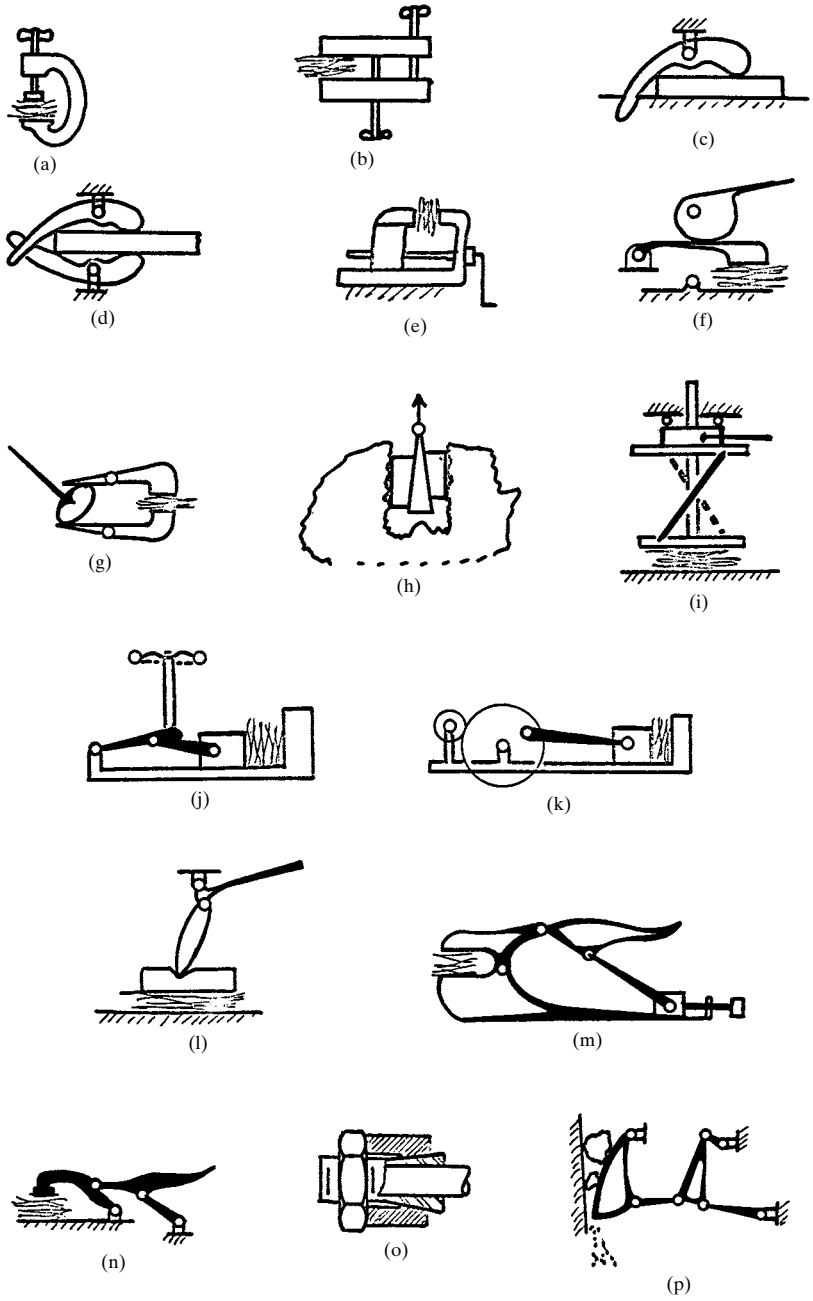

FIGURE 2.5 Clamping mechanisms. These devices are used to hold items for machining operations or to exert great forces for embossing or printing. (*a*) C clamp; (*b*) screw clamp; (*c*) cam clamp; (*d*) double cam clamp; (*e*) vise; (*f*) cam-operated clamp; (*g*) double cam-actuated clamp; (*h*) double wedge; (*i*) to (*l*) toggle press; (*m*) vise grips; (*n*) toggle clamp; (*o*) collet; (*p*) rock crusher.

A THESAURUS OF MECHANISMS

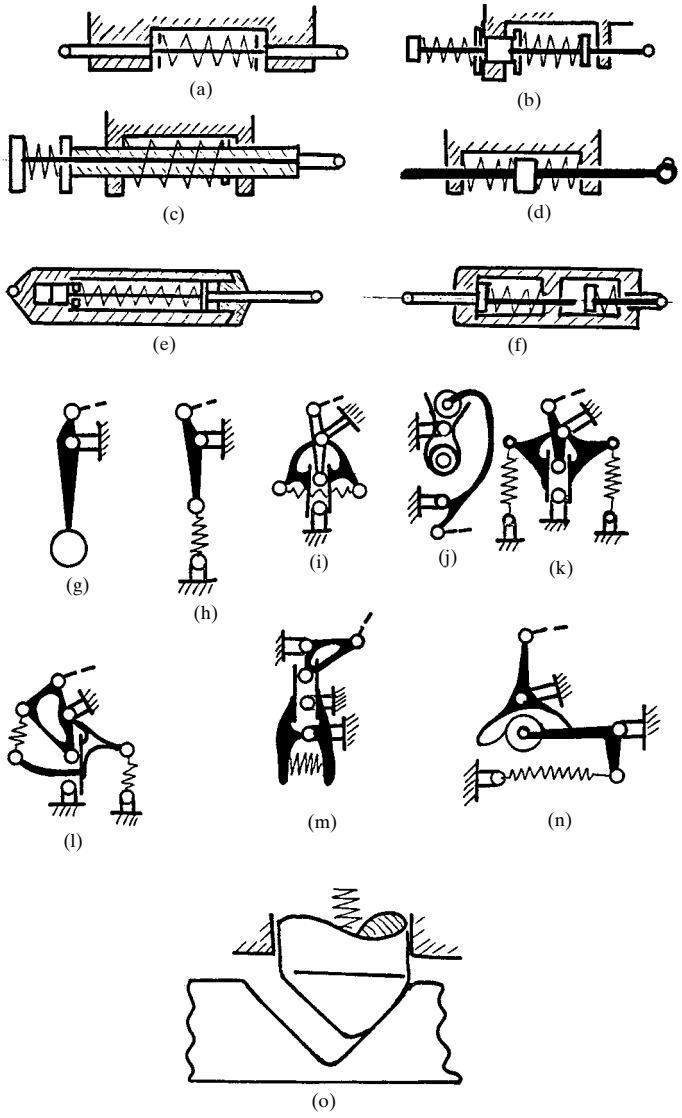

FIGURE 2.6 Locating mechanisms. These are devices which properly position a linkage member when the load is removed. (*a*) to (*f*) Self-centering linear devices; (*g*) to (*n*) self-centering angular devices; (*o*) detent.

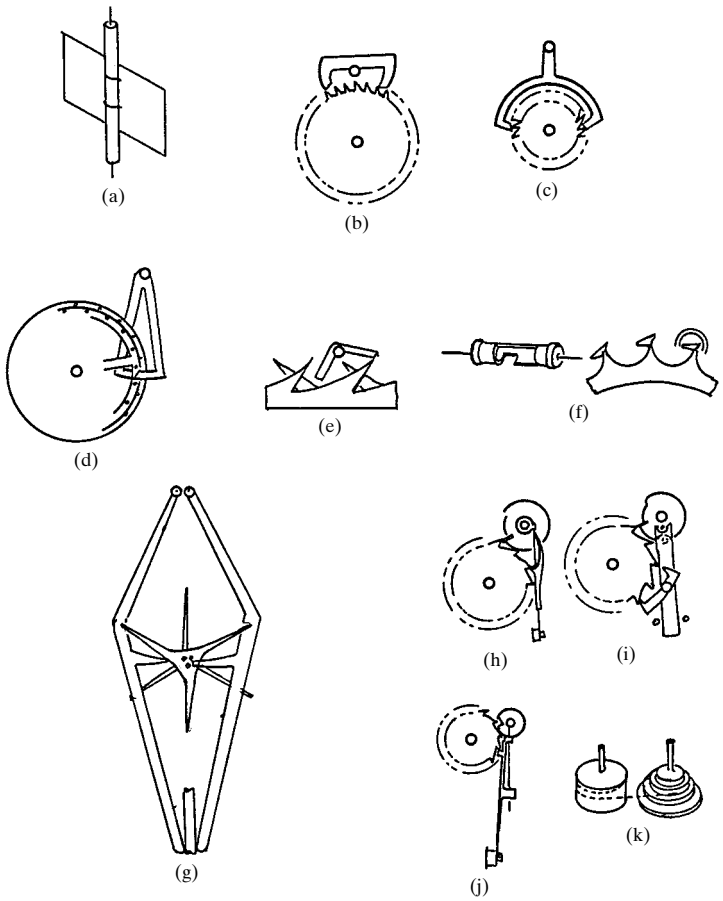

FIGURE 2.7 Escapements. These devices slowly release the potential energy stored in a spring to control devices such as clocks. (*a*) Paddle wheel; (*b*) recoil escapement; (*c*) dead-beat escapement; (*d*) stud escapement; (*e*) early anchor escapement; (*f*) cylinder escapement; (*g*) double three-legged escapement for tower clocks; (*h*) to (*j*) chronometer escapements; (*k*) fuse used to give uniform torque at escapement as the spring unwinds.

A THESAURUS OF MECHANISMS

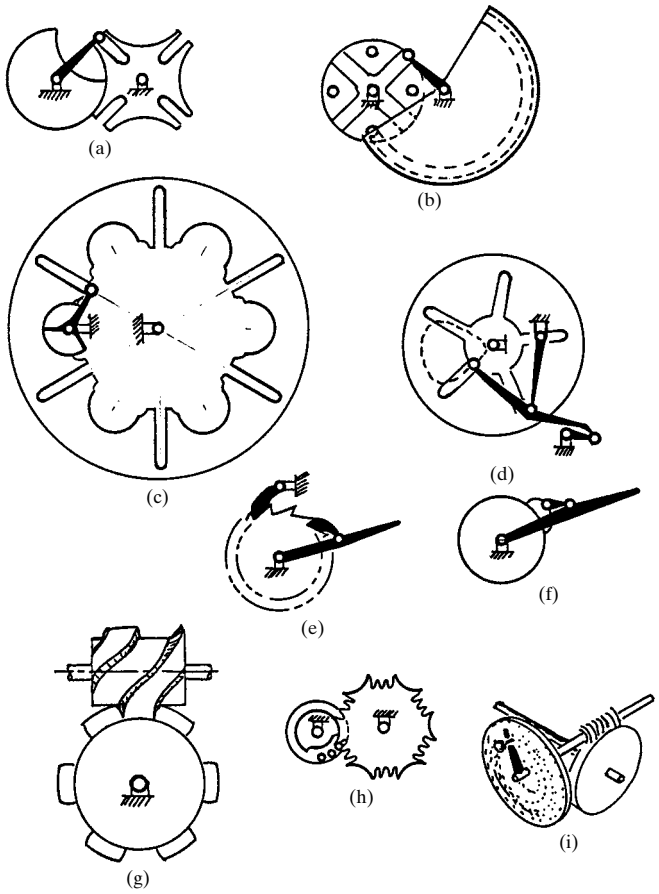

FIGURE 2.8 Indexing mechanisms. These mechanical devices advance a body to a specific position, hold it there for a period, and then advance it again. (*a*) to (*c*) Geneva stops; (*d*) four-bar links used to reduce jerk; (*e*) ratchet mechanism; (*f*) friction ratchet; (*g*) cylindrical cam-stop mechanism; (*h*) pin gearing used in indexing; (*i*) dividing head.

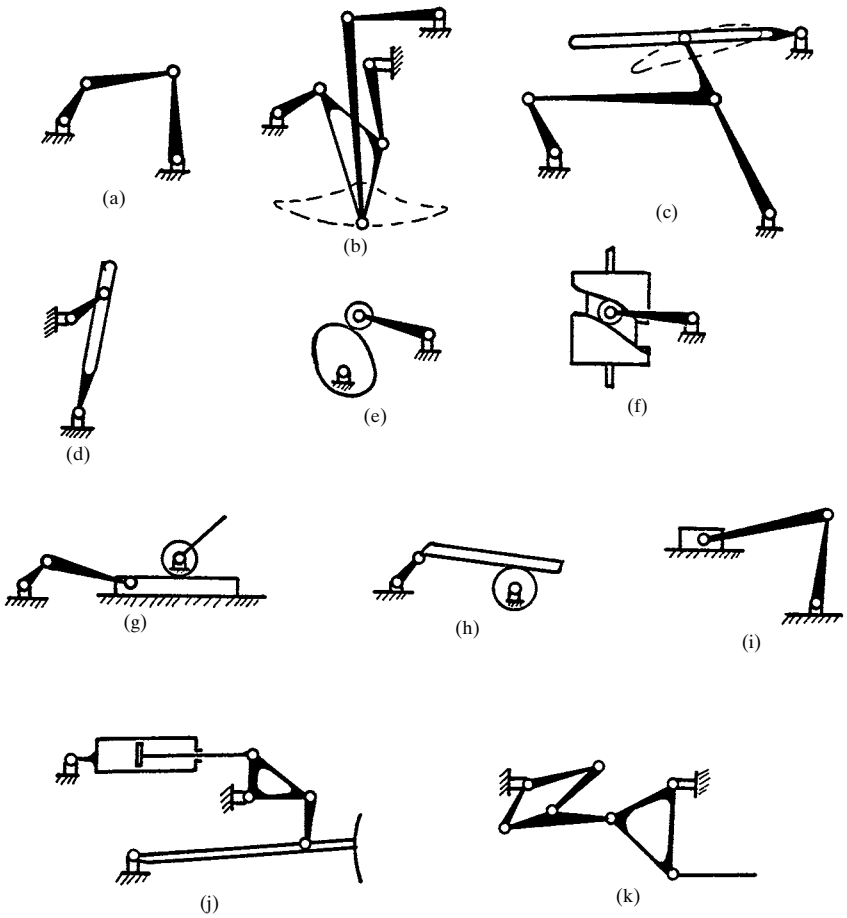

FIGURE 2.9 Oscillating mechanisms I. These mechanisms cause an output to repeatedly swing through a preset angle. (*a*) Four-bar linkage; (*b*) six-bar linkage; (*c*) six-bar linkage with pin in slot; (*d*) inverted slide-crank quick-return linkages; (*e*) radial cam and follower; (*f*) cylindrical cam; (*g*) geared slider crank; (*h*) geared inverted slider crank; (*i*) slider-driven crank; (*j*) bulldozer lift mechanism; (*k*) oscillator of the Corliss valve gear.

A THESAURUS OF MECHANISMS

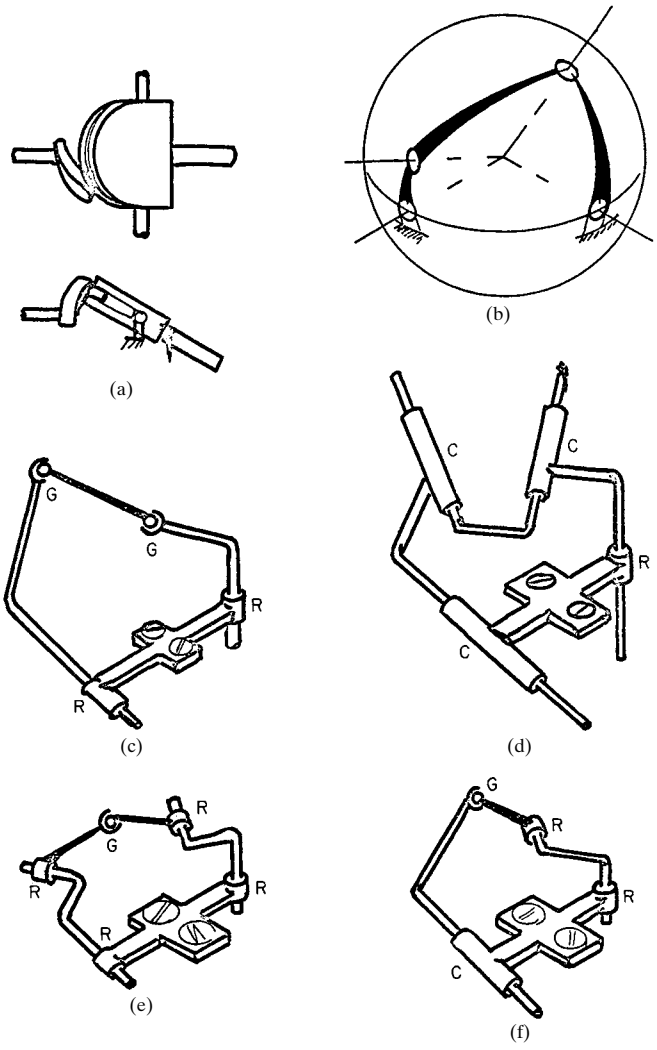

FIGURE 2.10 Oscillating mechanisms II. These all use spatial linkages. (*a*) Spatial pin and yoke; (*b*) spherical four-bar linkage; (*c*) spatial RGGR linkage; (*d*) spatial RCCC; (*e*) spatial RRGRR; (*f*) spatial RRGC.

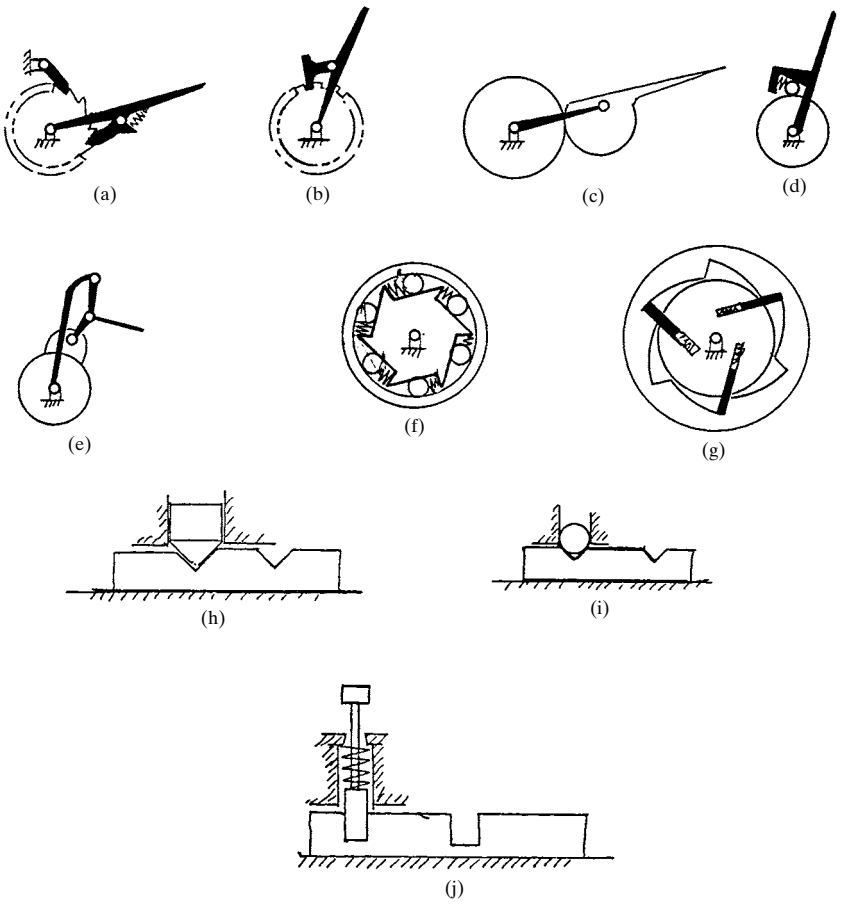

FIGURE 2.11 Ratchets and latches. These are mechanisms that advance or hold a machine member. (*a*) Ratchet and pawl; (*b*) reversible ratchet; (*c*) cam-lock ratchet; (*d*) ball-lock ratchet; (*e*) toggle ratchet; (*f*) overrunning clutch; (*g*) high-torque ratchet; (*h*), (*i*) detents; (*j*) locking bolts.

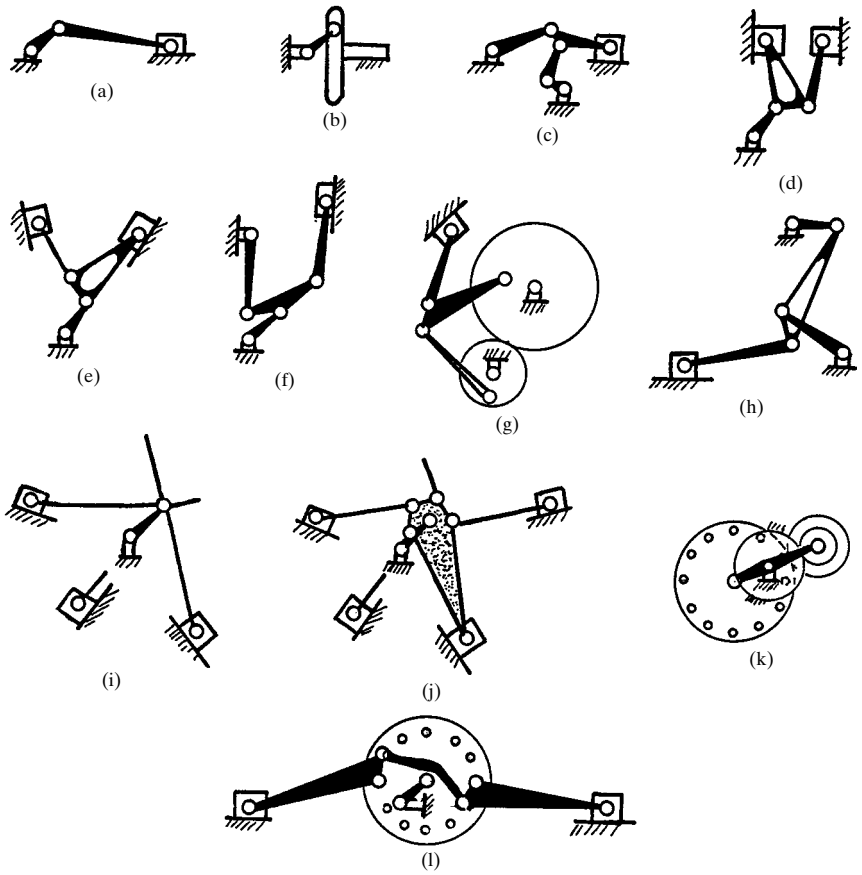

FIGURE 2.12 Reciprocating mechanisms I. These mechanical devices cause a member to translate on a straight line. (*a*) Slider crank; (*b*) Scotch yoke; (*c*) toggle mechanism; (*d*) Zoller engine; (*e*) V engine; (*f*) double-stroke engine; (*g*) geared engine; (*h*) Atkinson gas engine; (*i*) ideal radial engine; (*j*) practical radial engine; (*k*) geared Nordberg radial engine; (*l*) linked Nordberg radial engine.

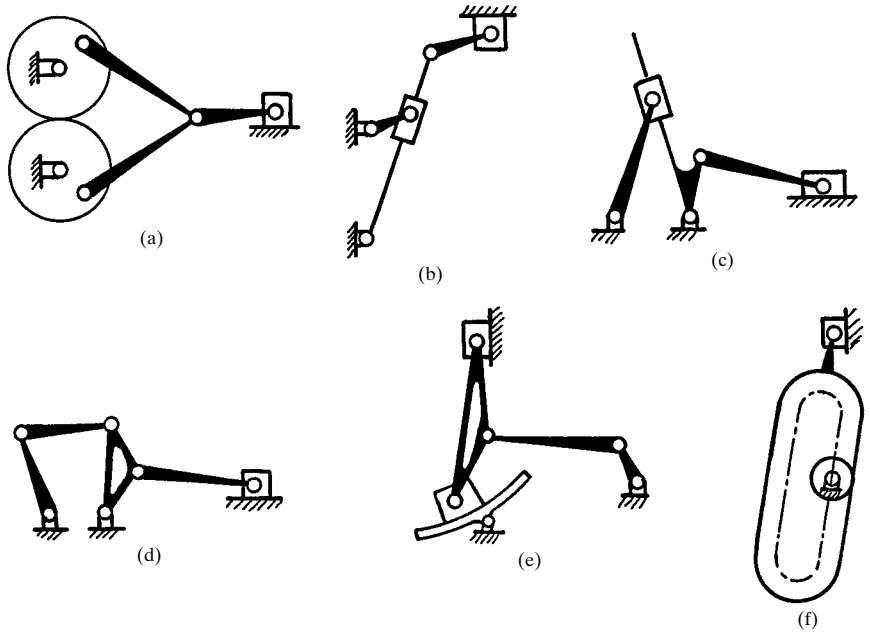

FIGURE 2.13 Reciprocating mechanisms II. (*a*) Geared cranks; (*b*) shaper mechanism; (*c*) slider on Whitworth quick-return mechanisms; (*d*) slider on drag-link mechanism; (*e*) variable-stroke engine; (*f*) gear-driven slider.

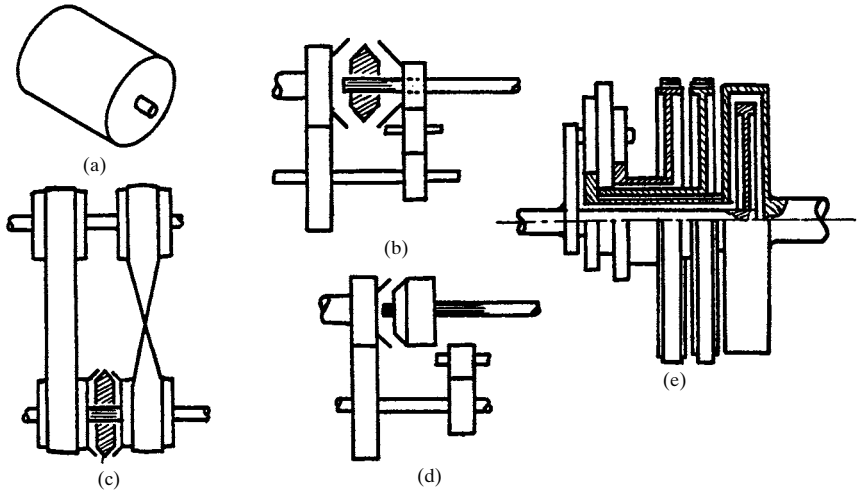

FIGURE 2.14 Reversing mechanism. These mechanical devices change the direction of rotation of the output. (*a*) Reversible prime movers; (*b*) reversing gears; (*c*) reversing belts; (*d*) transmission; (*e*) epicyclic gears as in Model T Ford.

A THESAURUS OF MECHANISMS

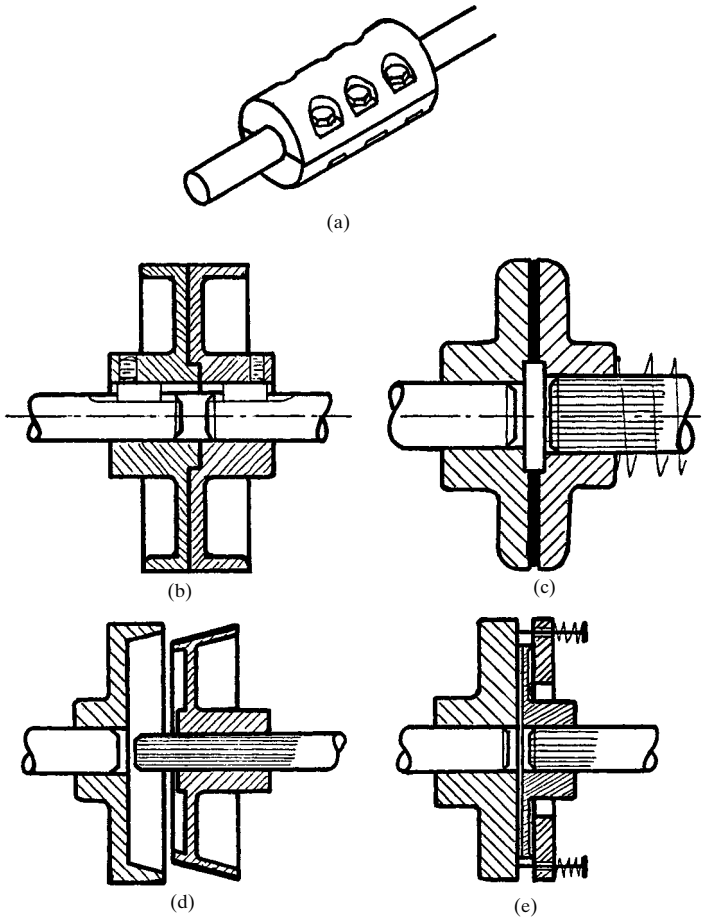

FIGURE 2.15 Couplings and connectors—axial. These are used to connect coaxial shafts. (*a*) Rigid coupling; (*b*) flanged coupling; (*c*) disk clutch; (*d*) cone clutch; (*e*) plate clutch.

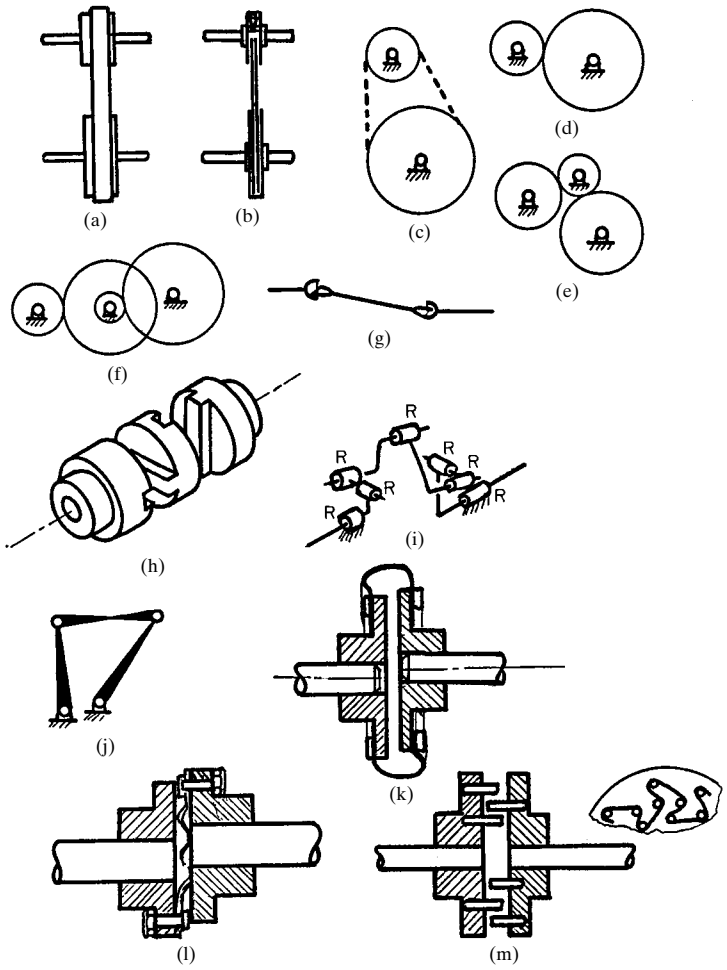

FIGURE 2.16 Couplings and connectors—parallel shafts. (*a*) Flat belt; (*b*) V belt; (*c*) chain; (*d*) to (*f*) gears; (*g*) Hooke joints; (*h*) Oldham coupling; (*i*) Hunt's constant-velocity coupling; (*j*) drag link; (*k*) to (*m*) flexible coupling.

A THESAURUS OF MECHANISMS

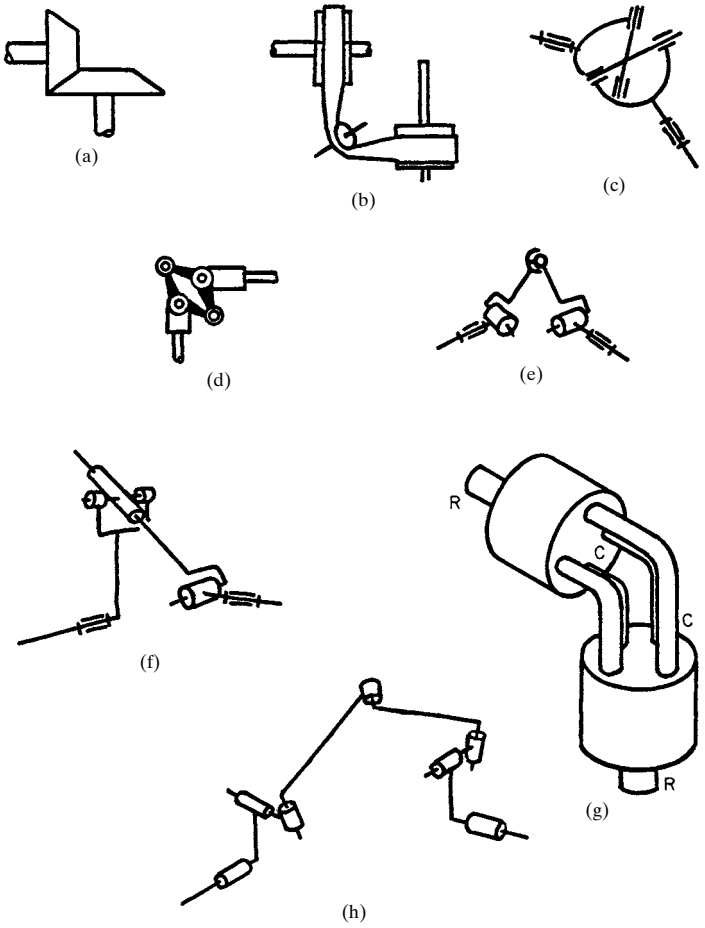

FIGURE 2.17 Couplings and connectors—intersecting shafts. (*a*) Bevel gears; (*b*) flat belts with idlers; (*c*) Hooke joint; (*d*) Hooke's coupling; (*e*) Clemens coupling; (*f*) Rouleaux coupling; (*g*) spatial RCCR; (*h*) Hunt's constant-velocity coupling.

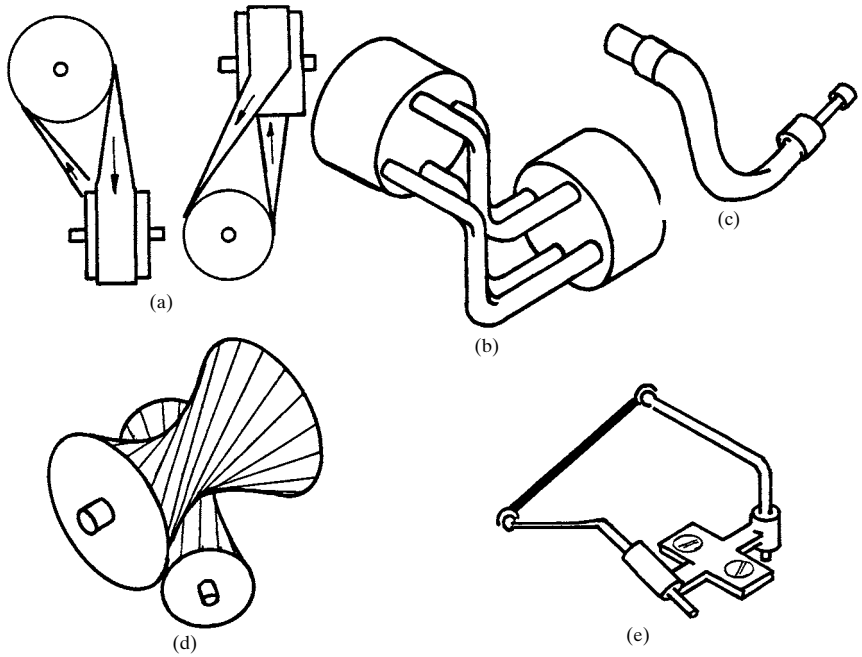

FIGURE 2.18 Couplings and connectors—skew shafts. (*a*) Flat belts; (*b*) spatial RCCR; (*c*) flexible shaft; (*d*) hypoid gears; (*e*) spatial RGGR.

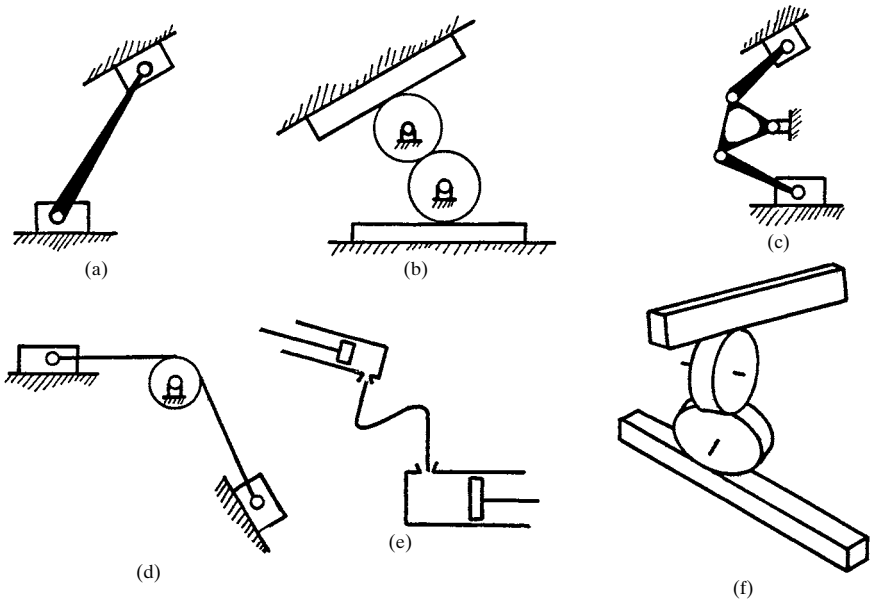

FIGURE 2.19 Slider connectors. These devices connect two or more reciprocating devices. (*a*) Elliptic trammel; (*b*) gears; (*c*) slider-crank-slider; (*d*) cable; (*e*) hydraulic; (*f*) helical gearing.

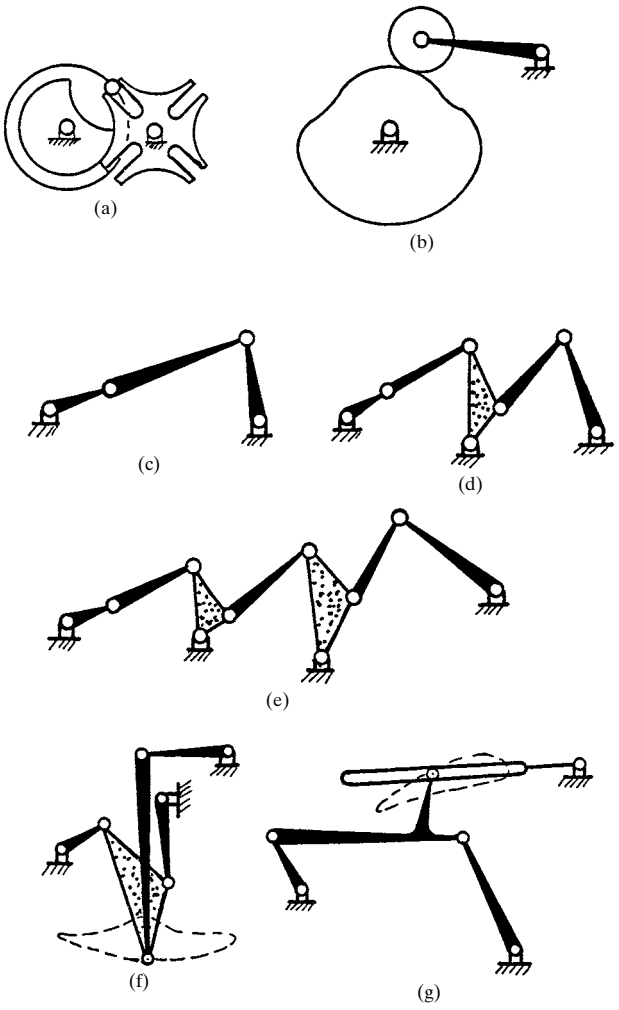

FIGURE 2.20 Stops, pauses, and hesitations. These machine elements cause an output to stop and dwell, to stop and return, to stop and advance, etc. The derivatives of the motion at the stop determine which category the motion fits. (*a*) Geneva stops (this includes all motions in Fig. 2.8); (*b*) cams; (*c*) linkage at extreme limits; (*d*), (*e*) combination of linkages at a limit; (*f*), (*g*) outputs derived from coupler curves.

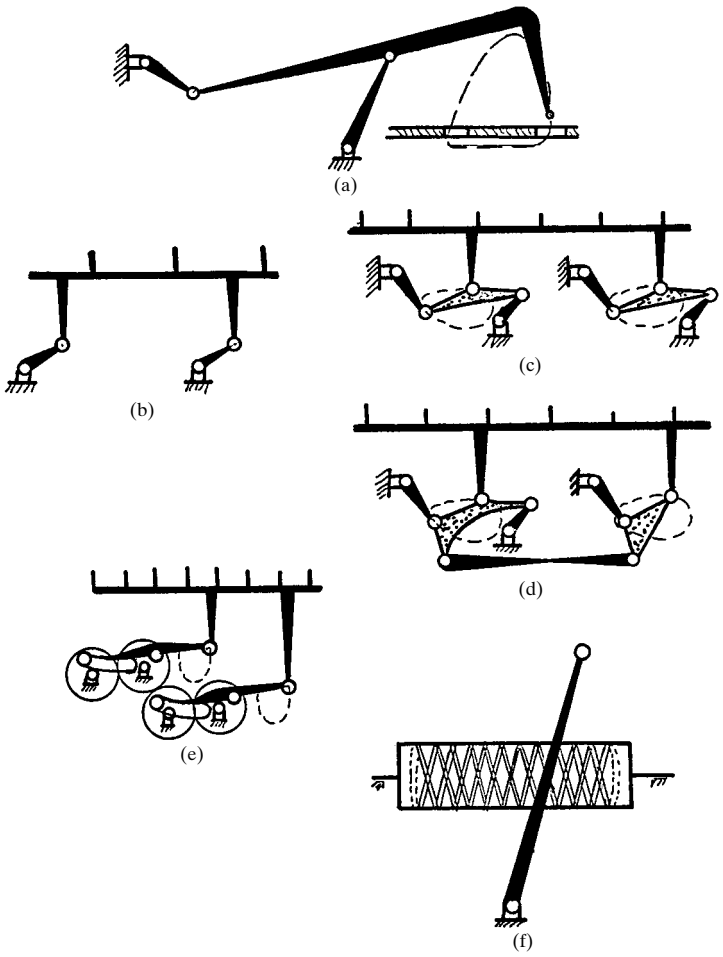

FIGURE 2.21 Transportation devices. These mechanisms move one or more objects a discrete distance in stepped motion. (*a*) Four-bar film advance; (*b*) circular-motion transport; (*c*), (*d*) coupler-curve transport; (*e*) geared linkage transport; (*f*) fishing-reel feed.

A THESAURUS OF MECHANISMS

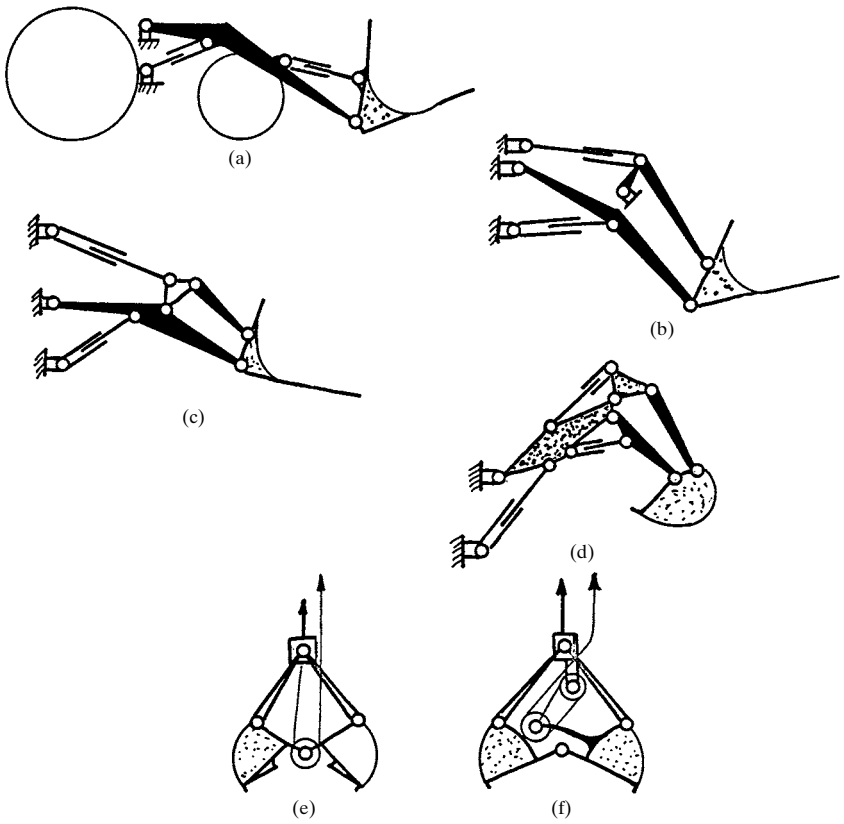

FIGURE 2.22 Loading and unloading mechanisms I. These mechanisms pick up material and transport it to another location. (*a*) to (*c*) Front-end loaders; (*d*) backhoe; (*e*), (*f*) clamshell loaders.

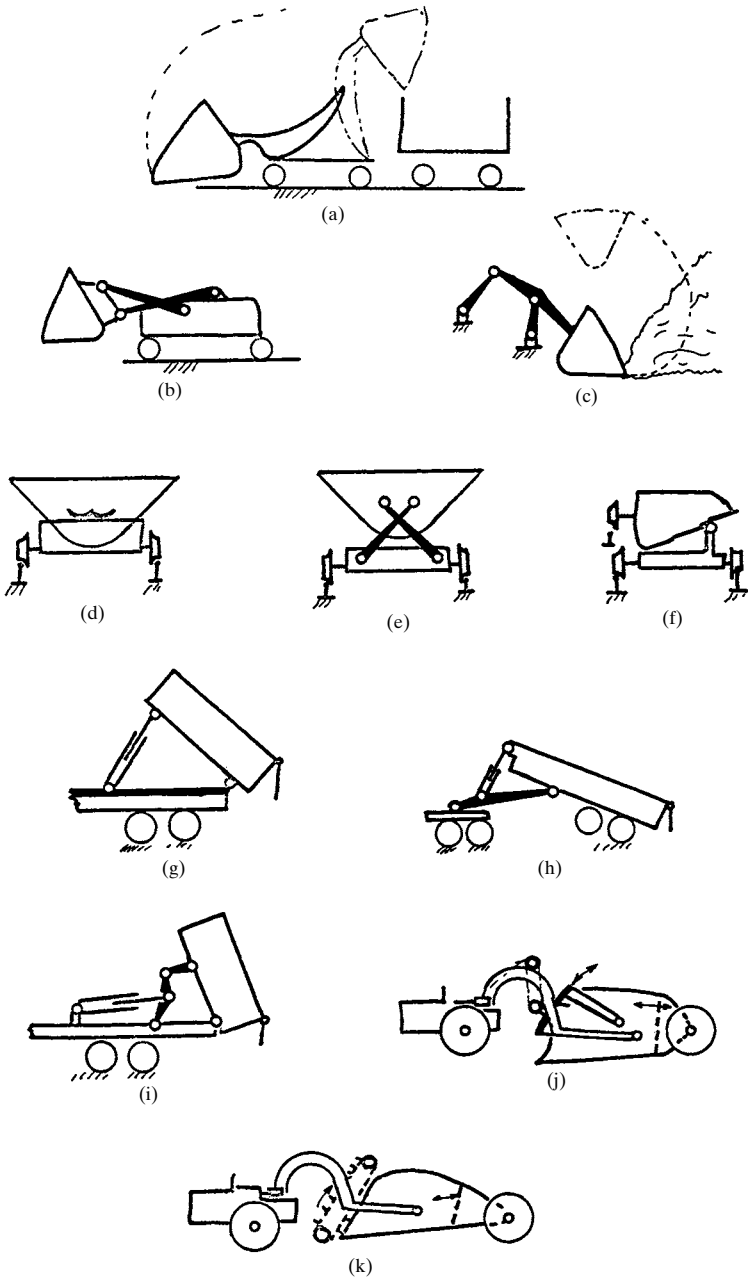

FIGURE 2.23 Loading and unloading mechanisms II. (*a*), (*b*) Mucking machines; (*c*) scooping mechanism; (*d*) to (*f*) dumping mine cars; (*g*) to (*i*) dump trucks; (*j*) motor scraper; (*k*) elevating scraper.

A THESAURUS OF MECHANISMS

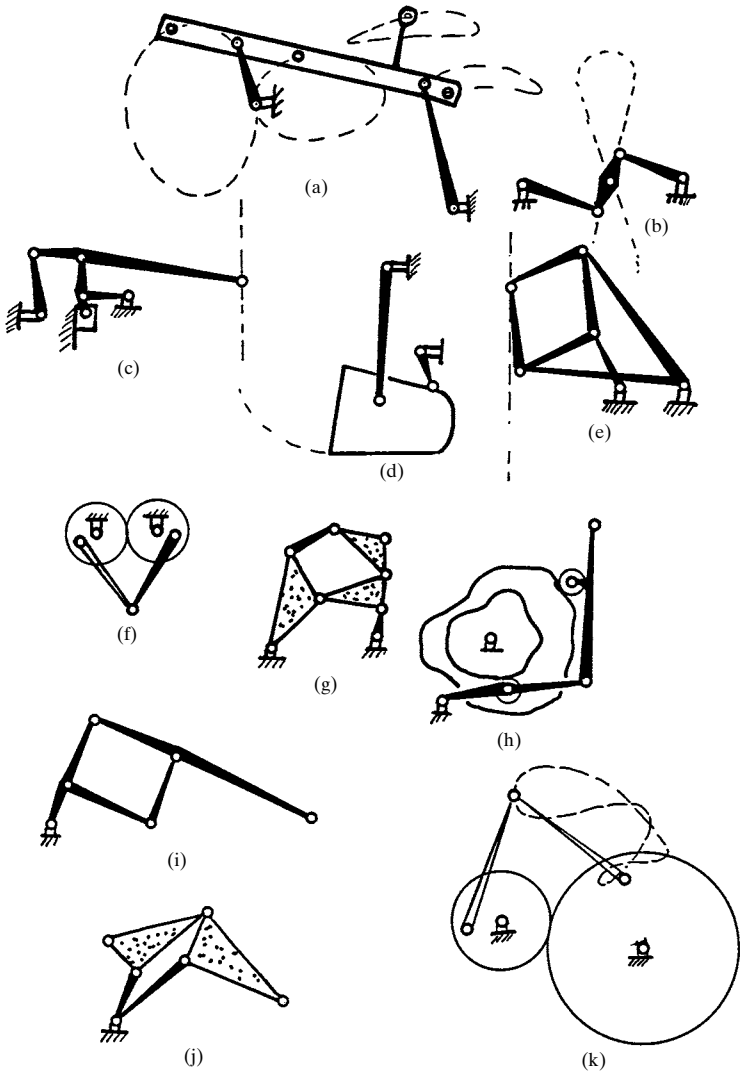

FIGURE 2.24 Path generators. These linkages approximately generate a required curve. (*a*) Four-bar coupler curve; (*b*) Watt straight-line linkage; (*c*) Crosby steam-engine indicator approximates straight line; (*d*) scooping mechanism; (*e*) Peaucellier exact straight-line linkage; (*f*) geared straight-line generators; (*g*) six-bar coupler curve; (*h*) double-cam line generator; (*i*) pantograph; (*j*) Sylvester skew pantograph; (*k*) geared linkage curve generator.

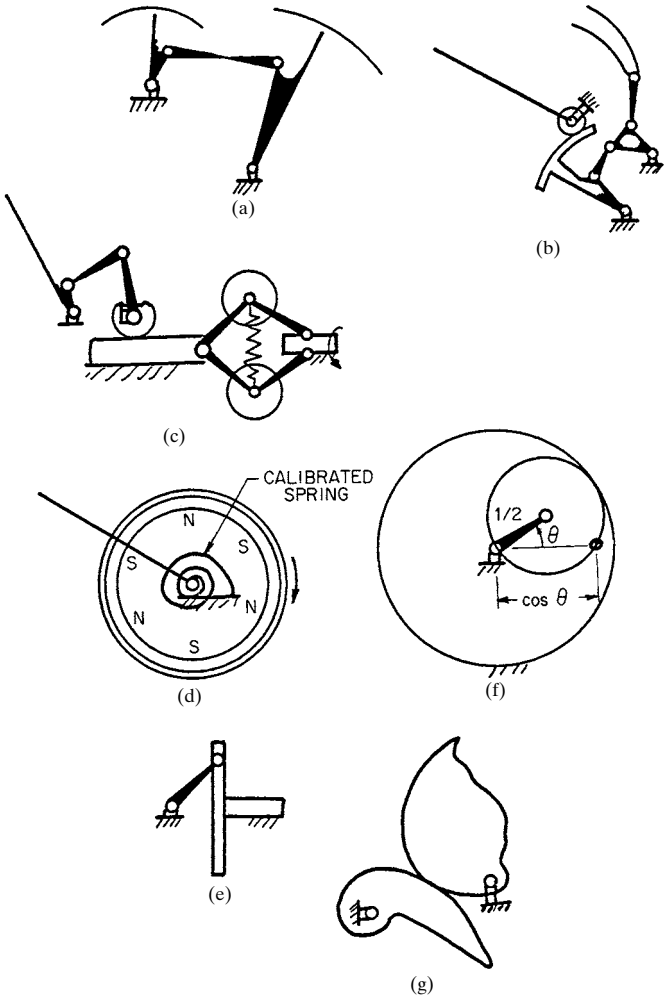

FIGURE 2.25 Function generators. These are mechanical devices in which the output moves as some function of the input $y = f(x)$. (*a*) Four-bar linkage function generator; (*b*) function generator in pressure gauge; (*c*), (*d*) function generator in a speedometer; (*e*) Scotch yoke sine-cosine generator; (*f*) epicyclic sine-cosine generator; (*g*) noncircular gears.

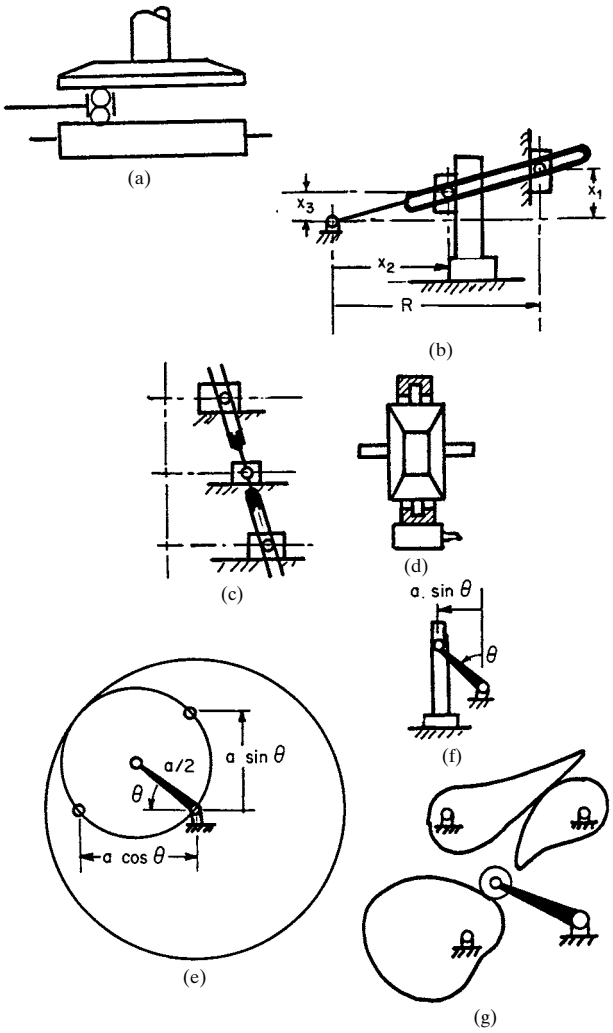

FIGURE 2.26 Computing mechanisms. These devices are used on mechanical computers for performing mathematical operations. (*a*) Ball disk integrator; (*b*) multiplier; (*c*), (*d*) adders; (*e*) epicyclic sine generators; (*f*) Scotch yoke sine generator; (*g*) noncircular gears; (*h*) special-function cams.

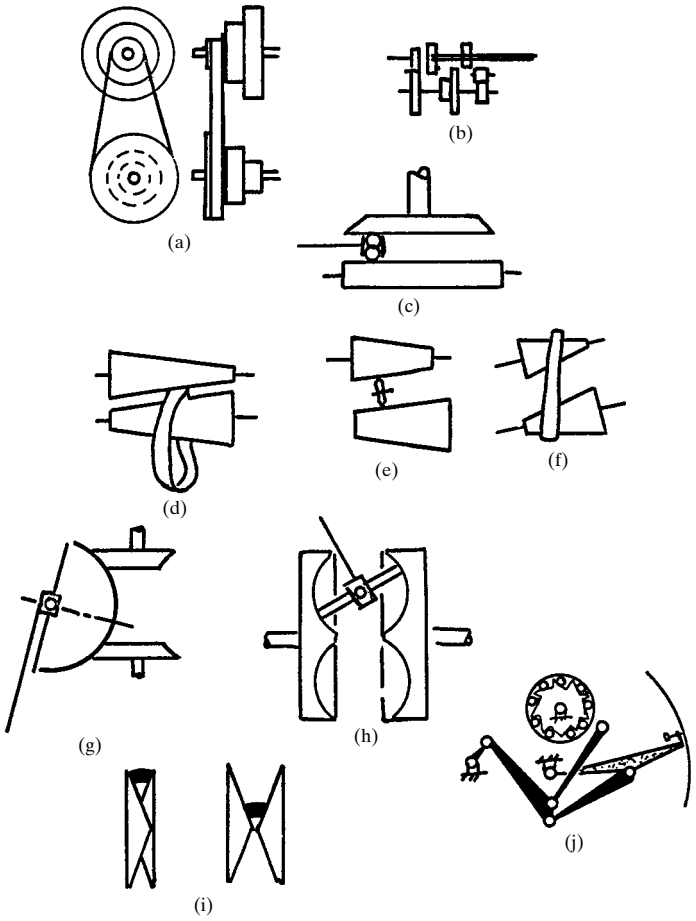

FIGURE 2.27 Speed-changing mechanisms. These devices change the speed of an output shaft while the input shaft has constant speed. (*a*) Stepped pulleys and flat belt; (*b*) geared transmission; (*c*) ball and disk speed changer; (*d*) to (*f*) cone drives; (*g*) sphere drive; (*h*) toroidal drive; (*i*) variable-pitch V belt; (*j*) zero maximum drive.

A THESAURUS OF MECHANISMS

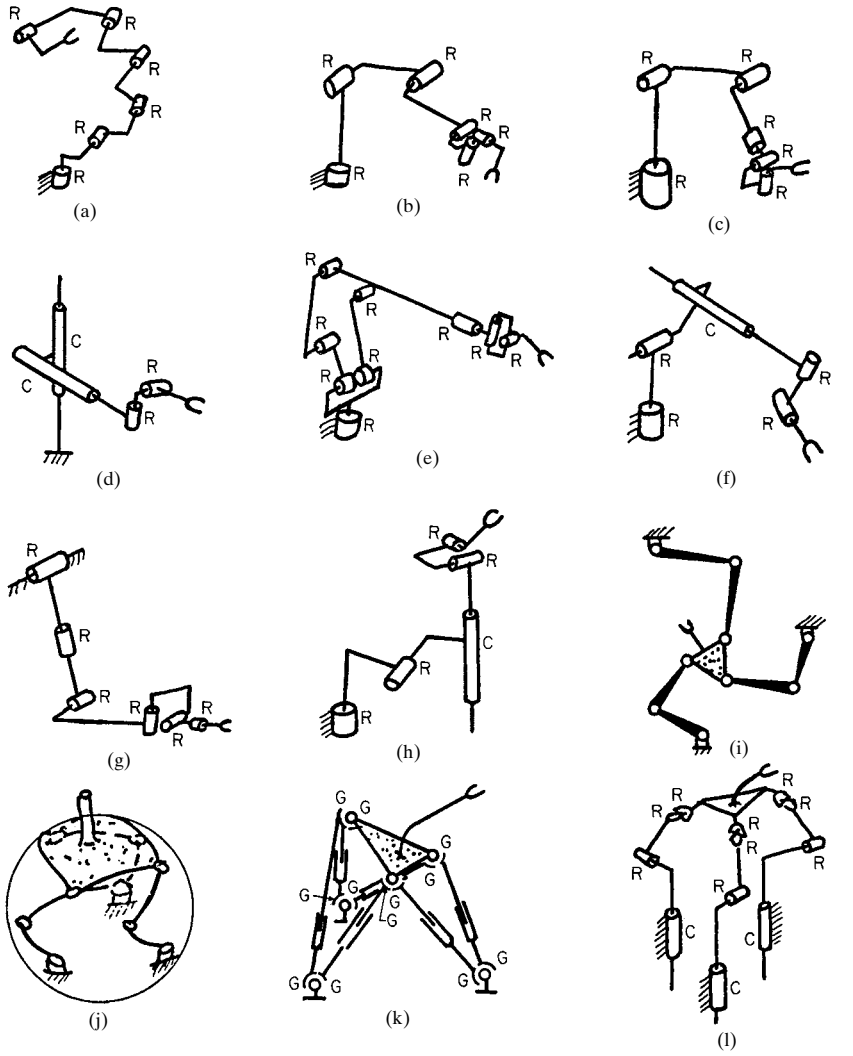

FIGURE 2.28 Robots. These are multidegree-of-freedom devices used for positioning or assembly of items. They usually have some degree of machine intelligence and work under computer control. (*a*) A general 6R robot; (*b*) to (*h*) some forms of existing robots; (*i*) parallel actuation of a planar 3-degrees-of-freedom robot; (*j*) Stewart platform which uses the 3-degrees-of-freedom principle; (*k*) Florida shoulder with parallel actuation; (*l*) general robot with parallel actuation.

CHAPTER 3
LINKAGES

Richard E. Gustavson
Technical Staff Member
The Charles Stark Draper Laboratory, Inc.
Cambridge, Massachusetts

Linkages are mechanical devices that appear very straightforward to both analyze and design. Given proper technique, that is generally the case. The methods described in this chapter reveal the complexity (and, I think, the beauty) of linkages. I have gained significant satisfaction during my 20 years of work with them from both theoretical and functioning hardware standpoints.

3.1 BASIC LINKAGE CONCEPTS

3.1.1 Kinematic Elements

A linkage is composed of rigid-body members, or *links,* connected to one another by rigid kinematic elements, or *pairs.* The nature of those connections as well as the shape of the links determines the kinematic properties of the linkage.

Although many kinematic pairs are conceivable and most do physically exist, only four have general practical use for linkages. In Fig. 3.1, the four cases are seen to include two with one degree of freedom ($f = 1$), one with $f = 2$, and one with $f = 3$. Single-degree-of-freedom pairs constitute joints in planar linkages or spatial linkages. The cylindrical and spherical joints are useful only in spatial linkages.

The links which connect these kinematic pairs are usually binary (two connections) but may be tertiary (three connections) or even more. A commonly used tertiary link is the *bell crank* familiar to most machine designers. Since our primary

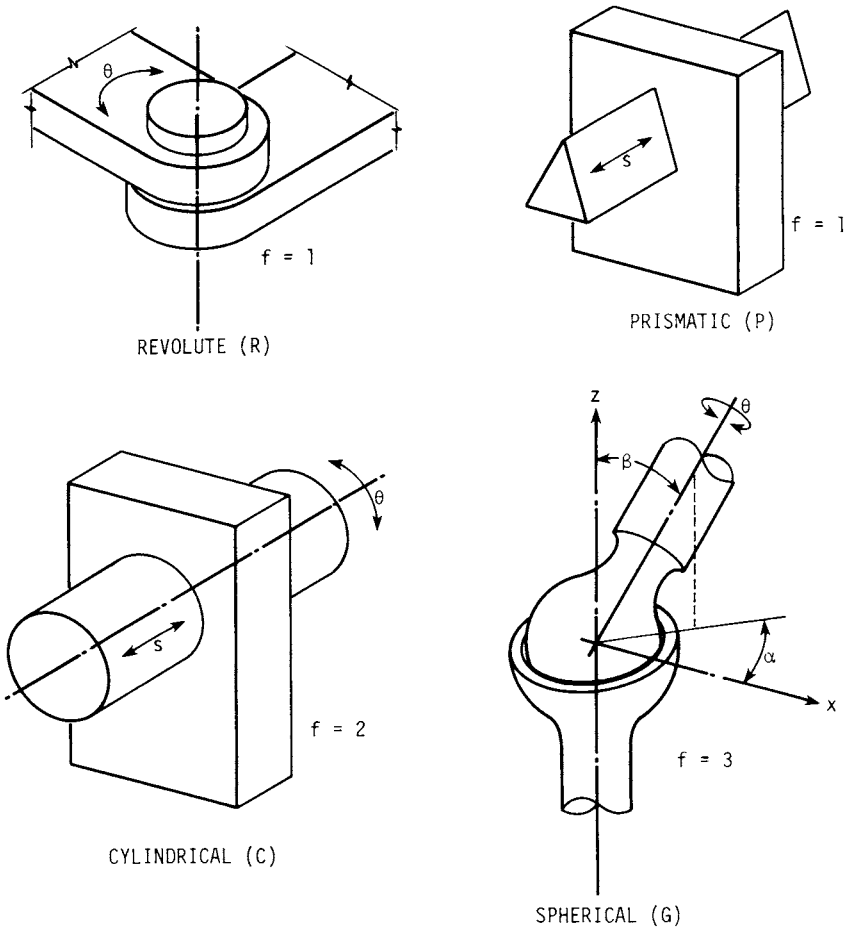

FIGURE 3.1 Kinematic pairs useful in linkage design. The quantity f denotes the number of degrees of freedom.

interest in most linkages is to provide a particular output for a prescribed input, we deal with closed kinematic chains, examples of which are depicted in Fig. 3.2. Considerable work is now under way on robotics, which are basically open chains. Here we restrict ourselves to the closed-loop type. Note that many complex linkages can be created by compounding the simple four-bar linkage. This may not always be necessary once the design concepts of this chapter are applied.

3.1.2 Freedom of Motion

The degree of freedom for a mechanism is expressed by the formula

$$F = \lambda(l - j - 1) + \sum_{i=1}^{j} f_i \tag{3.1}$$

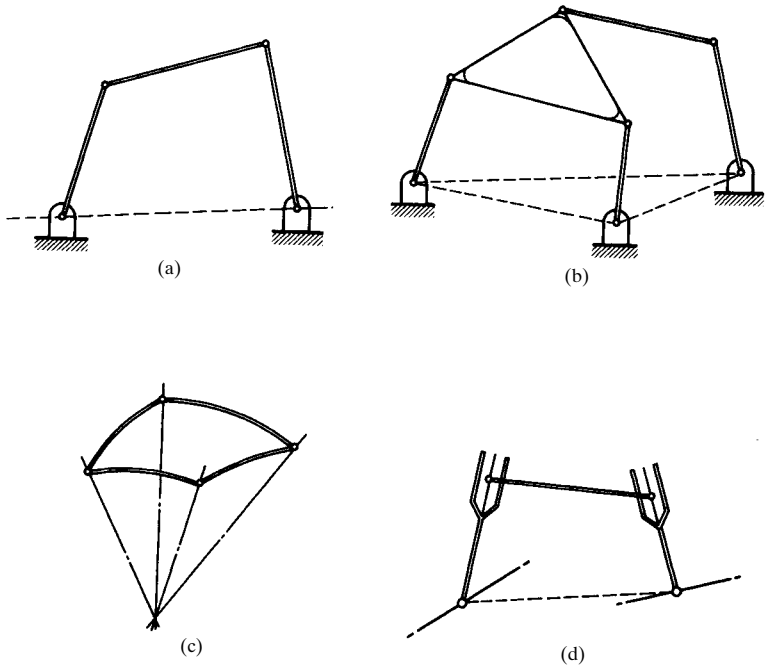

FIGURE 3.2 Closed kinematic chains. (*a*) Planar four-bar linkage; (*b*) planar six-bar linkage; (*c*) spherical four-bar linkage; (*d*) spatial RCCR four-bar linkage.

where l = number of links (fixed link included)
j = number of joints
f_i = f of ith joint
λ = integer
= 3 for plane, spherical, or particular spatial linkages
= 6 for most spatial linkages

Since the majority of linkages used in machines are planar, the particular case for plane mechanisms with one degree of freedom is found to be

$$2j - 3l + 4 = 0 \tag{3.2}$$

Thus, in a four-bar linkage, there are four joints (either revolute or prismatic). For a six-bar linkage, we need seven such joints. A peculiar special case occurs when a sufficient number of links in a plane linkage are parallel, which leads to such special devices as the pantograph.

Considerable theory has evolved over the years about numerous aspects of linkages. It is often of little help in creating usable designs. Among the best references available are Hartenberg and Denavit [3.9], Hall [3.8], Beyer [3.1], Hain [3.7], Rosenauer and Willis [3.10], Shigley and Uicker [3.11], and Tao [3.12].

3.1.3 Number Synthesis

Before you can dimensionally synthesize a linkage, you may need to use *number synthesis,* which establishes the number of links and the number of joints that are

required to obtain the necessary mobility. An excellent description of this subject appears in Hartenberg and Denavit [3.9]. The four-bar linkage is emphasized here because of its wide applicability.

3.2 MOBILITY CRITERION

In any given four-bar linkage, selection of any link to be the crank may result in its inability to fully rotate. This is not always necessary in practical mechanisms. A criterion for determining whether any link might be able to rotate 360° exists. Refer to Fig. 3.3, where *l, s, p,* and *q* are defined. *Grubler's criterion* states that

$$l + s < p + q \tag{3.3}$$

If the criterion is not satisfied, only double-rocker linkages are possible. When it is satisfied, choice of the shortest link as driver will result in a crank-rocker linkage; choice of any of the other three links as driver will result in a drag link or a double-rocker mechanism.

A significant majority of the mechanisms that I have designed in industry are the double-rocker type. Although they do not possess some theoretically desirable characteristics, they are useful for various types of equipment.

3.3 ESTABLISHING PRECISION POSITIONS

In designing a mechanism with a certain number of required precision positions, you will be faced with the problem of how to space them. In many practical situations, there will be no choice, since particular conditions must be satisfied.

If you do have a choice, Chebychev spacing should be used to reduce the structural error. Figure 3.4 shows how to space four positions within a prescribed interval [3.9]. I have found that the end-of-interval points can be used instead of those just inside with good results.

3.4 PLANE FOUR-BAR LINKAGE

3.4.1 Basic Parameters

The apparently simple four-bar linkage is actually an incredibly sophisticated device which can perform wonders once proper design techniques are known and used. Figure 3.5 shows the parameters required to define the general case. Such a linkage can be used for three types of motion:

1. *Crank-angle coordination.* Motion of driver link *b* causes prescribed motion of link *d.*
2. *Path generation.* Motion of driver link *b* causes point *C* to move along a prescribed path.
3. *Motion generation.* Movement of driver link *b* causes line *CD* to move in a prescribed planar motion.

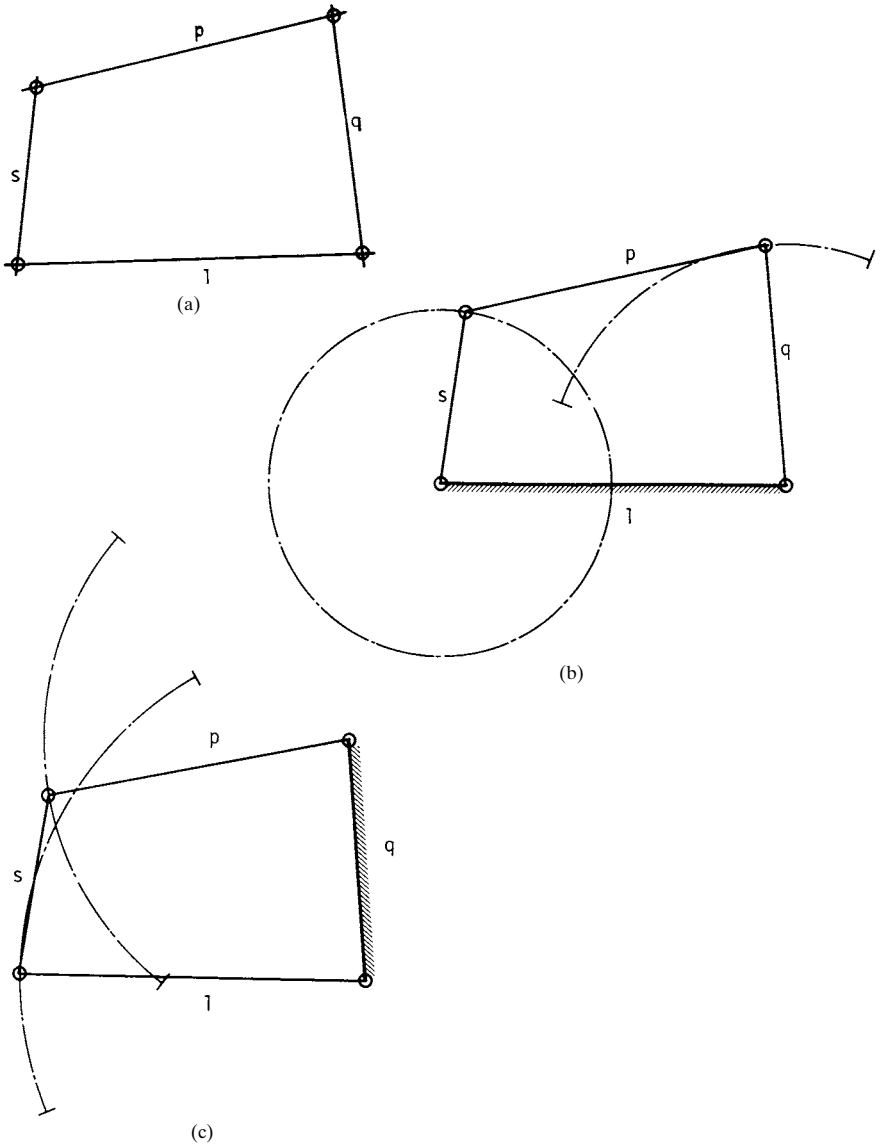

FIGURE 3.3 Mobility characteristics. (*a*) Closed four-link kinematic chain: *l* = longest link, *s* = shortest link, *p, q* = intermediate-length links; (*b*) crank-rocker linkage; (*c*) double-rocker linkage.

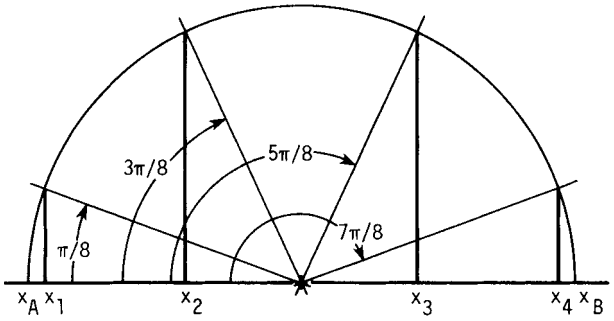

FIGURE 3.4 Four-precision-point spacing (Chebychev)

$$x_1 = x_A + 0.0381(x_B - x_A) \qquad x_2 = x_A + 0.3087(x_B - x_A)$$
$$x_3 = x_A + 0.6913(x_B - x_A) \qquad x_4 = x_A + 0.9619(x_B - x_A)$$

In general, for n precision points

$$x_j = \frac{1}{2}(x_A + x_B) - \frac{1}{2}(x_B - x_A)\cos\frac{\pi(2j-1)}{2n} \qquad j = 1, 2, \ldots, n$$

3.4.2 Kinematic Inversion

A very useful concept in mechanism design is that by inverting the motion, new interesting characteristics become evident. By imagining yourself attached to what is actually a moving body, you can determine various properties, such as the location of a joint which connects that body to its neighbor. This technique has been found useful in many industrial applications, such as the design of the four-bar automobile window regulator ([3.6]).

3.4.3 Velocity Ratio

At times the velocity of the output will need to be controlled as well as the corresponding position. When the motion of the input crank and the output crank is coordinated, it is an easy matter to establish the velocity ratio ω_d/ω_b. When you extend line AB in Fig. 3.5 until it intersects the line through the fixed pivots O_A and O_B in a point S, you find that

$$\frac{\omega_d}{\omega_b} = \frac{O_A S}{O_A O_B + O_A S} \tag{3.4}$$

Finding the linear velocity of a point on the coupler is not nearly as straightforward. A very good approximation is to determine the travel distance along the path of the point during a particular motion of the crank.

3.4.4 Torque Ratio

Because of the conservation of energy, the following relationship holds:

$$T_b d\phi = T_d d\psi \tag{3.5}$$

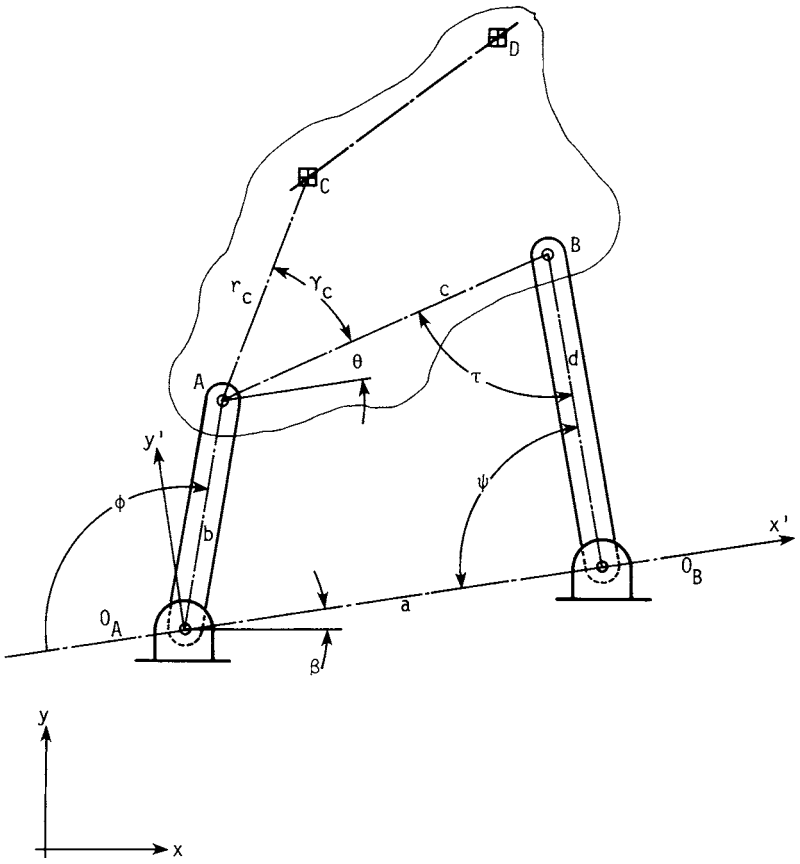

FIGURE 3.5 General four-bar linkage in a plane.

Since both sides of (3.5) can be divided by *dt,* we have, after some rearranging,

$$n = \frac{T_b}{T_d} = \frac{d\psi/dt}{d\phi/dt} = \frac{\omega_d}{\omega_b} \tag{3.6}$$

The torque ratio n is thus the inverse of the velocity ratio. Quite a few mechanisms that I have designed have made significant use of torque ratios.

3.4.5 Transmission Angle

For the four-bar linkage of Fig. 3.5, the transmission angle τ occurs between the coupler and the driven link. This angle should be as close to 90° as possible. Useful linkages for motion generation have been created with τ approaching 20°. When a crank rocker is being designed, you should try to keep $45° < \tau < 135°$. Double-rocker or drag link mechanisms usually have other criteria which are more significant than the transmission angle.

3.5 PLANE OFFSET SLIDER-CRANK LINKAGE

A variation of the four-bar linkage which is often seen occurs when the output link becomes infinitely long and the path of point B is a straight line. Point B becomes the slider of the slider-crank linkage. Although coupler b could have the characteristics shown in Fig. 3.6, it is seldom used in practice. Here we are interested in the motion of point B while crank a rotates. In general, the path of point B does not pass through the fixed pivot O_A, but is offset by dimension ε. An obvious example of the degenerate case ($\varepsilon \equiv 0$) is the piston crank in an engine.

The synthesis of this linkage is well described by Hartenberg and Denavit [3.9]. I have used the method many times after programming it for the digital computer.

3.6 KINEMATIC ANALYSIS OF THE PLANAR FOUR-BAR LINKAGE

3.6.1 Position Geometry

Refer to Fig. 3.7, where the parameters are defined. Given the link lengths a, b, c, and d and the crank position angle ϕ, the angular position of coupler c is

$$\theta = \pi - (\tau + \psi) \tag{3.7}$$

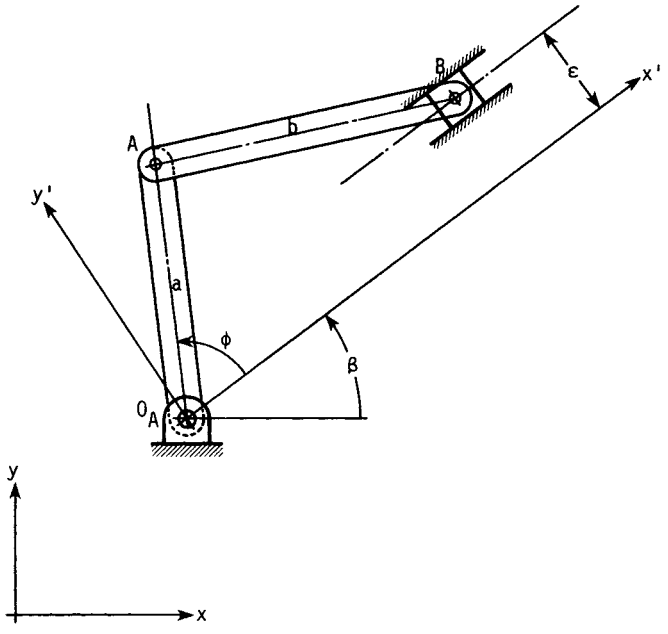

FIGURE 3.6 General offset slider-crank linkage.

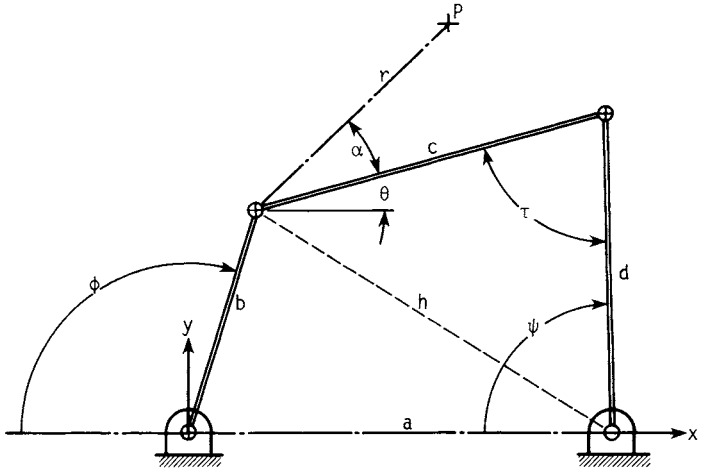

FIGURE 3.7 Parameters for analysis of a four-bar linkage.

The driven link d will be at angle

$$\psi = \cos^{-1}\frac{h^2 + a^2 - b^2}{2hb} + \cos^{-1}\frac{h^2 + d^2 - c^2}{2hd} \tag{3.8}$$

where

$$h^2 = a^2 + b^2 + 2ab\cos\phi \tag{3.9}$$

The transmission angle τ will be

$$\tau = \cos^{-1}\frac{c^2 + d^2 - a^2 - b^2 - 2ab\cos\phi}{2cd} \tag{3.10}$$

A point on coupler P has coordinates

$$\begin{aligned} P_x &= -b\cos\phi + r\cos(\theta + \alpha) \\ P_y &= b\sin\phi + r\sin(\theta + \alpha) \end{aligned} \tag{3.11}$$

3.6.2 Velocity and Acceleration

The velocity of the point on the coupler can be expressed as

$$\begin{aligned} \frac{dP_x}{dt} &= b\frac{d\phi}{dt}\sin\phi - r\frac{d\theta}{dt}\sin(\theta + \alpha) \\ \frac{dP_y}{dt} &= b\frac{d\phi}{dt}\cos\phi + r\frac{d\theta}{dt}\cos(\theta + \alpha) \end{aligned} \tag{3.12}$$

As you can see, the mathematics gets very complicated very rapidly. If you need to establish velocity and acceleration data, consult Ref. [3.1], [3.7], or [3.11]. Computer analysis is based on the closed vector loop equations of C. R. Mischke, developed at Pratt Institute in the late 1950s. See [3.19], Chap. 4.

3.6.3 Dynamic Behavior

Since all linkages have clearances in the joints as well as mass for each link, high-speed operation of a four-bar linkage can cause very undesirable behavior. Methods for solving these problems are very complex. If you need further data, refer to numerous theoretical articles originally presented at the American Society of Mechanical Engineers (ASME) mechanism conferences. Many have been published in ASME journals.

3.7 DIMENSIONAL SYNTHESIS OF THE PLANAR FOUR-BAR LINKAGE: MOTION GENERATION

3.7.1 Two Positions of a Plane

The line A_iB_i defines a plane (Fig. 3.8) which is to be the coupler of the linkage to be designed. When two positions are defined, you can determine a particular point, called the *pole* (in this case P_{12}, since the motion goes from position 1 to position 2). The significance of the pole is that it is the point about which the motion of the body is a simple rotation; the pole is seen to be the intersection of the perpendicular bisectors of A_1A_2 and B_1B_2.

A four-bar linkage can be created by choosing any point on a_1a_2 as O_A and any reasonable point on b_1b_2 as O_B. Note that you do not have a totally arbitrary choice for the fixed pivots, even for this elementary case. There are definite limitations, since the four-bar linkage must produce continuous motion between all positions. When a fully rotating crank is sought, the Grubler criterion must be adhered to. For double-rocker mechanisms, the particular link lengths still have definite criteria to meet. You have to check these for every four-bar linkage that you design.

3.7.2 Three Positions of a Plane

When three positions of a plane are specified by the location of line *CD,* as shown in Fig. 3.9, it is possible to construct the center of a circle through C_1, C_2, and C_3 and through D_1, D_2, and D_3. This is only one of an infinite combination of links that can be attached to the moving body containing line *CD.* If the path of one end of line *CD* lies on a circle, then the other end can describe points on a coupler path which correspond to particular rotation angles of the crank (Fig. 3.10); that is a special case of the motion generation problem.

The general three-position situation describes three poles P_{12}, P_{13}, and P_{23} which form a *pole triangle.* You will find this triangle useful since its interior angles ($\theta_{12}/2$ in Fig. 3.9) define precise geometric relationships between the fixed and moving pivots of links which can be attached to the moving body defined by line *CD.* Examples of this geometry are shown in Fig. 3.11, where you can see that

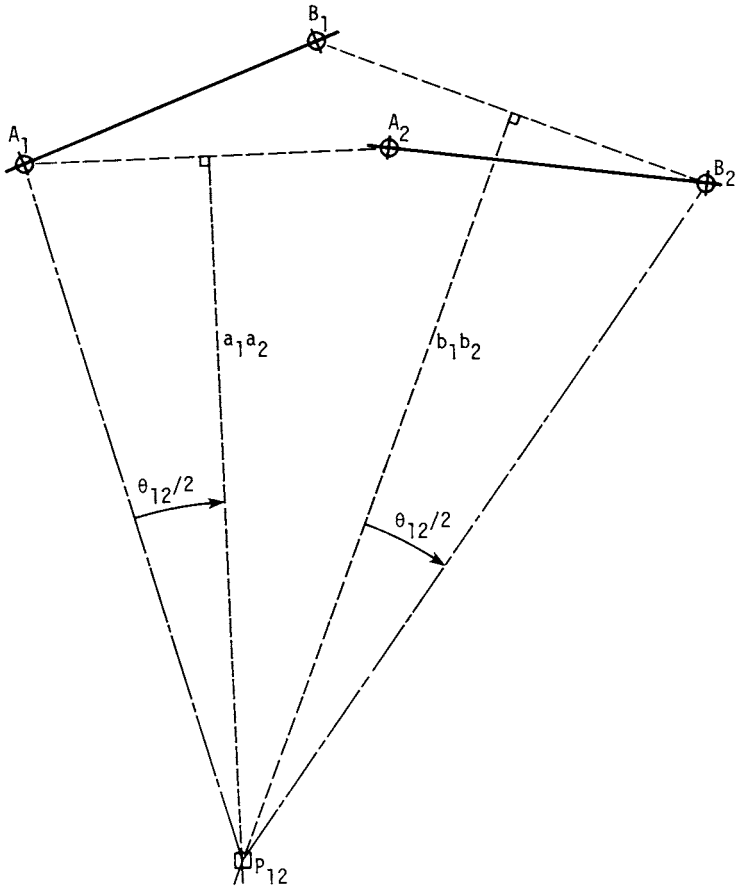

FIGURE 3.8 Two positions of a plane: definition of pole P_{12}.

$$\angle P_{13}P_{12}P_{23} \equiv \angle A_1P_{12}O_A \equiv \angle B_1P_{12}O_B \tag{3.13}$$

The direction in which these angles are measured is critical. For three positions, you may thus choose the fixed or the moving pivot and use this relationship to establish the location of the corresponding moving or fixed pivot, since it is also true that

$$\angle P_{12}P_{13}P_{23} = \angle A_1P_{13}O_A = \angle B_1P_{13}O_B \tag{3.14}$$

The intersection of two such lines (Fig. 3.12) is the required pivot point. Note that the lines defined by the pole triangle relationships extend in both directions from the pole; thus a pivot-point angle may appear to be ±180° from that defined within the triangle. This is perfectly valid.

It is important to observe that arbitrary choices for pivot locations are available when three positions, or less, of the moving plane are specified.

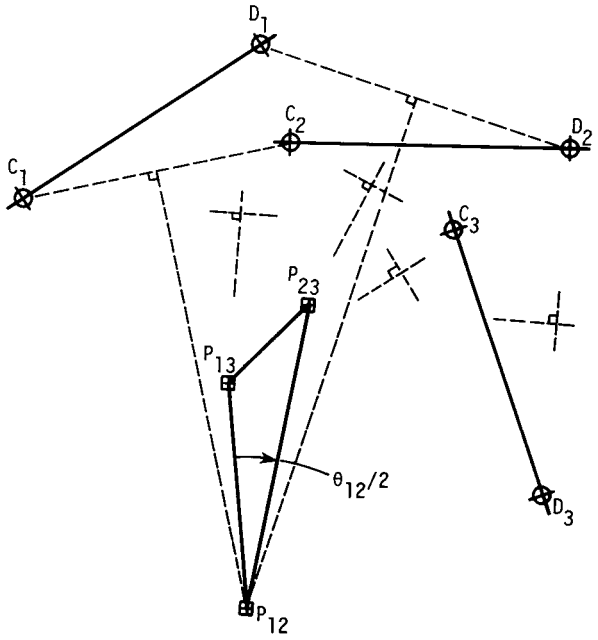

FIGURE 3.9 Three positions of a plane: definition of the pole triangle $P_{12}P_{13}P_{23}$.

3.7.3 Four Positions of a Moving Plane

When four positions are required, appropriate pivot-point locations are precisely defined by theories generated by Professor Burmester in Germany during the 1880s. His work [3.2] is the next step in using the poles of motion. When you define four positions of a moving plane containing line CD as shown in Fig. 3.13, six poles are defined:

$$P_{12} \quad P_{13} \quad P_{14} \quad P_{23} \quad P_{24} \quad P_{34}$$

By selecting opposite poles (P_{12}, P_{34} and P_{13}, P_{24}), you obtain a quadrilateral with significant geometric relationships. For practical purposes, this opposite-pole quadrilateral is best used to establish a locus of points which are the fixed pivots of links that can be attached to the moving body so that it can occupy the four prescribed positions. This locus is known as the *center-point curve* (Fig. 3.14) and can be found as follows:

1. Establish the perpendicular bisector of the two sides $P_{12}P_{24}$ and $P_{13}P_{34}$.
2. Determine points M and M' such that

$$\angle P_{12}MQ_2 \equiv \angle P_{13}M'Q_3$$

3. With M as center and MP_{12} as radius, create circle k. With M' as center and $M'P_{13}$ as radius, create circle k'.
4. The intersections of circles k and k' (shown as c_0 and c_0' in Fig. 3.14) are center points with the particular property that the link whose fixed pivot is c_0 or c_0' has a

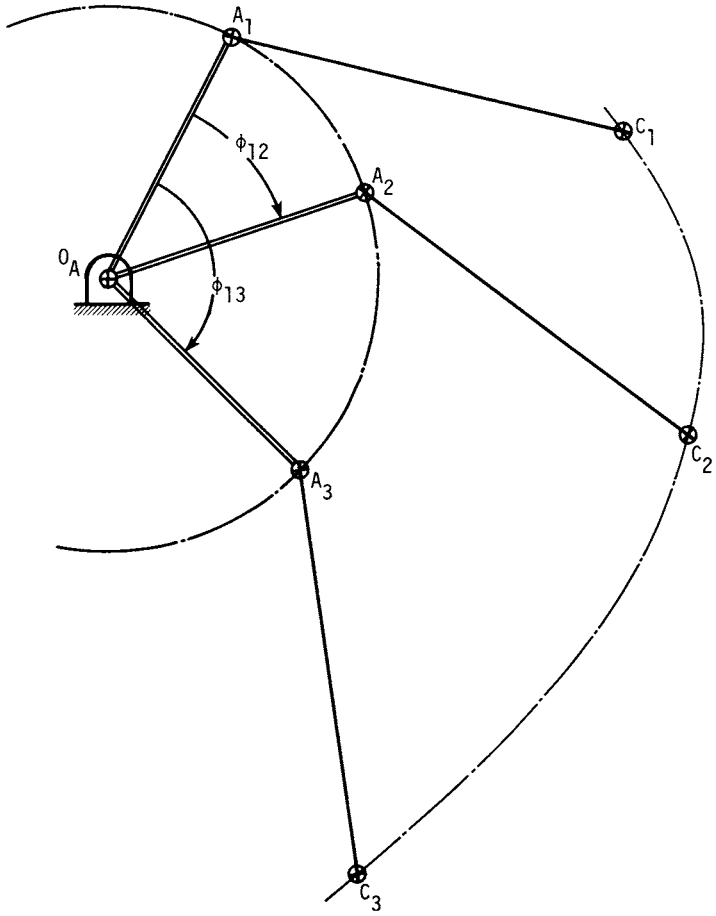

FIGURE 3.10 Path generation as a special case of motion generation.

total rotation angle twice the value defined by the angle(s) in step 2. The magnitude and direction of the link angle ϕ_{14} are defined in the figure.

Note that this construction can produce two, one, or no intersection points. Thus some link rotations are not possible. Depending on how many angles you want to investigate, there will still be plenty of choices. I have found it most convenient to solve the necessary analytic geometry and program it for the digital computer; as many accurate results as desired are easily determined.

Once a center point has been established, the corresponding moving pivot (circle point) can be established. For the first position of the moving body, you need to use the pole triangle $P_{12}P_{13}P_{23}$ angles to establish two lines whose intersection will be the circle point. In Fig. 3.15, the particular angles are

$$\angle P_{13}P_{12}P_{23} \equiv \angle c_1 P_{12} c_0$$

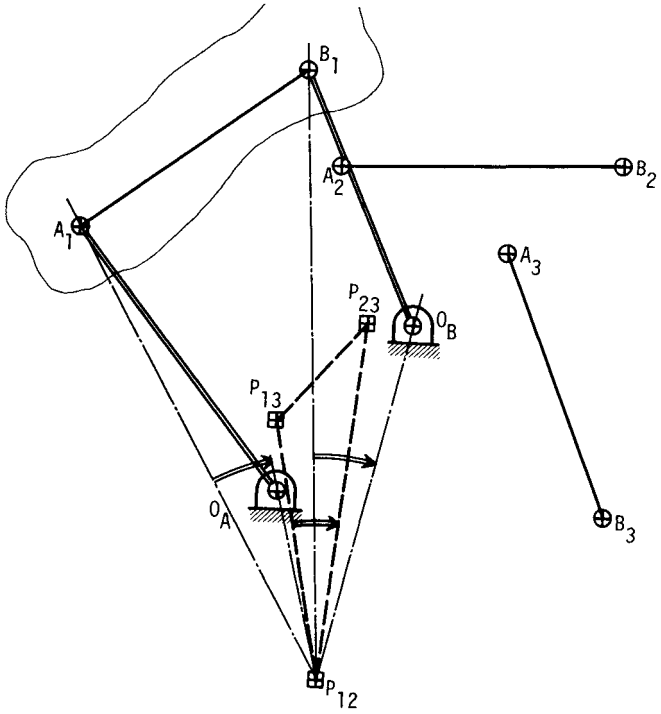

FIGURE 3.11 Geometric relationship between pole triangle angle(s) and location of link fixed and moving pivot points.

and

$$360° - \angle P_{23}P_{13}P_{12} \equiv \angle c_1P_{13}c_0$$

The second equality could also be written

$$\angle P_{23}P_{13}P_{12} \equiv \angle c_1P_{13}c_0 \pm 180°$$

A locus of points thus defined can be created as shown in Fig. 3.16. Each point on the circle-point curve corresponds to a particular point on the center-point curve. Some possible links are defined in Fig. 3.16; each has a known first-to-fourth-position rotation angle. Only those links whose length and/or pivot locations are within prescribed limits need to be retained.

The two intermediate positions of the link can be determined by establishing the location of the moving pivot (circle point) in the second and third positions of the moving body. Since the positions lie on the arc with center at the fixed pivot (center point) a and radius aa', it is easy to determine the link rotation angles as

$$\phi_{12} = \angle A_1O_AA_2 \qquad \phi_{13} = \angle A_1O_AA_3$$

Linkages need to be actuated or driven by one of the links. Knowing the three rotation angles allows you to choose a drive link which has the desired proportions

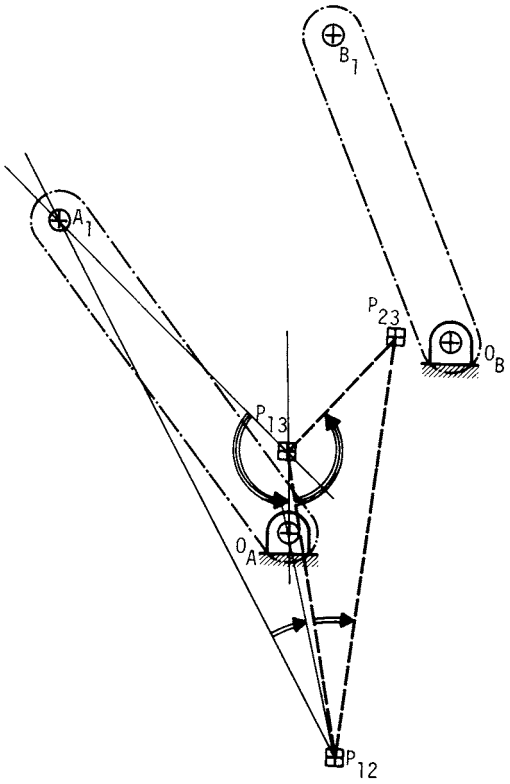

FIGURE 3.12 Determining the moving or fixed pivot by using the pole triangle.

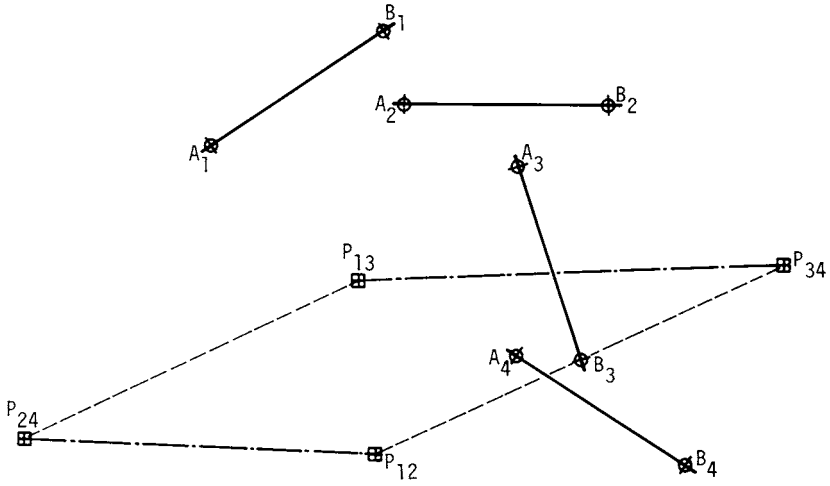

FIGURE 3.13 Four positions of a plane: definition of the opposite-pole quadrilateral formed by lines $P_{13}P_{24}$ and $P_{12}P_{34}$.

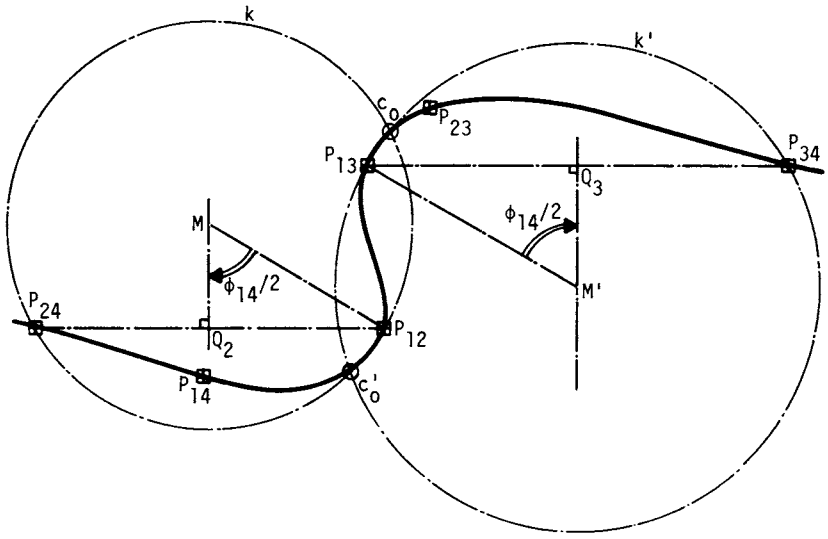

FIGURE 3.14 Determination of points on the center-point curve.

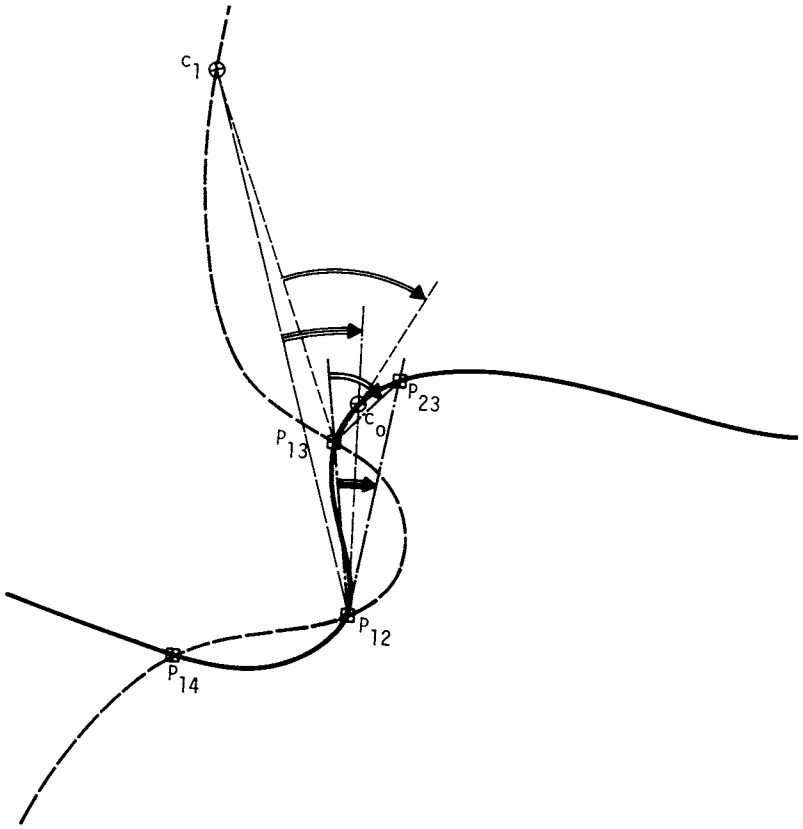

FIGURE 3.15 Determination of a circle point corresponding to a particular center point.

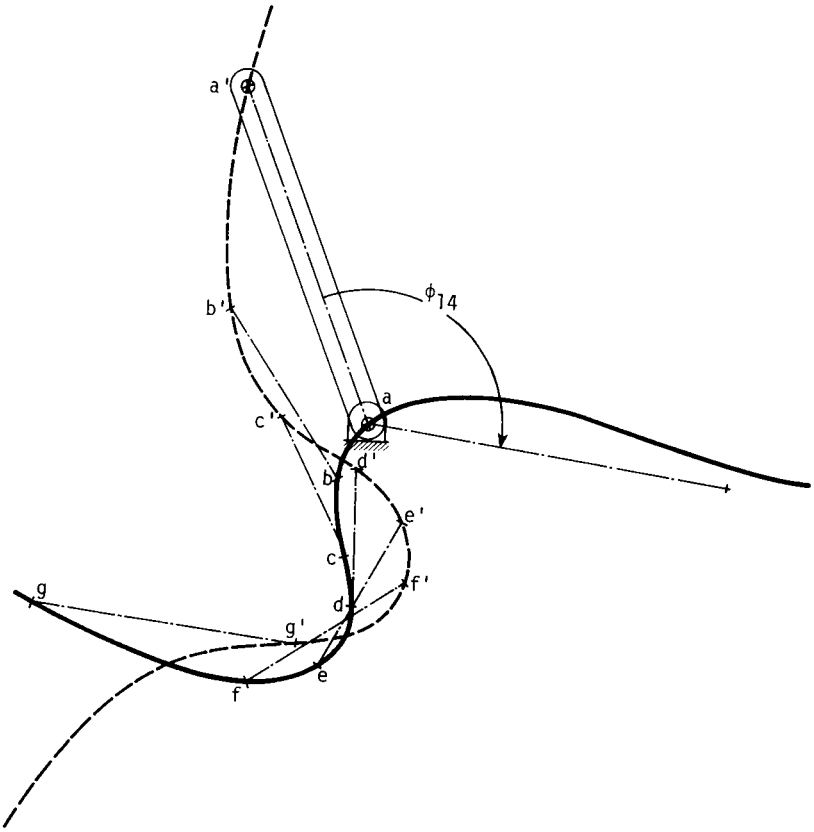

FIGURE 3.16 Some of the links which can be attached to the plane containing *CD*.

of motion. Proper care in selection of the two links will result in a smooth-running four-bar linkage.

3.7.4 Five Positions of a Plane

It would seem desirable to establish as many precision positions as possible. You can choose two sets of four positions (for example, 1235 and 1245) from which the Burmester curves can be created. The intersections (up to six) of those two center-point curves are the only fixed pivots which can be used to guide the moving body through the five positions. Since those pivots and/or link lengths have virtually always been outside the prescribed limits, I never use five-position synthesis.

3.7.5 Available Computer Programs

Two general-purpose planar linkage synthesis programs have been created: KINSYN ([3.17]) and LINCAGES ([3.18]). They involve the fundamentals described in

this section and can be valuable when time is limited. I have found it more advantageous to create my own design and analysis programs, since the general programs almost always need to be supplemented by routines that define the particular problem at hand.

3.8 DIMENSIONAL SYNTHESIS OF THE PLANAR FOUR-BAR LINKAGE: CRANK-ANGLE COORDINATION

Many mechanical movements in linkages depend on the angular position of the output crank. In general, you will have to design the four-bar linkage so that a prescribed input crank rotation will produce the desired output crank rotation. Significant work was performed in an attempt to generate functions ([3.9]) using the four-bar linkage until the advent of the microcomputer. Although it is seldom necessary to utilize the function capability, you will find many applications for crank-angle coordination. Two methods are possible: geometric and analytical.

3.8.1 Geometric Synthesis

In a manner similar to that for motion generation (Sec. 3.7), the concept of the pole is once again fundamental. Here, however, it is a *relative pole,* since it defines relative motions. Suppose that you need to coordinate the rotation angles ϕ_{12} for the crank (input) and ψ_{12} for the follower (output). Refer to Fig. 3.17, where the following steps have been drawn:

1. Establish convenient locations for the fixed pivots O_A and O_B.
2. Draw an extended fixed link O_AO_B.
3. With O_A as vertex, set off a line ℓ at angle $-\phi_{12}/2$ (half rotation angle, opposite direction).

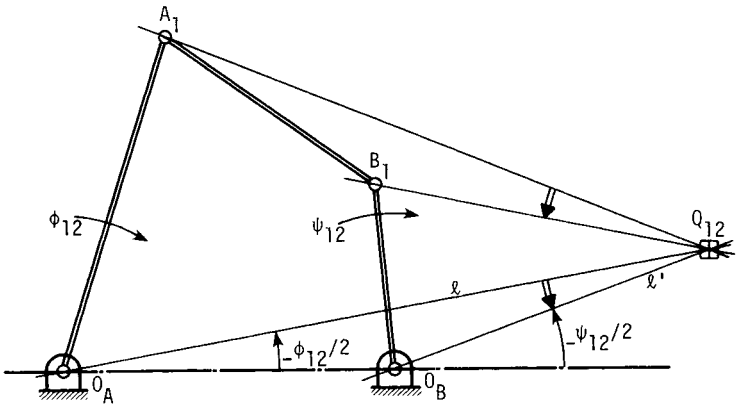

FIGURE 3.17 Crank-angle coordination: definition of relative pole Q_{12}.

4. With O_B as vertex, set off a line ℓ' at angle $-\psi_{12}/2$ (half rotation angle, opposite direction).
5. The intersection of ℓ and ℓ' is the relative pole Q_{12}.
6. Using Q_{12} as the vertex, set off the angle

$$\angle A_1 Q_{12} B_1 = \angle O_A Q_{12} O_B$$

in any convenient location, such as that shown.

When only two positions are required, you may choose A_1 and B_1 anywhere on the respective sides of the angle drawn in step 6. For three positions, two relative poles Q_{12} and Q_{13} are used. You may arbitrarily choose either A_1 or B_1, but the other pivot must be found geometrically. Figure 3.18 shows the necessary constructions.

3.8.2 Analytical Synthesis

Although four-bar linkages had been studied analytically for about 100 years, it was not until 1953 that Ferdinand Freudenstein [3.4] derived the now classic relationship

$$R_1 \cos \phi - R_2 \cos \psi + R_3 = \cos (\phi - \psi) \tag{3.15}$$

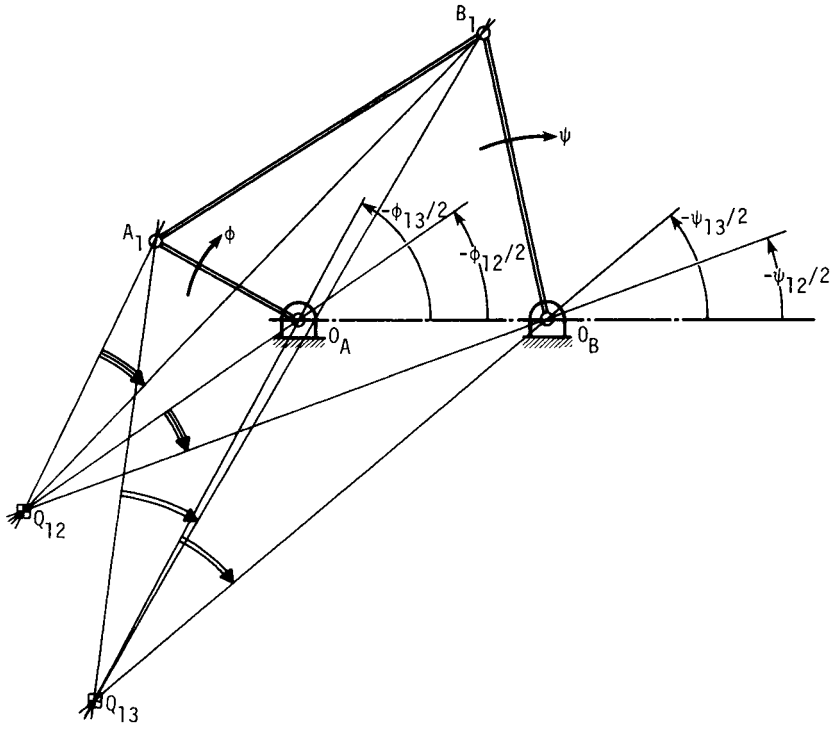

FIGURE 3.18 Geometric construction method for three crank-angle position coordination.

where

$$R_1 = \frac{a}{d} \qquad R_2 = \frac{a}{b} \qquad R_3 = \frac{b^2 - c^2 + d^2 + a^2}{2bd}$$

These link lengths are described in Fig. 3.7. With Eq. (3.15) you can establish a significant variety of linkage requirements. The first derivative of the Freudenstein equation is

$$(R_1 \sin \phi)\left(\frac{d\phi}{dt}\right) - (R_2 \sin \psi)\left(\frac{d\psi}{dt}\right) = \left(\frac{d\phi}{dt} - \frac{d\psi}{dt}\right) \sin (\phi - \psi) \tag{3.16}$$

which provides a relationship for the velocity or torque ratio. By using the relationship in Sec. 3.4.4, Eq. (3.16) becomes

$$R_1 \sin \phi - nR_2 \sin \psi = (1 - n) \sin (\phi - \psi) \tag{3.17}$$

where n is the torque or velocity ratio. A further derivative which would deal with accelerations has never been useful to me. If the need arises, see Ref. [3.9].

Since the problem is one of crank-angle coordination, there are potentially five unknowns (R_1, R_2, R_3, ϕ_1, and ψ_1) which you could determine. Combinations of ϕ_{1j}, ψ_{1j}, and n_j may be specified such that a series of equations of the form

$$R_1 \cos (\phi_1 + \phi_{1j}) - R_2 \cos (\psi_1 + \psi_{1j}) + R_3 = \cos (\phi_1 + \phi_{1j} - \psi_1 - \psi_{1j}) \tag{3.18}$$

and

$$R_1 \sin (\phi_1 + \phi_{1j}) - n_j R_2 \sin (\psi_1 + \psi_{1j}) = (1 - n_j) \sin (\phi_1 + \phi_{1j}) - \psi_1 - \psi_{1j}) \tag{3.19}$$

can be set up and solved. The nonlinear characteristic makes the solution complicated. Results for certain cases may be found in [3.9] and [3.11]. I have found it most useful in a digital computer program to vary ϕ_1 over the range 0 to π in four simultaneous equations. This produces loci for the moving pivot-point locations which go through the relative poles and are reminiscent of Burmester curves. The two sets of four conditions likely to be of practical interest are as follows:

1. Specify crank rotations ϕ_{12}, ϕ_{13}, ϕ_{14}, ψ_{12}, ψ_{13}, and ψ_{14}.
2. Specify crank rotations and velocity or torque ratios ϕ_{12}, n_1, ψ_{12}, and n_2.

3.9 POLE-FORCE METHOD

An extremely useful scheme for determining static balancing forces in a plane linkage was developed by Hain [3.7] and popularized by Tao [3.12]. Although it is potentially useful for design, I have used it primarily to analyze the requirements for counterbalance springs.

Statically balancing the force on the coupler of a four-bar linkage is a problem often encountered. The solution requires knowledge of the forces and/or torques acting on the four-bar linkage as well as determination of the instantaneous centers. Refer to Fig. 3.19*a,* in which the following constructions occur:

1. The intersection T_1 of forces F_{ab} and F_{ac} is found.
2. The intersection of the coupler (extended) with force F_{ab} is S_{ab} and with F_{ac} is S_{ac}.

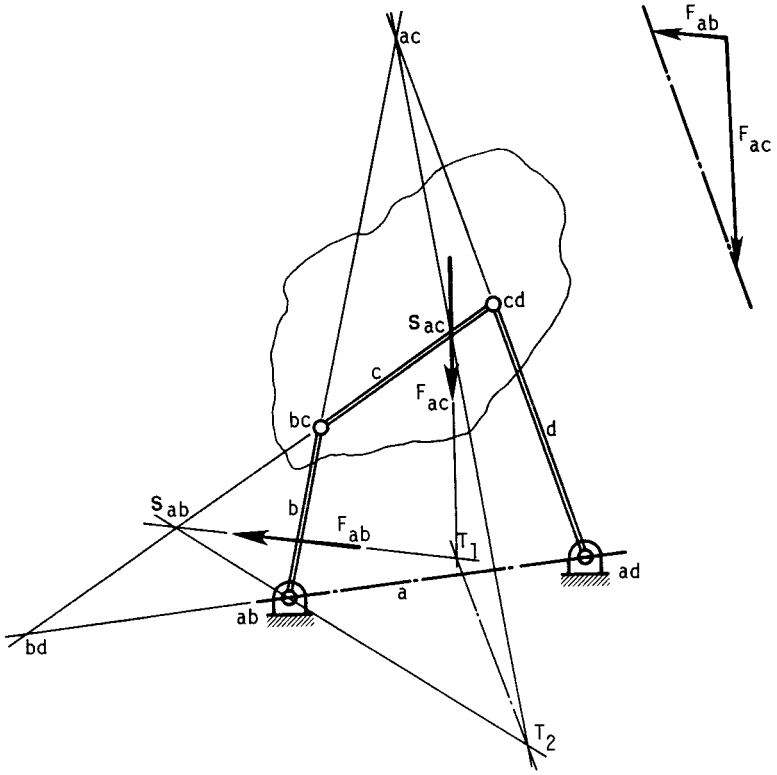

FIGURE 3.19 Pole-force method for balancing a force on the coupler of a four-bar linkage.

3. Determine lines $S_{ab}(ab)$ and $S_{ac}(ac)$; their intersection is T_2.
4. Line T_1T_2 closes the pole-force triangle, which is transferred to Fig. 3.19*b*.
5. The magnitude of F_{ab} required to balance the coupler force F_{ac} is easily found.

Many other cases, any of which you might encounter in practice, are shown by Tao [3.12].

3.10 SPATIAL LINKAGES

Most practical linkages have motion entirely in a plane or possibly in two parallel planes with duplicated mechanisms such as those in a backhoe or a front loader. Design procedures for some elementary types of spatial four-bar linkage have been created (Refs. [3.9] and [3.11]), principally for the RGGR type (Fig. 3.20).

Three principal mathematical methods for writing the loop-closure equation are vectors ([3.3]), dual-number quaternions ([3.14]), and matrices ([3.13]). These techniques have evolved into general-purpose computer programs such as IMP ([3.16])

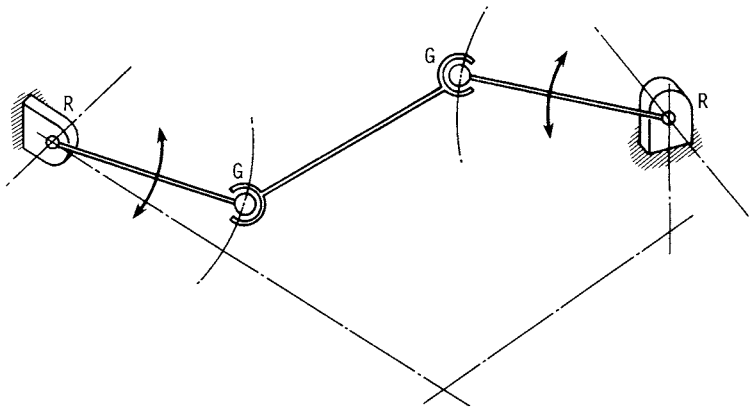

FIGURE 3.20 An RGGR spatial linkage; R designates a revolute joint, and G designates a spherical joint.

and ADAMS and DRAM ([3.5]); they will make your spatial linkage analysis much easier. With such tools available, you can design complex spatial mechanisms by iterative analysis.

REFERENCES

3.1 Rudolph A. Beyer, *Kinematic Synthesis of Mechanisms,* Herbert Kuenzel (trans.), McGraw-Hill, New York, 1964.

3.2 Ludwig Burmester, *Lehrbuch der Kinematick* (in German only), A. Felix, Leipzig, 1888.

3.3 Milton A. Chace, "Vector Analysis of Linkages," *J. Eng. Ind.,* ser. B, vol. 55, no. 3, August 1963, pp. 289–297.

3.4 Ferdinand Freudenstein, "Approximate Synthesis of Four-Bar Linkages," *Trans. ASME,* vol. 77, no. 6, 1955, pp. 853–861.

3.5 Ferdinand Freudenstein and George Sandor, "Kinematics of Mechanisms," in Harold A. Rothbart (ed.), *Mechanical Design and Systems Handbook,* 2d ed., McGraw-Hill, New York, 1985.

3.6 Richard E. Gustavson, "Computer-Designed Car-Window Linkage," *Mech. Eng.,* September 1967, pp. 45–51.

3.7 Kurt Hain, *Applied Kinematics,* 2d ed., Herbert Kuenzel, T. P. Goodman, et al. (trans.), McGraw-Hill, New York, 1967.

3.8 Allen S. Hall, Jr., *Kinematics and Linkage Design,* Prentice-Hall, Englewood Cliffs, N.J., 1961.

3.9 Richard S. Hartenberg and Jacques Denavit, *Kinematic Synthesis of Linkages,* McGraw-Hill, New York, 1964.

3.10 N. Rosenauer and A. H. Willis, *Kinematics of Mechanisms,* Dover, New York, 1967.

3.11 Joseph E. Shigley and John J. Uicker, Jr., *Theory of Machines and Mechanisms,* McGraw-Hill, New York, 1980.

3.12 D. C. Tao, *Applied Linkage Synthesis,* Addison-Wesley, Reading, Mass., 1964.

3.13 John J. Uicker, Jr., J. Denavit, and R. S. Hartenberg, "An Iterative Method for the Displacement Analysis of Spatial Linkages," *J. Appl. Mech.,* vol. 31, *ASME Trans.,* vol. 86, ser. E, 1964, pp. 309–314.

3.14 An T. Yang and Ferdinand Freudenstein, "Application of Dual-Number and Quaternion Algebra to the Analysis of Spatial Mechanisms," *J. Appl. Mech. ASME Trans.,* vol. 86, ser. E, 1964, pp. 300–308.

3.15 *ADAMS and DRAM, Automatic Dynamic Analysis of Mechanical Systems and Dynamic Response of Articulated Machinery,* developed by Chace at the University of Michigan.

3.16 *IMP, the Integrated Mechanisms Program,* developed by Uicker at the University of Wisconsin.

3.17 *KINSYN,* primarily for kinematic synthesis, developed by Kaufman while at M.I.T. (he is now at George Washington University).

3.18 *LINCAGES,* for kinematic synthesis and analysis, developed by Erdmann et al. at the University of Minnesota.

3.19 C. R. Mischke, *Elements of Mechanical Analysis,* Addison-Wesley, Reading, Mass., 1963.

LINKAGES

CHAPTER 4
CAM MECHANISMS

Andrzej A. Olędzki, D.Sc.[†]
Warsaw Technical University, Poland

SUMMARY

This chapter addresses the design of cam systems in which flexibility is not a consideration. Flexible, high-speed cam systems are too involved for handbook presentation. Therefore only two generic families of motion, trigonometric and polynomial, are discussed. This covers most of the practical problems.

The rules concerning the reciprocating motion of a follower can be adapted to angular motion as well as to three-dimensional cams. Some material concerns circular-arc cams, which are still used in some fine mechanisms. In Sec. 4.3 the equations necessary in establishing basic parameters of the cam are given, and the important problem of accuracy is discussed. Force and torque analysis, return springs, and contact stresses are briefly presented in Secs. 4.4 and 4.5, respectively.

The chapter closes with the logic associated with cam design to assist in creating a computer-aided cam design program.

4.1 CAM MECHANISM TYPES, CHARACTERISTICS, AND MOTIONS

Cam-and-follower mechanisms, as linkages, can be divided into two basic groups:

1. Planar cam mechanisms
2. Spatial cam mechanisms

In a planar cam mechanism, all the points of the moving links describe paths in parallel planes. In a spatial mechanism, that requirement is not fulfilled. The design of mechanisms in the two groups has much in common. Thus the fundamentals of planar cam mechanism design can be easily applied to spatial cam mechanisms, which

[†] Prepared while the author was Visiting Professor of Mechanical Engineering, Iowa State University, Ames, Iowa.

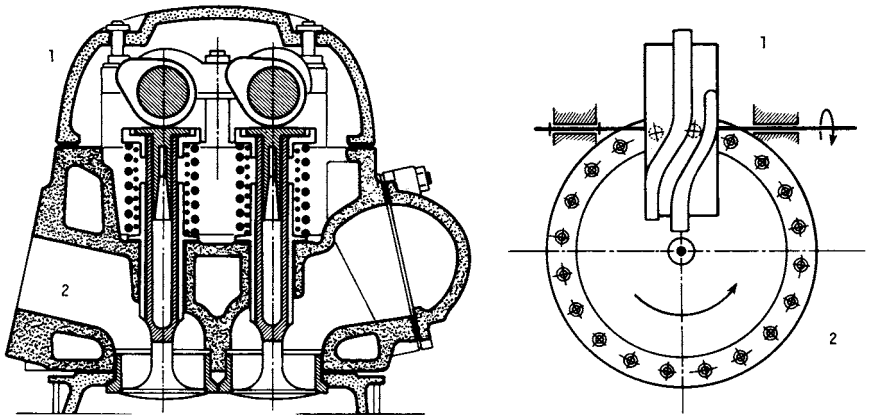

(a) (b)

FIGURE 4.1 (*a*) Planar cam mechanism of the internal-combustion-engine D-R-D-R type; (*b*) spatial cam mechanism of the 16-mm film projector R-D-R type.

is not the case in linkages. Examples of planar and spatial mechanisms are depicted in Fig. 4.1.

Planar cam systems may be classified in four ways: (1) according to the motion of the follower—reciprocating or oscillating; (2) in terms of the kind of follower surface in contact—for example, knife-edged, flat-faced, curved-shoe, or roller; (3) in terms of the follower motion—such as dwell-rise-dwell-return (D-R-D-R), dwell-rise-return (D-R-R), rise-return-rise (R-R-R), or rise-dwell-rise (R-D-R); and (4) in terms of the constraining of the follower—spring loading (Fig. 4.1*a*) or positive drive (Fig. 4.1*b*).

Plate cams acting with four different reciprocating followers are depicted in Fig. 4.2 and with oscillating followers in Fig. 4.3.

Further classification of reciprocating followers distinguishes whether the centerline of the follower stem is radial, as in Fig. 4.2, or offset, as in Fig. 4.4.

Flexibility of the actual cam systems requires, in addition to the operating speed, some data concerning the dynamic properties of components in order to find discrepancies between rigid and deformable systems. Such data can be obtained from dynamic models. Almost every actual cam system can, with certain simplifications, be modeled by a one-degree-of-freedom system, shown in Fig. 4.5, where m_e denotes

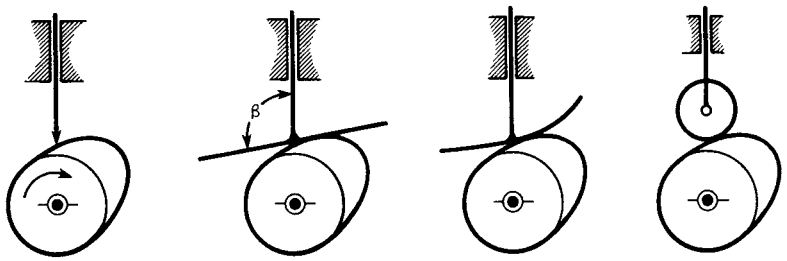

FIGURE 4.2 Plate cams with reciprocating followers.

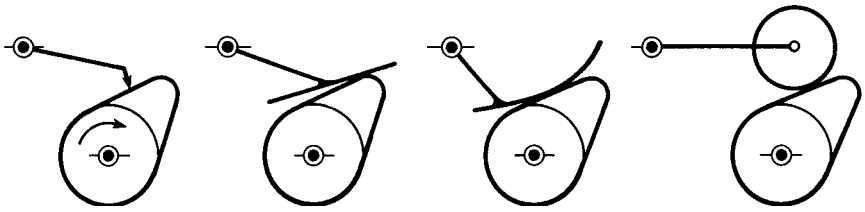

FIGURE 4.3 Plate cams with oscillating followers.

an equivalent mass of the system, k_e equals equivalent stiffness, and s and y denote, respectively, the input (coming from the shape of the cam profile) and the output of the system. The equivalent mass m_e of the system can be calculated from the following equation, based on the assumption that the kinetic energy of that mass equals the kinetic energy of all the links of the mechanism:

$$m_e = \sum_{i=1}^{i=n} \frac{m_i v_i^2}{\dot{s}^2} + \sum_{i=1}^{i=n} \frac{I_i \omega_i^2}{\dot{s}^2}$$

where m_i = mass of link i
v_i = linear velocity of center of mass of ith link
I_i = moment of inertia about center of mass for ith link
ω_i = angular velocity of ith link
$\dot{s}$ = input velocity

The equivalent stiffness k_e can be found from direct measurements of the actual system (after a known force is applied to the last link in the kinematic chain and the displacement of that link is measured), and/or by assuming that k_e equals the actual stiffness of the most flexible link in the chain. In the latter case, k_e can usually be calculated from data from the drawing, since the most flexible links usually have a simple form (for example, a push rod in the automotive cam of Fig. 4.16*c*). In such a

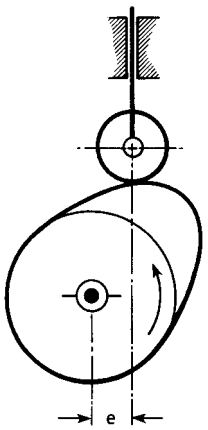

FIGURE 4.4 Plate cam with an offset reciprocating roller follower.

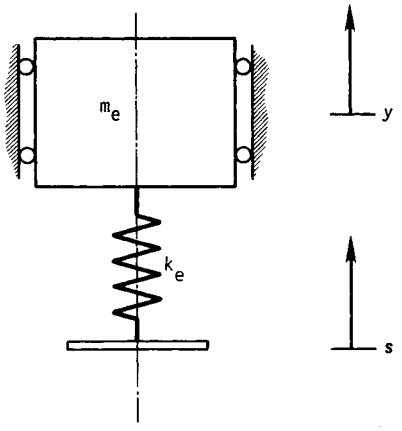

FIGURE 4.5 The one-degree-of-freedom cam system model.

model, the natural frequency of the mass m_e is $\omega_e = \sqrt{k_e/m_e}$ and should be equal to the fundamental frequency ω_n of the actual system.

The motion of the equivalent mass can be described by the differential equation

$$m_e\ddot{y} + k_e(y - s) = 0 \tag{4.1}$$

where $\ddot{y}$ denotes acceleration of the mass m_e. Velocity $\dot{s}$ and acceleration $\ddot{s}$ at the input to the system are

$$\dot{s} = \frac{ds}{dt} = \frac{ds}{d\theta}\frac{d\theta}{dt} = s'\omega \tag{4.2}$$

and

$$\ddot{s} = \frac{d}{dt}s'\omega = \frac{ds'}{dt}\omega + s'\frac{d\omega}{dt} = \frac{ds'}{d\theta}\frac{d\theta}{dt}\omega + s'\alpha$$
$$= s''\omega^2 + s'\alpha \tag{4.3}$$

where θ = angular displacement of cam
α = angular acceleration of cam
$s' = ds/d\theta$, the *geometric velocity*
$s'' = ds'/d\theta = d^2s/d\theta^2$, the *geometric acceleration*

When the cam operates at constant nominal speed $\omega = \omega_0$, $d\omega/dt = \alpha = 0$ and Eq. (4.3) simplifies to

$$\ddot{s} = s''\omega_0^2 \tag{4.4}$$

The same expressions can be used for the actual velocity $\dot{y}$ and for the actual acceleration $\ddot{y}$ at the output of the system. Therefore

$$\dot{y} = y'\omega \tag{4.5}$$

$$\ddot{y} = y''\omega^2 + y'\alpha \tag{4.6}$$

or

$$\ddot{y} = y''\omega_0^2 \qquad \omega = \omega_0 = \text{constant} \tag{4.7}$$

Substituting Eq. (4.7) into Eq. (4.1) and dividing by k_e gives

$$\mu_d y'' + y = s \tag{4.8}$$

where $\mu_d = (m_e/k_e)\omega_0^2$, the *dynamic factor* of the system.

Tesar and Matthew [4.10] classify cam systems by values of μ_d, and their recommendations for the cam designers, depending on the value of μ_d, are as follows:

$\mu_d \cong 10^{-6}$ (for low-speed systems; assume $s = y$)

$\mu_d \cong 10^{-4}$ (for medium-speed systems; use trigonometric, trapezoidal motion specifications, and/or similar ones; synthesize cam at design speed $\omega = \omega_0$, use good manufacturing practices, and investigate distortion due to off-speed operations)

$\mu_d \cong 10^{-2}$ (for high-speed systems; use polynomial motion specification and best available manufacturing techniques)

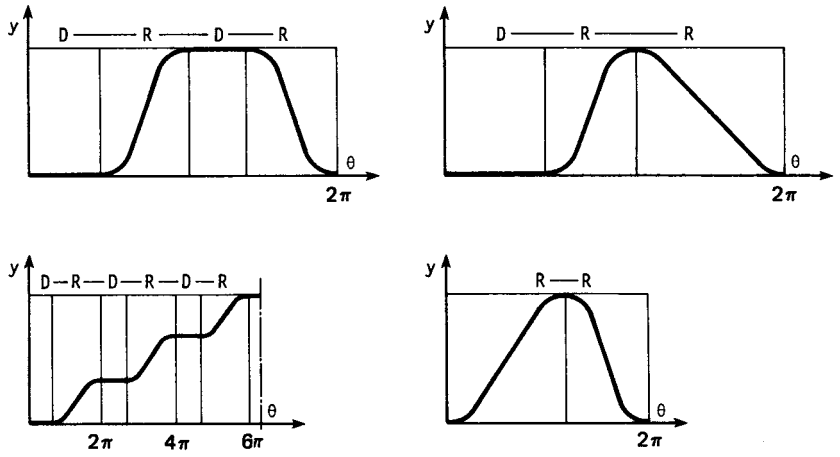

FIGURE 4.6 Types of follower motion.

In all the cases, increasing k_e and reducing m_e are recommended, because it reduces μ_d.

There are two basic phases of the follower motion, *rise* and *return.* They can be combined in different ways, giving types of cams classifiable in terms of the type of follower motion, as in Fig. 4.6.

For positive drives, the symmetric acceleration curves are to be recommended. For cam systems with spring restraint, it is advisable to use unsymmetric curves because they allow smaller springs. Acceleration curves of both the symmetric and unsymmetric types are depicted in Fig. 4.7.

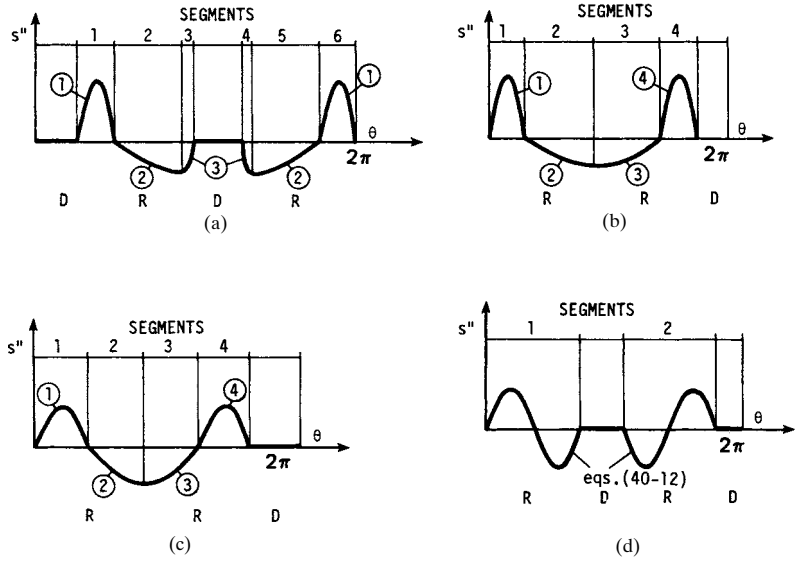

FIGURE 4.7 Acceleration diagrams: (*a*), (*b*) spring loading; (*c*), (*d*) positive drive.

4.2 BASIC CAM MOTIONS

Basic cam motions consist of two families: the trigonometric and the polynomial.

4.2.1 Trigonometric Family

This family is of the form

$$s'' = C_0 + C_1 \sin a\theta + C_2 \cos b\theta \tag{4.9}$$

where C_0, C_1, a, and b are constants.

For the low-speed systems where $\mu_d < 10^{-4}$, we can construct all the necessary diagrams, symmetric and unsymmetric, from just two curves: a sine curve and a cosine curve.

Assuming that the total rise or return motion s_0 occurs for an angular displacement of the cam $\theta = \beta_0$, we can partition acceleration curves into i separate segments, where $i = 1, 2, 3, \ldots$ with subtended angles $\beta_1, \beta_2, \beta_3, \ldots$ so that $\beta_1 + \beta_2 + \beta_3 + \cdots = \beta_0$. The sum of partial lifts $s_1, s_2, s_3, \ldots$ in the separate segments should be equal to the total rise or return s_0: $s_1 + s_2 + s_3 + \cdots = s_0$. If a dimensionless description θ/β of cam rotation is introduced into a segment, we will have the value of ratio θ/β equal to zero at the beginning of each segment and equal to unity at the end of each segment.

All the separate segments of the acceleration curves can be described by equations of the kind

$$s'' = A \sin \frac{n\pi\theta}{\beta} \qquad n = \frac{1}{2}, 1, 2 \tag{4.10}$$

or

$$s'' = A \cos \frac{\pi\theta}{2\beta} \tag{4.11}$$

where A is the maximum or minimum value of the acceleration in the individual segment.

The simplest case is when we have a positive drive with a symmetric acceleration curve (Fig. 4.7*d*). The complete rise motion can be described by a set of equations

$$\begin{aligned} s &= s_0 \left(\frac{\theta}{\beta} - \frac{1}{2\pi} \sin \frac{2\pi\theta}{\beta} \right) & s'' &= \frac{2\pi s_0}{\beta^2} \sin \frac{2\pi\theta}{\beta} \\ s' &= \frac{s_0}{\beta} \left(1 - \cos \frac{2\pi\theta}{\beta} \right) & s''' &= \frac{4\pi^2 s_0}{\beta^3} \cos \frac{2\pi\theta}{\beta} \end{aligned} \tag{4.12}$$

The last term is called *geometric jerk* ($\dddot{s} = \omega^3 s'''$). Traditionally, this motion is called *cycloidal.*

The same equations can be used for the return motion of the follower. It is easy to prove that

$$\begin{aligned} s_{\text{return}} &= s_0 - s_{\text{rise}} & s''_{\text{return}} &= -s''_{\text{rise}} \\ s'_{\text{return}} &= -s'_{\text{rise}} & s'''_{\text{return}} &= -s'''_{\text{rise}} \end{aligned} \tag{4.13}$$

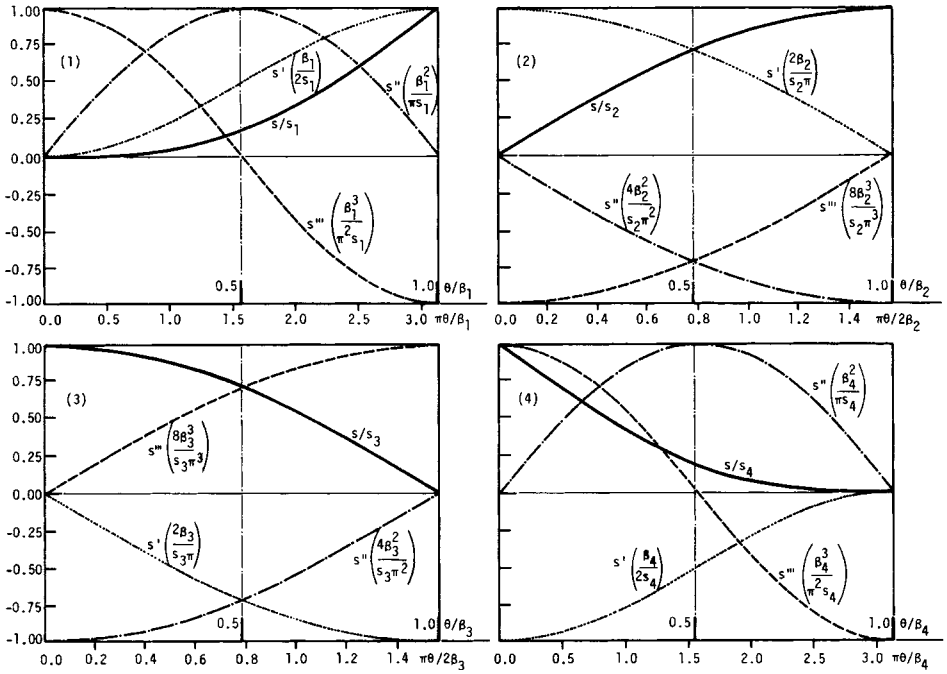

FIGURE 4.8 Trigonometric standard follower motions (according to the equation of Table 4.1, for $c = d = 0$).

All the other acceleration curves, symmetric and unsymmetric, can be constructed from just four trigonometric standard follower motions. They are denoted further by the numbers 1 through 4 (Fig. 4.8). These are displayed in Table 4.1.

Equations in Table 4.1 can be used to represent the different segments of a follower's displacement diagram. Derivatives of displacement diagrams for the adjacent segments should match each other; thus several requirements must be met in order to splice them together to form the motion specification for a complete cam. Motions 1 through 4 have the following applications:

Motion 1 is for the initial part of a rise motion.

Motion 2 is for the end and/or the middle part of a rise motion and the initial part of a return motion. The value c is a constant, equal to zero only in application to the end part of a rise motion.

Motion 3 is for the end part of a rise motion and/or the initial or middle part of a return motion. The value d is a constant, equal to zero only in application to the initial part of a return motion.

Motion 4 is for the end part of a return motion.

The procedure of matching the adjacent segments is best understood through examples.

Example 1. This is an extended version of Example 5-2 from Shigley and Uicker [4.8], p. 229. Determine the motion specifications of a plate cam with reciprocating fol-

TABLE 4.1 Standard Trigonometric Follower Motions

Parameter	Motion 1	Motion 2	Motion 3	Motion 4
s	$\frac{s_1}{\pi}\left(\frac{\pi\theta}{\beta_1} - \sin\frac{\pi\theta}{\beta_1}\right)$	$s_2 \sin\frac{\pi\theta}{2\beta_2} + c\frac{\theta}{\beta_2}$	$s_3 \cos\frac{\pi\theta}{2\beta_3} + d\left(\frac{\theta}{\beta_3} - \frac{1}{2}\right)$	$s_4\left(1 - \frac{\theta}{\beta_4} - \frac{1}{\pi}\sin\frac{\pi\theta}{\beta_4}\right)$
s'	$\frac{s_1}{\beta_1}\left(1 - \cos\frac{\pi\theta}{\beta_1}\right)$	$\frac{s_2\pi}{2\beta_2}\cos\frac{\pi\theta}{2\beta_2} + \frac{c}{\beta_2}$	$-\frac{s_3\pi}{2\beta_3}\sin\frac{\pi\theta}{2\beta_3} + \frac{d}{\beta_3}$	$-\frac{s_4}{\beta_4}\left(1 + \cos\frac{\pi\theta}{\beta_4}\right)$
s''	$\frac{\pi s_1}{\beta_1^2}\sin\frac{\pi\theta}{\beta_1}$	$-\frac{s_2\pi^2}{4\beta_2^2}\sin\frac{\pi\theta}{2\beta_2}$	$-\frac{s_3\pi^2}{4\beta_3^2}\cos\frac{\pi\theta}{2\beta_3}$	$\frac{\pi s_4}{\beta_4^2}\sin\frac{\pi\theta}{\beta_4}$
s'''	$\frac{\pi^2 s_1}{\beta_1^3}\cos\frac{\pi\theta}{\beta_1}$	$-\frac{s_2\pi^3}{8\beta_2^3}\cos\frac{\pi\theta}{2\beta_2}$	$\frac{s_3\pi^3}{8\beta_3^3}\sin\frac{\pi\theta}{2\beta_3}$	$\frac{\pi^2 s_4}{\beta_4^3}\cos\frac{\pi\theta}{\beta_4}$
$s'_{i,\text{ init}}\left(\frac{\theta}{\beta_i} = 0\right)$	. . .	$\frac{s_2\pi}{2\beta_2}$	$\frac{d}{\beta_3}$	$-\frac{2s_4}{\beta_4}$
$s'_{i,\text{ end}}\left(\frac{\theta}{\beta_i} = 1\right)$	$\frac{2s_1}{\beta_1}$	$\frac{c}{\beta_2}$	$-\frac{s_3\pi}{2\beta_3} + \frac{d}{\beta_3}$	
$s''_{\max};\ s''_{\min}$	$s''_{\max} = \frac{\pi s_1}{\beta_1^2}$	$s''_{\min} = -\frac{s_2\pi^2}{4\beta_2^2}$	$s''_{\min} = -\frac{s_3\pi^2}{4\beta_3^2}$	$s''_{\max} = \frac{\pi s_4}{\beta_4^2}$

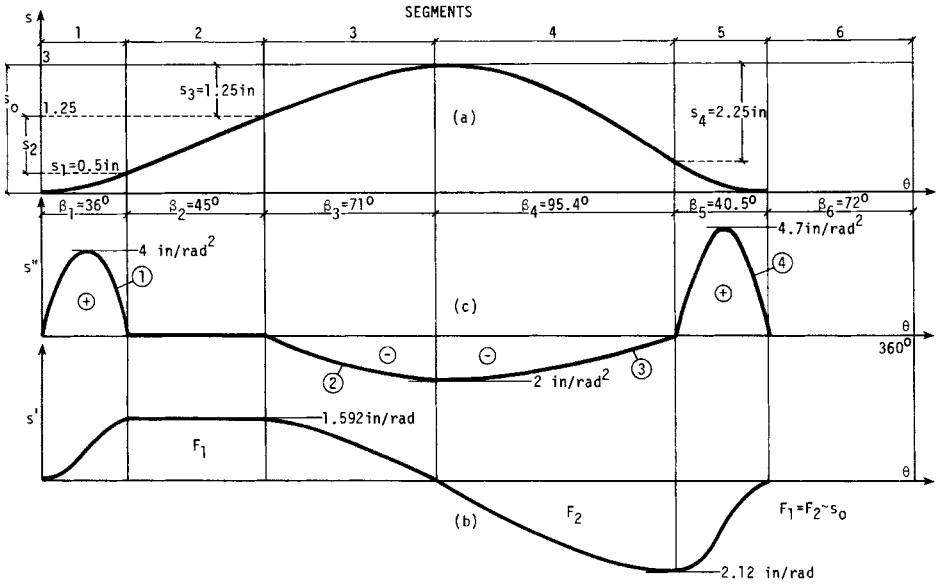

FIGURE 4.9 Example 1: (*a*) displacement diagram, in; (*b*) geometric velocity diagram, in/rad; (*c*) geometric acceleration diagram, in/rad^2.

lower and return spring for the following requirements: The speed of the cam is constant and equal to 150 r/min. Motion of the follower consists of six segments (Fig. 4.9):

1. Accelerated motion to $\dot{s}_{1,\text{end}} = 25$ in/s (0.635 m/s)
2. Motion with constant velocity 25 in/s, lasting for 1.25 in (0.03175 m) of rise
3. Decelerated motion (segments 1 to 3 describe rise of the follower)
4. Return motion
5. Return motion
6. Dwell, lasting for $t \geq 0.085$ s

The total lift of the follower is 3 in (0.0762 m).

Solution. Angular velocity $\omega = 150\pi/30 = 15.708$ radians per second (rad/s). The cam rotation for 1.25 in of rise is equal to $\beta_2 = 1.25$ in/$s_2' = 1.25$ in/1.592 in/rad = 0.785 rad = 45°, where $s_2' = 25/15.708 = 1.592$ in/rad.

The following decisions are quite arbitrary and depend on the designer:

1. Use motion 1; then $s_1 = 0.5$ in, $s''_{\max} = 0.05\pi/\beta_1^2 = 0.5\pi/(0.628)^2 = 4$ in/rad^2 (0.1016 m/rad^2). $s''_{1,\text{end}} = 2(0.5)/\beta_1$; so $\beta_1 = 1/1.592 = 0.628$ rad, or 36°.
2. For the motion with constant velocity, $s_2' = 1.592$ in/rad (0.4044 m/rad); $s_2 = 1.25$ in.
3. Motion type 2: $s_3 = s_2 = 1.25$ in, $s'_{3,\text{init}} = s_3\pi/(2\beta_3) = 1.592$ in/rad; therefore $\beta_3 = 1.25\pi/[2(1.592)] = 1.233$ rad $\cong 71°$, and $s'''_{3,\min} = -(1.25\pi^2)/[4(1.233)^2] = -2$ in/rad^2. (Points 1 through 3 describe the rise motion of the follower.)
4. Motion type 3: $s''_{4,\text{init}} = s_4\pi^2/(4\beta_r^2) = -2$ in/rad^2 (the same value as that of $s''_{3,\min}$), $s''_{4,\text{end}} = -\pi s_4/(2\beta_4)$, and $s_4 + s_5 = 3$ in.

5. Motion type 4: $s''_{5,\max} = \pi s_5/\beta_5^2$, and $s'_{5,\text{init}} = -s'_{4,\text{end}} = -2s_5/\beta_5$. We have here the four unknowns β_4, s_4, β_5, and s_5. Assuming time $t_6 = 0.85$ s for the sixth segment (a dwell), we can find $\beta_6 = \omega t_6 = 15.708(0.08) = 1.2566$ rad, or 72°. Therefore $\beta_4 + \beta_5 = 136°$, or 2.374 rad (Fig. 4.9). Three other equations are $s_4 + s_5 = 3$, $s_4\pi^2/(4\beta_4^2) = 2$, and $\pi s_4/(2\beta_4) = 2s_5/\beta_5$. From these we can derive the quadratic equation in β_4.

$$0.696\beta_4^2 + 6.044\beta_4 - 12 = 0$$

Solving it, we find $\beta_4 = 1.665\ 848$ rad $\cong 95.5°$ and $\beta_5 = 40.5°$. Since $s_4/s_5 = 4\beta_4/(\pi\beta_5) = 3.000\ 76$, it is easy to find that $s_5 = 0.75$ in (0.019 05 m) and $s_4 = 2.25$ in (0.057 15 m). Maximum geometric acceleration for the fifth segment $s''_{5,\max} = 4.7$ in/rad^2 (0.0254 m/rad^2), and the border (matching) geometric velocity $s'_{4,\text{end}} = s'_{5,\text{init}} = 2.12$ in/rad (0.253 m/rad).

Example 2. Now let us consider a cam mechanism with spring loading of the type D-R-D-R (Fig. 4.7*a*). The rise part of the follower motion might be constructed of three segments (1, 2, and 3) described by standard follower motions 1, 2, and 3 (Fig. 4.8). The values of constants c and d in Table 4.1 are no longer zero and should be found from the boundary conditions. (They are zero only in the motion case R-R-D, shown in Fig. 4.7*b,* where there is no dwell between the rise and return motions.)

For a given motion specification for the rise motion, the total follower stroke s_0, and the total angular displacement of the cam β_0, we have eight unknowns: β_1, s_1, β_2, s_2, β_3, s_3, and constants c and d. The requirements of matching the displacement derivatives will give us only six equations; thus two more must be added to get a unique solution. Two additional equations can be written on the basis of two arbitrary decisions:

1. The maximum value of the acceleration in segment 1, $s''_{1,\max}$, should be greater than that in segment 2 because of spring loading. So $s''_{1,\max} = -as''_{2,\min}$, where $s''_{2,\min}$ is the minimum value of the second-segment acceleration and a is any assumed number, usually greater than 2.

2. The end part of the rise (segment 3), the purpose of which is to avoid a sudden drop in a negative accelerative curve, should have a smaller duration than the basic negative part (segment 2). Therefore we can assume any number b (greater than 5) and write $\beta_2 = b\beta_3$. The following formulas were found after all eight equations for the eight unknowns were solved simultaneously:

$$\beta_1 = \frac{\beta_0}{1 + a + a/b} \qquad \beta_3 = \beta_0 \frac{a}{a(1+b) + b}$$

$$s_1 = s_0 \frac{\pi b^2}{b^2(\pi + 4a) + 4a(2a + 1)} \qquad s'_2 = s_1 \frac{4a}{\pi}$$

$$s_3 = s_1 \frac{4a}{\pi b^2} \qquad c = s_1 \frac{8a^2}{\pi b^2}$$

$$d = 2s_3 \qquad s_0 = s_1 + s'_2 + c + s_3$$

We can assume practical values for a and b (say $a = 2, b = 10$) and find from the above equations the set of all the parameters (as functions of s_0 and β_0) necessary to form

the motion specification for the rise motion of the follower and the shape of the cam profile. The whole set of parameters is as follows:

$$s_1 = 0.272\,198 s_0 \qquad \beta_1 = 0.312\,5\beta_0$$

$$s_2' = 0.693\,147 s_0 \qquad c = 0.027\,726 s_0$$

$$\beta_2 = 0.625\beta_0$$

$$s_3 = 0.006\,931 s_0 \qquad d = 2s_3 \quad \text{(always!)}$$

$$\beta_3 = 0.062\,5\beta_0$$

These can be used for calculations of the table $s = s(\theta)$, which is necessary for manufacturing a cam profile. For such a table, we use as a rule increments of θ equal to about 1° and accuracy of s up to 4×10^{-5} in 1 micrometer (μm). The data of such a table can be easily used for the description of both the return motion of the follower and a cam profile, providing $\beta_0(\text{return}) = \beta_0(\text{rise})$, and the acceleration diagram for the return motion is a mirror image of the acceleration diagram for the rise motion. Table 4.2 can be of assistance in calculating the return portion of the cam profile. The column s(return) is the same as the column s(rise).

TABLE 4.2 Data of Rise Motion Used for Calculations of Return Portion of Cam Profile

Rise		Return	
θ(rise)	s(rise)	θ(return)	s(return)
0	0	$2\beta_0 + \beta_d - 0$	0
⋮	⋮	⋮	⋮
θ_i	s_i	$2\beta_0 + \beta_d - \theta_i$	s_i
⋮	⋮	⋮	⋮
β_0	s_0	$2\beta_0 + \beta_d - \beta_0$	s_0

The trigonometric acceleration diagram for the positive drive was described at the beginning of this section by Eq. (4.12). The improved diagram (smaller maximum values of acceleration for the same values of s_0 and β_0[†]) can be obtained if we combine sine segments with segments of constant acceleration. Such a diagram, called a *modified trapezoidal acceleration curve,* is shown in Fig. 4.10. Segments 1, 3, 4, and 6 are the sinusoidal type. Sections 2 and 5 are with s'' = constant. It was assumed for that diagram that all the sine segments take one-eighth of the total angular displacement β_0 of the cam during its rise motion. The first half of the motion has three segments. The equations for the first segment are $0 \le \theta/\beta_0 \le \frac{1}{8}$, and so

[†] The maximum acceleration ratio is 4.9/6.28.

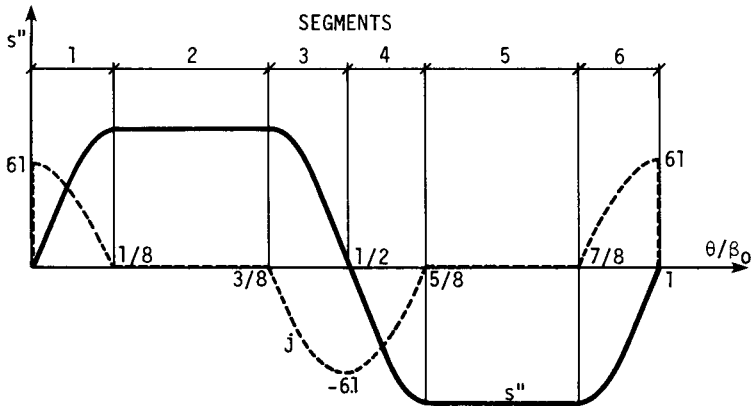

FIGURE 4.10 A modified trapezoidal acceleration diagram.

$$s = \frac{s_0'}{2\pi}\left(\frac{4\pi\theta}{\beta_0} - \sin\frac{4\pi\theta}{\beta_0}\right) \qquad s' = \frac{2s_0'}{\beta_0}\left(1 - \cos\frac{4\pi\theta}{\beta_0}\right)$$

$$s'' = 8\pi\frac{s_0'}{\beta_0^2}\sin\frac{4\pi\theta}{\beta_0} \qquad s''' = 32\pi^2\frac{s_0'}{\beta_0^3}\cos\frac{4\pi\theta}{\beta_0} \tag{4.14}$$

For the second segment, we have $\frac{1}{8} \le \theta/\beta_0 \le \frac{3}{8}$, and so

$$s = s_0'\left[-\frac{1}{2\pi} + \frac{2\theta}{\beta_0} + 4\pi\left(\frac{\theta}{\beta_0} - \frac{1}{8}\right)^2\right]$$

$$s' = \frac{s_0'}{\beta_0}\left[2 + 8\pi\left(\frac{\theta}{\beta_0} - \frac{1}{8}\right)\right] \tag{4.15}$$

$$s'' = \frac{8\pi s_0'}{\beta_0^2} \qquad s''' = 0$$

The relations for the third segment are $\frac{3}{8} \le \theta/\beta_0 \le \frac{4}{8}$ ([4.7]); therefore,

$$s = s_0'\left\{-\frac{\pi}{2} + 2(1+\pi)\frac{\theta}{\beta_0} - \frac{1}{2\pi}\sin\left[4\pi\left(\frac{\theta}{\beta_0} - \frac{2}{8}\right)\right]\right\}$$

$$s' = \frac{2s_0'}{\beta_0}\left\{1 + \pi - \cos\left[4\pi\left(\frac{\theta}{\beta_0} - \frac{2}{8}\right)\right]\right\}$$

$$s'' = \frac{8\pi s_0'}{\beta_0^2}\sin\left[4\pi\left(\frac{\theta}{\beta_0} - \frac{2}{8}\right)\right] \tag{4.16}$$

$$s''' = 32\pi^2\frac{s_0'}{\beta_0^3}\cos\left[4\pi\left(\frac{\theta}{\beta_0} - \frac{2}{8}\right)\right]$$

where $s_0' = s_0/(2+\pi) = 0.194\,492 s_0$.

Using Eqs. (4.14) through (4.16) for all three segments, we can calculate the s values for the first half of the rise motion, where $\theta/\beta_0 = \frac{1}{8}$ and $s = s_0/2$. Since the negative part of the acceleration diagram is a mirror image of the positive part, it is easy to calculate the s values for the second half of the rise motion from the data obtained for the first half. The necessary procedure for that is shown in Table 4.3. The procedure concerns the case with the modified trapezoidal acceleration diagram, but it could be used as well for all the cases with symmetric acceleration diagrams for the rise motion. For the return motion of the follower, when its acceleration diagram is a mirror image of the rise diagram, we can use again the technique shown in Table 4.2. All the calculations can be done simultaneously by the computer after a simple program is written.

TABLE 4.3 Data of First Half of Rise Motion Used for Calculations of Second Half

		$\gamma = \theta/\beta_o$	s	γ	s	
Segments	1	0 $\vdots$ γ_i $\vdots$ $\frac{1}{8}$	0 $\vdots$ s_i $\vdots$ $s_1 = s_0'(\pi/2 - 1)/2\pi$	1 $\vdots$ $1 - \gamma_i$ $\vdots$ $\frac{7}{8}$	s_0 $\vdots$ $s_0 - s_i$ $\vdots$ $s_0 - s_1$	6
	2	$\frac{1}{8}$ $\vdots$ γ_j $\vdots$ $\frac{3}{8}$	s_1 $\vdots$ s_j $\vdots$ $s_2 = s_0'(\frac{3}{4} - 1/2\pi + \pi/4)$	$\frac{7}{8}$ $\vdots$ $1 - \gamma_j$ $\vdots$ $\frac{5}{8}$	$s_0 - s_1$ $\vdots$ $s_0 - s_j$ $\vdots$ $s_0 - s_2$	5
	3	$\frac{3}{8}$ $\vdots$ γ_k $\vdots$ $\frac{4}{8}$	s_2 $\vdots$ s_k $\vdots$ $s_3 = s_0/2$	$\frac{5}{8}$ $\vdots$ $1 - \gamma_k$ $\vdots$ $\frac{4}{8}$	$s_0 - s_2$ $\vdots$ $s_0 - s_k$ $\vdots$ $s_0 - s_3 = s_0/2$	4

All the trigonometric curves of this section were calculated with finite values of jerk, which is of great importance for the dynamic behavior of the cam mechanism. An example of the jerk diagram is given in Fig. 4.10. The jerk curve j was plotted by using the dimensionless expression

$$j = \frac{s'''}{s_0/\beta_0^3} \tag{4.17}$$

This form of the jerk description can also be used to compare properties of different acceleration diagrams.

4.2.2 Polynomial Family

The basic polynomial equation is

$$s = C_0 + C_1\frac{\theta}{\beta_0} + C_2\left(\frac{\theta}{\beta_0}\right)^2 + C_3\left(\frac{\theta}{\beta_0}\right)^3 + \cdots \tag{4.18}$$

with constants C_i depending on assumed initial and final conditions.

This family is especially useful in the design of flexible cam systems, where values of the dynamic factor are $\mu_d \geq 10^{-2}$. Dudley (1947) first used polynomials for the synthesis of flexible systems, and his ideal later was improved by Stoddart [4.9] in application to automotive cam gears.

The shape factor s of the cam profile can be found by this method after a priori decisions are made about the motion y of the last link in the kinematic chain. Cams of that kind are called *polydyne cams*.

When flexibility of the system can be neglected, the initial and final conditions ([4.3], [4.4], and [4.8]) might be as follows (positive drive):

1. Initial conditions for full-rise motion are

$$\frac{\theta}{\beta_0} = 0 \qquad s = 0 \qquad s' = 0 \qquad s'' = 0$$

2. Final (end) conditions are

$$\frac{\theta}{\beta_0} = 1 \qquad s = s_0 \qquad s' = 0 \qquad s'' = 0$$

The first and second derivatives of Eq. (4.18) are

$$\begin{aligned} s' &= C_1 + 2C_2\frac{\theta}{\beta_0} + 3C_3\left(\frac{\theta}{\beta_0}\right)^2 + 4C_4\left(\frac{\theta}{\beta_0}\right)^3 + \cdots \\ s'' &= 2C_2 + 6C_3\frac{\theta}{\beta_0} + 12C_4\left(\frac{\theta}{\beta_0}\right)^2 + \cdots \end{aligned} \tag{4.19}$$

Substituting six initial and final conditions into Eqs. (4.18) and (4.19) and solving them simultaneously for unknowns C_0, C_1, C_2, C_3, C_4, and C_5, we have

$$\begin{aligned} s &= 10s_0\left[\left(\frac{\theta}{\beta_0}\right)^3 - 1.5\left(\frac{\theta}{\beta_0}\right)^4 + 0.6\left(\frac{\theta}{\beta_0}\right)^5\right] \\ s' &= 30\frac{s_0}{\beta_0}\left[\left(\frac{\theta}{\beta_0}\right)^2 - 2\left(\frac{\theta}{\beta_0}\right)^3 + \left(\frac{\theta}{\beta_0}\right)^4\right] \\ s'' &= 60\frac{s_0}{\beta_0^2}\left[\frac{\theta}{\beta_0} - 3\left(\frac{\theta}{\beta_0}\right)^2 + 2\left(\frac{\theta}{\beta_0}\right)^3\right] \end{aligned} \tag{4.20}$$

and for a jerk $s''' = ds''/d\theta$, or

$$s''' = 60\frac{s_0}{\beta_0^3}\left[1 - 6\frac{\theta}{\beta_0} + 6\left(\frac{\theta}{\beta_0}\right)^2\right]$$

This is called the polynomial 3-4-5, since powers 3, 4, and 5 remain in the displacement equation. It provides a fairly good diagram for the positive drives.

Equations for the full-return polynomial are

$$s(\text{return}) = -s(\text{rise}) + s_0 \qquad s''(\text{return}) = -s'(\text{rise})$$
$$s''(\text{return}) = -s''(\text{rise}) \qquad s'''(\text{return}) = -s'''(\text{rise}) \tag{4.21}$$

All the characteristic curves of the full-rise 3-4-5 polynomial are shown in Fig. 4.11. They were generated by the computer for $s_0 = 1$ displacement unit (inches or centimeters) and $\beta_0 = 1$ rad.

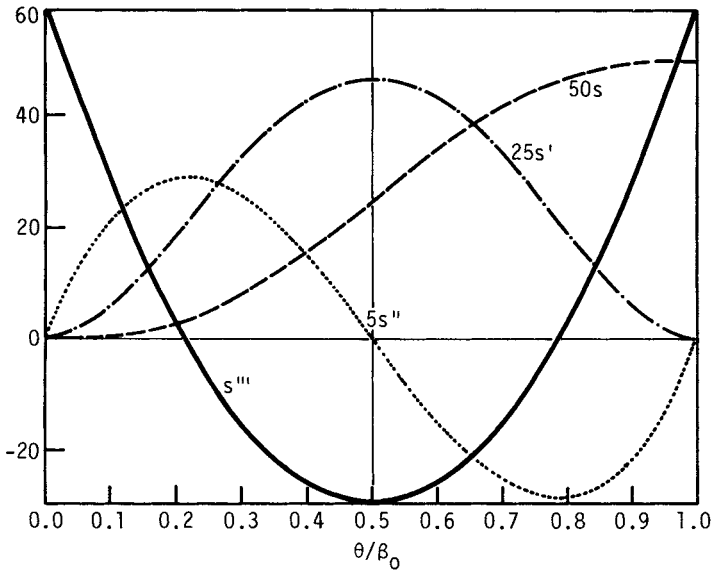

FIGURE 4.11 Full-rise 3-4-5 polynomial motion.

After a proper set of initial and final conditions is established, the basic equation [Eq. (4.18)] can be used for describing any kind of follower motion with an unsymmetric acceleration diagram. Details concerning the necessary procedure can be found in Rothbart [4.7].

4.2.3 Other Cam Motions

The basic cam motions described in the previous sections cover most of the routine needs of the contemporary cam designer. However, sometimes the cost of manufacturing the cam profile may be too high and the dynamic properties of the cam motion may not be severe. This is the case of cams used for generating functions. There is a very effective approach, described by Mischke [4.2], concerning an optimum design of simple eccentric cams. They are very inexpensive, yet can be used even for generating very complicated functions.

The other approach, when we are interested in inexpensive cams, is to use *circular-arc* cams or *tangent* cams. They are still used in low-speed diesel IC engines since the cost of their manufacture is low (compare with Fig. 4.15). An extensive review of these cams can be found in Rothbart [4.7]. They were used quite frequently in the past when the speed of machines was low, but today they are not often recommended because their dynamic characteristics are poor. The only exception can be made for fine- or light-duty mechanisms, such as those of 8- and 16-mm film projectors, where circular-arc cams are still widely used. Those cams are usually of the positive drive kind, where the breadth of the cam is constant. The cam drives a reciprocating follower with two flat working surfaces a fixed distance apart, which contact opposite sides of the cam.

The constant-breadth cam is depicted in Fig. 4.12. For given values of radius ρ, total angle of cam rotation β_0, and total lift of the follower s_0, the basic dimensions of the cam can be found from the relations ([4.11])

$$R_1 = \frac{\rho - b(s_0 + \rho)}{1 - b} \qquad r = R_1 - s_0 \tag{4.22}$$

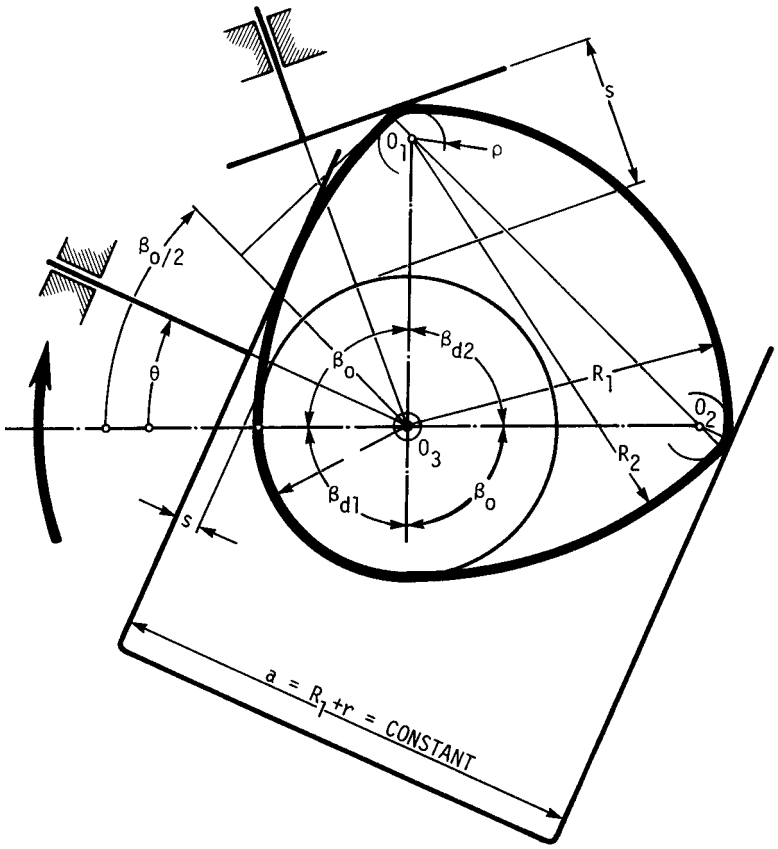

FIGURE 4.12 Constant-breadth circular-arc cam.

where $b = \cos 0.25\beta_0/\cos 0.75\beta_0$. Cam motions for full rise ($0 \geq \theta \geq \beta_0$) are described in Table 4.4. Such cams are symmetric; therefore, β_0(rise) = β_0(return), and the two dwells β_{d1} and β_{d2} are the same and equal to $180° - \beta_0$. Table 4.4 can also be used for calculation of full-return motion. Dimensions of the cam (R_1) and maximum values of the acceleration increase with a decrease in β_0. Acceleration diagrams for different values of β_0 are shown in Fig. 4.13.

TABLE 4.4 Basic Equations for a Constant-Breadth Circular-Arc Cam, Using $A = R_1 - \rho$

Parameter	$0 \leq \theta \leq \beta_0/2$	$\beta_0/2 \leq \theta \leq \beta_0$
s	$A(1 - \cos\theta)$	$A\cos(\beta_0 - \theta) - (r - \rho)$
s'	$A\sin\theta$	$A\sin(\beta_0 - \theta)$
s''	$A\cos\theta$	$-A\cos(\beta_0 - \theta)$
s'''	$-A\sin\theta$†	$-A\sin(\beta_0 - \theta)$†

† Both equations are valid, however, only inside the partitions. For $\theta = 0$, $\beta_0/2$, and β_0, $s''' \to \infty$.

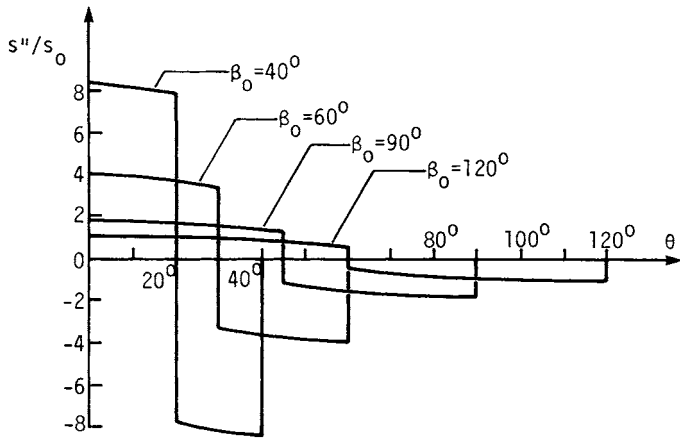

FIGURE 4.13 Acceleration diagrams.

4.3 LAYOUT AND DESIGN; MANUFACTURING CONSIDERATIONS

The cam profile is an inner envelope of the working surface of the follower. After the displacement diagram is determined, the cam layout can be found by using the usual graphical approach or by computer graphics with a rather simple computer program.

In the design of a plate cam with a reciprocating flat-face follower, the geometric parameters necessary for its layout are the prime-circle radius R_0, the minimum

width of the follower face F, and the offset e of the follower face. The value R_0 can be found from

$$R_0 > (\rho_{min} - s'' - s)_{max} \tag{4.23}$$

where ρ_{min} is a minimum value of the radius ρ of the cam-profile curvature. Its value for such practical reasons as contact stresses might be assumed equal to 0.2 to 0.25 in [5 to 6 millimeters (mm)]. Since s is always positive, we should examine that part of the follower acceleration diagram for the rise motion where acceleration is negative.

The face width F can be calculated from

$$F > s'_{max} - s'_{min} \tag{4.24}$$

To avoid undercutting cams with a roller follower, the radius R_r of the roller must always be smaller than $|\rho|$, where ρ is the radius of curvature.

The pressure angle γ (Fig. 4.14) is an angle between a common normal to both the roller and the cam profile and the direction of the follower motion. This angle can be calculated from

$$\tan \gamma = \frac{s'}{s + R_0 + R_r} \tag{4.25}$$

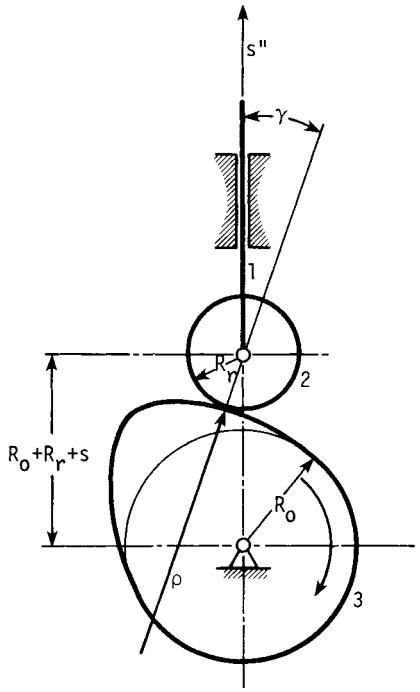

FIGURE 4.14 Cam mechanism with reciprocating roller follower.

It is a common rule of thumb to assume for the preliminary calculation that γ_{max} is not greater than 30° for the reciprocating follower motion (or 45° for the oscillating one). Acceptable values of γ_{max} that can be used without causing difficulties depend, however, on the particular cam mechanism design and should be found for any actual mechanism from the dynamic analysis.

After establishing the value of γ_{max} and R_r in accordance with the preliminary layout of the mechanism, we can find the value of the prime-circle radius R_0 from the equation

$$R_0 \geq \left(\frac{s'}{\tan \gamma_{max}} - s - R_r \right)_{max} \tag{4.26}$$

Now check whether the assumed value of R_r is small enough to avoid undercutting of the cam profile. It can be done ([4.7]) by using Eq. (4.27):

$$R_r \leq \left[\frac{|s'|}{\sin^3 \gamma_{max} \left(\frac{1}{\sin^3 \gamma_{max}} + 2 - \frac{s''}{|s'| \tan \gamma_{max}} - \frac{1}{|s'|} \right)} \right]_{min} - \rho_{min} \tag{4.27}$$

The primary choice of the follower motion should always be guided by a good understanding of the planned manufacturing technique. *Tracer cutting* and *incremental cutting* are two very common methods of cam manufacture. Incremental cutting consists of manufacturing the profile by intermittent cuts based on a table with accurate values of angular cam displacement θ (cam blank) and linear displacement $s(\theta)$ of the follower (cutter). This method is used for making master cams or cams in small numbers. In the tracer control cutting method, the cam surface is milled, shaped, or ground, with the cutter or grinder guided continuously by either a master cam or a computer system. This is the best method for producing large numbers of accurate cam profiles.

In the process of cam and follower manufacturing, several surface imperfections may occur, such as errors, waviness, and roughness. These surface irregularities may induce shock, noise, wear, and vibrations of the cam and follower systems. Imperfections of actual profile cannot exceed an accepted level. Therefore, highly accurate inspection equipment is commonly used in production inspection. Actual displacements of the follower are measured as a function of the cam rotation; then the resulting data can be compared with tabulated theoretical values. By application of the method of finite differences (Sec. 4.3.1), these data can be transformed to actual acceleration curves and compared with theoretical ones. There is, however, a drawback in such a method in that it is based on static measurements.

An example of results obtained from a widely used production inspection method is shown in Fig. 4.15 ([4.5]). Line 1 was obtained from some accurate data from a table of θ values and the corresponding $s(\theta)$ values. Next, two boundary curves were obtained from the basis curve by adding and subtracting 10 percent. This was an arbitrary decision, it being assumed that any acceleration curve contained between such boundaries would be satisfactory. These are shown as upper and lower bounds in Fig. 4.15. The main drawback of the method is that only maximum values of actual acceleration diagrams have been taken into account. It is important to realize that waviness of the real acceleration curve may cause more vibration troubles than will single local surpassing of boundary curves.

A much better method is that of measuring the real acceleration of the follower in an actual cam mechanism at the operating speed of the cam by means of high-quality

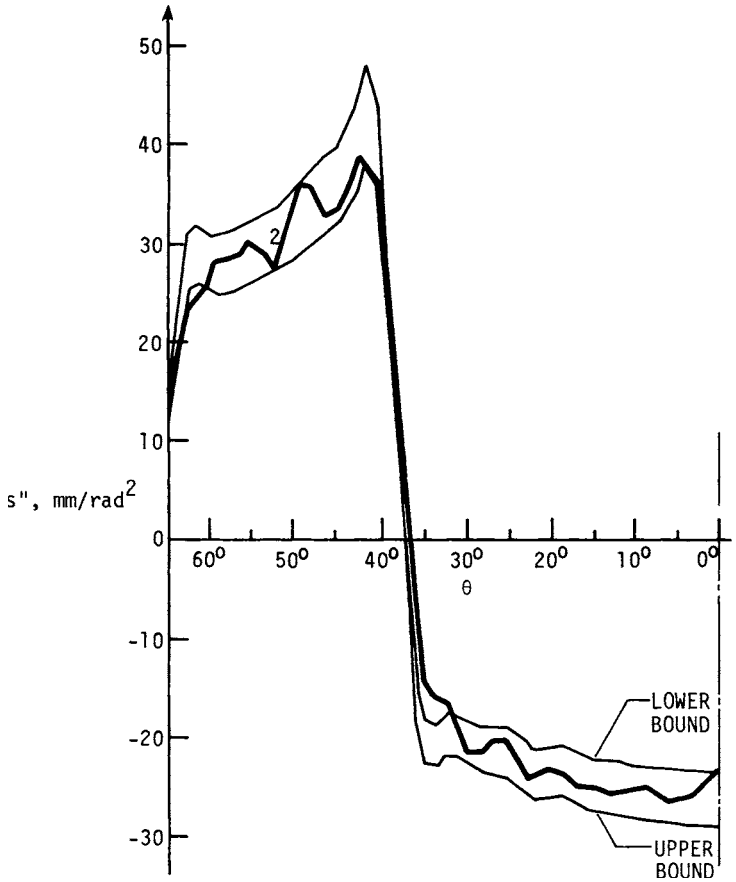

FIGURE 4.15 Example of inspection technique based on acceleration diagram obtained from accurate static measurements of the cam of the Henschel internal combustion engine.

accelerometers and electronic equipment. To illustrate the importance of proper measurements of the cam profile, we show the results of an investigation of the mechanism used in the Fiat 126 engine ([4.6]). Those results are shown in Figs. 4.16 and 4.17. The acceleration diagram of Fig. 4.16*a* was obtained from designer data by using Eq. (4.29). The diagram plotted as a broken line (1) in Fig. 4.16*b* comes from accurate measurements of a new profile. Here again Eq. (4.29) was applied. The same profile was measured again after 1500 hours (h) of operation, and the acceleration diagram is plotted by a solid line (2) in Fig. 4.16*b*. Comparing curves 1 and 2 of Fig. 4.16*b*, we can see that the wear of the cam smoothed somewhat the waviness of the negative part of the diagram. Accelerations of the follower induced by the same new cam in the actual mechanism (Fig. 4.16*c*) were measured as well by electronic equipment at the design speed, and results of that experiment are presented in Fig. 4.16*d* and *e*. It is obvious from comparison of the diagrams in Fig. 4.16*b* and *d* that the response of the system differs to a considerable extent from the actual input.

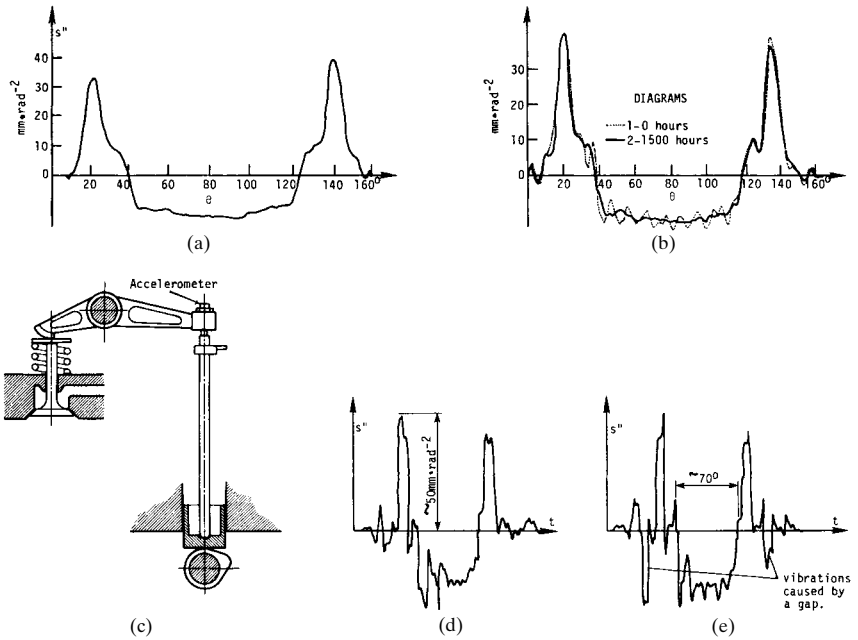

FIGURE 4.16 Comparison between results obtained from static measurements of the Fiat 126 cam profile [(*a*) and (*b*)] and acceleration curves obtained at design speed on the actual engine [(*d*) and (*e*)]. Diagram *d* was obtained for a zero value of backlash and diagram *e* for the factory-recommended 0.2-mm backlash.

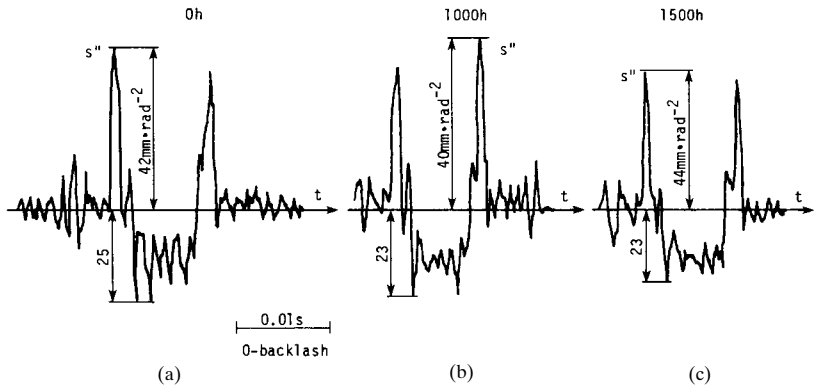

FIGURE 4.17 Changes of acceleration diagram caused by the wear of the cam profile of the Fiat 126.

Eight new cams of the same engine were later used in two separate laboratory stands to find the influence of cam-surface wear on dynamic properties of the cam system. Some of the obtained results are presented in Fig. 4.17. We can observe there that some smoothing of the negative part of the curve (registered as well by statistical measurements) took place after 1500 h. The general character of the acceleration curve remained unchanged, however. (That observation was confirmed later by a Fourier analysis of all the acceleration signals.) The conclusion derived from that single experiment is that dynamic imperfections of the cam system introduced by the process of cam manufacturing may last to the end of the cam life.

4.3.1 Finite-Difference Method

Geometric acceleration of the follower s'' may be estimated by using accurate values of its displacement s from a table of θ versus $s(\theta)$, which comes from the designer's calculations and/or from accurate measurements of the actual cam profile. Denoting as s_{i-1}, s_i, and s_{i+1} three adjacent values of s in such a table, and designating their second finite difference as Δ_i'', we have

$$s_i'' \cong \frac{1}{(\Delta\theta)^2}\,\Delta_i'' = \frac{s_{i-1} - 2s_i + s_{i+1}}{(\Delta\theta)^2} \tag{4.28}$$

where $\Delta\theta$ = constant increment of the cam's angular displacement θ. A more accurate value of s_i'' can be found from the *average weighted value* (Oderfeld [4.3]) by using entries of 11 adjacent Δ'' from the table of s versus $s(\theta)$:

$$s_i'' = \frac{1}{(\Delta\theta)^2} \sum_{j=-5}^{i=5} W_j \Delta_{i+j}'' \tag{4.29}$$

The weights W_j are given in Table 4.5.

TABLE 4.5 Weights Used in the Improved Finite-Difference Method

j	0	±1	2	±3	±4	±5
W_j	0.31	0.25	0.13	0.015	−0.025	−0.025

An example of an acceleration diagram $s''(\theta)$ of a certain cam obtained using the finite-difference method is presented in Fig. 4.18.

4.4 FORCE AND TORQUE ANALYSIS

A typical approach to dynamic analysis of a rigid cam system can be illustrated by an example of a mechanism with a reciprocating roller follower.† A schematic drawing of such a mechanism is depicted in Fig. 4.19*a*. For the upward motion of the follower,

† Suggestion of Professor Charles R. Mischke, Iowa State University.

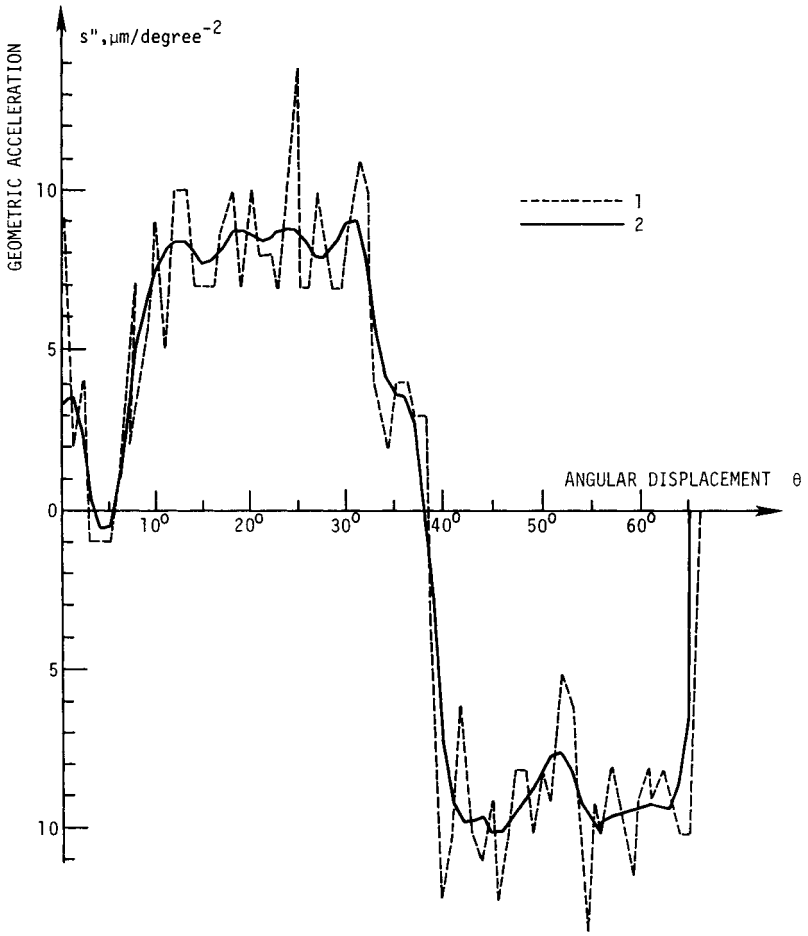

FIGURE 4.18 Acceleration diagrams obtained in the static way. Curve 1 is from Eq. (4.28), curve 2 from Eq. (4.29).

we assume that the follower's stem 4 contacts its guideway at points B and C. As a result of its upward motion, the Coulomb friction at B and C is fully developed and $\tan \psi = \mu$. The free-body diagram of links 3 and 4 is shown in Fig. 4.19*b*. The cam force F_{23} can be resolved into two components: P_{cr} in the critical-angle (γ_{cr}) direction to sustain motion against friction, and P_y in the y direction to produce accelerated motion or to oppose other forces.

It can be found from the geometry of the follower that

$$\gamma_{cr} = \frac{\pi}{2} - \tan^{-1} \mu \left(\frac{2a - \mu d}{l} - \frac{2s}{l} - 1 \right) \tag{4.30}$$

where $a = l_B - R_0 - R_r$. For $\gamma > \gamma_{cr}$, the cam-follower system is self-locking, and motion is impossible. From the force triangle in Fig. 4.19*b* and the rule of sines,

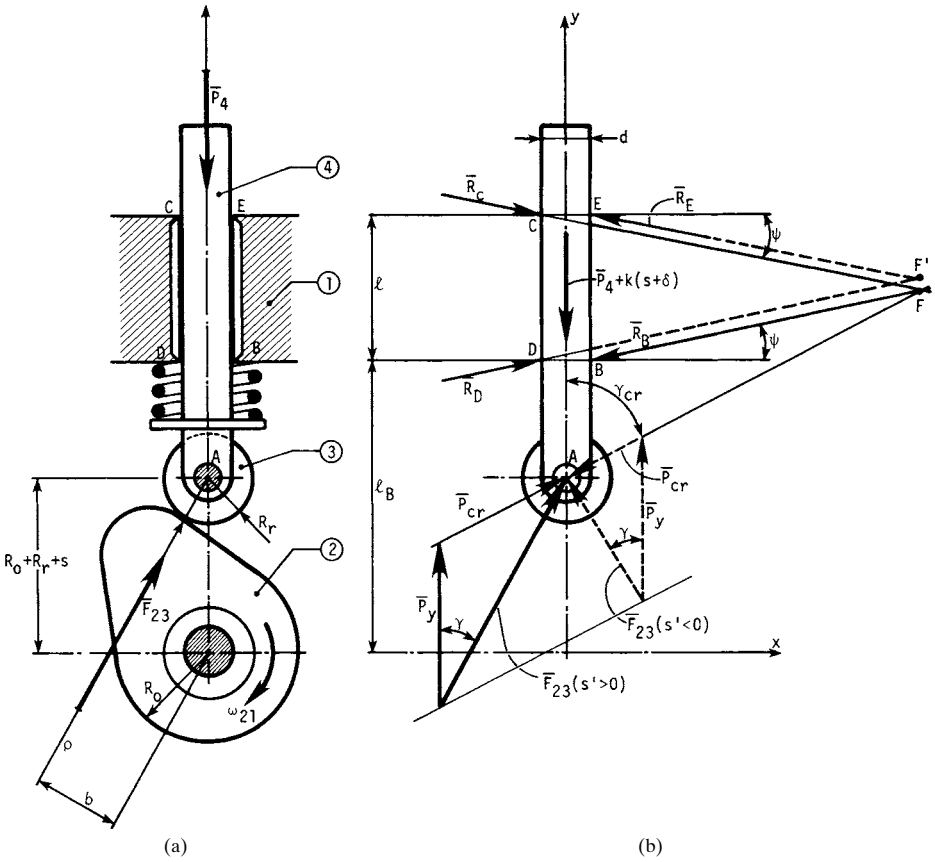

FIGURE 4.19 Force analysis of reciprocating roller-follower cam system.

$$P_y = F_{23}\frac{\sin(\gamma_{cr}-\gamma)}{\sin\gamma_{cr}} \tag{4.31}$$

After finding the vertical component P_y for constant ω_{21} from the force-equilibrium equation, substituting into Eq. (4.31), and solving for F_{23}, we have

$$F_{23} = \frac{\sin\gamma_{cr}(m\omega_{21}^2 s'' + ks + P_4')}{\sin(\gamma_{cr}-\gamma)} \tag{4.32}$$

where m = mass of follower
k = spring rate of retaining spring
$P_4' = P_4 + k\delta$
δ = preset of spring
$k\delta = P_0$; this force is called *preload* of spring

For $F_{23} = 0$, roller and cam lose their contact. The result is called *jump* ([4.7], [4.8]). Assuming $F_{23} = 0$, we can find the jump speed of the cam from Eq. (4.31). The jump occurs for the upward movement of the follower at

$$\omega_{21} \geq \sqrt{\frac{-ks - P_4'}{ms''}} \tag{4.33}$$

Since s is always positive, jump may occur only for negative values of s''. To prevent jump, we increase preload P_0 or the spring rate or both. The driving torque is

$$T_{12} = \frac{\sin \gamma_{cr} \sin \gamma}{\sin (\gamma_{cr} - \gamma)} (R_0 + R_r + s)(m\omega_{21}^2 s'' + ks + P_4') \tag{4.34}$$

We recall that according to Eq. (4.25),

$$\gamma = \tan^{-1} \frac{s'}{s + R_0 + R_r} \tag{4.35}$$

When motion is downward, the contact point of mating surfaces goes to the right side of the roller, cam force F_{23} changes inclination, and new contact points D and E in the follower's guideway replace old ones (B and C, respectively). The new point of concurrency is now at F'. Since in most practical cases points F and F' almost coincide, we can assume that both the point of concurrency and the line of action of force P_{cr} are unchanged. A new vector P_{cr} (broken line) is rotated by 180° with respect to the old one. It is easy to see in Fig. 4.19*b* that F_{23} for downward motion, when γ and P_y equal those for the upward motion, is always smaller than F_{23} for upward motion.

4.4.1 Springs

In cam-follower systems, the follower must contact the cam at all times. This is accomplished by a positive drive or a retaining spring. Spring forces should always prevent the previously described jump of the follower for all the operating speeds of the cam. Thus the necessary preload P_0 of the spring and its spring rate k should be chosen for the highest possible velocity of the cam. By plotting inertial and spring forces, we can find values of preload P_0 and spring rate k that will ensure sufficient load margin for the total range of the follower displacement. We use here only the negative portion of the acceleration curve. Since the follower must be held in contact with the cam, even while operating the system with temporary absence of applied forces, that part of the cam-system synthesis may be accomplished without applied forces. At the critical location, where both curves are in closest proximity, the spring force should exceed the inertial force with friction corrections included by not less than 25 to 50 percent.

4.5 CONTACT STRESS AND WEAR: PROGRAMMING

Let us consider the general case of two cylinderlike surfaces in contact. They are represented by a cam and a follower. The radius of curvature of the follower ρ_1 is equal to the radius of the roller R_r for the roller follower, and it goes to infinity for a flat

follower. The radius of the cam's curvature ρ_2 can be found from the following equation [compare to Eq. (4.23)]:

$$\rho_2 = R_0 + s'' + s \tag{4.36}$$

Equating $d\rho_2/d\theta = s''' + s'$ to zero, we can find the position of the cam, where a minimum of ρ_2 occurs, and find its value from Eq. (4.36). Assuming perfect alignment of the contacting bodies, we have conditions described by Hertz and can check maximum compressive stress σ_c from his well-known equation

$$\sigma_c = 0.558 \sqrt{\frac{P(1/\rho_1 + 1/\rho_2)}{L[(1-\mu_1^2)/E_1 + (1-\mu_2^2)/E_2]}} \tag{4.37}$$

where P = normal load between cam and follower
L = actual thickness of contacting follower and cam
μ_1, μ_2 = Poisson's ratios for follower and cam, respectively
E_1, E_2 = moduli of elasticity of follower and cam, respectively

Some selected data concerning properties of materials for cams and followers are given in [4.7].

Equation (4.37) may be used for finding the minimum permissible value ρ_{min} of the cam's profile radius of curvature. We recall that ρ_{min} was necessary for calculating the values of R_0 and R_r from Eqs. (4.23) and (4.26), respectively.

Rearranging Eq. (4.37) gives, for a roller follower,

$$\rho_{min} \geq \left[3.2\, S_c^2 \frac{L}{P} \left(\frac{1-\mu_1^2}{E_1} + \frac{1-\mu_2^2}{E_2} \right) - \frac{1}{R_r} \right]^{-1} \tag{4.38}$$

The same equation holds true for a flat-faced follower, where $1/R_r = 0$.

Using Eq. (4.38), we can easily check to see if the commonly recommended and used value $\rho_{min} = 0.25$ in (6 mm) is justified in the particular design.

Elements of a cam system, as well as of other machine parts, are subject to wear. The proper choice of metal combinations may increase the life of kinematic pairs of the cam system and decrease their wear. Some experience is necessary in choosing materials to fulfill the requirements of satisfactory cam action with low wear over a long period. Designers, as a rule, prefer to make the follower of softer or first-worn-out material, since manufacturing of the follower is less expensive than manufacturing of the cam profile. There are, however, cases where the cam is cheaper and thus is made of softer material.

4.5.1 Programming of Cam Systems

The steps shown in Fig. 4.20 are as follows:

1. Make a preliminary sketch of your cam system, and estimate the dynamic factor $\mu_d = m_e\omega_c^2/k_e$, according to Eq. (4.8).
2. If your system is a positive drive, go to step 3; otherwise go to step 4.
3. Choose a proper symmetric diagram $s''(\theta)$, and write equations for $s''(\theta)$, $s'(\theta)$, and $s(\theta)$. Write a computer program for θ and $s(\theta)$ with increments of θ equal to 1°.
4. Choose a proper unsymmetric diagram $s''(\theta)$, and proceed as in step 3.
5. Print table of θ and $s(\theta)$.

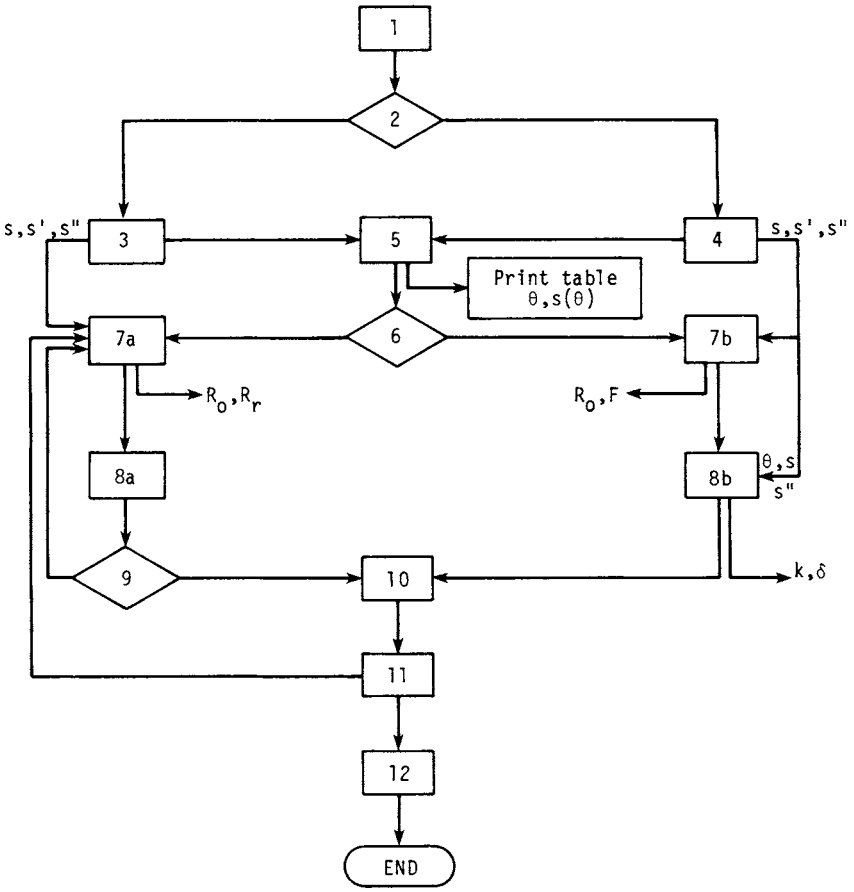

FIGURE 4.20 Programming of cam systems.

6. If you decided to use a roller follower, go to step 7*a;* otherwise go to step 7*b.*

7. *a.* Establish the radius of the roller R_r and the value of maximum pressure angle γ_{max} ($\gamma_{max} \leq 30°$ for the reciprocating follower and $\gamma_{max} \leq 40°$ for the oscillating one). Find the value of θ for which $s'/\tan \gamma_{max} - s - R_r$ is maximum, by equating $s''/\tan \gamma_{max} - s'$ to zero. Calculate the value of the radius R_0 of the prime circle from Eq. (4.26). Go to step 8*a.*

b. Find the value of θ for which $\rho_{min} - s'' - s$ is maximum, by setting $-(s''' + s')$ to zero. Calculate the value of the radius R_0 of the prime circle from Eq. (4.23). Calculate the face width F from Eq. (4.24). Go to step 8*b.*

8. *a.* Check undercutting of the cam profile from Eq. (4.27).

b. Find the spring rate of the retaining spring. Go to step 10.

9. If the assumed value R_r is satisfactory, go to step 10; otherwise, assume a new value of R_r and return to step 7*a.*

10. Draw a final version of your cam system (a complete drawing).

11. Write equations describing all the forces in the kinematic pairs, and check the maximum stresses. Find the values of γ_{max} and ρ_{min} for your particular design (if you have a roller follower), and determine whether the actual values of γ and ρ in your design are far enough from γ_{max} and ρ_{min}, respectively; otherwise, return to step 7*a*.

12. Make final corrections in your design.

13. END.

REFERENCES

4.1 M. P. Koster, *Vibrations of Cam Mechanisms,* Philips Technical Library, Macmillan Press, London, 1974.

4.2 C. R. Mischke, *Mathematical Model Building,* Iowa State University Press, Ames, 1980, pp. 316–322.

4.3 J. Oderfeld, "On Application of the Finite-Difference Method for Kinematics of Mechanisms," *Zastosowania Matematyki IV* (in Polish), 1958, pp. 176–195.

4.4 A. A. Olędzki, "Cam Mechanisms," *Wydawnictwa Naukowo Techniczne* (in Polish), Warsaw, Poland, 1966.

4.5 A. A. Olędzki, M. Krawczyński, I. Siwicki, and F. Źrudelny, "On the Automation of Cam-Profile Control," *IFAC Manufacturing Technology Symposium,* Tokyo, 1977.

4.6 A. A. Olędzki and T. Klimowicz, "An Experimental Attempt to Find the Influence of Cam-Profile Wear on the Kinematics of the Cam-Mechanism," *Archiwum Budowy Maszyn* (in Polish), 1979.

4.7 H. A. Rothbart, *Cams—Design, Dynamics, and Accuracy,* John Wiley & Sons, New York, 1956.

4.8 J. E. Shigley and J. J. Uicker, *Theory of Machines and Mechanisms,* 2d ed., McGraw-Hill, New York, 1995.

4.9 D. A. Stoddart, "Polydyne Cam Design," *Machine Design,* January 1953, p. 124; February 1953, p. 146; March 1953, p. 149.

4.10 D. Tesar and G. K. Matthew, *The Dynamic Synthesis, Analysis, and Design of Modeled Cam Systems,* D. C. Heath, Lexington, Mass., 1976.

CHAPTER 5
GEAR TRAINS

Harold L. Johnson, Ph.D.
Associate Professor Emeritus
School of Mechanical Engineering
Georgia Institute of Technology
Atlanta, Georgia

5.1 ORDINARY GEAR TRAINS

Gear trains consist of two or more gears meshed for the purpose of transmitting motion from one axis to another. Ordinary gear trains have axes, relative to the frame, for all gears making up the train. Figure 5.1*a* shows a simple ordinary train in which there is only one gear for each axis. In Fig. 5.1*b,* a compound ordinary train is seen to be one in which two or more gears may rotate about a single axis.

The ratio of the angular velocities of a pair of gears is the inverse of their numbers of teeth. The equations for each mesh in the simple train are

$$n_3 = \frac{N_2}{N_3} n_2 \qquad n_4 = \frac{N_3}{N_4} n_3 \qquad n_5 = \frac{N_4}{N_5} n_4 \tag{5.1}$$

where n is in revolutions per minute (r/min) and N = number of teeth. These equations can be combined to give the velocity ratio of the first gear in the train to the last gear:

$$n_5 = \frac{N_4}{N_5} \frac{N_3}{N_4} \frac{N_2}{N_3} n_2 \tag{5.2}$$

Note that the tooth numbers in the numerator are those of the driving gears, and the tooth numbers in the denominator belong to the driven gears. Gears 3 and 4 both drive and are, in turn, driven. Thus, they are called *idler gears.* Since their tooth numbers cancel, idler gears do not affect the magnitude of the input-output ratio, but they do change directions of rotation. Note the directional arrows in the figure. Idler gears can also produce a saving of space and money. In Fig. 5.2, the simple train of the previous figure has been repeated. In dotted outline is shown a pair of gears on the same center distance as gears 2 and 5 and having the same input-output ratio as the simple train.

Finally, Eq. (5.2) is simplified to become

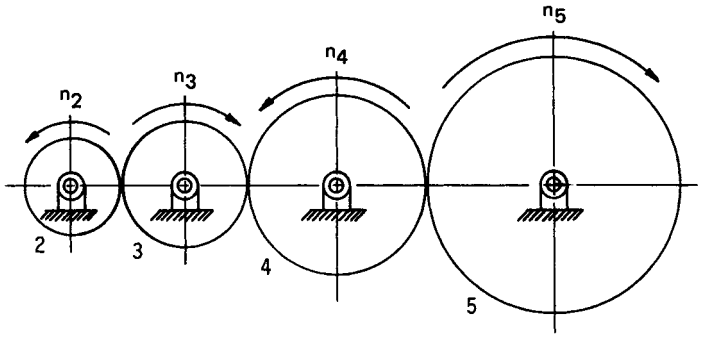

(a)

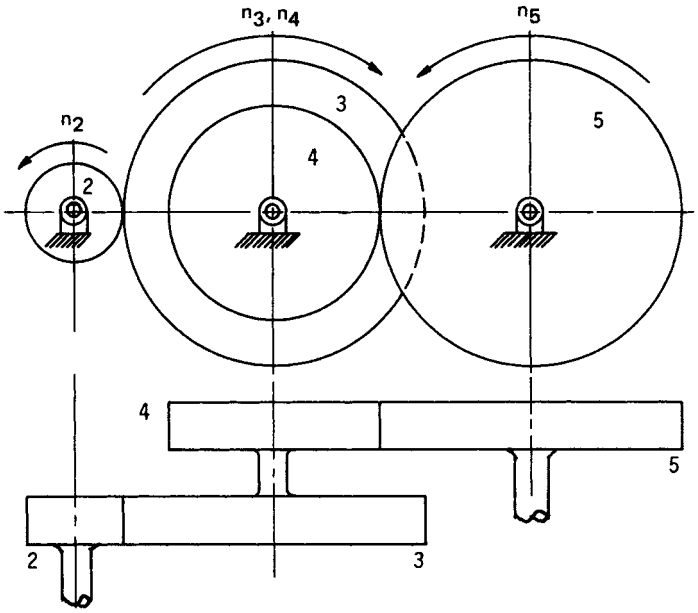

(b)

FIGURE 5.1 Ordinary gear trains. (*a*) Simple; (*b*) compound.

$$n_5 = -\frac{N_2}{N_5} n_2 \tag{5.3}$$

where the minus sign is now introduced to indicate contrarotation of the two gears.

The compound train in Fig. 5.1*b* has the following velocity ratios for the pairs of driver and driven gears:

$$n_3 = -\frac{N_2}{N_3} n_2 \qquad \text{and} \qquad n_5 = -\frac{N_4}{N_5} n_4 \tag{5.4}$$

and, of course, $n_4 = n_3$. Combining the equations yields

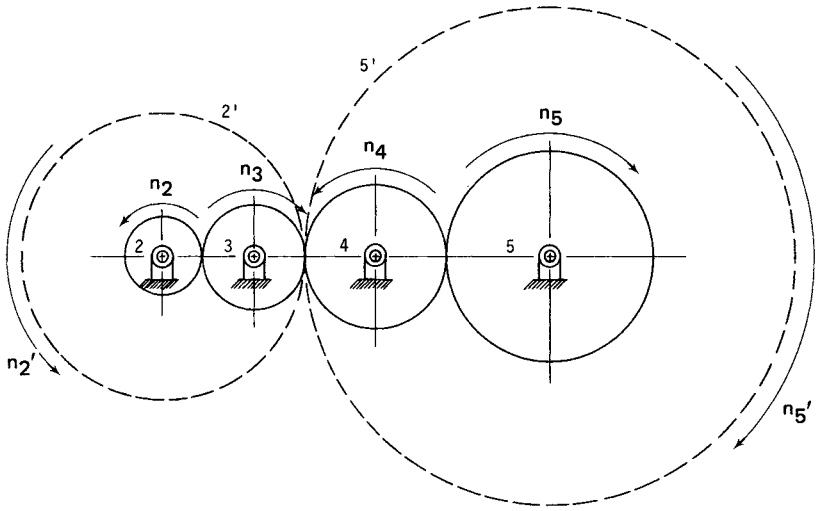

FIGURE 5.2 Gears 2′ and 5′ are required if idler gears are not used.

$$n_5 = \frac{N_2 N_4}{N_3 N_5} n_2 \tag{5.5}$$

and the thing worthy of note here is that the numbers of teeth of all gears constituting a mesh with a compounded pair are required to determine the velocity ratio through the system. Compound gear trains have an advantage over simple gear trains whenever the speed change is large. For example, if a reduction of 12/1 is required, the final gear in a simple train will have a diameter 12 times that of the first gear.

5.2 GEAR TYPE SELECTION

The disposition of the axes to be joined by the gear train often suggests the type of gear to choose. If the axes are parallel, the choices can be spur gears or helical gears. If the axes intersect, bevel gears can be used. If the axes are nonparallel and nonintersecting, then crossed helicals, worm and gear, or hypoid gears will work. In Fig. 5.3, a train having various types of gears is shown. Gears 2 and 3, parallel helical gears, have a speed ratio

$$n_3 = -\frac{N_2}{N_3} n_2 \tag{5.6}$$

Gears 4 and 5, bevel gears, have a speed ratio

$$n_5 = -\frac{N_4}{N_5} n_4 \tag{5.7}$$

Gears 6 and 7, worm and gear, are considered in a slightly different manner. A worm is generally spoken of as having threads, one, two, three or more (see Chap. 12). A

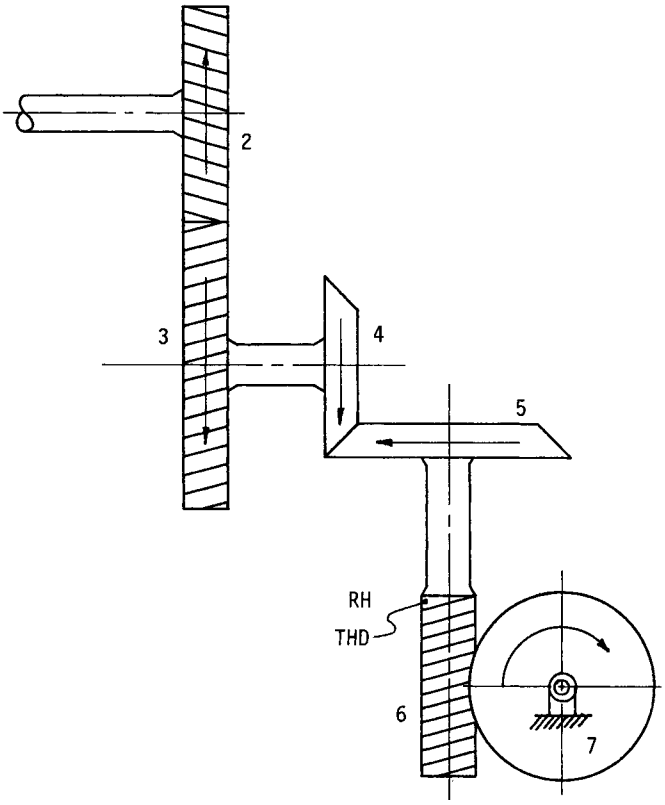

FIGURE 5.3 Various gears used in a train.

worm with one thread would have a lead equal to the pitch of the thread. A worm with two threads would have a lead equal to twice the pitch of the thread. Thus

$$n_7 = \frac{\text{number of threads on 6}}{N_7}\, n_6 \tag{5.8}$$

Joining Eqs. (5.6), (5.7), and (5.8), we find

$$n_7 = \frac{N_6}{N_7}\frac{N_4}{N_5}\frac{N_2}{N_3}\, n_2 \tag{5.9}$$

where N_6 represents the number of threads of the worm gear.

To determine the direction of rotation of gear 7, an inversion technique can be used. Fix gear 7 and allow the worm to translate along its axis as it rotates. Here it is necessary to note the hand of the worm, which can be either right or left. In the figure, gear 6 rotates in the same direction as gear 5 and, having a right-hand thread, will move downward (in the drawing). Now, inverting back to the original mechanism, the worm is moved in translation to its proper position, and by doing so, gear 7 is seen to rotate clockwise.

5.3 PLANETARY GEAR TRAINS

Planetary gear trains, also referred to as *epicyclic gear trains,* are those in which one or more gears orbit about the central axis of the train. Thus, they differ from an ordinary train by having a moving axis or axes. Figure 5.4 shows a basic arrangement that is functional by itself or when used as a part of some more complex system. Gear 2 is called a *sun gear,* gear 4 is a *planet,* link 3 is an *arm,* or *planet carrier,* and gear 5 an internal-toothed *ring gear.*

Planetary gear trains are, fundamentally, two-degree-of-freedom systems. Therefore, two inputs are required before they can be uniquely analyzed. Quite frequently a fixed gear is included in the train. Its velocity is zero, but this zero velocity constitutes one of the input values. Any link in the train shown except the planet can serve as an input or an output link. If, for example, the rotations of link 2 and link 5 were the input values, the rotation of the arm would be the output. The term *link* refers to the individual machine elements comprising a mechanism or linkage, and gear trains are included in this broad array of systems. Each link is paired, or joined, with at least two other links by some form of connection, such as pin points, sliding joints, or

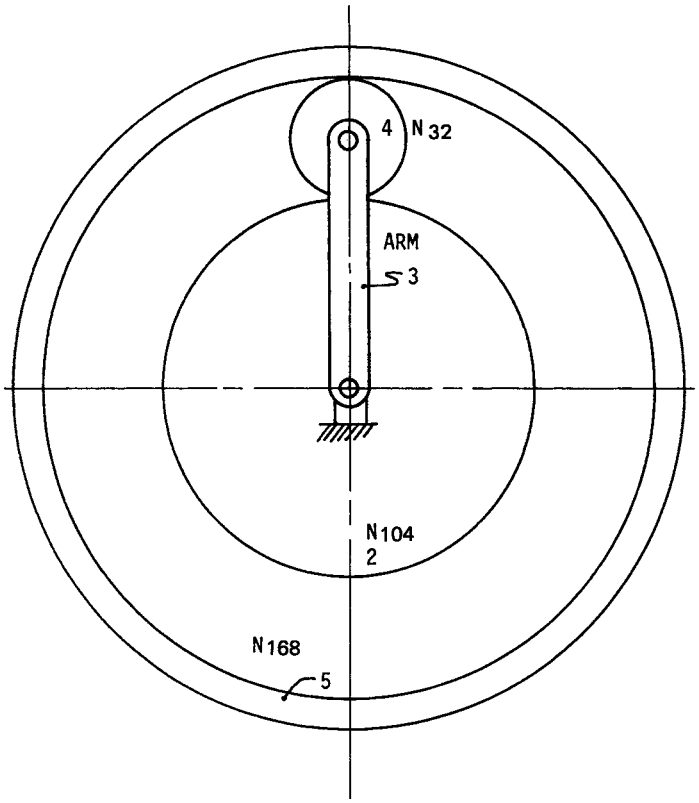

FIGURE 5.4 A basic planetary train.

direct contact, a pairing that is prevalent in cam-and-gear systems. An explanation and an illustration of the *joint* types are found in Refs. [5.1] and [5.2] as well as others (see Chap. 3).

There are several methods for analyzing planetary trains. Among these are instant-centers, formula, and tabular methods. By instant centers, as in Ref. [5.3] and on a face view of the train, draw vectors representing the velocities of the instant centers for which input information is known. Then, by simple graphical construction, the velocity of another center can be found and converted to a rotational speed. Figure 5.5 illustrates this technique.

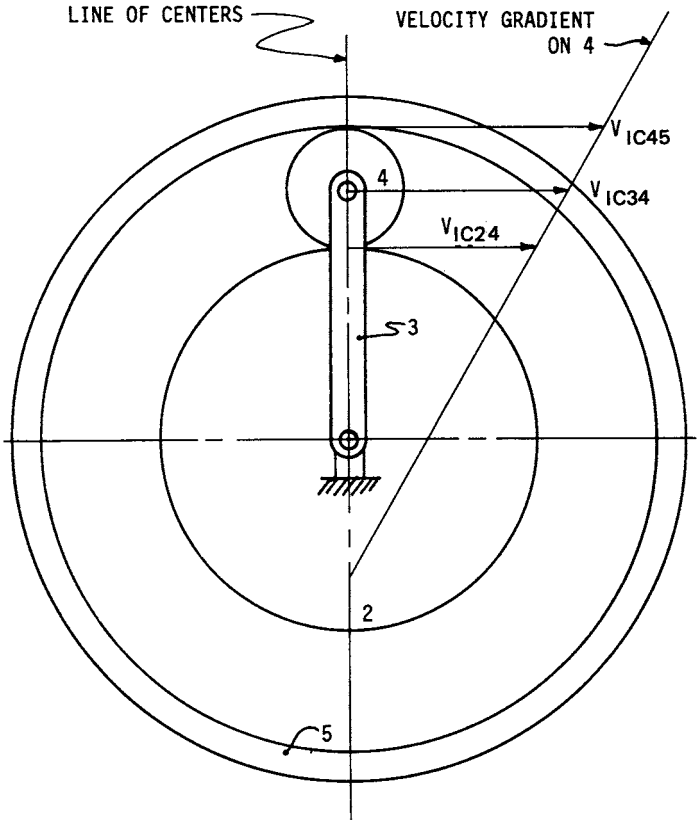

FIGURE 5.5 Instant-centers method of velocity analysis.

Calculate V_{IC24} and V_{IC45} from

$$V = r\omega \tag{5.10}$$

where r = radius dimension and ω = angular velocity in radians per second (rad/s). Draw these vectors to scale in the face view of the train. Then V_{IC24} and V_{IC45} will emanate from their instant-center positions. Now draw a straight line through the

termini of the velocity vectors.† The velocity of IC34 will be a vector perpendicular to the line of centers and having its terminus on the velocity gradient. Determine ω of link 3 by using Eq. (5.10). Thus,

$$V_{IC24} = r_2\omega_2 \qquad \text{and} \qquad V_{IC45} = r_5\omega_5$$

Choose a scale and construct the two vectors. Next, draw the gradient line and construct V_{IC34}. Scale its magnitude and determine n_3 according to

$$n_3 = \frac{V_{IC34}}{2\pi r_3} 60 \tag{5.11}$$

where r_3 = radius of the arm and n_3 is in revolutions per minute.

If gear 5 is fixed, then $V_{IC45} = 0$; using V_{IC24}, connect the terminus of V_{IC24} and IC45 with a straight line, and find V_{IC34} as before. See Fig. 5.6.

† This line can be called a *velocity gradient* for link 4.

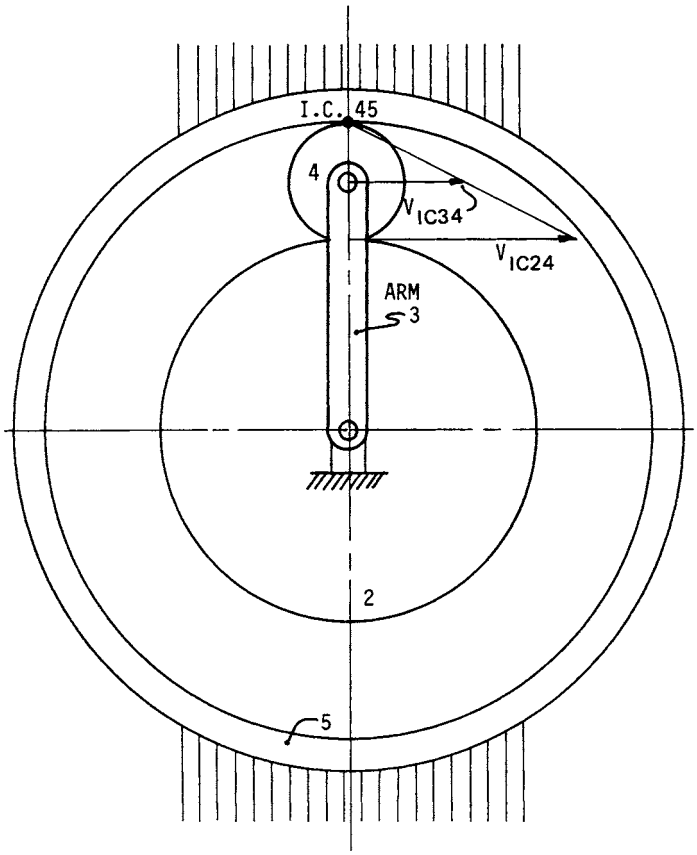

FIGURE 5.6 Gear 5 is fixed.

By formula, the relative-motion equation will establish the velocity of the gears relative to the arm; that is,

$$n_{23} = n_2 - n_3 \tag{5.12}$$

$$n_{53} = n_5 - n_3 \tag{5.13}$$

Then, dividing (5.13) by (5.12), we see that

$$\frac{n_{53}}{n_{23}} = \frac{n_5 - n_3}{n_2 - n_3} \tag{5.14}$$

which represents the ratio of the relative velocity of gear 5 to that of gear 2 with both velocities related to the arm. The right-hand side of the equation is called the *train value.* If the arm should be held fixed, then the ratio of output to input speeds for an ordinary train is obtained.

The equation for train value, which is seen in most references, can be written

$$e = \frac{n_L - n_A}{n_F - n_A} \tag{5.15}$$

where n_F = speed of first gear in train
n_L = speed of last gear in train
n_A = speed of arm

The following example will illustrate the use of Eq. (5.15).

Example 1. Refer to the planetary train of Fig. 5.4. The tooth numbers are $N_2 = 104$, $N_4 = 32$, and $N_5 = 168$. Gear 2 is driven at 250 r/min in a clockwise *negative* direction, and gear 5 is driven at 80 r/min in a counterclockwise *positive* direction. Find the speed and direction of rotation of the arm.

Solution. $n_F = n_2 = -250$ r/min $\quad n_L = n_5 = +80$ r/min

$$e = \left(-\frac{N_2}{N_4}\right)\left(\frac{N_4}{N_5}\right) = \left(-\frac{104}{32}\right)\left(\frac{32}{168}\right) = -\frac{13}{21}$$

In Eq. (5.15),

$$-\frac{13}{21} = \frac{80 - n_3}{-250 - n_3} \qquad n_3 = -46.2 \text{ r/min}$$

By tabular method, a table is first formed according to the following:

1. Include a column for any gear centered on the planetary axis.
2. Do not include a column for any gear whose axis of rotation is fixed and different from the planetary axis.
3. A column for the arm is not necessary.
4. The planet, or planets, may be included in a column or not, as preferred.

Gears which fit rule 2 are treated as ordinary gear train elements. They are used as input motions to the planetary system, or they may function as output motions.

The table contains three rows arranged so that each entry in a column will constitute one term of the relative-motion equation

TABLE 5.1 Solution by Tabulation

Step	Gear 2	Gear 5
1. Gears locked	n_3	n_3
2. Arm fixed	$n_2 - n_3$	$-\frac{N_2}{N_4}\left(\frac{N_4}{N_5}\right)(n_2 - n_3)$
3. Results	n_2	n_5

$$n_y + n_{xy} = n_x \tag{5.16}$$

This is best shown by example. Using the planetary train of the previous example, we form Table 5.1, and the equation from the column for gear 5 is

$$n_3 - \frac{N_2 N_4}{N_4 N_5}(n_2 - n_3) = n_5$$

Rearranging and canceling N_4, we find

$$n_3\left(1 + \frac{N_2}{N_5}\right) - n_2\frac{N_2}{N_5} = n_5 \tag{5.17}$$

This is the characteristic equation of the planetary train, as shown in Fig. 5.4.

Note that three rotational quantities appear—n_3, n_2, and n_5. There must be two input rotations in order to solve for the output. This is easily done when the input rotations and the tooth numbers are inserted. When a positive sense is assigned to counterclockwise and a negative sense to clockwise rotation, the sign of the output rotation indicates its sense of direction.

Note that planet 4 was not included in the table (it could have been); however, gear 4 served its purpose by acting as an idler to change a direction of rotation. This is evidenced by the presence of a negative sign in the second row of the column for gear 5.

A convenient means of representing a planetary train was shown by Levai [5.4]. Type A of Fig. 5.7*a* shows an edge view of the planetary train first seen in Fig. 5.4. It and the other 11 configurations represent all possible variations for a planetary train. The equations in Table 5.2 are the characteristic equations of the 12 types.

An examination of the equations and their corresponding types reveals that certain ones are identical. Types C and D in Fig. 5.7*b* are identical because of the arrangement of gears. Whereas in type C the meshes of 2 and 4 and of 7 and 8 are external, the input and output meshes are internal in type D. The same relationship can be seen in types G and H in Fig. 5.7*c*. Certain pair types are alike in equation form but differ in sign. Compare types E and K and F and L in Fig. 5.7*b* and *d*, and B and G (or B and H) in Fig. 5.7*a* and *c*.

The speed of a planet gear relative to the frame or relative to the arm may be required. If appreciable speeds and forces are involved, this information will facilitate the selection of bearings. Using type A as an example, set up Table 5.3. Row 2 in the column for gear 4 is the speed of gear 4 relative to the arm, and row 3 in the column for gear 4 is its speed relative to the frame.

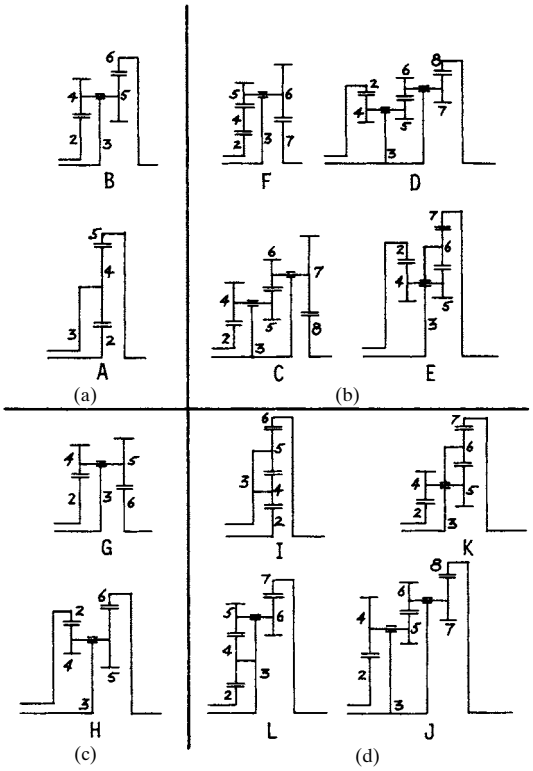

FIGURE 5.7 Twelve variations of planetary trains.

Example 2. Figure 5.8 shows a planetary gear train with input at gear 2. Also, gear 6′ is seen to be part of the frame, in which case its rotation is zero. For $n_2 = 100$ r/min clockwise (negative), find output rotation n_6.

Solution. Gears 2, 4, 5, and 6 and arm 3 form a type B planetary train:

$$n_3\left(1+\frac{N_2N_5'}{N_4N_6'}\right)-n_2\frac{N_2N_6'}{N_4N_6'}=n_6'$$

Solving for n_3 yields

$$n_3\left(1+\frac{1}{8}\right)-(-100)\left(\frac{1}{8}\right)=0$$

$$n_3=-\frac{100}{9}\text{ r/min}$$

For type G:

$$n_3\left(1-\frac{N_2N_5}{N_4N_6}\right)+\left(n_2\frac{N_2N_5}{N_4N_6}\right)=n_6$$

Then we solve type G for n_6:

TABLE 5.2 Characteristic Equations for 12 Planetary Trains of Fig. 5.7

Type	Equation
A	$n_3\left(1+\frac{N_2}{N_5}\right)-n_2\frac{N_2}{N_5}=n_5$
B	$n_3\left(1+\frac{N_2N_5}{N_4N_6}\right)-n_2\frac{N_2N_5}{N_4N_6}=n_6$
C	$n_3\left(1+\frac{N_2N_5N_7}{N_4N_6N_8}\right)-n_2\frac{N_2N_5N_7}{N_4N_6N_8}=n_8$
D	$n_3\left(1+\frac{N_2N_5N_7}{N_4N_6N_8}\right)-n_2\frac{N_2N_5N_7}{N_4N_6N_8}=n_8$
E	$n_3\left(1+\frac{N_2N_5}{N_4N_7}\right)-n_2\frac{N_2N_5}{N_4N_7}=n_7$
F	$n_3\left(1+\frac{N_2N_6}{N_5N_7}\right)-n_2\frac{N_2N_6}{N_5N_7}=n_7$
G	$n_3\left(1-\frac{N_2N_5}{N_4N_6}\right)+n_2\frac{N_2N_5}{N_4N_6}=n_6$
H	$n_3\left(1-\frac{N_2N_5}{N_4N_6}\right)+n_2\frac{N_2N_5}{N_4N_6}=n_6$
I	$n_3\left(1-\frac{N_2}{N_6}\right)+n_2\frac{N_2}{N_6}=n_6$
J	$n_3\left(1-\frac{N_2N_5N_7}{N_4N_6N_8}\right)+n_2\frac{N_2N_5N_7}{N_4N_6N_8}=n_8$
K	$n_3\left(1-\frac{N_2N_5}{N_4N_7}\right)+n_2\frac{N_2N_5}{N_4N_7}=n_7$
L	$n_3\left(1-\frac{N_2N_6}{N_5N_7}\right)+n_2\frac{N_2N_6}{N_5N_7}=n_7$

TABLE 5.3 Solution of Type A Train

Step	Gear 2	Gear 4	Gear 5
1. Gears locked	n_3	n_3	n_3
2. Arm fixed	n_3-n_2	$-\frac{N_2}{N_4}(n_3-n_2)$	$-\frac{N_2}{N_5}(n_3-n_2)$
3. Results	n_3	n_4	n_5

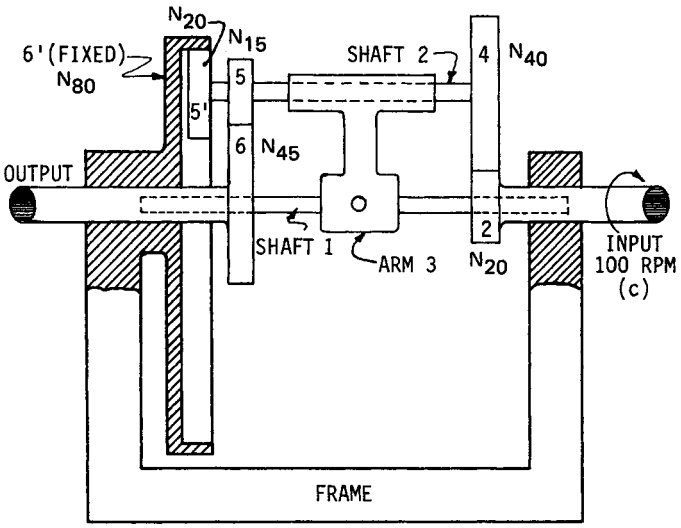

(a)

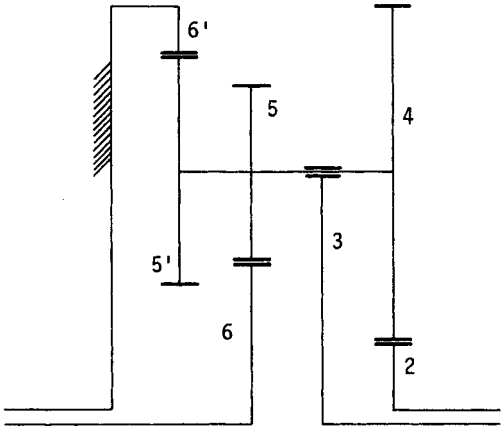

(b)

FIGURE 5.8 (*a*) View of a gear train and (*b*) its symbolic notation.

$$-\frac{100}{9}\left(1-\frac{1}{6}\right)+(-100)\left(\frac{1}{6}\right)=n_6$$

$$n_6 = -25.93 \text{ r/min}$$

Example 3. Figure 5.9 shows a type I planetary train, Ref. [5.2]. Here, if $n_2 = 100$ r/min clockwise and $n_3 = 200$ r/min clockwise, both considered negative, determine n_4, n_5, and n_6.

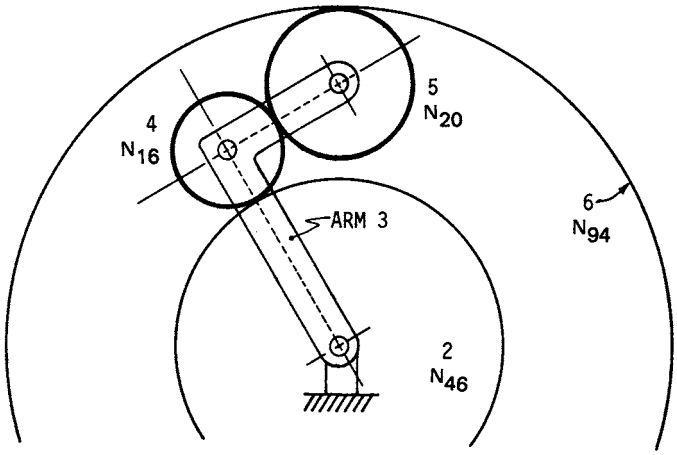

(a)

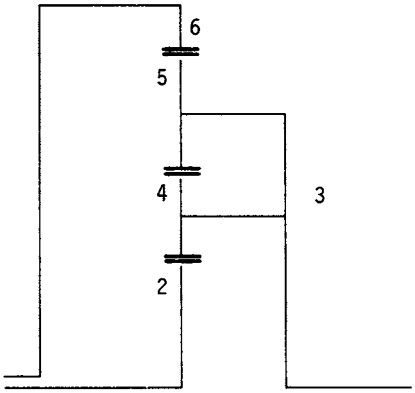

(b)

FIGURE 5.9 (*a*) Planetary train; (*b*) symbolic notation.

TABLE 5.4 Solution of Type I Train

Step	Gear 2	Gear 4	Gear 5	Gear 6
1	n_3	n_3	n_3	n_3
2	$n_2 - n_3$	$-\frac{N_2}{N_4}(n_2 - n_3)$	$+\frac{N_2}{N_5}(n_2 - n_3)$	$+\frac{N_2}{N_6}(n_2 - n_3)$
3	n_2	n_4	n_5	n_6

Solution. To determine the angular speeds for the planet, form Table 5.4. The speed of gear 4 can be found by writing the equation in the column for gear 4. Thus,

$$n_3\left(1+\frac{N_2}{N_4}\right)-n_2\frac{N_2}{N_4}=n_4$$

$$-200\left(1+\frac{46}{16}\right)-(-100)\left(\frac{46}{16}\right)=n_4$$

$$n_4=-487.5 \text{ r/min}$$

For gear 5,

$$n_3\left(1-\frac{N_2}{N_5}\right)+n_2\frac{N_2}{N_5}=n_5$$

$$-200\left(1-\frac{46}{20}\right)+(-100)\left(\frac{46}{20}\right)=n_5$$

$$n_5=+30 \text{ r/min}$$

For gear 6,

$$n_3\left(1-\frac{N_2}{N_6}\right)+n_2\frac{N_2}{N_6}=n_6$$

$$-200\left(1-\frac{46}{94}\right)+(-100)\left(\frac{46}{94}\right)=n_6$$

$$n_6=-151 \text{ r/min}$$

5.4 DIFFERENTIAL TRAINS

Differential gear trains are useful as mechanical computing devices. In Fig. 5.10, if ω_4 and ω_6 are input angular velocities and V_A and V_B are the resulting linear velocities of points A and B, respectively, then the velocity of point C on the carrier is

$$V_C=\frac{V_A+V_B}{2} \tag{5.18}$$

The differential gear train also finds application in the wheel-axle system of an automobile. The planet carrier rotates at the same speed as the wheels when the automobile is traveling in a straight line. When the car goes into a curve, however, the inside wheel rotates at a lesser speed than the outside wheel because of the differential gear action. This prevents tire drag along the road during a turn.

Example 4. See Ref. [5.2], page 329. The tooth numbers for the automotive differential shown in Fig. 5.11 are $N_2=17$, $N_3=54$, $N_4=11$, and $N_5=N_6=16$. The drive shaft turns at 1200 r/min. What is the speed of the right wheel if it is jacked up and the left wheel is resting on the road surface?

GEAR TRAINS

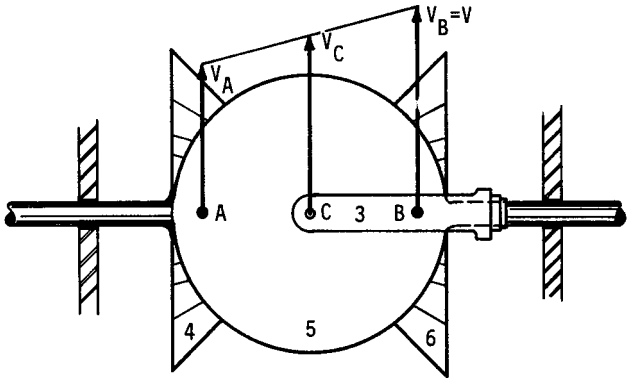

(a)

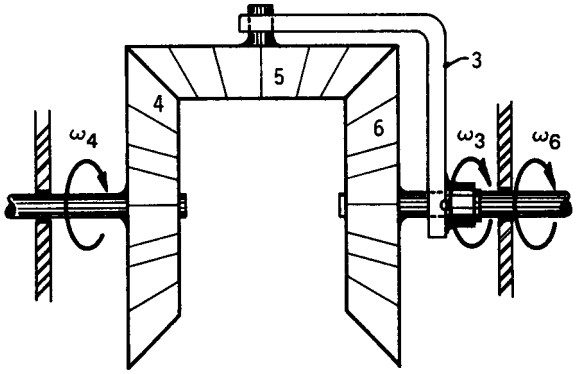

(b)

FIGURE 5.10 (*a*) Top and (*b*) front views of a bevel-gear differential used as a mechanical averaging linkage. Point *A* is the pitch point of gears 4 and 5. Point *B* is the pitch point of gears 5 and 6.

Solution. The planet carrier, gear 3, is rotating according to the following equation:

$$n_3 = \frac{N_2}{N_3} n_2 = \frac{17}{54} (1200) = 377.78 \text{ r/min}$$

Since the r/min of the left wheel is zero, the pitch point of gears 4 and 5 has a linear velocity twice that of the pin which supports the planet. Therefore, the r/min of the right wheel is twice that of the planet, or

$$n_6 = 2n_3 = 755.56 \text{ r/min}$$

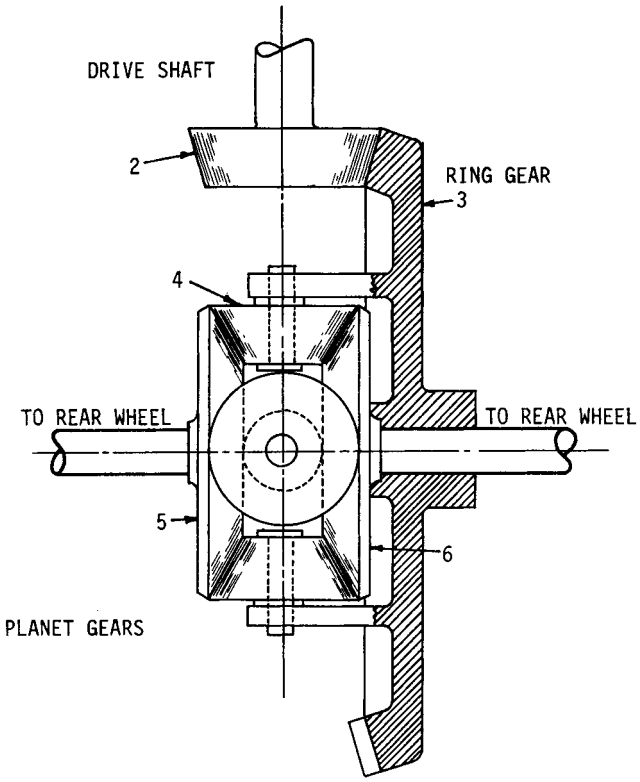

FIGURE 5.11 Schematic drawing of a bevel-gear automotive differential.

REFERENCES

5.1 Richard S. Hartenberg and Jacques Denavit, *Kinematic Synthesis of Linkages,* McGraw-Hill, New York, 1964.

5.2 J. E. Shigley and J. J. Uicker, Jr., *Theory of Machines and Mechanisms,* 2d ed., McGraw-Hill, New York, 1995.

5.3 Virgil M. Faires and Robert M. Keown, *Mechanism,* 5th ed., McGraw-Hill, New York, 1960.

5.4 Z. L. Levai, "Theory of Epicyclic Gears and Epicyclic Change-Speed Gears," Technical University of Building, Civil and Transport Engineering, Budapest, 1966.

P · A · R · T · 2

MACHINE ELEMENTS THAT ABSORB AND STORE ENERGY

CHAPTER 6
SPRINGS

Robert E. Joerres
Applications Engineering Manager
Associated Spring, Barnes Group, Inc.
Bristol, Connecticut

GENERAL NOMENCLATURE[†]

A	Area, mm^2 (in^2)
b	Width, mm (in)
C	Spring index, D/d
d	Wire diameter, mm (in)
D	Mean diameter (OD minus wire diameter), mm (in)
E	Modulus of elasticity in tension or Young's modulus, MPa (psi)
f	Deflection, mm (in)
g	Gravitational constant, 9.807 m/s^2 (386.4 in/s^2)
G	Shear modulus or modulus of rigidity, MPa (psi)
I	Moment of inertia, mm^4 (in^4)
ID	Inside diameter, mm (in)
k	Spring rate, N/mm (lb/in) or N·mm/r (lb·in/r)

[†] The symbols presented here are used extensively in the spring industry. They may differ from those used elsewhere in this Handbook.

K	Design constant
K_w	Stress correction factor for helical springs
L	Length, mm (in)
L_f	Free length, mm (in)
L_s	Length at solid, mm (in)
M	Moment or torque, N·mm (lb·in)
n	Frequency, Hz
N_a	Number of active coils or waves
N_t	Total number of coils
OD	Outside diameter, mm (in)
P	Load, N (lbf)
r	Radius, mm (in)
S	Stress, MPa (psi)
TS	Tensile strength, MPa (psi)
t	Thickness, mm (in)
YS	Yield strength, MPa (psi)
ρ	Density, g/cm^3 (lb/in^3)
θ	Angular deflection, expressed in number of revolutions
μ	Poisson's ratio

6.1 INTRODUCTION

Spring designing is a complex process. It is an interactive process which may require several iterations before the best design is achieved. Many simplifying assumptions have been made in the design equations, and yet they have proved reliable over the years. When more unusual or complex designs are required, designers should rely on the experience of a spring manufacturer.

The information in this chapter is offered for its theoretical value and should be used accordingly.

6.2 GLOSSARY OF SPRING TERMINOLOGY

active coils: those coils which are free to deflect under load.

baking: heating of electroplated springs to relieve hydrogen embrittlement.

buckling: bowing or lateral displacement of a compression spring; this effect is related to slenderness ratio *L/D*.

closed and ground ends: same as *closed ends,* except that the first and last coils are ground to provide a flat bearing surface.

closed ends: compression spring ends with coil pitch angle reduced so that they are square with the spring axis and touch the adjacent coils.

close-wound: wound so that adjacent coils are touching.

deflection: motion imparted to a spring by application or removal of an external load.

elastic limit: maximum stress to which a material may be subjected without permanent set.

endurance limit: maximum stress, at a given stress ratio, at which material will operate in a given environment for a stated number of cycles without failure.

free angle: angular relationship between arms of a helical torsion spring which is not under load.

free length: overall length of a spring which is not under load.

gradient: see *rate.*

heat setting: a process to prerelax a spring in order to improve stress-relaxation resistance in service.

helical springs: springs made of bar stock or wire coiled into a helical form; this category includes compression, extension, and torsion springs.

hooks: open loops or ends of extension springs.

hysteresis: mechanical energy loss occurring during loading and unloading of a spring within the elastic range. It is illustrated by the area between load-deflection curves.

initial tension: a force that tends to keep coils of a close-wound extension spring closed and which must be overcome before the coils start to open.

loops: formed ends with minimal gaps at the ends of extension springs.

mean diameter: in a helical spring, the outside diameter minus one wire diameter.

modulus in shear or torsion (modulus of rigidity *G*): coefficient of stiffness used for compression and extension springs.

modulus in tension or bending (Young's modulus *E*): coefficient of stiffness used for torsion or flat springs.

moment: a product of the distance from the spring axis to the point of load application and the force component normal to the distance line.

natural frequency: lowest inherent rate of free vibration of a spring vibrating between its own ends.

pitch: distance from center to center of wire in adjacent coils in an open-wound spring.

plain ends: end coils of a helical spring having a constant pitch and with the ends not squared.

plain ends, ground: same as *plain ends,* except that wire ends are ground square with the axis.

rate: spring gradient, or change in load per unit of deflection.

residual stress: stress mechanically induced by such means as set removal, shot peening, cold working, or forming; it may be beneficial or not, depending on the spring application.

set: permanent change of length, height, or position after a spring is stressed beyond material's elastic limit.

set point: stress at which some arbitrarily chosen amount of set (usually 2 percent) occurs; set percentage is the set divided by the deflection which produced it.

set removal: an operation which causes a permanent loss of length or height because of spring deflection.

solid height: length of a compression spring when deflected under load sufficient to bring all adjacent coils into contact.

spiral springs: springs formed from flat strip or wire wound in the form of a spiral, loaded by torque about an axis normal to the plane of the spiral.

spring index: ratio of mean diameter to wire diameter.

squared and ground ends: see *closed and ground ends.*

squared ends: see *closed ends.*

squareness: angular deviation between the axis of a compression spring in a free state and a line normal to the end planes.

stress range: difference in operating stresses at minimum and maximum loads.

stress ratio: minimum stress divided by maximum stress.

stress relief: a low-temperature heat treatment given springs to relieve residual stresses produced by prior cold forming.

torque: see *moment.*

total number of coils: the sum of the number of active and inactive coils in a spring body.

6.3 SELECTION OF SPRING MATERIALS

6.3.1 Chemical and Physical Characteristics

Springs are resilient structures designed to undergo large deflections within their elastic range. It follows that the materials used in springs must have an extensive elastic range.

Some materials are well known as spring materials. Although they are not specifically designed alloys, they do have the elastic range required. In steels, the medium- and high-carbon grades are suitable for springs. Beryllium copper and phosphor bronze are used when a copper-base alloy is required. The high-nickel alloys are used when high strength must be maintained in an elevated-temperature environment.

The selection of material is always a cost-benefit decision. Some factors to be considered are costs, availability, formability, fatigue strength, corrosion resistance, stress relaxation, and electric conductivity. The right selection is usually a compromise among these factors. Table 6.1 lists some of the more commonly used metal alloys and includes data which are useful in material selection.

Surface quality has a major influence on fatigue strength. This surface quality is a function of the control of the material manufacturing process. Materials with high surface integrity cost more than commercial grades but must be used for fatigue applications, particularly in the high cycle region.

6.3.2 Heat Treatment of Springs

Heat treatment is a term used in the spring industry to describe both low- and high-temperature heat treatments. Low-temperature heat treatment, from 350 to 950°F (175 to 510°C), is applied to springs after forming to reduce unfavorable residual stresses and to stabilize parts dimensionally.

When steel materials are worked in the spring manufacturing process, the yield point is lowered by the unfavorable residual stresses. A low-temperature heat treatment restores the yield point. Most heat treatment is done in air, and the minor oxide that is formed does not impair the performance of the springs.

When hardened high-carbon-steel parts are electroplated, a phenomenon known as *hydrogen embrittlement* occurs, in which hydrogen atoms diffuse into the metallic lattice, causing previously sound material to crack under sustained stress. Low-temperature baking in the range of 375 to 450°F (190 to 230°C) for times ranging from 0.5 to 3 h, depending on the type of plating and the degree of embrittlement, will reduce the concentration of hydrogen to acceptable levels.

High-temperature heat treatments are used to strengthen annealed material after spring forming. High-carbon steels are austenitized at 1480 to 1652°F (760 to 900°C), quenched to form martensite, and then tempered to final hardness. Some nickel-base alloys are strengthened by high-temperature aging. Oxidation will occur at these temperatures, and it is advisable to use a protective atmosphere in the furnace.

Heat treatments for many common materials are listed in Table 6.2. Unless otherwise noted, 20 to 30 min at the specified temperature is sufficient. Thin, flimsy cross-sectional springs can be distorted by the heat-treatment operation. Pretempered materials are available for use in such cases.

6.3.3 Relaxation

The primary concern in elevated-temperature applications is stress relaxation. *Stress relaxation* is the loss of load or spring length that occurs when a spring is held at load or cycled under load. Heat affects modulus and tensile strength. In addition to the factors of stress, time, and temperature which affect relaxation, other controllable factors are

1. Alloy type—the highly alloyed materials are generally more temperature-resistant.
2. Residual stresses—such stresses remaining from forming operations are detrimental to relaxation resistance. Use the highest practical stress-relief temperature.
3. Heat setting—procedures employed to expose springs under some load to stress and heat to prepare them for a subsequent exposure. The effect is to remove the first stage of relaxation.

6.3.4 Corrosion

The specific effect of a corrosive environment on spring performance is difficult to predict. In general, if the environment causes damage to the spring surface, the life and the load-carrying ability of the spring will be reduced.

The most common methods of combating corrosion are to use materials that are resistant or inert to the particular corrosive environment or to use coatings that slow

TABLE 6.1 Typical Properties of Common Spring Materials

Common Name	Young's Modulus E (1) MPa 10^3	Young's Modulus E (1) psi 10^6	Modulus of Rigidity G (1) MPa 10^3	Modulus of Rigidity G (1) psi 10^6	Density (1) g/cm^3	Density (1) lb/in^3	Electrical Conductivity (1) % IACS	Sizes Normally Available (2) Min. mm	Sizes Normally Available (2) Min. in.	Sizes Normally Available (2) Max. mm	Sizes Normally Available (2) Max. in.	Typical Surface Quality (3)	Maximum Service Temperature (4) °C	Maximum Service Temperature (4) °F
Carbon Steel Wires:														
Music (5)	207	(30)	79.3	(11.5)	7.86	(0.284)	7	0.10	(0.004)	6.35	(0.250)	a	120	250
Hard Drawn (5)	207	(30)	79.3	(11.5)	7.86	(0.284)	7	0.13	(0.005)	16	(0.625)	c	150	250
Oil Tempered	207	(30)	79.3	(11.5)	7.86	(0.284)	7	0.50	(0.020)	16	(0.625)	c	150	300
Valve Spring	207	(30)	79.3	(11.5)	7.86	(0.284)	7	1.3	(0.050)	6.35	(0.250)	a	150	300
Alloy Steel Wires:														
Chrome Vanadium	207	(30)	79.3	(11.5)	7.86	(0.284)	7	0.50	(0.020)	11	(0.435)	a,b	220	425
Chrome Silicon	207	(30)	79.3	(11.5)	7.86	(0.284)	5	0.50	(0.020)	9.5	(0.375)	a,b	245	475
Stainless Steel Wires:														
Austenitic Type 302	193	(28)	69.0	(10.)	7.92	(0.286)	2	0.13	(0.005)	9.5	(0.375)	b	260	500
Precipitation Hardening 17-7 PH	203	(29.5)	75.8	(11)	7.81	(0.282)	2	0.08	(0.002)	12.5	(0.500)	b	315	600
NiCr A286	200	(29)	71.7	(10.4)	8.03	(0.290)	2	0.40	(0.016)	5	(0.200)	b	510	950
Copper Base Alloy Wires:														
Phosphor Bronze (A)	103	(15)	43.4	(6.3)	8.86	(0.320)	15	0.10	(0.004)	12.5	(0.500)	b	95	200
Silicon Bronze (A)	103	(15)	38.6	(5.6)	8.53	(0.308)	7	0.10	(0.004)	12.5	(0.500)	b	95	200
Silicon Bronze (B)	117	(17)	44.1	(6.4)	8.75	(0.316)	12	0.10	(0.004)	12.5	(0.500)	b	95	200
Beryllium Copper	128	(18.5)	48.3	(7.0)	8.26	(0.298)	21	0.08	(0.003)	12.5	(0.500)	b	205	400
Spring Brass, CA260	110	(16)	42.0	(6.0)	8.53	(0.308)	17	0.10	(0.004)	12.5	(0.500)	b	95	200
Nickel Base Alloys:														
Inconel® Alloy 600	214	(31)	75.8	(11)	8.43	(0.304)	1.5	0.10	(0.004)	12.5	(0.500)	b	320	700
Inconel Alloy X750	214	(31)	79.3	(11.5)	8.25	(0.298)	1	0.10	(0.004)	12.5	(0.500)	b	595	1100
Ni-Span-C®	186	(27)	62.9	(9.7)	8.14	(0.294)	1.6	0.10	(0.004)	12.5	(0.500)	b	95	200
Monel® Alloy 400	179	(26)	66.2	(9.6)	8.83	(0.319)	3.5	0.05	(0.002)	9.5	(0.375)	b	230	450
Monel Alloy K500	179	(26)	66.2	(9.6)	8.46	(0.306)	3	0.05	(0.002)	9.5	(0.375)	b	260	500

Carbon Steel Strip:												
AISI 1050	207	(30)	79.3	(11.5)	7.86	(0.284)	7	0.25 (0.010)	3	(0.125)	b	95	200
1065	207	(30)	79.3	(11.5)	7.86	(0.284)	7	0.08 (0.003)	3	(0.125)	b	95	200
1074, 1075	207	(30)	79.3	(11.5)	7.86	(0.284)	7	0.08 (0.003)	3	(0.125)	b	120	250
1095	207	(30)	79.3	(11.5)	7.86	(0.284)	7	0.08 (0.003)	3	(0.125)	b	120	250
Stainless Steel Strip:												
Austenitic Types 301, 302	193	(28)	69.0	(10)	7.92	(0.286)	2	0.08 (0.003)	1.5	(0.063)	b	315	600
Precipitation Hardening 17-7 PH	203	(29.5)	75.8	(11)	7.81	(0.282)	2	0.08 (0.003)	3	(0.125)	b	370	700
Copper Base Alloy Strip:												
Phosphor Bronze (A)	103	(15)	43	(6.3)	8.86	(0.320)	15	0.08 (0.003)	5	(0.188)	b	95	200
Beryllium Copper	128	(18.5)	48	(7.0)	8.26	(0.298)	21	0.08 (0.003)	9.5	(0.375)	b	205	400

(1) Elastic moduli, density and electrical conductivity can vary with cold work, heat treatment and operating stress. These variations are usually minor but should be considered if one or more of these properties is critical.
(2) Sizes normally available are diameters for wire; thicknesses for strip.
(3) Typical surface quality ratings. (For most materials, special processes can be specified to upgrade typical values.)
a. Maximum defect depth: 0 to 0.5% of d or t.
b. Maximum defect depth: 1.0% of d or t.
c. Defect depth: less than 3.5% of d or t.
(4) Maximum service temperatures are guidelines and may vary due to operating stress and allowable relaxation.
(5) Music and hard drawn are commercial terms for patented and cold-drawn carbon steel spring wire.

SOURCE: Associated Spring, Barnes Group Inc.

INCONEL, MONEL and NI-SPAN-C are registered trademarks of International Nickel Company, Inc.

TABLE 6.2 Typical Heat Treatments for Springs after Forming

Materials	Heat Treatment °C	°F
Patented and Cold-Drawn Steel Wire	190–230	375–450
Tempered Steel Wire:		
Carbon	260–400	500–750
Alloy	315–425	600–800
Austenitic Stainless Steel Wire	230–510	450–950
Precipitation Hardening Stainless Wire (17–7 PH):		
Condition C	480/1 hour	900/1 hour
Condition A to TH 1050	760/1 hour cool to 15°C followed by 565/1 hour	1400/1 hour, cool to 60°F followed by 1050/1 hour
Monel:		
Alloy 400	300–315	575–600
Alloy K500, Spring Temper	525/4 hours	980/4 hours
Inconel:		
Alloy 600	400–510	750–950
Alloy X-750:		
#1 Temper	730/16 hours	1350/16 hours
Spring Temper	650/4 hours	1200/4 hours
Copper Base, Cold Worked (Brass, Phosphor Bronze, etc.)	175–205	350–400
Beryllium Copper:		
Pretempered (Mill Hardened)	205	400
Solution Annealed, Temper Rolled or Drawn	315/2-3 hours	600/2–3 hours
Annealed Steels:		
Carbon (AISI 1050 to 1095)	800–830*	1475–1525*
Alloy (AISI 5160H 6150, 9254)	830–885*	1525–1625*

*Time depends on heating equipment and section size. Parts are austenitized then quenched and tempered to the desired hardness.

SOURCE: Associated Spring, Barnes Group Inc.

down the rate of corrosion attack on the base metal. The latter approach is most often the most cost-effective method.

Spring Wire. The tensile strength of spring wire varies inversely with the wire diameter (Fig. 6.1).

Common spring wires with the highest strengths are ASTM A228 (music wire) and ASTM A401 (oil-tempered chrome silicon). Wires having slightly lower tensile strength and with surface quality suitable for fatigue applications are ASTM A313 type 302 (stainless steel), ASTM A230 (oil-tempered carbon valve-spring-quality steel), and ASTM A232 (oil-tempered chrome vanadium). For most static applica-

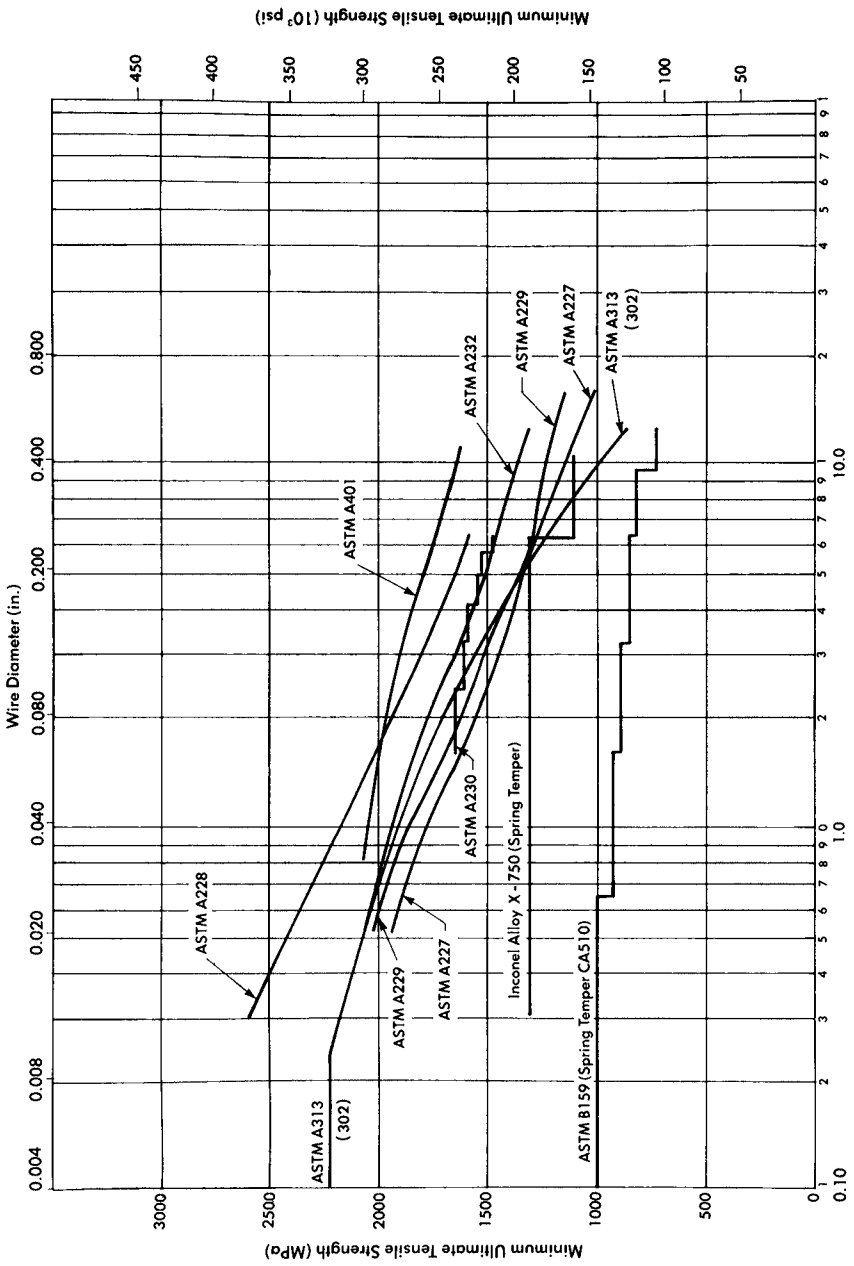

FIGURE 6.1 Minimum tensile strengths of spring wire. *(Associated Spring, Barnes Group Inc.)*

tions ASTM A227 (hard-drawn carbon steel) and ASTM A229 (oil-tempered carbon steel) are available at lower strength levels. Table 6.3 ranks the relative costs of common spring materials based on hard-drawn carbon steel as 1.0.

Spring Strip. Most "flat" springs are made from AISI grades 1050, 1065, 1074, and 1095 steel strip. Strength and formability characteristics are shown in Fig. 6.2, covering the range of carbon content from 1050 to 1095. Since all carbon levels can be obtained at all strength levels, the curves are not identified by composition. Figure 6.3 shows the tensile strength versus Rockwell hardness for tempered carbon-steel strip. Edge configurations for steel strip are shown in Fig. 6.4.

Formability of annealed spring steels is shown in Table 6.4, and typical properties of various spring-tempered alloy strip materials are shown in Table 6.5.

6.4 HELICAL COMPRESSION SPRINGS

6.4.1 General

A helical compression spring is an open-pitch spring which is used to resist applied compression forces or to store energy. It can be made in a variety of configurations and from different shapes of wire, depending on the application. Round, high-carbon-steel wire is the most common spring material, but other shapes and compositions may be required by space and environmental conditions.

Usually the spring has a uniform coil diameter for its entire length. Conical, barrel, and hourglass shapes are a few of the special shapes used to meet particular load-deflection requirements.

TABLE 6.3 Ranking of Relative Costs of Common Spring Wires

Wire	Specification	Relative Cost of 2 mm (0.079") Dia.	
		Mill Quantities	Ware-House Lots
Patented and Cold Drawn	ASTM A227	1.0	1.0
Oil Tempered	ASTM A229	1.3	1.3
Music	ASTM A228	2.6	1.4
Carbon Valve Spring	ASTM A230	3.1	1.9
Chrome Silicon Valve	ASTM A401	4.0	3.9
Stainless Steel (Type 302)	ASTM A313 (302)	7.6	4.7
Phosphor Bronze	ASTM	8.0	6.7
Stainless Steel (Type 631) (17–7 PH)	ASTM A 313 (631)	11	8.7
Beryllium Copper	ASTM B197	27	17
Inconel Alloy X–750		44	31

SOURCE: Associated Spring, Barnes Group Inc.

Helical compression springs are stressed in the torsional mode. The stresses, in the elastic range, are not uniform about the wire's cross section. The stress is greatest at the surface of the wire and, in particular, at the inside diameter (ID) of the spring.

In some circumstances, residual bending stresses are present as well. In such cases, the bending stresses become negligible after set is removed (or the elastic limit is exceeded) and the stresses are redistributed more uniformly about the cross section.

6.4.2 Compression Spring Terminology

The definitions that follow are for terms which have evolved and are commonly used in the spring industry. Figure 6.5 shows the relationships among the characteristics.

Wire Diameter d. Round wire is the most economical form. Rectangular wire is used in situations where space is limited, usually to reduce solid height.

Coil Diameter. The outside diameter (OD) is specified when a spring operates in a cavity. The inside diameter is specified when the spring is to operate over a rod. The mean diameter D is either OD minus the wire size or ID plus the wire size.

The coil diameter increases when a spring is compressed. The increase, though small, must be considered whenever clearances could be a problem. The diameter increase is a function of the spring pitch and follows the equation

$$\text{OD}_{\text{at solid}} = \sqrt{D^2 + \frac{p^2 - d^2}{\pi^2}} + d \tag{6.1}$$

where p = pitch and d = wire size.

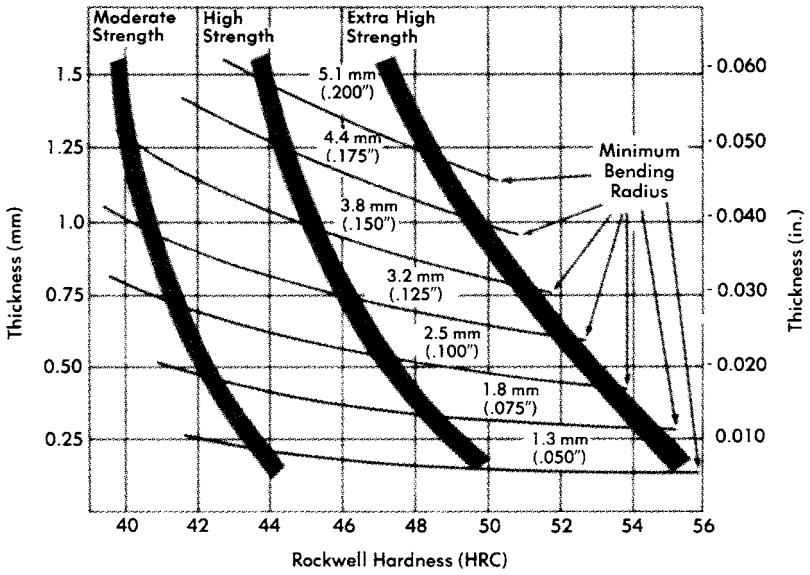

FIGURE 6.2 Minimum transverse bending radii for various tempers and thicknesses of tempered spring steel. *(Associated Spring, Barnes Group Inc.)*

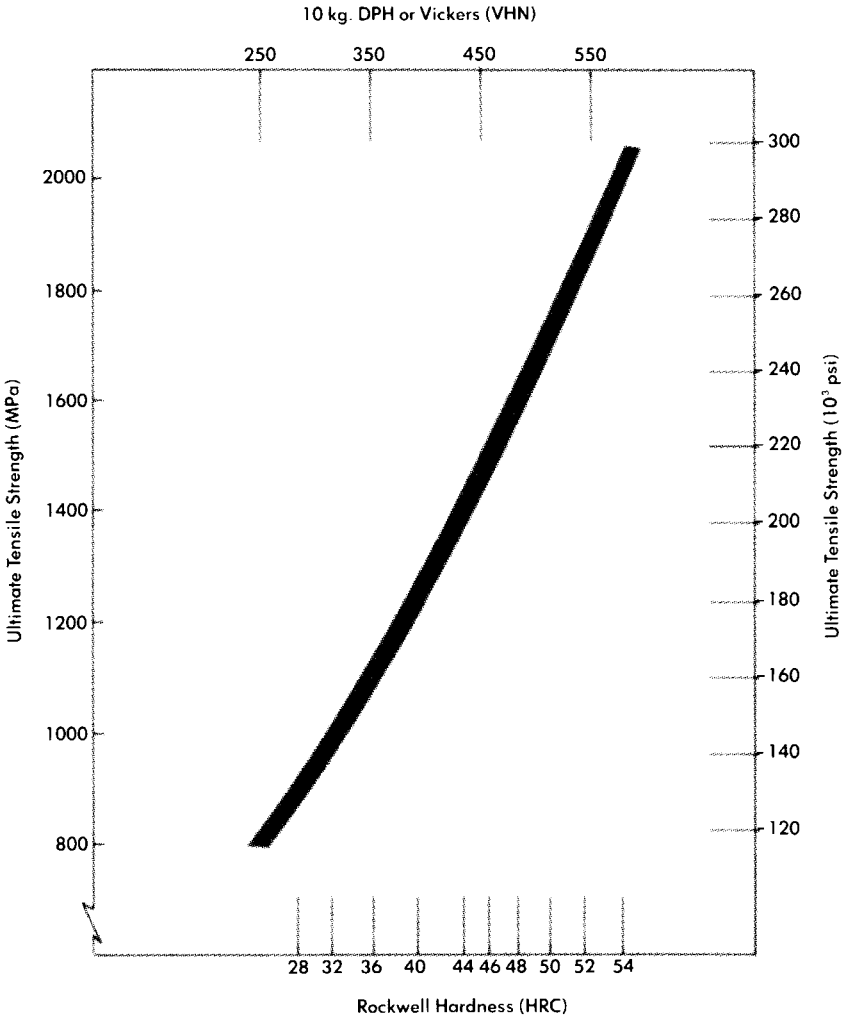

FIGURE 6.3 Tensile strength versus hardness of quenched and tempered spring steel. *(Associated Spring, Barnes Group Inc.)*

Spring Index. Spring index C is the ratio of the mean diameter to the wire diameter (or to the radial dimension if the wire is rectangular). The preferred range of index is 5 to 9, but ranges as low as 3 and as high as 15 are commercially feasible. The very low indices are hard to produce and require special setup techniques. High indices are difficult to control and can lead to spring tangling.

Free Length. Free length L_f is the overall length measured parallel to the axis when the spring is in a free, or unloaded, state. If loads are not given, the free length should be specified. If they are given, then free length should be a reference dimension which can be varied to meet the load requirements.

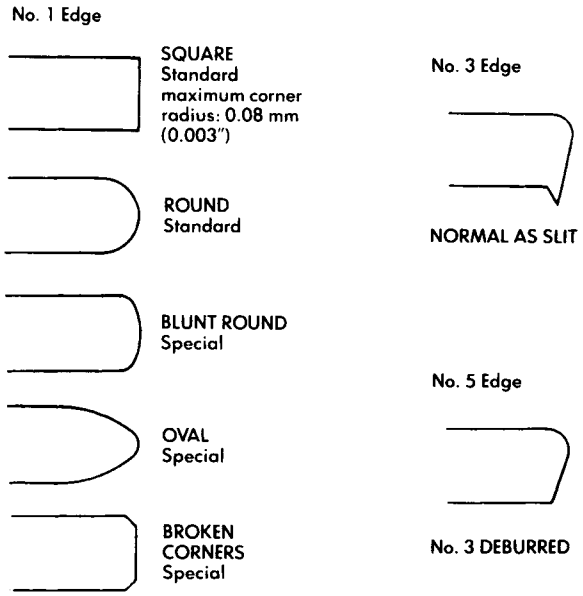

FIGURE 6.4 Edges available on steel strip. *(Associated Spring, Barnes Group Inc.)*

Types of Ends. Four basic types of ends are used: closed (squared) ends, closed (squared) ends ground, plain ends, and plain ends ground. Figure 6.6 illustrates the various end conditions. Closed and ground springs are normally supplied with a ground bearing surface of 270 to 330°.

Number of Coils. The number of coils is defined by either the total number of coils N_t or the number of active coils N_a. The difference between N_t and N_a equals the number of inactive coils, which are those end coils that do not deflect during service.

Solid Height. The solid height L_s is the length of the spring when it is loaded with enough force to close all the coils. For ground springs, $L_s = N_t d$. For unground springs, $L_s = (N_t + 1)d$.

Direction of the Helix. Springs can be made with the helix direction either right or left hand. Figure 6.7 illustrates how to define the direction. Springs that are nested one inside the other should have opposite helix directions. If a spring is to be assembled onto a screw thread, the direction of the helix must be opposite to that of the thread.

Spring Rate. Spring rate k is the change in load per unit deflection. It is expressed as

$$k = \frac{P}{f} = \frac{Gd^4}{8D^3N_a} \tag{6.2}$$

where G = shear modulus.

TABLE 6.4 Formability of Annealed Spring Steels

Thickness (t) mm (in.)	Direction of Bend	AISI 1050 N_t/t		AISI 1065 N_t/t		AISI 1074 N_t/t	AISI 1095 N_t/t
		Annealed (standard lowest max.)	WBS* Barco-Form®	Annealed (standard lowest max.)	WBS Barco-Form	Annealed (standard lowest max.)	Annealed (standard lowest max.)
1.9 mm (0.076)-over	⊥	2	0	2	0	2	3
	∥	4	3	4	3	4	5
0.9–1.89 mm (0.036–0.075″)	⊥	1	0	1	0	1	2
	∥	2	1	2	1	2	3
0.37–0.89 mm (0.015–0.035″)	⊥	0	0	0	0	1	1
	∥	1	0	1 1/2	1	1 1/2	2
0.2–0.36 mm (0.008–0.014″)	⊥	0	0	0	0	1	1
	∥	0	0	0	0	1	1

Formability is determined by slowly bending a sample over 180° until its ends are parallel. The measured distance between the ends is N_t.
For example, if $N_t = 4$ and $t = 2$, then $N_t/t = 2$
*Wallace Barnes Steel.

SOURCE: Associated Spring, Barnes Group Inc.

TABLE 6.5 Typical Properties of Spring-Tempered Alloy Strip

Material	Tensile Strength MPa (10^3 psi)	Rockwell Hardness	Elongation(1) Percent	Bend Factor (1) (2r/t trans. bends)	Modulus of Elasticity 10^4 MPa (10^6 psi)	Poisson's Ratio
Steel, spring temper	1700 (246)	C50	2	5	20.7 (30)	0.30
Stainless 301	1300 (189)	C40	8	3	19.3 (28)	0.31
Stainless 302	1300 (189)	C40	5	4	19.3 (28)	0.31
Monel 400	690 (100)	B95	2	5	17.9 (26)	0.32
Monel K500	1200 (174)	C34	40	5	17.9 (26)	0.29
Inconel 600	1040 (151)	C30	2	2	21.4 (31)	0.29
Inconel X-750	1050 (152)	C35	20	3	21.4 (31)	0.29
Copper-Beryllium	1300 (189)	C40	2	5	12.8 (18.5)	0.33
Ni- Span-C	1400 (203)	C42	6	2	18.6 (27)	—
Brass CA 260	620 (90)	B90	3	3	11 (16)	0.33
Phosphor Bronze	690 (100)	B90	3	2.5	10.3 (15)	0.20
17–7 PH RH950	1450 (210)	C44	6	flat	20.3 (29.5)	0.34
17–7 PH Condition C	1650 (239)	C46	1	2.5	20.3 (29.5)	0.34

(1) Before heat treatment.

SOURCE: Associated Spring, Barnes Group Inc.

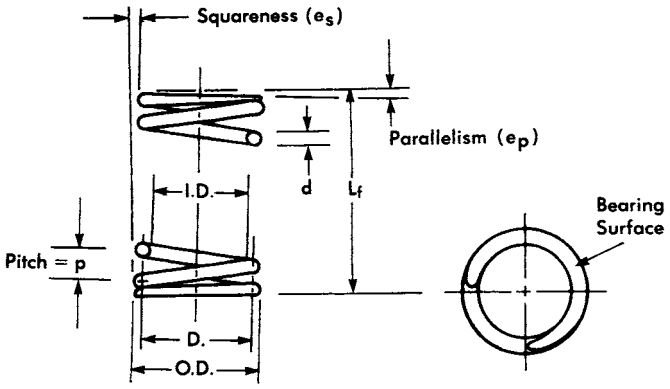

FIGURE 6.5 Dimensional terminology for helical compression springs. *(Associated Spring, Barnes Group Inc.)*

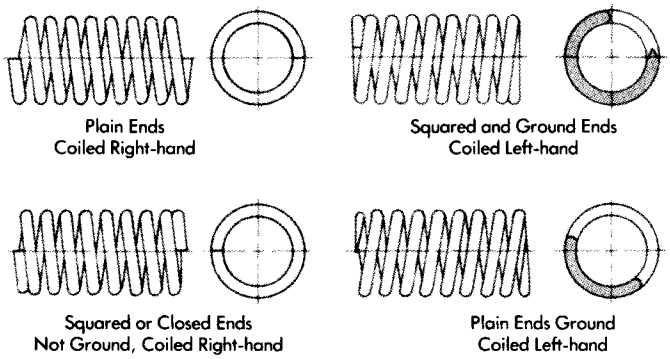

FIGURE 6.6 Types of ends for helical compression springs. *(Associated Spring, Barnes Group Inc.)*

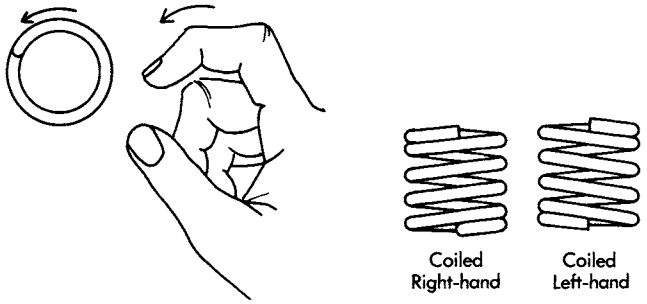

FIGURE 6.7 Direction of coiling of helical compression springs. *(Associated Spring, Barnes Group Inc.)*

The rate equation is accurate for a deflection range between 15 and 85 percent of the maximum available deflection. When compression springs are loaded in parallel, the combined rate of all the springs is the sum of the individual rates. When the springs are loaded in series, the combined rate is

$$k = \frac{1}{1/k_1 + 1/k_2 + 1/k_3 + \cdots + 1/k_n} \tag{6.3}$$

This relationship can be used to design a spring with variable diameters. The design method is to divide the spring into many small increments and calculate the rate for each increment. The rate for the whole spring is calculated as in Eq. (6.3).

Stress. Torsional stress S is expressed as

$$S = \frac{8K_w PD}{\pi d^3} \tag{6.4}$$

Under elastic conditions, torsional stress is not uniform around the wire's cross section because of the coil curvature and direct shear loading.

The highest stress occurs at the surface in the inside diameter of the spring, and it is computed by using the stress factor K_w. In most cases, the correction factor is expressed as

$$K_{w_1} = \frac{4C - 1}{4C - 4} + \frac{0.615}{C} \tag{6.5}$$

The stress-concentration factor K_{w_1} becomes K_{w_2} after a spring has been set out because stresses become more uniformly distributed after subjecting the cross section to plastic flow during set-out:

$$K_{w_2} = 1 + \frac{0.5}{C} \tag{6.6}$$

The appropriate stress correction factor is discussed in Sec. 6.4.3.

Loads. If deflection is known, the load is found by multiplying deflection by the spring rate. When the stress is either known or assumed, loads can be obtained from the stress equation.

Loads should be specified at a test height so that the spring manufacturer can control variations by adjustments of the free length. The load-deflection curve is not usually linear at the start of deflection from free position or when the load is very close to solid height. It is advisable to specify loads at test heights between 15 and 85 percent of the load-deflection range.

Loads can be conveniently classified as static, cyclic, and dynamic. In static loading, the spring will operate between specified loads only a few times. In other instances, the spring may remain under load for a long time. In cyclic applications, the spring may typically be required to cycle between load points from 10^4 to more than 10^9 times. During dynamic loading, the rate of load application is high and causes a surge wave in the spring which usually induces stresses higher than calculated from the standard stress equation.

Buckling. Compression springs with a free length more than 4 times the mean coil diameter may buckle when compressed. Guiding the spring, either in a tube or over

a rod, can minimize the buckling but can result in additional friction which will affect loads, especially when the L_f/D ratio is high.

Buckling conditions are shown in Figs. 6.8 and 6.9 for springs loaded axially and with squared and ground ends. Buckling occurs at points above and to the right of the curves. Curve *A* is for the springs with one end on a fixed, flat surface and the other end free to tip. Curve *B* is for springs with both ends on fixed, flat surfaces. The tendency to buckle is clearly less for curve *B* springs.

6.4.3 Choice of Operating Stress

The choice of operating stress depends on whether the application is static or cyclic. For static applications, yield strength or stress-relaxation resistance of the material limits the load-carrying ability of the springs. The required cycles are few, if any, and the velocity of the end coils is so low as to preclude surging or impact conditions.

The maximum allowable torsional stresses for static applications are shown in Table 6.6 as percentages of tensile strengths for common spring materials. To calculate the stress before set removal, use the K_{w_1} correction factor. If the calculated stress is greater than the indicated percentage of the tensile strength, then the spring will take a permanent set when deflected to solid. The amount of set is a function of the amount by which the calculated stress exceeds the tabular percentage.

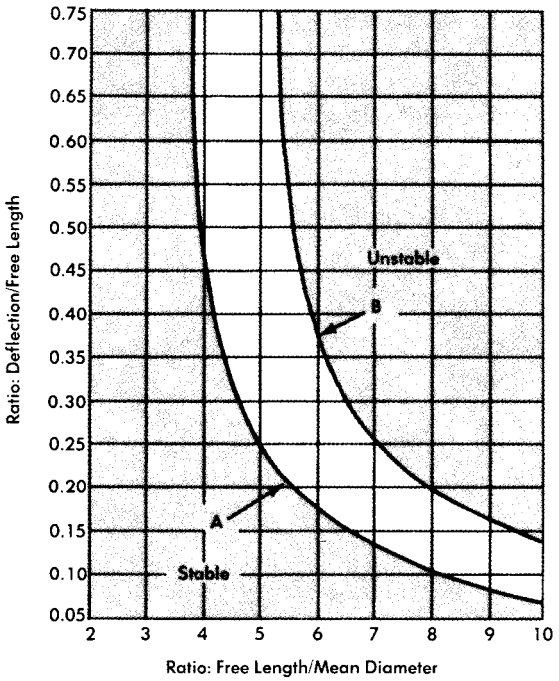

FIGURE 6.8 Critical buckling curves. *(Associated Spring, Barnes Group Inc.)*

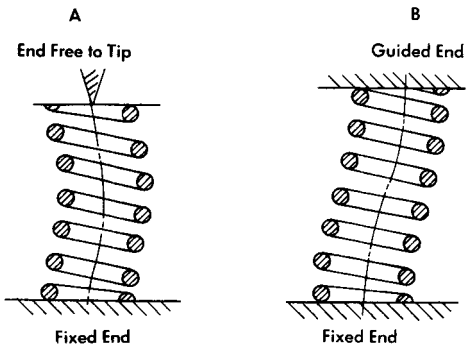

FIGURE 6.9 End conditions used to determine critical buckling. *(Associated Spring, Barnes Group Inc.)*

It is common practice, in static applications, to increase the load-carrying capability of a spring by making it longer than the desired free length and then compressing it to solid. The spring *sets* to its final desired length. This procedure is called *removing set.* It induces favorable residual stresses which allow for significantly higher stresses than in springs not having the set removed. The loss of the length should be at least 10 percent to be effective (see Fig. 6.10).

Note that set removal causes stresses to be more uniformly distributed about the cross section. Therefore, stress after set removal is calculated by using the K_{w_2} correction factor. If the stress calculated by using the K_{w_2} correction factor exceeds the percentage of tensile strength shown in Table 6.6, the spring cannot be made. It is then necessary either to lower the design stress or to select a higher-strength material.

For cyclic applications, the load-carrying ability of the spring is limited by the fatigue strength of the material. To select the optimum stress level, spring costs must be balanced against reliability. The designer should know the operating environ-

TABLE 6.6 Maximum Allowable Torsional Stresses for Helical Compression Springs in Static Applications

Materials	Maximum % of Tensile Strength	
	Before Set Removed (K_{W1})	After Set Removed (K_{W2})
Patented and cold drawn carbon steel	45%	65–75%
Hardened and tempered carbon and low alloy steel	50%	
Austenitic stainless steels	35%	
Nonferrous alloys	35%	

SOURCE: Associated Spring, Barnes Group Inc.

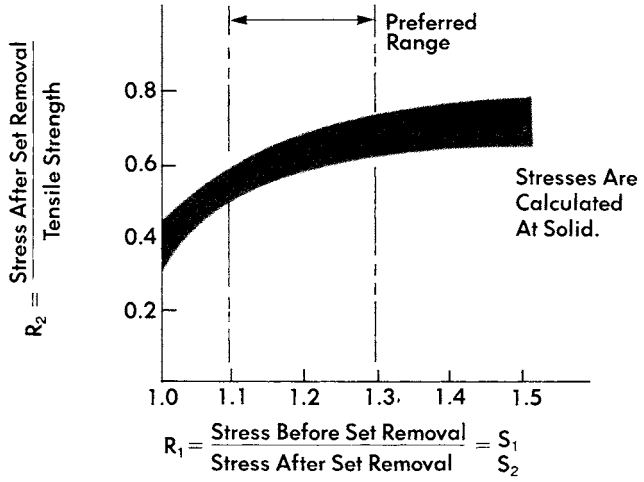

FIGURE 6.10 Spring load-carrying ability versus amount of set removed. *(Associated Spring, Barnes Group Inc.)*

ment, desired life, stress range, frequency of operation, speed of operation, and permissible levels of stress relaxation in order to make a cost-reliability decision.

Fatigue life can be severely reduced by pits, seams, or tool marks on the wire surface where stress is at a maximum. Shot peening improves fatigue life, in part, by minimizing the harmful effects of surface defects. It does not remove them. Additionally, shot peening imparts favorable compression stresses to the surface of the spring wire.

Maximum allowable stresses for fatigue applications should be calculated by using the K_{w_1} stress correction factor. Table 6.7 shows the estimated fatigue life for common spring materials. Note the significant increase in fatigue strength from shot peening.

TABLE 6.7 Maximum Allowable Torsional Stress for Round-Wire Helical Compression Springs in Cyclic Applications

Fatigue Life (cycles)	Percent of Tensile Strength			
	ASTM A228, Austenitic Stainless Steel and Nonferrous		ASTM A230 and A232	
	Not Shot-Peened	Shot-Peened	Not Shot-Peened	Shot-Peened
10^5	36	42	42	49
10^6	33	39	40	47
10^7	30	36	38	46

This information is based on the following conditions: no surging, room temperature and noncorrosive environment.

Stress ratio in fatigue $= \frac{S \text{ minimum}}{S \text{ maximum}} = 0$

SOURCE: Associated Spring, Barnes Group Inc.

The fatigue life estimates in Table 6.7 are guideline values which should be used only where specific data are unavailable. The values are conservative, and most springs designed using them will exceed the anticipated lives.

6.4.4 Dynamic Loading under Impact

When a spring is loaded or unloaded, a surge wave is established which transmits torsional stress from the point of load along the spring's length to the point of restraint. The surge wave will travel at a velocity approximately one-tenth that of a normal, torsional-stress wave. The velocity of the torsional-stress wave V_T, in meters per second (m/s) [inches per second (in/s)], is given by

$$V_T = 10.1\sqrt{\frac{Gg}{\rho}} \quad \text{m/s} \qquad \text{or} \qquad V_T = \sqrt{\frac{Gg}{\rho}} \quad \text{in/s} \tag{6.7}$$

The velocity of the surge wave V_s varies with material and design but is usually in the range of 50 to 500 m/s. The surge wave limits the rate at which a spring can absorb or release energy by limiting the impact velocity *V. Impact velocity* is defined as the spring velocity parallel to the spring axis and is a function of stress and material as shown:

$$V \simeq 10.1S\sqrt{\frac{g}{2\rho G}} \quad \text{m/s} \qquad \text{or} \qquad V \simeq S\sqrt{\frac{g}{2\rho G}} \quad \text{in/s} \tag{6.8}$$

For steel, this reduces to

$$V = \frac{S}{35.5} \quad \text{m/s} \qquad \text{or} \qquad V = \frac{S}{131} \quad \text{in/s} \tag{6.9}$$

If a spring is compressed to a given stress level and released instantaneously, the maximum spring velocity is the stress divided by 35.5. Similarly, if the spring is loaded at known velocity, the instantaneous stress can be calculated. At very high load velocities, the instantaneous stress will exceed the stress calculated by the conventional equation. This will limit design performance. Since the surge wave travels the length of the spring, springs loaded at high velocity often are subject to resonance.

6.4.5 Dynamic Loading—Resonance

A spring experiences resonance when the frequency of cyclic loading is near the natural frequency or a multiple of it. Resonance can cause an individual coil to deflect to stress levels above those predicted by static stress analysis. Resonance can also cause the spring to bounce, resulting in loads lower than calculated. To avoid these effects, the natural frequency should be a minimum of 13 times the operating frequency.

For a compression spring with both ends fixed and no damper, the natural frequency in International System (SI) units is

$$n = \frac{1.12(10^3)d}{D^2 N_a}\sqrt{\frac{Gg}{\rho}} \tag{6.10}$$

For steel, this equation becomes

$$n = \frac{3.5(10^5)d}{D^2 N_a} \tag{6.11}$$

where n = frequency in hertz (Hz). The corresponding equation in U.S. Customary System (USCS) units is

$$n = \frac{d}{9D^2 N_a}\sqrt{\frac{Gg}{\rho}} \tag{6.12}$$

and for steel we have

$$n = \frac{14(10^3)d}{D^2 N_a} \tag{6.13}$$

If the spring cannot be designed to have a natural frequency more than 13 times the operating frequency, energy dampers may be employed. They are generally friction devices which rub against the coils. Often, variable-pitch springs are used to minimize resonance effects.

6.4.6 Rectangular-Wire Springs

In applications where high loads and relatively low stresses are required but solid height is also restricted, rectangular wire can be used to increase the material volume while maintaining the maximum solid-height limitation.

Springs made of rectangular wire with the long side of the wire cross section perpendicular to the axis of the coils can store more energy in a smaller space than an equivalent, round-wire spring.

When rectangular wire is coiled, it changes from a rectangular to a keystone shape, as shown in Fig. 6.11. Similarly, if the wire is made to the keystone shape, it will become rectangular after coiling. The cross-sectional distortion can be approximated by

$$t_1 = t\frac{C + 0.5}{C} \tag{6.14}$$

where t_1 = wider end of keystone section and t = original, smaller dimension of rectangle.

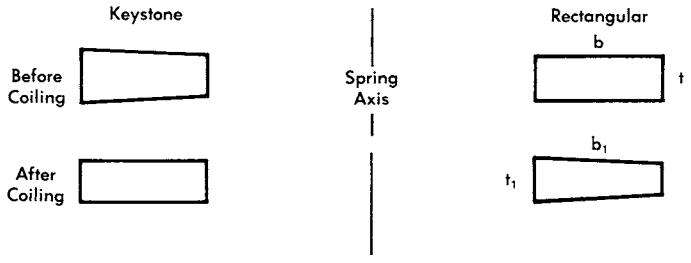

FIGURE 6.11 Wire cross section before and after coiling. *(Associated Spring, Barnes Group Inc.)*

The spring rate for a rectangular-wire spring is

$$k = \frac{P}{f} = \frac{K_2 G b t^3}{N_a D^3} \tag{6.15}$$

Since the wire is loaded in torsion, it makes no difference whether the wire is wound on the flat or on edge. See Fig. 6.12.

Stress is calculated by

$$S = \frac{K_E P D}{K_1 b t^2} \quad \text{or} \quad S = \frac{K_F P D}{K_1 b t^2} \tag{6.16}$$

Values for K_1 and K_2 are found in Fig. 6.13, and those for K_E and K_F are found in Figs. 6.15 and 6.14, respectively.

When a round wire cannot be used because the solid height exceeds the specification, the approximate equivalent rectangular dimensions are found from

$$t = \frac{2d}{1 + b/t} \tag{6.17}$$

where d = round-wire diameter.

6.4.7 Variable-Diameter Springs

Conical, hourglass, and barrel-shaped springs, shown in Fig. 6.16, are used in applications requiring a low solid height and an increased lateral stability or resistance to surging. Conical springs can be designed so that each coil nests wholly or partly within an adjacent coil. Solid height can be as low as one wire diameter. The rate for conical springs usually increases with deflection (see Fig. 6.17) because the number of active coils decreases progressively as the spring approaches solid. By varying the pitch, conical springs can be designed to have a uniform rate. The rate for conical springs is calculated by considering the spring as many springs in series. The rate for

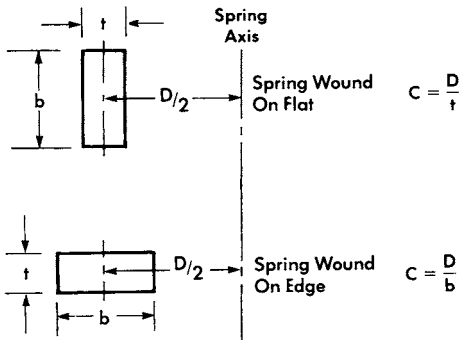

FIGURE 6.12 Rectangular-wire compression spring wound on flat or edge. *(Associated Spring, Barnes Group Inc.)*

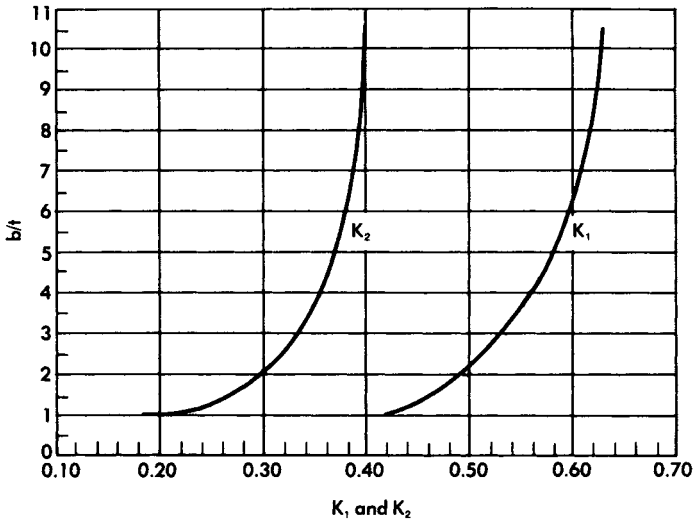

FIGURE 6.13 Constants for rectangular wire in torsion. *(Associated Spring, Barnes Group Inc.)*

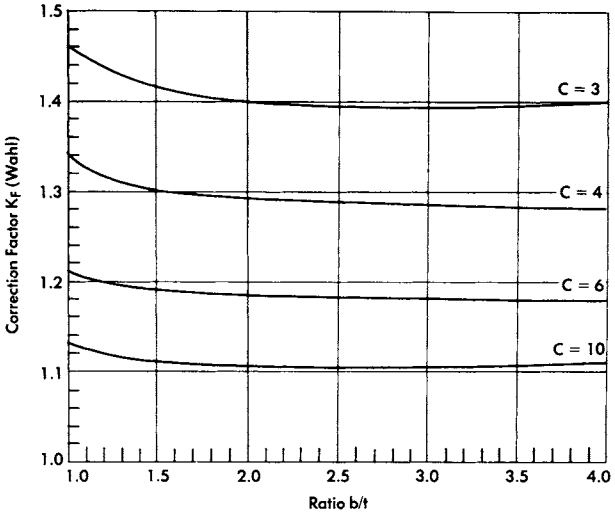

FIGURE 6.14 Stress correction factors for rectangular-wire compression springs wound on flat. *(Associated Spring, Barnes Group Inc.)*

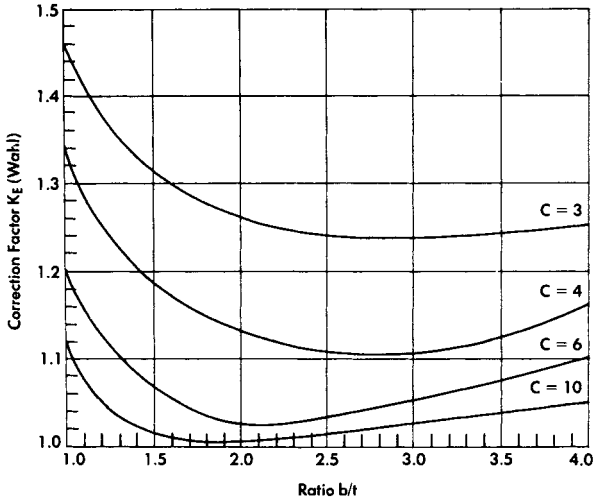

FIGURE 6.15 Stress correction factors for rectangular-wire compression springs wound on edge. *(Associated Spring, Barnes Group Inc.)*

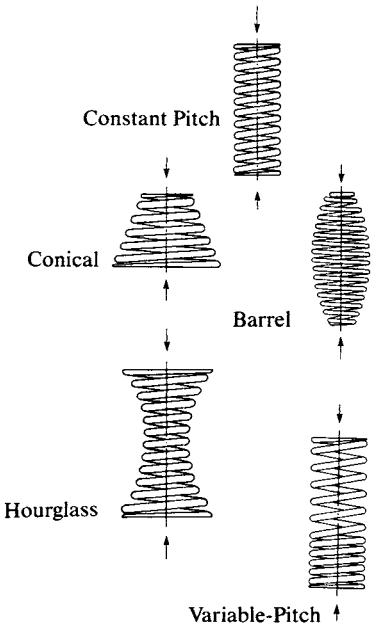

FIGURE 6.16 Various compression-spring body shapes. *(Associated Spring, Barnes Group Inc.)*

each turn or fraction of a turn is calculated by using the standard rate equation. The rate for a complete spring is then determined, given that the spring rate follows the series relationship in Eq. (6.3).

To calculate the highest stress at a given load, the mean diameter of the largest active coil at load is used. The solid height of a uniformly tapered, but not telescoping, spring with squared and ground ends made from round wire can be estimated from

$$L_S = N_a \sqrt{d^2 - u^2} + 2d \qquad (6.18)$$

where u = OD of large end minus OD of small end, divided by $2N_a$.

Barrel- and hourglass-shaped springs are calculated as two conical springs in series.

6.4.8 Commercial Tolerances

Standard commercial tolerances are presented in Tables 6.8, 6.9, and 6.10 for free length, coil diameter, and load tolerances, respectively. These tolerances represent the best tradeoffs between manufacturing costs and performance.

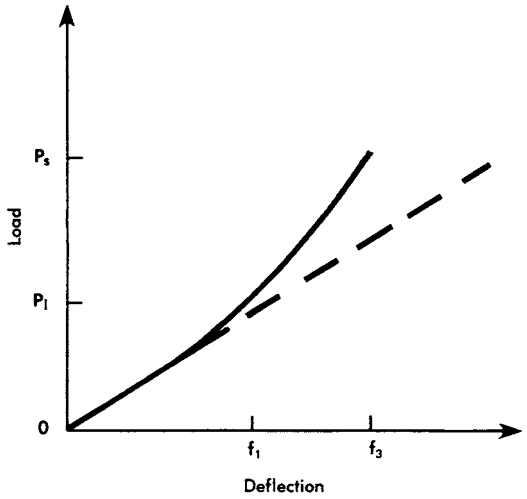

FIGURE 6.17 Typical load-deflection curve for variable-diameter springs (solid line). *(Associated Spring, Barnes Group Inc.)*

TABLE 6.8 Free-Length Tolerances of Squared and Ground Helical Compression Springs

Number of Active coils per mm(in.)	Tolerances: ±mm/mm (in./in.) of Free Length						
	Spring Index (D/d)						
	4	6	8	10	12	14	16
0.02 (0.5)	0.010	0.011	0.012	0.013	0.015	0.016	0.016
0.04 (1)	0.011	0.013	0.015	0.016	0.017	0.018	0.019
0.08 (2)	0.013	0.015	0.017	0.019	0.020	0.022	0.023
0.2 (4)	0.016	0.018	0.021	0.023	0.024	0.026	0.027
0.3 (8)	0.019	0.022	0.024	0.026	0.028	0.030	0.032
0.5 (12)	0.021	0.024	0.027	0.030	0.032	0.034	0.036
0.6 (16)	0.022	0.026	0.029	0.032	0.034	0.036	0.038
0.8 (20)	0.023	0.027	0.031	0.034	0.036	0.038	0.040

For springs less than 12.7 mm (0.500″) long, use the tolerances for 12.7 mm (0.500″). For closed ends not ground, multiply above values by 1.7.

SOURCE: Associated Spring, Barnes Group Inc.

TABLE 6.9 Coil Diameter Tolerances of Helical Compression and Extension Springs

Wire Dia., mm(in.)	Tolerances: ±mm (in.)						
	Spring Index (D/d)						
	4	6	8	10	12	14	16
0.38 (0.015)	0.05 (0.002)	0.05 (0.002)	0.08 (0.003)	0.10 (0.004)	0.13 (0.005)	0.15 (0.006)	0.18 (0.007)
0.58 (0.023)	0.05 (0.002)	0.08 (0.003)	0.10 (0.004)	0.15 (0.006)	0.18 (0.007)	0.20 (0.008)	0.25 (0.010)
0.89 (0.035)	0.05 (0.002)	0.10 (0.004)	0.15 (0.006)	0.18 (0.007)	0.23 (0.009)	0.28 (0.011)	0.33 (0.013)
1.30 (0.051)	0.08 (0.003)	0.13 (0.005)	0.18 (0.007)	0.25 (0.010)	0.30 (0.012)	0.38 (0.015)	0.43 (0.017)
1.93 (0.076)	0.10 (0.004)	0.18 (0.007)	0.25 (0.010)	0.33 (0.013)	0.41 (0.016)	0.48 (0.019)	0.53 (0.021)
2.90 (0.114)	0.15 (0.006)	0.23 (0.009)	0.33 (0.013)	0.46 (0.018)	0.53 (0.021)	0.64 (0.025)	0.74 (0.029)
4.34 (0.171)	0.20 (0.008)	0.30 (0.012)	0.43 (0.017)	0.58 (0.023)	0.71 (0.028)	0.84 (0.033)	0.97 (0.038)
6.35 (0.250)	0.28 (0.011)	0.38 (0.015)	0.53 (0.021)	0.71 (0.028)	0.90 (0.035)	1.07 (0.042)	1.24 (0.049)
9.53 (0.375)	0.41 (0.016)	0.51 (0.020)	0.66 (0.026)	0.94 (0.037)	1.17 (0.046)	1.37 (0.054)	1.63 (0.064)
12.70 (0.500)	0.53 (0.021)	0.76 (0.030)	1.02 (0.040)	1.57 (0.062)	2.03 (0.080)	2.54 (0.100)	3.18 (0.125)

SOURCE: Associated Spring, Barnes Group Inc.

6.5 HELICAL EXTENSION SPRINGS

6.5.1 General

Helical extension springs store energy and exert a pulling force. They are usually made from round wire and are close-wound with initial tension. They have various types of end hooks or loops by which they are attached to the loads.

Like compression springs, extension springs are stressed in torsion in the body coils. The design procedures for the body coil are similar to those discussed in Sec. 6.4 except for the initial tension and the hook stresses.

Most extension springs are made with the body coils held tightly together by a force called *initial tension.* The measure of initial tension is the load required to overcome the internal force and start coil separation.

Extension springs, unlike compression springs, seldom have set removed. Furthermore, they have no solid stop to prevent overloading. For these reasons, the design stresses are normally held to lower values than those for compression springs.

The pulling force exerted by an extension spring is transmitted to the body coils through hooks or loops. Careful attention must be given to the stresses in the hooks. The hook ends must be free of damaging tool marks so that spring performance will not be limited by hook failure.

TABLE 6.10 Load Tolerances of Helical Compression Springs

Length Tolerance ± mm (in.)	Tolerances: ±% of Load. Start with Tolerance from Table 6-8 Multiplied by L_F.														
	Deflection from Free Length to Load, mm (in.)														
	1.27 (0.050)	**2.54 (0.100)**	**3.81 (0.150)**	**5.08 (0.200)**	**6.35 (0.250)**	**7.62 (0.300)**	**10.2 (0.400)**	**12.7 (0.500)**	**19.1 (0.750)**	**25.4 (1.00)**	**38.1 (1.50)**	**50.8 (2.00)**	**76.2 (3.00)**	**102 (4.00)**	**152 (6.00)**
0.13 (0.005)	12.	7.	6.	5.	—	—	—	—	—	—	—	—	—	—	—
0.25 (0.010)	—	12.	8.5	7.	6.5	5.5	5.	—	—	—	—	—	—	—	—
0.51 (0.020)	—	22.	15.5	12.	10.	8.5	7.	6.	5.	—	—	—	—	—	—
0.76 (0.030)	—	—	22.	17.	14.	12.	9.5	8.	6.	5.	—	—	—	—	—
1.0 (0.040)	—	—	—	22.	18.	15.5	12.	10.	7.5	6.	5.	—	—	—	—
1.3 (0.050)	—	—	—	—	22.	19.	14.5	12.	9.	7.	5.5	—	—	—	—
1.5 (0.060)	—	—	—	—	25.	22.	17.	14.	10.	8.	6.	5.	—	—	—
1.8 (0.070)	—	—	—	—	—	25.	19.5	16.	11.	9.	6.5	5.5	—	—	—
2.0 (0.080)	—	—	—	—	—	—	22.	18.	12.5	10.	7.5	6.	5.	—	—
2.3 (0.090)	—	—	—	—	—	—	25.	20.	14.	11.	8.	6.	5.	—	—
2.5 (0.100)	—	—	—	—	—	—	—	22.	15.5	12.	8.5	7.	5.5	—	—
5.1 (0.200)	—	—	—	—	—	—	—	—	—	22.	15.5	12.	8.5	7.	5.5
7.6 (0.300)	—	—	—	—	—	—	—	—	—	—	22.	17.	12.	9.5	7.
10.2 (0.400)	—	—	—	—	—	—	—	—	—	—	—	21.	15.	12.	8.5
12.7 (0.500)	—	—	—	—	—	—	—	—	—	—	—	25.	18.5	14.5	10.5

First load test at not less than 15% of available deflection.
Final load test at not more than 85% of available deflection.

SOURCE: Associated Spring, Barnes Group Inc.

6.5.2 Initial Tension

Initial tension is illustrated in Fig. 6.18. The point of intersection on the ordinate is initial tension P_I. The amount of initial tension is governed by the spring index, material, method of manufacture, and the post-stress-relief heat treatment temperature. Note that a high stress-relief temperature can reduce the initial tension. This is sometimes used as a means to control initial tension in low-stress, low-index springs. It follows that an extension spring requiring no initial tension can be made either by removing the initial tension with heat treatment or by keeping the coils open during coiling. The levels of initial tension obtainable are shown in Fig. 6.19.

6.5.3 Types of Ends

Extension springs require a means of attachment to the system which is to be loaded. A variety of end configurations have been developed over the years. The configurations most commonly used are shown in Fig. 6.20. Loops or hooks longer than recommended will require special setup and are more expensive. Specifying an angular relationship for the loops may also add to the cost. Allow a random relationship of loops whenever possible.

Stresses in the loops are often higher than those in the body coils. In such cases, the loops are the performance limiters, particularly in cyclic applications. Generous bend radii, elimination of tool marks, and a reduced diameter of end coils are methods used to reduce loop stresses. In a full-twist loop, stress reaches a maximum in bending at point A (Fig. 6.21) and a maximum in torsion at point B. The stresses at these locations are complex, but useful approximations are, for bending,

$$S_A = \frac{16K_1DP}{\pi d^3} + \frac{4P}{\pi d^2} \tag{6.19}$$

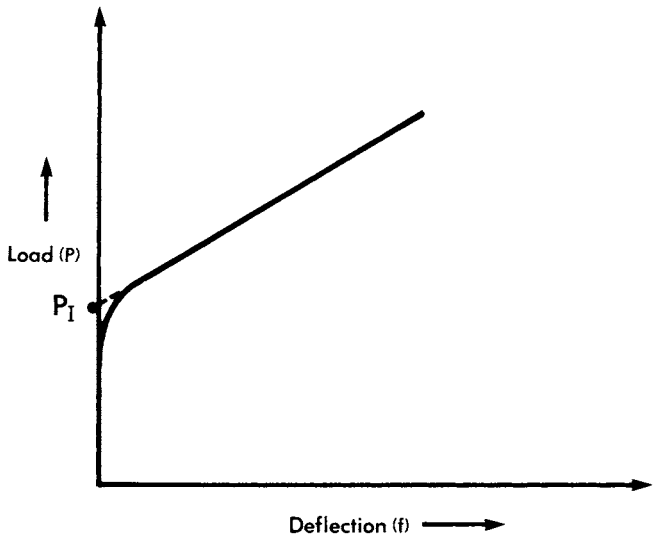

FIGURE 6.18 Load-deflection curve for a helical extension spring with initial tension. *(Associated Spring, Barnes Group Inc.)*

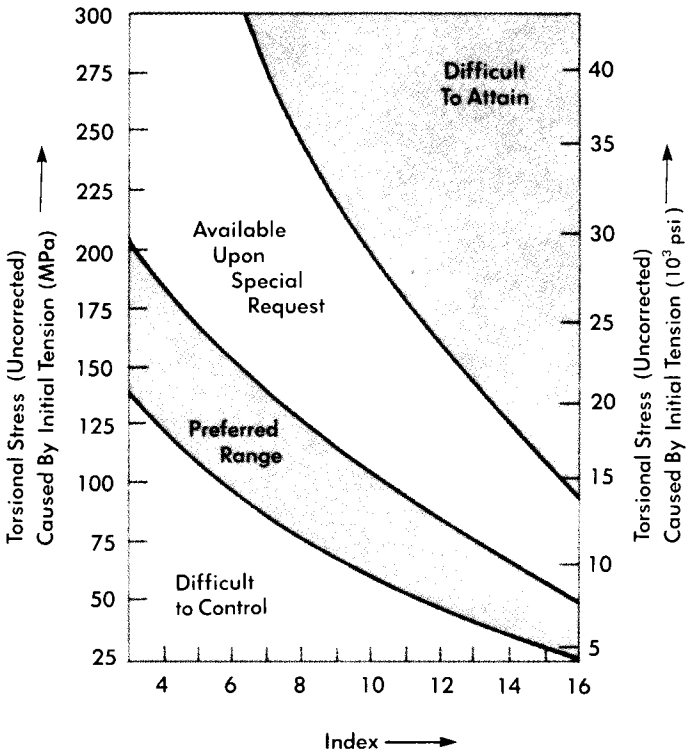

FIGURE 6.19 Torsional stress resulting from initial tension as a function of index in helical extension springs. *(Associated Spring, Barnes Group Inc.)*

where the constants are

$$K_1 = \frac{4C^2 - C_1 - 1}{4C_1(C_1 - 1)} \tag{6.20}$$

and

$$C_1 = \frac{2R_1}{d} \tag{6.21}$$

The torsional stresses are

$$S_B = \frac{8DP}{\pi d^3} \frac{4C_2 - 1}{4C_2 - 4} \tag{6.22}$$

where

$$C_2 = \frac{2R_2}{d} \tag{6.23}$$

General practice is to make C_2 greater than 4.

Type	Configurations	Recommended Length Min.-Max.
Twist Loop or Hook		0.5-1.7 I.D.
Cross Center Loop or Hook	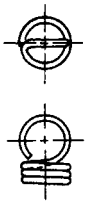	I.D.
Side Loop or Hook	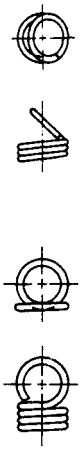	0.9-1.0 I.D.
Extended Hook		1.1 I.D. and up, as required by design
Special Ends	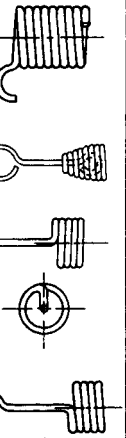	As required by design

FIGURE 6.20 Common end configurations for helical extension springs. Recommended length is distance from last body coil to inside of end. ID is inside diameter of adjacent coil in spring body. *(Associated Spring, Barnes Group Inc.)*

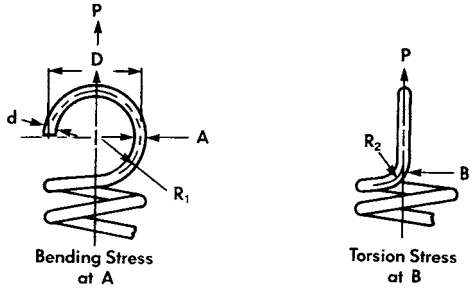

FIGURE 6.21 Location of maximum bending and torsional stresses in twist loops. *(Associated Spring, Barnes Group Inc.)*

6.5.4 Extension Spring Dimensioning

The dimensioning shown in Fig. 6.22 is generally accepted for extension springs. The free length is the distance between the inside surfaces of the loops. The body length is $L_B = d(N + 1)$. The loop opening, or gap, can be varied. The number of active coils is equal to the number of coils in the body of the spring. However, with special ends such as threaded plugs or swivel hooks, the number of active coils will be less than the number of body coils.

6.5.5 Design Equations

The design equations are similar to those for compression springs with the exception of initial tension and loop stresses. The rate is given by

$$k = \frac{P - P_I}{f} = \frac{Gd^4}{8D^3N_a} \tag{6.24}$$

where P_I is initial tension. Stress is given by

$$S = \frac{K_w 8PD}{\pi d^3} \tag{6.25}$$

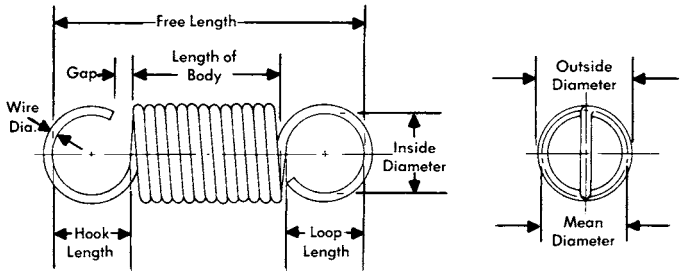

FIGURE 6.22 Typical extension-spring dimensions. *(Associated Spring, Barnes Group Inc.)*

Dynamic considerations discussed previously are generally applicable to extension springs. Natural frequency with one end fixed, in SI units, is

$$n = \frac{560d}{D^2 N_a} \sqrt{\frac{Gg}{\rho}} \tag{6.26}$$

For steel, this equation becomes

$$n = \frac{176\,000d}{N_a D^2} \tag{6.27}$$

where n = frequency in hertz. The corresponding equation in USCS units is

$$n = \frac{d}{18D^2 N_a} \sqrt{\frac{Gg}{\rho}} \tag{6.28}$$

And for steel we have

$$n = \frac{7000d}{N_a D^2} \tag{6.29}$$

6.5.6 Choice of Operating Stress—Static

The maximum stresses recommended for extension springs in static applications are given in Table 6.11. Note that extension springs are similar to compression springs without set removed. For body coil stresses in springs that cannot be adequately stress-relieved because of very high initial-tension requirements, use the maximum recommended stress in torsion, given for the end loops.

6.5.7 Choice of Operating Stress—Cyclic

Table 6.12 presents the maximum stresses for extension springs used in cyclic applications. The data are for stress-relieved springs with initial tension in the preferred range.

TABLE 6.11 Maximum Allowable Stresses (K_{w_1} Corrected) for Helical Extension Springs in Static Applications

Materials	Percent of Tensile Strength		
	In Torsion		In Bending
	Body	End	End
Patented, cold-drawn or hardened and tempered carbon and low alloy steels	45–50	40	75
Austenitic stainless steel and nonferrous alloys	35	30	55

This information is based on the following conditions: set not removed and low temperature heat treatment applied.
For springs that require high initial tension, use the same percent of tensile strength as for end.

SOURCE: Associated Spring, Barnes Group Inc.

TABLE 6.12 Maximum Allowable Stresses for ASTM A228 and Type 302 Stainless-Steel Helical Extension Springs in Cyclic Applications

Number of Cycles	Percent of Tensile Strength		
	In Torsion		In Bending
	Body	End	End
10^5	36	34	51
10^6	33	30	47
10^7	30	28	45

This information is based on the following conditions: not shot-peened, no surging and ambient environment with a low temperature heat treatment applied. Stress ratio = 0.

SOURCE: Associated Spring, Barnes Group Inc.

6.5.8 Tolerances

Extension springs do not buckle or require guide pins when they are deflected, but they may vibrate laterally if loaded or unloaded suddenly. Clearance should be allowed in these cases to eliminate the potential for noise or premature failure. The load tolerances are the same as those given for compression springs. Tolerances for free length and for angular relationship of ends are given in Tables 6.13 and 6.14.

6.6 HELICAL TORSION SPRINGS

Helical springs that exert a torque or store rotational energy are known as *torsion springs*. The most frequently used configuration of a torsion spring is the single-body type (Fig. 6.23). Double-bodied springs, known as double-torsion springs, are sometimes used where dictated by restrictive torque, stress, and space requirements. It is often less costly to make a pair of single-torsion springs than a double-torsion type.

TABLE 6.13 Commercial Free-Length Tolerances for Helical Extension Springs with Initial Tension

Spring Free Length (inside hooks) mm (in.)	Tolerance ± mm (in.)
Up to 12.7 (0.500)	0.51 (0.020)
Over 12.7 to 25.4 (0.500 to 1.00)	0.76 (0.030)
Over 25.4 to 50.8 (1.00 to 2.00)	1.0 (0.040)
Over 50.8 to 102 (2.00 to 4.00)	1.5 (0.060)
Over 102 to 203 (4.00 to 8.00)	2.4 (0.093)
Over 203 to 406 (8.00 to 16.0)	4.0 (0.156)
Over 406 to 610 (16.0 to 24.0)	5.5 (0.218)

SOURCE: Associated Spring, Barnes Group Inc.

TABLE 6.14 Tolerances on Angular Relationship of Extension Spring Ends

Angular Tolerance per Coil: ± Degrees									
Index									
4	5	6	7	8	9	10	12	14	16
0.75	0.9	1.1	1.3	1.5	1.7	1.9	2.3	2.6	3

For example, tolerance for a 10-coil spring with an index of 8 is $10 \times \pm 1.5 = \pm 15°$.
If angular tolerance is greater than ± 45°, or if closer tolerances than indicated must be held, consult with Associated Spring.

SOURCE: Associated Spring, Barnes Group Inc.

Torsion springs are used in spring-loaded hinges, oven doors, clothespins, window shades, ratchets, counterbalances, cameras, door locks, door checks, and many other applications. Torsion springs are almost always mounted on a shaft or arbor with one end fixed. They can be wound either right or left hand.

In most cases the springs are not stress-relieved and are loaded in the direction that winds them up or causes a decrease in body diameter. The residual forming stresses which remain are favorable in that direction. Although it is possible to load a torsion spring in the direction to unwind and enlarge the body coils, ordinarily it is not good design practice and should be avoided. Residual stresses in the unwind direction are unfavorable. Torsion springs which are plated or painted and subsequently baked or are stress-relieved will have essentially no residual stresses and can be loaded in either direction, but at lower stress levels than springs which are not heat-treated.

Correlation of test results between manufacturer and user may be difficult because there are few, if any, standardized torsion-spring testing machines. The springs will have varying degrees of intercoil friction and friction between the mounting arbor and the body coils. Often, duplicate test fixtures must be made and test methods coordinated.

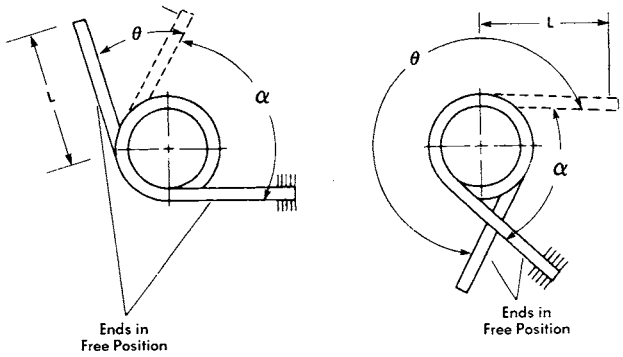

FIGURE 6.23 Specifying load and deflection requirements for torsion spring: α = angle between ends; P = load on ends at α; L = moment arm; θ = angular deflection from free position. *(Associated Spring, Barnes Group Inc.)*

Spring ends most commonly used are shown in Fig. 6.24, although the possible variations are unlimited. In considering spring mounting, it must be recognized that for each turn of windup, the overall length L of the spring body will increase as

$$L_1 = d(N_a + 1 + \theta) \tag{6.30}$$

where θ = deflection in revolutions.

Also note that the body coil diameter will be reduced to

$$D = \frac{D_I N_a}{Na + \theta} \tag{6.31}$$

where D_I = initial mean coil diameter. Experience indicates that the diameter of the arbor over which the spring operates should be approximately 90 percent of the smallest inside diameter to which the spring is reduced under maximum load. Too large an arbor will interfere with deflection, while too small an arbor will provide too little support. Both conditions lead to unexpectedly early failure. Coil diameter tolerances are given in Table 6.17.

6.6.1 Spring Rate

The spring rate, or moment per turn, is given by

$$k = \frac{M}{\theta} = \frac{Ed^4}{10.8DN_a} \tag{6.32}$$

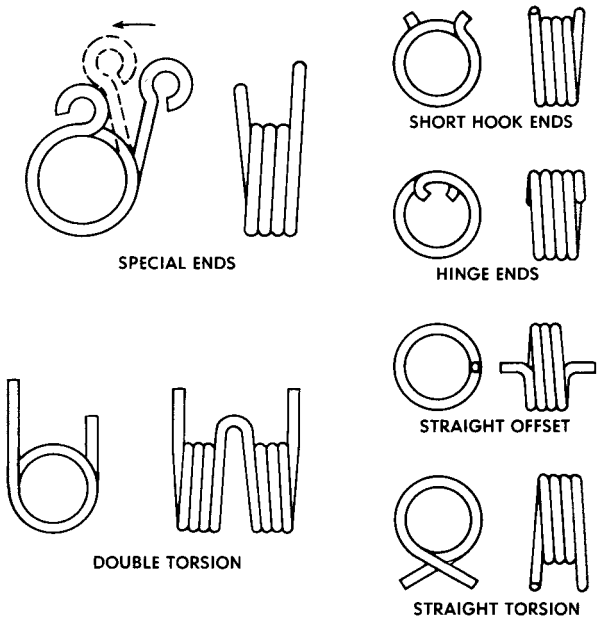

FIGURE 6.24 Common helical torsion-spring end configurations. *(Associated Spring, Barnes Group Inc.)*

The number of coils is equal to the number of body coils plus a contribution from the ends. The effect is more pronounced when the ends are long. The number of equivalent coils in the ends is

$$N_e = \frac{L_1 + L_2}{3\pi D} \tag{6.33}$$

where L_1 and L_2 = lengths of ends, and so $N_a = N_b + N_e$, where N_b = number of body coils.

The load should be specified at a fixed angular relationship of the spring ends rather than at a specific angular deflection from free or load positions. Helical torsion springs are stressed in bending. Rectangular sections are more efficient than round sections, but round sections are normally used because there is usually a premium cost for rectangular wire.

6.6.2 Stresses

Stress in round-wire torsion springs is given by

$$S = \frac{32K_B M}{\pi d^3} \tag{6.34}$$

where K_B = a stress correction factor. Stress is higher on the inner surface of the coil. A useful approximation of this factor is

$$K_B = \frac{4C - 1}{4C - 4} \tag{6.35}$$

6.6.3 Rectangular-Wire Torsion Springs

When rectangular wire is formed into coils, it approaches a keystone according to the relation

$$b_I = b\,\frac{C + 0.5}{C} \tag{6.36}$$

where b_I = axial dimension b after keystoning. The radial dimension is always t. The rate equation is

$$k = \frac{M}{\theta} = \frac{Ebt^3}{6.6DN_a} \tag{6.37}$$

Stress in rectangular-wire torsion springs is given by

$$S = \frac{6K_B M}{bt^2} \tag{6.38}$$

where $K_{B_{1D}} = 4C/(4C - 3)$ and b = axial dimension of rectangular cross section. Maximum recommended stresses are given in Table 6.15 for static applications and in Table 6.16 for cyclic applications.

TABLE 6.15 Maximum Recommended Bending Stresses for Helical Torsion Springs in Static Applications

Material	Percent of Tensile Strength	
	Stress-Relieved (1) (K_B Corrected)	With Favorable Residual Stress (2) (No Correction Factor)
Patented and Cold Drawn	80	100
Hardened and Tempered Carbon and Low Alloy Steels	85	100
Austenitic Stainless Steels and Non-Ferrous Alloys	60	80

(1) Also for springs without residual stresses.
(2) Springs that have not been stress-relieved and which have bodies and ends loaded in a direction that decreases the radius of curvature.

SOURCE: Associated Spring, Barnes Group Inc.

TABLE 6.16 Maximum Recommended Bending Stresses (K_B Corrected) for Helical Torsion Springs in Cyclic Applications

Fatigue Life (cycles)	ASTM A228 and Type 302 Stainless Steel		ASTM A230 and A232	
	Not Shot-Peened	Shot-Peened*	Not Shot-Peened	Shot-Peened*
10^5	53	62	55	64
10^6	50	60	53	62

This information is based on the following conditions: no surging, springs are in the "as-stress-relieved" condition
*Not always possible.

SOURCE: Associated Spring, Barnes Group Inc.

6.6.4 Tolerances

The tolerances for coil diameter and end position are given in Tables 6.17 and 6.18, respectively. Use them as guides.

6.7 BELLEVILLE SPRING WASHER

Belleville washers, also known as *coned-disk springs,* take their name from their inventor, Julian F. Belleville. They are essentially circular disks formed to a conical shape, as shown in Fig. 6.25. When load is applied, the disk tends to flatten. This elastic deformation constitutes the spring action.

TABLE 6.17 Commercial Tolerances for Torsion-Spring Coil Diameters

Wire Diameter mm (in.)	Tolerance: ± mm (in.) Spring Index D/d						
	4	6	8	10	12	14	16
0.38 (0.015)	0.05 (0.002)	0.05 (0.002)	0.05 (0.002)	0.05 (0.002)	0.08 (0.003)	0.08 (0.003)	0.10 (0.004)
0.58 (0.023)	0.05 (0.002)	0.05 (0.002)	0.05 (0.002)	0.08 (0.003)	0.10 (0.004)	0.13 (0.005)	0.15 (0.006)
0.89 (0.035)	0.05 (0.002)	0.05 (0.002)	0.08 (0.003)	0.10 (0.004)	0.15 (0.006)	0.18 (0.007)	0.23 (0.009)
1.30 (0.051)	0.05 (0.002)	0.08 (0.003)	0.13 (0.005)	0.18 (0.007)	0.20 (0.008)	0.25 (0.010)	0.31 (0.012)
1.93 (0.076)	0.08 (0.003)	0.13 (0.005)	0.18 (0.007)	0.23 (0.009)	0.31 (0.012)	0.38 (0.015)	0.46 (0.018)
2.90 (0.114)	0.10 (0.004)	0.18 (0.007)	0.25 (0.010)	0.33 (0.013)	0.46 (0.018)	0.56 (0.022)	0.71 (0.028)
4.37 (0.172)	0.15 (0.006)	0.25 (0.010)	0.33 (0.013)	0.51 (0.020)	0.69 (0.027)	0.86 (0.034)	1.07 (0.042)
6.35 (0.250)	0.20 (0.008)	0.36 (0.014)	0.56 (0.022)	0.76 (0.030)	1.02 (0.040)	1.27 (0.050)	1.52 (0.060)

SOURCE: Associated Spring, Barnes Group Inc.

TABLE 6.18 End-Position Tolerances (for *D/d* Ratios up to and Including 16)

Total Coils	Tolerance: ± Degrees*
Up to 3	8
Over 3–10	10
Over 10–20	15
Over 20–30	20
Over 30	25

*Closer tolerances available

SOURCE: Associated Spring, Barnes Group Inc.

Belleville springs are used in two broad types of applications. First, they are used to provide very high loads with small deflections, as in stripper springs for punch-press dies, recoil mechanisms, and pressure-relief valves. Second, they are used for their special nonlinear load-deflection curves, particularly those with a constant-load portion. In loading a packing seal or a live center for a lathe, or in injection molding machines, Belleville washers can maintain a constant force throughout dimensional changes in the mechanical system resulting from wear, relaxation, or thermal change.

The two types of performance depend on the ratio of height to thickness. Typical load-deflection curves for various height-thickness ratios are shown in Fig. 6.26. Note that the curve for a small h/t ratio is nearly a straight line. At $h/t = 1.41$ the curve shows a nearly constant load for approximately the last 50 percent of deflection

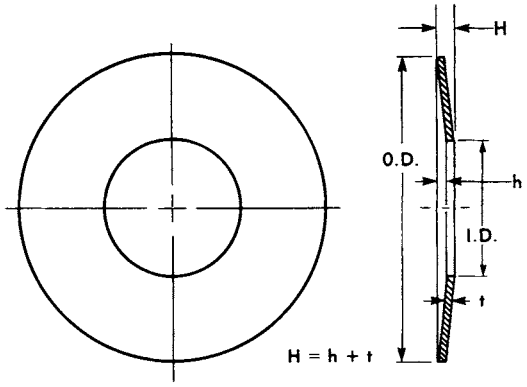

FIGURE 6.25 Belleville washer. *(Associated Spring, Barnes Group Inc.)*

before the flat position. Above $h/t = 1.41$ the load decreases after reaching a peak. When h/t is 2.83 or more, the load will go negative at some point beyond flat and will require some force to be restored to its free position. In other words, the washer will turn inside out.

The design equations given here are complex and may present a difficult challenge to the occasional designer. Use of charts and the equation transpositions presented here have proved helpful. Note that these equations are taken from the mathematical analysis by Almen and Laszlo [6.5]. The symbols used here are those originally used by the authors and may not necessarily agree with those used elsewhere in the text.

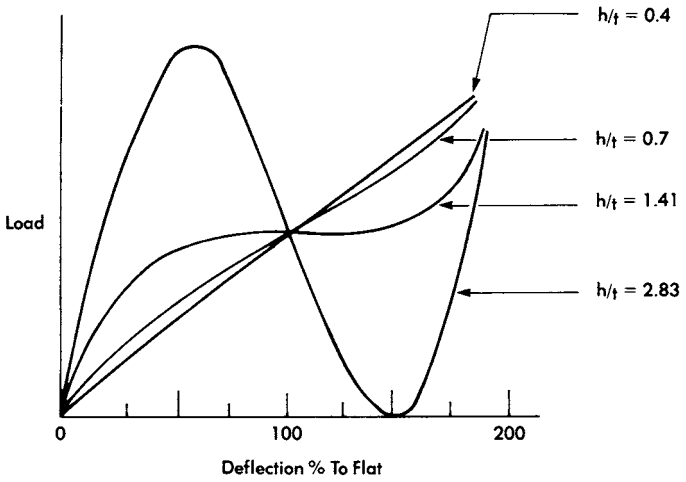

FIGURE 6.26 Load-deflection curves for Belleville washers with various h/t ratios. *(Associated Spring, Barnes Group Inc.)*

6.7.1 Nomenclature

a	OD/2, mm (in)
C_1	Compressive stress constant (see formula and Fig. 6.28)
C_2	Compressive stress constant (see formula and Fig. 6.28)
E	Modulus of elasticity (see Table 6.19), MPa (psi)
f	Deflection, mm (in)
h	Inside height, mm (in)
ID	Inside diameter, mm (in)
M	Constant
OD	Outside diameter, mm (in)
P	Load, N (lb)
P_f	Load at flat position, N (lb)
R	OD/ID
S_c	Compressive stress (Fig. 6.27), MPa (psi)
S_{T_1}	Tensile stress (Fig. 6.27), MPa (psi)
S_{T_2}	Tensile stress (Fig. 6.27), MPa (psi)
t	Thickness, mm (in)
T_1	Tensile stress constant (see formula and Fig. 6.29)
T_2	Tensile stress constant (see formula and Fig. 6.29)
μ	Poisson's ratio (Table 6.19)

6.7.2 Basic Equations

$$P = \frac{Ef}{(1-\mu^2)Ma^2}\left[(h-f)\left(h-\frac{f}{2}\right)t+t^3\right] \tag{6.39}$$

$$P_F = \frac{Eht^3}{(1-\mu^2)Ma^2} \tag{6.40}$$

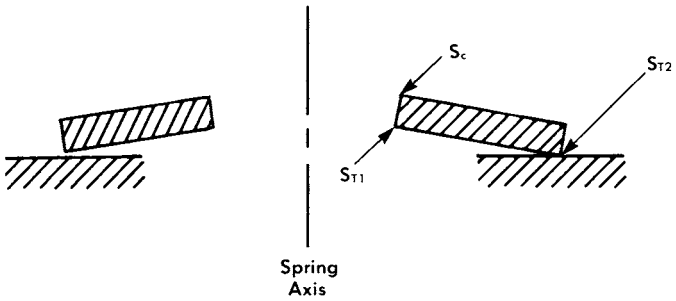

FIGURE 6.27 Highest-stressed regions in Belleville washers. *(Associated Spring, Barnes Group Inc.)*

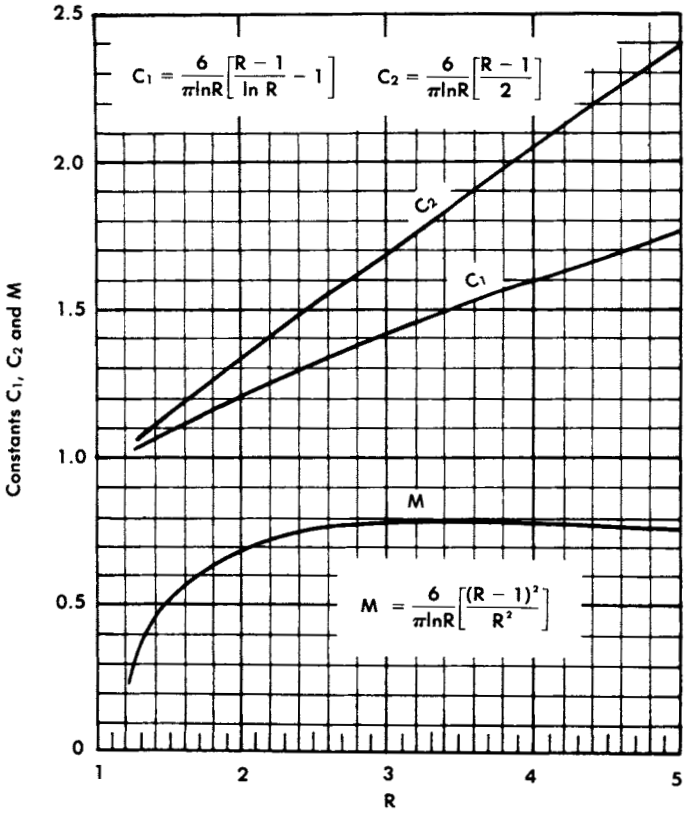

FIGURE 6.28 Compressive stress constants for Belleville washers. *(Associated Spring, Barnes Group Inc.)*

TABLE 6.19 Elastic Constants of Common Spring Materials

Material	Modulus of Elasticity *E*		Poisson's ratio μ
	Mpsi	GPa	
Steel	30	207	0.30
Phosphor bronze	15	103	0.20
17-7 PH stainless	29	200	0.34
302 stainless	28	193	0.30
Beryllium copper	18.5	128	0.33
Inconel	31	214	0.29
Inconel X	31	214	0.29

SOURCE: Associated Spring, Barnes Group Inc.

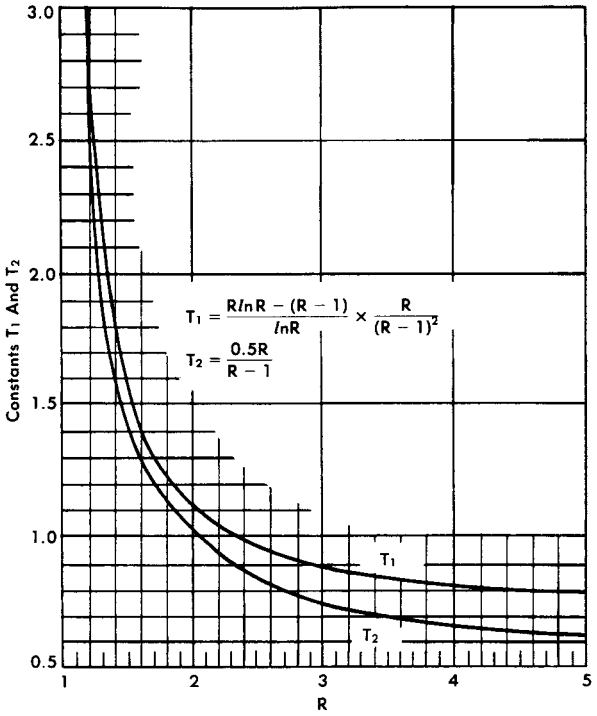

FIGURE 6.29 Tensile stress constants for Belleville washers. *(Associated Spring, Barnes Group Inc.)*

$$S_c = \frac{Ef}{(1-\mu^2)Ma^2}\left[C_1\left(h-\frac{f}{2}\right)+C_2 t\right] \tag{6.41}$$

$$S_{T_1} = \frac{Ef}{(1-\mu^2)Ma^2}\left[C_1\left(h-\frac{f}{2}\right)-C_2 t\right] \tag{6.42}$$

$$S_{T_2} = \frac{Ef}{(1-\mu^2)a^2}\left[T_1\left(h-\frac{f}{2}\right)+T_2 t\right] \tag{6.43}$$

The design approach recommended here depends on first determining the loads and stresses at flat position, as shown in Fig. 6.30. Intermediate loads are determined from the curves in Fig. 6.31.

Figure 6.30 gives the values graphically for compressive stresses S_c at flat position. The stress at intermediate stages is approximately proportional to the deflection. For critical applications involving close tolerances or unusual proportions, stresses should be checked by using the equation before the design is finalized.

The stress level for static applications is evaluated in accordance with Eq. (6.41). This equation has been used most commonly for appraising the design of a Belleville spring because it gives the highest numerical value. It gives the compressive stress at the point shown in Fig. 6.27.

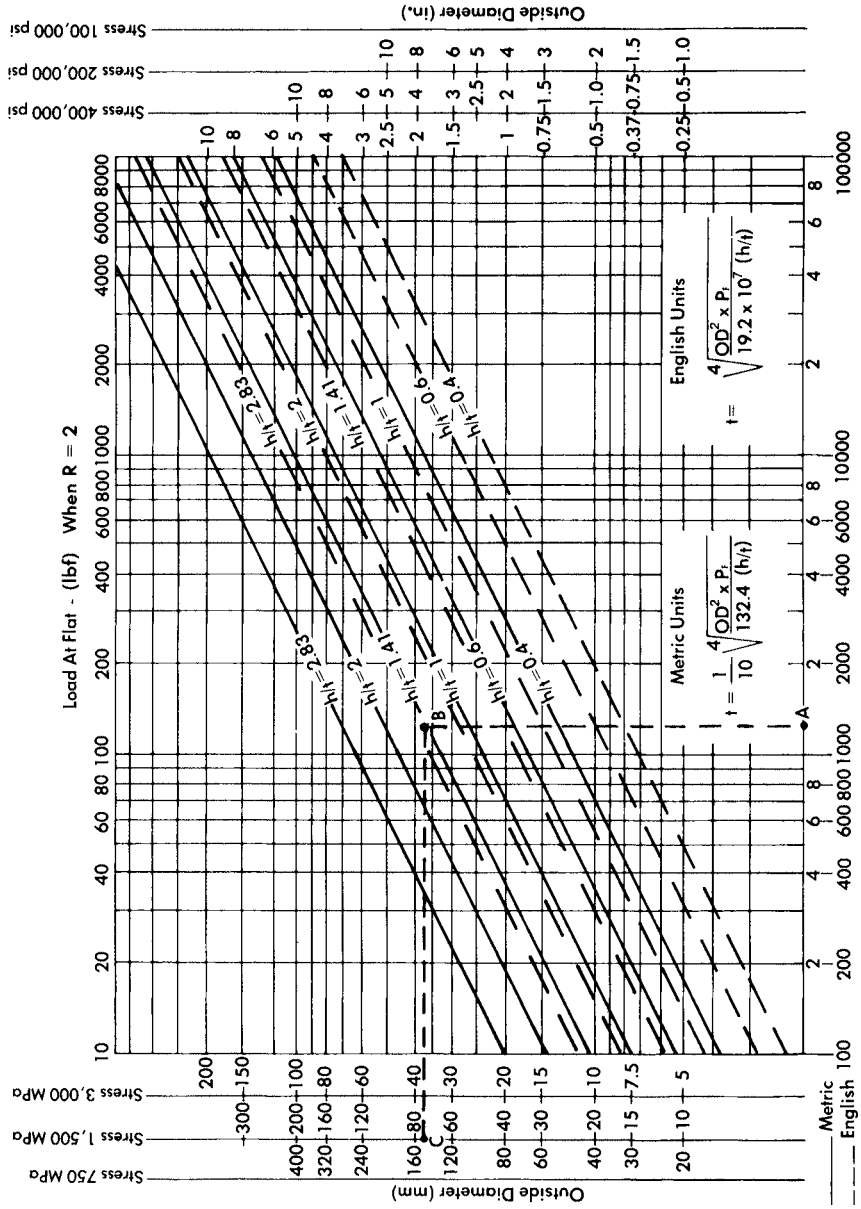

FIGURE 6.30 Loads and compressive stresses S_c for Belleville washers with various outside diameters and h/t ratios. *(Associated Spring, Barnes Group Inc.)*

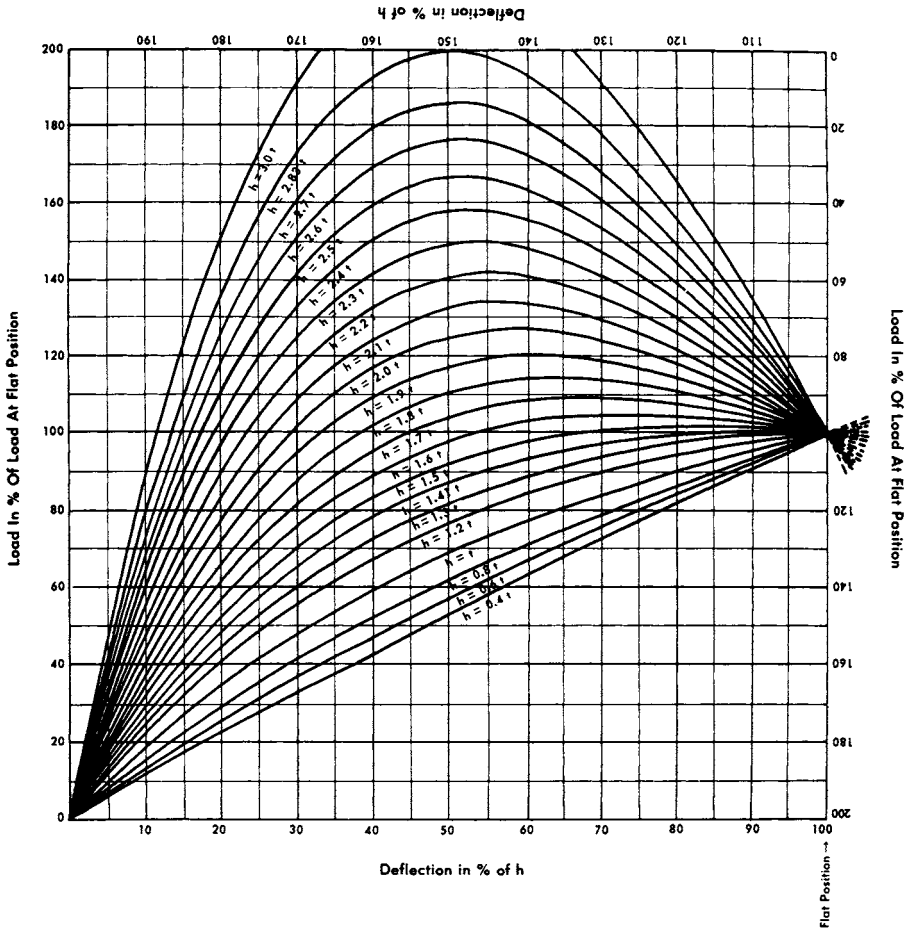

FIGURE 6.31 Load-deflection characteristics for Belleville washers. If a washer is supported and loaded at its edges so that it is deflected beyond the flat position, then the greatest possible deflection can be utilized. Since the load-deflection curve beyond the horizontal position is symmetric with the first part of the curve, this chart has been labeled at the right and top to be read upside down for deflection beyond horizontal. Dotted lines extending beyond the chart indicate continuation of curves beyond flat. *(Associated Spring, Barnes Group Inc.)*

A Belleville spring washer should be designed so that it can be compressed flat by accidental overloading, without setting. This can be accomplished either by using a stress so low that the spring will not set or by forming the spring higher than the design height and removing set by compressing flat or beyond flat (see Table 6.21). The table values should be reduced if the washers are plated or used at elevated temperatures.

For fatigue applications it is necessary to consider the tensile stresses at the points marked S_{T_1} and S_{T_2} in Fig. 6.27. The higher value of the two can occur at either

the ID or the OD, depending on the proportions of the spring. Therefore, it is necessary to compute both values.

Fatigue life depends on the stress range as well as the maximum stress value. Figure 6.32 predicts the endurance limits based on either S_{T_1} or S_{T_2}, whichever is higher. Fatigue life is adversely affected by surface imperfections and edge fractures and can be improved by shot peening.

Since the deflection in a single Belleville washer is relatively small, it is often necessary to combine a number of washers. Such a combination is called a *stack*.

The deflection of a series stack (Fig. 6.33) is equal to the number of washers times the deflection of one washer, and the load of the stack is equal to that of one washer. The load of a parallel stack is equal to the load of one washer times the number of washers, and the deflection of the stack is that of one washer.

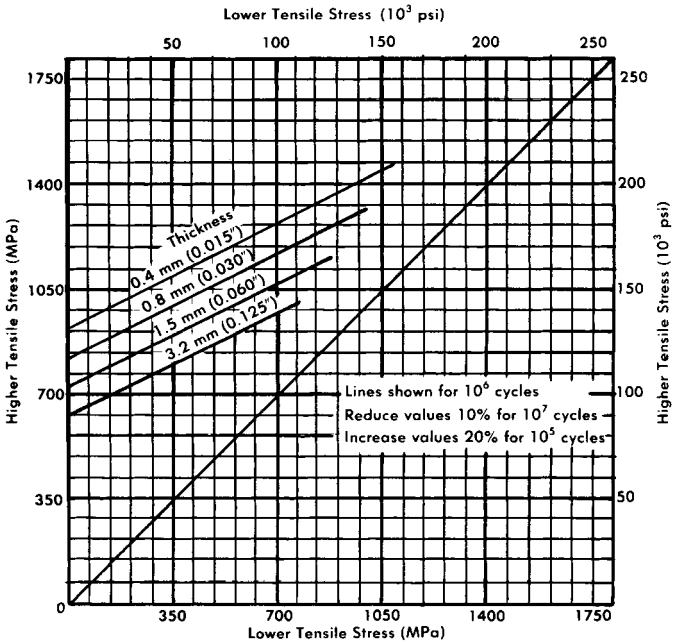

FIGURE 6.32 Modified Goodman diagram for Belleville washers; for carbon and alloy steels at 47 to 49 R_c with set removed, but not shot-peened. *(Associated Spring, Barnes Group Inc.)*

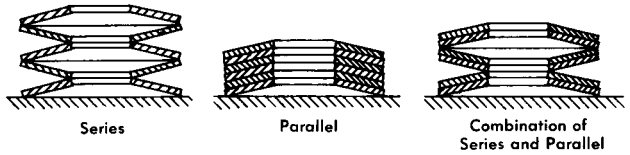

FIGURE 6.33 Stacks of Belleville washers. *(Associated Spring, Barnes Group Inc.)*

Because of production variations in washer parameters, both the foregoing statements carry cautionary notes. In the series stack, springs of the constant-load type ($h/t = 1.41$) may actually have a negative rate in some portion of their deflection range. When such a series stack is deflected, some washers will snap through, producing jumps in the load-deflection curve. To avoid this problem, the h/t ratio in a series stack design should not exceed 1.3.

In the parallel stack, friction between the washers causes a hysteresis loop in the load-deflection curve (Fig. 6.34). The width of the loop increases with each washer added to the stack but may be reduced by adding lubrication as the washers burnish each other during use.

Stacked washers normally require guide pins or sleeves to keep them in proper alignment. These guides should be hardened steel at HRC 48 minimum hardness. Clearance between the washer and the guide pin or sleeve should be about 1.5 percent of the appropriate diameter.

6.7.3 Tolerances

Load tolerances should be specified at test height. For carbon-steel washers with $h/t < 0.25$, use load tolerance of ±15 percent. For washers with $h/t > 0.25$, use ±10 percent. The recommended load tolerance for stainless steel and nonferrous washers is ±15 percent. See Table 6.20 for outside- and inside-diameter tolerances.

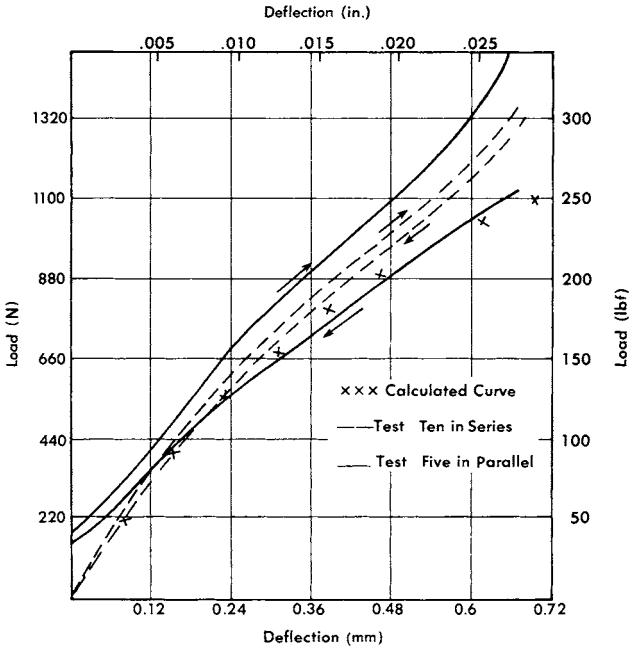

FIGURE 6.34 Hysteresis in stacked Belleville washers. *(Associated Spring, Barnes Group Inc.)*

TABLE 6.20 Belleville Washer Diameter Tolerances

Diameter, mm (in.)	O.D. mm (in.)	I.D. mm (in.)
	+0.00	−0.00
Up to 5 (0.197)	−0.20 (−0.008)	+0.20 (+0.008)
5–10 (0.197–0.394)	−0.25 (−0.010)	+0.25 (+0.010)
10–25 (0.394–0.984)	−0.30 (−0.012)	+0.30 (+0.012)
25–50 (0.984–1.969)	−0.40 (−0.016)	+0.40 (+0.016)
50–100 (1.969–3.937)	−0.50 (−0.020)	+0.50 (+0.020)

Based on R = 2, increased tolerances are required for lower R ratios.
SOURCE: Associated Spring, Barnes Group Inc.

Example. In a clutch, a minimum pressure of 202 lb (900 N) is required. This pressure must be held nearly constant as the clutch facing wears down 0.31 in (7.9 mm). The washer OD is 2.99 in (76 mm). The material washer OD is 2.99 in (76 mm). The material selected for the application is spring steel HRC 47-50.

Solution

1. Base the load on a value 10 percent above the minimum load, or 202 + 10 percent = 223 lb (998 N). Assume OD/ID = 2. From Fig. 6.31, select a load-deflection curve which gives approximately constant load between 50 and 100 percent of deflection to flat. Choose the $h/t = 1.41$ curve.
2. From Fig. 6.31, the load at 50 percent of deflection to flat is 88 percent of the flat load.
3. Flat load is $P_F = 223/0.88 = 252$ lb (1125 N).
4. From Fig. 6.30 [follow line AB from 1125 N to $h/t = 1.41$ and line BC to approximately 76-mm (2.99-in) OD], the estimated stress is 1500 MPa [218 kilopounds per square inch (kpsi)].
5. From Table 6.21 maximum stress without set removed is 120 percent of tensile strength. From Fig. 6.3, the tensile strength at HRC 48 will be approximately 239 kpsi (1650 MPa). Yield point without residual stress will be (239 kpsi)(1.20) = 287 kpsi. Therefore 218 kpsi stress is less than the maximum stress of 287 kpsi.
6. Stock thickness is

$$t = \sqrt[4]{\frac{\text{OD}^2(P_F)}{19.2(10^7)(h/t)}} = 0.054 \text{ in } (1.37 \text{ mm})$$

TABLE 6.21 Maximum Recommended Stress Levels for Belleville Washers in Static Applications

Material	Percent of Tensile Strength	
	Set Not Removed	Set Removed
Carbon or Alloy Steel	120	275
Nonferrous and Austenitic Stainless Steel	95	160

SOURCE: Associated Spring, Barnes Group Inc.

7. $$h = 1.41t = 1.41(0.054) = 0.076 \text{ in}$$

$$H = h + t = 0.076 + 0.054 = 0.130 \text{ in}$$

8. Refer to Fig. 6.31. The load of 202 lb will be reached at $f_1 = 50$ percent of maximum available deflection. And $f_1 = 0.50(0.076) = 0.038$ in deflection, or the load of 223 lb will be reached at $H_1 = H - f_1 = 0.130 - 0.038 = 0.092$ in height at load. To allow for wear, the spring should be preloaded at $H_2 = H_1 - f(\text{wear}) = 0.092 - 0.032 = 0.060$ in height. This preload corresponds to a deflection $f_2 = H - H_2 = 0.130 - 0.060 = 0.070$ in. Then $f_2/h = 0.070/0.076 = 0.92$, or 92 percent of h.

9. Because 92 percent of h exceeds the recommended 85 percent (the load-deflection curve is not reliable beyond 85 percent deflection when the washer is compressed between flat surfaces), increase the deflection range to 40 to 85 percent. From Fig. 6.31, the load at 40 percent deflection is 78.5 percent, and $P_F = 223/0.785 = 284$ lb. Repeat previous procedures 4, 5, 6, 7, and 8, and find that $100(f_2/h) = 81$ percent of h. The final design is as follows:

Material: AISI 1074

OD = 2.99 in (76 mm)

ID = 1.50 in (38 mm)

$t = 0.055$ in (1.40 mm) nominal

$h = 0.078$ in (1.95 mm) nominal

Tensile stress $S_{T_1} = -29.5$ kpsi (–203 MPa) at $f_2 = 85$ percent of h

Tensile stress $S_{T_2} = 103$ kpsi (710 MPa) at $f_2 = 85$ percent of h

6.8 SPECIAL SPRING WASHERS

Spring washers are being used increasingly in applications where there is a requirement for miniaturization and compactness of design. They are used to absorb vibrations and both side and end play, to distribute loads, and to control end pressure.

Design equations have been developed for determining the spring characteristics of curved, wave, and Belleville washers. There are no special design equations for slotted and finger washers. They are approximated by using Belleville and cantilever equations and then are refined through sampling and testing.

6.8.1 Curved Washers

These springs (Fig. 6.35) exert relatively light thrust loads and are often used to absorb axial end play. The designer must provide space for diametral expansion which occurs as the washer is compressed during loading. Bearing surfaces should be hard, since the washer edges tend to dig in. The spring rate is approximately linear up to 80 percent of the available deflection. Beyond that the rate will be much higher than calculated. Load tolerance should not be specified closer than ±20 percent.

Approximate equations are

$$P = \frac{4fEt^3}{\text{OD}^2(K)} \tag{6.44}$$

and

$$S = \frac{1.5KP}{t^2} \tag{6.45}$$

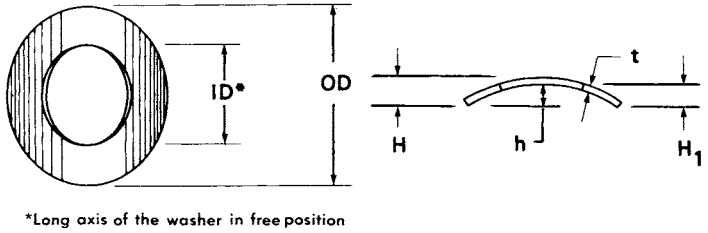

FIGURE 6.35 Curved washer. *(Associated Spring, Barnes Group Inc.)*

where K is given in Fig. 6.36 and f is 80 percent of h or less.

Maximum recommended stress levels for static operations are given in Table 6.22. Favorable residual stresses can be induced by shot peening and, to a lesser extent, by removing set. The maximum recommended stresses for cyclic applications are given in Table 6.23.

Tensile strengths for carbon steel are obtained from Fig. 6.3.

6.8.2 Wave Washer

These spring washers (Fig. 6.37) are regularly used in thrust loading applications, for small deflections, and for light to medium loads. The rate is linear between 20 and 80 percent of available deflection. Load tolerances should be no less than ±20 percent. In the most commonly used range of sizes, these washers can have three, four, or six waves.

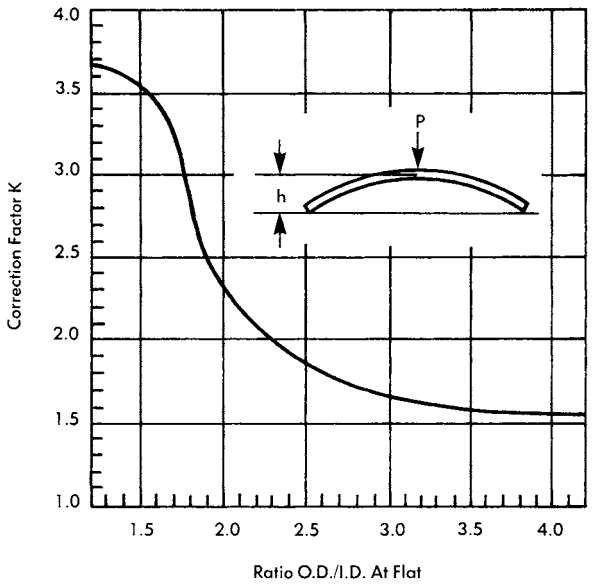

FIGURE 6.36 Empirical correction factor K for curved spring washers. *(Associated Spring, Barnes Group Inc.)*

TABLE 6.22 Maximum Recommended Operating Stress Levels for Special Spring Washers in Static Applications

Material	Percent of Tensile Strength	
	Stress-Relieved	With Favorable Residual Stresses
Steels, Alloy Steels	80	100
Nonferrous Alloys and Austenitic Steel	—	80

Finger washers are not generally supplied with favorable residual stresses.
SOURCE: Associated Spring, Barnes Group Inc.

TABLE 6.23 Maximum Recommended Operating Stress Levels for Steel Curved and Wave Washers in Cyclic Applications

Life (Cycles)	Percent of Tensile Strength
	Maximum Stress
10^4	80
10^5	53
10^6	50

This information is based on the following conditions: ambient environment, free from sharp bends, burrs, and other stress concentrations. AISI 1075
SOURCE: Associated Spring, Barnes Group Inc.

Design equations are

$$\frac{P}{f} = \frac{Ebt^3N^4(\text{OD})}{2.4D^3(\text{ID})} \tag{6.46}$$

and

$$S = \frac{3\pi PD}{4bt^2N^2} \tag{6.47}$$

where $D = \text{OD} - b$. The washer expands in diameter when compressed, according to the formula

$$D' = \sqrt{D^2 + 0.458h^2N^2} \tag{6.48}$$

Maximum recommended stress levels for static applications are given in Table 6.22. Favorable residual stresses are induced by shot peening or removing set. Table 6.23 gives the maximum recommended stress levels for cyclic applications. Figure 6.3 provides tensile strengths for carbon steel.

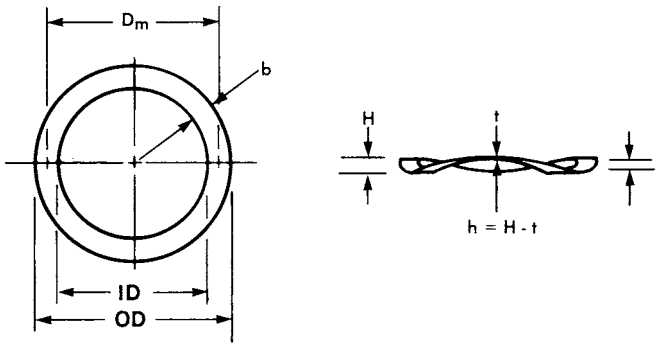

FIGURE 6.37 Typical wave spring washer. *(Associated Spring, Barnes Group Inc.)*

6.8.3 Finger Washers

Finger washers (Fig. 6.38) have both the flexibility of curved washers and the distributed points of loading of wave washers. They are calculated, approximately, as groups of cantilever springs; then samples are made and tested to prove the design. They are most frequently used in static applications such as applying axial load to ball-bearing races to reduce vibration and noise. These washers are not used in cyclic applications because of the shear cuts.

6.8.4 Slotted Washers

These are more flexible than plain dished washers but should be designed to maintain a constant pressure rather than to operate through a deflection range (see Fig. 6.39).

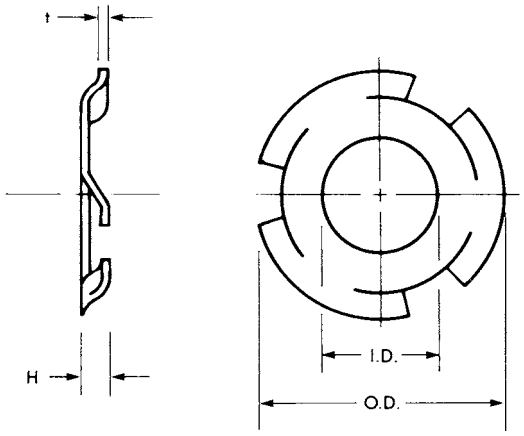

FIGURE 6.38 Finger washer. *(Associated Spring, Barnes Group Inc.)*

6.9 FLAT SPRINGS

6.9.1 Introduction

The classification *flat springs* applies to a wide range of springs made from sheet, strip, or plate material. Exceptions to this classification are power springs and washers. Flat springs may contain bends and forms. Thus the classification refers to the raw material and not to the spring itself.

Flat springs can perform functions beyond normal spring functions. A flat spring may conduct electricity, act as a latch, or hold a part in position. In some flat springs, only a portion of the part may have a spring function.

FIGURE 6.39 Slotted washers. *(Associated Spring, Barnes Group Inc.)*

Most flat springs are custom designs, and the tooling is often a major cost consideration. Flat springs can be cantilever or simple elliptical beams or combinations of both. These two elementary forms are discussed in this section. For a description of the methods used to compute complex flat-spring designs, see [6.6].

Load specification in flat springs is closely connected with the dimensioning of the form of the spring. From the equations it can be seen that the deflection and load vary in proportion to the third power of the material thickness. The important factors in load control are first, the material thickness and second, the deflection. Where close load control is required, the material may have to be selected to restricted thickness tolerance, and/or the free shape may be trued.

6.9.2 Cantilever Springs

The basic type of cantilever is a rectangular spring as shown in Fig. 6.40. The maximum bending stress occurs at the clamping point, and the stress is not uniform through the section. This stress is

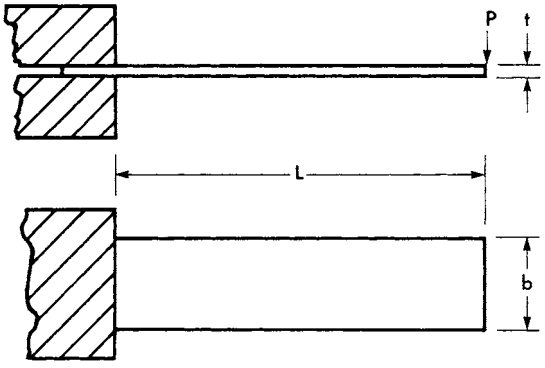

FIGURE 6.40 Rectangular cantilever spring. *(Associated Spring, Barnes Group Inc.)*

$$S = \frac{6PL}{bt^2} \tag{6.49}$$

The load is given by

$$P = \frac{fEbt^3}{4L^3} \tag{6.50}$$

These equations are satisfactory when the ratio of deflection to length f/L is less than 0.3. For larger deflections, use the method described in Fig. 6.41.

In cantilever springs with a trapezoidal or triangular configuration (Fig. 6.42), the stress is uniform throughout and is

$$S = \frac{6PL}{b_o t^2} \tag{6.51}$$

The corresponding load is

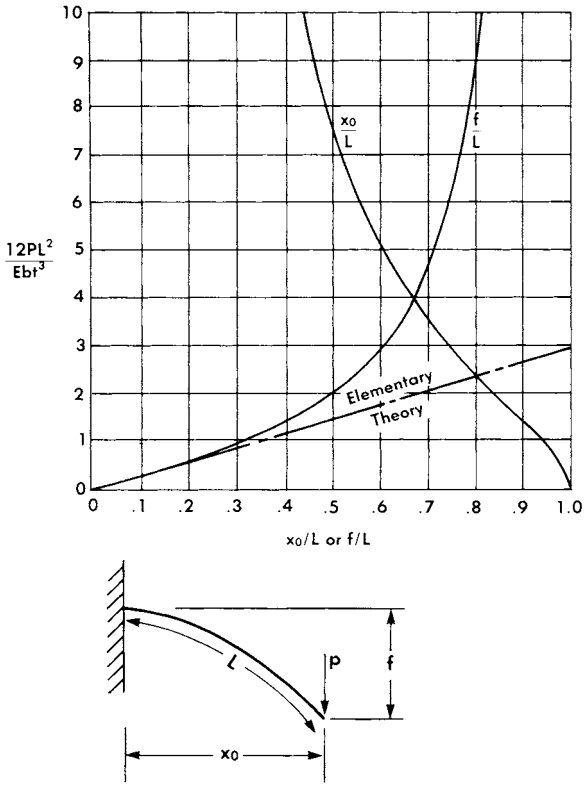

FIGURE 6.41 Calculating large deflection in cantilever beams [6.7]. To utilize this figure for any load P, first calculate the quantity $12PL^3/Ebt^3$. Using this value, from the curves find f/L and x_o/L, where x_o is the moment arm of the load P. Deflection then equals L multiplied by f/L. The maximum stress is reduced in the ratio x_o/L. *(Associated Spring, Barnes Group Inc.)*

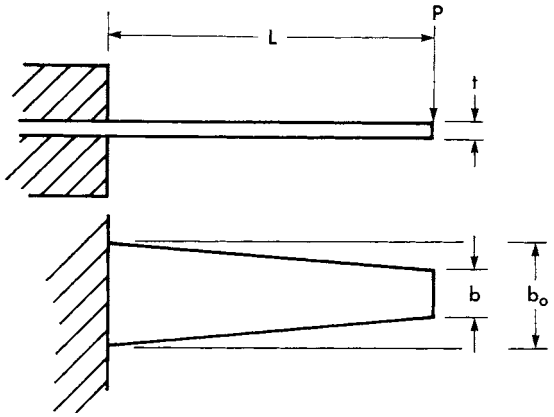

FIGURE 6.42 Trapezoidal cantilever spring. *(Associated Spring, Barnes Group Inc.)*

$$P = \frac{fEb_o t^3}{4L^3 K} \tag{6.52}$$

where K = constant based on the ratio b/b_o (Fig. 6.43). These equations are valid for f/L ratios of less than 0.3.

6.9.3 Simple Beams or Elliptical Springs

Simple beams are usually rectangular and are formed into an arc as in Fig. 6.44. If holes are introduced for clamping purposes, stress will increase at the hole and at the clamping point owing to stress concentration.

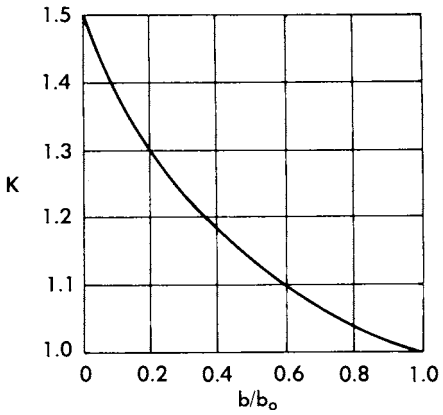

FIGURE 6.43 Correction factor for trapezoidal beam-load equation. *(Associated Spring, Barnes Group Inc.)*

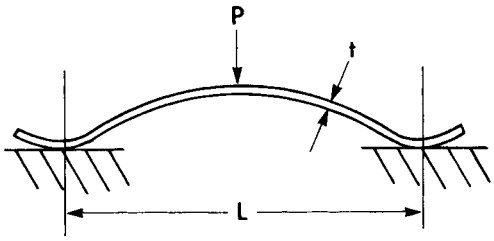

FIGURE 6.44 Simple beam spring. *(Associated Spring, Barnes Group Inc.)*

When ends are free to move laterally, the equation for load is

$$P = \frac{4fEbt^3}{L^3} \tag{6.53}$$

and stress is given by

$$S = \frac{1.5PL}{bt^2} \tag{6.54}$$

These equations apply when the ratio f/L is less than 0.15.

Stress Considerations. The maximum design stresses for cantilevers and simple beams are given in Table 6.24 for static applications and in Table 6.25 for cyclic applications. These recommendations do not apply when holes, sharp corners, notches, or abrupt changes in cross section are incorporated in the design, and should be used for guidance only.

6.10 CONSTANT-FORCE SPRINGS

A constant-force spring is a roll of prestressed material which exerts a nearly constant restraining force to resist uncoiling. Its unique characteristic is *force independent of deflection.* The force required to produce a unit deflection is the same for

TABLE 6.24 Maximum Design Stresses for Cantilever and Simple Beam Springs in Static Applications

Percent of Tensile Stength			
Ferrous Material		Nonferrous Material	
No Residual Stress	Maximum Residual Stress	No Residual Stress	Maximum Residual Stress
80	100	75	80

SOURCE: Associated Spring, Barnes Group Inc.

TABLE 6.25 Maximum Design Stresses for Carbon-Steel Cantilever and Simple Beam Springs in Cyclic Applications

Number of Cycles	Percent of Tensile Strength	
	Not Shot-Peened	Shot-Peened*
10^5	53	62
10^6	50	60
10^7	48	58

*Shot peening is not recommended for thin materials and complex shapes. This information is based on an ambient environment. Stress ratio = 0.

SOURCE: Associated Spring, Barnes Group Inc.

each increment of coil because the radius of curvature of each increment is the same as any other.

Although these springs are not constant-load or constant-torque springs in the precise meaning of those terms, they produce a more nearly constant load over a greater deflection than any other spring design covered here. See Fig. 6.45. Constant-force springs are made of both type 301 stainless steel and ultra-high-strength high-carbon steels, with many of the applications using stainless steel because of its inherent resistance to corrosion.

One of the most severe limitations on the use of constant-force springs is their relatively short operating life. The most efficient use of material will produce a life of about 3000 cycles. Although life of hundreds of thousands of cycles is possible,

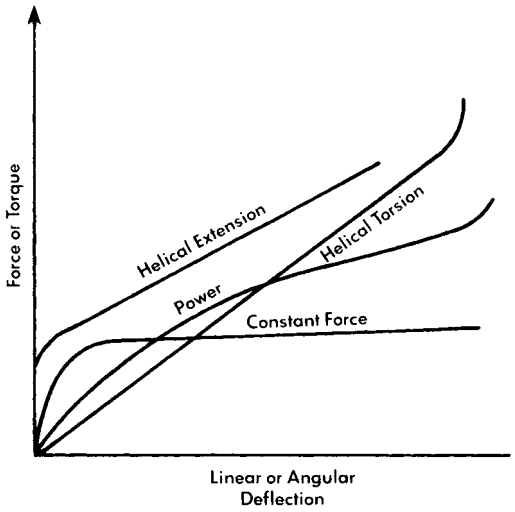

FIGURE 6.45 Load-deflection curves for various spring configurations. *(Associated Spring, Barnes Group Inc.)*

most applications fall into the range of 3000 to 30 000 cycles. Figure 6.46 shows the relationship between stress and fatigue life. These curves are derived from experimentally obtained data.

Some applications involving constant-force and constant-torque springs are simple extension springs, window sash counterbalances, camera motors, toys, machine carriage returns, constant-pressure electric-motor brush springs, space vehicle applications, and retraction devices.

6.10.1 Extension Type

This type of spring is a spiral spring made of strip material wound on the flat with an inherent curvature such that, in repose, each coil wraps tightly on its inner neighbor. In use the strip is extended with the free end loaded and the inner end supported on a drum or arbor. Very long deflections are possible, but the strip becomes unstable in long deflections and must be guided or supported to avoid kinking or snarling on the return stroke.

The rated load is not reached until after an initial deflection of 1.25 times the drum diameter, as shown in Fig. 6.47. Idler pulleys can be used but should be no smaller in diameter than the natural diameter of the coils and should never be used in a direction to cause backbending against the strip curvature.

6.10.2 Design Equations

$$P = \frac{Ebt^3}{6.5D_n^2} \qquad \text{for } N \le 10 \tag{6.55}$$

$$P = \frac{Ebt^3}{6.5D_1}\left(\frac{2}{D_n} - \frac{1}{D_1}\right) \qquad \text{for } N > 10 \tag{6.56}$$

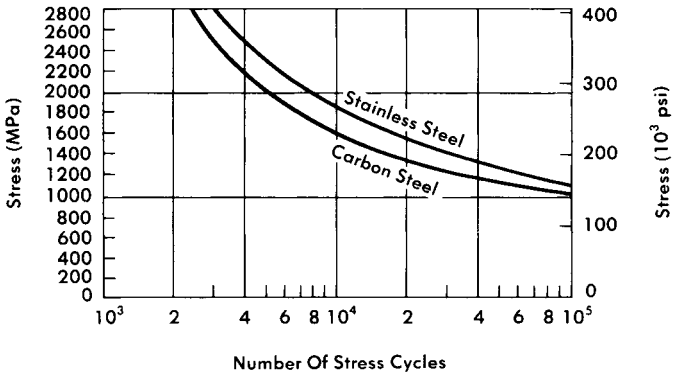

FIGURE 6.46 Maximum bending stress versus number of stress cycles for constant-force springs. These curves are based on no. 1 round-edge strip. *(Associated Spring, Barnes Group Inc.)*

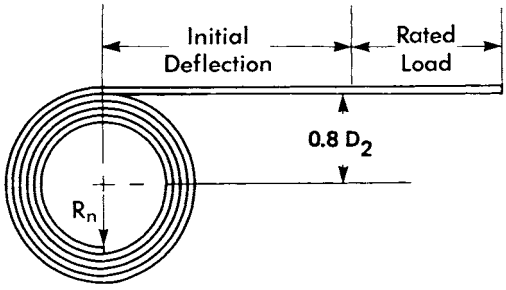

FIGURE 6.47 Typical constant-force extension spring (extension form). *(Associated Spring, Barnes Group Inc.)*

If unknown, let $b/t = 100/1$, $D_2 = 1.2\ D_n$,

$$S = \frac{Et}{D_n} \tag{6.57}$$

and

$$L = 1.57N(D_1 + D_2) \qquad \text{or} \qquad L \simeq f + 5D_2$$

where N = number of turns
D_1 = outside coil diameter
D_2 = drum (arbor) diameter
D_n = natural diameter
E = modulus of elasticity

6.10.3 Spring Motor Type

When a constant-force spring is mounted on two drums of different diameters and the spring is backbent onto the larger diameter, the result is a constant-force spring motor. The strip is in repose on the smaller (storage) drum and is backbent onto the larger (output) drum. Torque is taken from the output drum shaft as shown in Fig. 6.48.

Note here that constant torque does not mean constant speed. Constant torque implies uniform acceleration, and the mechanism so driven will continue to speed up unless restrained by a governor mechanism. Load tolerances are normally held within ±10 percent.

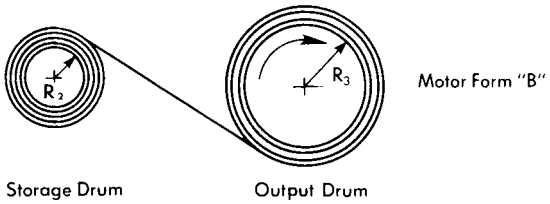

FIGURE 6.48 Typical constant-torque motor spring. *(Associated Spring, Barnes Group Inc.)*

6.10.4 Design Equations

$$M = \frac{Ebt^3 D_3}{13}\left(\frac{1}{D_n} + \frac{1}{D_3}\right)^2 \tag{6.58}$$

$$S = Et\left(\frac{1}{D_n} + \frac{1}{D_3}\right) \tag{6.59}$$

$$L = \pi N(D_3 + Nt) + 10D_3 \tag{6.60}$$

$$R_c = R_n\sqrt{4 + \frac{4R_3}{R_n} + \frac{R_n}{R_3} + \left(\frac{R_3}{R_n}\right)^2} \tag{6.61}$$

Design Suggestions. Let

$$\frac{b}{t} = 100 \qquad \frac{D_n}{t} = 250 \qquad \frac{D_3}{D_n} = 2 \qquad \frac{D_3}{D_2} = 1.6$$

where D_n = natural diameter
R_n = natural radius
D_2 = storage-drum diameter
D_3 = output-drum diameter
R_3 = output-drum radius
N = number of revolutions
R_c = minimum center-to-center distance of drums

6.11 TORSION BARS

Torsion bars used as springs are usually straight bars of spring material to which a twisting couple is applied. The stressing mode is torsional. This type of spring is very efficient in its use of material to store energy. The major disadvantage with the torsion bar is that unfavorable stress concentrations occur at the point where the ends are fastened.

Although both round and rectangular bar sections are used, the round section is used more often.

6.11.1 Design Equations: Round Sections

$$\phi = \frac{584ML}{d^4 G} \tag{6.62}$$

$$S = \frac{16M}{\pi d^3} \tag{6.63}$$

where ϕ = rotation angle in degrees
S = shear stress
L = active length

6.11.2 Design Equations: Rectangular Sections

$$\phi = \frac{57.3ML}{K_1 bt^3 G} \tag{6.64}$$

$$S = \frac{M}{K_2 bt^2} \tag{6.65}$$

where factors K_1 and K_2 are taken from Table 6.26.

The assumptions used in deriving these equations are (1) the bar is straight, (2) the bar is solid, and (3) loading is in pure torsion.

Torsion-bar springs are often preset in the direction in which they are loaded by twisting the bar beyond the torsional elastic limit. Care must be taken in the use of a preset bar: It must be loaded in the same direction in which it was preset; otherwise, excessive set will occur.

6.12 POWER SPRINGS

Power springs, also known as clock, motor, or flat coil springs, are made of flat strip material which is wound on an arbor and confined in a case. Power springs store and release rotational energy through either the arbor or the case in which they are retained. They are unique among spring types in that they are almost always stored in a case or housing while unloaded. Figure 6.49 shows typical retainers, a case, and various ends.

6.12.1 Design Considerations

Power springs are stressed in bending, and stress is related to torque by

$$S = \frac{6M}{bt^2} \tag{6.66}$$

Load-deflection curves for power springs are difficult to predict. As a spring is wound up, material is wound onto the arbor. This material is drawn from that which

TABLE 6.26 Factors for Computing Rectangular Bars in Torsion

b/t	K_1	K_2
1.0	0.140	0.208
1.5	0.196	0.231
2.0	0.229	0.246
2.5	0.249	0.258
3.0	0.263	0.267
5.0	0.291	0.291

SOURCE: A. M. Wahl, *Mechanical Springs*, 2d ed., McGraw-Hill Book Company, New York, 1963.

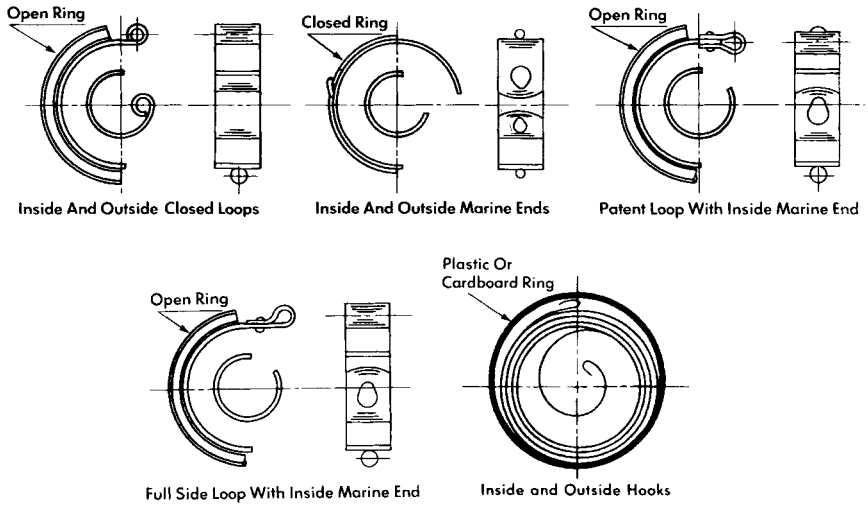

FIGURE 6.49 Typical power spring retainers and ends. *(Associated Spring, Barnes Group Inc.)*

was at rest against the case. Thus, the length of active material is constantly changing, which makes it difficult to develop a workable expression for the spring rate. For these reasons, ratios, tables, and graphical presentations are used to develop the design criteria.

The ratio of arbor diameter to thickness D_a/t is sometimes called the *life factor.* If it is too small, fatigue life will suffer. The life factor is usually maintained from 15 to 25. The ratio of active strip length to thickness L/t determines the flatness of the spring-gradient (torque-revolution) curve. The curve is flatter when L is longer. The usual range of the L/t ratio is from 5000 to 10 000. The ratio of the inside diameter of cup (case or housing) to thickness D_c/t is the *turns factor.* This determines the motion capability of the spring or indicates how much space is available between the arbor and the material lying against the inside of the case.

6.12.2 Design Procedure

In order to design a power spring that will deliver a given torque and number of turns, first determine its maximum torque in the fully wound condition. If a spring is required to deliver a minimum torque of 0.5 N·m for 10 revolutions (r) of windup and 10 r equals 80 percent unwound from solid, then from Fig. 6.50 we see that the torque at that point is 50 percent of the fully wound. Thus the fully wound torque is 1.0 N·m. Table 6.27 shows that a strip of steel 0.58 mm thick and 10 mm wide will provide 1.0 N·m of torque at the fully wound position per 10 mm of strip width.

Figure 6.51 shows that the average maximum solid stress for 0.58-mm-thick stock is about 1820 MPa. At the hardness normally supplied in steel strip for power springs, this is about 95 percent of tensile strength.

In Fig. 6.52, 10 turns relate to a length-to-thickness L/t ratio of 4300. With $t = 0.58$, L equals 2494 mm. Similarly, 4300 L/t relates to a D_c/t ratio of 107. Then $D_c = 62.06$ mm. If

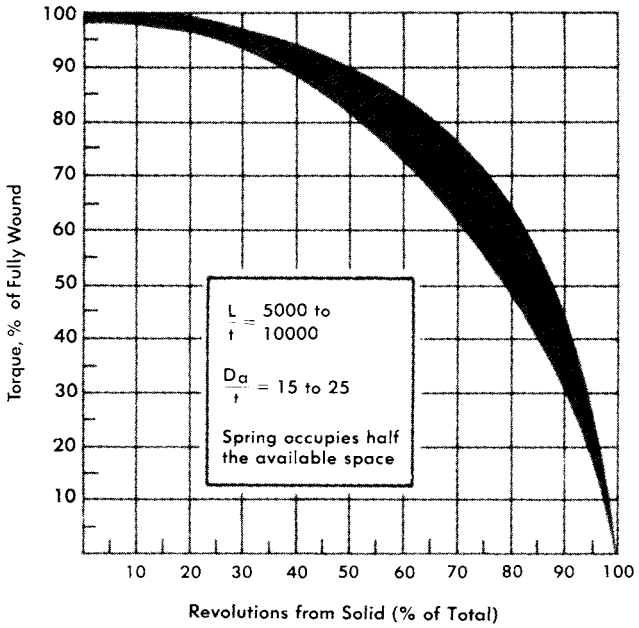

FIGURE 6.50 Typical normalized torque-revolution curve for power springs. *(Associated Spring, Barnes Group Inc.)*

$$L = \frac{D_c^2 - D_a^2}{2.55t} \tag{6.67}$$

then $D_a = \sqrt{D_c^2 - 2.55Lt} = 12.72$ mm and $D_a/t = 22$.

The equation for the number of turns a power spring will deliver, when it occupies half the space between arbor and case, is

$$\theta = \frac{\sqrt{2(D_c^2 + D_a^2)} - (D_c + D_a)}{2.55t} \tag{6.68}$$

In this example $\theta = 10$ r.

Experience shows that highly stressed power springs, made from pretempered AISI 1095 steel with a hardness of HRC 50 to 52 and stressed to 100 percent of tensile strength, could be expected to provide approximately 10 000 full-stroke life cycles. If the maximum stress were 50 percent of tensile strength at full stroke, then a life of about 100 000 cycles could be expected.

The final design is as follows:

$t = 0.023$ in (0.58 mm)

1095 carbon steel, HRC 51, no. 1 round edge

$b = 0.394$ in (10 mm)

$L = 98.188$ in (2494 mm)

$D_a = 0.501$ in (12.72 mm)

$D_c = 2.443$ in (62.06 mm)

TABLE 6.27 Torque per Unit of Width at Maximum Allowable Stress for Steel; L/t Range Is 5000 to 10 000

Thickness t		Unit Torque M		Thickness t		Unit Torque M	
mm	in	N·m/10 mm of width	lb·in/in of width	mm	in	N·m/10 mm of width	lb·in/in of width
0.127	0.005	0.0587	1.32	1.30	0.051	4.132	92.90
0.152	0.006	0.0841	1.89	1.37	0.054	4.541	102.1
0.178	0.007	0.1094	2.46	1.45	0.057	4.991	112.2
0.203	0.008	0.1419	3.19	1.60	0.063	5.947	133.7
0.229	0.009	0.1775	3.99	1.70	0.067	6.619	148.8
0.254	0.010	0.2171	4.88	1.83	0.072	7.504	168.7
0.279	0.011	0.2620	5.89	1.93	0.076	8.282	186.2
0.305	0.012	0.3074	6.91	2.03	0.080	8.981	201.9
0.330	0.013	0.3567	8.02	2.18	0.086	10.37	233.2
0.356	0.014	0.4101	9.22	2.34	0.092	11.74	264.0
0.381	0.015	0.4679	10.52	2.49	0.098	13.12	295
0.406	0.016	0.5271	11.85	2.67	0.105	14.86	334
0.432	0.017	0.5876	13.21	2.84	0.112	16.59	373
0.457	0.018	0.6530	14.68	3.05	0.120	18.82	423
0.483	0.019	0.7215	16.22	3.18	0.125	20.24	455
0.508	0.020	0.7953	17.88	3.43	0.135	23.35	525
0.584	0.023	1.025	23.05	3.58	0.141	25.35	570
0.635	0.025	1.189	26.72	3.76	0.148	27.76	624
0.711	0.028	1.452	32.65	3.96	0.156	30.69	690
0.813	0.032	1.841	41.40	4.11	0.162	33.00	742
0.889	0.035	2.144	48.20	4.50	0.177	39.23	882
1.041	0.041	2.824	63.50	4.75	0.187	43.81	985
1.19	0.047	3.585	80.60				

SOURCE: Associated Spring, Barnes Group Inc.

6.13 HOT-WOUND SPRINGS

6.13.1 Introduction

Springs are usually cold-formed when bar or wire diameters are less than 10 mm (approximately ⅜ in). When the bar diameter exceeds 16 mm (approximately ⅝ in), cold forming becomes impractical and springs are hot-wound.

Hot winding involves heating the steel into the austenitic range, winding hot, quenching to form martensite, and then tempering to the required properties. Although the most common types of hot-wound springs are compression springs for highway, off-highway, and railroad-vehicle suspension applications, torsion and extension springs can also be hot-wound.

6.13.2 Special Design Considerations

Design equations for hot-wound springs are the same as those for cold-formed springs except for the use of an empirical factor K_H which adjusts for effects related to hot-winding springs. Multiply the spring rate by K_H.

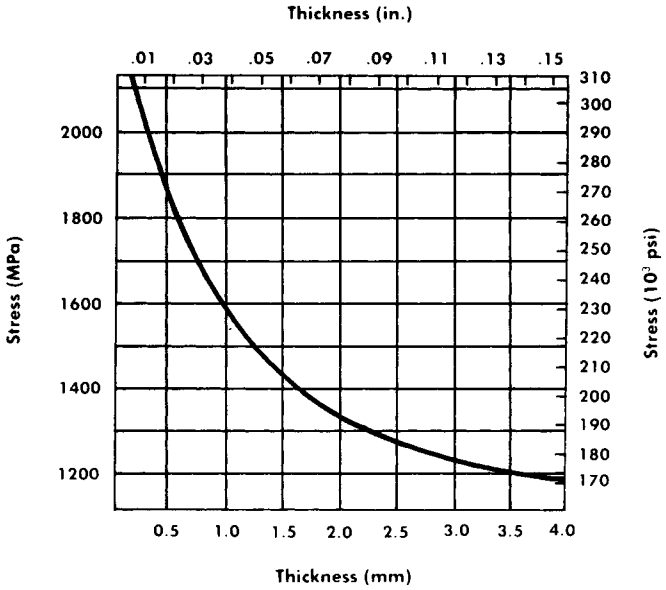

FIGURE 6.51 Average maximum solid stress in carbon-steel power springs. *(Associated Spring, Barnes Group Inc.)*

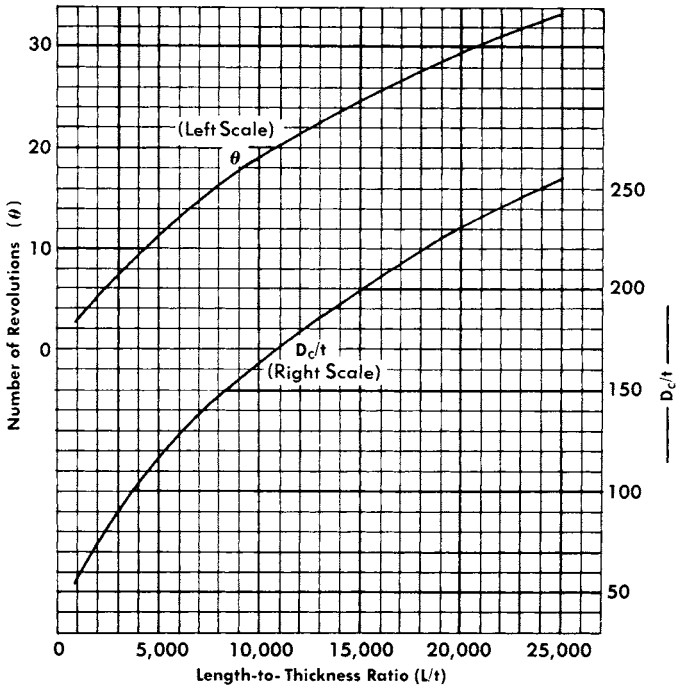

FIGURE 6.52 Relationships among number of revolutions, case diameter, strip length, and thickness for power springs. *(Associated Spring, Barnes Group Inc.)*

The values for factor K_H are 0.91 for springs made from hot-rolled carbon or low-alloy steel, *not* centerless ground; 0.96 for springs made from hot-rolled carbon or low-alloy steel, centerless ground; and 0.95 for torsion springs made from carbon or low-alloy steel.

The ends of hot-wound springs can be open or squared or either ground or not ground. Solid height is calculated in the same way as for cold-wound springs; but when space is limited, L_s can be reduced to $(N_t - 0.5)d$ by using a heavy grind.

The end configurations of extension or torsion springs must be formed hot at the same time as the spring is wound. If the configuration is complex, they may become cool in the process, and the whole spring may have to be reheated into the austenitic range. Note that hot-wound extension springs cannot have initial tension.

6.13.3 Materials

The common hot-wound alloys are AISI 5160, 5160H, and 1095 steels. The normal range of hardness is from HRC 44 to 48. Corresponding tensile strengths are 1430 to 1635 MPa.

The hot-rolled wire used in hot-wound springs is produced in standard sizes. Bar diameter variation and bar out-of-roundness tolerances are approximated in Table 6.28.

6.13.4 Choice of Operating Stress

Static Applications. The stress is calculated as in cold-wound springs. Use Table 6.29 for set-point information.

Cyclic Applications. Hot-wound springs made from hot-rolled wire are used in cyclic applications because rolled bars are subject to a variety of characteristic material defects mostly related to the bar surface condition. Therefore Table 6.30 can be

TABLE 6.28 Diameter and Out-of-Roundness Tolerances for Hot-Rolled Carbon-Steel Bars

Diameter mm(in.) Over	Through	Tolerance ± mm(in.)	Out-of-Roundness mm(in.)
	8 (0.315)	0.13 (0.005)	0.20 (0.008)
8 (0.315)	10 (0.394)	0.15 (0.006)	0.22 (0.009)
10 (0.394)	15 (0.591)	0.18 (0.007)	0.27 (0.011)
15 (0.591)	20 (0.787)	0.20 (0.008)	0.30 (0.012)
20 (0.787)	25 (0.984)	0.23 (0.009)	0.34 (0.013)
25 (0.984)	30 (1.181)	0.25 (0.010)	0.38 (0.015)
30 (1.181)	35 (1.378)	0.30 (0.012)	0.45 (0.018)
35 (1.378)	40 (1.575)	0.35 (0.014)	0.52 (0.020)
40 (1.575)	60 (2.362)	0.40 (0.016)	0.60 (0.024)
60 (2.362)	80 (3.150)	0.60 (0.024)	0.90 (0.035)

SOURCE: Associated Spring, Barnes Group Inc.

TABLE 6.29 Maximum Allowable Torsional Stress for Hot-Wound Helical Compression Springs in Static Applications

Before Set Removal	After Set Removal
50% of TS	65–75% of TS

Torsional stress after set removal depends on material size and amount of set removed.

SOURCE: Associated Spring, Barnes Group Inc.

TABLE 6.30 Maximum Allowable Torsional Stress for Hot-Wound Helical Compression Springs in Cyclic Applications

Fatigue Life (Cycles)	Percent of Tensile Strength	
	Not Shot-Peened	Shot-Peened
10^5	40	48
10^6	38	46
10^7	35	43

This information is based on **centerless ground** AISI 5160, 5160H and 1095, HRC 44 to 48, 25 mm (1″) diameter. Set has not been removed. Conditions are: no surging, room temperature and non-corrosive environment.

$$\text{Stress ratio in fatigue} = \frac{\text{S Minimum}}{\text{S Maximum}} = 0.$$

SOURCE: Associated Spring, Barnes Group Inc.

used only for centerless ground alloy bars. Practical manufacturing tolerances for hot-wound springs can be found in ASTM A125.

REFERENCES

6.1 Leonard G. Johnson, *The Statistical Treatment of Fatigue Experiments,* Elsevier Publishing Co., New York, 1964.

6.2 R. E. Little and E. H. Jebe, *Statistical Design of Fatigue Experiments,* John Wiley & Sons, New York, 1975.

6.3 A. M. Wahl, *Mechanical Springs,* 2d ed., McGraw-Hill, New York, 1963.

6.4 W. R. Berry, *Spring Design: A Practical Treatment,* Emmot & Co., London, 1961.

6.5 J. O. Almen and A. Laszlo, "The Uniform Section Disc Spring," *ASME Transactions,* vol. 58, no. 4, May 1936, pp. 305–314.

6.6 A. Blake, *Design of Curved Members for Machines,* Industrial Press, New York, 1966.

6.7 K. E. Bisshopp and D. C. Drucker, "Large Deflections of Cantilever Beams," *Quarterly of Applied Mathematics,* vol. 3, no. 3, 1945, p. 272.

6.8 J. H. Maker, "Steel Springs," *Metals Handbook,* 9th ed., vol. 1, American Society for Metals, Metals Park, Ohio, 1978, pp. 283–313.

6.9 *Design and Manufacture of Volute Springs,* SAE, New York, 1945.

6.10 R. E. Peterson, *Stress Concentration Design Factors,* John Wiley & Sons, New York, 1953, p. 102.

6.11 Karl W. Maier, "Dynamic Loading of Compression Springs," *Product Engineering,* January 1954, pp. 162–167; "Dynamic Loading of Compression Springs," *Product Engineering,* March 1955, pp. 162–172; "Surge Waves in Compression Springs," *Product Engineering,* August 1957, pp. 167–174.

CHAPTER 7
FLYWHEELS

Daniel M. Curtis, Ph.D.
Senior Mechanical Engineer
NKF Engineering, Inc.
Reston, Virginia

LIST OF SYMBOLS

a	Constant, lb·s·ft/rad (J·s/rad)
A	Cross-sectional area of rim, in^2 (m^2)
A_s	Cross-sectional area of spoke, in^2 (m^2)
A_j, B_j, C_j	Difference coefficients
b	Constant, lb·ft (J)
C_s	Coefficient of speed fluctuation
C_u	Coefficient of energy fluctuation
D_j	Difference coefficient, lb (kN)
f_i	Intermediate variable
F	Stress function ($= rt\sigma_r$), lb (kN)
F_s	Geometric shape factor
g	Acceleration of gravity, 32.2 ft/s^2 (9.80 m/s^2)
I	Second moment of area, in^4 (m^4)
j	Index
J	Polar-mass moment of inertia, lb·s^2·ft (N·s^2·m)
K	Coefficient, 33 000 lb·ft·rpm/hp [2π J·rad/(W·s)]
n	Engine speed, rpm (rad/s)
N_c	Number of cylinders
N_s	Number of spokes
P	Power, hp (W)
r	Radial distance, in (m)

Δr	Radial-distance increment, in (m)
r_h	Hub radius, in (m)
r_a	Average radius of rim, in (m)
r_i	Inner radius of rim, in (m)
r_o	Outer radius of rim, in (m)
R	Specific energy, in (m)
S_y	Yield strength, psi (MPa)
t	Time, s
Δt	Time increment, s
T	Torque, lb·ft (J)
T_a	Angle-dependent torque, lb·ft (J)
T_s	Speed-dependent torque, lb·ft (J)
T_j	Torque at end of interval *j,* lb·ft (J)
U	Difference between the flywheel energy at maximum speed and at minimum speed, lb·ft (J)
V	Rim velocity, ft/s (m/s)
W	Weight, lb (kN)
z	Thickness, in (m)
z'	Radial derivative of flywheel thickness (= dz/dr)
z_0	Thickness at center, in (m)
Z_r	Section modulus of rim, in^3 (m^3)
Z_s	Section modulus of spoke, in^3 (m^3)
2α	Angle between adjacent spokes (see Fig. 7.6), rad
β	Angle, rad
θ	Angular position, rad
θ_{max}	Maximum angular deviation from constant-speed position, rad
θ_0	Angular position at start of machine cycle, rad
$\Delta\theta$	Angular increment, rad
ν	Poisson's ratio
ξ	Time, s
ρ	Weight density, lb/in^3 (kN/m^3)
σ	Stress, psi (MPa)
σ_0	Stress constant, psi (MPa)
σ_r	Radial stress, psi (MPa)
σ_t	Tangential stress, psi (MPa)
ω	Rotational speed, rad/s
ω_{max}, ω_{min}	Maximum and minimum speed, rad/s
ω_{avg}	Average speed [= $0.5(\omega_{max} + \omega_{min})$], rad/s
ω_0	Speed at start of machine cycle, rad/s
$\Delta\omega$	Maximum deviation of speed from average value, rad/s
ω_j	Speed at end of interval *j,* rad/s

The energy-storage capacity of a flywheel is determined from its polar moment of inertia J and its maximum safe running speed. The necessary inertia depends on the cyclic torque variation and the allowable speed variation or, in the case of energy-storage flywheels, the maximum energy requirements. The safe running speed depends on the geometry and material properties of the flywheel.

7.1 FLYWHEEL USAGE

Flywheels store energy. Indeed, flywheels are used as energy reservoirs, and this use will be discussed in Sec. 7.4. Their principal use in machine design, however, is to smooth the variations in shaft speed that are caused by loads or power sources that vary in a cyclic fashion. By using its stored kinetic energy $0.5J\omega^2$ to absorb the variations in torque during a machine cycle, a flywheel smooths the fluctuating speed of a machine and reduces undesirable transient loads. The effect of a flywheel is therefore fundamentally different from that of a regulator: A flywheel limits the speed variation over one cycle and has minimal effect on the average speed; a regulator uses negative feedback to maintain a selected average speed with only secondary effects on the speed during a cycle.

The flywheel has other features which have to be considered in design. Its size, speed, and windage effect can all be used to advantage in providing a secondary function as part of a clutch, gear, belt pulley, cooling fan, pump, gyroscope, or torsional damper.

7.2 SIZING THE FLYWHEEL

7.2.1 Coefficient of Speed Variation

A certain amount of fluctuation in shaft speed will not cause harmful torques or reduce the usefulness of a machine. The *coefficient of speed fluctuation* C_s is defined as

$$C_s = \frac{\omega_{max} - \omega_{min}}{\omega_{avg}} \tag{7.1}$$

where ω = rotational speed at the flywheel and ω_{avg} = average of ω_{max} and ω_{min}. Ranges for C_s for several categories of speed variation are given in Table 7.1. Assume that the system is stiff (the speeds of all shafts are proportional), that the external torque input or load is constant, and that ω_{avg} is close to the constant speed at which the energy from the average torque balances the external energy (this is usually a good assumption for values of C_s up to about 0.2). The energy equation $U = 0.5J(\omega_{max}^2 - \omega_{min}^2)$ and the definition of C_s combine to give the equation for the required mass moment of inertia [7.11]:

$$J = \frac{U}{\omega_{avg}^2 C_s} \tag{7.2}$$

This inertia includes the flywheel inertia and the inertia of all rotating parts, referred to the flywheel speed by multiplying by the square of the ratio of the shaft speeds.

TABLE 7.1 Suggested Values for the Coefficient of Speed Fluctuation C_s

Required speed uniformity	C_s
Very uniform	≤0.003
Moderately uniform	0.003–0.012
Some variation acceptable	0.012–0.05
Moderate variation	0.05–0.2
Large variation acceptable	≥0.2

Example 1. During each punching cycle, the cranking shaft for a punching operation does 270 J of work while rotating 30 degrees, as shown in Fig. 7.1. No work is done during the remaining 330 degrees. What size flywheel is necessary if the speed at the location of the flywheel is 20 rad/s and the inertia of the other rotating parts referred to the flywheel is 0.51 $N \cdot s^2 \cdot m$?

The average work required is $270/(2\pi) = 43.0$ J/rad. The motor will supply this constant torque throughout the cycle. Referring to Fig. 7.1, the flywheel will give up some of its stored energy during the 30 degrees of actual punching. This is the shaded area above the average-torque line; the motor will supply the additional 43 J/rad. During the remaining 330 degrees, the motor will resupply the flywheel, as shown by the shaded area below the average-torque line. The flywheel speed reaches its maximum and minimum where the loading torque crosses the average-torque line.

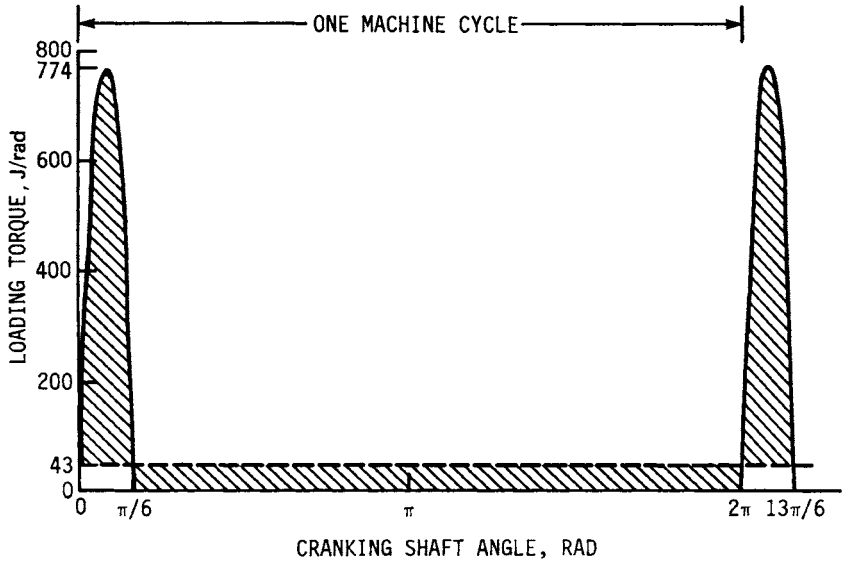

FIGURE 7.1 Torque-angle curve for punching operation in Example 1. The dashed line indicates the average torque of 43 J/rad, and the shaded areas are each equal to the maximum energy variation of 247 J.

Since the torque-angle curve is steep at both ends, the area above the average torque line is the total area minus the small rectangle below the average. The energy variation is then

$$U = 270 - 43.0\left(\frac{\pi}{6}\right) = 247 \text{ J} \tag{7.3}$$

The relative speed between the cranking shaft and the flywheel is unimportant since the energy (torque times angle) is the same at either speed. Letting $C_s = 0.10$ for a moderate speed variation, Eq. (7.2) gives the necessary flywheel inertia:

$$J = \frac{247}{20^2(0.10)} - 0.51 = 5.67 \text{ N}\cdot\text{s}^2\cdot\text{m} \tag{7.4}$$

For a steel-rim-type flywheel, assuming that 10 percent of the inertia is provided by the hub and spokes, the flywheel rim with a 0.5-m average rim diameter will weigh approximately

$$W = \frac{Jg}{r_a^2} = \frac{0.9(5.67)(9.80)}{0.25^2(1000)} = 0.800 \text{ kN} \tag{7.5}$$

Using a density of 76.5 kN/m^3, the necessary cross-sectional area is then given by

$$A = \frac{Jg}{2\pi\rho r_a^3} = \frac{0.9(5.67)(9.80)}{2\pi(76.5)(0.25)^3(1000)} = 0.006\,66 \text{ m}^2 \tag{7.6}$$

Assuming that the speed is at its average during the peak torque of 774 J, the peak power required without any flywheel effect would be

$$P = T\omega = 774(20)(0.001) = 15.5 \text{ kW} \tag{7.7}$$

Without a flywheel, the design limitation on the speed fluctuation would have to be met using a nonuniform input torque. With the flywheel, the required power is determined from the average torque of 43.0 J:

$$P = T\omega = 43.0(20)(0.001) = 0.9 \text{ kW} \tag{7.8}$$

This shows that in addition to smoothing the machine operation, the flywheel actually reduces the size of the motor required.

7.2.2 Integration of the Torque-Angle Relation

If the torque-angle curve for a machine cycle is available from experimental data or a dynamic analysis, U is determined from the areas between the curve and the average-torque line. If the external torque input or load is not constant, it can be combined with the torque-angle curve for the machine. If the loading torque and the driving torque are not synchronized or have an unknown phase difference, a worst-case combination should be used. The areas under the curve can be determined using a planimeter or by graphic or numerical integration. (See Example 4.) Unless C_s is accurately known and the curve is from a worst case or is highly repeatable, precision in integrating is not warranted.

Example 2. An engine has the torque-angle curve given in Fig. 7.2. If the average speed at the flywheel is 2000 rpm and the output speed is allowed to vary by ±2.5 percent, how large a flywheel is necessary if the loading torque is assumed constant? The inertia of the other rotating parts, referred to the flywheel, is 0.11 lb·s^2·ft.

The net area under the curve, using a planimeter, is 1156 lb·ft. One machine cycle for the four-stroke engine consists of two crankshaft cycles. The average torque is therefore 1156/(4π) = 92.0 lb·ft. This average torque is shown as the dashed line in Fig. 7.2. The maximum and minimum velocities will occur at the points where the curve crosses this line. Each area between crossover points is measured and tabulated (see Table 7.2). The relative maxima and minima of the speed occur at the crossover points; therefore, the largest energy difference between any two crossover points will determine U. Since these two points will not necessarily be adjacent to each other, a running sum of the individual areas $A + I$ through H is formed, starting at an arbitrary crossover point. The largest energy difference is then the maximum sum minus the minimum sum; in this case, $U = 1106 - (-95) = 1201$ lb·ft. With $\omega = 2\pi(2000)/60 = 209.4$ rad/s and $C_s = 2(0.025) = 0.05$, Eq. (7.2) gives

$$J = \frac{1201}{209.4^2(0.05)} - 0.11 = 0.438 \text{ lb}\cdot\text{s}^2\cdot\text{ft} \tag{7.9}$$

Note that if the engine were operated at a slower speed, Eq. (7.2) indicates that a larger flywheel would be necessary even if the torque-angle curve did not change.

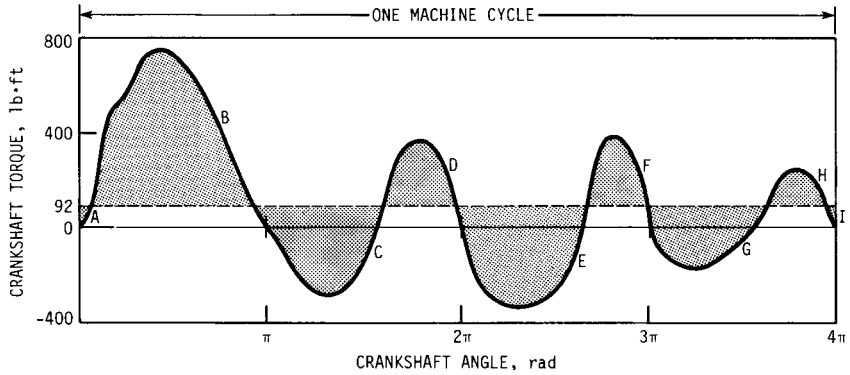

FIGURE 7.2 Torque-angle curve for the engine in Example 2. The dashed line indicates the average torque of 92.0 lb·ft, and the shaded areas are the energy variations from the average speed. Sections A and I correspond to the values given in Table 7.2.

TABLE 7.2 Area Sums for Example 2

Section	$A + I$	B	C	D	E	F	G	H
Area, lb·ft	−18	1124	−550	242	−710	208	−391	95
Sum, lb·ft	−18	1106	556	798	88	296	−95	0
Extreme values, lb·ft		1106					−95	

7.2.3 Coefficient of Energy Variation

The torque-angle relationship for an engine depends on the fuel, gas pressures, reciprocating masses, speed, and engine geometry [7.2]. The large variation that is possible between different engine designs shows that dynamic measurement or kinematic analysis is necessary to determine the torque fluctuation. It is often necessary, however, to come up with a rough estimate for preliminary design purposes or for checking the reasonableness of calculated values. For these purposes, the energy variation for an internal-combustion engine can be estimated by

$$U = C_u \frac{KP}{\omega} \tag{7.10}$$

where $K = 33\,000$ lb·ft·rpm/hp [2π J·rad/(W·s)]. The coefficient of energy variation C_u can be approximated for a two-stroke engine with from 1 to 8 cylinders using the equation

$$C_u = \frac{7.46}{(N_c + 1)^3} \tag{7.11}$$

and for a four-stroke engine with from 1 to 16 cylinders using the two-branched equation

$$C_u = \frac{0.8}{|N_c - 1.4|^{1.3}} - 0.015 \tag{7.12}$$

Example 3. A 150-hp four-cylinder, four-stroke engine has a flywheel speed of 1000 rpm. Estimate the flywheel necessary for a 2 percent speed variation with a uniform load at an engine speed of 3000 rpm, neglecting the flywheel effect of the other rotating parts.

Using Eq. (7.12),

$$C_u = \frac{0.8}{|4 - 1.4|^{1.3}} - 0.015 = 0.22 \tag{7.13}$$

Then from Eq. (7.10),

$$U = 0.22 \frac{33\,000(150)}{3000} = 363 \text{ lb·ft} \tag{7.14}$$

so that from Eq. (7.2), with $\omega = 2\pi(1000)/60 = 105$ rad/s,

$$J = \frac{363}{105^2(0.02)} = 1.6 \text{ lb·s}^2\text{·ft} \tag{7.15}$$

7.2.4 Angular Fluctuation

Certain machines, such as electric generators and magnetic digital storage systems, must maintain their angular position within a close tolerance of the constant-speed position. If the torque is known as a function of time, it can be integrated to deter-

mine the angular velocity, and then the angular velocity can be integrated to give the angular position:

$$\omega(t) = \int_0^t \frac{T(\xi)}{J}\, d\xi + \omega_0 \tag{7.16}$$

$$\theta(t) = \int_0^t \omega(\xi)\, d\xi + \omega_0 t + \theta_0 \tag{7.17}$$

where the $\omega_0 t + \theta_0$ term represents the constant-speed position.

In the more usual instance, the torque is known only as a function of angle. For small values of C_s, however, the torque-time curve is indistinguishable from the torque-angle curve with the angle coordinate divided by ω_{avg}.

Example 4. A generator with the input torque given in Fig. 7.3*a* must maintain an angular position within ±0.25 degrees of the uniform 200-rpm position. Assuming a uniform load, what flywheel inertia is necessary?

For illustration purposes, the machine cycle will be divided into 10 intervals of $\Delta t = 0.03$ s each, as shown in Fig. 7.3*a.* For an accurate solution, the problem would be programmed with perhaps 20 intervals.

The torque at each step is tabulated (column 3 in Table 7.3), and then the average torque in each interval is placed in column 4. This value, if multiplied by Δt, would be the area below the curve using the trapezoid rule. Adding these average torques (column 5) and dividing by 10 intervals gives the average torque for the curve, 902 lb·ft (column 6), shown as the dashed line in Fig. 7.3*a.* Subtracting this average, the constant loading torque, from column 4 gives column 7, the average excess of supplied torque in each interval. The running sum of these values (column 8) performs the integration, to give $J\omega/\Delta t$ (see Fig. 7.3*b*). The relative speed at the end of each interval is therefore the value in column 8 times $\Delta t/J$.

The procedure is repeated for the second integration, giving columns 9 through 13. Column 13 is then $J\theta/(\Delta t)^2$ (Fig. 7.3*c*), so that the relative angular position is the value in column 13 times $\Delta t^2/J$. The maximum range in column 13 is 6915 – (–7725) = 14 640 lb·ft. The maximum angular deviation from the mean position is calculated from half the maximum range, so that

$$\theta_{max} = \frac{(\Delta t)^2(14\,640)}{J(2)} \tag{7.18}$$

For $\theta_{max} = 0.25$ degrees = 0.004 36 rad deviation, this gives

$$J = \frac{0.03^2(14\,640)}{0.004\,36(2)} = 1511 \text{ lb}\cdot\text{s}^2\cdot\text{ft} \tag{7.19}$$

The speed variation is determined as a by-product of the process. The maximum range in column 8 is 9878 – 0 = 9878 lb·ft. The maximum speed variation is then

$$\omega_{max} - \omega_{min} = \frac{\Delta t(9878)}{J} = \frac{0.03(9878)}{1511} = 0.196 \text{ rad/s} \tag{7.20}$$

For $\omega_{avg} = 2\pi(200)/60 = 20.94$ rad/s, the coefficient of speed fluctuation is then, from Eq. (7.1),

$$C_s = \frac{0.196}{20.94} = 0.009\,36 \tag{7.21}$$

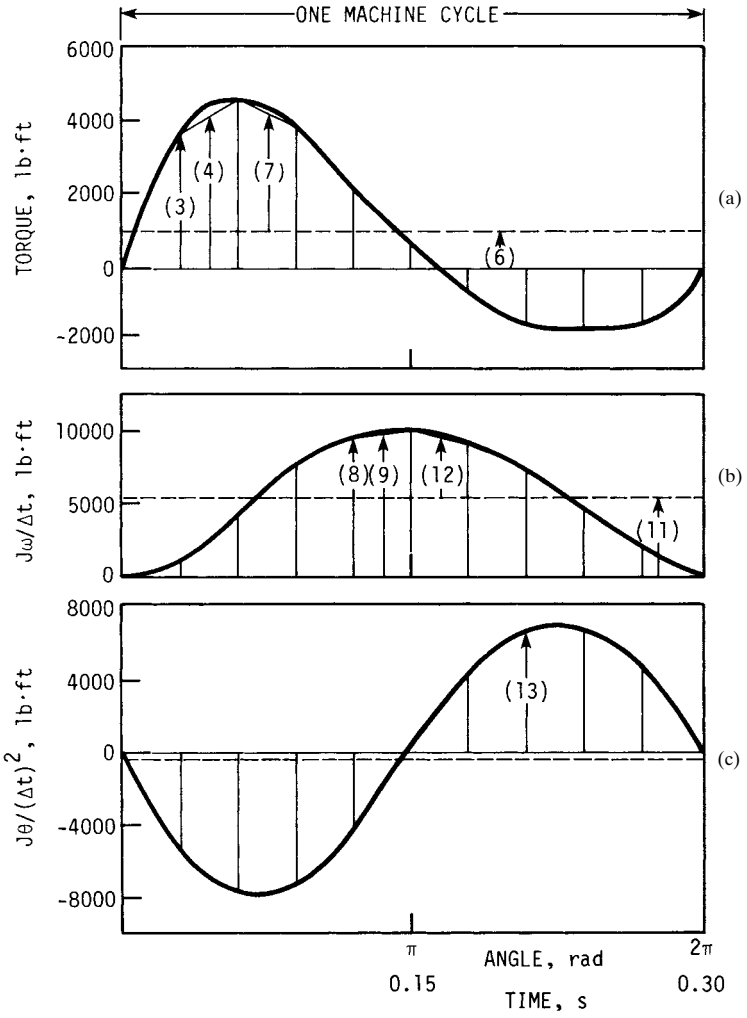

FIGURE 7.3 (*a*) Torque-angle or torque-time curve for Example 4. Dashed lines indicate average values, and the numbers in parentheses represent typical values found in Table 7.3. (*b*) Calculated rotational speed. (*c*) Calculated rotation angle.

7.2.5 Speed-Dependent Torques

The input and loading torques are in reality a function of angle, time, speed, acceleration, and other factors. In most cases, the assumption that they are functions of angle only is a good one. In some applications, however, different assumptions are necessary.

Figure 7.4 shows the torque-speed relationship for an induction motor. The curve can be approximated by a straight line $T_s = a\omega + b$ in the recommended operating

TABLE 7.3 Numerical Integration for Example 4

j (1)†	t, s (2)	T, lb·ft (3)	Area, $[(3)_j + (3)_{j-1}]/2$, lb·ft (4)	Area − Avg. [(4) − (6)], lb·ft (7)	Sum Σ (7), lb·ft (8)	Area $[(8)_j + (8)_{j-1}]/2$, lb·ft (9)	Area − Avg. [(9) − (11)], lb·ft (12)	Sum Σ (12), lb·ft (13)
0	0	0	0	0	0	0	0	0
1	0.03	3670	1835‡	933	933	467	−4908	−4908
2	0.06	4628	4149	3247	4181	2557	−2818	−7725
3	0.09	3830	4229	3327	7508	5845	470	−7256
4	0.12	1931	2881	1979	9487	8498	3123	−4132
5	0.15	654	1293	391	9878	9683	4308	175
6	0.18	−734	−40	−942	8936	9407	4033	4208
7	0.21	−1628	−1181	−2083	6854	7895	2521	6729
8	0.24	−1739	−1684	−2585	4269	5561	187	6915
9	0.27	−1596	−1668	−2569	1700	2984	−2390	4525
10	0.30	0	−798	−1700	0	850	−4525	0
			(5) Sum 9016			(10) Sum 53 746		
			(6) Avg. 902			(11) Avg. 5375		

†See Example 4 and Fig. 7-3 for a description of each column.
‡The table entries were calculated to a higher precision and rounded.

range [7.7]. If the torque-angle curve is known for the loading torque T_a, the speed equation is

$$\omega^2(\theta) - \omega_0^2 = \frac{2}{J}\int_0^{\theta} [a\omega(\beta) + b - T_a(\beta)]\, d\beta \tag{7.22}$$

This equation is implicit in ω, and the initial value ω_0 is unknown. Dividing the angle for one cycle into intervals $\Delta\theta$ long and letting ω_j denote the speed at the end of j intervals, the trapezoidal rule gives

$$\omega_j^2 - \omega_0^2 = \frac{2}{J}\left(\frac{a(\omega_0 + 2\omega_1 + 2\omega_2 + \cdots + 2\omega_{j-1} + \omega_j)}{2} + jb - \frac{T_0 + 2T_1 + 2T_2 + \cdots + 2T_{j-1} + T_j}{2}\right)\Delta\theta \tag{7.23}$$

where T_0 through T_j are the values of T_a at the end of each interval. The unknowns in this equation are ω_j and ω_0. If a value for ω_0 is assumed, the quadratic equation gives

$$\omega_j = A_j + \sqrt{A_j^2 + B_j} \tag{7.24}$$

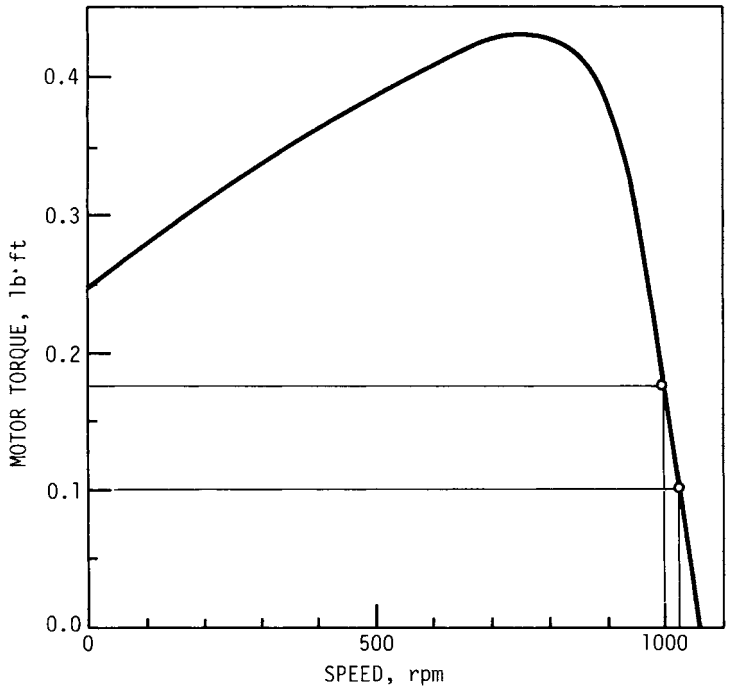

FIGURE 7.4 Torque-speed curve for the induction motor of Example 5. The curve can be approximated by a straight line near the recommended full-torque operating speed of 1000 rpm.

where

$$A_j = \frac{a\,\Delta\theta}{2J} \tag{7.25}$$

$$B_j = \omega_0^2 + \left[\frac{a}{2}\left(\omega_0 + 2\omega_1 + \cdots + 2\omega_{j-1}\right) + C_j\right]\frac{2\,\Delta\theta}{J} \tag{7.26}$$

and

$$C_j = jb - \frac{T_0 + 2T_1 + 2T_2 + \cdots + 2T_{j-1} + T_j}{2} \tag{7.27}$$

Equation (7.24) is solved successively for each j. The calculated value of ω at the end of the final interval will not in general equal the value that was originally assumed for ω_0. If the calculation is rerun with this final speed as the assumed value for ω_0, the numbers will be closer. After a few calculation cycles, the answers will converge.

Example 5. An induction motor provides 0.175 lb·ft of torque at the recommended full-load operating speed of 1000 rpm. The linear portion of the torque-speed curve also goes through the point of 0.102 lb·ft torque at 1025 rpm. Using the torque-angle curve for the load given in Fig. 7.5, find C_s if the load has the same 200-rpm speed as the flywheel and $J = 0.085$ lb·s^2·ft referred to the flywheel.

The motor has been chosen so that the average loading torque balances the motor torque at the recommended speed; since the speed of the motor is 1000/200 = 5 times the speed of the load, the average load should be approximately $T = 5(0.175) = 0.875$ lb·ft.

Referring the motor torques and speeds to the flywheel speed, the two points on the torque-speed curve become 0.175(5) = 0.875 lb·ft at 1000/5 = 200 rpm and 0.102(5) = 0.510 lb·ft at 1025/5 = 205 rpm. With 200 rpm = 2π(200)/60 = 20.944 rad/s

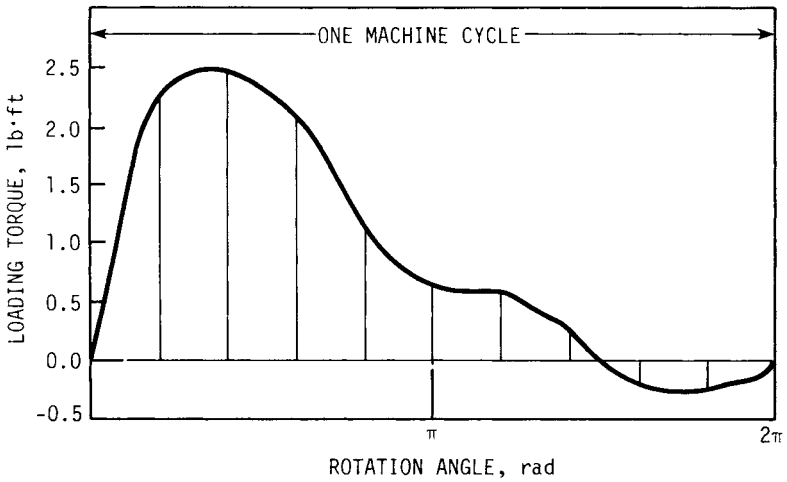

FIGURE 7.5 Torque-angle curve for the load in Example 5.

and 205 rpm = $2\pi(205)/60 = 21.468$ rad/s, the equation for the linear part of the torque-speed curve for the motor, referred to the flywheel, is given by the two-point formula

$$\frac{T_s - 0.875}{\omega - 20.944} = \frac{0.510 - 0.875}{21.468 - 20.944} \tag{7.28}$$

or

$$T_s = -0.697\omega + 15.46 \tag{7.29}$$

Therefore, $a = -0.697$ lb·s·ft/rad and $b = 15.46$ lb·ft.

For illustration purposes, the machine cycle will be divided into 10 intervals of $\pi/5$ rad each (see Fig. 7.5). For an accurate solution, the problem would be programmed on a computer with perhaps 50 intervals. The loading torque at the end of each interval is first tabulated as shown in column 3 in Table 7.4. The average torque in each interval, $0.5(T_{j-1} + T_j)$, is placed in column 4, and the cumulative sum of these numbers is placed in column 5. The values in column 5 thus represent the T summation in Eq. (7.27). In column 6 these values are subtracted from $jb = j(15.46)$ to form C_j. The values in columns 1 through 6 will not be changed in the iteration process.

For the first iteration, a value of $\omega_0 = 20.944$ rad/s is chosen as an initial guess of the speed at the start of the cycle. For $j = 1$, $\omega_{j-1} = \omega_0 = 20.944$ rad/s is placed in column 7. As column 7 is filled, column 8 will be formed as the summation $\omega_0 + 2\omega_1 + 2\omega_2 + \cdots + 2\omega_{j-1}$ required in Eq. (7.26). B_j is then evaluated from Eq. (7.26) using the values of a, C_j, ω_0, and $2\,\Delta\theta/J = 2(\pi/5)/0.085 = 14.784$ rad/(lb·s^2·ft) and placed in column 9. With $A_j = -0.697(\pi/5)(0.5)/0.085 = -2.576$ rad/s, Eq. (7.24) can be evaluated to give ω_j. For $j = 1$, $\omega_1 = 20.87$ rad/s is thus placed in column 10. This value is then brought over to column 7 for $j = 2$ and the process is repeated until column 10 is filled. The last value in column 10, 21.59 rad/s, is the speed at the end of the cycle using the initial guess for ω_0. Then 21.59 rad/s is used as the ω_0 value for the second iteration, producing columns 11 through 14. This process is repeated until the final speed for the cycle equals the initial speed that was assumed. In this example this takes three iterations, giving the speed variation given in column 18.

The maximum and minimum speeds, from column 18, are 21.64 rad/s and 20.32 rad/s. From Eq. (7.1), C_s is then this range divided by the average:

$$C_s = \frac{\omega_{max} - \omega_{min}}{0.5(\omega_{max} + \omega_{min})} = \frac{21.64 - 20.32}{0.5(21.64 + 20.32)} = 0.063 \tag{7.30}$$

7.3 STRESS

7.3.1 Rim-Type: No Bending

If interaction with the spokes is ignored, the stress in a thin-rim flywheel is the uniform hoop stress:

$$\sigma = \frac{\rho r_a^2 \omega^2}{g} = \frac{\rho V^2}{g} \tag{7.31}$$

Since the stress is a function of velocity, the strength of flywheel materials can be given in terms of maximum rim velocity (see Sec. 7.5.1).

TABLE 7.4 Numerical Tabulation for Example 5

j	θ, rad	T	Avg.	Sum	C_j	ω_{j-1}	Sum†	B_j, (rad/s)^2	ω_j, rad/s	ω_{j-1}	Sum†	B_j, (rad/s)^2	ω_j, rad/s	ω_{j-1}	Sum†	B_j, (rad/s)^2	ω_j, rad/s
		lb·ft				rad/s				rad/s				rad/s			
(1)‡	(2)	(3)	(4)	(5)	(6)	(7)	(8)	(9)	(10)	(11)	(12)	(13)	(14)	(15)	(16)	(17)	(18)
0	0	0.00	0.000	0.000	. . . .	. . . .	. . . .	. . . .	20.94	. . . .	. . . .	. . . .	21.59	. . . .	. . . .	. . . .	21.64
1	$\pi/5$	2.22	1.110§	1.110	14.35	20.94	20.94	542.89	20.87	21.59	21.59	566.90	21.37	21.64	21.64	568.89	21.41
2	$2\pi/5$	2.43	2.325	3.435	27.49	20.87	62.68	522.07	20.42	21.37	64.33	540.86	20.82	21.41	64.47	542.42	20.86
3	$3\pi/5$	2.06	2.245	5.680	40.70	20.42	103.51	507.05	20.09	20.82	105.98	521.67	20.41	20.86	106.18	522.88	20.44
4	$4\pi/5$	1.08	1.570	7.250	54.59	20.09	143.69	505.40	20.05	20.41	146.79	516.71	20.30	20.44	147.05	517.66	20.32
5	π	0.62	0.850	8.100	69.20	20.05	183.79	514.77	20.26	20.30	187.40	523.52	20.45	20.32	187.69	524.25	20.46
6	$6\pi/5$	0.55	0.585	8.685	84.08	20.26	224.31	525.93	20.50	20.45	228.29	532.72	20.65	20.46	228.62	533.29	20.66
7	$7\pi/5$	0.23	0.390	9.075	99.15	20.50	265.31	537.47	20.75	20.65	269.59	542.75	20.86	20.66	269.94	543.19	20.87
8	$8\pi/5$	−0.20	0.015	9.090	114.59	20.75	306.81	551.99	21.06	20.86	311.31	556.11	21.15	20.87	311.69	556.45	21.15
9	$9\pi/5$	−0.26	−0.230	8.860	130.28	21.06	348.93	566.95	21.37	21.15	353.61	570.17	21.44	21.15	353.99	570.44	21.45
10	2π	0.00	−0.130	8.730	145.87	21.37	391.68	577.19	21.59	21.44	396.49	579.72	21.64	21.45	396.89	579.93	21.64
						$\omega_0 = 21.59$				$\omega_0 = 21.64$				$\omega_0 = 21.64$			

†$\omega_1 + 2\omega_2 + 2\omega_3 + \cdots + 2\omega_{j-1}$
‡See Example 5 for a description of each column.
§The table entries were calculated to a higher precision and rounded.

Example 6. An alloy of density 26.6 kN/m^3 has an allowable stress of 70 MPa. For a flywheel speed of 200 rad/s, what is the largest possible average radius, overlooking the additional stress caused by the spokes?

From Eq. (7.31),

$$V = \sqrt{\frac{g\sigma}{\rho}} = \sqrt{\frac{9.80(70)(1000)}{26.6}}$$

$$= 160.6 \text{ m/s} \tag{7.32}$$

and

$$r_a = \frac{V}{\omega} = \frac{160.6}{200} = 0.803 \text{ m} \tag{7.33}$$

7.3.2 Rim-Type: With Bending

If the effects of the spoke are taken into account, Timoshenko showed that the tensile stress in the thin rim (Fig. 7.6), including bending but neglecting the effect of the curvature on the bending stress and assuming spokes of constant cross-sectional area, can be calculated from beam theory using Castigliano's theorem [7.10], giving

$$\sigma = \frac{\rho r_a^2 \omega^2}{g}\left[1 - \frac{f_4}{3} + \frac{A r_a}{3 Z_r}\left(f_4 - \frac{1}{f_3 \alpha}\right)\right] \tag{7.34}$$

where

$$f_1 = \frac{1}{2\sin^2\alpha}\left(\frac{\sin 2\alpha}{4} + \frac{\alpha}{2}\right) \qquad f_2 = f_1 - \frac{1}{2\alpha} \tag{7.35}$$

$$f_3 = \frac{A r_a^2 f_2}{I} + f_1 + \frac{A}{A_s} \qquad f_4 = \frac{\cos\beta}{f_3 \sin\alpha} \tag{7.36}$$

and the section modulus of the rim Z_r is positive for the outer face of the rim and negative for the inner face. The stress in the spokes is given by

$$\sigma = \frac{\rho r_a^2 \omega^2}{6g}\left(3 + \frac{4A}{f_3 A_s} - \frac{3r^2}{r_a^2}\right) \tag{7.37}$$

In addition, there will be bending stresses in the spokes as power is exchanged with the flywheel. This torque might be determined by the maximum shaft torque, by the minimum braking time from full speed, or, if the flywheel also serves as a pulley, by the difference in belt force between the power and slack sides.

Depending on how thick the rim is, the spoke will behave as something between an end-loaded cantilever and a guided cantilever. For a thin rim, the maximum bending stress on the spokes will occur at the hub, assuming that they do not taper more than the usual 10 to 25 percent. This bending stress is

$$\sigma = \frac{T(r_a - r_h)}{Z_s N_s r_a} \tag{7.38}$$

If the flywheel serves as a pulley, the torque is not equally distributed to the spokes; the value for N_s should be halved in this case. For a flywheel with a large rim

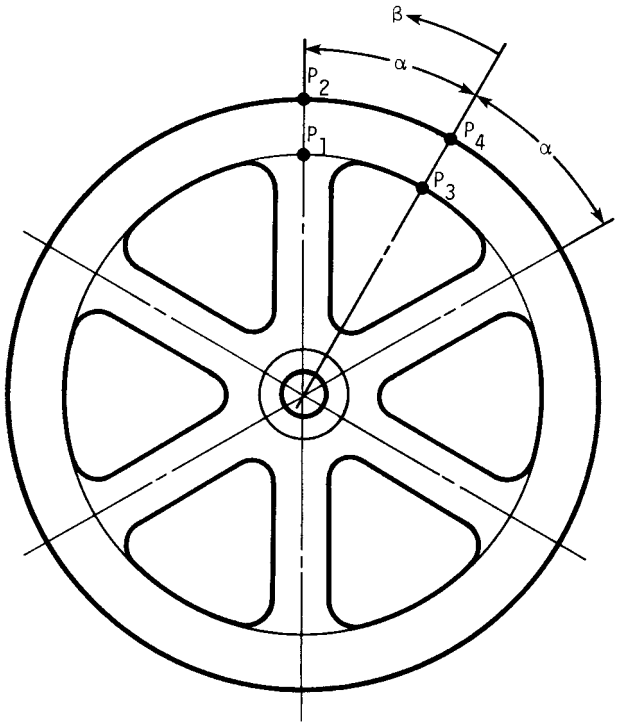

FIGURE 7.6 Rim-type flywheel. The angular position β is measured from the center line bisecting the adjacent spoke locations. Points P_1 through P_4 correspond to the values given in Table 7.5.

section in comparison to the spokes, the spokes act as guided cantilevers and have a maximum bending stress that is half the value given by Eq. (7.38).

Example 7. A cast-iron flywheel with a rectangular rim 5 in thick and 11 in wide has an average radius of 48 in. If the hub has a 5.2-in radius and each of the 8 spokes has an area of 11 in^2, what are the maximum stresses at a speed of 400 rpm? The maximum torque possible is 4000 lb·ft at full speed.

The area $A = (5)(11) = 55$ in^2, $\omega = 2\pi(400)/60 = 41.9$ rad/s, $I = 11(5)^3/12 = 114.6$ in^4, and $Z_r = 11(5)^2/6 = 45.8$ in^3. The angle α is 22.5 degrees, or π/8, and the maximum rim stress occurs at the inner surface of the rim with $\beta = \pi/8$. From Eqs. (7.34) through (7.36), using a density of 0.283 lb/in^3,

$$f_1 = \frac{1}{2\sin^2(\pi/8)}\left[\frac{\sin(\pi/4)}{4} + \frac{\pi/8}{2}\right] = 1.274 \tag{7.39}$$

$$f_2 = 1.274 - \frac{1}{\pi/4} = 7.600 \times 10^{-4} \tag{7.40}$$

$$f_3 = \frac{55(48)^2 7.600 \times 10^{-4}}{114.6} + 1.274 + \frac{55}{11} = 7.11 \tag{7.41}$$

$$f_4 = \frac{\cos(\pi/8)}{7.11 \sin(\pi/8)} = 0.340 \tag{7.42}$$

$$\sigma = \frac{0.283(48)^2(41.9)^2}{32.2(12)}\left[1 - \frac{0.340}{3} + \frac{55(48)}{3(-45.8)}\left(0.340 - \frac{1}{7.11\pi/8}\right)\right] = 3660 \text{ psi} \tag{7.43}$$

Table 7.5 shows the values for points P_1, P_2, P_3, and P_4, giving additional digits for checking computer programs. Although the stress formulation was based on a spoke of length r_a, the maximum tension stress in the spoke is found for the hub radius, 5.2 in. From Eq. (7.37),

$$\sigma = \frac{0.283(48)^2(41.9)^2}{6(32.2)(12)}\left[3 + \frac{4(55)}{7.11(11)} - \frac{3(5.2)^2}{(48)^2}\right] = 2850 \text{ psi} \tag{7.44}$$

If the spokes are of standard design, an elliptical cross section twice as long in the direction of motion as in the axial direction, the dimensions for an 11-in^2 spoke would be $\sqrt{2(11)/\pi}$ = 2.65 in by 5.29 in. The section modulus is then Z_s = $\pi(2.65)(5.29)^2/32$ = 7.28 in^3, and the bending stress in the spokes, from Eq. (7.38), would be

$$\sigma = \frac{4000(48 - 5.2)}{7.28(8)(48)} = 61 \text{ psi} \tag{7.45}$$

The combined stress for the spoke is then $\sigma = 2850 + 61 = 2910$ psi.

7.3.3 Thin Disk

If a thin disk has a large radius in comparison to its thickness, the stress can be assumed constant across the thickness. Defining the stress function F as

$$F = rz\sigma_r \tag{7.46}$$

the stress equation for a thin disk of variable thickness $z(r)$ is

$$r^2\frac{d^2F}{dr^2} + r\frac{dF}{dr} - F + (3+\nu)\frac{\rho\omega^2 r^3 z}{g} - \frac{r}{z}\frac{dz}{dr}\left(r\frac{dF}{dr} - \nu F\right) = 0 \tag{7.47}$$

and

$$\sigma_t = \frac{1}{z}\frac{dF}{dr} + \rho\omega^2 r^2 \tag{7.48}$$

TABLE 7.5 Rim Stress for Example 7

Term	P_1	P_2	P_3	P_4
Z_r, in^3	−45.833 3	45.844 3	−45.833 3	45.833 3
β	$\pi/8$	$\pi/8$	0	0
f_1	1.273 93	1.273 93	1.273 93	1.273 93
f_2 ($\times 10^{-4}$)	6.932 02	6.932 02	6.932 02	6.932 02
f_3	7.040 56	7.040 56	7.040 56	7.040 56
f_4	0.342 901	0.342 901	0.371 153	0.371 153
σ, psi	3690.32	1554.43	2056.37	3132.62

The boundary conditions for the center or inner radius and the outer radius are both $F = 0$. If there is a central bore, a finite value for r_i is used in the formulation, and for an infinitesimal hole, the limit is taken later. At the center of the solid disk, $\sigma_r = \sigma_t$. The inertia for a disk is given by

$$J = \int_{r_i}^{r_o} \frac{2\pi\rho r^3 z}{g}\, dr \tag{7.49}$$

Equations (7.46) through (7.48) can be solved explicitly for the uniform and hyperbolic profiles [7.4]. For the general case, using a difference approximation for dz/dr and F leads to a tractable banded set of linear simultaneous equations. Divide the radius into equal intervals of length Δr. Determine the z derivative for each point using

$$z'_j = \frac{z_{j+1} - z_{j-1}}{2\,\Delta r} \tag{7.50}$$

except at the two boundaries, where, for the same accuracy,

$$z'_j = \frac{2z_{j+3} - 9z_{j+2} + 18z_{j+1} - 11z_j}{6\,\Delta r} \tag{7.51}$$

at the center or inner radius and

$$z'_j = \frac{11z_j - 18z_{j-1} + 9z_{j-2} - 2z_{j-3}}{6\,\Delta r} \tag{7.52}$$

at the outer radius. The stress equation then becomes the set of equations

$$A_j F_{j-1} + B_j F_j + C_j F_{j+1} = D_j \tag{7.53}$$

where

$$A_j = \frac{r_j}{\Delta r}\left(\frac{r_j}{\Delta r} - \frac{1}{2} + \frac{r_j}{2}\frac{z'_j}{z_j}\right) \tag{7.54}$$

$$B_j = -2\left(\frac{r_j}{\Delta r}\right)^2 + \nu r_j\left(\frac{z'_j}{z_j}\right) - 1 \tag{7.55}$$

$$C_j = \frac{r_j}{\Delta r}\left(\frac{r_j}{\Delta r} + \frac{1}{2} - \frac{r_j}{2}\frac{z'_j}{z_j}\right) \tag{7.56}$$

$$D_j = -(3+\nu)\frac{r_j^3 z_j \rho\omega^2}{g} \tag{7.57}$$

At the two boundary points the equation is identically satisfied, leaving $(r_o - r_i)/\Delta r - 1$ equations. For the inner equation, $A_j = 0$, and for the outer equation, $C_j = 0$. The simultaneous equations are solved for F_j, and the stresses are found from Eqs. (7.46) and (7.48). See the user's guide for your computer for a convenient method of solving linear simultaneous equations.

7.3.4 Disk of Constant Thickness

The solutions for a disk of uniform thickness are simplified if a constant is defined as

$$\sigma_0 = \frac{\rho r_o^2 \omega^2 (3+\nu)}{8g} \tag{7.58}$$

For a constant-thickness disk without a central hole, the radial and tangential stresses are then given by

$$\sigma_r = \sigma_0\left(1 - \frac{r^2}{r_o^2}\right) \tag{7.59}$$

$$\sigma_t = \sigma_0\left(1 - \frac{1+3\nu}{3+\nu}\frac{r^2}{r_o^2}\right) \tag{7.60}$$

and the maximum stress, at $r = 0$, is

$$\sigma_{r,\max} = \sigma_{t,\max} = \sigma_0 \tag{7.61}$$

For a disk with a central hole, the stresses are given by

$$\sigma_r = \sigma_0\left(1 - \frac{r^2}{r_o^2} + \frac{r_i^2}{r_o^2} - \frac{r_i^2}{r^2}\right) \tag{7.62}$$

$$\sigma_t = \sigma_0\left(1 - \frac{1+3\nu}{3+\nu}\frac{r^2}{r_o^2} + \frac{r_i^2}{r_o^2} + \frac{r_i^2}{r^2}\right) \tag{7.63}$$

The maximum radial stress, at $r = \sqrt{r_o r_i}$, is

$$\sigma_{r,\max} = \sigma_0\left(1 - \frac{r_i}{r_o}\right)^2 \tag{7.64}$$

and the maximum tangential stress, at $r = r_i$, is

$$\sigma_{t,\max} = \sigma_0\left(2 + \frac{2-2\nu}{3+\nu}\frac{r_i^2}{r_o^2}\right) \tag{7.65}$$

The inertia is

$$J = \frac{\pi\rho z}{2g}(r_o^4 - r_i^4) \tag{7.66}$$

Example 8. A steel disk of uniform thickness and outer radius 0.6 m rotates at 30 rad/s. Find the maximum stress in the disk if it has an integral shaft, neglecting stress rises due to the geometry change at the shaft. What is the maximum disk stress if the disk is bored for a shaft of 0.025-m radius?

The stress is independent of thickness. From Eqs. (7.58) and (7.61) with $\rho = 76.5$ kN/m^3 and $\nu = 0.3$,

$$\sigma_{r,\max} = \sigma_{t,\max} = \sigma_0$$
$$= \frac{76.5(0.6)^2(30)^2(3+0.3)}{8(9.80)(1000)} = 1.043 \text{ MPa} \tag{7.67}$$

For the bored disk, the maximum radial stress occurs at $r = \sqrt{0.6(0.025)} = 0.122$ m. From Eq. (7.64),

$$\sigma_{r,\max} = 1.043\left(1 - \frac{0.025}{0.6}\right)^2 = 0.958 \text{ MPa} \tag{7.68}$$

The maximum tangential stress occurs at the hub. From Eq. (7.65),

$$\sigma_{t,\max} = 1.043\left[2 + \frac{2-2(0.3)}{3+0.3}\,\frac{(0.025)^2}{(0.6)^2}\right]$$

$$= 2.09 \text{ MPa} \tag{7.69}$$

7.4 FLYWHEELS FOR ENERGY STORAGE

The flywheel can be used as an energy reservoir, with energy being supplied at a slow constant rate or when it is available and being withdrawn when desired. A flywheel might, for example, be used to give good acceleration to an automobile that is underpowered by present standards. Regenerative breaking, power storage for peak-demand periods, and mechanical replacements for battery banks are all potential uses for the flywheel. The high charging and discharging rates of a flywheel system give it an advantage over other portable sources of power, such as batteries.

Although the concepts developed in the previous sections are still true for energy-storage flywheels, the purpose is now to store as much kinetic energy, $0.5J\omega^2$, as possible. In most applications, the flywheel speed does not vary over 50 percent, so that only about 75 percent of this total energy is actually recoverable. The design of the ordinary flywheel is usually dictated by the allowable diameter, governed by the machine size, and the maximum speed, governed by the practicalities of a speed-increasing drive and higher bearing speeds. These constraints can result in a low peripheral speed, causing the economics to favor a rim-type flywheel design. The economics change with the energy-storage flywheel, since (1) larger values of total stored energy are usually involved, requiring heavier flywheels or more energy per unit weight of flywheel, (2) the weight of a heavy flywheel and the correspondingly heavy bearings and other components may be unacceptable, especially in mobile applications, and (3) the design constraints imposed in a machine where the flywheel limits the speed variation can be relaxed when the flywheel is the main component, encouraging optimization. Depending on the application, the energy per dollar, energy per weight, or energy per swept volume is usually maximized [7.1].

7.4.1 Isotropic and Anisotropic Designs

The stress equations for the thin disk given in Sec. 7.3.3 can be solved with $\omega_r = \omega_t$ to give the shape for a fully stressed thin isotropic disk with no central bore:

$$z = z_0 \exp\left(-\frac{\rho\omega^2 r^2}{2gS_y}\right) \tag{7.70}$$

where S_y = allowable strength, for example, the yield strength of the material. Define the energy stored per unit weight as

$$R = F_s\,\frac{S_y}{\rho} \tag{7.71}$$

where F_s is a dimensionless factor that depends only on the shape of the flywheel. Using Eqs. (7.46) through (7.49), it turns out that the efficiency or geometric shape

factor $F_s = 1.0$ for the fully stressed profile. As Eq. (7.70) indicates, this profile has an infinite outer radius; truncating the profile reduces F_s substantially. Modifying the profile can improve the efficiency, increasing F_s to 0.97 (see Table 7.6), but that is the limit for a homogeneous isotropic design. To avoid this basic limitation and to take advantage of the higher strength-to-weight and stiffness-to-weight ratio of composite materials, recent efforts have concentrated on anisotropic designs ([7.1], [7.8]). Figure 7.7 describes a few of the many designs that are being developed.

7.4.2 Special Considerations

Energy-storage flywheels have special problems which are related to their high speed, flexibility, and anisotropy. The increased operational speed requires high-speed power transmission and bearings as well as special attention to drag forces and the critical vibration speeds of the torsional system. A continuously variable transmission and operation in a vacuum are usually required. Forward whirling is a potentially serious problem that may limit the operating range or require external damping [7.3]. The flexibility can cause flywheel vibration modes with frequencies in the operating range and can also cause significant imbalance to occur as the flywheel deforms with speed. Anisotropy can cause failure in the weak direction (matrix failure or delamination) before the full strength in the strong direction is utilized.

7.5 STRENGTH AND SAFETY

7.5.1 Materials

Neglecting gravity and other secondary loads, the stresses in a flywheel will be proportional to $V^2 = (r_o\omega)^2$. Two flywheels of the same design but of different size will therefore have the same rim stress when their rim velocities are equal. Also, since the stress is proportional to V^2, a 10 percent increase in rotational speed will cause a 21 percent increase in stress. Although the strengths of flywheel materials are sometimes given in terms of their maximum rim velocities, these strengths include generous factors of safety to account for all the possible variations in the material properties, design details, and methods of manufacture. A rational approach would

TABLE 7.6 Shape Factor for Several Isotropic Flywheel Shapes

Shape	F_s
Fully stressed, infinite radius	1.00
Optimum, finite radius	0.97
Exponential or truncated conical (approximate)	0.8
Uniform thickness	0.61
Thin-rim type	0.50
Bar	0.33
Uniform thickness, central bore	0.31

SOURCE: From Gilbert et al. [7.5], by permission.

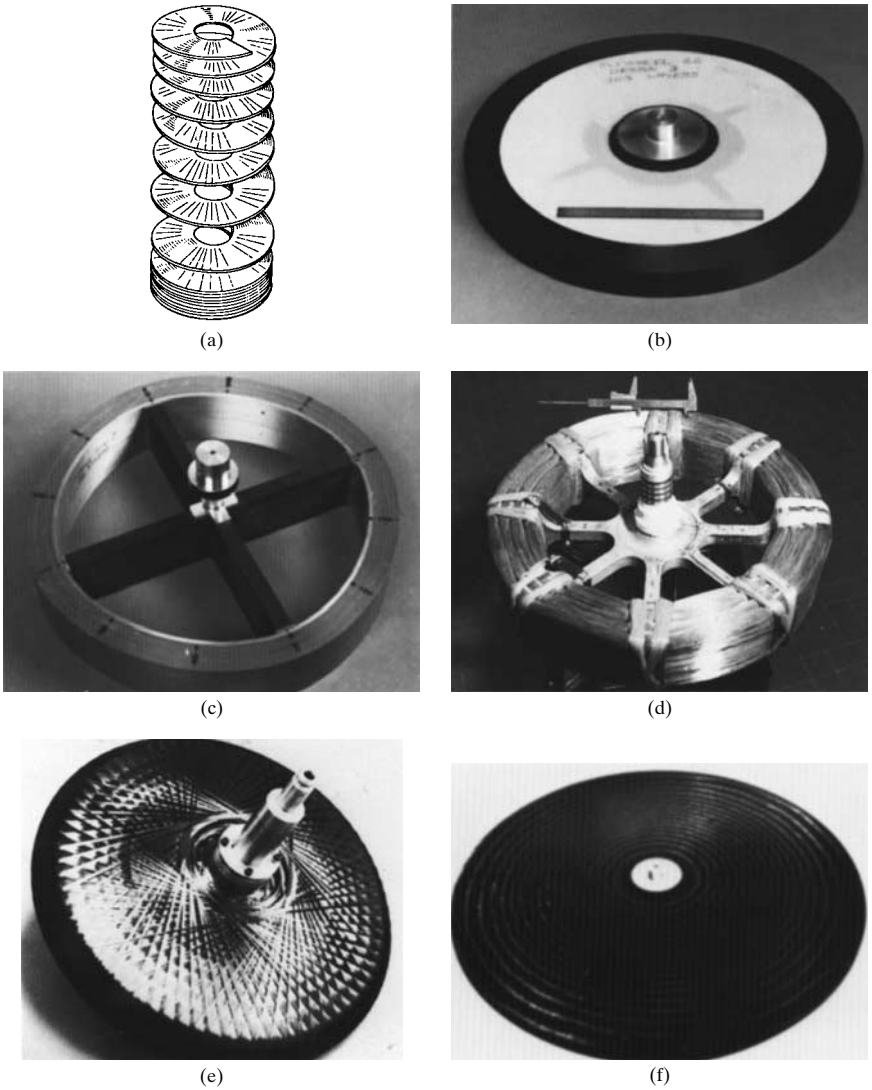

FIGURE 7.7 Energy-storage flywheel designs. (*a*) Flywheel of helically woven fabric with variable properties in the radial and circumferential directions (*exploded view*) (*Avco Systems Division*); (*b*) filament-wound graphite/epoxy rim with laminated S2-glass/epoxy disk (*General Electric Company*); (*c*) subcircular multilayer rim of S-glass and Kevlar, with graphite/epoxy spokes (*Garrett AiResearch Corporation*); (*d*) bare-filament Kevlar rim with aluminum hub (*Istituto della Motorizzazione, Torino, Italy, built by Industrie Pirelli S.p.A. and sponsored by the Italian National Research Council*); (*e*) graphite/epoxy and steel-filament/epoxy rim with a woven graphite/epoxy overwrap (*MAN Advanced Technology, Munich, Germany*); (*f*) variable-thickness graphite/epoxy laminated disk (*Lawrence Livermore National Laboratory*).

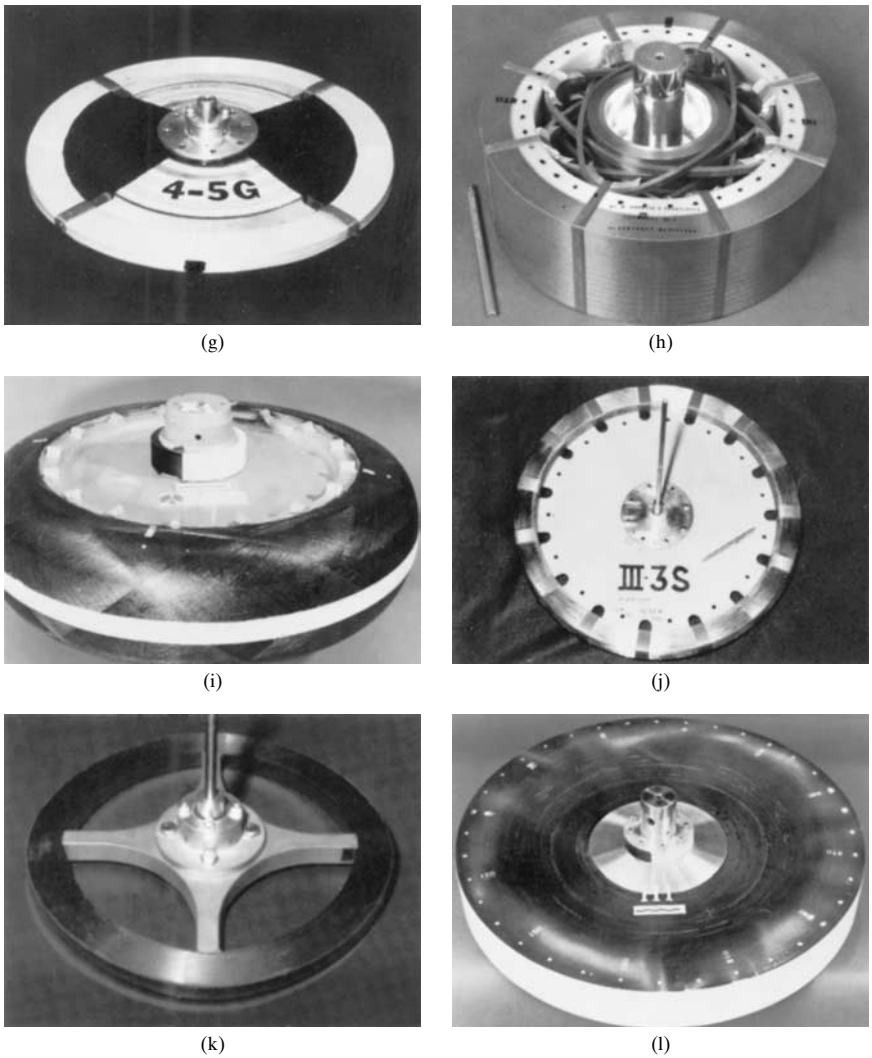

(g) (h)

(i) (j)

(k) (l)

FIGURE 7.7 *(Continued)* Energy-storage flywheel designs. (*g*) bare-filament high-strength steel-wire rim, as used in steel-belted radial tires, with fiberglass hub (*The Johns Hopkins University Applied Physics Laboratory*); (*h*) multilayer rim of S-glass and Kevlar, with catenary tension-balanced spokes (*William M. Brobeck and Associates*); (*i*) graphite/epoxy-wound rim with overwrap over an aluminum liner with two contoured-aluminum hubs (*Rockwell International/Rocketdyne Division*); (*j*) vinyl-coated S-glass rim with Russian birch hub (*The Johns Hopkins University Applied Physics Laboratory*); (*k*) Metglas (amorphous steel) ribbon rim with aluminum spokes (*The Johns Hopkins University Applied Physics Laboratory*); (*l*) contoured graphite/epoxy filament-wound disk (*Hercules Aerospace*). (Kevlar is a registered trademark of E. I. du Pont de Nemours and Company, Inc.; Metglas is a registered trademark of The Allied Corporation.) (*Photographs assembled with the assistance of W. Wilkinson, The Johns Hopkins University Applied Physics Laboratory, and S. Kulkarni, The Lawrence Livermore National Laboratory; by permission.*)

be to assign risk factors to each unknown in the specific flywheel design and multiply the resulting factors of safety or, if sufficient data are available, to use a probabilistic or statistical approach [7.6].

Cast iron has often been chosen as a flywheel material on the basis of cost per pound. However, this criterion is valid only if the design constraints on radius and speed dictate a low rim stress. Otherwise the higher strength-to-weight ratio of other materials may make them less expensive. With any cast flywheel there is the possibility of brittleness, of blowholes, and of other casting flaws; shrinkage stresses in the casting must also be controlled. To reduce shrinkage stresses, one-piece flywheels larger than a few feet in diameter are often cast with a split hub, i.e., with each separate arc of the hub allowed to move with the attached spokes. After cooling, the hub is then bolted together using spacer plates.

The rim is sometimes cast separately from the spokes, and special care must be taken to design an efficient joint between the two. On flywheels larger than 10 ft in diameter, the rim is sometimes fabricated in two or more sections, usually for transportation reasons. The joint efficiency in these cases can be as low as 30 percent, and so extreme care should be taken in designing the joint. The more efficient designs rely on bow tie or ring shrink-fit connectors placed at the spoke locations. A more advanced study should be made unless the calculated stresses are markedly low; a photoelastic or finite-element model [7.9] might be constructed, for example.

Cast steel is stronger than cast iron and is widely used. Flame-cut steel-plate flywheels are relatively inexpensive to manufacture, and their simplicity may make up for their inefficient shape. Flywheels welded from steel plate are inherently stronger than cast flywheels as long as proper care is taken to control flaws and residual weld stresses.

7.5.2 Safety

If the designer can reduce the uncertainty in any of the design unknowns, the necessary factor of safety will be less and a lighter flywheel will result. Design unknowns include (1) material properties, (2) analysis error, (3) loading, and (4) installation. The material properties of the finished flywheel may vary due to welds, porous casting, or lamination flaws. The analysis may have been an elementary beam calculation or a detailed finite-element/fatigue/fracture mechanics study. The input and output loads and speeds may be estimated, calculated, or measured values. The skill or care used in installation may be unknown or well controlled. Improvement in any of these areas will give a better design.

Another way to reduce the necessary factor of safety is through testing. Both destructive and nondestructive tests of the material are excellent tools in answering questions about material properties and fabrication technique. The spin test, of course, is the primary proof of the material, fabrication, and design. Although it will not ordinarily answer questions of fatigue or cycled loads, a destructive spin test gives the best indication of the true safety margin. Long-term cyclic life tests are very helpful if a realistic load cycle can be devised.

A third way to reduce the necessary factor of safety is to reduce the physical and financial harm that would be caused by a flywheel failure. No matter what material is used, any flywheel will break if it is rotated fast enough. If this failure can be controlled in some way, the design speed of the flywheel can be closer to the failure speed without undue risk. Standard steel rim-type and disk flywheels usually burst into three to six pieces at failure; each piece travels with quite a bit of kinetic energy. One method to control failure is therefore to force a breakup into smaller pieces;

many composite flywheels shred, for example. Another method used with the energy-storage flywheel relies on centrifugal force to separate the outer circular sections of the flywheel from the spokes or inner hub section before the material begins to fail. If a benign failure mode cannot be introduced into the design, a heavier containment enclosure could serve the same purpose, lessening the consequence of a flywheel failure.

REFERENCES

7.1 *1980 Flywheel Technology Symposium,* October 1980, Scottsdale, Arizona, University of California Lawrence Livermore National Laboratory, Livermore, Calif., NTIS CONF-801022.

7.2 Rowland S. Benson and N. D. Whitehouse, *Internal Combustion Engines,* Pergamon, New York, 1979.

7.3 C. W. Bert and G. Ramunujam, "Design Guide for Composite-Material Flywheels: Rotor Dynamic Considerations, Part I," University of Oklahoma, Norman, Okla., September 1981, UCRL-15420.

7.4 J. P. Den Hartog, *Advanced Strength of Materials,* McGraw-Hill, New York, 1952.

7.5 R. R. Gilbert, et al., "Flywheel Feasibility Study and Demonstration," Lockheed Missiles and Space Company, Sunnyvale, Calif., April 1971, NTIS PB-200143.

7.6 Edward B. Haugen, *Probabilistic Approaches to Design,* John Wiley & Sons, New York, 1968.

7.7 Charles R. Mischke, *Elements of Mechanical Analysis,* Addison-Wesley, Reading, Mass., 1963.

7.8 R. P. Nimmer, K. Torossian, and W. W. Wilkening, "Laminated Composite Disk Flywheel Development," General Electric Company, Schenectady, N.Y., UCRL-15383.

7.9 M. Saraph, A. Midha, and J. C. Wambold, "Automated Stress Analysis of Mechanical Sheaves and Pulleys," *Computers in Mechanical Engineering,* pp. 34–42, October 1982.

7.10 Joseph E. Shigley and Charles R. Mischke, *Mechanical Engineering Design,* 5th ed., McGraw-Hill, New York, 1989.

7.11 Joseph Edward Shigley and John Joseph Uicker, Jr., *Theory of Machines and Mechanisms,* 2d ed. McGraw-Hill, New York, 1995.

FLYWHEELS

CHAPTER 8
CLUTCHES AND BRAKES

John R. Zimmerman, Ph.D.
Professor of Mechanical and Aerospace Engineering
University of Delaware
Newark, Delaware

GLOSSARY OF SYMBOLS

a	Vehicle deceleration, ft/s^2 (m/s^2)
a	Location of shoe pivot, in (m)
a	Lever arm for larger band force, in (m)
A	Area, in^2 (m^2)
b	Percentage of grade
b	Width of band, shoe, or web, in (m)
c	Lever arm for smaller band force, in (m)
C	Center of pressure
C	Specific heat, Btu/(lbm · °F) [J/(kg · °C)]
d	Inside disk diameter, in (m)
D	Outside disk diameter, in (m)
D	Pitch diameter of gear, in (m)
D_{max}	Maximum roll diameter, in (m)
e	Radius to center of circular brake pad, in (m)
E	Total energy dissipated, ft · lb or Btu (J)
f	Coefficient of friction
f_v	Ventilation factor

F	Actuating force, lb (N)
F_D	Prime-mover factor
F^l	Actuating force on leading shoe, lb (N)
F_L	Load factor
F_n	Normal force, lb (N)
F_S	Starting factor
F_t	Tension force on web, lb (N)
F^t	Actuating force on trailing shoe, lb (N)
g	Local acceleration of gravity, ft/s^2 (m/s^2)
g_c	Gravitational constant, 32.174 lbm · ft/(lb · s^2) [1 kg · m/(N · s^2)]
h	Overall heat transfer coefficient, Btu/(in^2 · s · °F) [W/(m^2 · °C)]
h_c	Convection heat transfer coefficient, Btu/(in^2 · s · °F) [W/(m^2 · °C)]
h_r	Radiation heat transfer coefficient, Btu/(in^2 · s · °F) [W/(m^2 · °C)]
H_{av}	Average rate of heat dissipation, lb · ft/s or Btu/s (W)
I	Mass moment of inertia, lb · in · s^2 (kg · m^2)
I_L	Mass moment of inertia on load side, lb · in · s^2 (kg · m^2)
I_P	Mass moment of inertia on prime-mover side, lb · in · s^2 (kg · m^2)
K_S	Service factor
ℓ	Moment arm of actuating force (drum brake); length of actuating lever in a band brake, in (m)
m	Mass, lbm (kg)
M_a	Moment of actuating force, lb · in (N · m)
M_f	Moment of resultant friction force, lb · in (N · m)
M_n	Moment of resultant normal force, lb · in (N · m)
n	Shaft speed, r/s (Hz) or r/min
N	Number of pairs of friction surfaces in disk clutches or brakes
N	Number of shoes in centrifugal clutch
p	Normal pressure, psi (MPa) or r/min
p_{av}	Average contact pressure, psi (MPa)
p_h	Hydraulic pressure, psi (MPa)
p_{max}	Maximum contact pressure, psi (MPa)
p^{ℓ}_{max}	Maximum contact pressure on leading shoe, psi (MPa)
p^{t}_{max}	Maximum contact pressure on trailing shoe, psi (MPa)
P	Resultant normal force between drum and shoe, lb (N)
P	Power, Btu/s or hp (kW)
P_x	Component of normal force in x direction, lb (N)
P_y	Component of normal force in y direction, lb (N)
P_1	Larger band tension, lb (N)
P_2	Smaller band tension, lb (N)
q	Rate of energy dissipation during clutch slip, Btu/s (W)

Q	Actuating force (band brake), lb (N)
r	Brake drum radius, in (m)
r	Radius to point on disk, in (m)
r_f	Radius to center of pressure, in (m)
R	Tire-rolling radius, in (m)
R	Reaction force (drum brake), lb (N)
R	Radius to rim of centrifugal brake, in (m)
R_e	Effective friction radius, in (m)
R_i	Inside radius, in (m)
R_o	Outside radius, in (m)
s	Total stopping distance, ft (m)
S	Initial tension, lb (n)
S	Stops per hour
t	Web thickness, mils (mm)
t_d	Combined delay time for driver reaction and brake system reaction, s
t_s	Total stopping time, s
T	Torque; nominal torque, lb · ft (N · m)
T_a	Temperature of surrounding air, °F (°C)
T_d	Disk temperature, °F (°C)
ΔT	Temperature rise, °F (°C)
T_{des}	Design torque, lb · ft (N · m)
T_L	Load torque, lb · ft (N · m)
$T_{\max}$	Maximum torque, lb · ft (N · m)
T_P	Prime mover torque, lb · ft (N · m)
V	Rubbing velocity, ft/s (m/s)
V_o	Initial velocity, ft/s (m/s)
V_f	Final velocity, ft/s (m/s)
V_w	Web velocity, ft/s (m/s)
w	Web tension per unit thickness and unit width, lb/(mil · in) [N/(mm · m)]
W	Vehicle weight, lb (N)
α	Cone angle, deg
δ	Multiplier for circular disk brake pads
ε	Angular position of actuation force, deg
θ	Angle of wrap, deg
θ	Angular position, deg
θ_1	Starting position of brake shoe lining, deg
θ_2	Ending position of brake shoe lining, deg
ω	Shaft speed, rad/s
ω_e	Engagement speed, rad/s
ω_o	Initial shaft speed, rad/s

ω_f Final shaft speed, rad/s
Ω_L Initial shaft speed on load side of clutch, rad/s
Ω_P Initial shaft speed on prime-mover side of clutch, rad/s

This chapter begins with an introduction to brakes and clutches, the various types and their applications. The problem of energy dissipation and temperature rise is discussed along with the proper selection of friction materials. Design methods are presented for almost every type of brake and clutch. A discussion of the actuation problems of brakes and clutches, including electromagnetic devices, is also presented.

8.1 TYPES, USES, ADVANTAGES, AND CHARACTERISTICS

8.1.1 Types of Clutches

The characteristic use of a clutch is to connect two shafts rotating at different speeds and bring the output shaft up to the speed of the input shaft smoothly and gradually.

Classifying clutches is done by distinguishing (1) the physical principle used to transmit torque from one member to another and (2) the means by which the members are engaged or by which their relative speed is controlled. Here, we classify clutches as follows:

1. Engagement or actuation method
  a. Mechanical
  b. Pneumatic
  c. Hydraulic
  d. Electrical
  e. Automatic
2. Basic operating principle
  a. Positive contact
    (1) Square jaw
    (2) Spiral jaw
    (3) Toothed
  b. Friction
    (1) Axial
    (2) Radial
    (3) Cone
  c. Overrunning
    (1) Roller
    (2) Sprag
    (3) Wrap-spring
  d. Magnetic
    (1) Magnetic particle
    (2) Hysteresis
    (3) Eddy current
  e. Fluid coupling
    (1) Dry fluid
    (2) Hydraulic

Coupling Methods. *Positive-contact clutches* have interlocking engaging surfaces to form a rigid mechanical junction. Three types of positive-contact clutches are shown in Fig. 8.1.

Frictional clutches are used most frequently. Two opposing surfaces are forced into firm frictional contact. Figures 8.2, 8.3, and 8.4 show *axial, radial,* and *cone* types.

Overrunning clutches are used when two members are to run freely relative to each other in one direction but are to lock in the other. Roller, sprag, and wrap-spring types are shown in Fig. 8.5. In the *roller-ramp clutch* (Fig. 8.5*a*), the members are locked together when the rollers (or balls) ride on a race with a slight cam profile. Eccentric cams are pinched between concentric races in the *sprag-type clutches* (Fig. 8.5*b*). And in the basic *wrap-spring clutch* (Fig. 8.5*c*), the spring's inside diameter is slightly smaller than the outside diameters of the input and output hubs. When the spring is forced over the two hubs, rotation of the input hub in

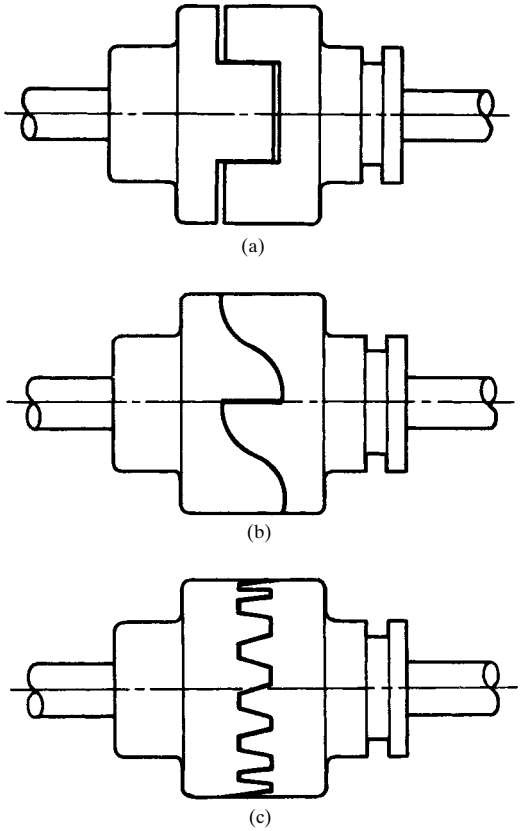

FIGURE 8.1 Positive-contact clutches. (*a*) Square-jaw—the square teeth lock into recesses in the facing plate; (*b*) spiral-jaw—the sloping teeth allow smoother engagement and one-way drive; (*c*) toothed-clutch—engagement is made by the radial teeth.

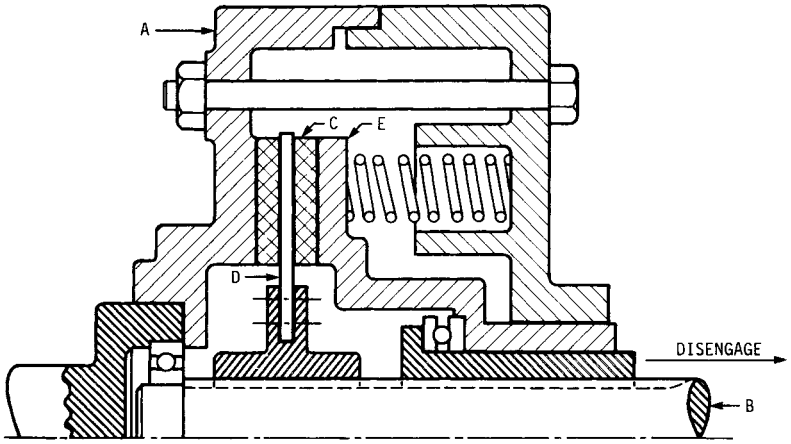

FIGURE 8.2 Schematic drawing of an axial clutch; *A,* driving member; *B,* driven shaft; *C,* friction plates; *D,* driven plate; *E,* pressure plate.

the drive direction causes the spring to tighten down on the hubs. Torque is then transmitted. But rotation in the opposite direction opens the spring, and no torque is transmitted.

A *magnetic clutch* (Sec. 8.8) uses magnetic forces to couple the rotating members or to provide the actuating force for a friction clutch.

Fluid couplings may make use of a hydraulic oil or a quantity of heat-treated steel shot. In the *dry-fluid coupling,* torque is developed when the steel shot is thrown centrifugally to the outside housing (keyed to the input shaft) as the input

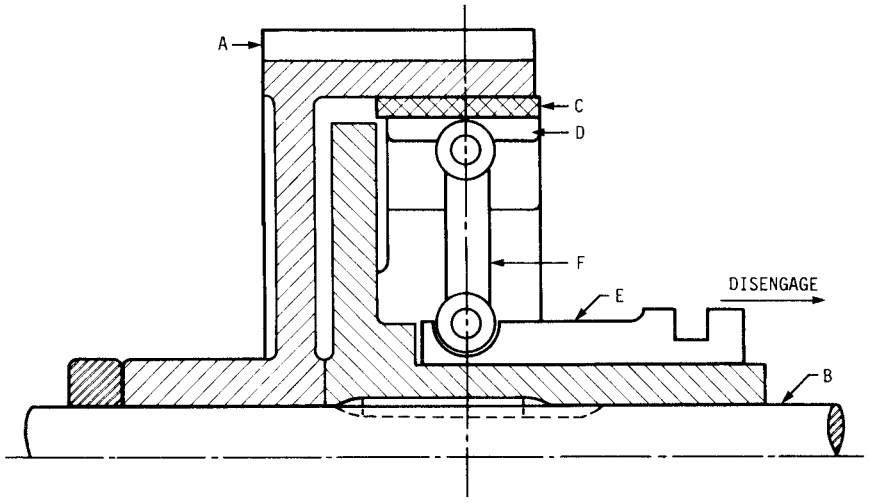

FIGURE 8.3 Schematic drawing of a radial clutch built within a gear; *A,* gear, the driving member; *B,* driven shaft; *C,* friction plate; *D,* pressure plate; *E,* movable sleeve; *F,* toggle link. This type of clutch can also be made within a V-belt sheave.

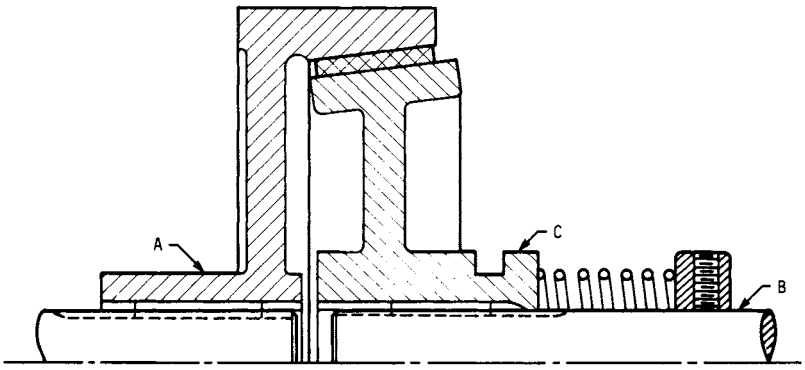

FIGURE 8.4 Schematic drawing of a cone clutch; *A,* driving member; *B,* driven shaft; *C,* movable sleeve.

shaft begins to rotate. At the design speed the shot is solidly packed, and the housing and rotor lock together.

Control Methods. *Mechanical control* is achieved by linkages or by balls or rollers working over cams or wedges. The actuating force can be supplied manually or by solenoid, electric motor, air cylinder, or hydraulic ram.

Electrical control of friction or tooth clutches often involves engaging the clutch electrically and releasing it by spring force. Thus the clutch is *fail-safe:* If power fails, the clutch is disengaged automatically. But where shafts are coupled for much longer periods than they are uncoupled, the opposite arrangement may be used: spring force to engage, electromagnetic force to disengage.

Pneumatic, or *hydraulic, control* is accomplished in several ways. Actuating pistons may be used either to move the actuating linkage or to directly apply a normal force between frictional surfaces. In other designs an inflatable tube or bladder is used to apply the engagement force. Such designs permit close control of torque level.

Automatic control of clutches implies that they react to predetermined conditions rather than simply respond to an external command. Hydraulic couplings and eddy-current clutches both have torque regulated by the slip. *Centrifugal clutches* (Fig. 8.6) use speed to control torque.

8.1.2 Selecting Clutches

A starting point is a selection table constructed by Proctor [8.5] and reproduced here as Table 8.1. Four additional tables in Proctor's article also are useful for preliminary decisions. Designers will have to consult the manufacturers before making final decisions.

8.1.3 Types of Brakes

Physically, brakes and clutches are often nearly indistinguishable. If two shafts initially at different speeds are connected by a device to bring them to the same speed,

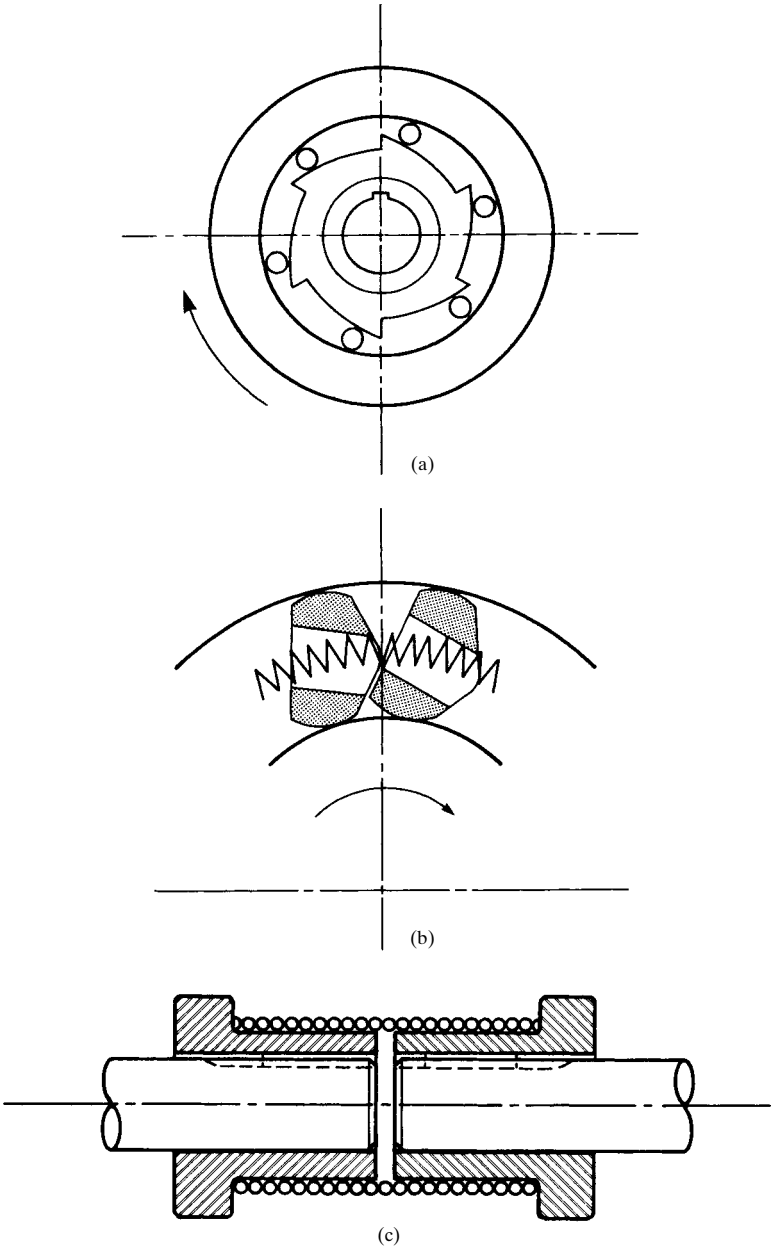

FIGURE 8.5 Overrunning clutches. (*a*) Roller-ramp clutch; springs are often used between the rollers and the stops. (*b*) Portion of a Formsprag clutch. Rockers or *sprags*, acting as cams, are pushed outward by garter springs at both ends of the prismatic sprags. (*c*) Torsion spring winds up when the clutch is in "drive" and grips both hubs. Larger-torque loads can be carried by making the springs of rectangular-section wire.

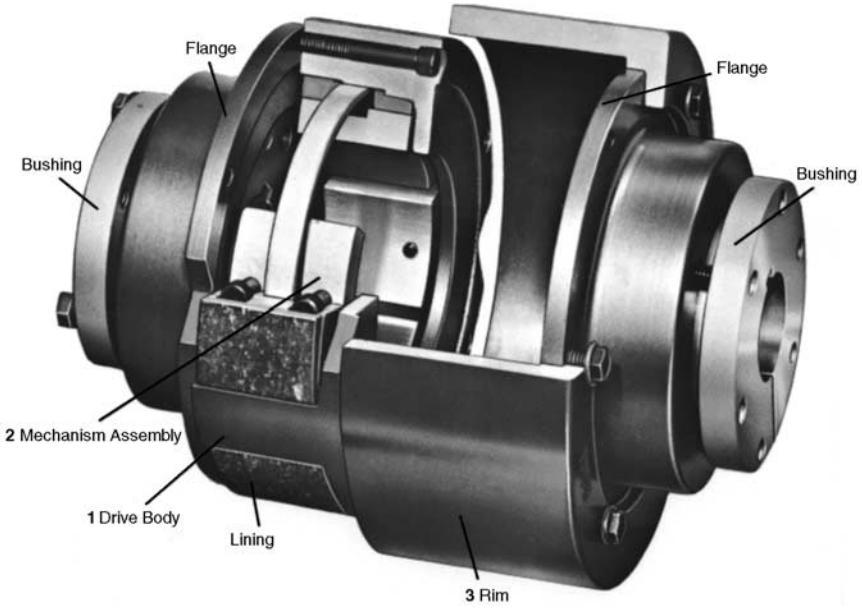

FIGURE 8.6 Centrifugal clutch. *(BLM Automatic Clutch Limited.)*

it is a clutch. If one member is fixed and the torque is used to slow down or stop the rotating member, the device is a brake. A classification scheme for brakes is presented in Fig. 8.7.

Brake Configuration. *Band brakes* can be made *simple* (not self-energizing) or *differential* (self-energizing). In designing a differential band brake (Fig. 8.19), care must be taken to ensure that the brake is not self-locking.

Short-shoe brakes have been used for hoists. Centrifugal brakes employ speed as the actuating signal for short-shoe internal-block brakes and are used in a wide variety of applications.

Drum brakes (Fig. 8.8) are used principally for vehicles, although seldom on the front axles of passenger cars. On the rear axles, drum brakes supply high braking torque for a given hydraulic pressure because one or both of the long shoes can be made self-energizing.

For a *leading shoe,* the friction moment exerted on the shoe by the drum assists in actuating the shoe. The friction moment on a *trailing shoe* opposes the actuating moment. Thus a leading shoe is *self-energizing,* but a trailing shoe is *self-deenergizing.*

The *leading-shoe trailing-shoe* design (Fig. 8.8) provides good braking torque in forward or reverse. The *two-leading-shoe* design has an even higher braking torque in forward, but a much lower braking capacity in reverse. Very high braking torque is available from the *duo-serve* design. Here the friction force on the "leading shoe" assists in actuating the "trailing shoe."

One difficulty with drum brakes is instability. If a brake's output is not sensitive to small changes in the coefficient of friction, the brake is *stable.* But if small changes

TABLE 8.1 Selecting the Right Clutch

Load characteristic or clutch function	Type of clutch				
	General utility	Centrifugal and fluid self-actuating	Continuous slip		Overrunning or freewheeling
			Automatic	Variable	
1. No-load start					
a. Manual or externally controlled	✓	...	...	...	✓
b. Automatic	...	✓			
2. Smooth load pickup					
a. Normal load	✓	✓	...	...	✓
b. High-inertia load	...	✓	...	✓	
c. High breakaway load (more than 100% running torque)	...	✓	...	✓	
d. Automatic delayed pickup	...	✓	...	✓	
e. Extended acceleration	...	✓	...	✓	
f. Auxiliary starter	...	...	...	...	✓
3. Running operation					
a. Normal load (no slip at full load, full speed)	✓	✓	✓		
b. Control variable-torque load	...	...	...	✓	
c. Control constant-torque load	...	...	✓	✓	
d. Control constant-tension load	...	...	...	✓	
4. Overload protection and stopping					
a. General protection: transient and infrequent overloads	✓	✓			
b. Limit speed (prevent runaway load)	...	✓	...	...	✓
c. Limit torque	...	✓	✓	...	✓
d. Automatic overload release	✓	...	...	...	✓
e. Dynamic braking	...	✓	...	...	✓
f. Backstopping	...	✓	...	...	✓
5. Intermittent operation					
a. On-off, with driver at speed	✓	...	...	...	✓
b. Inching and jogging	✓				
c. Indexing and load positioning	...	...	...	...	✓
6. Dual-drive and standby operation	...	✓	...	...	✓

SOURCE: Ref. [8.5].

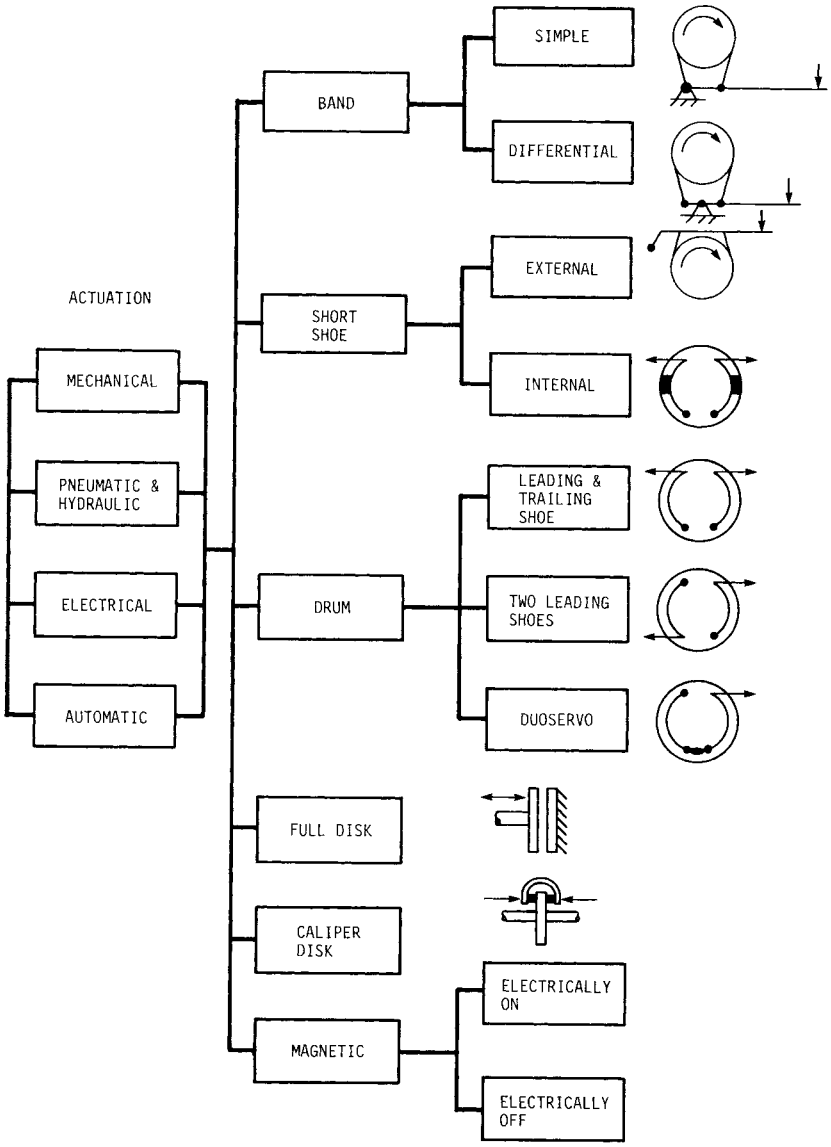

FIGURE 8.7 Classification of brakes.

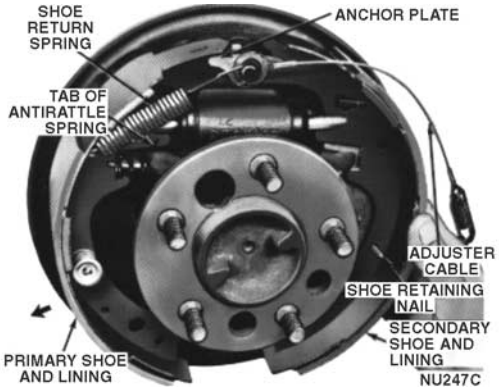

FIGURE 8.8 Drum brake. *(Chrysler Corporation.)*

in the friction coefficient cause large changes in brake torque, the brake is *unstable.* It will tend to grab and squeal if the coefficient of friction increases. But if the coefficient decreases (say, because of a temperature increase), there will be a noticeable drop in capacity.

Full disk brakes are used principally for industrial machinery. They are very much like full disk clutches in construction. Indeed, they are found in *clutch-brake combination drives* where both members of the drive are full disk in construction.

Caliper disk brakes (Fig. 8.9) are now familiar components of vehicles, but they find applications in industrial equipment as well. The Chrysler brake shown uses a floating caliper. In this design, an automatic mechanism to adjust for pad wear can be incorporated easily.

Generally caliper disk brakes are not self-energizing, although they can be. An advantage of the non-self-energizing disk brake is its great stability; it is relatively insensitive to changes in the coefficient of friction.

Brake Actuation. Four principal actuation methods are shown in the classification chart of Fig. 8.7: mechanical, pneumatic (or hydraulic), electric, and automatic. Sometimes the methods are combined.

The drum brake of Fig. 8.8 and the disk brake of Fig. 8.9 are both *hydraulically operated.* Both are intended for vehicles. In industrial applications, air is often the actuating fluid. The air-tube configuration in Fig. 8.10 can be used for a *pneumatically operated* clutch or brake.

Electrically operated brakes most commonly use electromagnetic forces to actuate a full-disk-friction brake. However, a number of other designs are found (see Sec. 8.8).

Automatically operated brakes are used for both transportation and industrial equipment. Sometimes manual operation is overridden by automatic actuation. Truck brakes are available with spring actuators that engage if the air pressure is lost. The air brake, as originally conceived by George Westinghouse for railroad applications, was of this *fail-safe* design. Electrically, hydraulically, and pneumatically operated brakes can all be designed for automatic operation. Antiskid brakes for automobiles and trucks superimpose on the usual manual control an automatic control that releases braking pressure if lockup and skidding are imminent.

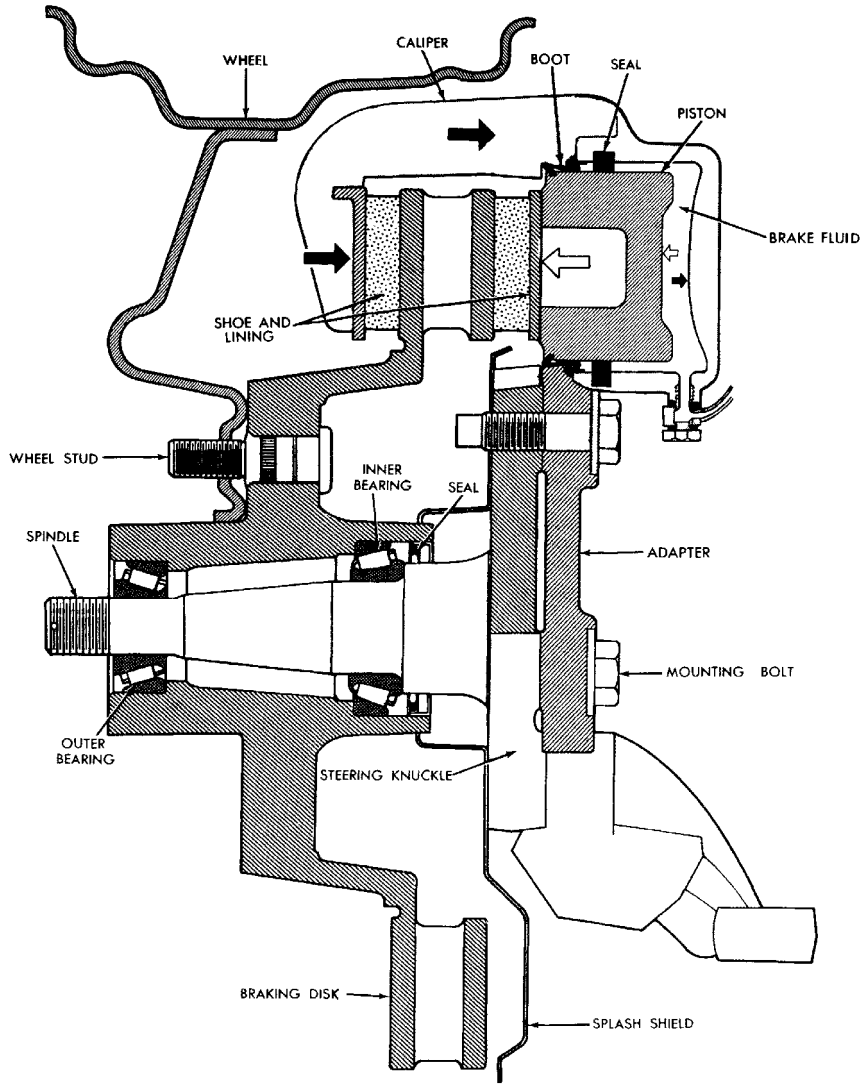

FIGURE 8.9 Automotive disk brake. *(Chrysler Corporation.)*

8.1.4 Selecting a Brake

To help narrow the choice of a brake, Table 8.2 has been provided. Some general indicators are given for performance requirements and environmental conditions. Typical applications are listed as well. The *brake factor* is the ratio of the frictional braking force developed to the actuating force.

Note that temperature considerations have been omitted from the environmental conditions in Table 8.2. For high temperatures, the capacity of all brakes listed is limited by the type of friction material. The performance of all brakes listed is con-

FIGURE 8.10 A pneumatically actuated brake using an expandable tube. *(Eaton Corporation.)*

sidered *good* for low temperatures, but ice buildup must be avoided.

8.2 TORQUE AND ENERGY CONSIDERATIONS

In selecting or designing a clutch, the torque requirement, energy dissipation, and temperature rise are the principal factors to be considered. The torque requirement and energy dissipation are covered in this section. Estimating temperature rise is the subject of Sec. 8.3.

8.2.1 Torque Requirement: Clutches

The torque requirement of a clutch will have to be substantially greater than the nominal torque it is transmitting in order to accelerate the load. The character of the prime-mover output torque and of the load torque also influences the designer's selection of torque capacity.

Gagne [8.4] recommended the following technique for calculating clutch capacity for design purposes. Calculate the design torque as a multiple of the nominal torque T:

$$T_{\text{des}} = K_S T \tag{8.1}$$

where K_S = service factor taking into account the load inertia, the character of the prime mover's output torque, and the character of the load torque. The service factor K_S is

$$K_S = (F_S^2 + F_D^2 + F_L^2 - 2)^{1/2} \tag{8.2}$$

where F_S, F_D, and F_L are the starting, prime-mover, and load factors, respectively. Recommended values for these factors are given in Tables 8.3 to 8.5. Note that if each factor is unity, the service factor is unity also.

But the service factor K_S will usually be greater than unity. Indeed, an old rule of thumb was that the clutch should be designed for a torque capacity at least twice the nominal torque.

Example 1. A multicylinder diesel engine is used to drive an electric generator in a hospital's emergency-power facility. What service factor should be used?

Solution. From Table 8.3, a reasonable selection of values for the torque factors is $F_S = 2$, $F_D = 1.5$, and $F_L = 1.0$. The corresponding service factor is

$$K_S = [2^2 + (1.5)^2 + (1.0)^2 - 2]^{1/2} = 2.29$$

TABLE 8.2 Selecting the Right Brake

Type of brake	Performance requirements			Environmental conditions		Typical applications
	Maximum operating temperature	Brake factor	Stability	Wet and humid	Dust and dirt	
Differential band brake	Low	Very high	Very low	Unstable but still effective	Good	Winches, hoists, excavators, tractors, etc.
External drum brake (leading-trailing edge)	Low	Moderate	Moderate	Unstable if humid; poor performance if wet	Good	Mills, elevators, winders
Internal drum brake (leading-trailing edge)	Higher than external brake	Moderate	Moderate	Unstable if humid; completely ineffective if wet	Very good if sealed	Vehicles (rear axles on passenger cars)
Internal drum brake (two leading shoes)	Higher than external brake	High	Low	Unstable if humid; completely ineffective if wet	Very good if sealed	Vehicles (rear axles on passenger cars)
Internal drum brake (duo-servo)	Low	Very high	Low	Unstable if humid; completely ineffective if wet	Very good if sealed	Vehicles (rear axles on passenger cars)
Caliper disk brake	High	Low	High	Good	Poor; should be shielded	Vehicles and industrial machinery
Full disk brake	High	Low	High	Good	Poor; should be shielded	Machine tools and other industrial machinery

SOURCE: Ref. [8.6].

TABLE 8.3 Suggested Values of Torque Starting Factor F_S for Friction Clutches

Type of load	F_S
Free start; no load	1.0
Average inertia load	2.0
High inertia load	3.0

SOURCE: Ref. [8.4].

TABLE 8.4 Suggested Values of Torque Drive (Prime-Mover) Factor F_D for Friction Clutches

Type of drive	F_D
Nonpulsating, such as three-phase motors	1.0
Moderate pulsation—single-phase motors, multicylinder engines, etc.	1.5
Severe pulsation, such as a single-cylinder gas engine	2.0

SOURCE: Ref. [8.4].

TABLE 8.5 Suggested Values of Torque Load Factor F_L for Friction Clutches

Type of load	F_L
Nonpulsating—blowers, centrifugal pumps, generators under steady load, etc.	1.0
Moderate shock, such as a multicylinder pump	1.5–1.75
Severe shock—crane, shovel, single-cylinder compressor, rock crusher, etc.	2.0–3.0

SOURCE: Ref. [8.4].

8.2.2 Equivalent Inertias

Two shafts geared together and rotating at different speeds are shown in Fig. 8.11*a*. The inertias I_1 and I_2 are each assumed to include the corresponding shaft and gear. For design calculations, it is necessary to have an equivalent inertia for the whole system referred to a single shaft. Figure 8.11*b* and *c* shows this. In each case an equivalent inertia has been added to the shaft. So I_2' is the equivalent inertia on shaft 1 of shaft 2 and its hardware. Similarly, I_1' is the equivalent inertia on shaft 2 of shaft 1 and its hardware.

A simple way to find the equivalent inertia is to equate the kinetic energies of the actual and equivalent inertias. Thus, to find the equivalent inertia I_2' referred to shaft 1 (Fig. 8.11*b*), we write

$$\frac{1}{2}I_2'\omega_1^2 = \frac{1}{2}I_2\omega_2^2$$

Thus

$$I_2' = \left(\frac{\omega_2}{\omega_1}\right)^2 I_2 \tag{8.3}$$

CLUTCHES AND BRAKES

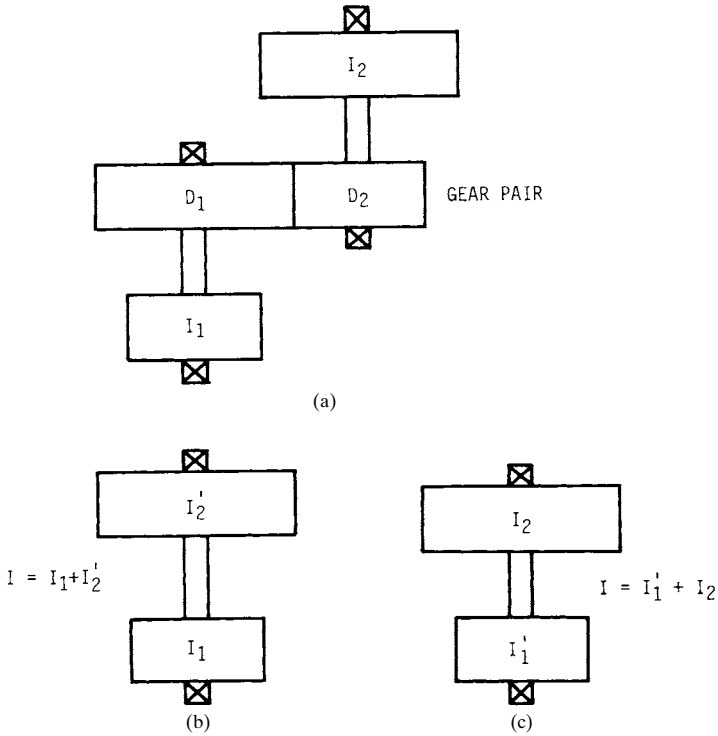

FIGURE 8.11 Equivalent inertia. I_1, I_2 = inertia of input and output shafts, respectively; I' = equivalent inertia. (*a*) Original configuration; (*b*) equivalent system referred to input shaft; (*c*) equivalent system referred to output shaft. For a more extensive treatment of equivalent inertias, see "Suggested Reading" list, Mischke.

Similarly,

$$I_1' = \left(\frac{\omega_1}{\omega_2}\right)^2 I_1 \tag{8.4}$$

In general,

$$I_i' = \left(\frac{\omega_i}{\omega_j}\right)^2 I_i = \left(\frac{n_i}{n_j}\right)^2 I_i \tag{8.5}$$

where the equivalent inertia of the *i*th shaft is referred to the *j*th shaft. Equation (8.5) can be used to reduce a machine with several shafts connected by gears or flexible connectors to a single equivalent shaft.

Example 2. For the two-shaft machine in Fig. 8.11*a*, the inertias are I_1 = 2.88 pound-inch-square seconds (lb · in · s^2) [0.3254 kilogram-square meters (kg · m^2)] and I_2 = 0.884 lb · in · s^2 (0.09988 kg · m^2). The pitch diameters of the gears are D_1 = 4 in [0.102 meter (m)] and D_2 = 7 in (0.178 m). What is the equivalent inertia of shaft 2 referred to shaft 1?

Solution. Equation (8.3) can be used once the speed ratio ω_2/ω_1 is known. For spur or helical gears,

$$\frac{\omega_2}{\omega_1} = \frac{D_1}{D_2} = \frac{4}{7} = 0.5714$$

Thus

$$I_2' = (0.5714)^2(0.884) = 0.2887 \text{ lb} \cdot \text{in} \cdot \text{s}^2 \ (0.0326 \text{ kg} \cdot \text{m}^2)$$

8.2.3 Torque Requirement: Brakes

Industrial Brakes. The torque to bring a rotating machine from an initial speed ω_o to a lower one ω_f (perhaps to rest) in a slowdown time of t_S is

$$T = \frac{I(\omega_o - \omega_f)}{t_S} \tag{8.6}$$

Vehicle Brakes. The braking torque to stop a vehicle of weight W at a deceleration rate a on a grade of b percent can be estimated as

$$T = \frac{WR}{g}\left(\frac{a}{g} + \frac{b}{100}\right) \tag{8.7}$$

Here R is the tire-rolling radius. This is a conservative approach; both tire-rolling resistance and air resistance have been neglected. Of course, this torque capacity T must be allocated to the several brakes in a rational way (for example, in proportion to the weight of the vehicle supported by the corresponding wheel during a panic stop).

For parking-brake capacity, simply set $a = 0$ in Eq. (8.7).

The required acceleration rate a can be determined by setting either a total stopping time t_S or a total stopping distance s:

$$a = \frac{V_o}{t_S - t_d} \tag{8.8}$$

$$a = \frac{V_o^2}{2(s - V_o t_d)} \tag{8.9}$$

In these equations, t_d is the combined delay time (about 1 s for a passenger car) for driver reaction and brake system reaction.

8.2.4 Energy Dissipation: Clutches

A simple model of a clutch connecting a prime mover and a load is shown in Fig. 8.12. The clutch capacity is T, the driving torque provided by the prime mover is T_P, and the load torque is T_L. The inertias I_P and I_L include all rotating masses on their respective sides of the clutch.

If the two sides of the clutch are initially rotating at Ω_P and Ω_L radians per second (rad/s) when the clutch is actuated, the duration of the slip period is

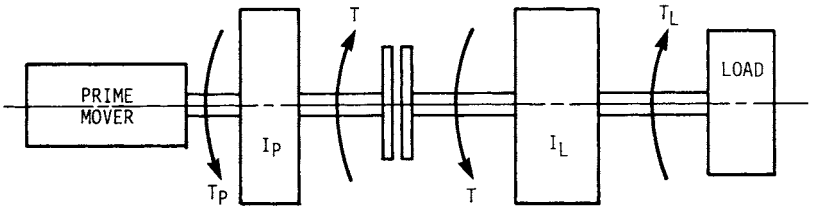

FIGURE 8.12 Abstract model of a machine using a clutch.

$$t_S = \frac{I_P I_L (\Omega_P - \Omega_L)}{T(I_P + I_L) - (I_L T_P + I_P T_L)} \tag{8.10}$$

The rate at which energy is dissipated during the slip period is, at t s from the beginning,

$$q(t) = T\left[\frac{I_L T_P + I_P T_L - T(I_P + I_L)t}{I_P I_L + \Omega_P - \Omega_L}\right] \tag{8.11}$$

And the total energy dissipated in one actuation operation is

$$E = \frac{T(\Omega_P - \Omega_L)^2 I_P I_L}{2T(I_P + I_L) - (I_L T_P + I_P T_L)} \tag{8.12}$$

8.2.5 Energy Dissipation: Brakes

Vehicle Brakes. When a vehicle of weight W is slowed from an initial velocity V_o to a final velocity V_f, the heat energy that the brakes must dissipate is equal to the change of kinetic energy E:

$$E = \frac{W}{2g}(V_o^2 - V_f^2) \tag{8.13}$$

In dealing with individual brakes, let W be that portion of the vehicle's weight for which the brake is responsible.

Example 3. A sports car weighing 3185 lb [14.2 kilonewtons (kN)] has 62 percent of its weight on the front axle during an emergency stop. What energy must each of the front-wheel brakes dissipate in braking from 55 miles per hour (mph) [88 kilometers per hour (km/h)] to rest? Local acceleration of gravity is 32.17 feet per second (ft/s) (9.81 m/s).

Solution. Each front brake is responsible for a weight of

$$W = 0.5(0.62)(3185) = 987 \text{ lb } (4.39 \text{ kN})$$

The initial velocity is

$$V_o = 55\left(\frac{88}{60}\right) = 80.7 \text{ ft/s } (24.6 \text{ m/s})$$

Finally, the energy to be dissipated is

$$E = \frac{W}{2g}(V_o^2 - V_f^2) = \frac{987}{2(32.17)}[(80.7)^2 - 0^2]$$

$$= 99\,900 \text{ lb} \cdot \text{ft } (135.5 \text{ kN} \cdot \text{m})$$

$$= 128.4 \text{ Btu } [135.5 \text{ kilojoules (kJ)}]$$

Industrial Brakes. The approach is the same as for vehicular brakes. The heat energy the brake must dissipate equals the change in kinetic energy of the rotating machine:

$$E = \frac{I}{2}(\omega_o^2 - \omega_f^2) \tag{8.14}$$

where, with n in rev/min,

$$\omega = \frac{2\pi n}{60} \tag{8.15}$$

In many industrial applications, the brakes are applied frequently. The average rate of heat dissipation is, for S stops per hour,

$$H_{av} = \frac{ES}{3600} \tag{8.16}$$

Tensioning Applications. In tensioning applications, a continuous application of the brake is required, for example, in unwinding a roll of aluminum foil. The maximum torque occurs at the maximum roll diameter D_{max}. It is

$$T_{max} = \frac{D_{max} F_t}{2} \tag{8.17}$$

The tension F_t is, for material width b and thickness t,

$$F_t = wtb \tag{8.18}$$

Typical values of tension per unit width and per unit thickness for a few materials are given in Table 8.6.

TABLE 8.6 Tension Data for Typical Materials

Material	Unit tension, lb/mil per inch of web width
Aluminum foil	1.00
Cellophane	0.75
Mylar	0.60
Polystyrene	1.00

SOURCE: The Carlson Company, Inc., Wichita, Kansas.

The rate at which heat is generated by the brake friction is

$$H_{av} = F_t V_w \tag{8.19}$$

Example 4. A printing press is to print on Mylar 0.002 in [0.051 millimeter (mm)] thick. The web velocity is 4000 ft/min (20.3 m/s). The maximum roll diameter is 55 in (1.4 m). The web is 54 in wide. Find the necessary braking torque and the rate at which heat is generated by braking.

Solution. For Mylar the unit tension is 0.60 lb/mil per inch (379.2 kN/mm per meter). So the web tension is

$$F = wtb = 0.60(2)(54) = 64.8 \text{ lb } (288 \text{ N})$$

The maximum brake torque is

$$T_{max} = \frac{D_{max} F_t}{2} = \frac{55(64.8)}{2} = 1782 \text{ in} \cdot \text{lb } (201 \text{ N} \cdot \text{m})$$

The rate at which the brake must dissipate heat is, by Eq. (8.19),

$$H_{av} = F_t V_w$$

The web velocity is

$$V_w = \frac{4000}{60} = 66.67 \text{ ft/s } (20.3 \text{ m/s})$$

So H_{av} is

$$H_{av} = 64.8(66.67) = 4320 \text{ ft} \cdot \text{lb/s } [5855 \text{ watts (W)}]$$

$$= 5.55 \text{ Btu/s}$$

8.3 TEMPERATURE CONSIDERATIONS

8.3.1 Intermittent Operation: Clutches and Brakes

The temperature rise can be estimated as

$$\Delta T = \frac{E}{Cm} \tag{8.20}$$

where m [pounds mass (lbm) or kilograms (kg)] = mass of the parts adjacent to the friction surfaces. The specific heat C for steel or cast iron is about 0.12 Btu/(lbm · °F) [500 J/(kg · °C)].

8.3.2 Frequent Operation: Caliper Disk Brakes

The average rate at which heat must be dissipated can be calculated by Eq. (8.16). The disk is capable of dissipating heat by a combination of convection and radiation.

And the convection-heat transfer is sensitive to the velocity of air moving over the disk. The rate at which the disk can dissipate heat is

$$H_{\text{diss}} = hA(T_d - T_a) \tag{8.21}$$

The overall heat transfer coefficient h is

$$h = h_r + f_v h_c \tag{8.22}$$

The heat transfer coefficients for radiation h_r and convection h_c are plotted in Fig. 8.13 against the temperature rise of the disk above the surrounding air. The ventilation factor f_v is plotted against the velocity of the moving air in Fig. 8.14.

Example 5. An industrial caliper brake is used 19 times per hour on average to stop a machine with a rotating inertia of $I = 328$ lb · in · s^2 (37.06 kg · m^2) from a speed of 315 rev/min. The mean air velocity over the disk will be 30 ft/s (9.14 m/s). What minimum exposed area on the disk is needed to limit the disk's temperature rise to 200°F (111°C)?

Solution. From Figs. 8.13 and 8.14, $h_r = 3.1 \times 10^{-6}$ Btu/(in^2 · s · °F), $h_c = 2.0 \times 10^{-6}$ Btu/(in^2 · s · °F), and $f_v = 5.25$. The overall heat transfer coefficient is

$$h = 3.1 \times 10^{-6} + 5.25(2.0 \times 10^{-6}) = 13.6 \times 10^{-6} \text{ Btu/(in}^2 \cdot \text{s} \cdot \text{°F)}$$

The energy the brake must dissipate per stop is, by Eq. (8.14),

$$E = \frac{I}{2}(\omega_o^2 - \omega_f^2)$$

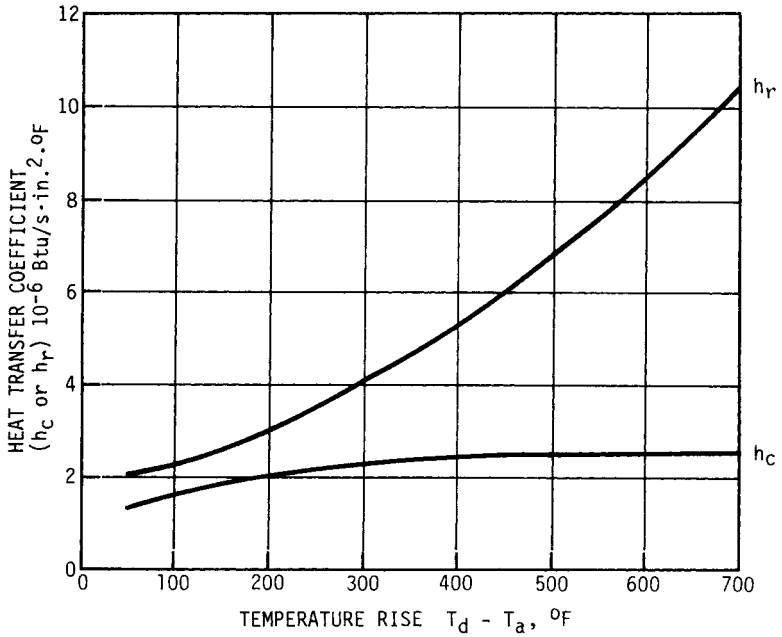

FIGURE 8.13 Heat transfer coefficients in still air. *(Tol-o-matic.)*

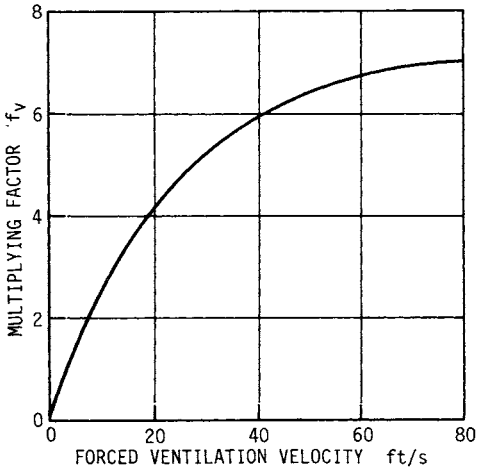

FIGURE 8.14 Ventilation factors. *(Tol-o-matic.)*

Here

$$\omega_o = \frac{2\pi}{60}(315) = 33 \text{ rad/s} \qquad \omega_f = 0$$

Therefore,

$$E = \frac{328}{2}(33^2) = 178.6 \times 10^3 \text{ lb} \cdot \text{in}$$

$$= 19.1 \text{ Btu } (20.150 \text{ kJ})$$

The average rate of energy generation is found by Eq. (8.16):

$$H_{\text{av}} = \frac{ES}{3600} = \frac{19.1(19)}{3600} = 0.101 \text{ Btu/s } (107 \text{ W})$$

The disk area needed can be calculated by using Eq. (8.21) and setting $H_{\text{av}} = H_{\text{diss}} = 0.101$ Btu/s. Thus

$$A = \frac{H_{\text{diss}}}{h(T_d - T_a)} = \frac{0.101}{(13.6 \times 10^{-6})(200)} = 37.1 \text{ in}^2 \ (0.0239 \text{ m}^2)$$

8.4 FRICTION MATERIALS

To help in preliminary design, Tables 8.7 and 8.8 have been compiled, principally from data supplied by British and U.S. manufacturers of friction materials. Although these data are representative, they are hardly exhaustive. And they should be used

TABLE 8.7 Characteristics of Friction Materials for Brakes and Clutches

Material	Friction coefficient μ	Maximum pressure p_{max}, psi	Maximum temperature		Maximum velocity V_{max}, ft/min	Applications
			Instantaneous, °F	Continuous, °F		
Cermet	0.32	150	1500	750		Brakes and clutches
Sintered metal (dry)	0.29–0.33	300–400	930–1020	570–660	3600	Clutches and caliper disk brakes
Sintered metal (wet)	0.06–0.08	500	930	570	3600	Clutches
Rigid molded asbestos (dry)	0.35–0.41	100	660–750	350	3600	Drum brakes and clutches
Rigid molded asbestos (wet)	0.06	300	660	350	3600	Industrial clutches
Rigid molded asbestos pads	0.31–0.49	750	930–1380	440–660	4800	Disk brakes
Rigid molded nonasbestos	0.33–0.63	100–150		500–750	4800–7500	Clutches and brakes
Semirigid molded asbestos	0.37–0.41	100	660	300	3600	Clutches and brakes
Flexible molded asbestos	0.39–0.45	100	660–750	300–350	3600	Clutches and brakes
Wound asbestos yarn and wire	0.38	100	660	300	3600	Vehicle clutches
Woven asbestos yarn and wire	0.38	100	500	260	3600	Industrial clutches and brakes
Woven cotton	0.47	100	230	170	3600	Industrial clutches and brakes
Resilient paper (wet)	0.09–0.15	400	300		$PV < 500\,000$ psi·ft/min	Clutches and transmission bands

SOURCES: Ferodo Ltd., Chapel-en-le-frith, England; Scan-pac, Mequon, Wisc.; Raybestos, New York, N.Y. and Stratford, Conn.; Gatke Corp., Chicago, Ill.; General Metals Powder Co., Akron, Ohio; D. A. B. Industries, Troy, Mich.; Friction Products Co., Medina, Ohio.

TABLE 8.8 Area of Friction Material Required for a Given Average Braking Power

Duty cycle	Typical applications	Ratio of area to average braking power, $in^2/(Btu/s)$		
		Band and drum brakes	Plate disk brakes	Caliper disk brakes
Infrequent	Emergency brakes	0.85	2.8	0.28
Intermittent	Elevators, cranes, and winches	2.8	7.1	0.70
Heavy-duty	Excavators, presses	5.6–6.9	13.6	1.41

SOURCES: Refs. [8.6], Sec. A51, and [8.7].

for preliminary design estimates only. A friction materials manufacturer should be consulted both to learn of additional options and to get more authoritative data.

Although Table 8.7 lists maximum recommended values for contact pressure and rubbing velocity, it is not very likely that you can go the limit on both parameters at once. And a careful distinction must be made between the maximum temperature permissible for a short time and the safe temperature level for continuous operation. The temperature limit for continuous operation is much lower than that for a brief temperature peak.

Preliminary design of brakes is aided by calculating the lining area needed for the average rate at which energy has to be dissipated by the brakes (*braking power*). Table 8.8 lists values that are typical of modern design practice. Again, after using these data to make some preliminary design estimates, you will need to contact the manufacturers of the friction materials before making final design decisions.

8.5 TORQUE AND FORCE ANALYSIS OF RIM CLUTCHES AND BRAKES

8.5.1 Long-Shoe Rim Brake

One shoe of an internal expanding rim brake is shown in Fig. 8.15. Usually there is a second shoe as well. The shoe is pivoted about the fixed point *A*. It is actuated by a force *F* which can be provided in a number of ways: mechanically, hydraulically, pneumatically, electromagnetically, or by some combination of these.

The forces on the shoe include the actuating force *F,* a reaction force *R* at the pivot, the distributed normal force, and the distributed friction force, the latter two exerted by the drum on the shoe.

For purposes of analysis, the distributed normal and frictional forces on the shoe can be replaced by a resultant normal force *P* and a resultant frictional force *fP.* Use of these fictional concentrated forces simplifies the analysis. There is one odd consequence, however. The resultant frictional force *fP* has to be regarded as acting beyond the surface of the shoe at some point *C,* the *center of pressure.* Figure 8.16 shows the shoe subjected to this equivalent force system.

Pressure Distribution along Lining. A first step in developing an equation for the torque capacity of the shoe is to adopt a model for the pressure distribution along

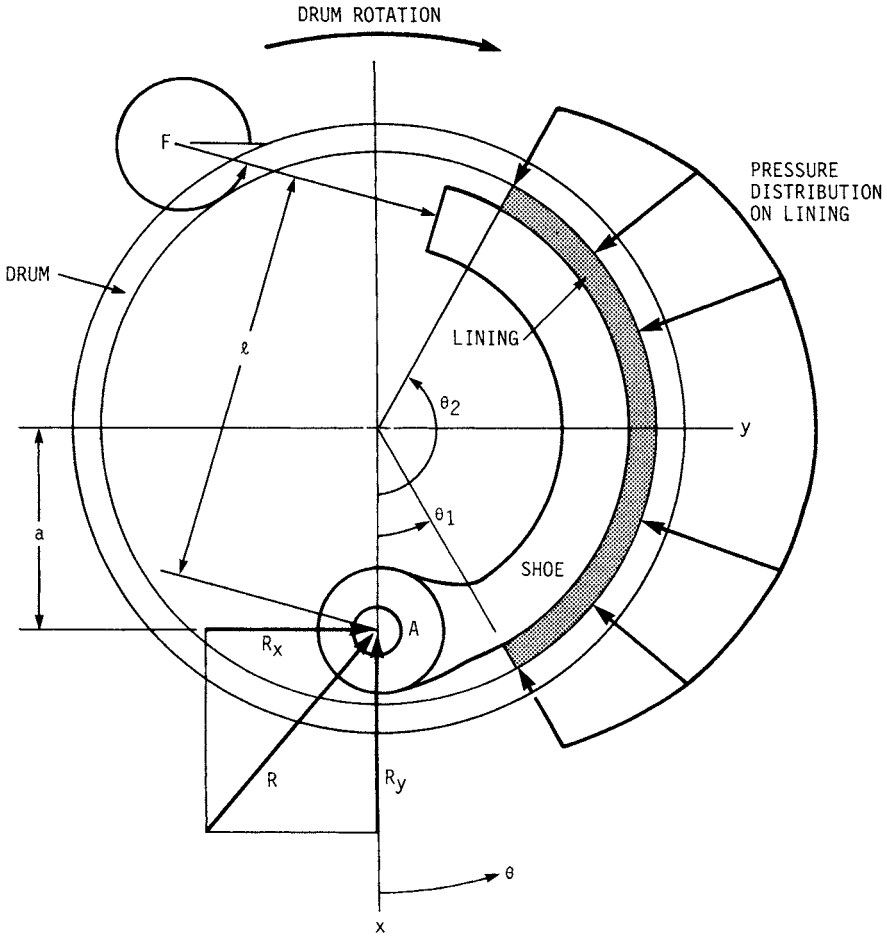

FIGURE 8.15 Forces on an internal long shoe.

the lining of the shoe. Assuming that the lining is elastic and of uniform thickness, but that the drum is perfectly rigid, the expression for the normal pressure p on the lining at any angular position θ is

$$p = \frac{p_{\max} \sin \theta}{(\sin \theta)_{\max}} \tag{8.23}$$

In the usual case, the shoe straddles the $\theta = 90°$ position and $(\sin \theta)_{\max} = 1$.

The variation of contact pressure along the lining is significant. To assume a uniform pressure is to oversimplify. For example, for a shoe extending from $\theta = 30°$ to $\theta = 165°$, the pressure varies from $0.5p_{\max}$ at 30° to $p_{\max}$ at 90°, and to $0.26p_{\max}$ at 165°.

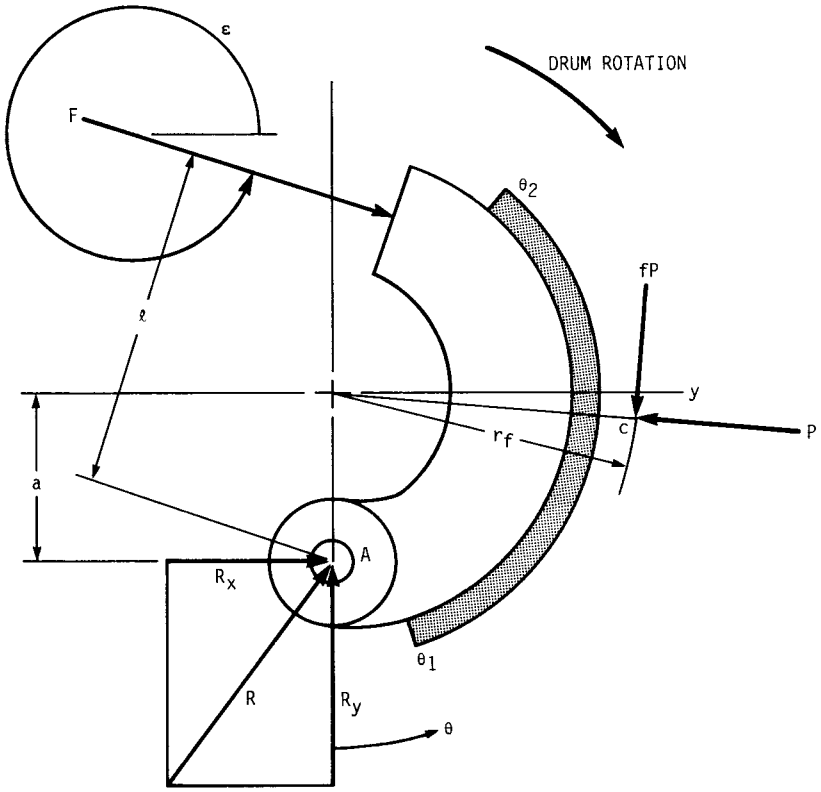

FIGURE 8.16 Equivalent force system on a long internal shoe.

Torque Capacity. With a model for contact pressure variation in hand, the friction torque exerted by the shoe on the drum can be found by a simple integration:

$$T = \int_{\theta_1}^{\theta_2} fpbr^2 \, d\theta \tag{8.24}$$

where b = width of lining. Substituting for p from Eq. (8.23) and integrating, we get

$$T = \frac{p_{\max}}{(\sin\theta)_{\max}} fbr^2(\cos\theta_1 - \cos\theta_2) \tag{8.25}$$

Normal Force. To determine the actuating force and the pin reaction, it is necessary first to find the normal force P. The components of P are

$$P_x = \int_{\theta_1}^{\theta_2} pbr \, d\theta \sin\theta \tag{8.26}$$

and

$$P_y = \int_{\theta_1}^{\theta_2} pbr \, d\theta \cos\theta \tag{8.27}$$

Again, substituting for p from Eq. (8.23) and integrating, we find

$$P_x = \frac{brp_{\max}}{2(\sin\theta)_{\max}} (\theta_2 - \theta_1 + \sin\theta_1 \cos\theta_1 - \sin\theta_2 \cos\theta_2) \tag{8.28}$$

and

$$P_y = \frac{brp_{\max}}{2(\sin\theta)_{\max}} (\cos^2\theta_1 - \cos^2\theta_2) \tag{8.29}$$

The resultant normal force P has the magnitude

$$P = (P_x^2 + P_y^2)^{1/2} \tag{8.30}$$

and is located at the angle θ_p, where

$$\theta_p = \tan^{-1}\frac{P_x}{P_y} \tag{8.31}$$

Effective Friction Radius. The location r_f of the center of pressure C is found by equating the moment of a concentrated frictional force fP to the torque capacity T:

$$T = fPr_f \qquad \text{or} \qquad r_f = \frac{T}{fP} \tag{8.32}$$

Brake-Shoe Moments. The last basic task is to find a relation among actuating force F, normal force P, and the equivalent friction force fP. The moments about the pivot point A are

$$M_a - M_n + M_f = 0 \tag{8.33}$$

where

$$M_a = F\ell \tag{8.34}$$

$$M_n = Pa\sin\theta_p \tag{8.35}$$

$$M_f = P(r_f - a\cos\theta_p) \tag{8.36}$$

Self-energizing Shoes. The brake shoe in Fig. 8.16 is said to be *self-energizing,* for the frictional force fP exerts a clockwise moment about point A, thus assisting the actuating force. On vehicle brakes, this would also be called a *leading shoe.* Suppose a second shoe, a *trailing shoe,* were placed to the left of the one shown in Fig. 8.16. For this shoe, the frictional force would exert a counterclockwise moment and oppose the action of the actuating force. Equation (8.33) can be written in a form general enough to apply to both shoes and to external shoes as well:

$$M_a - M_n \pm M_f = 0 \tag{8.37}$$

Burr [8.2], p. 84, proposes this simple rule for using Eq. (8.37): "If to seat a shoe more firmly against the drum it would have to be rotated in the same sense as the

drum's rotation, use the positive sign for the M_f term. Otherwise, use the negative sign."

Pin Reaction. At this point in the analysis, the designer should sketch a free-body diagram of each shoe, showing the components of the actuating force *F,* the normal force *P,* and the friction force *fP.* Then the components of the pin reaction can be found by setting to zero the sum of the force components in each direction (x and y).

Design. The design challenge is to produce a brake with a required torque capacity *T.* A scale layout will suggest tentative values for the dimensions θ_1, θ_2, a, ℓ, and ε. From the lining manufacturer we learn the upper limit on maximum contact pressure p_{max} and the expected range for values of the frictional coefficient *f.* The designer must then determine values for lining width b and the actuating force F for each shoe.

Since the friction force assists in seating the shoe for a self-energizing shoe but opposes the actuating moment for a self-deenergizing shoe, a much larger actuating force would be needed to provide as large a contact pressure for a trailing shoe as for a leading shoe. Or if, as is often the case, the same actuating force is used for each shoe, a smaller contact pressure and a smaller torque capacity are achieved for the trailing shoe.

The lining manufacturer will usually specify a likely range of values for the coefficient of friction. It is wise to use a low value in estimating the torque capacity of the shoe.

In checking the design, make sure that a self-energizing shoe is not, in fact, self-locking. For a *self-locking* shoe, the required actuating force is zero or negative. That is, the lightest touch would cause the brake to seize. A brake is self-locking when

$$M_n \le M_f \tag{8.38}$$

As a design rule, make sure that self-locking could occur only if the coefficient of friction were 25 to 50 percent higher than the maximum value cited by the lining manufacturer.

Example 6. Figure 8.17 shows a preliminary layout of an automotive brake with one leading shoe and one trailing shoe. The contact pressure on the lining shall not exceed 1000 kilopascals (kPa). The lining manufacturer lists the coefficient of friction as 0.34 ± 0.02. The brake must be able to provide a braking torque of 550 N · m. Two basic design decisions have already been made: The same actuating force is used on each shoe, and the lining width is the same for each.

Check dimension a to make sure that self-locking will not occur. Determine the lining width b, the actuating force F, and the maximum contact pressure p_{max} for each shoe.

Solution. One way to proceed is to express the braking torque T, the normal moment M_n, and the frictional moment M_f in terms of lining width b and maximum contact pressure p_{max}. Then the design can be completed by equating the actuating force for the two shoes, setting the sum of the braking torques to 550 N · m, and selecting the lining width b so that the maximum contact pressure is within bounds.

1. The dimension a is

$$a = (83^2 + 25^2)^{1/2} = 86.7 \text{ mm} = 0.0867 \text{ m}$$

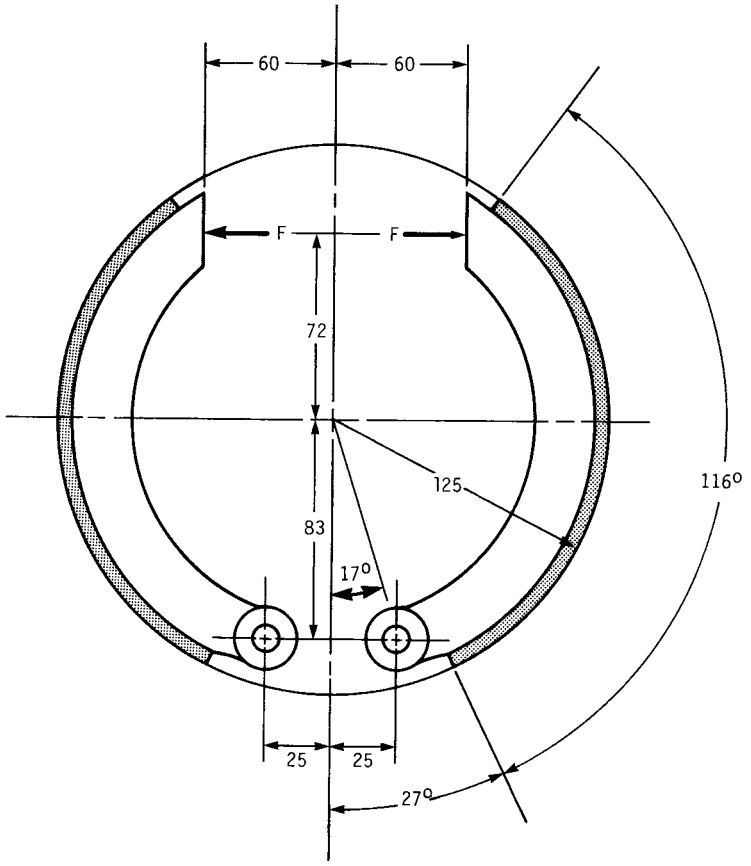

FIGURE 8.17 A leading-shoe trailing-shoe automotive brake.

2. For either shoe the braking torque can be written in terms of the coefficient of friction, the lining width, and the maximum contact pressure. From Eq. (8.25),

$$T = \frac{p_{\max}}{(\sin\theta)_{\max}} fbr^2(\cos\theta_1 - \cos\theta_2)$$

$$= \frac{p_{\max}}{1} fb(0.125)^2(\cos 10° - \cos 126°)$$

$$= 0.024\,57 fbp_{\max}$$

The numerical values of T are different for the two shoes, since $p_{\max}$ differs.

3. Now the normal force P must be calculated. Equations (8.28), (8.29), (8.30), and (8.31) are used:

$$P_x = \frac{brp_{\max}}{2(\sin\theta)_{\max}}(\theta_2 - \theta_1 + \sin\theta_1\cos\theta_1 - \sin\theta_2\cos\theta_2)$$

$$= \frac{b(0.125)p_{\max}}{2(1)}\left(\frac{126° - 10°}{57.296°} + \sin 10°\cos 10° - \sin 126°\cos 126°\right)$$

$$= 0.1671bp_{\max}$$

$$P_y = \frac{brp_{\max}}{2(\sin\theta)_{\max}}(\cos^2\theta_1 - \cos^2\theta_2)$$

$$= \frac{b(0.125)p_{\max}}{2(1)}(\cos^2 10° - \cos^2 126°) = 0.0390bp_{\max}$$

$$P = (P_x^2 + P_y^2)^{1/2} = 0.1716bp_{\max}$$

$$\theta_p = \tan^{-1}\frac{P_x}{P_y} = \tan^{-1}\frac{0.1671}{0.0390} = 76.85°$$

4. The effective friction radius r_f is, by Eq. (8.32),

$$r_f = \frac{T}{fP} = \frac{0.024\,57fbp_{\max}}{f(0.1716bp_{\max})} = 0.1432\text{ m} = 143.2\text{ mm}$$

5. The moments about pivot point A are found by Eqs. (8.34) to (8.36):

$$M_a = F\ell = F(0.072 + 0.083) = 0.155F$$

$$M_n = Pa\sin\theta_p = 0.1716bp_{\max}(0.0867)(\sin 76.85°) = 0.014\,49bp_{\max}$$

$$M_f = fP(r_f - a\cos\theta_p)$$

$$= f(0.1716bp_{\max})(0.1432 - 0.0867\cos 76.85°)$$

$$= 0.021\,19fbp_{\max}$$

6. For the leading (self-energizing) shoe, the proper form of Eq. (8.37) is

$$M_a - M_n + M_f = 0$$

Therefore

$$0.155F^l - 0.014\,49bp^l_{\max} + 0.021\,19fbp^l_{\max} = 0$$

The superscript l has been used to designate the leading shoe.

7. For the trailing shoe, Eq. (8.37) has the form

$$M_a - M_n - M_f = 0$$

Thus

$$0.155F^t - 0.014\,49bp^t_{\max} - 0.021\,19fbp^t_{\max} = 0$$

8. Since the same actuating force is used for each shoe, $F^l = F^t$. After substituting from the two moment equations, we obtain

$$\frac{0.014\,49bp^l_{\max} - 0.021\,19fbp^l_{\max}}{0.155} = \frac{0.014\,49bp^t_{\max} + 0.021\,19fbp^t_{\max}}{0.155}$$

After cancellation and substitution of $f = 0.32$ (the most pessimistic assumption),

$$p^l_{\max} = 2.759p^t_{\max}$$

9. The torque capacities of the shoe must sum to 550 N · m:

$$T^l + T^t = 550$$

$$(0.024\,57)(0.32)b(p^l_{\max} + p^t_{\max}) = 550$$

Then

$$b(p^l_{\max} + p^t_{\max}) = 69.95 \text{ kN} \cdot \text{m}$$

10. Enough information has been accumulated to begin to specify the design. Since $p^l_{\max} = 1000$ kPa, $p^t_{\max} = 1000/2.759 = 362.4$ kPa. Now the distance b can be found. Since

$$b(p^l_{\max} + p^t_{\max}) = 69.95$$

we have

$$b = \frac{69.95 \times 10^3}{(1000 + 362.4)(10^3)} = 0.0513 \text{ m, or about 51 mm}$$

11. The actuating force F ($F^l = F^t$) can be found from either shoe's moment equation. For the leading shoe,

$$0.155F^l - 0.014\,49bp^l_{\max} + 0.021\,19fbp^l_{\max} = 0$$

Substituting values of b, f, and $p^l_{\max}$ gives $F = 2.55$ kN. Thus $F = F^l = F^t = 2.55$ kN.

12. Now we determine whether the leading shoe is self-locking or too close to self-locking for safety. The moment equation used above in step 11 is used again, but this time with an f value 50 percent higher than the maximum value cited by the lining manufacturer. Use

$$f = 1.5(0.34 + 0.02) = 0.54$$

Then by substituting into the moment equation, the corresponding value of F can be found:

$$0.155F^l - (0.014\,49)(0.0513)(1000) + (0.021\,19)(0.54)(0.0513)(1000) = 0$$

Solving gives $F^l = F^t = 1.001$ kN. Since a large positive force is required to activate the leading shoe even for this very high coefficient of friction, the brake is in no danger of self-locking.

8.5.2 Centrifugal Clutches

The simple centrifugal clutch shown in Fig. 8.18 has a number of shoes which can move radially and against the drum as the input shaft speed increases. A garter spring regulates the engagement speed. At engagement speed the weights contact the drum's inner surface and begin to drive it, and the attached pulley, by means of friction to bring it up to speed.

Design Equations. The normal force between each shoe and the inner circumference of the drum is principally due to centrifugal force. However, the garter spring exerts some inward force. The net normal force [8.1] is

$$F_n = \frac{mr\omega^2}{g_c} - 2S\cos\left(90° - \frac{180°}{N_s}\right) \tag{8.39}$$

Engagement occurs at the shaft speed ω_e when $F = 0$. The proper initial tension S for the garter spring is found by setting $\omega = \omega_e$ and $F = 0$ in Eq. (8.39). The engagement speed is selected by the designer (for example, about 70 percent of running speed). The required value for S is

$$S = \frac{mr\omega_e^2}{2g_c\cos\,(90° - 180°/N_s)} \tag{8.40}$$

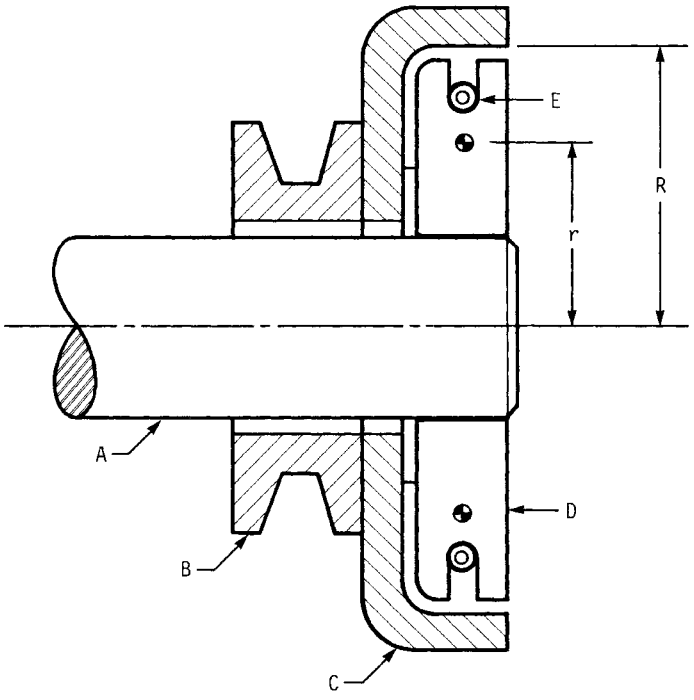

FIGURE 8.18 Free-shoe centrifugal clutch with garter spring to regulate engagement speed. *A,* input shaft; *B,* output pulley; *C,* drum; *D,* weights; *E,* garter spring.

The torque capacity at any shaft speed ω is

$$T = fF_n RN_s \tag{8.41}$$

Example 7. A centrifugal clutch is being considered for an application where the running speed is 3000 rev/min and engagement is to begin at 1000 rev/min. It is planned to use four shoes, each with a mass of 140 grams (g). A coefficient of friction $f = 0.3$ can be achieved. The inner diameter of the drum is 75 mm, and the radius R to the center of gravity of each shoe is 25 mm. (1) What should be the initial tension of the garter spring? (2) What is the normal force on each shoe at running speed? (3) What is the torque capacity at running speed? (4) What is the power capacity at running speed if a service factor of 2.25 is required?

Solution.

1. The initial tension of the garter spring is found from Eq. (8.40):

$$S = \frac{0.140(0.025)[1000(2\pi/60)]^2}{2(1)\cos(90° - 180°/4)} = 27.1 \text{ N}$$

2. The normal force on each shoe at 3000 rev/min is, by Eq. (8.39),

$$F_n = \frac{(0.140)(0.025)[(2\pi/60)(3000)]^2}{1} - 2(27.1)\cos(90° - 180°/4)$$

$$= 307.1 \text{ N}$$

3. The torque capacity at running speed is

$$T = fF_n RN_s = (0.3)(307.1)\left(\frac{0.075}{2}\right)(4) = 13.8 \text{ N} \cdot \text{m}$$

4. The power capacity uncorrected for service factor is

$$P = \frac{Tn}{9550} = \frac{13.8(3000)}{9550} = 4.34 \text{ kW}$$

Correcting for service factor, we see the power rating is

$$P_{\text{rating}} = \frac{P}{K_S} = \frac{4.34}{2.25} = 1.93 \text{ kW}$$

8.6 BAND AND CONE BRAKES AND CLUTCHES

8.6.1 Band Brakes

A typical design for a band brake is shown in Fig. 8.19. A flexible metal band lined with a friction material contacts the drum over an angle of wrap θ and exerts a braking torque T on the drum. This particular design is self-energizing, since the moment exerted on the lever by force P_1 assists in actuating the brake.

CLUTCHES AND BRAKES

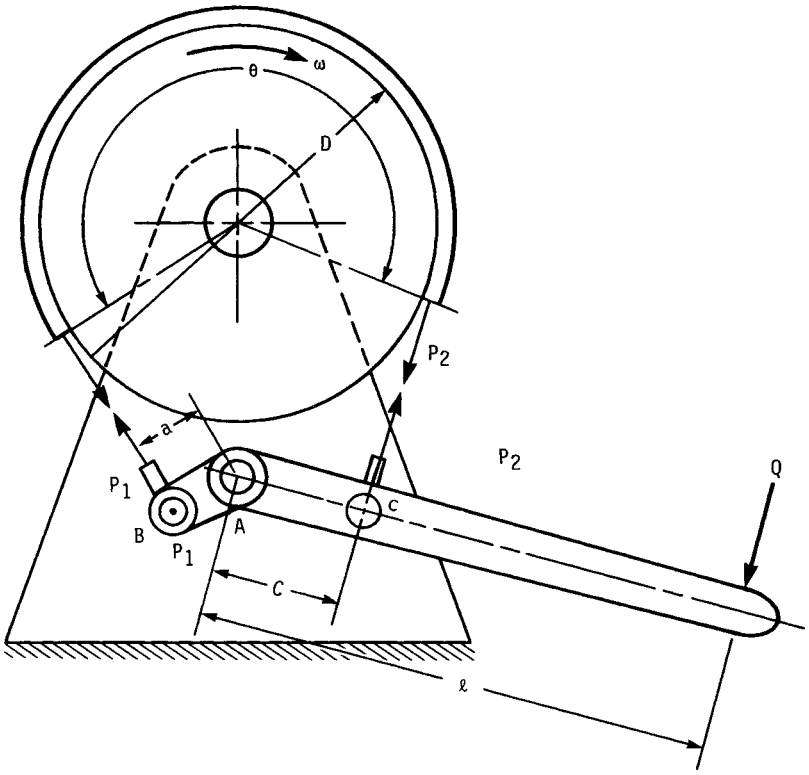

FIGURE 8.19 Forces on a band brake; b = bandwidth.

Four basic relationships are needed for analysis or design. For a band wrapped around a drum, the ratio of tensions is

$$\frac{P_1}{P_2} = e^{f\theta} \tag{8.42}$$

where the notation is indicated in Fig. 8.19. The net torque exerted on the drum by the band is

$$T = (P_1 - P_2\left(\frac{D}{2}\right) \tag{8.43}$$

The maximum contact pressure between the band and the drum occurs at the more taut P_1 end of the band:

$$p_{\max} = \frac{2P_1}{bD} \tag{8.44}$$

Finally, it is necessary to sum moments on the lever about pivot A to get the relationship involving the actuating force Q:

$$Q\ell - P_2 c + P_1 a = 0 \tag{8.45}$$

After substituting for P_1 and P_2 in terms of p_{max}, f, and θ, we get the following equation for actuating force:

$$Q = \frac{bDp_{max}}{2\ell}\left(\frac{c}{e^{f\theta}} - a\right) \tag{8.46}$$

For p_{max} you should use the value suggested by the lining manufacturer.

This brake could be self-locking if the designer were to get careless. The actuating force Q should always be positive. If it were zero or negative, the slightest touch on the lever would cause the brake to lock abruptly. The expression in the parentheses in Eq. (8.46) must always be positive. Thus, as a rule, design the brake so that

$$a < \frac{c}{e^{f\theta}} \tag{8.47}$$

In checking for self-locking, use a value for f that is 25 to 50 percent greater than the maximum value cited by the lining manufacturer.

Example 8. A band brake like that in Fig. 8.19 is needed to exert a braking torque of 3100 lb · in (350 N · m) on a drum with 10-in (0.254-m) diameter. The actuating force Q (exerted by the operator's foot) should not have to exceed 25 lb (111 N). Limit the maximum contact pressure to 60 pounds per square inch (psi) [0.414 megapascal (MPa)]. The value for f is 0.31 ± 0.03. (1) Make sure the brake will not be self-locking for an f value 30 percent above the maximum value. (2) Calculate the bandwidth b to limit the contact pressure. (3) Find the length ℓ for the operating lever. (4) For the same actuating force, what is the braking torque if the drum's rotation is reversed?

Solution. A scale layout indicates that $a = 1$ in (0.0254 m) and $\theta = 200°$ are feasible values when the lever's pivot point A is placed directly below the center of the drum. Then $c = 5$ in (0.127 m), corresponding to the drum's radius.

1. First make sure that the brake will not be self-locking. Use $f = 1.3(0.31 + 0.03) = 0.442$ and $\theta = 200°/57.296 = 3.491$ rad. Then, from Eq. (8.47),

$$a < \frac{5}{0.442(3.491)} \qquad \text{or} \qquad a < 1.069 \text{ in}$$

So the dimension $a = 1$ in will do nicely.

2. Now select a bandwidth b so that p_{max} does not exceed 60 psi (0.414 MPa). By Eqs. (8.42) and (8.43),

$$\frac{P_1}{P_2} = e^{0.28(3.491)} = 2.658$$

$$3100 = (P_1 - P_2)\left(\frac{10}{2}\right)$$

Solving these for P_1 and P_2 gives $P_1 = 994$ lb (4420 N) and $P_2 = 374$ lb (1664 N). So, by Eq. (8.44), the bandwidth is

$$b = \frac{2P_1}{p_{max}D} = \frac{2(994)}{60(10)} = 3.31 \text{ in (say 3.5 in)}$$

3. Next the moment arm length ℓ for the actuating force Q must be found from Eq. (8.45):

$$\ell = \frac{P_2 c - P_1 a}{Q} = \frac{374(5) - 994(1)}{25} = 35 \text{ in}$$

4. Finally, the torque capacity of the brake for the same actuating force, but with the drum rotating counterclockwise, can be evaluated. Since the drum turns counterclockwise, the braking torque must be clockwise. Thus, forces P_1 and P_2 are interchanged. The larger force P_1 is applied at point *C,* and the force P_2 is applied at point *B.* Equation (8.45), suitably rewritten, is

$$P_1 c - P_2 a - Q\ell = 0$$

But Eqs. (8.42) and (8.43) do not need to be changed:

$$P_1(5) - P_2(1) - 25(35) = 0$$

or

$$5P_1 - P_2 = 875$$

$$\frac{P_1}{P_2} = e^{f\theta} = 2.658$$

Then $P_1 = 189$ lb and $P_2 = 70$ lb. And the net braking torque is

$$T = (P_1 - P_2)\left(\frac{D}{2}\right) = (189 - 70)\left(\frac{10}{2}\right) = 595 \text{ lb} \cdot \text{in}$$

This is considerably less than the 3100-lb · in capacity for clockwise rotation of the drum.

8.6.2 Cone Brakes and Clutches

Two mating cones kept in contact by an axial force can be used as a clutch, as in Fig. 8.20, or as a brake, as in Fig. 8.21. A small cone angle α produces a wedging action, and a large torque capacity is achieved for a small actuating force. But if the cone angle is too small, it becomes difficult to disengage the cones. A cone angle of 10° to 15° is a reasonable compromise.

Basic Relationships. A cone is shown schematically in Fig. 8.22 with three elementary quantities indicated: area dA, normal contact force dP, and actuating force dF. From these it follows that the elementary torque dT is

$$dT = fr\, dP = frp\, \frac{2\pi r\, dr}{\sin \alpha} = \frac{2\pi f p r^2\, dr}{\sin \alpha} \tag{8.48}$$

Similarly, the elementary actuating force dF is

$$dF = dP \sin \alpha = 2\pi p r\, dr \tag{8.49}$$

The actuating force F and the torque capacity T are found by integrating in Eqs. (8.49) and (8.48) from the inside radius $d/2$ to the outside radius $D/2$:

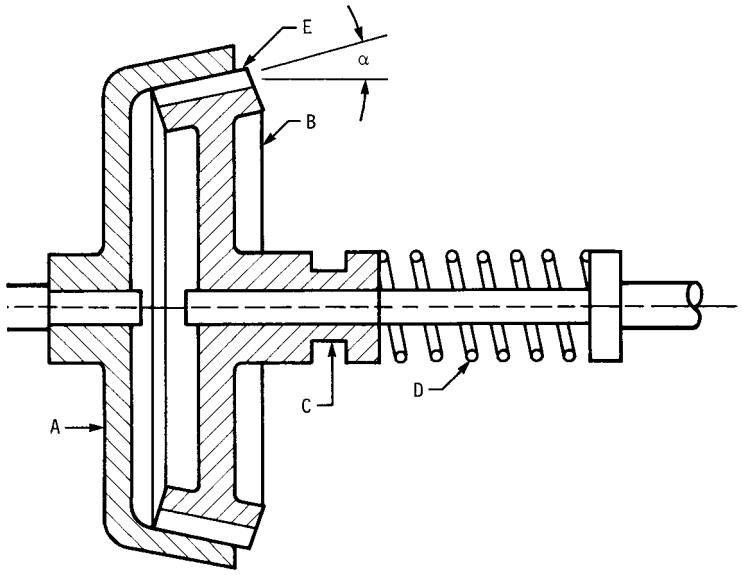

FIGURE 8.20 Cone clutch; *A,* cup; *B,* cone; *C,* shifting groove; *D,* spring; *E,* friction lining; α = cone angle.

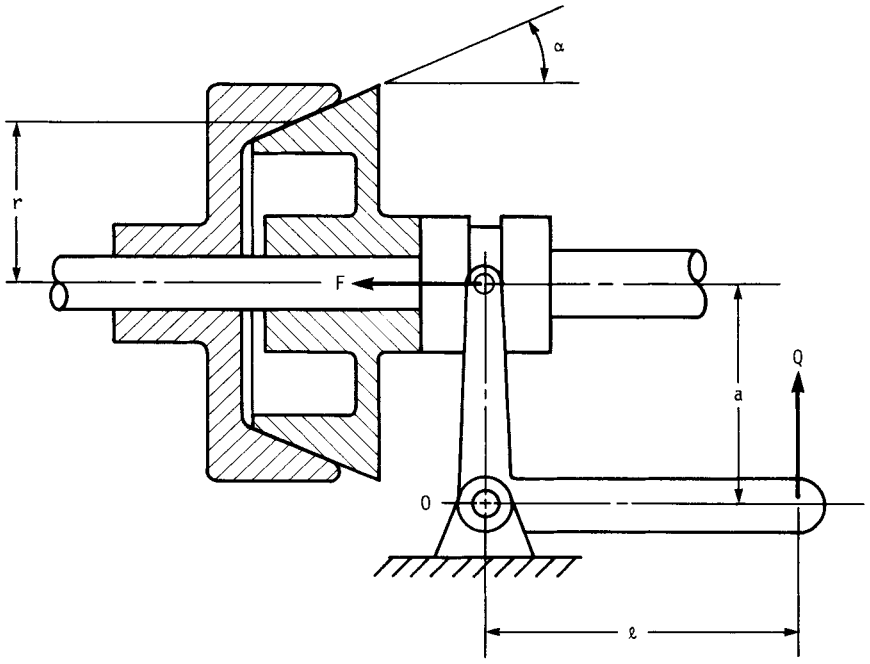

FIGURE 8.21 Cone brake; α = cone angle.

CLUTCHES AND BRAKES

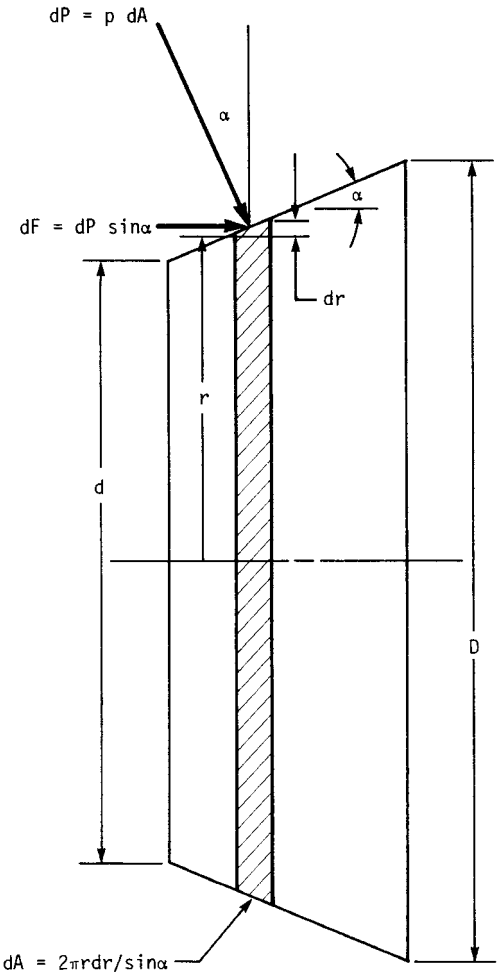

FIGURE 8.22 Elementary quantities on conical surface.

$$F = 2\pi \int_{d/2}^{D/2} pr\, dr \tag{8.50}$$

$$T = \frac{2\pi}{\sin \alpha} \int_{d/2}^{D/2} fpr^2\, dr \tag{8.51}$$

Before these integrations can be carried out, assumptions have to be made about the way in which contact pressure p and friction coefficient f vary across the active face of the cone. In what follows, the variations of f with pressure and rubbing velocity have been neglected. Only the variation in contact pressure p is used.

Contact-Pressure Distribution. When the friction surfaces are new, the pressure is fairly uniform across the clutch face. But after an initial wear-in period, the pressure

accommodates itself to a uniform rate of wear. We assume that the wear rate is proportional to the frictional work per unit area, that is, to fpV. If the variations in f are neglected, then the wear rate is proportional simply to pV, the product of contact pressure and rubbing velocity. We can write

$$pV = 2\pi r\omega p = \text{constant} \tag{8.52}$$

Thus across the face the product pr is constant, implying that p_{max} occurs at the inner radius $d/2$. In general,

$$p = \frac{p_{max} d}{2r} \tag{8.53}$$

A typical pressure distribution is shown in Fig. 8.23.

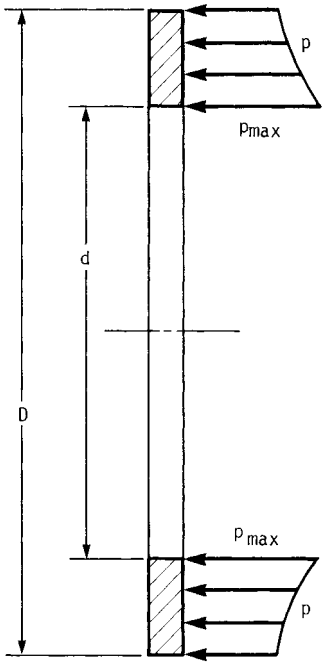

FIGURE 8.23 Contact-pressure distribution on face of cone after wear-in period (for constant f).

Torque Capacity. By substituting for p from Eq. (8.53) in Eq. (8.51) and carrying out the integration, we find the torque capacity T:

$$T = \frac{\pi f p_{max} d}{8 \sin \alpha} (D^2 - d^2) \tag{8.54}$$

Actuating Force. Equation (8.50) can be integrated to yield

$$F = \frac{\pi p_{max} d}{2} (D - d) \tag{8.55}$$

The last two equations can be combined to produce the useful result

$$T = \frac{Ff}{4 \sin \alpha} (D + d) \tag{8.56}$$

The last equation indicates that for the uniform-wear assumption, the mean friction radius is simply the average radius.

Moment Equation for Brake Lever. The axial actuating force for the cone brake shown in Fig. 8.21 can be found by summing moments on the lever about the pivot point O and solving for F. Thus

$$F = \frac{Q\ell}{a} \tag{8.57}$$

8.7 DISK CLUTCHES AND BRAKES

8.7.1 Multidisk Clutches and Brakes

The multidisk clutch in Fig. 8.24 is intended for wet operation using an oil coolant. Similar clutches are built for dry operation. Disk brakes are similar in construction

to the disk clutch. In either case, an axial force is applied to the flat surfaces of the elements to produce tangential frictional forces. Typically not more than the outer 40 percent of the radius is used. The ratio of inside to outside diameters may be as high as 0.80/1.

Contact-Pressure Distribution. The reasoning used to establish pressure distribution on the annular clutch or brake plate is the same as that used for cone clutches and brakes. After an initial wear-in period, the pressure distribution accommodates itself to a constant rate of wear across the active portion of the disk (Fig. 8.25). Equations (8.52) and (8.53) apply here also.

Axial Actuating Force. For a given set of dimensions and a permissible contact pressure, the corresponding actuating force is given by Eq. (8.55), which was developed for cone clutches and brakes.

Torque Capacity. For this pressure distribution, the torque capacity is

$$T = \frac{1}{8}[\pi f p_{\max} d(D^2 - d^2)N_p] \tag{8.58}$$

Although the torque equation could be derived independently, it can also be derived directly from Eq. (8.54) by setting the cone angle $\alpha = 90°$ and inserting N_p, the num-

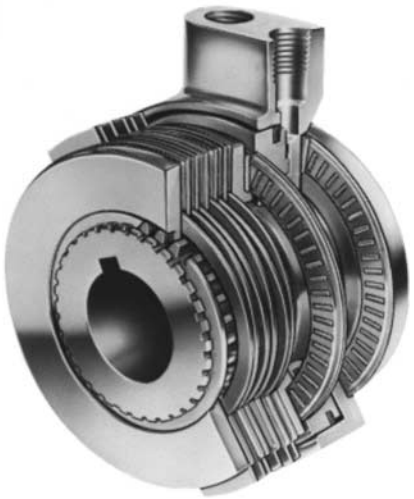

FIGURE 8.24 An oil-actuated multiple-disk clutch for enclosed operation in an oil spray or bath. *(Twin Disc, Inc.)*

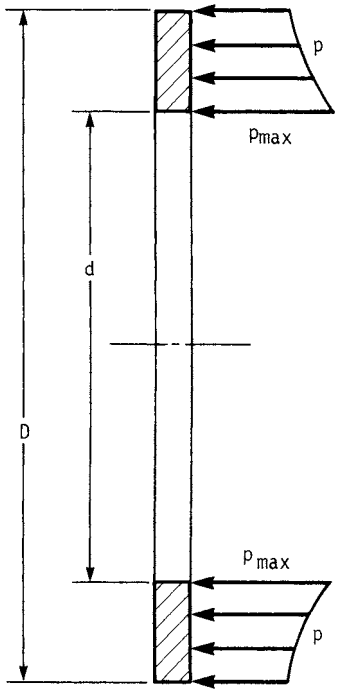

FIGURE 8.25 A friction member of a multiple-disk clutch or brake with the pressure distribution for uniform wear.

ber of pairs of contacting disk faces. Torque capacity can also be expressed in terms of the actuating force *F:*

$$T = \frac{FfN_p}{4}(D + d) \tag{8.59}$$

8.7.2 Caliper Disk Brakes

The automotive caliper disk brake shown in Fig. 8.9 is hydraulically operated. Two pads are pressed against opposite sides of the brake disk to provide a braking torque. The principle of operation is shown schematically in Fig. 8.26*a.*

Usually each pad is nearly the annular shape, illustrated in Fig. 8.26*b,* but occasionally a circular pad ("puck" or "button") is used (Fig. 8.26*c*).

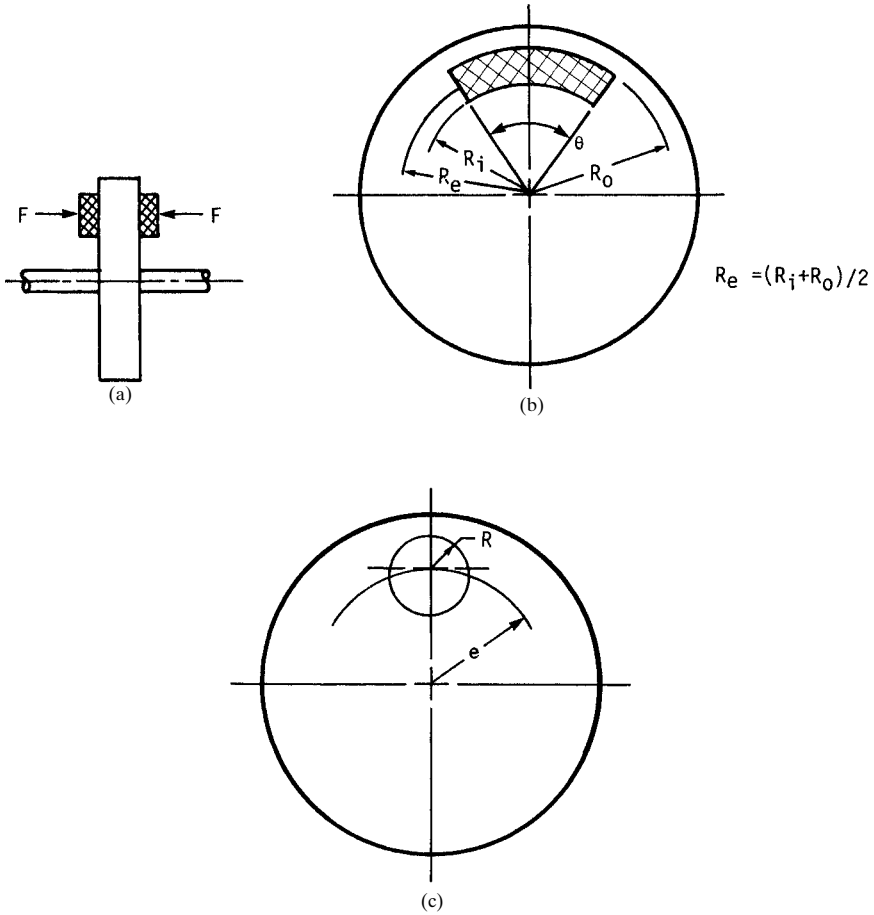

FIGURE 8.26 Caliper disk brake. (*a*) Principle of operation; (*b*) annular pad; (*c*) circular pad.

Torque Capacity. The torque capacity *per pad* is

$$T = fFR_e \tag{8.60}$$

If two pads are used, then the torque capacity is double the value calculated by Eq. (8.60).

This torque equation is quite simple. A friction force fF acting at an effective friction radius R_e produces a braking torque T. The practical issues are (1) the value to use for the effective friction radius R_e and (2) the maximum contact pressure p_{max} developed.

Actuating Force for Annular Pad. Brake designers often assume that the contact pressure does not vary very much over the annular pad. But you may prefer to use the uniform-wear approach as more realistic. Both approaches are given here.

The following two equations are used to calculate the actuating force for the constant-contact-pressure and the uniform-wear approaches, respectively:

$$F = p_{av}\theta \frac{R_o^2 - R_i^2}{2} \tag{8.61}$$

$$F = p_{max}\theta R_i(R_o - R_i) \tag{8.62}$$

The notation is shown in Fig. 8.26*a* and *b*.

The relation between average and maximum contact pressures for the uniform-wear approach is

$$\frac{p_{av}}{p_{max}} = \frac{2R_i/R_o}{1 + R_i/R_o} \tag{8.63}$$

In the limit, the average and maximum pressures become equal as the inner radius approaches the outer one. For $R_i/R_o = 0.60$, $p_{av} = 0.75p_{max}$; but for $R_i/R_o = 0.80$, $p_{av} = 0.89p_{max}$.

The uniform-wear assumption is the more conservative approach. For a given actuating force, it implies a smaller torque capacity.

Effective Friction Radius for Annular Pad. If the contact pressure is assumed to be constant over the pad, the effective friction radius is

$$R_e = \frac{2}{3}\frac{R_o^3 - R_l^3}{R_o^2 - R_l^2} \tag{8.64}$$

When the uniform-wear assumption is made, the effective friction radius is simply

$$R_e = \frac{R_i + R_o}{2} \tag{8.65}$$

Circular Pads. Fazekas [8.3] has derived the basic equations for circular pads. The effective friction radius is

$$R_e = \delta e \tag{8.66}$$

where e = radius from the center of the disk to the center of the pad and δ = multiplier found in Table 8.9. Also tabulated in Table 8.9 is the ratio of maximum to average contact pressure.

TABLE 8.9 Design Factors for Caliper Disk Brakes with Circular Pads

R/e	$\delta = R_e/e$	p_{max}/p_{av}
0	1.000	1.000
0.1	0.983	1.093
0.2	0.969	1.212
0.3	0.957	1.367
0.4	0.947	1.578
0.5	0.938	1.875

SOURCE: Ref. [8.3].

The actuating force on each pad is

$$F = \pi R^2 p_{av} \tag{8.67}$$

The torque capacity per pad is found by using Eq. (8.60) after F and R_e have been calculated.

Example 9. A sports car requires disk brakes for the front wheels. It has been decided to use two annular pads per wheel with $R_i = 3.875$ in, $R_o = 5.5$ in, and $\theta = 108°$. The friction material supplier guarantees a coefficient of friction of at least $f = 0.37$. Each pad is actuated by two hydraulic cylinders, each 1.5 in in diameter. Each front-wheel brake provides a braking torque capacity of 13×10^3 lb · in. What hydraulic pressure is needed at the wheel cylinders? What are the average and the maximum contact pressures? Assume uniform wear.

Solution

1. The torque capacity per pad has to be $(13 \times 10^3)/2 = 6500$ lb · in. Given uniform wear, the effective friction radius is, by Eq. (8.65),

$$R_e = \frac{R_i + R_o}{2} = \frac{3.875 + 5.5}{2} = 4.69 \text{ in}$$

The corresponding actuating force is, by Eq. (8.60),

$$T = \frac{T}{fR_e} = \frac{6500}{0.37(4.69)} = 3750 \text{ lb per pad}$$

or

$$F = 1875 \text{ lb per wheel cylinder}$$

The hydraulic pressure at the wheel cylinder has to be

$$p_h = \frac{F}{A_p} = \frac{4F}{\pi d_p^2} = \frac{4(1875)}{\pi(1.5)^2} = 1060 \text{ psi}$$

2. Equation (8.62) can be used to find the maximum contact pressure:

$$p_{max} = \frac{F}{\theta R_i (R_o - R_i)} = \frac{3750}{(108°/57.296)(3.875)(5.5 - 3.875)} = 316 \text{ psi}$$

For finding the average contact pressure, use Eq. (8.63):

$$p_{av} = p_{max} \frac{2R_i/R_o}{1 + R_i/R_o} = 316 \frac{2(3.875)/5.5}{1 + 3.875/5.5} = 261 \text{ psi}$$

8.8 ELECTROMAGNETIC TYPES

Electromagnetic forces are used in a variety of ways to couple two sides of a clutch or a brake. The use of electrically generated forces implies relatively easy means of automatic control.

8.8.1 Magnetically Actuated Friction Clutches and Brakes

The most common use of electromagnetic forces is to provide the actuating force for a friction brake or clutch. The configuration shown in Fig. 8.27 can be used either as a clutch or as a brake. When power is applied to the coil, the magnet, faced with a friction material, attracts the armature. Torque can be varied by using a potentiometer. If one member is fixed, the device functions as a brake; otherwise, it is a clutch.

The combination clutch-brake in Fig. 8.28 uses a single solenoid coil. When the coil is deenergized, the clutch is disengaged and springs prevent the release of the brake. When the coil is energized, the clutch is engaged and the brake is released. An arrangement of opposing mechanical springs ensures that the input-side clutch is fully engaged for a brief time before the brake is released. This is done by making the springs assisting clutch engagement weaker than those resisting brake release.

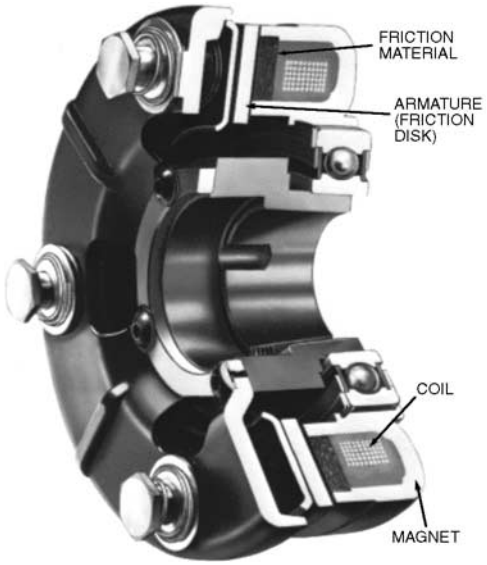

FIGURE 8.27 Electromagnetic friction clutches and brakes. *(Warner Electric Brake and Clutch Co.)*

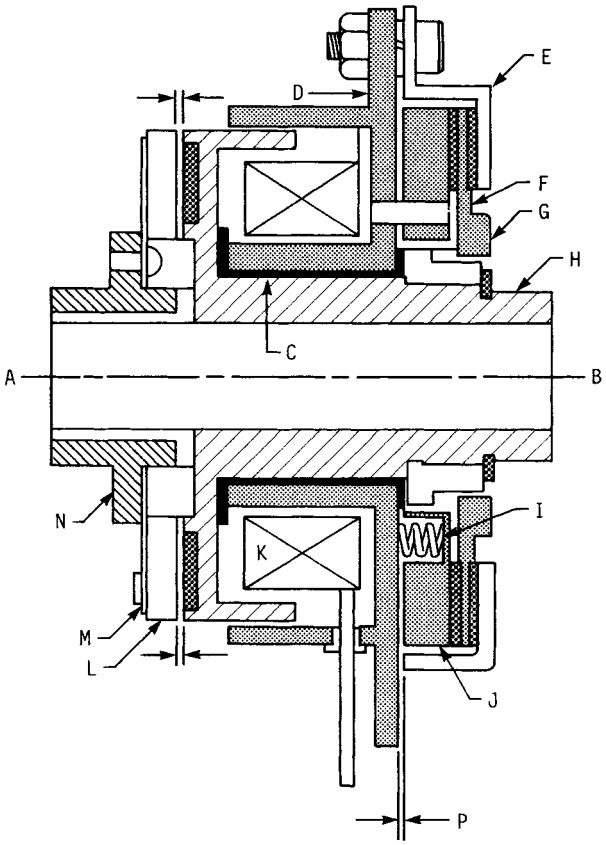

FIGURE 8.28 Clutch-brake transmission. *A,* input; *B,* output; *C,* field coil bearing; *D,* field coil assembly; *E,* pressure cup; *F,* brake plate; *G,* hub spring; *H,* rotor assembly; *I,* brake spring; *J,* brake armature; *K,* field coil; *L,* clutch armature; *M,* clutch spring; *N,* drive plate; *P,* air gap. *(Electroid Corporation.)*

8.8.2 Magnetic Clutches

The operating characteristics of three types of magnetic clutches are shown in Fig. 8.29.

Magnetic-particle clutches (Fig. 8.29*a*) use an iron powder mixed with a lubricant to partially fill the annular gap between members. When a direct-current (dc) coil induces a magnetic field, the iron particles form chains and provide the means to transmit torque. There is a nearly linear relation between coil current and torque.

Hysteresis clutches (Fig. 8.29*b*) directly couple the two members as long as the load does not exceed the torque rating. They can also slip continuously to maintain a constant-torque output independent of speed.

The *eddy-current clutch* (Fig. 8.29*c*) is rather like the hysteresis clutch in construction. Torque is developed if there is slip. The torque is associated with dissipation of eddy currents in the rotor ring's electric resistance.

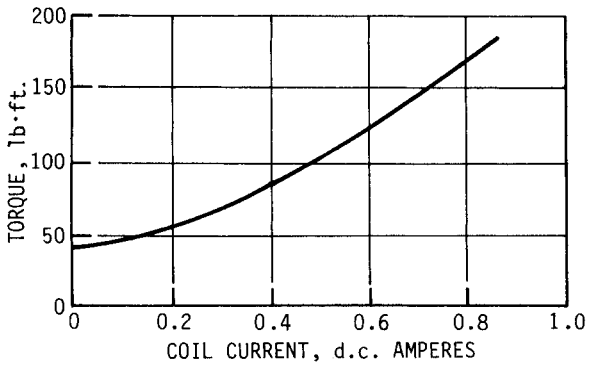

(a)

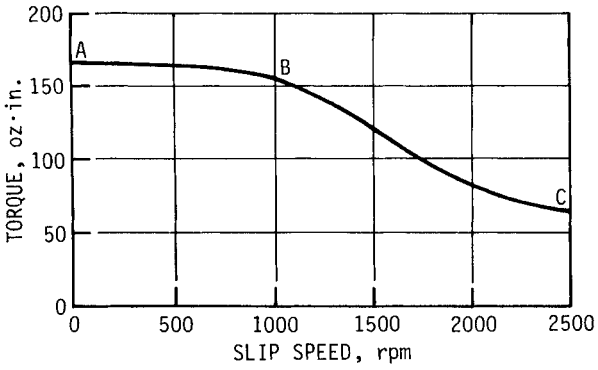

(b)

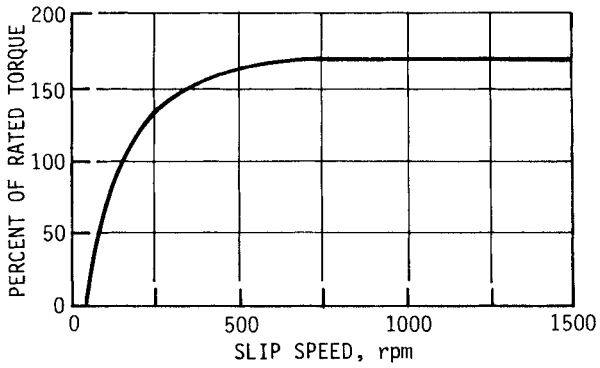

(c)

FIGURE 8.29 Torque characteristics of magnetic clutches. (*a*) Magnetic-particle clutch has a characteristic that is independent of slip and increases almost linearly with coil current. (*b*) Hysteresis clutch exhibits almost a constant torque out to the thermal, which begins at *B;* temperature then limits the torque capacity from *B* to *C.* (*c*) Eddy-current clutch exhibits a constant-torque characteristic at rated slip speed. *(From Ref. [8.5].)*

8.8.3 Dynamic Braking

When it is necessary to bring a motor-driven load from operating speed to rest in less than the normal coasting time, braking is necessary. However, for motors, the braking can be done by purely electrical means through dynamic braking. Electric braking, or *dynamic braking,* is done by altering the connections to the motor. It may be done with or without the aid of an external power source. Dynamic braking is available for fractional-horsepower motors. The designer should keep this option in mind.

8.9 ACTUATION PROBLEMS

8.9.1 General

Table 8.10 lists the characteristics of four basic brake actuation methods. Note that many brakes are made to operate on the fail-safe principle. This means that the brake is applied by using strong springs and that the method of actuation releases or holds off the brake. Thus, a reduction, say, in hydraulic pressure would cause the brake to be applied.

8.9.2 Brake Actuation Systems for Vehicles

The hydraulic system shown schematically in Fig. 8.30 is suitable for a passenger vehicle using disk brakes on the front axles and drum brakes on the rear. The pedal force, multiplied by the leverage ratio, is applied to the *master cylinder* to produce a

TABLE 8.10 Characteristics of Various Methods of Actuating Band, Drum, and Disk Brakes

Actuation method	Advantages	Disadvantages	Possible difficulties
Mechanical	Robust; simple; manual operation gives good control	Large leverage needed	Friction losses at pins and pivots
Pneumatic	Large forces available	Compressed air supply needed; brake chambers may be bulky; slow response time	Length of stroke (particularly if diaphragm type)
Hydraulic†	Compact; large forces available; quick response and good control	Special fluid needed; temperatures must not be high enough to vaporize fluid	Seals
Electric‡	Suitable for automatic control; quick response	On/off operation	Air gap

†Used for spot-type disk brakes.
‡Used for spot- and plate-type disk brakes.
SOURCE: Ref. [8.6].

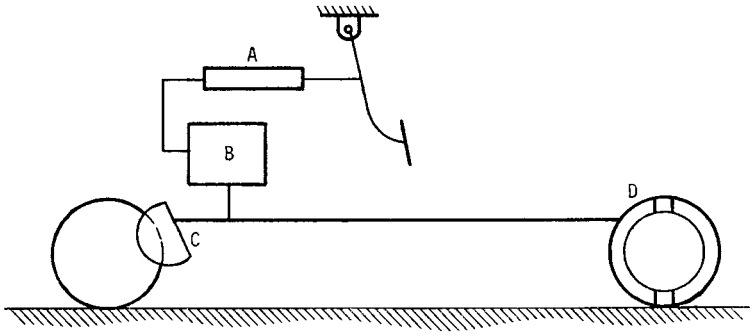

FIGURE 8.30 Hydraulic system with indirect servo. *A,* master cylinder; *B,* slave cylinder and servo; *C,* disk brake; *D,* leading-trailing shoe brake.

hydraulic pressure. This hydraulic pressure can itself be multiplied by a *power-brake assist unit* which uses either the intake manifold's vacuum or a positive hydraulic pressure from the power-steering pump to create a pressure differential.

In a *split system,* the master cylinder has two pistons and two reservoirs, one for the front-wheel brakes, the other for the rear. When the primary piston is pushed forward, the secondary piston is pushed forward as well by the primary piston spring and the buildup of pressure between the two pistons. Thus hydraulic pressure is built up in both systems. The springs return the pistons when the brake-pedal force is removed.

With the split system, one set of brakes can function even if the hydraulic system for the other set of brakes is damaged. For example, if the hydraulic system of the front brakes fails, no hydraulic pressure is built up in the front-brake system, and the secondary piston continues to move until its nose butts against the end of the cylinder. The primary piston continues to move and build up pressure between the primary and secondary pistons to actuate the rear brakes.

Most hydraulic brake systems are equipped with automatic valves:

1. *Pressure-differential valve* to turn on a warning light if either of the hydraulic systems (front or rear) fails.
2. *Proportioning valve* to improve the braking balance between the front and rear brakes and prevent skidding resulting from the rear brakes locking up before the front brakes.
3. *Metering valve* to delay the flow of brake fluid to the front-brake calipers until the system pressure has risen sufficiently. The motives are to overcome the tension of the retracting springs at the rear-brake shoes, expand the shoes, and supply the rear brakes before the front brakes. The metering valve prevents front-brake lockup during light braking on slippery or icy roads.

All three functions may be merged into a *combination valve* mounted near the master cylinder.

A *vacuum-brake booster* functions in three modes: released, applied, and holding. When the brake pedal is released, the engine intake manifold pulls air from the front shell through a check valve. There is a vacuum on both sides of the diaphragm, and the pressures are equal. The diaphragm is held to the rear by its spring. No force is exerted on the master cylinder by the push rod.

When the brake pedal is depressed, the valve rod pushes the valve plunger forward to close the vacuum port and open the atmospheric port. With atmospheric pressure on the rear side of the diaphragm and a vacuum at its front side, the diaphragm moves forward and pushes against the push rod. This is the *applied position.*

To provide gradual braking when needed (*holding position*), a position between the released and the applied positions is provided. The driver has control over the degree of braking.

8.9.3 Antiskid Brakes

In an antiskid braking system, the brakes are normally under manual control; but if wheel lockup is imminent, the antiskid system takes corrective action.

Whenever a rear wheel starts to lock, a wheel sensor detects an abrupt deceleration. A computer then causes the pressure in the rear braking system to decrease slightly, allowing the wheels to accelerate. When the wheel speed approaches its normal level for the vehicle's speed, the wheel cylinder pressure is restored. The antiskid system goes into action repeatedly to prevent wheel lockup and skidding until the vehicle speed drops to about 5 miles per hour (mph).

REFERENCES

8.1 Karl Beach, "Try These Formulas for Centrifugal Clutches," *Product Engineering,* July 9, 1962.

8.2 Arthur H. Burr, *Mechanical Analysis and Design,* Elsevier, New York, 1981.

8.3 G. A. Fazekas, "On Circular Spot Brakes," *Journal of Engineering for Industry, ASME Transactions,* August 1972.

8.4 A. F. Gagne, Jr., "Torque Capacity and Design of Cone and Disk Clutches," *Product Engineering,* December 1953.

8.5 John Proctor, "Selecting Clutches for Mechanical Drives," *Product Engineering,* June 1961.

8.6 M. J. Neale (ed.), *The Tribology Handbook,* 2d ed., Butterworth, London, 1996.

8.7 Ferodo Limited, *Friction Materials for Engineers,* Chapel-en-le-Frith, England, 1968.

SUGGESTED READING

Crouse, William H.: "Automotive Brakes," *Automotive Chassis and Body,* 4th ed., McGraw-Hill, New York, 1971.

Mathews, G. P.: "Art and Science of Braking Heavy Duty Vehicles," special publication SP-251, Society of Automotive Engineers, Warrendale, Pa., 1964.

Mischke, Charles R., *Elements of Mechanical Analysis*, Addison-Wesley, Reading, Mass., 1963, pp. 55–65.

Mischke, Charles R., *Mathematical Model Building*, 2d rev. ed., Iowa State University Press, Ames, 1980, pp. 338–344.

Remling, John: *Brakes,* Wiley, New York, 1978.

Wong, J. Y.: *Theory of Ground Vehicles,* Wiley, New York, 1978.

P · A · R · T · 3

GEARING

CHAPTER 9
SPUR GEARS

Joseph E. Shigley
Professor Emeritus
The University of Michigan
Ann Arbor, Michigan

9.1 DEFINITIONS

Spur gears are used to transmit rotary motion between parallel shafts. They are cylindrical, and the teeth are straight and parallel to the axis of rotation.

The *pinion* is the smaller of two mating gears; the larger is called the *gear* or the *wheel.*

The *pitch circle, B* in Fig. 9.1, is a theoretical circle upon which all calculations are based. The *operating pitch circles* of a pair of gears in mesh are tangent to each other.

The *circular pitch, p* in Fig. 9.1, is the distance, measured on the theoretical pitch circle, from a point on one tooth to a corresponding point on an adjacent tooth. The circular pitch is measured in inches or in millimeters. Note, in Fig. 9.1, that the circular pitch is the sum of the *tooth thickness t* and the *width of space.*

The *pitch diameter, d* for the pinion and *D* for the gear, is the diameter of the pitch circle; it is measured in inches or in millimeters.

The *module m* is the ratio of the theoretical pitch diameter to the number of teeth *N.* The module is the metric index of tooth sizes and is always given in millimeters.

The *diametral pitch* P_d is the ratio of the number of teeth on a gear to the theoretical pitch diameter. It is the index of tooth size when U.S. customary units are used and is expressed as teeth per inch.

The *addendum a* is the radial distance between the top land *F* and the pitch circle *B* in Fig. 9.1. The *dedendum b* is the radial distance between the pitch circle *B* and the *root circle D* in Fig. 9.1. The *whole depth* h_t is the sum of the addendum and dedendum.

The clearance circle *C* in Fig. 9.1 is tangent to the addendum circle of the mating gear. The distance from the clearance circle to the bottom land is called the *clearance c.*

Backlash is the amount by which the width of a tooth space exceeds the thickness of the engaging tooth measured on the pitch circle.

Undercutting (see distance *u* in Fig. 9.1) occurs under certain conditions when a small number of teeth are used in cutting a gear.

Table 9.1 lists all the relations described above. Additional terminology is shown in Fig. 9.2. Here line *OP* is the *line of centers* connecting the rotation axes of a pair of

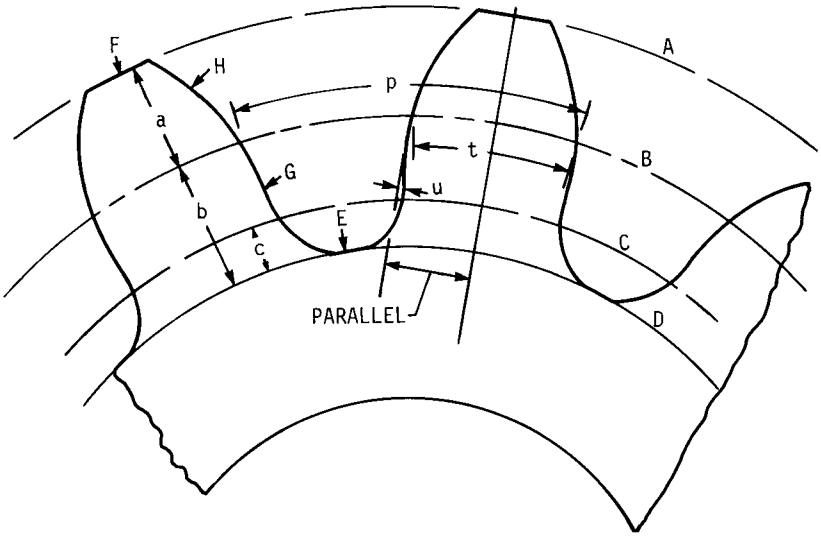

FIGURE 9.1 Terminology of gear teeth. *A,* addendum circle; *B,* pitch circle; *C,* clearance circle; *D,* dedendum circle; *E,* bottom land; *F,* top land; *G,* flank; *H,* face; a = addendum distance; b = dedendum distance; c = clearance distance; p = circular pitch; t = tooth thickness; u = undercut distance.

meshing gears. Line E is the *pressure line,* and the angle ϕ is the *pressure angle.* The resultant force vector between a pair of operating gears acts along this line.

The pressure line is tangent to both *base circles C* at points *F.* The operating diameters of the pitch circles depend on the center distance used in mounting the gears, but the base circle diameters are constant and depend only on how the tooth forms were generated, because they form the *base* or the starting point of the involute profile.

TABLE 9.1 Basic Formulas for Spur Gears

Quantity desired	Formula	Equation number
Diametral pitch P_d	$P_d = \dfrac{N}{d}$	(9.1)
Module m	$m = \dfrac{d}{N}$	(9.2)
Circular pitch p	$p = \dfrac{\pi d}{N} = \pi m$	(9.3)
Pitch diameter, d or D	$d = \dfrac{N}{P_d} = mN$	(9.4)

SPUR GEARS

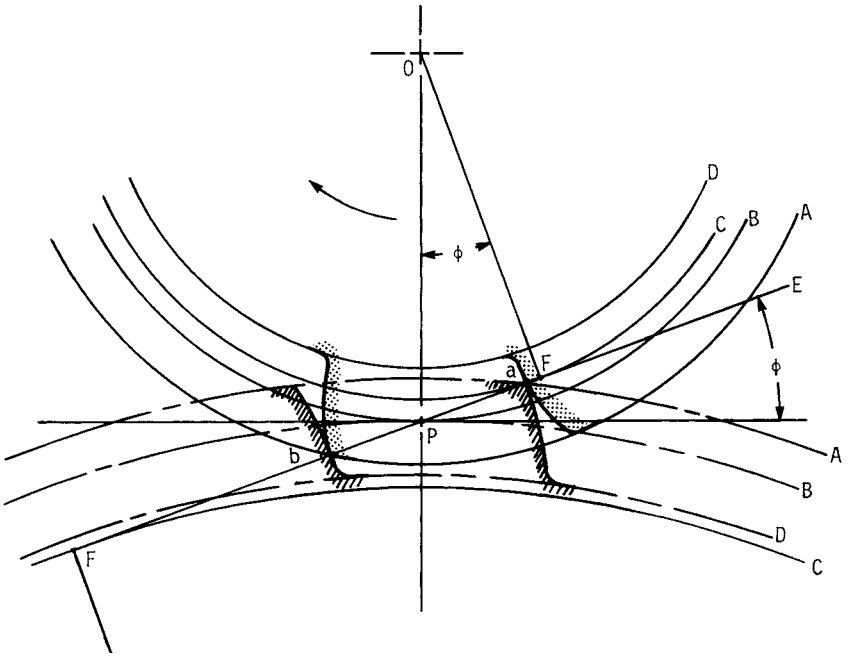

FIGURE 9.2 Layout drawing of a pair of spur gears in mesh. The pinion is the driver and rotates clockwise about the axis at *O. A,* addendum circles; *B,* pitch circles; *C,* base circles; *D,* dedendum circles; *E,* pressure line; *F,* tangent points; *P,* pitch point; *a,* initial point of contact; *b,* final point of contact.

Line *aPb* is the *line of action.* Point *a* is the *initial point of contact.* This point is located at the intersection of the addendum circle of the gear with the pressure line. Should point *a* occur on the other side of point *F* on the pinion base circle, the pinion flank would be *undercut* during generation of the profile.

Point *b* of Fig. 9.2 is the *final point of contact.* This point is located at the intersection of the addendum circle of the pinion with the pressure line. For no undercutting of the gear teeth, point *b* must be located between the pitch point *P* and point *F* on the base circle of the gear.

Line *aP* represents the *approach* phase of tooth contact; line *Pb* is the *recess* phase. Tooth contact is a sliding contact throughout the line of action except for an instant at *P* when contact is pure rolling. The nature of the sliding is quite different during the approach action and the recess action; bevel-gear teeth, for example, are generated to obtain more recess action, thus reducing wear.

Instead of using the theoretical pitch circle as an index of tooth size, the base circle, which is a more fundamental distance, can be used. The result is called the *base pitch* p_b. It is related to the circular pitch p by the equation

$$p_b = p \cos \phi \tag{9.5}$$

If, in Fig. 9.2, the distance from *a* to *b* exactly equals the base pitch, then, when one pair of teeth are just beginning contact at *a,* the preceding pair will be leaving contact at *b.* Thus, for this special condition, there is never more or less than one pair

of teeth in contact. If the distance *ab* is greater than the base pitch but less than twice as much, then when a pair of teeth come into contact at *a,* another pair of teeth will still be in contact somewhere along the line of action *ab.* Because of the nature of this tooth action, usually one or two pairs of teeth in contact, a useful criterion of tooth action, called the *contact ratio* m_c, can be defined. The formula is

$$m_c = \frac{L_{ab}}{p_b} \tag{9.6}$$

where L_{ab} = distance *ab,* the length of the line of action. Do not confuse the contact ratio m_c with the module m.

9.2 TOOTH DIMENSIONS AND STANDARDS

The American Gear Manufacturer's Association (AGMA) publishes much valuable reference data.† The details on nomenclature, definitions, and tooth proportions for spur gears can be found in ANSI/AGMA 1012-F90. Table 9.2 contains the most used tooth proportions. The hob tip radius r_f varies with different cutters; $0.300/P_d$ or $0.300m$ is the usual value. Tables 9.3 and 9.4 list the modules and pitches in general use. Cutting tools can be obtained for all these sizes.

† See Chap. 10 for a special note on AGMA.

TABLE 9.2 Standard and Commonly Used Tooth Systems for Spur Gears

Tooth system	Pressure angle ϕ, deg	Addendum a	Dedendum b
Full depth	20	$1/P_d$ or $1m$	$1.25/P_d$ or $1.25m$ $1.35/P_d$ or $1.35m$
	$22\frac{1}{2}$	$1/P_d$ or $1m$	$1.25/P_d$ or $1.25m$ $1.35/P_d$ or $1.35m$
	25	$1/P_d$ or $1m$	$1.25/P_d$ or $1.25m$ $1.35/P_d$ or $1.35m$
Stub	20	$0.8/P_d$ or $0.8m$	$1/P_d$ or $1m$

TABLE 9.3 Diametral Pitches in General Use

Coarse pitch	2, $2\frac{1}{4}$, $2\frac{1}{2}$, 3, 4, 6, 8, 10, 12, 16
Fine pitch	20, 24, 32, 40, 48, 64, 96, 120, 150, 200

TABLE 9.4 Modules in General Use

Preferred	1, 1.25, 1.5, 2, 2.5, 3, 4, 5, 6, 8, 10, 12, 16, 20, 25, 32, 40, 50
Next choice	1.125, 1.375, 1.75, 2.25, 2.75, 3.5, 4.5, 5.5, 7, 9, 11, 14, 18, 22, 28, 36, 45

9.3 FORCE ANALYSIS

In Fig. 9.3 a gear, not shown, exerts force W against the pinion at pitch point P. This force is resolved into two components, a radial force W_r, acting to separate the gears, and a tangential component W_t, which is called the *transmitted load.*

Equal and opposite to force W is the shaft reaction F, also shown in Fig. 9.3. Force F and torque T are exerted by the shaft on the pinion. Note that torque T opposes the force couple made up of W_t and F_x separated by the distance $d/2$. Thus

$$T = \frac{W_t d}{2} \tag{9.7}$$

where T = torque, lb · in (N · m)
W_t = transmitted load, lb (N)
d = operating pitch diameter, in (m)

The *pitch-line velocity* v is given by

$$v = \frac{\pi d n_P}{12} \quad \text{ft/min} \qquad v = \frac{\pi d n_P}{60} \quad \text{m/s} \tag{9.8}$$

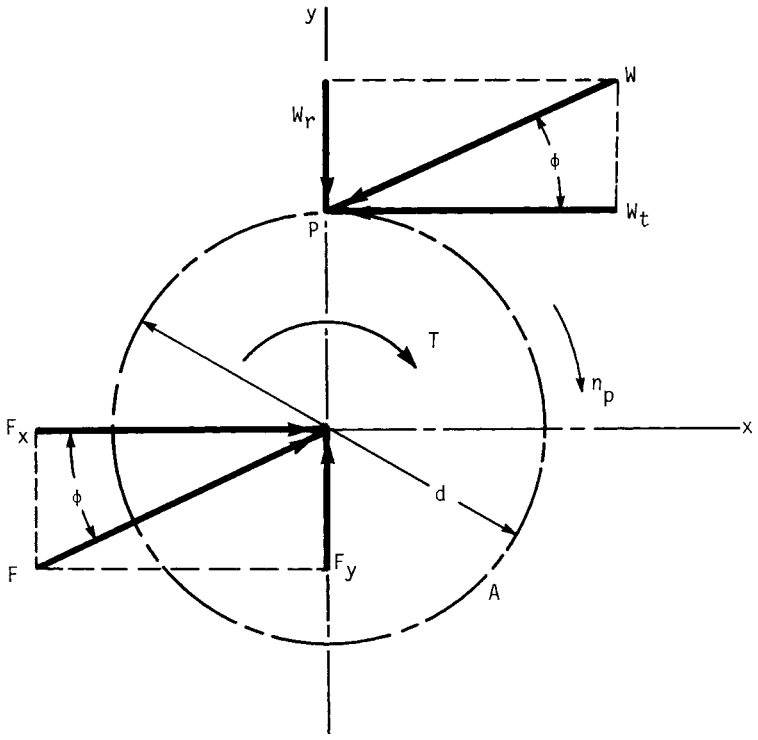

FIGURE 9.3 Force analysis of a pinion. *A,* operating pitch circle; *d,* operating pitch diameter; n_p, pinion speed; ϕ, pressure angle; W_t, transmitted tangential load; W_r, radial tooth load; W, resultant tooth load; T, torque; F, shaft force reaction.

where n_P = pinion speed in revolutions per minute (r/min). The power transmitted is

$$P = \begin{cases} \dfrac{W_t v}{33\,000} & \text{hp} \\ W_t v & \text{kW} \end{cases} \tag{9.9}$$

9.4 FUNDAMENTAL AGMA RATING FORMULAS†

Many of the terms in the formulas that follow require lengthy discussions and considerable space to list their values. This material is considered at length in Chap. 10 and so is omitted here.

9.4.1 Pitting Resistance

The basic formula for *pitting resistance,* or *surface durability,* of gear teeth is

$$s_c = C_p \left(\frac{W_t C_a}{C_v} \frac{C_s}{dF} \frac{C_m C_f}{I} \right)^{1/2} \tag{9.10}$$

where s_c = contact stress number, lb/in^2 (MPa)
C_p = elastic coefficient, (lb/in^2)$^{1/2}$ [(MPa)$^{1/2}$]; see Eq. (10.77) and Table 10.4
W_t = transmitted tangential load, lb (N)
C_a = application factor for pitting resistance; see Table 10.3
C_s = size factor for pitting resistance; use 1.0 or more until values are established
C_m = load distribution factor for pitting resistance; use Tables 9.5 and 9.6
C_f = surface condition factor; use 1.0 or more until values are established
C_v = dynamic factor for pitting resistance; use Fig. 10.4; multiply v in meters per second by 197 to get feet per minute
d = operating pitch diameter of pinion, in (mm)
= $2C/(m_G + 1.0)$ for external gears
= $2C/(m_G - 1.0)$ for internal gears
C = operating center distance, in (mm)
m_G = gear ratio (never less than 1.0)
F = net face width of narrowest member, in (mm)
I = geometry factor for pitting resistance; use Eq. (10.24) with $C_\psi = 1.0$

Allowable Contact Stress Number. The contact stress number s_c, used in Eq. (9.10), is obtained from the *allowable contact stress number* s_{ac} by making several adjustments as follows:

$$s_c \le s_{ac} \frac{C_L C_H}{C_T C_R} \tag{9.11}$$

† See Ref. [10.1].

TABLE 9.5 Load-Distribution Factors C_m and K_m for Spur Gears Having a Face Width of 6 in (150 mm) and Greater†

Face-diameter ratio F/d	Contact	C_m, K_m
1 or less	95% face width contact at one-third torque	1.4 at one-third torque
	95% face width contact at full torque	1.1 at full torque
	75% face width contact at one-third torque	1.8 at one-third torque
	95% face width contact at full torque	1.3 at full torque
	35% face width contact at one-third torque	3.0 at one-third torque
	95% face width contact at full torque	1.9 at full torque
	20% face width contact at one-third torque	5.0 at one-third torque
	75% face width contact at full torque	2.5 at full torque
	Teeth are crowned:	
	35% face width contact at one-third torque	2.5 at one-third torque
	85% face width contact at full torque	1.7 at full torque
Over 1 and less than 2	Calculated combined twist and bending of pinion not over 0.001 in (0.025 mm) over entire face:	
	Pinion not over 250 bhn hardness:	
	75% face width contact at one-third torque	2.0 at one-third torque
	95% face width contact at full torque	1.4 at full torque
	30% face width contact at one-third torque	4.0 at one-third torque
	75% face width contact at full torque	3.0 at full torque

†For an alternate approach see Eq. (10.21).

SOURCE: ANSI/AGMA 2001-C95.

where s_{ac} = allowable contact stress number, lb/in^2 (MPa); see Fig.10.40
C_L = life factor for pitting resistance; use Fig.10.49
C_H = hardness ratio factor; use Figs. 10.47 and 10.48
C_T = temperature factor for pitting resistance; use 1.0 or more, but see Sec.10.5.1
C_R = reliability factor for pitting resistance; use Table 10.6

TABLE 9.6 Load-Distribution Factors C_m and K_m for Spur Gears

Condition of support	Face width			
	Up to 2 in (50 mm)	6 in (150 mm)	9 in (225 mm)	Over 16 in (400 mm)
Accurate mounting, low bearing clearances, minimum elastic deflection, precision gears	1.3	1.4	1.5	1.8
Less rigid mountings, less accurate gears, contact across full face	1.6	1.7	1.8	2.0
Accuracy and mounting such that less than full-face contact exists	Over 2.0			

SOURCE: ANSI/AGMA 2001-C95. For an alternate approach see Eq. (10.21).

Pitting Resistance Power Rating. The allowable power rating P_{ac} for pitting resistance is given by

$$P_{ac} = \begin{cases} \dfrac{n_P F}{126\,000} \dfrac{IC_v}{C_s C_m C_f C_a} \left(\dfrac{ds_{ac}}{C_p} \dfrac{C_L C_H}{C_T C_R} \right)^2 & \text{hp} \\ \dfrac{n_P F}{1.91(10^7)} \dfrac{IC_v}{C_s C_m C_f C_a} \left(\dfrac{ds_{ac}}{C_p} \dfrac{C_L C_H}{C_T C_R} \right)^2 & \text{kW} \end{cases} \tag{9.12}$$

9.4.2 Bending Strength

The basic formula for the bending stress number in a gear tooth is

$$S_t = \begin{cases} \dfrac{W_t K_a}{K_v} \dfrac{P_d}{F} \dfrac{K_s K_m}{J} & \text{lb/in}^2 \\ \dfrac{W_t K_a}{K_v} \dfrac{1.0}{Fm} \dfrac{K_s K_m}{J} & \text{MPa} \end{cases} \tag{9.13}$$

where s_t = bending stress number, lb/in^2 (MPa)
K_a = application factor for bending strength; use Table 10.3
K_s = size factor for bending strength; use 1.0 or more until values are established
K_m = load distribution factor for bending strength; use Tables 9.5 and 9.6
K_v = dynamic factor for bending strength; use Fig.10.4; multiply v in meters per second by 197 to get feet per minute
J = geometry factor for bending strength; use Eq. (10.46) with $C_\psi = 1.0$ and Figs.10.11 to 10.22
m = module, mm
P_d = nominal diametral pitch, teeth per inch

Allowable Bending Stress Number. The bending stress number s_t in Eq. (9.13) is related to the *allowable bending stress number* s_{at} by

$$s_t \le \frac{s_{at} K_L}{K_T K_R} \tag{9.14}$$

where s_{at} = allowable bending stress number, lb/in^2 (MPa); use Fig. 10.41
K_L = life factor for bending strength; use Figs. 10.49 and 10.50
K_T = temperature factor for bending strength; use 1.0 or more; see Sec. 10.5.1
K_R = reliability factor for bending strength; use Table 10.6

Bending Strength Power Rating. The allowable power rating P_{at} for bending strength is given by

$$P_{at} = \begin{cases} \dfrac{n_P d K_v}{126\,000 K_a} \dfrac{FJ}{P_d K_s K_m} \dfrac{s_{at} K_L}{K_R K_T} & \text{hp} \\ \dfrac{n_P d K_v}{1.91(10)^7 K_a} Fm \dfrac{J}{K_s K_m} \dfrac{S_{at} K_L}{K_R K_T} & \text{kW} \end{cases} \tag{9.15}$$

SPUR GEARS

CHAPTER 10
HELICAL GEARS

Raymond J. Drago, P.E.
Senior Engineer, Advanced Power Train Technology
Boeing Vertol Company
Philadelphia, Pennsylvania

The following is quoted from the Foreword of Ref. [10.1]:

> This AGMA Standard and related publications are based on typical or average data, conditions, or applications. The standards are subject to continual improvement, revision, or withdrawal as dictated by increased experience. Any person who refers to AGMA technical publications should be sure that he has the latest information available from the Association on the subject matter.
>
> Tables or other self-supporting sections may be quoted or extracted in their entirety. Credit line should read: "Extracted from ANSI/AGMA #2001-C95 Fundamental Rating Factors and Calculation Methods for Involute Spur and Helical Gear Teeth, with the permission of the publisher, American Gear Manufacturers Association, Alexandria, Virginia."

This reference is cited because numerous American Gear Manufacturer's Association (AGMA) tables and figures are used in this chapter. In each case, the appropriate publication is noted in a footnote or figure caption.

10.1 INTRODUCTION

Helical gearing, in which the teeth are cut at an angle with respect to the axis of rotation, is a later development than spur gearing and has the advantage that the action is smoother and tends to be quieter. In addition, the load transmitted may be somewhat larger, or the life of the gears may be greater for the same loading, than with an equivalent pair of spur gears. Helical gears produce an end thrust along the axis of the shafts in addition to the separating and tangential (driving) loads of spur gears. Where suitable means can be provided to take this thrust, such as thrust collars or ball or tapered-roller bearings, it is no great disadvantage.

Conceptually, helical gears may be thought of as stepped spur gears in which the size of the step becomes infinitely small. For external parallel-axis helical gears to

mesh, they must have the same helix angle but be of different hand. An external-internal set will, however, have equal helix angle with the same hand.

Involute profiles are usually employed for helical gears, and the same comments made earlier about spur gears hold true for helical gears.

Although helical gears are most often used in a parallel-axis arrangement, they can also be mounted on nonparallel noncoplanar axes. Under such mounting conditions, they will, however, have limited load capacity.

Although helical gears which are used on crossed axes are identical in geometry and manufacture to those used on parallel axes, their operational characteristics are quite different. For this reason they are discussed separately at the end of this chapter. All the forthcoming discussion therefore applies only to helical gears operating on parallel axes.

10.2 TYPES

Helical gears may take several forms, as shown in Fig. 10.1:

1. Single
2. Double conventional
3. Double staggered
4. Continuous (herringbone)

Single-helix gears are readily manufactured on conventional gear cutting and grinding equipment. If the space between the two rows of a double-helix gear is wide enough, such a gear may also be cut and ground, if necessary, on conventional equipment. Continuous or herringbone gears, however, can be cut only on a special shaping machine (Sykes) and usually cannot be ground at all.

Only single-helix gears may be used in a crossed-axis configuration.

10.3 ADVANTAGES

There are three main reasons why helical rather than straight spur gears are used in a typical application. These are concerned with the noise level, the load capacity, and the manufacturing.

10.3.1 Noise

Helical gears produce less noise than spur gears of equivalent quality because the total contact ratio is increased. Figure 10.2 shows this effect quite dramatically. However, these results are measured at the mesh for a specific test setup; thus, although the trend is accurate, the absolute results are not.

Figure 10.2 also brings out another interesting point. At high values of helix angle, the improvement in noise tends to peak; that is, the curve flattens out. Had data been obtained at still higher levels, the curve would probably drop drastically. This is due to the difficulty in manufacturing and mounting such gears accurately enough to take full advantage of the improvement in contact ratio. These effects at

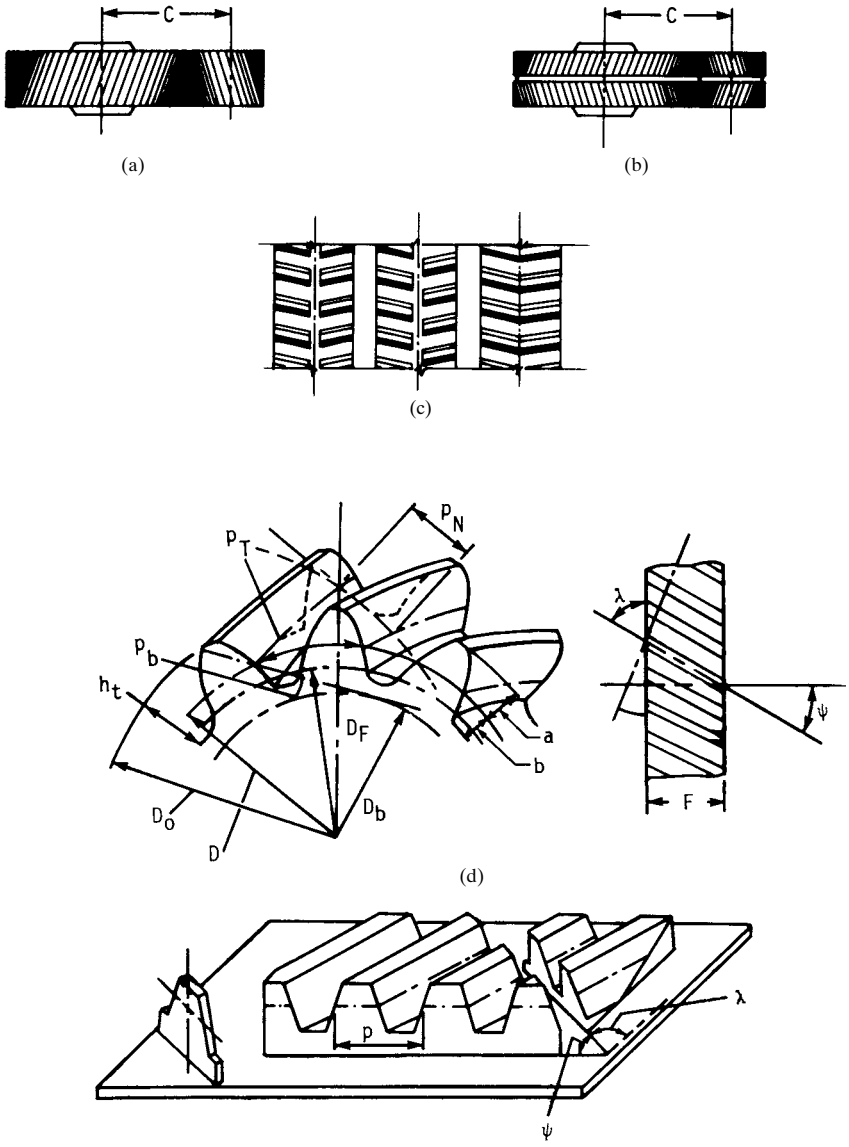

FIGURE 10.1 Terminology of helical gearing. (*a*) Single-helix gear. (*b*) Double-helix gear. (*c*) Types of double-helix gears: left, conventional; center, staggered; right, continous or herringbone. (*d*) Geometry. (*e*) Helical rack.

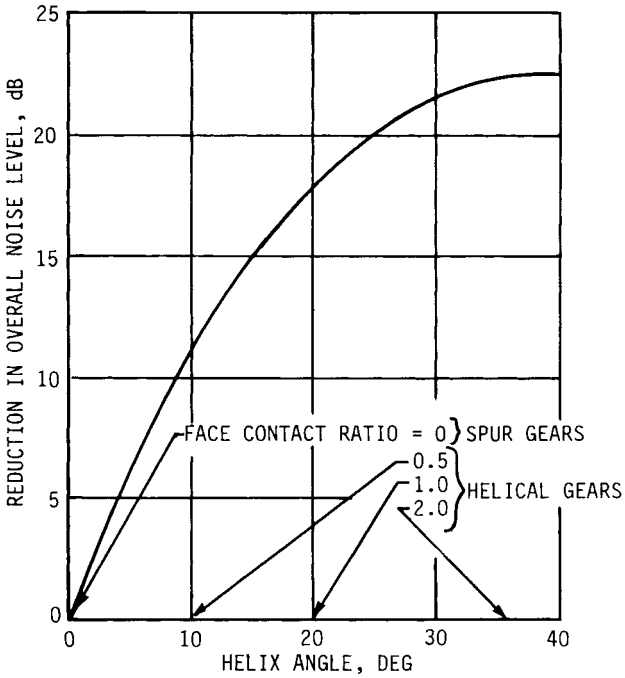

FIGURE 10.2 Effect of face-contact ratio on noise level. Note that increased helix angles lower the noise level.

very high helix angles actually tend to reduce the effective contact ratio, and so noise increases. Since helix angles greater than 45° are seldom used and are generally impractical to manufacture, this phenomenon is of academic interest only.

10.3.2 Load Capacity

As a result of the increased total area of tooth contact available, the load capacity of helical gears is generally higher than that of equivalent spur gears. The reason for this increase is obvious when we consider the contact line comparison which Fig. 10.3 shows. The most critical load condition for a spur gear occurs when a single tooth carries all the load at the highest point of single-tooth contact (Fig. 10.3*c*). In this case, the total length of the contact line is equal to the face width. In a helical gear, since the contact lines are inclined to the tooth with respect to the face width, the total length of the line of contact is increased (Fig. 10.3*b*), so that it is greater than the face width. This lowers unit loading and thus increases capacity.

10.3.3 Manufacturing

In the design of a gear system, it is often necessary to use a specific ratio on a specific center distance. Frequently this results in a diametral pitch which is nonstandard. If

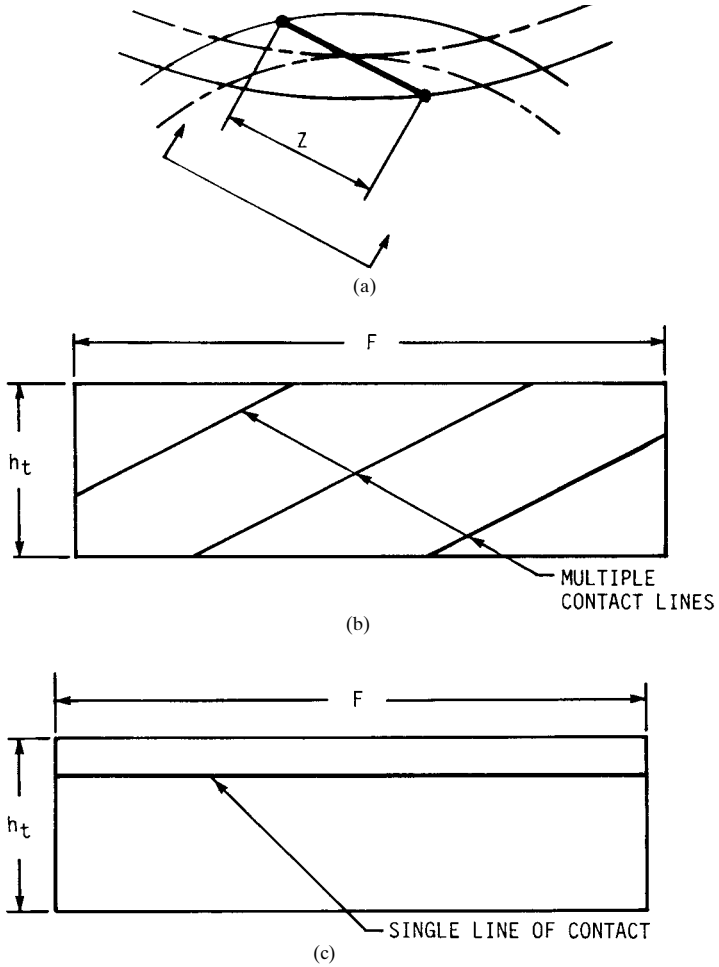

FIGURE 10.3 Comparison of spur and helical contact lines. (*a*) Transverse section; (*b*) helical contact lines; (*c*) spur contact line.

helical gears are employed, a limited number of standard cutters may be used to cut a wide variety of transverse-pitch gears simply by varying the helix angle, thus allowing virtually any center-distance and tooth-number combination to be accommodated.

10.4 GEOMETRY

When considered in the transverse plane (that is, a plane perpendicular to the axis of the gear), all helical-gear geometry is identical to that for spur gears. Standard tooth proportions are usually based on the normal diametral pitch, as shown in Table 10.1.

TABLE 10.1 Standard Tooth Proportions for Helical Gears

Quantity†	Formula	Quantity†	Formula
Addendum	$\frac{1.00}{P_N}$	External gears:	
Dedendum	$\frac{1.25}{P_N}$	Standard center distance	$\frac{D+d}{2}$
Pinion pitch diameter	$\frac{N_P}{P_N \cos \psi}$	Gear outside diameter	$D + 2a$
Gear pitch diameter	$\frac{N_G}{P_N \cos \psi}$	Pinion outside diameter	$d + 2a$
Normal arc tooth thickness	$\frac{\pi}{P_N} - \frac{B_N}{2}$	Gear root diameter	$D - 2b$
Pinion base diameter	$d \cos \phi_T$	Pinion root diameter	$d - 2b$
Gear base diameter	$D \cos \phi_T$	Internal gears:	
Base helix angle	$\tan^{-1} (\tan \psi \cos \phi_T)$	Center distance	$\frac{D-d}{2}$
		Inside diameter	$d - 2a$
		Root diameter	$D + 2b$

†All dimensions in inches, and angles are in degrees.

It is frequently necessary to convert from the normal plane to the transverse plane and vice versa. Table 10.2 gives the necessary equations. All calculations previously defined for spur gears with respect to transverse or profile-contact ratio, top land, lowest point of contact, true involute form radius, nonstandard center, etc., are valid for helical gears if only a transverse plane section is considered.

For spur gears, the profile-contact ratio (ratio of contact to the base pitch) must be greater than unity for uniform rotary-motion transmission to occur. Helical gears, however, provide an additional overlap along the axial direction; thus their profile-contact ratio need not necessarily be greater than unity. The sum of both the profile-

TABLE 10.2 Conversions between Normal and Transverse Planes

Parameter (normal/transverse)	Normal to transverse	Transverse to normal
Pressure angle (ϕ_N/ϕ_T)	$\phi_T = \tan^{-1} \frac{\tan \phi_N}{\cos \psi}$	$\phi_N = \tan^{-1} (\tan \phi_T \cos \psi)$
Diametral pitch (P_N/P_d)	$P_d = P_N \cos \psi$	$P_N = \frac{P_d}{\cos \psi}$
Circular pitch (p_N/p_T)	$P_T = \frac{P_N}{\cos \psi}$	$P_N = P_T \cos \psi$
Arc tooth thickness (T_N/T_T)	$T_T = \frac{T_N}{\cos \psi}$	$T_N = T_T \cos \psi$
Backlash (B_N/B_T)	$B_T = \frac{B_N}{\cos \psi}$	$B_N = B_T \cos \psi$

contact ratio and the axial overlap must, however, be at least unity. The axial overlap, also often called the *face-contact ratio,* is the ratio of the face width to the axial pitch. The face-contact ratio is given by

$$m_F = \frac{P_{do} F \tan \psi_o}{\pi} \tag{10.1}$$

where P_{do} = operating transverse diametral pitch
ψ_o = helix angle at operating pitch circle
F = face width

Other parameters of interest in the design and analysis of helical gears are the base pitch p_b and the length of the line of action Z, both in the transverse plane. These are

$$p_b = \frac{\pi}{P_d} \cos \phi_T \tag{10.2}$$

and

$$Z = (r_o^2 - r_b^2)^{1/2} + (R_o^2 - R_b^2)^{1/2} - C_o \sin \phi_o \tag{10.3}$$

This equation is for an external gear mesh. For an internal gear mesh, the length of the line of action is

$$Z = (R_l^2 - R_b^2)^{1/2} - (r_o^2 - r_b^2)^{1/2} + C_o \sin \phi_o \tag{10.4}$$

where P_d = transverse diametral pitch as manufactured
ϕ_T = transverse pressure angle as manufactured, degrees (deg)
r_o = effective pinion outside radius, inches (in)
R_o = effective gear outside radius, in
R_l = effective gear inside radius, in
ϕ_o = operating transverse pressure angle, deg
r_b = pinion base radius, in
R_b = gear base radius, in
C_o = operating center distance, in

The operating transverse pressure angle ϕ_o is

$$\phi_o = \cos^{-1}\left(\frac{C}{C_o} \cos \phi_T\right) \tag{10.5}$$

The manufactured center distance C is simply

$$C = \frac{N_P + N_G}{2P_d} \tag{10.6}$$

for external mesh; for internal mesh, the relation is

$$C = \frac{N_G - N_P}{2P_d} \tag{10.7}$$

The contact ratio m_P in the transverse plane (profile-contact ratio) is defined as the ratio of the total length of the line of action in the transverse plane Z to the base pitch in the transverse plane p_b. Thus

$$m_P = \frac{Z}{p_b} \tag{10.8}$$

The diametral pitch, pitch diameters, helix angle, and normal pressure angle at the operating pitch circle are required in the load-capacity evaluation of helical gears. These terms are given by

$$P_{do} = \frac{N_P + N_G}{2C_o} \tag{10.9}$$

for external mesh; for internal mesh,

$$P_{do} = \frac{N_G - N_P}{2C_o} \tag{10.10}$$

Also,

$$d = \frac{N_P}{P_{do}} \qquad D = \frac{N_G}{P_{do}} \tag{10.11}$$

$$\psi_B = \tan^{-1} (\tan \psi \cos \phi_T) \tag{10.12}$$

$$\psi_o = \tan^{-1} \frac{\tan \psi_B}{\cos \phi_o} \tag{10.13}$$

$$\phi_{No} = \sin^{-1} (\sin \phi_o \cos \psi_B) \tag{10.14}$$

where P_{do} = operating diametral pitch
ψ_B = base helix angle, deg
ψ_o = helix angle at operating pitch point, deg
ϕ_{No} = operating normal pressure angle, deg
d = operating pinion pitch diameter, in
D = operating gear pitch diameter, in

10.5 LOAD RATING

Reference [10.1] establishes a coherent method for rating external helical and spur gears. The treatment of strength and durability provided here is derived in large part from this source.

Four factors must be considered in the load rating of a helical-gear set: strength, durability, wear resistance, and scoring probability. Although strength and durability must always be considered, wear resistance and scoring evaluations may not be required for every case. We treat each topic in some depth.

10.5.1 Strength and Durability

The strength of a gear tooth is evaluated by calculating the bending stress index number at the root by

$$s_t = \frac{W_t K_a}{K_v} \frac{P_d}{F_E} \frac{K_b K_m}{J} \tag{10.15}$$

where s_t = bending stress index number, pounds per square inch (psi)
K_a = bending application factor
F_E = effective face width, in
K_m = bending load-distribution factor
K_v = bending dynamic factor
J = bending geometry factor
P_d = transverse operating diametral pitch
K_b = rim thickness factor

The calculated bending stress index number s_t must be within safe operating limits as defined by

$$s_t \le \frac{s_{at} K_L}{K_T K_R} \tag{10.16}$$

where s_{at} = allowable bending stress index number
K_L = life factor
K_T = temperature factor
K_R = reliability factor

Some of the factors which are used in these equations are similar to those used in the durability equations. Thus we present the basic durability rating equations before discussing the factors:

$$s_c = C_p \sqrt{\frac{W_t C_a}{C_v} \frac{1}{d F_N} \frac{C_m}{I}} \tag{10.17}$$

where s_c = contact stress index number
C_a = durability application factor
C_v = durability dynamic factor
d = operating pinion pitch diameter
F_N = net face width, in
C_m = load-distribution factor
C_p = elastic coefficient
I = durability geometry factor

The calculated contact stress index number must be within safe operating limits as defined by

$$s_c \le \frac{s_{ac} C_L C_H}{C_T C_R} \tag{10.18}$$

where s_{ac} = allowable contact stress index number
C_L = durability life factor
C_H = hardness ratio factor
C_T = temperature factor
C_R = reliability factor

To utilize these equations, each factor must be evaluated. The tangential load W_t is given by

$$W_t = \frac{2T_P}{d} \tag{10.19}$$

where T_P = pinion torque in inch-pounds (in · lb) and d = pinion operating pitch diameter in inches. If the duty cycle is not uniform but does not vary substantially, then the maximum anticipated load should be used. Similarly, if the gear set is to operate at a combination of very high and very low loads, it should be evaluated at the maximum load. If, however, the loading varies over a well-defined range, then the cumulative fatigue damage for the loading cycle should be evaluated by using Miner's rule. For a good explanation, see Ref. [10.2].

Application Factors $\mathbf{C_a}$ ***and*** $\mathbf{K_a}$. The application factor makes the allowances for externally applied loads of unknown nature which are in excess of the nominal tangential load. Such factors can be defined only after considerable field experience has been established. In a *new* design, this consideration places the designer squarely on the horns of a dilemma, since "new" presupposes limited, if any, experience. The values shown in Table 10.3 may be used as a guide if no other basis is available.

TABLE 10.3 Application Factor Guidelines

	Character of load on driven machine		
Power source	Uniform	Moderate shock	Heavy shock
Uniform	1.15	1.25	At least 1.75
Light shock	1.25	1.50	At least 2.00
Medium shock	1.50	1.75	At least 2.50

The application factor should never be set equal to unity except where clear experimental evidence indicates that the loading will be absolutely uniform. Wherever possible, the actual loading to be applied to the system should be defined. One of the most common mistakes made by gear system designers is assuming that the motor (or engine, etc.) "nameplate" rating is also the gear unit rating point.

Dynamic Factors $\mathbf{C_v}$ ***and*** $\mathbf{K_v}$. These factors account for internally generated tooth loads which are induced by nonconjugate meshing action. This discontinuous motion occurs as a result of various tooth errors (such as spacing, profile, and runout) and system effects (such as deflections). Other effects, such as system torsional resonances and gear blank resonant responses, may also contribute to the overall dynamic loading experienced by the teeth. The latter effects must, however, be separately evaluated. The effect of tooth accuracy may be determined from Fig. 10.4, which is based on both pitch line velocity and gear quality Q_n as specified in Ref. [10.3]. The pitch line velocity of a gear is

$$v_t = 0.2618nD \tag{10.20}$$

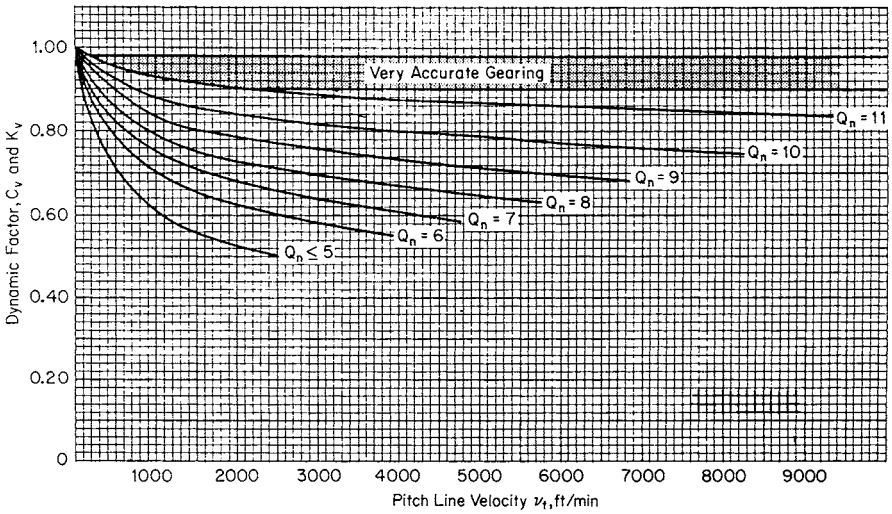

FIGURE 10.4 Dynamic factors C_v and K_v. *(From Ref. [10.1].)*

where v_t = pitch line velocity, feet per minute (ft/min)
n = gear speed, revolutions per minute (r/min)
D = gear pitch diameter, in

Effective and Net Face Widths $\mathbf{F_E}$ ***and*** $\mathbf{F_N}$. The net minimum face width of the narrowest member should always be used for F_N. In cases where one member has a substantially larger face width than its mate, some advantage may be taken of this fact in the bending stress calculations, but it is unlikely that a very narrow tooth will fully transfer its tooth load across the face width of a much wider gear. At best, the effective face width of a larger-face-width gear mating with a smaller-face-width gear is limited to the minimum face of the smaller member plus some allowance for the extra support provided by the wide face. Figure 10.5 illustrates the definition of net and effective face widths for various cases.

Rim Thickness Factor $\mathbf{K_b}$. The basic bending stress equations were developed for a single tooth mounted on a rigid support so that it behaves as a short cantilever beam. As the rim which supports the gear tooth becomes thinner, a point is reached at which the rim no longer provides "rigid" support. When this occurs, the bending of the rim itself combines with the tooth bending to yield higher total alternating stresses than would be predicted by the normal equations. Additionally, when a tooth is subjected to fully reversed bending loads, the alternating stress is also increased because of the additive effect of the compressive stress distribution on the normally unloaded side of the tooth, as Fig. 10.6 shows. Both effects are accounted for by the rim thickness factor, as Fig. 10.7 indicates.

It must be emphasized that the data shown in Fig. 10.7 are based on a limited amount of analytical and experimental (photoelastic and strain-gauge) measurements and thus must be used judiciously. Still, they are the best data available to date and are far better than nothing at all; see Refs. [10.4] and [10.5].

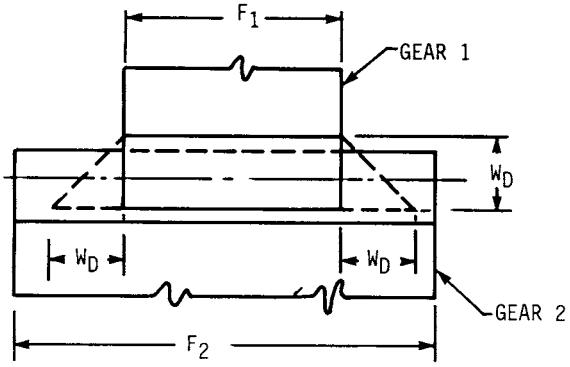

(a)

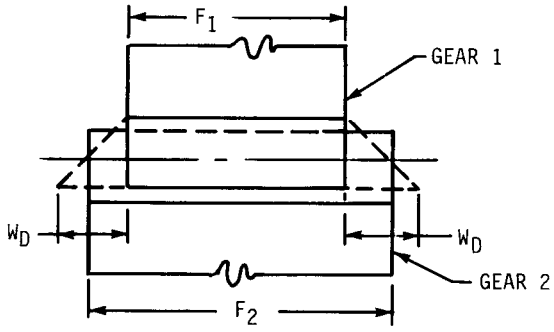

(b)

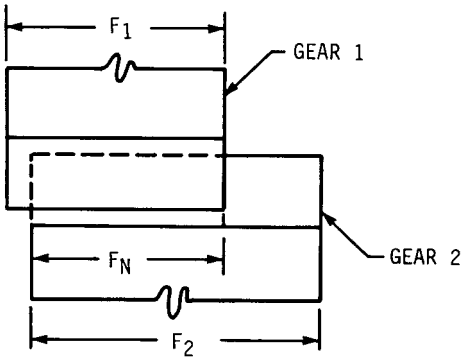

(c)

FIGURE 10.5 Definition of effective face width. (*a*) $F_{E1} = F_1, F_{E2} = F_1 + 2W_D; F_N = F_1$; (*b*) $F_{E1} = F_1, F_{E2} = F_2, F_N = F_1$; (*c*) $F_{E1} = F_{E2} = F_N$.

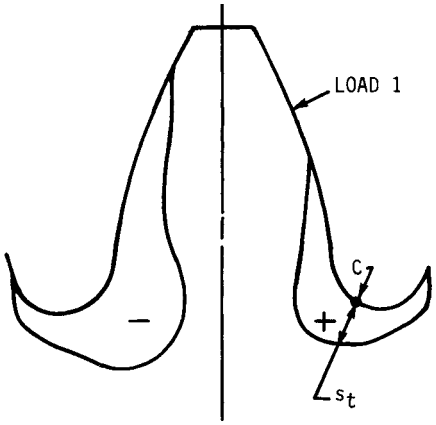

(a)

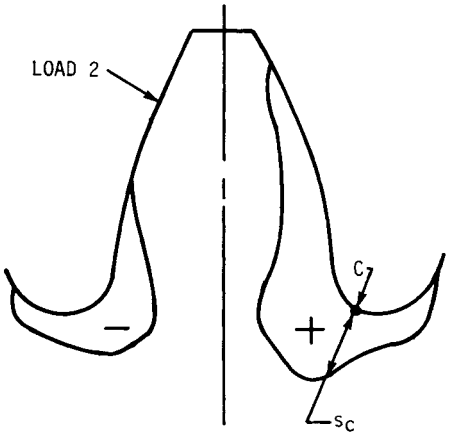

(b)

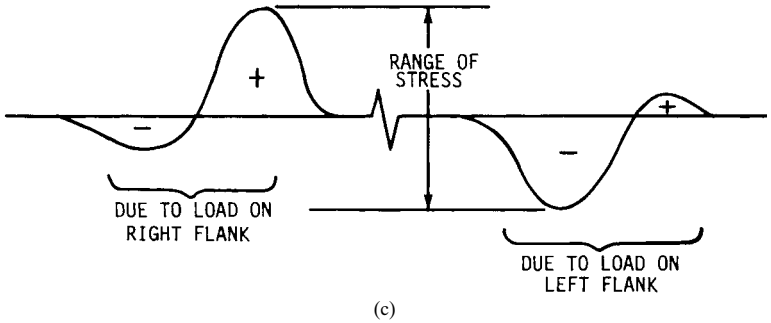

(c)

FIGURE 10.6 Stress condition for reversing (as with an idler) loading. (*a*) Load on right flank; (*b*) load on left flank; (*c*) typical waveform for strain gauge at point *C*.

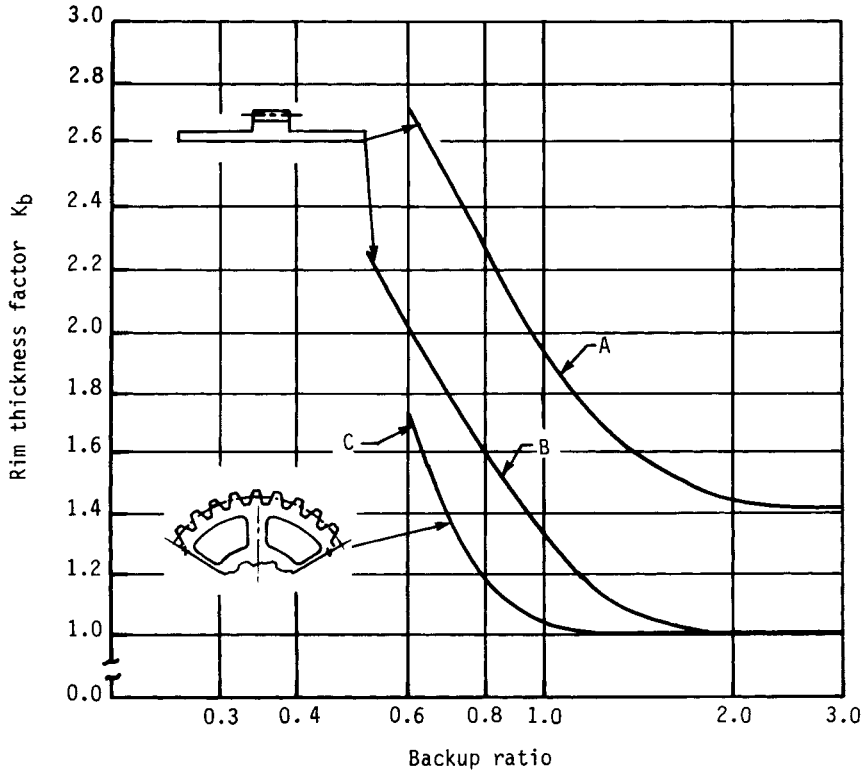

FIGURE 10.7 Rim thickness factor K_b. The *backup ratio* is defined as the ratio of the rim thickness to the tooth height. Curve *A* is fully reversed loading; curves *B* and *C* are unidirectional loading.

For gear blanks which utilize a T-shaped rim and web construction, the web acts as a hard point, if the rim is thin, and stresses will be higher over the web than over the ends of the T. The actual value which should be used for such constructions depends greatly on the relative proportions of the gear face width and the web. If the web spans 70 to 80 percent of the face width, the gear may be considered as having a rigid backup. Thus the backup ratio will be greater than 2.0, and any of the curves shown may be used (that is, curve *C* or *B,* both of which are identical above a 2.0 backup ratio, for unidirectional loading or curve *A* for fully reversed loading). If the proportions are between these limits, the gear lies in a gray area and probably lies somewhere in the range defined by curves *B* and *C.* Some designer discretion should be exercised here.

Finally, note that the rim thickness factor is equal to unity only for unidirectionally loaded, rigid-backup helical gears. For fully reversed loading, its value will be at least 1.4, even if the backup is rigid.

Load-Distribution Factors $\mathbf{K_m}$ ***and*** $\mathbf{C_c}$. These factors modify the rating equations to account for the manner in which the load is distributed on the teeth. The load on a set of gears will never be exactly uniformly distributed. Factors which affect the load distribution include the accuracy of the teeth themselves; the accuracy of the

housing which supports the teeth (as it influences the alignment of the gear axes); the deflections of the housing, shafts, and gear blanks (both elastic and thermal); and the internal clearances in the bearings which support the gears, among others.

All these and any other appropriate effects must be evaluated in order to define the total effective alignment error e_t for the gear pair. Once this is accomplished, the load-distribution factor may be calculated.

In some cases it may not be possible to fully define or even estimate the value of e_t. In such cases an empirical approach may be used. We discuss both approaches in some detail.

The empirical approach requires only minimal data, and so it is the simplest to apply. Several conditions must be met, however, prior to using this method:

1. Net face width to pinion pitch diameter ratios must be less than or equal to 2.0. (For double-helix gears, the gap is not included in the face width.)
2. The gear elements are mounted between bearings (not overhung).
3. Face width can be up to 40 in.
4. There must be contact across the full face width of the narrowest member when loaded.
5. Gears are not highly crowned.

The empirical expression for the load-distribution factor is

$$C_m = K_m = 1.0 + C_{mc}(C_{pf}C_{pm} + C_{ma}C_e) \tag{10.21}$$

where C_{mc} = lead correction factor
C_{pf} = pinion proportion factor
C_{pm} = pinion proportion modifier
C_{ma} = mesh alignment factor
C_e = mesh alignment correction factor

The lead correction factor C_{mc} modifies the peak loading in the presence of slight crowning or lead correction as follows:

$$C_{mc} = \begin{cases} 1.0 & \text{for gear with unmodified leads} \\ 0.8 & \text{for gear with leads properly modified by crowning or lead correction} \end{cases}$$

Figure 10.8 shows the pinion proportion factor C_{pf}, which accounts for deflections due to load. The pinion proportion modifier C_{pm} alters C_{pf} based on the location of the pinion relative to the supporting bearings. Figure 10.9 defines the factors S and S_1. And C_{pm} is defined as follows:

$$C_{pm} = \begin{cases} 1.0 & \text{when } S_1/S < 0.175 \\ 1.1 & \text{when } S_1/S \geq 0.175 \end{cases}$$

The mesh alignment factor C_{ma} accounts for factors other than elastic deformations. Figure 10.10 provides values for this factor for four accuracy groupings. For double-helix gears, this figure should be used with F equal to half of the total face width. The mesh alignment correction factor C_e modifies the mesh alignment factor to allow for the improved alignment which may be obtained when a gear set is adjusted at assembly or when the gears are modified by grinding, skiving, or lapping to more closely match their mates at assembly (in which case, pinion and gear

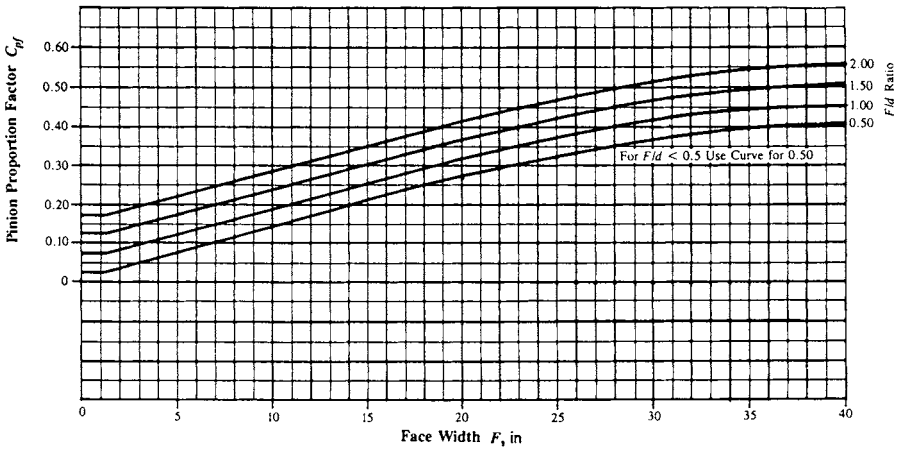

FIGURE 10.8 Pinion proportion factor C_{pf}. *(From Ref. [10.1].)*

become a matched set). Only two values are permissible for C_e—either 1.0 or 0.8, as defined by the following requirements:

$$C_e = \begin{cases} 0.80 & \text{when the compatibility of the gearing is improved by lapping, grinding, or skiving after trial assembly to improve contact} \\ 0.80 & \text{when gearing is adjusted at assembly by shimming support bearings and/or housing to yield uniform contact} \\ 1.0 & \text{for all other conditions} \end{cases}$$

If enough detailed information is available, a better estimate of the load-distribution factor may be obtained by using a more analytical approach. This method, however, requires that the total alignment error e_t be calculated or estimated. Depending on the contact conditions, one of two expressions is used to calculate the load-distribution factor.

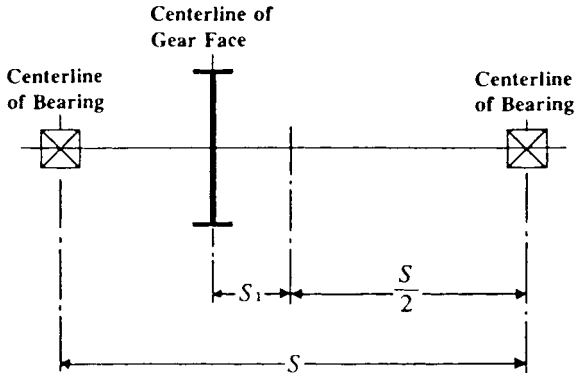

FIGURE 10.9 Definition of distances S and S_1. Bearing span is distance S; pinion offset from midspan is S_1. *(From Ref. [10.1].)*

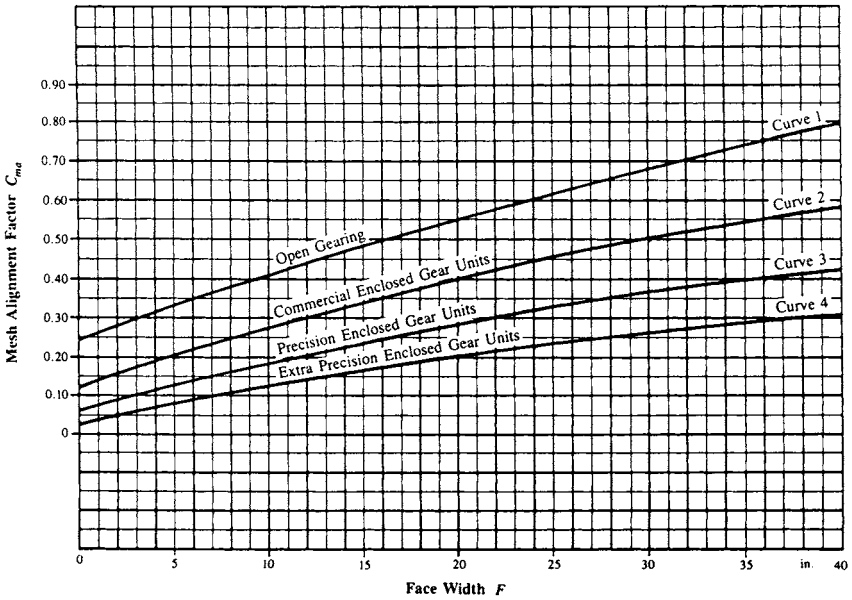

FIGURE 10.10 Mesh alignment factor C_{ma}. For analytical method for determination of C_{ma}, see Eq. (10.21). *(From Ref. [10.1].)*

If the tooth contact pattern at normal operating load essentially covers the entire available tooth face, Eq. (10.22) should be used. If the tooth contact pattern does not cover the entire available tooth face (as would be the case for poorly aligned or high-crowned gears) at normal operating loads, then Eq. (10.23) must be used:

$$C_m = 1.0 + \frac{Ge_t ZF}{4W_t p_b} \tag{10.22}$$

and

$$C_m = \sqrt{\frac{Ge_t ZF}{W_t p_b}} \tag{10.23}$$

where W_t = tangential tooth load, pounds (lb)
G = tooth stiffness constant, (lb/in)/in of face
Z = length of line of contact in transverse plane
e_t = total effective alignment error, in/in
p_b = transverse base pitch, in
F = net face width of narrowest member, in

The value of G will vary with tooth proportions, tooth thickness, and material. For steel gears of standard or close to standard proportions, it is normally in the range of 1.5×10^6 to 2.0×10^6 psi. The higher value should be used for higher-pressure-angle teeth, which are normally stiffer, while the lower value is representative of more flexible teeth. The most conservative approach is to use the higher value in all cases.

For double-helix gears, each half should be analyzed separately by using the appropriate values of F and e_t and by assuming that half of the tangential tooth load is transmitted by each half (the values for p_b, Z, and G remain unchanged).

***Geometry Factor* I.** The geometry factor I evaluates the radii of curvature of the contacting tooth profiles based on the pressure angle, helix, and gear ratio. Effects of modified tooth proportions and load sharing are considered. The I factor is defined as follows:

$$I = \frac{C_c C_x C_\psi^2}{m_N} \tag{10.24}$$

where C_c = curvature factor at operating pitch line
C_x = contact height factor
C_ψ = helical overlap factor
m_N = load-sharing ratio

The curvature factor is

$$C_c = \frac{\cos \phi_o \sin \phi_o}{2} \frac{N_G}{N_G + N_P} \tag{10.25}$$

for external mesh; for internal mesh,

$$C_c = \frac{\cos \phi_o \sin \phi_o}{2} \frac{N_G}{N_G - N_P} \tag{10.26}$$

The contact height factor C_x adjusts the location on the tooth profile at which the critical contact stress occurs (i.e., face-contact ratio > 1.0). The stress is calculated at the mean diameter or the middle of the tooth profile. For low-contact-ratio helical gears (that is, face-contact ratio ≤ 1.0), the stress is calculated at the lowest point of single-tooth contact in the transverse plane and C_x is given by Eq. (10.27):

$$C_x = \frac{R_1 R_2}{R_P R_G} \tag{10.27}$$

where R_P = pinion curvature radius at operating pitch point, in
R_G = gear curvature radius at operating pitch point, in
R_1 = pinion curvature radius at critical contact point, in
R_2 = gear curvature radius at critical contact point, in

The required radii are given by

$$R_P = \frac{d}{2} \sin \phi_o \qquad R_G = \frac{D}{2} \sin \phi_o \tag{10.28}$$

where d = pinion operating pitch diameter, in
D = gear operating pitch diameter, in
ϕ_o = operating pressure angle in transverse plane, deg

$$R_1 = R_P - Z_c \tag{10.29}$$

and

$$R_2 = R_G + Z_c \tag{10.30}$$

for external gears; for internal gears,

$$R_2 = R_G - Z_c \tag{10.31}$$

where Z_c is the distance along the line of action in the transverse plane to the critical contact point. The value of Z_c is dependent on the transverse contact ratio. For helical gears where the face-contact ratio ≤ 1.0, Z_c is found by using Eq. (10.32). For normal helical gears where the face-contact ratio is > 1.0, Eq. (10.33) is used:

$$Z_c = p_b - 0.5[(d_o^2 - d_b^2)^{1/2} - (d^2 - d_b^2)^{1/2}] \qquad m_F \le 1.0 \tag{10.32}$$

and

$$Z_c = 0.5\,[(d^2 - d_b^2)^{1/2} - (d_m^2 - d_b^2)^{1/2}] \qquad m_F > 1.0 \tag{10.33}$$

where p_b = base pitch, in
d_o = pinion outside diameter, in
d_b = pinion base diameter, in
d_m = pinion mean diameter, in

The pinion mean diameter is defined by Eq. (10.34) or (10.35). For external mesh,

$$d_m = C_o - \frac{D_o - d_o}{2} \tag{10.34}$$

For internal mesh,

$$d_m = \frac{D_I + d_o}{2} - C_o \tag{10.35}$$

where D_o = external gear outside diameter and D_I = internal gear inside diameter.

The helical factor C_ψ accounts for the partial helical overlap action which occurs in helical gears with a face-contact ratio $m_F \le 1.0$. For helical gears with a face-contact ratio > 1.0, C_ψ is set equal to unity; for low-contact helical gears, it is

$$C_\psi = \sqrt{1 - m_F + \frac{C_{xn} Z m_F^2}{C_x F \sin \psi_b}} \tag{10.36}$$

where Z = total length of line of action in transverse plane, in
F = net minimum face width, in
m_F = face-contact ratio
C_x = contact height factor [Eq. (10.27)]
C_{xn} = contact height factor for equivalent normal helical gears [Eq. (10.37)]
ψ_b = base helix angle, deg

The C_{xn} factor is given by

$$C_{xn} = \frac{R_{1n} R_{2n}}{R_P R_G} \tag{10.37}$$

where R_{1n} = curvature radius at critical point for equivalent normal helical pinion, in
R_{2n} = curvature radius at critical contact point for equivalent normal helical gear, in

The curvature radii are given by

$$R_{1n} = R_P - Z_c \tag{10.38}$$

$$\begin{aligned} R_{2n} &= R_G + Z \qquad \text{external gears} \\ R_{2n} &= R_G - Z_c \qquad \text{internal gears} \end{aligned} \tag{10.39}$$

where Eq. (10.38) applies to external gears and Eq. (10.39) to either, as appropriate. Also, the term Z_c is obtained from Eq. (10.32).

The load-sharing ratio m_N is the ratio of the face width to the minimum total length of the contact lines:

$$m_N = \frac{F}{L_{\min}} \tag{10.40}$$

where m_N = load-sharing ratio
F = minimum net face width, in
$L_{\min}$ = minimum total length of contact lines, in

The calculation of $L_{\min}$ is a rather involved process. For most helical gears which have a face-contact ratio of at least 2.0, a conservative approximation for the load-sharing ratio ratio m_N may be obtained from

$$m_N = \frac{P_N}{0.95Z} \tag{10.41}$$

where p_N = normal circular pitch in inches and Z = length of line of action in the transverse plane in inches. For helical gears with a face-contact ratio of less than 2.0, it is imperative that the actual value of $L_{\min}$ be calculated and used in Eq. (10.40). The method for doing this is shown in Eqs. (10.42) through (10.45):

$$L_{\min} = \frac{1}{\sin \psi_b} [(P_1 - Q_1) + (P_2 - Q_2) + \cdots + (P_i - Q_i) + \cdots + (P_n - Q_n)] \tag{10.42}$$

where n = limiting number of lines of contact, as given by

$$n = \frac{(Z/\tan \psi_b) + F}{p_x} \tag{10.43}$$

Also, P_i = sum of base pitches in inches. The ith term of P_i is the lesser of

$$ip_x \tan \psi_b \qquad \text{or} \qquad Z \tag{10.44}$$

Finally, Q_i = remainder of base pitches in inches. Its value is

$$Q_i = 0 \qquad \text{if } ip_x \le F$$

But when $ip_x > F$, then Q_i is the ith term and is the lesser of

$$(ip_x - F) \tan \psi_b \qquad \text{or} \qquad Z \tag{10.45}$$

***Geometry Factor* J.** The bending strength geometry factor is

$$J = \frac{YC_\psi}{K_f m_N} \tag{10.46}$$

where Y = tooth form factor
K_f = stress correction factor
C_ψ = helical factor
m_N = load-distribution factor

The helical and load-distribution factors were both defined in the discussion of the geometry factor *I*. The calculation of Y is also a long, tedious process. For helical gears in which load sharing exists among the teeth in contact and for which the face-contact ratio is at least 2.0, the value of Y need not be calculated, since the value for J may be obtained directly from the charts shown in Figs. 10.11 through 10.25 with Eq. (10.47):

$$J = J' Q_{TR} Q_{TT} Q_A Q_H \tag{10.47}$$

where J' = basic geometry factor
Q_{TR} = tool radius adjustment factor
Q_{TT} = tooth thickness adjustment factor
Q_A = addendum adjustment factor
Q_H = helix-angle adjustment factor

In using these charts, note that the values of addendum, dedendum, and tool-tip radius are given for a 1-normal-pitch gear. Values for any other pitch may be obtained by dividing the factor by the actual normal diametral pitch. For example, if an 8-normal-pitch gear is being considered, the parameters shown on Fig. 10.11 are

$$\text{Addendum } a = \frac{1.0}{8} = 0.125 \text{ in}$$

$$\text{Dedendum } b = \frac{1.35}{8} = 0.168\,75 \text{ in}$$

$$\text{Tool (hob) tip radius } r_T = \frac{0.42}{8} = 0.0525 \text{ in}$$

The basic geometry factor J' is found from Figs. 10.11 through 10.25. The tool radius adjustment factor Q_{TR} is found from Figs. 10.14 through 10.16 if the edge radius on the tool is other than $0.42/P_d$, which is the standard value used in calculating J'. Similarly, for gears with addenda other than $1.0/P_d$ or tooth thicknesses other than the standard value of $\pi/(2P_d)$, the appropriate factors may be obtained from these charts. In the case of a helical gear, the adjustment factor Q_H is obtained from Figs. 10.23 through 10.25. If a standard helical gear is being considered, Q_{TR}, Q_{TT}, and Q_A remain equal to unity, but Q_H must be found from Figs. 10.23 to 10.25.

These charts are computer-generated and, when properly used, produce quite accurate results. Note that they are also valid for spur gears if Q_H is set equal to unity (that is, enter Figs. 10.23 through 10.25 with 0° helix angle).

The charts shown in Figs. 10.11 through 10.25 assume the use of a standard full-radius hob. Additional charts, still under the assumption that the face-contact ratio is

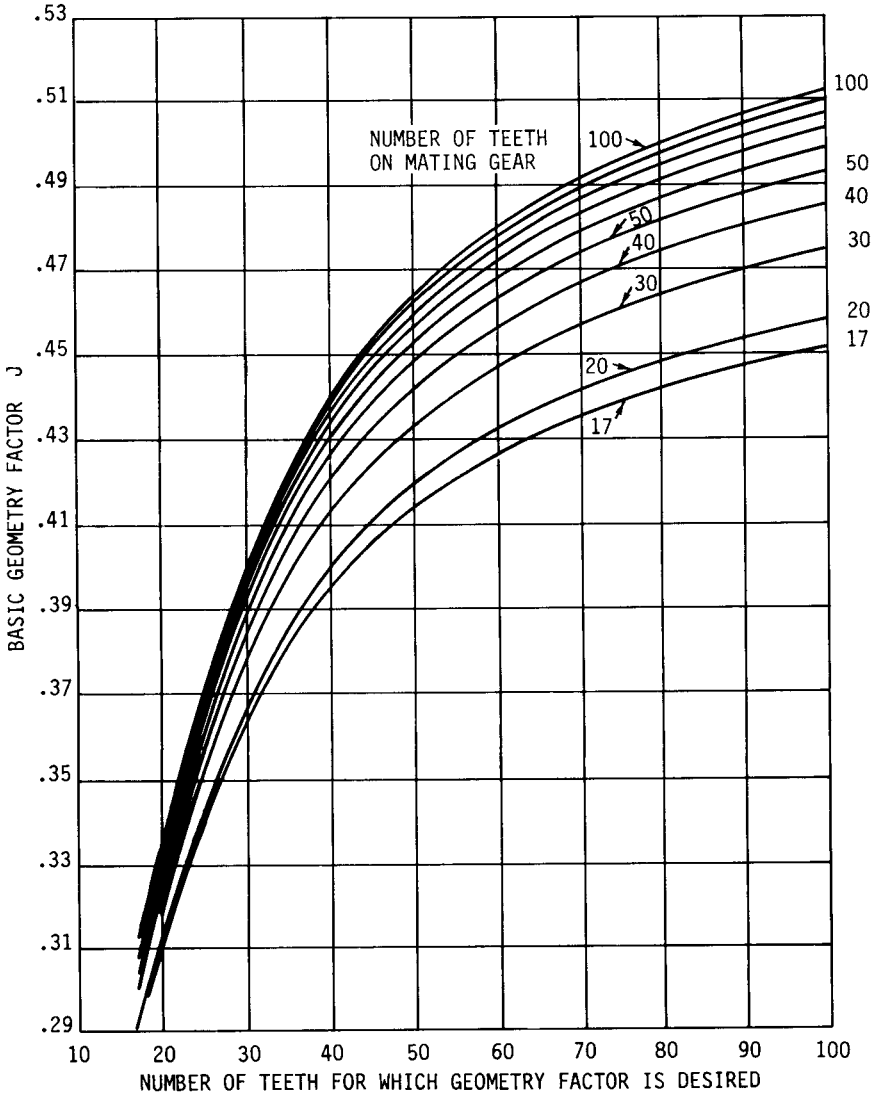

FIGURE 10.11 Basic geometry factors for 20° spur teeth; $\phi_N = 20°$, $a = 1.00$, $b = 1.35$, $r_T = 0.42$, $\Delta t = 0$.

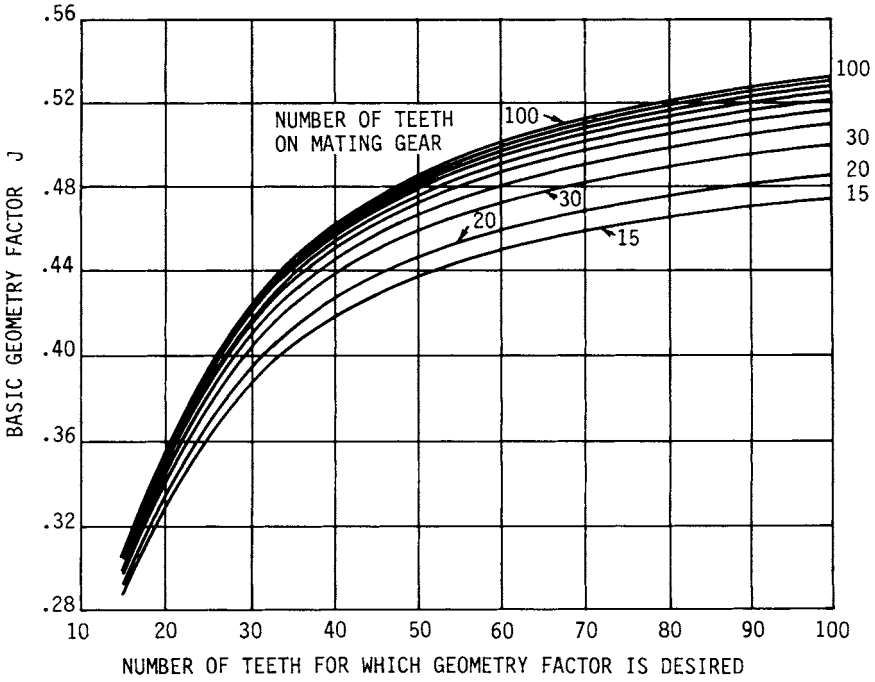

FIGURE 10.12 Basic geometry factors for 22½° spur teeth; $\phi_N = 22½°$, $a = 1.00$, $b = 1.35$, $r_T = 0.34$, $\Delta t = 0$.

at least 2.0 for other cutting-tool configurations, are shown in Figs. 10.26 through 10.36.† For these figures,

$$m_N = \frac{P_N}{0.95Z} \tag{10.48}$$

where the value of Z is for an element of indicated number of teeth and a 75-tooth mate. Also, the normal tooth thicknesses of pinion and gear teeth are each reduced 0.024 in, to provide 0.048 in of total backlash corresponding to a normal diametral pitch of unity. Note that these charts are limited to standard addendum, dedendum, and tooth thickness designs.

If the face-contact ratio is less than 2.0, the geometry factor must be calculated in accordance with Eq. (10.46); thus, it will be necessary to define Y and K_f. The definition of Y may be accomplished either by graphical layout or by a numerical iteration procedure. Since this Handbook is likely to be used by the machine designer with an occasional need for gear analysis, rather than by the gear specialist, we present the direct graphical technique. Readers interested in preparing computer codes or calculator routines might wish to consult Ref. [10.6].

The following graphical procedure is abstracted directly from Ref. [10.1] with permission of the publisher, as noted earlier. The Y factor is calculated with the aid

† These figures are extracted from AGMA 908-B89 with the permission of the AGMA.

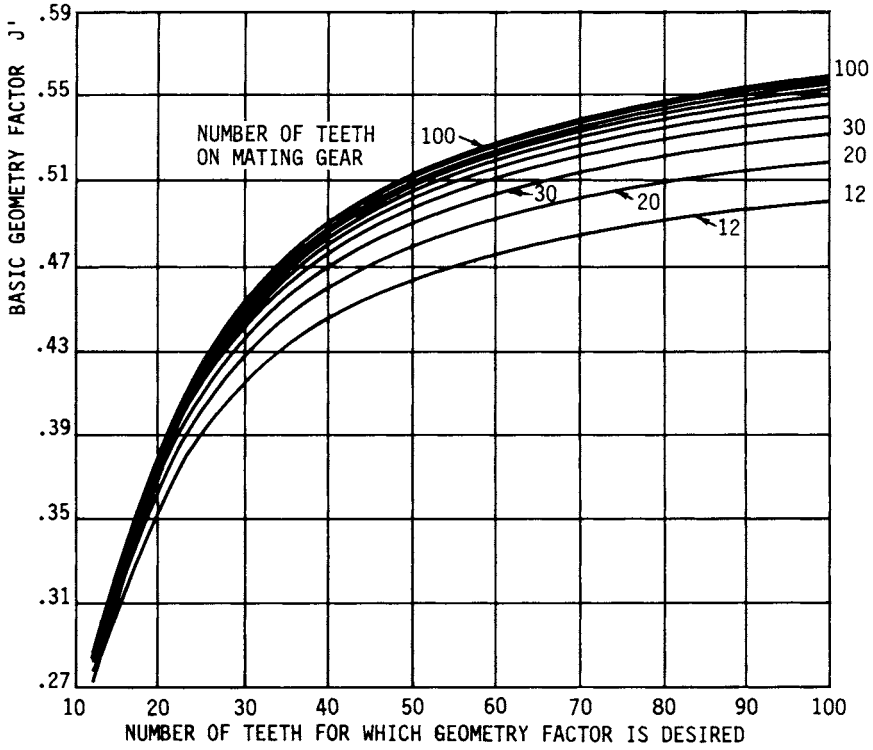

FIGURE 10.13 Basic geometry factors for 25° spur teeth; $\phi_N = 25°$, $a = 1.00$, $b = 1.35$, $r_T = 0.24$, $\Delta t = 0$.

of dimensions obtained from an accurate layout of the tooth profile in the normal plane at a scale of 1 normal diametral pitch. Actually, any scale can be used, but the use of 1 normal diametral pitch is most convenient. Depending on the face-contact ratio, the load is considered to be applied at the highest point of single-tooth contact (HPSTC), Fig. 10.37, or at the tooth tip, Fig. 10.38. The equation is

$$Y = \frac{K_\psi P_s}{[\cos(\phi_L)/\cos(\phi_{No})][(1.5/uC_h) - \tan(\phi_L)/t]} \tag{10.49}$$

The terms in Eq. (10.49) are defined as follows:

K_ψ = helix-angle factor
ϕ_{No} = normal operating pressure angle [Eq. (10.14)]
ϕ_L = load angle
C_h = helical factor
t = tooth thickness from layout, in
u = radial distance from layout, in
P_s = normal diametral pitch of layout (scale pitch), usually 1.0 in^{-1}

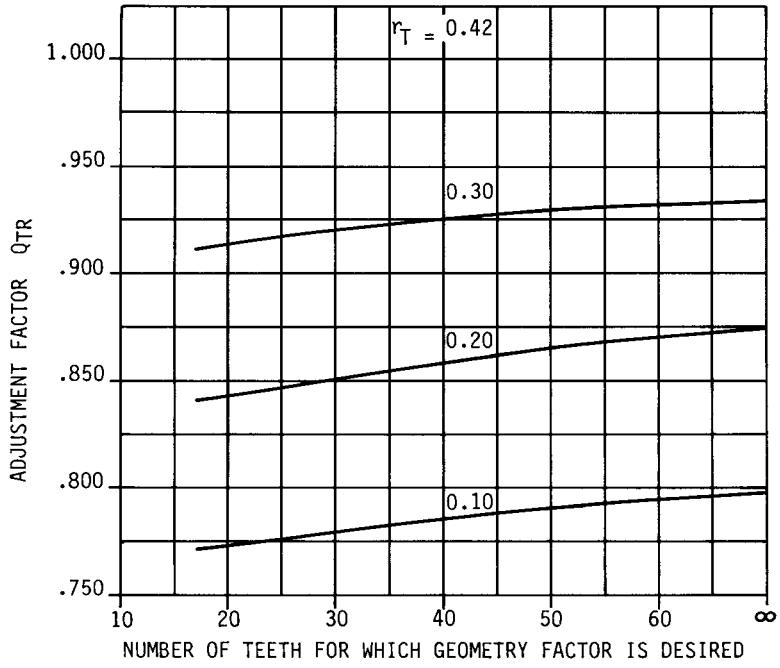

FIGURE 10.14 Tool-tip radius adjustment factor for 20° spur teeth. Tool-tip radius = r_T for a 1-diametral-pitch gear.

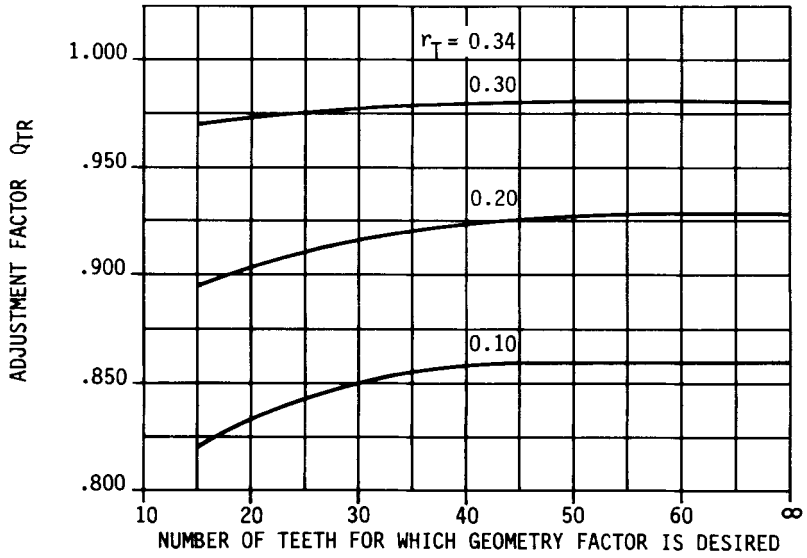

FIGURE 10.15 Tool-tip radius adjustment factor for 22½° spur teeth. Tool-tip radius = r_T for a 1-diametral-pitch gear.

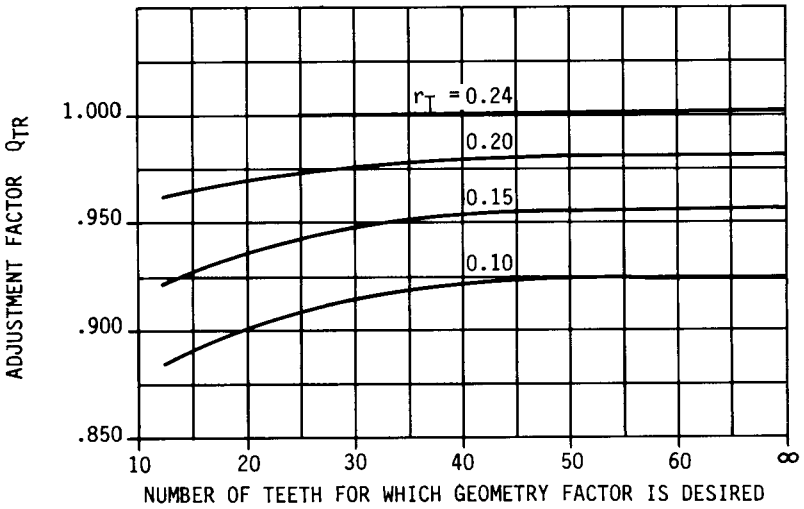

FIGURE 10.16 Tool-tip radius adjustment factor for 25° spur teeth. Tool-tip radius = r_T for a 1-diametral-pitch gear.

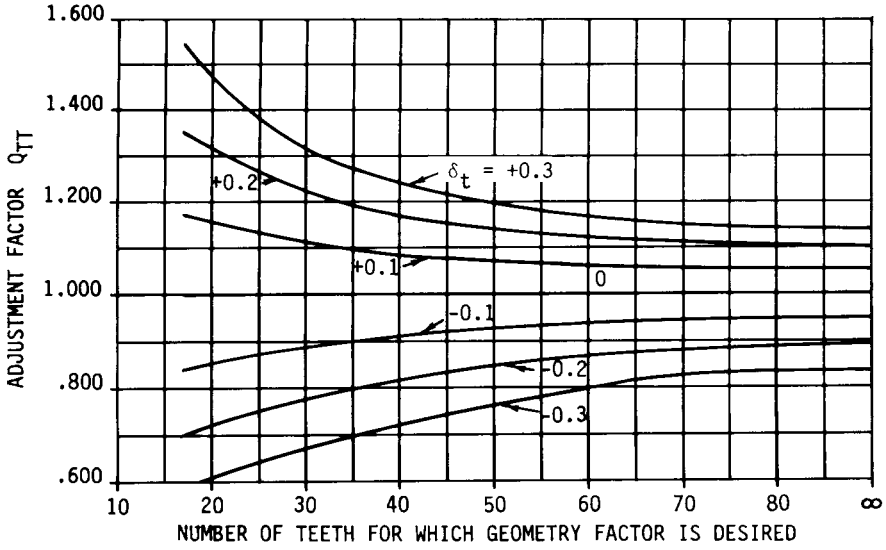

FIGURE 10.17 Tooth thickness adjustment factor Q_{TT} for 20° spur teeth. Tooth thickness modification = δ_t for 1-diametral-pitch gears.

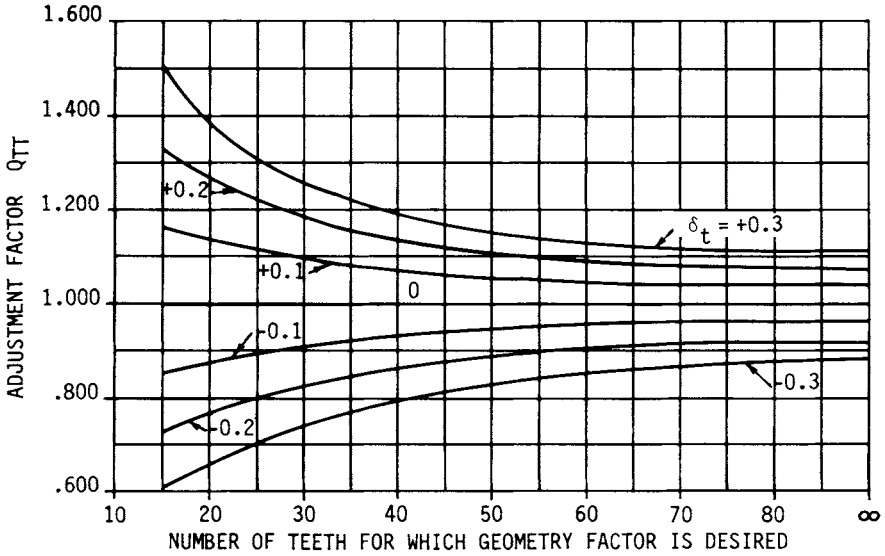

FIGURE 10.18 Tooth thickness adjustment factor Q_{TT} for 22½° spur teeth. Tooth thickness modification = δ_t for 1-diametral-pitch gears.

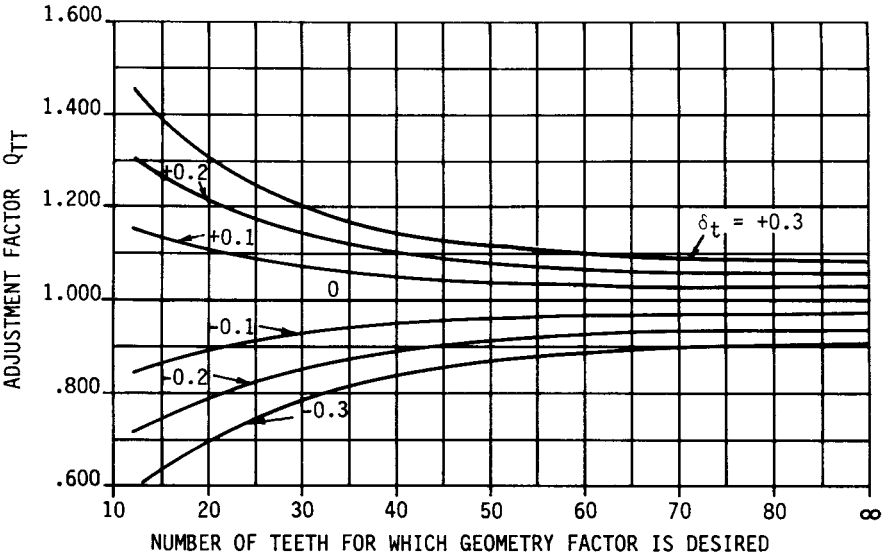

FIGURE 10.19 Tooth thickness adjustment factor Q_{TT} for 25° spur teeth. Tooth thickness modification = δ_t for 1-diametral-pitch gears.

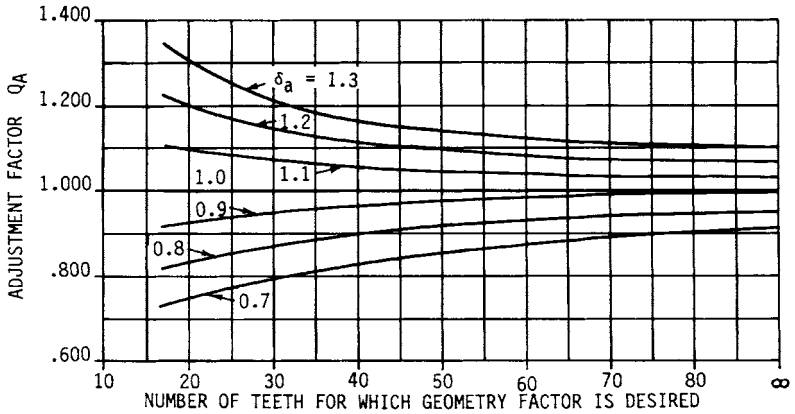

FIGURE 10.20 Addendum adjustment factor Q_A for 20° spur teeth. Addendum factor modification = δ_a for 1-diametral-pitch gears.

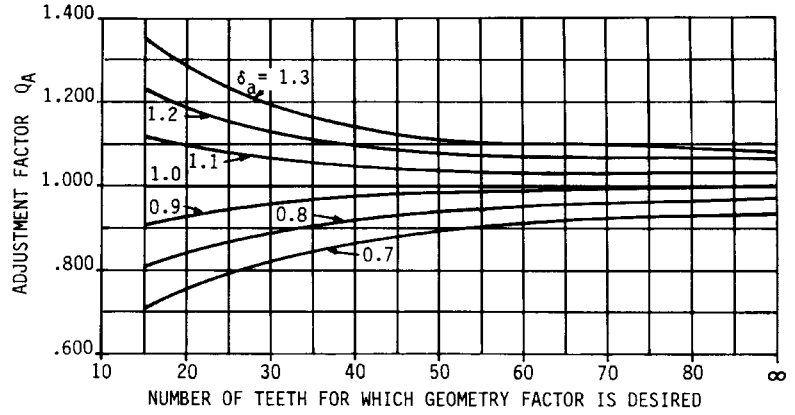

FIGURE 10.21 Addendum adjustment factor Q_A for 22½° spur teeth. Addendum factor modification = δ_a for 1-diametral-pitch gears.

To make the Y factor layout for a helical gear, an equivalent normal-plane gear tooth must be created, as follows:

$$N_e = \frac{N_P}{\cos^3 \psi} \tag{10.50}$$

$$d_c = \frac{dP_{nd}}{\cos^2 \psi} \tag{10.51}$$

$$d_{be} = d_e \cos \phi_n = N_e \cos \phi_c \tag{10.52}$$

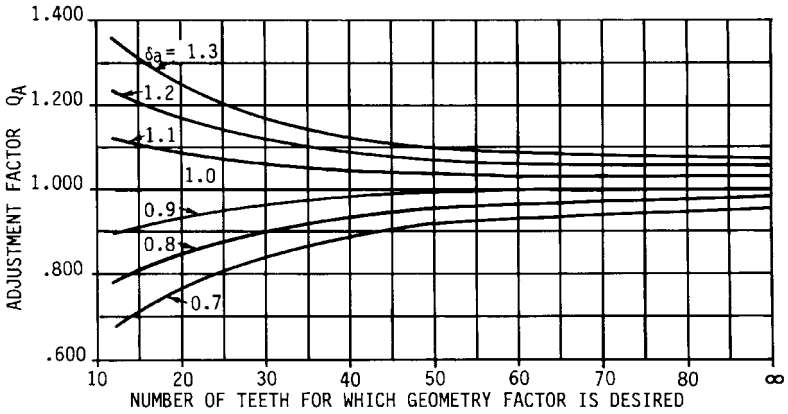

FIGURE 10.22 Addendum adjustment factor Q_A for 25° spur teeth. Addendum factor modification = δ_a for 1-diametral-pitch gears.

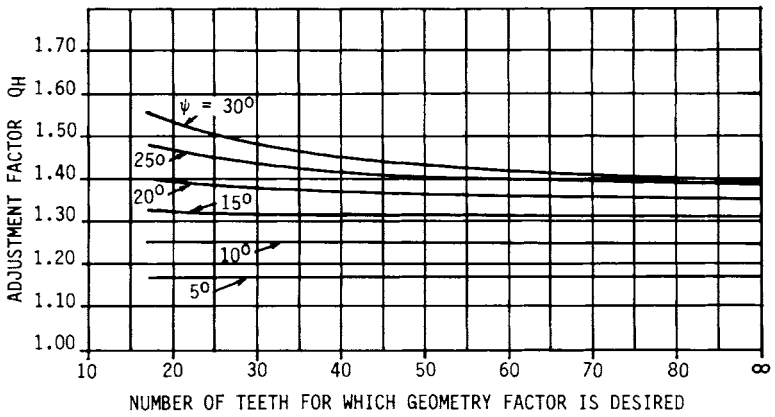

FIGURE 10.23 Helix-angle adjustment factor Q_H for $\phi_N = 20°$.

$$a = \frac{d_o - d}{2} P_{nd} \tag{10.53}$$

$$b = \frac{d - d_R}{2} P_{nd} \tag{10.54}$$

$$d_{oe} = d_e + 2a \tag{10.55}$$

$$d_{Re} = d_e - 2b \tag{10.56}$$

$$r_1 = \frac{(b - r_{Te})^2}{R_o + b - r_{Te}} \tag{10.57}$$

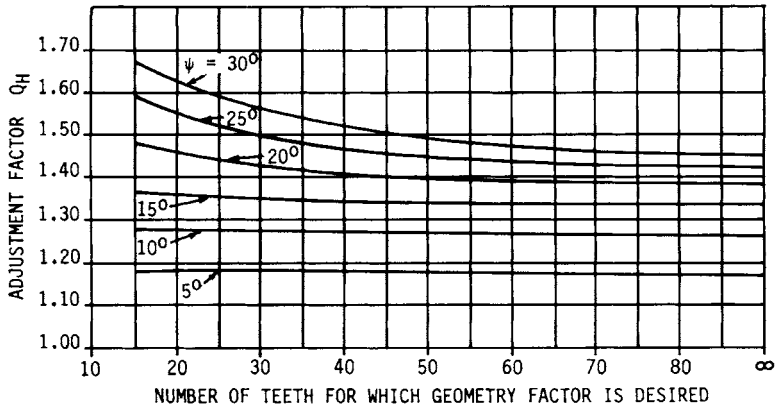

FIGURE 10.24 Helix-angle adjustment factor Q_H for $\phi_N = 22\frac{1}{2}°$.

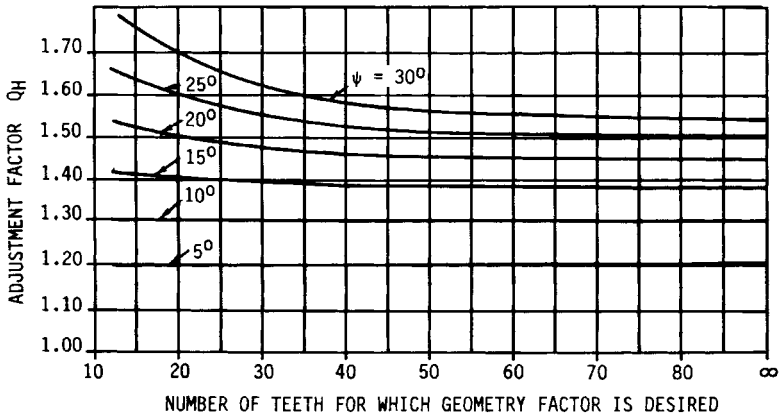

FIGURE 10.25 Helix-angle adjustment factor Q_H for $\phi_N = 25°$.

$$r_f = r_1 + r_{Te} \tag{10.58}$$

$$r_{Te} = r_T P_{nd} \tag{10.59}$$

For a hob or rack-shaped cutting tool,

$$R_o = \frac{d_{se}}{2} \tag{10.60}$$

For a pinion-shaped cutting tool,

$$R_o = \frac{d_{se} D_c P_{nd}}{2(d_{se} + D_c P_{nd})} \tag{10.61}$$

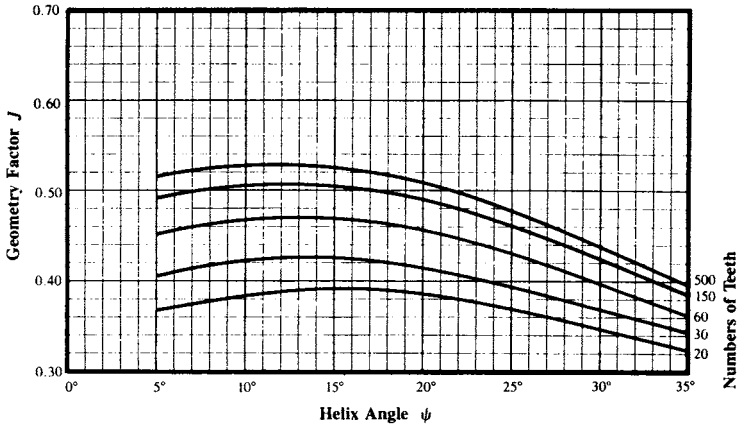

FIGURE 10.26 Geometry factor J for a 14½° normal-pressure-angle helical gear. These factors are for a standard addendum finishing hob as the final machining operation. See Fig. 10.27*a*. *(From AGMA 908-B89.)*

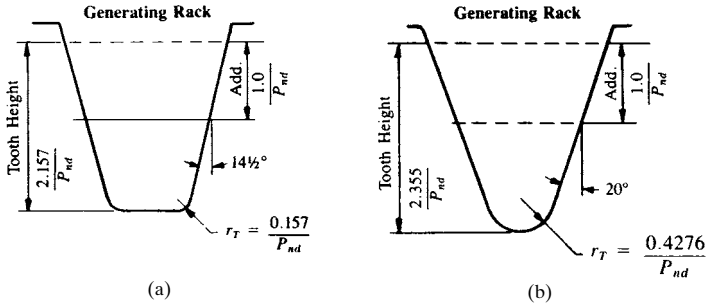

FIGURE 10.27 Generating racks. (*a*) For teeth of Fig. 10.26; (*b*) for teeth of Fig. 10.29. *(From AGMA 218.01.)*

$$D_e = \frac{DP_{nd}}{\cos^2 \psi} \tag{10.62}$$

$$A = \frac{D_o - D}{2} P_{nd} \tag{10.63}$$

$$D_{oe} = D_e + 2A \tag{10.64}$$

$$D_{be} = D_e \cos \phi_n \tag{10.65}$$

$$d_{se} = \frac{N_e}{P_s} \tag{10.66}$$

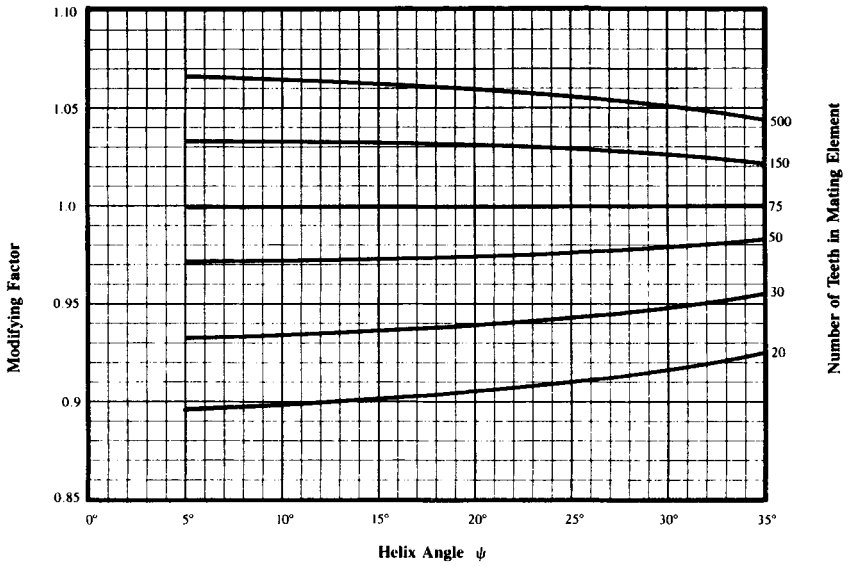

FIGURE 10.28 *J* factor multipliers for 14½° normal-pressure-angle helical gear. These factors can be applied to the *J* factor when other than 75 teeth are used in the mating element. *(From AGMA 908-B89.)*

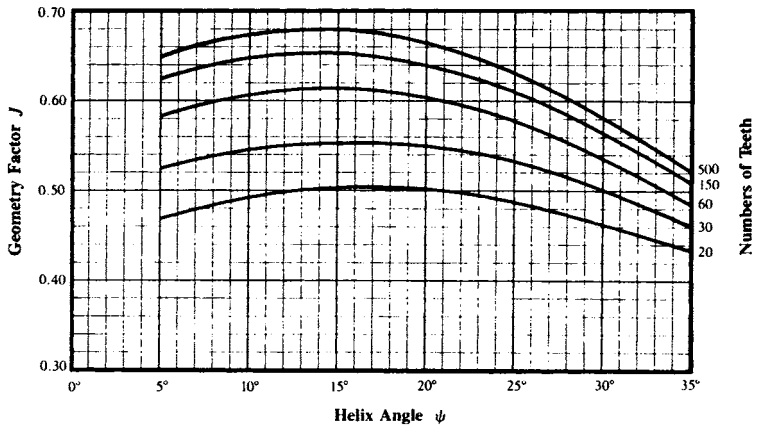

FIGURE 10.29 Geometry factor *J* for a 20° normal-pressure-angle helical gear. These factors are for standard addendum teeth cut with a full-fillet hob. See Fig. 10.27*b*. *(From AGMA 908-B89.)*

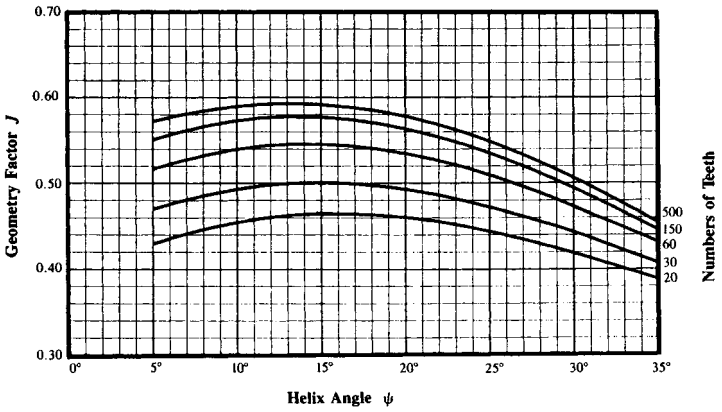

FIGURE 10.30 Geometry factor J for a 20° normal-pressure-angle helical gear. These factors are for standard addendum teeth cut with a finishing hob as the final machining operation. See Fig. 10.31*a*. *(From AGMA 908-B89.)*

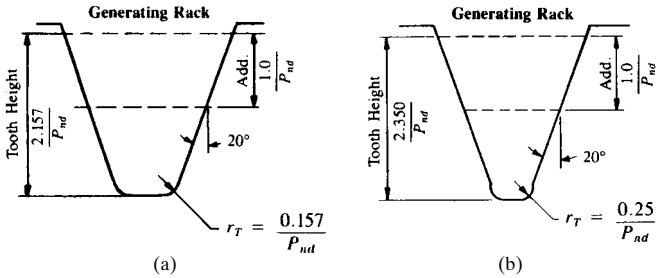

FIGURE 10.31 Generating racks. (*a*) For teeth of Fig. 10.30; (*b*) for teeth of Fig. 10.32. *(From AGMA 908-B89.)*

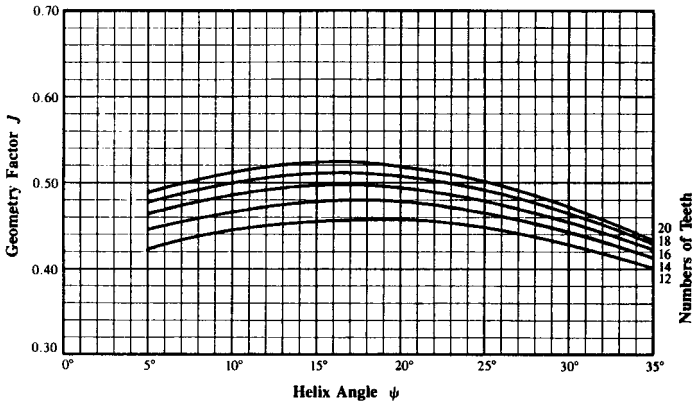

FIGURE 10.32 Geometry factor J for 20° normal-pressure-angle helical gear. These factors are for long-addendum (125 percent of standard) shaved teeth cut with a preshave hob. See Fig. 10.31*b*. *(From AGMA 908-B89.)*

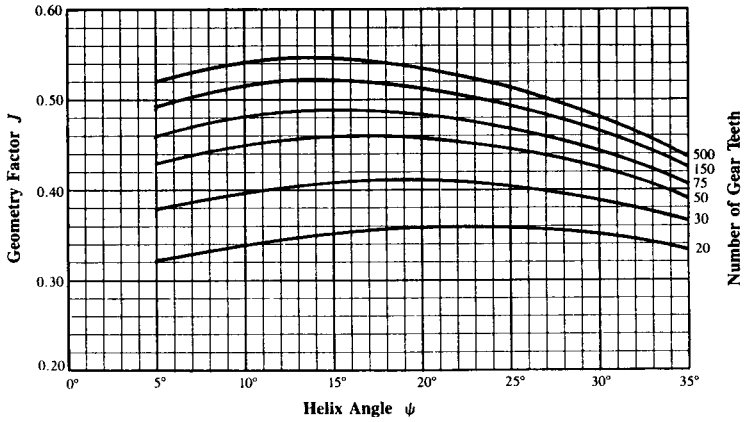

FIGURE 10.33 Geometry factor J for 20° normal-pressure-angle helical gear. These factors are for short-addendum teeth (75 percent of standard) cut with a preshave hob. See Fig. 10.34. *(From AGMA 908-B89.)*

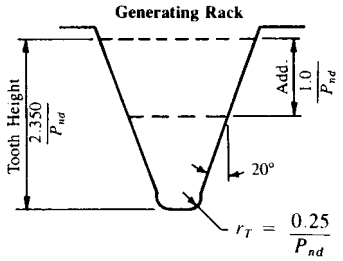

FIGURE 10.34 Generating rack for teeth of Fig. 10.33. *(From AGMA 908-B89.)*

where N_e = equivalent number of pinion teeth
d_{se} = equivalent generating pitch diameter, in
d_R = root diameter for actual number of teeth and generated pitch, in
d_{Re} = equivalent root diameter for equivalent number of teeth, in
d_{be} = equivalent base diameter for equivalent number of teeth, in
d_e = equivalent operating pitch diameter for equivalent number of teeth, in
d_{oe} = equivalent outside diameter for equivalent number of teeth, in
a = operating addendum of pinion at 1 normal diametral pitch, in
b = operating dedendum of pinion at 1 normal diametral pitch, in
r_f = minimum fillet radius at root circle of layout, in
r_T = edge radius of cutting tool, in
r_{Te} = equivalent edge radius of cutting tool, in
R_o = relative radius of curvature of pitch circle of pinion and pitch line or circle of cutting tool, in
D_c = pitch diameter of pinion-shaped cutting tool, in
D_e = equivalent operating pitch diameter of mating gear for equivalent number of teeth, in

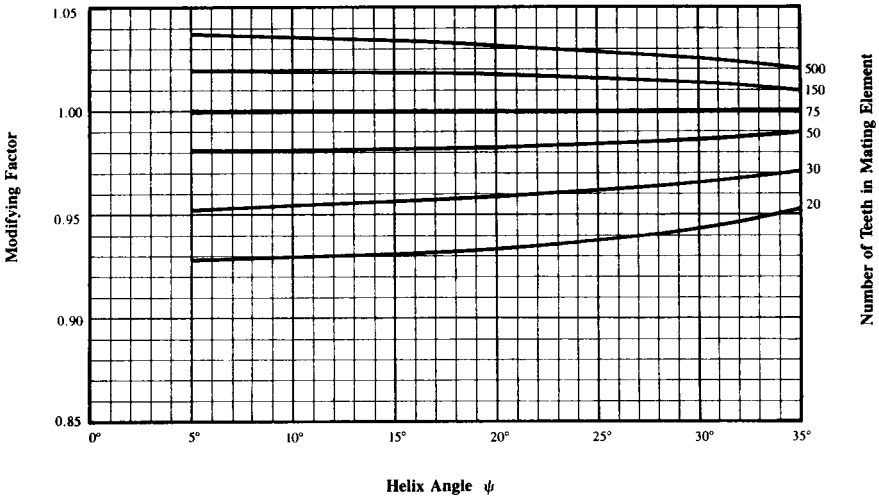

FIGURE 10.35 *J* factor multipliers for 20° normal-pressure-angle helical gears. These factors can be applied to the *J* factor when other than 75 teeth are used in the mating element. *(From Ref. [10.1].)*

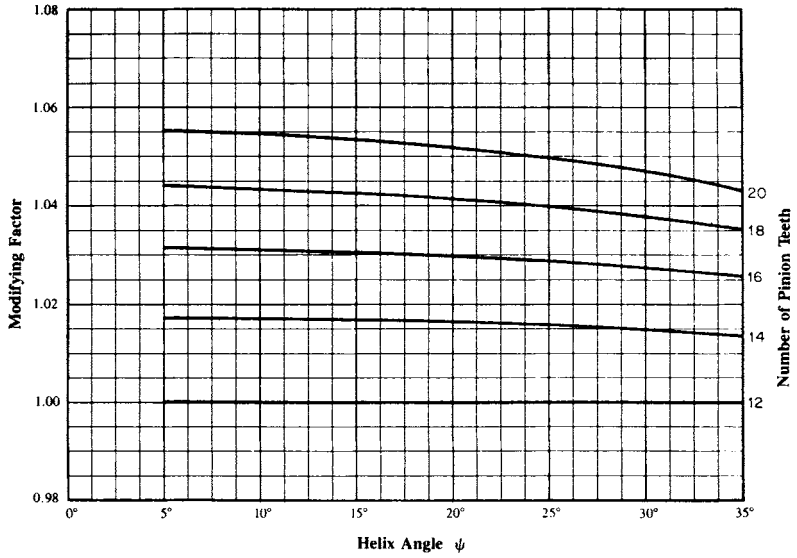

FIGURE 10.36 *J* factor multipliers for 20° normal-pressure-angle helical gears with short addendum (75 percent of standard). These factors can be applied to the *J* factor when other than 75 teeth are used in the mating element. *(From Ref. [10.1].)*

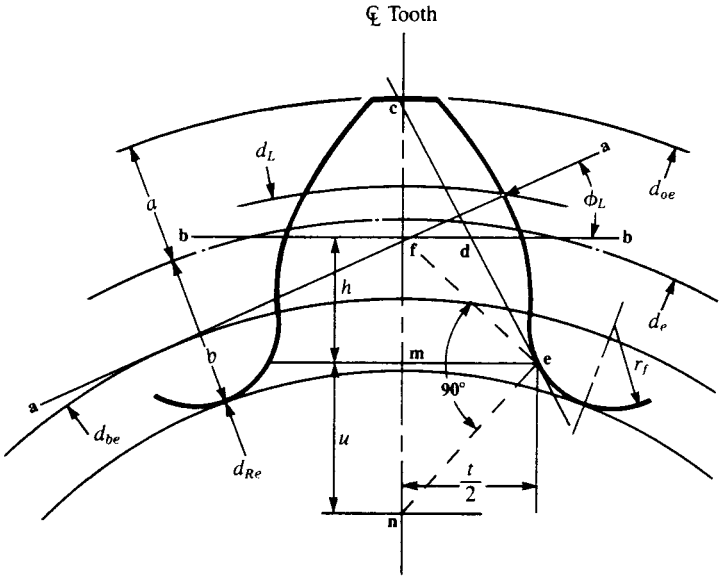

FIGURE 10.37 Tooth form factor with load at highest point of single-tooth contact (HPSTC) shown in the normal plane through the pitch point. Note that r_f occurs at the point where the trochoid meets the root radius. *(From Ref. [10.1].)*

D_{oe} = equivalent outside diameter of mating gear for equivalent number of teeth, in
D_{be} = equivalent base diameter of mating gear for equivalent number of teeth, in
A = operating addendum of mating gear at 1 normal diametral pitch, in

The dimensions defined by Eqs. (10.50) through (10.66) are then used to make a tooth-stress layout, as shown in either Fig. 10.37 or 10.38 as required by the face-contact ratio. That is, helical gears with low face-contact ratio ($m_F \le 1.0$) are assumed to be loaded at the highest point of single-tooth contact; normal helical gears ($m_F > 1.0$) use tip loading, and the C_h factor compensates for the actual loading on the oblique line.

To find Y from the above data, a graphical construction, as follows, is required. For low-contact-ratio helical gears (with $m_F \le 1.0$), using Fig. 10.37, draw a line $\overline{aa}$ through point p, the intersection of diameter d_L with the profile, and tangent to the base diameter d_{be}:

$$d_L = 2\left\{\left[\sqrt{\left(\frac{d_e}{2}\right)^2 - \left(\frac{d_{be}}{2}\right)^2} + Z_d\right]^2 + \left(\frac{d_{be}}{2}\right)^2\right\}^{1/2} \tag{10.67}$$

where Z_d = distance on line of action from highest point of single-tooth contact to pinion operating pitch circle, in inches, and so

$$Z_d = \pi \cos \phi_c - Z_e \tag{10.68}$$

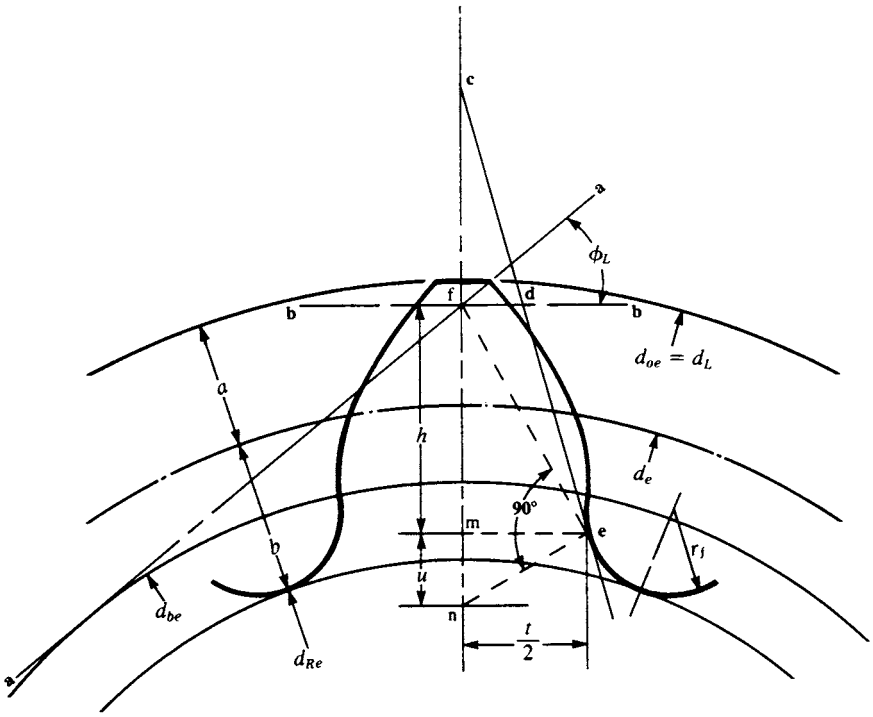

FIGURE 10.38 Tooth form factor layout with load at tooth tip; shown in normal plane through the pitch point. *(From Ref. [10.1].)*

Letting Z_e = distance on line of action from gear outside diameter to pinion operating pitch circle, in inches, we have

$$Z_e = \sqrt{\left(\frac{D_{oe}}{2}\right)^2 - \left(\frac{D_{be}}{2}\right)^2} - \sqrt{\left(\frac{D_e}{2}\right)^2 - \left(\frac{D_{be}}{2}\right)^2} \tag{10.69}$$

For normal helical gears with $m_F > 1.0$, using Fig. 10.38, we find $D_L = d_{oe}$. Draw a line $\overline{aa}$ through point p, the tip of the tooth profile, and tangent to the base diameter d_{be}. Continue the layout for all gear types as follows:

Through point f, draw a line $\overline{bb}$ perpendicular to the tooth centerline. The included angle between lines $\overline{aa}$ and $\overline{bb}$ is load angle ϕ_L.

Draw line $\overline{cde}$ tangent to the tooth fillet radius r_f at e, intersecting line $\overline{bb}$ at d and the tooth centerline at c so that $\overline{cd} = \overline{de}$.

Draw line $\overline{fe}$.

Through point e, draw a line perpendicular to $\overline{fe}$, intersecting the tooth centerline at n.

Through point e, draw a line $\overline{me}$ perpendicular to the tooth centerline.

Measure the following in inches from the tooth layout:

$$\overline{mn} = u \qquad \overline{me} = \frac{t}{2}$$

and

$$\overline{mf} = h \qquad \text{(required for calculating } K_f\text{)}$$

The helix-angle factor K_ψ is set equal to unity for helical gears with $m_F \le 1.0$, but for helical gears with $m_F > 1.0$, it is given by

$$K_\psi = \cos \psi_o \cos \psi \tag{10.70}$$

where ψ_o = helix angle at operating pitch diameter [from Eq. (10.13)] and ψ = helix angle at standard pitch diameter.

The helical factor C_h is the ratio of the root bending moment produced by the same intensity of loading applied along the actual oblique contact line (Fig. 10.39). If the face width of one gear is substantially larger than that of its mate, then full buttressing may exist on the wider face gear. If one face is wider than its mate by at least one addendum on *both* sides, then the value of C_h defined below may be increased by 10 percent only. The helical factor is given by either Eq. (10.71) for low-contact-ratio helical gears ($m_F \le 1.0$) or Eq. (10.72) for normal-contact-ratio ($m_F > 1.0$) helicals. These equations are valid only for helix angles up to 30°:

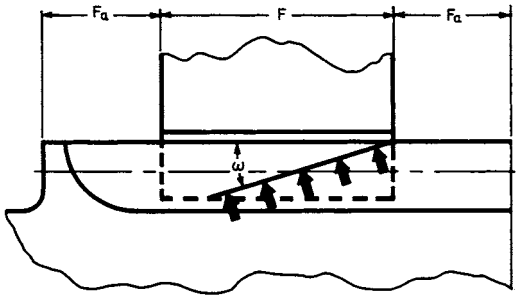

FIGURE 10.39 Oblique contact line. Full buttressing exists when $F_a \ge$ one addendum.

$$C_h = 1.0 \tag{10.71}$$

$$C_h = \frac{1.0}{1 - [(\omega/100)\ (1 - \omega/100)]^{1/2}} \tag{10.72}$$

where $\omega = \tan^{-1} (\tan \psi_o \sin \phi_{No})$ = inclination angle, deg
ψ_o = helix angle at operating pitch diameter, deg [Eq. (10.13)]
ϕ_{No} = operating normal pressure angle, deg [Eq. (10.14)]

The tooth form factor Y may now be calculated from Eq. (10.49).

The stress correction factor is the last item which must be calculated prior to finding a value for the bending geometry factor J. Based on photoelastic studies by Dolan and Broghamer, the empirical relations shown in Eqs. (10.73) through (10.76) were developed:

$$K_f = H + \left(\frac{t}{r_f}\right)^L \left(\frac{t}{h}\right)^m \tag{10.73}$$

$$H = 0.18 - 0.008(\phi_{No} - 20) \tag{10.74}$$

$$L = H - 0.03 \tag{10.75}$$

$$m = 0.45 + 0.010(\phi_{No} - 20) \tag{10.76}$$

Elastic Coefficient $\mathbf{C_p}$. This factor accounts for the elastic properties of various gear materials. It is given by Eq. (10.77). Table 10.4 provides values directly for C_p for various material combinations, for which Poisson's ratio is 0.30.

TABLE 10.4 Values of Elastic Coefficient C_p for Helical Gears with Nonlocalized Contact and for $\upsilon = 0.30$

Pinion material	Gear material					
	Steel	Malleable iron	Nodular iron	Cast iron	Aluminum bronze	Tin bronze
Steel, E = 30†	2300	2180	2160	2100	1950	1900
Malleable iron, E = 25	2180	2090	2070	2020	1900	1850
Nodular iron, E = 24	2160	2070	2050	2000	1880	1830
Cast iron, E = 22	2100	2020	2000	1960	1850	1800
Aluminum bronze, E = 17.5	1950	1900	1880	1850	1750	1700
Tin bronze, E = 16	1900	1850	1830	1800	1700	1650

†Modulus of elasticity E is in megapounds per square inch (Mpsi).

$$C_p = \left\{ \frac{1}{\pi[(1 - \nu_P^2)/E_P + (1 - \nu_G^2)/E_G]} \right\}^{1/2} \tag{10.77}$$

where ν_P, ν_G = Poisson's ratio for pinion and gear, respectively
E_P, E_G = modulus of elasticity for pinion and gear, respectively

Allowable Stresses $\mathbf{s_{ac}}$ ***and*** $\mathbf{s_{at}}$. The allowable stresses depend on many factors, such as chemical composition, mechanical properties, residual stresses, hardness, heat treatment, and cleanliness. As a guide, the allowable stresses for helical gears may be obtained from Tables 10.5 and 10.6 or Figs. 10.40 and 10.41. Where a range of values is shown, the lowest values are used for general design. The upper values may be used only when the designer has certified that

1. High-quality material is used.
2. Section size and design allow maximum response to heat treatment.
3. Proper quality control is effected by adequate inspection.
4. Operating experience justifies their use.

Surface-hardened gear teeth require adequate case depth to resist the subsurface shear stresses developed by tooth contact loads and the tooth root fillet tensile stresses. But depths must not be so great as to result in brittle tooth tips and high residual tensile stress in the core.

TABLE 10.5 Allowable Bending Stress Numbers s_{at} and Contact Stress Numbers s_{ac} for a Variety of Materials

AGMA class	Commercial designation	Heat treatment	Minimum hardness		s_{at}, kpsi	s_{ac}, kpsi
			Surface	Core		
Steel						
A-1 through A-5		Through-hardened and tempered (Fig. 10-40)	180 H_B and less		25–33	85–95
			240 H_B		31–41	105–115
			300 H_B		36–47	120–135
			360 H_B		40–52	145–160
			400 H_B		42–56	155–170
		Flame- or induction-hardened† with type A pattern (Fig. 10-45)	50–54 R_C		45–55	170–190
		Flame- or induction-hardened with type B pattern (Fig. 10-45)			22	
		Carburized† and case-hardened†	55 R_C		55–65	180–200
			60 R_C		55–70	200–225
	AISI 4140	Nitrided†‡	48 R_C	300 H_B	35–45	155–180
	AISI 4340	Nitrided†‡	46 R_C	300 H_B	36–47	150–175
	Nitralloy 135M	Nitrided†‡	60 R_C	300 H_B	38–48	170–195
	2½% chrome	Nitrided†‡	54–60 R_C	350 H_B	55–65	155–216

Cast iron						
20		As cast			5	50–60
30		As cast	175 H_B		8.5	65–75
40		As cast	200 H_B		13	75–85
Nodular (ductile) iron						
A-7-a	60-40-18	Annealed,	140 H_B		22–33	77–92
A-7-c	80-55-06	quenched, and	180 H_B		22–33	77–92
A-7-d	100-70-03	tempered	230 H_B		27–40	92–112
A-7-e	120-90-02		270 H_B		31–44	103–126
Malleable iron (pearlitic)						
A-8-c	45007		165 H_B		10	72
A-8-e	50005		180 H_B		13	78
A-8-f	53007		195 H_B		16	83
A-8-i	80002		240 H_B		21	94
Bronze						
Bronze 2	AGMA 2C	Sand-cast	Min. tensile strength 40 kpsi		5.7	30
Al/Br 3	ASTM B-148-52 Alloy 9C	Heat-treated	Min. tensile strength 90 kpsi		23.6	65

† The range of allowable stress numbers indicated corresponds to grade 1 and grade 2 steels. See tables 14-6 and 14-9 to 14-11 of source.

‡ The overload capacity of nitrided gears is low, since the shape of the effective SN curve is flat. The sensitivity to shock should be investigated before proceeding with the design.

SOURCE: **Ref. [10.1].**

TABLE 10.6 Reliability Factors K_R and C_R

	Probabilities, %	
Factor, K_R or C_R	Success	Failure
1.50	99.99	0.01
1.25	99.90	0.10
1.00	99.00	1.00
0.85	90.00	10.00

The effective case depth for carburized and induction-hardened gears is defined as the depth below the surface at which the Rockwell C hardness has dropped to 50 R_C or to 5 points below the surface hardness, whichever is lower.

The values and ranges shown in Fig. 10.42 have had a long history of successful use for carburized gears and can be used as guides. For gearing in which maximum performance is required, detailed studies must be made of the application, loading, and manufacturing procedures to obtain desirable gradients of both hardness and internal stress. Furthermore, the method of measuring the case, as well as the allowable tolerance in case depth, should be a matter of agreement between the customer and the manufacturer.

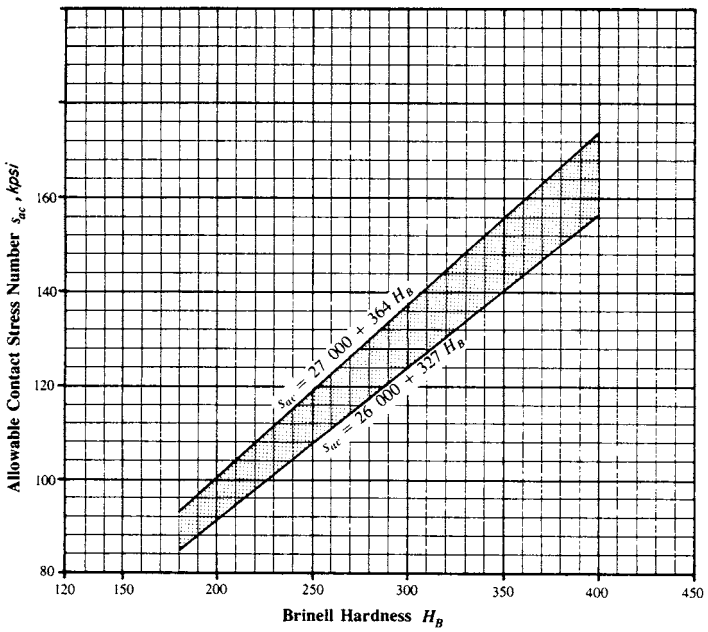

FIGURE 10.40 Allowable contact stress number s_{ac} for steel gears. Lower curve is maximum for grade 1 and upper curve is maximum for grade 2. *(From Ref. [10.1].)*

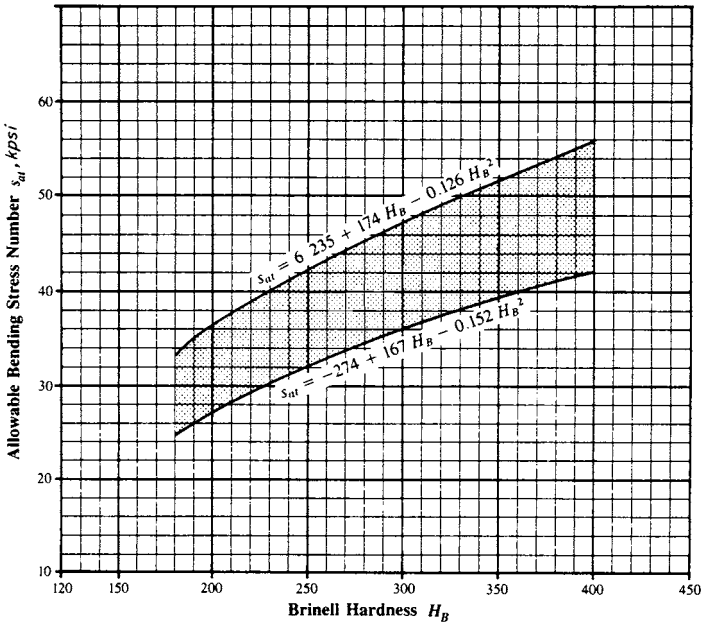

FIGURE 10.41 Allowable bending stress number s_{at} for steel gears. Lower curve is maximum for grade 1 and upper curve is maximum for grade 2. *(From Ref. [10.1].)*

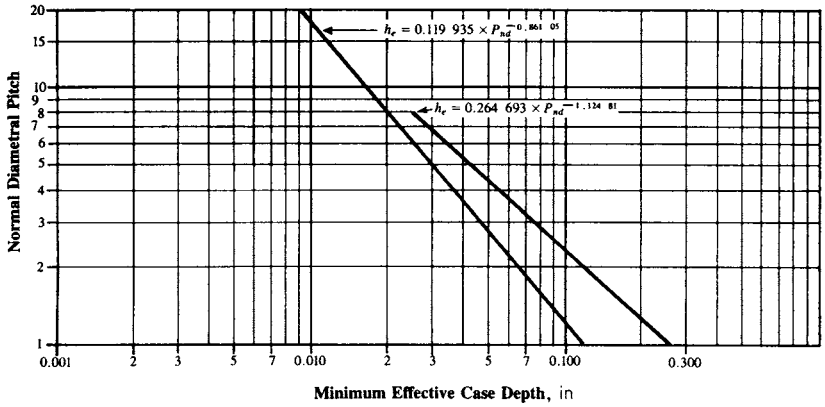

FIGURE 10.42 Effective case depth h_e for carburized gears based on normal diametral pitch. The effective case depth is defined as the depth of case which has a minimum hardness of 50 R_C. The total case depth to core carbon is about $1.5h_e$. The values and ranges shown on the case depth curves are to be used as guides. For gearing in which maximum performance is required, detailed studies must be made of the application, loading, and manufacturing procedures to obtain desirable gradients of both hardness and internal stress. Furthermore, the method of measuring the case as well as the allowable tolerance in case depth should be a matter of agreement between the customer and the manufacturer. *(From Ref. [10.1].)*

A guide for minimum effective case depth h_e at the pitch line for carburized and induction-hardened teeth, based on the depth of maximum shear from contact loading, is given by

$$h_e = \frac{C_G s_c d \sin \phi_o}{U_H \cos \psi_b} \tag{10.78}$$

where h_e = minimum effective case depth in inches and U_H = hardening process factor in pounds per square inch. In Eq. (10.78), $U_H = 6.4 \times 10^6$ psi for carburized teeth and 4.4×10^6 psi for tooth-to-tooth induction-hardened teeth.

You should take care when using Eq. (10.78) that adequate case depths prevail at the tooth root fillet, and that tooth tips are not overhardened and brittle. A suggested value of maximum effective case depth $h_{e,\max}$ at the pitch line is

$$h_{e,\max} = \frac{0.4}{P_d} \qquad \text{or} \qquad h_{e,\max} = 0.56 t_o \tag{10.79}$$

where $h_{e,\max}$ = suggested maximum effective case depth in inches and t_o = normal tooth thickness at top land of gear in question, in inches.

For nitrided gears, case depth is specified as total case depth h_c, and h_c is defined as the depth below the surface at which the hardness has dropped to 110 percent of the core hardness.

For gearing requiring maximum performance, especially large sizes, coarse pitches, and high contact stresses, detailed studies must be made of application, loading, and manufacturing procedures to determine the desirable gradients of hardness, strength, and internal residual stresses throughout the tooth.

A guide for minimum case depth for nitrided teeth, based on the depth of maximum shear from contact loading, is given by

$$h_c = \frac{C_G U_c s_c d \sin \phi_o}{(1.66 \times 10^7)(\cos \psi_b)} \tag{10.80}$$

where h_c = minimum total case depth in inches and U_c = core hardness coefficient, from Fig. 10.43.

If the value of h_c from Eq. (10.80) is less than the value from Fig. 10.44, then the minimum value from Fig. 10.44 should be used. The equation for the lower or left-hand curve in Fig. 10.44 is

$$h_c = (4.328\ 96)(10^{-2}) - P_{nd}(9.681\ 15)(10^{-3}) + P_{nd}^2(1.201\ 85)(10^{-3}) - P_{nd}^3(6.797\ 21)(10^{-5}) + P_{nd}^4(1.371)(10^{-6}) \tag{10.81}$$

The equation of the right-hand curve is

$$h_c = (6.600\ 90)(10^{-2}) - P_{nd}(1.622\ 24)(10^{-2}) + P_{nd}^2(2.093\ 61)(10^{-3}) - P_{nd}^3(1.177\ 55)(10^{-4}) + P_{nd}^4(2.331\ 60)(10^{-6}) \tag{10.82}$$

Note that other treatments of the subject of allowable gear-tooth bending recommend that the value obtained from Table 10.6 or Fig. 10.41 be multiplied by 0.70 for teeth subjected to reversed bending. This is not necessary within the context of this analysis, since the rim thickness factor K_b accounts for reversed bending.

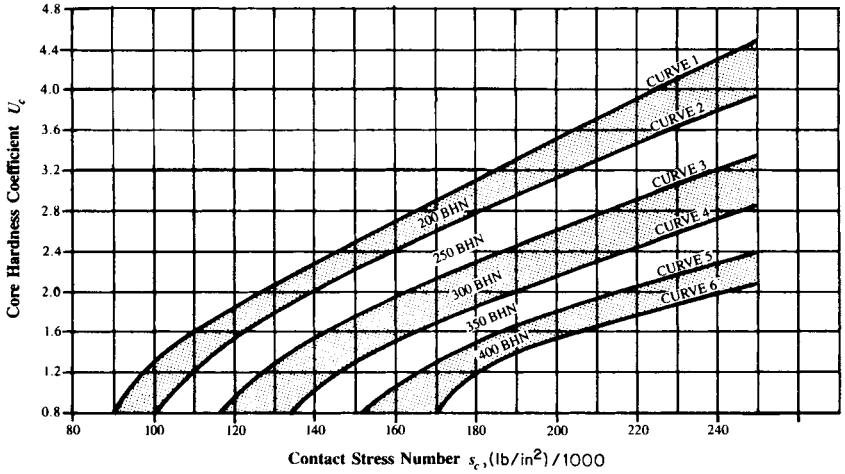

FIGURE 10.43 Core-hardness coefficient U_c as a function of the contact stress number s_c. The upper portion of the core-hardness bands yields heavier case depths and is for general design purposes; use the lower portion of the bands for high-quality material. *(From Ref. [10.1].)*

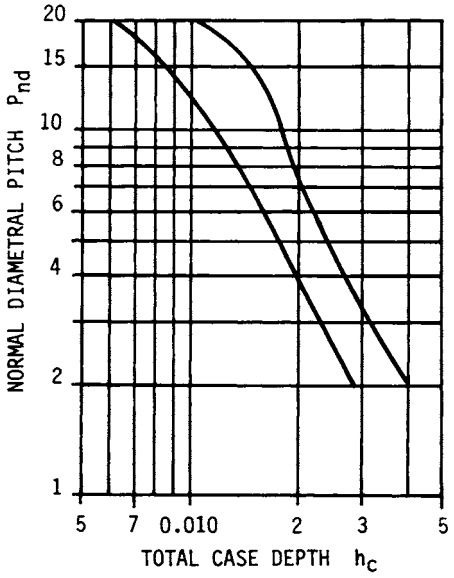

FIGURE 10.44 Minimum total case depth h_c for nitrided gears based on the normal diametral pitch. *(From Ref. [10.1].)*

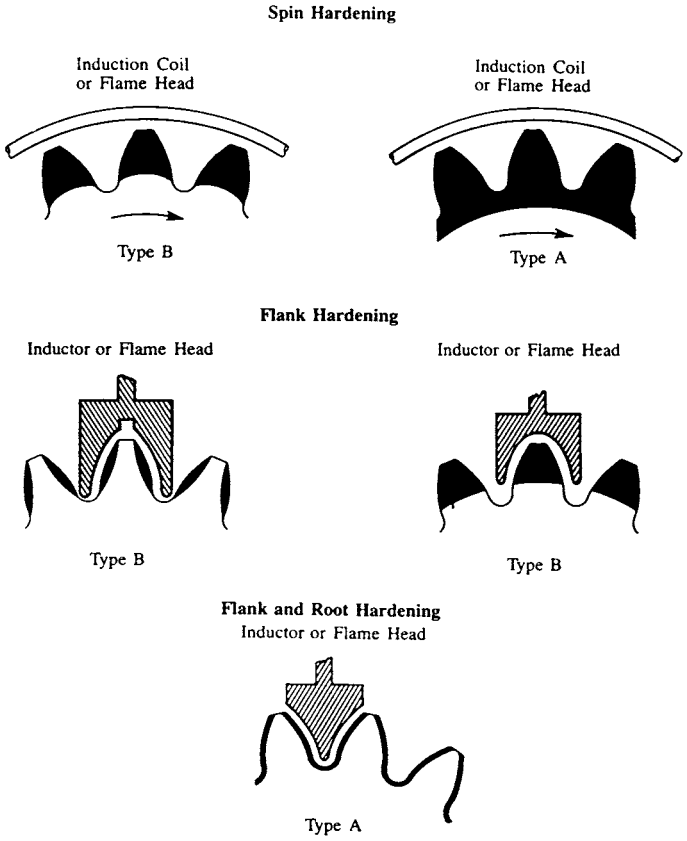

FIGURE 10.45 Variations in hardening patterns obtainable with flame or induction hardening. *(From Ref. [10.1].)*

For through-hardened gears, the yield stress at maximum peak stress should also be checked as defined by Eq. (10.83):

$$S_{ay}K_y \geq \frac{W_{t,\max}K_a}{K_v}\frac{P_d}{F}\frac{K_m}{K_f} \tag{10.83}$$

where $W_{t,\max}$ = peak tangential tooth load, lb
K_a = application factor
K_v = dynamic factor
F = minimum net face width, in
K_m = load-distribution factor
K_f = stress correction factor
K_y = yield strength factor
s_{ay} = allowable yield strength number, psi (from Fig. 10.46)

The yield strength factor should be set equal to 0.50 for conservative practice or to 0.75 for general industrial use.

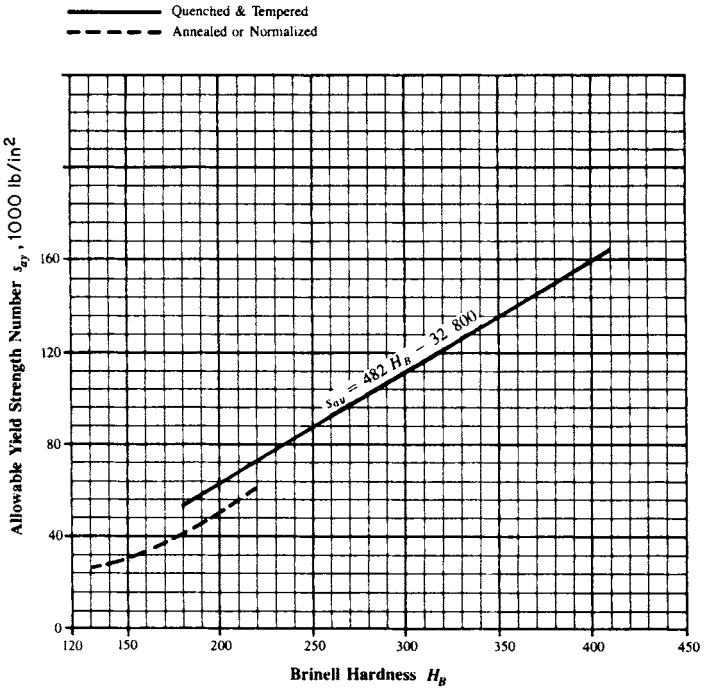

FIGURE 10.46 Allowable yield strength number s_{ay} for steel gears. *(From Ref. [10.1].)*

***Hardness Ratio Factor* C_H.** It is common practice in using through-hardened gear sets to utilize a higher hardness on the pinion than on the gear. The pinion typically sees many more cycles than the gear; thus a more economical overall design is obtained by balancing the surface durability and wear rate in this manner. Similarly, surface-hardened pinions may be used with through-hardened gears to provide improved overall capacity through the work-hardening effect which a "hard" pinion has on a "soft" gear. The hardness ratio factor adjusts the allowable stresses for this effect.

For through-hardened gear sets, C_H can be found from Fig. 10.47, while Fig. 10.48 provides values for surface-hardened pinions mating with through-hardened gears.

***Life Factors* K_L *and* C_L.** The allowable stresses shown in Tables 10.5 and 10.6 and Figs. 10.40 and 10.41 are based on 10 000 000 load cycles. The life factor adjusts the allowable stresses for design lives other than 10 000 000 cycles. A unity value for the life factor may be used for design lives beyond 10 000 000 cycles only when it is justified by experience with similar designs.

Insufficient specific data are available to define life factors for most materials. For steel gears, however, experience has shown that the curves shown in Figs. 10.49 and 10.50 are valid.

In utilizing these charts, care should be exercised whenever the product of K_L and s_{at} equals or exceeds s_{ay}, as shown on Fig. 10.46, since this indicates that localized yielding may occur. For low-speed gears without critical noise vibration or transmis-

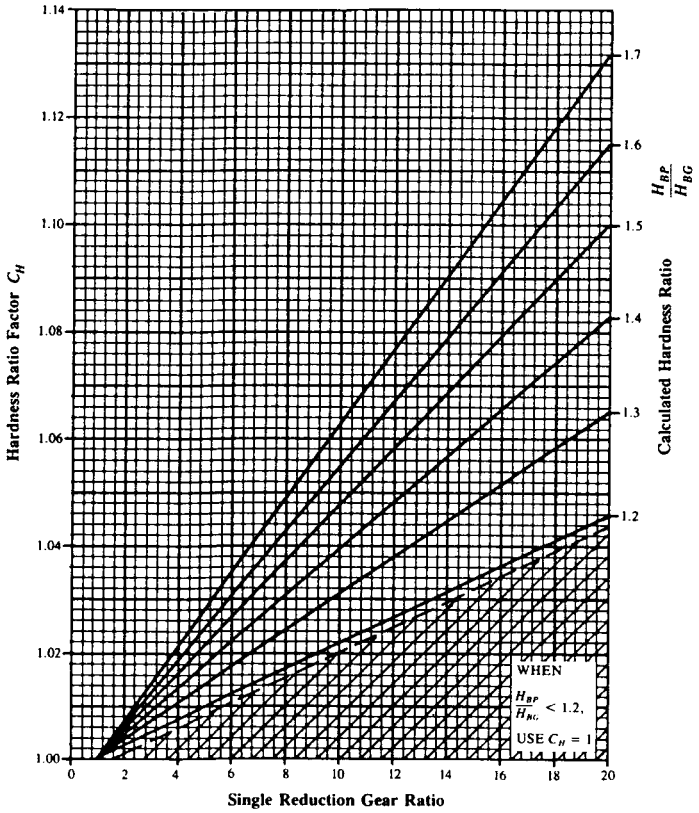

FIGURE 10.47 Hardness ratio factor C_H for through-hardened gears. In this chart, H_{BP} is the Brinell hardness of the pinion, and H_{BG} is the Brinell hardness of the gear. *(From Ref. [10.1].)*

sion accuracy requirements, local yielding may be acceptable, but it should be avoided in general.

***Reliability Factors* C_R *and* K_R.** The allowable stress levels are not absolute parameters. Rather, a specific probability of failure is associated with each allowable level. The values shown in Figs. 10.40 and 10.41 and Table 10.5 are based on a 99 percent probability of success (or a 1 percent probability of failure). This means that in a *large* population, at least 99 percent of the gears designed to a particular listed allowable stress will run for at least 10 000 000 cycles without experiencing a failure in the mode (that is, bending or durability) addressed.

In some cases it is desirable to design to higher or lower failure probabilities. Table 10.6 provides values for C_R and K_R which will permit the designer to do so. Before deciding on the reliability factor which is appropriate for a particular design, the analyst should consider what is meant by a "failure." In the case of a durability failure, a failure is said to have occurred when the first pit, or spall, is observed. Obviously a long time will elapse between the occurrence of a durability failure and the time at which the gear will cease to perform its normal power-transmission function.

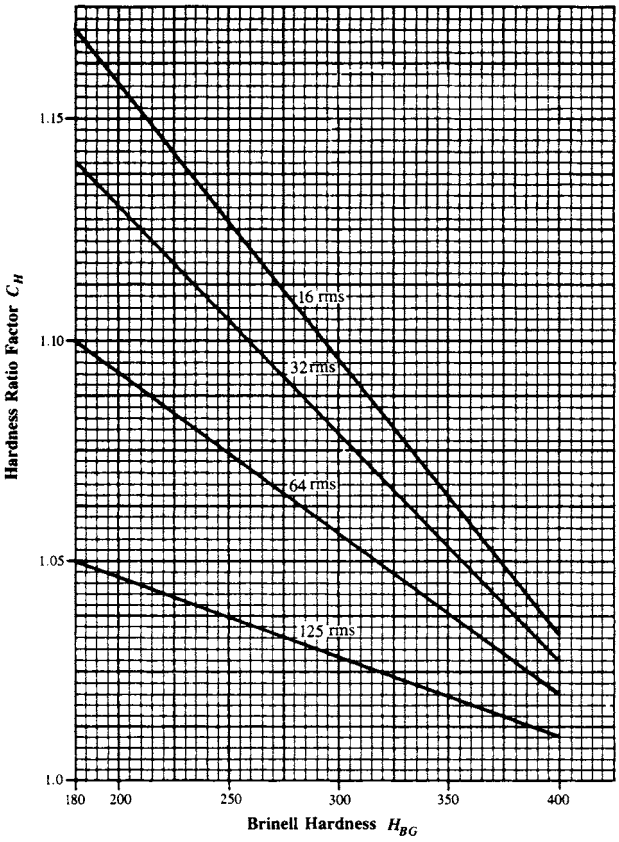

FIGURE 10.48 Hardness ratio factor C_H for surface-hardened teeth. The rms values shown correspond to the surface finish of the pinion f_p in microinches. *(From Ref. [10.1].)*

In the case of a bending failure, the appearance of a crack in the fillet area is the criterion. In most cases, and for most materials, the progression of this crack to the point at which a tooth or a piece of tooth fractures is rather quick. A bending failure will almost always progress to the point where function is lost much more rapidly than a durability failure. For this reason it is sometimes desirable to use a higher value for K_R than for C_R.

Because of the load sharing which occurs on most normal helical gears, a complete fracture of a full single tooth, as often occurs on a spur gear, is not usually the mode of failure on a helical gear. A certain redundancy is built into a helical gear, since initially only a piece of a tooth will normally fracture.

Temperature Factors $\mathbf{C_T}$ ***and*** $\mathbf{K_T}$**.** At gear blank operating temperatures below 250°F and above freezing, actual operating temperature has little effect on the allowable stress level for steel gears; thus a temperature factor of unity is used. At higher or lower temperatures, the allowable stress levels are altered considerably. Unfortunately, few hard data are available to define these effects. At very low tem-

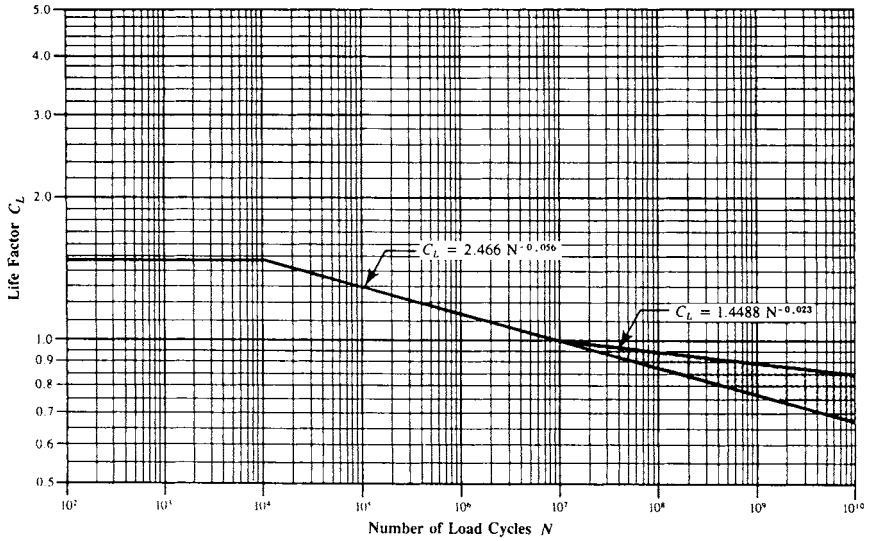

FIGURE 10.49 Pitting-resistance life factor C_L. This curve does not apply where a service factor C_{SF} is used. *Note:* The choice of C_L above 10^7 cycles is influenced by lubrication regime, failure criteria, smoothness of operation required, pitch line velocity, gear material cleanliness, material ductility and fracture toughness, and residual stress. *(From Ref. [10.1].)*

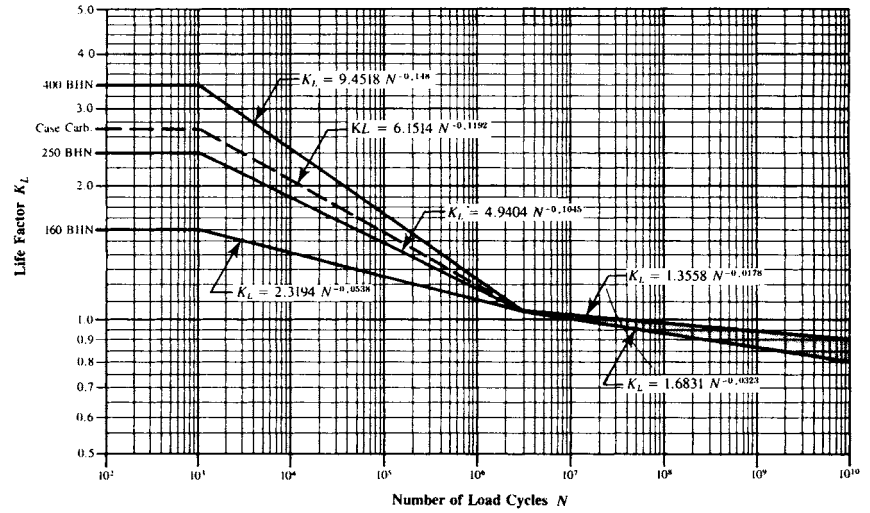

FIGURE 10.50 Bending-strength life factor K_L. This chart does not apply where a service factor K_{SF} is used. *Note:* The choice of K_L above 3×10^6 cycles is influenced by pitch line velocity, gear material cleanliness, residual stress, gear material ductility, and fracture toughness. *(From Ref. [10.1].)*

peratures, the impact resistance and fracture toughness of most materials are reduced; thus special care must be exercised in such designs if nonuniform loading is expected. A temperature factor greater than unity should be used in such cases. Although no specific data are available, a value between 1.25 and 1.50 is recommended for gears which must transmit full power between 0 and –50°F.

At high temperatures, most materials experience a reduction in hardness level. Nonmetallic gears are not ordinarily used at high temperatures; thus our comments are restricted to steel gearing. The temperature factor should be chosen on the basis of the hot hardness curve for the particular material in use. That is, the temperature factor is equal to the allowable stress at room-temperature hardness divided by the allowable stress at the hardness corresponding to the higher temperature. For information related to typical trends, Fig. 10.51 shows the hardness-temperature characteristics for two gear steels (AISI 9310 and VASCO-X2). Two typical bearing steels (M-50 and SAE 52100) are also shown for reference purposes.

Once the strength and durability analyses have been completed, the wear and scoring resistance of the gears must be defined. Wear (see Chap. 34) is usually a concern only for relatively low-speed gears, whereas scoring is a concern only for relatively high-speed gears.

Wear. Gear-tooth wear is a very difficult phenomenon to predict analytically. Fortunately, it is not a major problem for most gear drives operating in the moderate- to

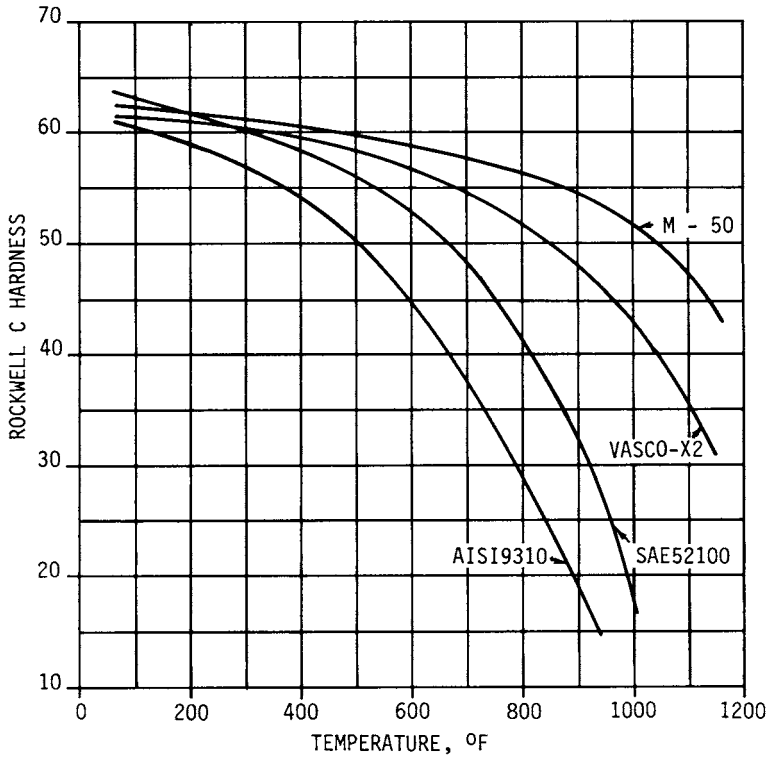

FIGURE 10.51 Hardness as a function of temperature for several steels.

high-speed range. In the case of low-speed gears, however, not only is wear a significant problem, but also it can be the limiting factor in defining the load capacity of the mesh.

In low-speed gear drives, the film which separates the mating tooth surfaces is insufficient to prevent metal-to-metal contact; thus wear occurs. In higher-speed gears, the film becomes somewhat thicker, and gross contact of the mating surfaces is prevented. Indeed, grinding lines are still visible on many aircraft gears after hundreds of hours of operation. The type of surface distress which will occur in a gear set is dependent, to a certain extent, on the pitch line velocity. As shown in Fig. 10.52, wear predominates in the lower-speed range, while scoring rules the upper-speed range. In the midrange, pitting controls the gear life.

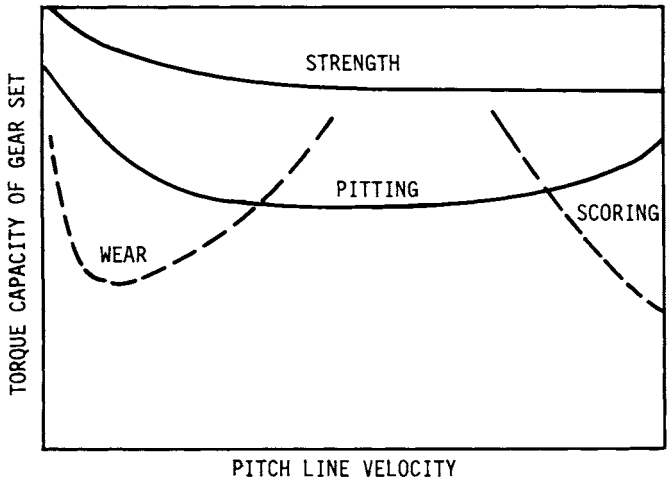

FIGURE 10.52 Gear distress as a function of pitch line velocity.

The elastohydrodynamic (EHD) film thickness can provide some guidance in the evaluation of the wear potential of a gear set. Care must be used in the application of these methods, since the existing data are far from complete and there are many instances of contradictory results. One of the simplest approaches is due to Dowson; see Ref. [10.7] and Chap. 20. The equation is

$$\frac{h}{R'} = \frac{(4.46 \times 10^{-5})(\alpha E')^{0.54}[\mu_o u/(E'R')]^{0.70}}{[w/(E'R')]^{0.13}} \tag{10.84}$$

where h = calculated minimum film thickness, in
R' = relative radius of curvature in transverse plane at pitch point, in
α = lubricant pressure-viscosity coefficient, in^2/lb
E' = effective elastic modulus, psi
μ_o = sump lubricant viscosity, centipoise (cP)
u = rolling velocity in transverse plane, inches per second (in/s)
w = load per unit length of contact, lb/in

Wellauer and Holloway ([10.8]) present a nomograph to compute the film thickness at the pitch point; but this nomograph is quite detailed and is not included here.

The parameter of interest in our discussion is not the film thickness itself, but rather the ratio of the film thickness to the relative surface roughness. This ratio is defined as the *specific film thickness* and is given by

$$\lambda = \frac{h}{S'} \tag{10.85}$$

The relative surface roughness [root-mean-square (rms)] is given by

$$S' = \frac{S_P + S_G}{2} \tag{10.86}$$

Typical values for various gear manufacturing processes are shown in Table 10.7.

TABLE 10.7 Tooth Surface Texture in the As-Finished Condition

Finish method	Surface texture in microinches (rms)	
	Range	Typical
Hobbed	30–80	50
Shaved	10–45	35
Lapped	20–200	93
Lapped and run in	20–100	53
Ground (soft)	5–35	25
Ground (hard)	5–35	15
Honed and polished	4–15	5

Once the specific film thickness has been determined, the probability of surface distress occurring can be determined through the use of Fig. 10.53.

Although the data presented thus far can be quite useful, several factors must be kept in mind in applying them to actual design. Most of the experimental data on which this information is based were obtained from through-hardened gear sets operating with petroleum-based oils. Gears operating with synthetic oils appear able to operate successfully at film thicknesses much less than those predicted by this analysis. The same is true for case-hardened gears of 59 R_C and higher hardness. The results may be further altered by the use of friction modifiers or EP additives in the oil. Finally, wear, of and by itself, is not necessarily a failure. In many cases, wear is an acceptable condition; it is simply monitored until it reaches some predetermined level, at which time the gears are replaced.

Perhaps the most useful application for this analysis is as a comparative, relative rating tool, rather than as an absolute design criterion.

The occurrence of wear is difficult to predict, but the rate of wear is even more so. Equation (10.87) may be useful as a guide in predicting wear, but its accuracy has not been rigorously verified:

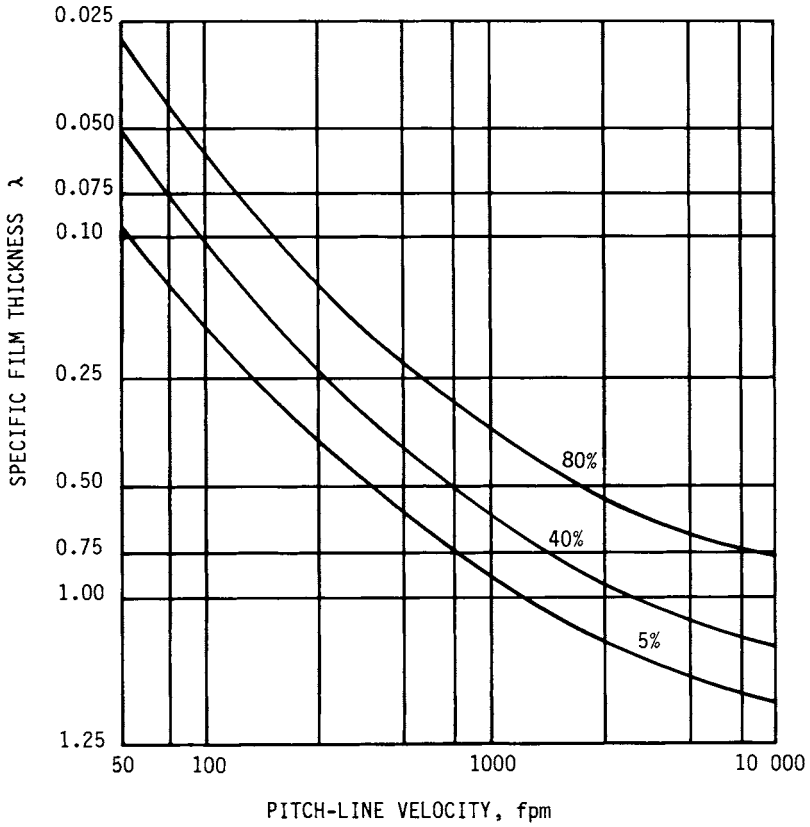

FIGURE 10.53 Surface-distress probability chart as a function of pitch line velocity and specific film thickness. Curves represent 80, 40, and 5 percent probability of distress. The region above the 80 percent line is unsatisfactory; the region below the 5 percent line is good.

$$q = \frac{KW_t n_T}{FS_y} \tag{10.87}$$

where q = wear, in
n_T = number of cycles
S_y = yield strength of gear material, psi
K = factor from Eq. (10.88)

and

$$3.1 \geq K\lambda^{1.645} \times 10^9 \geq 1.8 \tag{10.88}$$

In applying these equations, greater emphasis should be placed on the trend indicated than on the absolute value of the numbers. For example, a new design might be compared with an existing similar design for which the wear characteristics have been established. This could be accomplished by calculating the q value for each by

Eqs. (10.87) and (10.88) and then comparing them, rather than looking at absolute values of either. The ratio of the two q values is far more accurate than the absolute value of either.

Scoring. Very few data concerning the scoring behavior of gears are available in an easily usable form. Scoring is normally a problem for heavily loaded, high-speed steel gears. The exact mechanism by which scoring occurs is not yet fully understood.

At high speeds, the calculated film thickness is often quite large. Yet a wearlike failure mode sometimes occurs. Under high-speed conditions, the sliding motion of one gear tooth on another may create instantaneous conditions of temperature and pressure which destroy the film of oil separating the tooth flanks. When this occurs, the asperities on the surfaces of the mating teeth instantaneously weld. As the gears continue to rotate, these welds break and drag along the tooth flanks, causing scratches, or "score" marks, in the direction of sliding. If the damage which occurs is very slight, it is often referred to as *scuffing* or *frosting.* In some cases, light frosting may heal over and not progress; however, scoring is generally progressively destructive. Though never a catastrophic failure itself, scoring destroys the tooth surface, which leads to accelerated wear, pitting, and spalling. If scoring is allowed to progress unchecked, tooth fracture may ultimately occur.

Note that scoring is not a fatigue phenomenon; that is, its occurrence is not time-dependent. In general, if scoring does not occur within 15 to 25 minutes (min) at a certain operating condition, usually it will not occur *at that condition* at all. Only a change in operating condition, and not the accumulation of cycles, will cause scoring.

A theory known as the *critical-temperature theory,* originally proposed by Harmen Blok, is usually used in the evaluation of scoring hazard for a set of helical gears.

If we consider a simple analogy, the concept of critical temperature will become clear. Consider the old method of making fire by rubbing two sticks together. If the sticks are held together with only light pressure and/or they are rubbed slowly, they will simply wear. If, however, the pressure is increased and the sticks are rubbed more rapidly, then the temperature at the mating surfaces will increase. If the pressure (load) and the rubbing speed (sliding velocity) are progressively increased, eventually the sticks will ignite. At the point of ignition, the sticks have reached their *critical* temperature. Quite obviously, the critical temperature will vary with the type of wood, its moisture content, and other factors.

In a similar manner, as gear-tooth sliding velocity and load are increased, eventually a point will be reached at which the temperature at the conjunction attains a critical value, and then the film separating the tooth flanks will be destroyed. At this point the teeth are in metal-to-metal contact, and instantaneous welding of the surface asperities occurs. The continued rotation of the mesh rips apart these microscopic welds and produces the scored appearance from which this failure derives its name. The critical temperature varies with the type of gear material, surface hardness, surface finish, type and viscosity of oil, additives in the oil, etc. When the film is destroyed, it is sometimes referred to as *flashing;* thus the parameter used to evaluate this condition has come to be known as the *flash* temperature. When the flash temperature reaches its *critical* value, failure by scoring will occur. Note that the flash temperature referred to here is not related in any way to the flash point of the oil, and the oil flash point shown on some manufacturers' specification sheets is in no way related to the allowable flash temperature discussed here.

Many refinements have been made to Blok's original theory, and it is currently accepted as the best method available for evaluating scoring resistance for spur, helical, and bevel gears. Reference [10.9] presents a method of analysis for steel spur and

helical gears based on Blok's method. The scoring hazard is evaluated by calculating a flash temperature rise ΔT_{Fi}. The flash temperature rise is added to the gear blank temperature T_B and compared with the allowable tooth flash temperature for the particular material and lubricant combination being used.

The flash temperature rise is given by

$$\Delta T_{Fi} = \left(\frac{W_{ti} C_a C_m}{F C_v}\right)^{0.75} \left(\frac{n_P^{0.5}}{P_d^{0.25}}\right) (\mu Z_{ti}) \left(\frac{50}{50 - S'}\right) \tag{10.89}$$

where T_{Fi} = flash temperature rise at ith contact point along line of action, °F
W_{ti} = tangential tooth load at ith contact point, lb
F = net minimum face width, in
C_a = application factor
C_m = load-distribution factor
C_v = dynamic factor
n_P = pinion speed, revolutions per minute (r/min)
P_d = transverse diametral pitch
S' = relative surface roughness, Eq. (10.86)
Z_{ti} = scoring geometry factor at ith contact point along line of action

The factors C_a, C_v, and C_m are the same as those used in the durability formula [Eq. (10.17)].

The scoring geometry factor is given by

$$Z_{ti} = \frac{0.2917[\rho_{Pi}^{1/2} - (N_P \rho_{Gi}/N_G)^{1/2}] P_d^{1/4}}{(\cos \phi_i)^{0.75} [\rho_{Pi} \rho_{Gi}/(\rho_{Pi} + \rho_{Gi})]^{0.25}} \tag{10.90}$$

where ρ_{Pi}, ρ_{Gi} = radius of curvature of pinion and gear, respectively, at ith contact point, in
N_P, N_G = tooth numbers of pinion and gear, respectively
P_d = transverse diametral pitch
ϕ_i = pressure angle at ith contact point, deg

The tooth flash temperature is then calculated by

$$T_{Fi} = T_B + \Delta T_{Fi} \tag{10.91}$$

TABLE 10.8 Allowable Flash Temperatures for Some Gear Materials and for Spur and Helical Gears

The surface hardness is 60 R_C for all materials listed.

Gear material	Oil type	Allowable flash temperature, °F
AISI 9310	MIL-L-7808	295
	MIL-L-23699	295
	XAS 2354	335†
VASCO-X2	MIL-L-7808	350
	MIL-L-23699	350
	XAS 2354	375†

†Conservative estimate based on limited current data.

In most cases the blank temperature will be very close to the oil inlet temperature. Thus, unless the actual blank temperature is known, the oil inlet temperature may be used for T_B. Table 10.8 gives allowable values of the total flash temperature.

Equations (10.89) through (10.91) refer to the *i*th contact point. In utilizing these equations, the entire line of contact should be examined on a point-by-point basis to define the most critical contact point. Depending on the pitch of the tooth, 10 to 25 divisions should be adequate. For hand calculations, this could be quite burdensome. A quick look at the highest and lowest points of single-tooth contact (based on a transverse-plane slice of the helical set) will provide a reasonable approximation.

The range of materials and oils shown in Table 10.8 is limited. Generally, scoring is a problem only in high-speed, high-load applications.

The most likely applications to be affected are aerospace types. This being the case, the material choice is limited to those shown, and usually either MIL-L-23699 or MIL-L-7808 oil is used. Some of the new XAS-2354 oils will provide much improved scoring resistance, but hard data are not presently available.

REFERENCES

10.1 ANSI/AGMA 2001-C95, "Fundamental Rating Factors and Calculation Methods for Involute Spur and Helical Gear Teeth."

10.2 "Design Guide for Vehicle Spur and Helical Gears," AGMA publ. 6002-B93.

10.3 *Gear Handbook,* vol. 1, *Gear Classification, Materials, and Measuring Methods for Unassembled Gears,* AGMA publ. 2000-A88.

10.4 Raymond J. Drago, "Results of an Experimental Program Utilized to Verify a New Gear Tooth Strength Analysis," AGMA publ. 229.27, October 1983.

10.5 Raymond J. Drago, "An Improvement in the Conventional Analysis of Gear Tooth Bending Fatigue Strength," AGMA publ. 229.24, October 1982.

10.6 R. Errichello, "An Efficient Algorithm for Obtaining the Gear Strength Geometry Factor on a Programmable Calculator," AGMA publ. 139.03, October 1981.

10.7 D. Dowson, "Elastohydrodynamic Lubrication: Interdisciplinary Approach to the Lubrication of Concentrated Contacts," NASA SP-237, 1970.

10.8 E. J. Wellauer and G. Holloway, "Application of EHD Oil Film Theory to Industrial Gear Drives," ASME paper no. 75PTG-1, 1975.

10.9 "Information Sheet—Gear Scoring Design Guide for Aerospace Spur and Helical Involute Gear Teeth," AGMA publ. 217.

HELICAL GEARS

CHAPTER 11
BEVEL AND HYPOID GEARS

Theodore J. Krenzer, M.S.
Director of Research and Development
Gleason Machine Division
Rochester, New York

Robert G. Hotchkiss, B.S.
Director, Gear Technology
Gleason Machine Division
Rochester, New York

11.1 INTRODUCTION

This chapter provides you with information necessary to design a bevel- or hypoid-gear set. It includes guidelines for selecting the type and size of a gear set to suit the application requirements. Equations and graphs are provided for calculating gear-tooth geometry, strength, surface durability, and bearing loads.

Although the text provides sufficient data to design a gear set, reference is also made to appropriate American Gear Manufacturer's Association (AGMA) publications and software available for computer-aided design.

11.2 TERMINOLOGY

11.2.1 Types of Bevel and Hypoid Gears

Straight-bevel gears are the simplest form of bevel gears. The teeth are straight and tapered, and if extended inward, they would pass through the point of intersection of the axes. See Fig. 11.1.

Spiral-bevel gears have teeth that are curved and oblique to their axes. The contact begins at one end of the tooth and progresses to the other. See Fig. 11.2.

Zerol bevel gears have teeth that are in the same general direction as straight-bevel gears and are curved similarly to spiral-bevel gears. See Fig. 11.3.

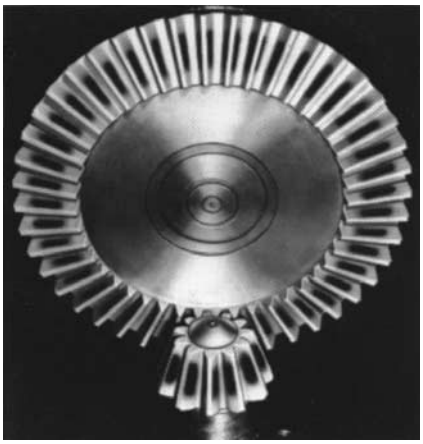

FIGURE 11.1 Straight-bevel set. *(Gleason Machine Division.)*

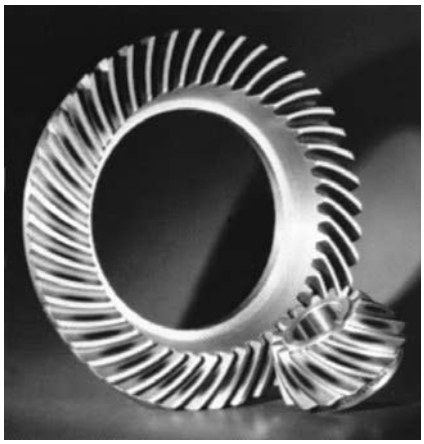

FIGURE 11.2 Spiral-bevel set. *(Gleason Machine Division.)*

Hypoid gears are similar in appearance to spiral-bevel gears. They differ from spiral-bevel gears in that the axis of the pinion is offset from the axis of the gear. See Fig. 11.4.

11.2.2 Tooth Geometry

The nomenclature used in this chapter relative to bevel and hypoid gears is illustrated in Figs. 11.5, 11.6, and 11.7.

The following terms are used to define the geometry:

Addendum of pinion (gear) a_p (a_G) is the height that the tooth projects above the pitch cone.

Backlash allowance B is the amount by which the circular tooth thicknesses are reduced to provide the necessary backlash in assembly.

Clearance c is the amount by which the dedendum in a given gear exceeds the addendum of its mating gear.

Cone distance, mean A_m is the distance from the apex of the pitch cone to the middle of the face width.

Cone distance, outer A_o is the distance from the apex of the pitch cone to the outer ends of the teeth.

Control gear is the term adopted for bevel gearing in place of the term *master gear,* which implies a gear with all tooth specifications held to close tolerances.

Crown to crossing point on the pinion (gear) x_o (X_o) is the distance in an axial section from the crown to the crossing point, measured in an axial direction.

Cutter radius r_c is the nominal radius of the face-type cutter or cup-shaped grinding wheel that is used to cut or grind the spiral-bevel teeth.

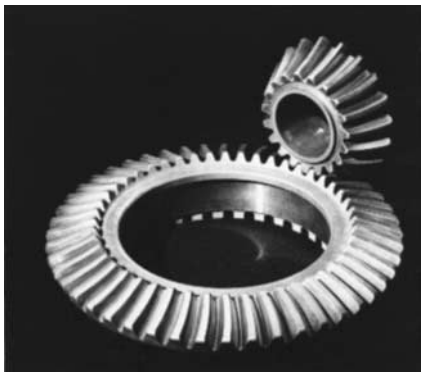

FIGURE 11.3 Zerol bevel set. *(Gleason Machine Division.)*

FIGURE 11.4 Hypoid set. *(Gleason Machine Division.)*

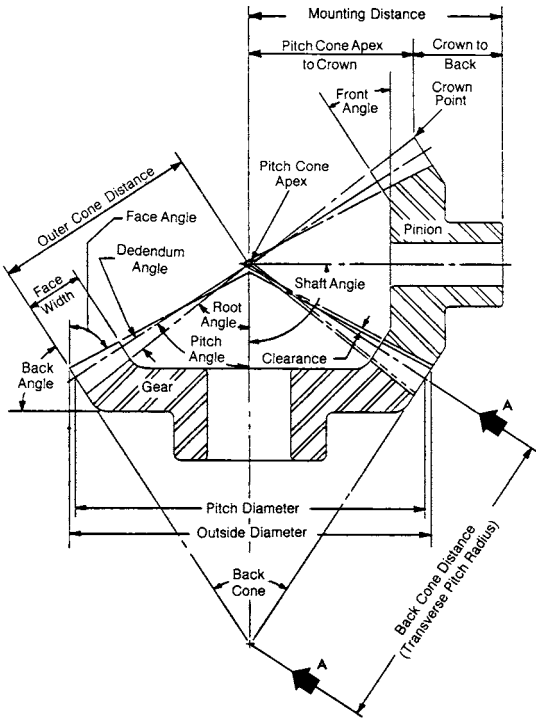

FIGURE 11.5 Bevel-gear nomenclature—axial plane. Section A-A is illustrated in Fig. 11.6.

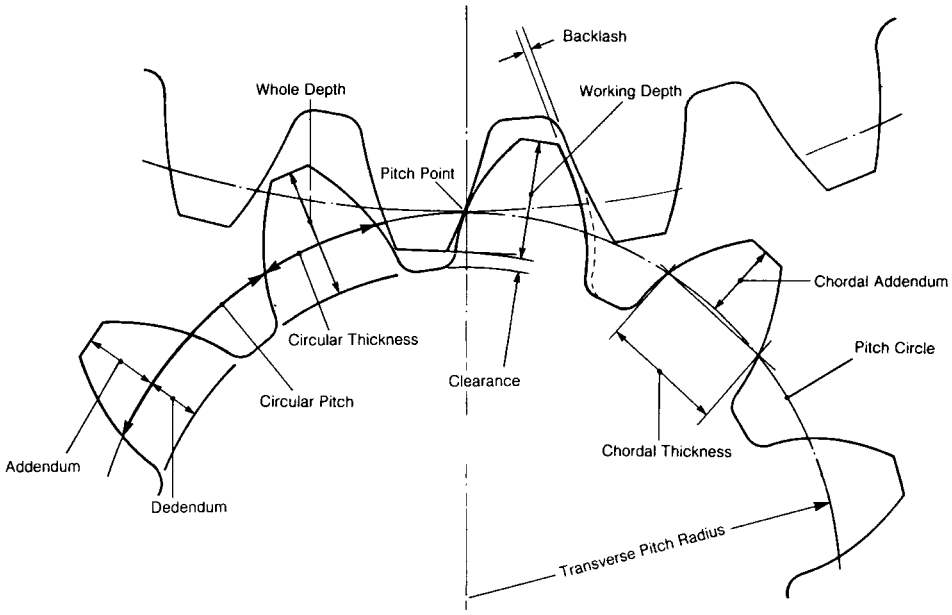

FIGURE 11.6 Bevel-gear nomenclature—mean transverse section AA in Fig. 11.5.

Dedendum angle of pinion (gear) δ_P (δ_G) is the angle between elements of the root cone and pitch cone.

Dedendum angles, sum of $\Sigma\delta$ is the sum of the pinion and gear dedendum angles.

Dedendum of pinion (gear) b_p (b_G) is the depth of the tooth space below the pitch cone.

Depth, mean whole h_m is the tooth depth at midface.

Depth, mean working h is the depth of engagement of two gears at midface.

Diametral pitch P_d is the number of gear teeth per unit of pitch diameter.

Face angle of pinion (gear) blank γ_o (Γ_o) is the angle between an element of the face cone and its axis.

Face apex beyond crossing point on the pinion (gear) G_o (Z_o) is the distance between the face apex and the crossing point on a bevel or hypoid set.

Face width F is the length of the teeth measured along a pitch-cone element.

Factor, mean addendum c_1 is the addendum modification factor.

Front crown to crossing point on the pinion (gear) x_i (X_i) is the distance in an axial section from the front crown to the crossing point, measured in the axial direction.

Hypoid offset E is the distance between two parallel planes, one containing the gear axis and the other containing the pinion axis of a hypoid-gear set.

Number of teeth in pinion (gear) n (N) is the number of teeth contained in the whole circumference of the pitch cone.

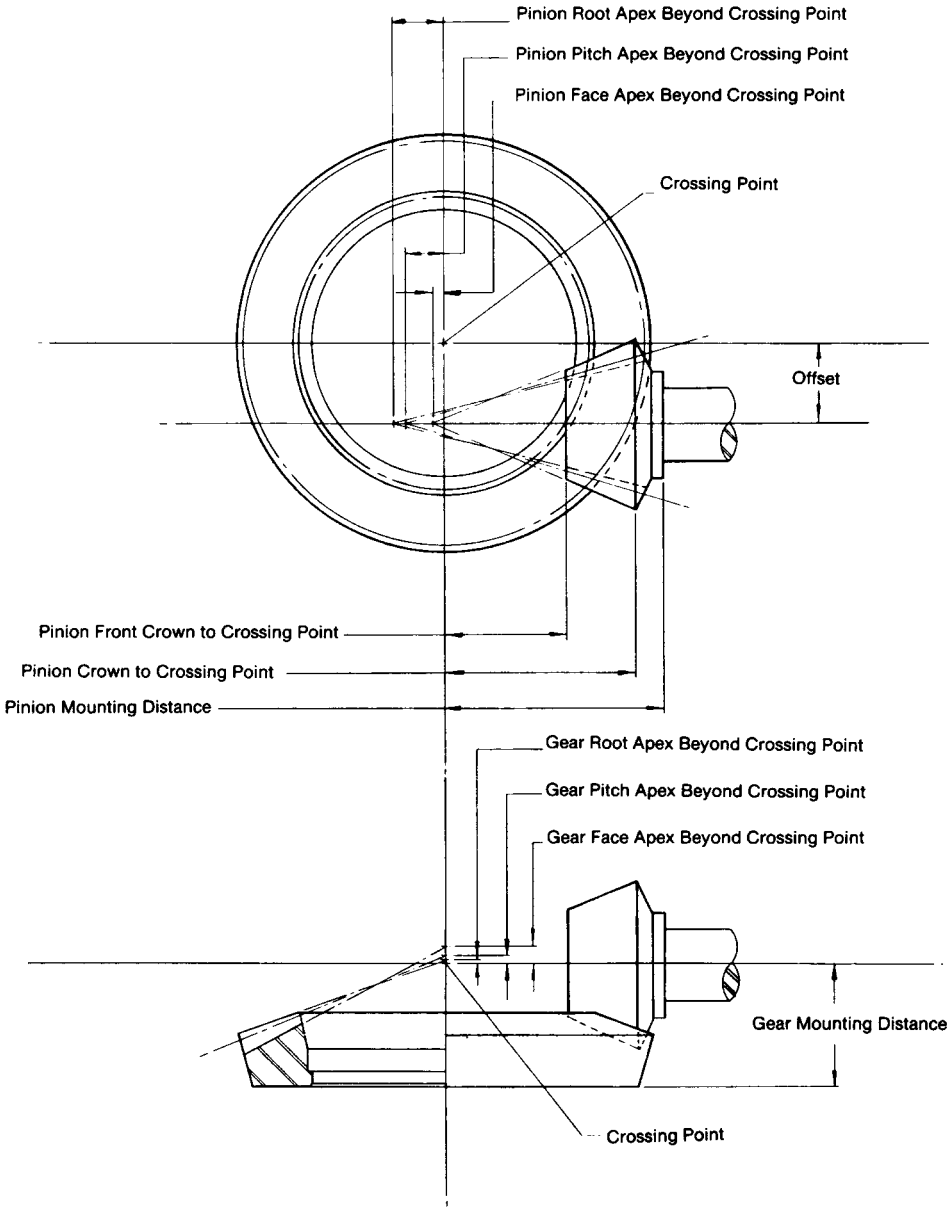

FIGURE 11.7 Hypoid gear nomenclature.

Pitch angle of pinion (gear) $\gamma\,(\Gamma)$ is the angle between an element of the pitch cone and its axis.

Pitch apex beyond crossing point on the pinion (gear) $G\ (Z)$ is the distance between the pitch apex and the crossing point on a hypoid set.

Pitch diameter of pinion (gear) $d\ (D)$ is the diameter of the pitch cone at the outside of the blank.

Pitch, mean circular p_m is the distance along the pitch circle at the mean cone distance between corresponding profiles of adjacent teeth.

Pressure angle ϕ is the angle at the pitch point between the line of pressure which is normal to the tooth surface and the plane tangent to the pitch surface. It is specified at the mean cone distance.

Ratio, gear m_G is the ratio of the number of gear teeth to the number of pinion teeth.

Root angle of pinion (gear) $\gamma_R\ (\Gamma_R)$ is the angle between an element of the root cone and its axis.

Root apex beyond crossing point on the pinion (gear) $G_R\ (Z_R)$ is the distance between the root apex and the crossing point on a bevel or hypoid set.

Shaft angle Σ is the angle between the axes of the pinion shaft and the gear shaft.

Spiral angle ψ is the angle between the tooth trace and an element of the pitch cone. It is specified at the mean cone distance.

Spiral-bevel gear, left-hand is one in which the outer half of a tooth is inclined in the counterclockwise direction from the axial plane through the midpoint of the tooth, as viewed by an observer looking at the face of the gear.

Spiral-bevel gear, right-hand is one in which the outer half of a tooth is inclined in the clockwise direction from the axial plane through the midpoint of the tooth, as viewed by an observer looking at the face of the gear.

Tangential force W_t is the force applied to a gear tooth at the mean cone distance in a direction tangent to the pitch cone and normal to a pitch-cone element.

Thickness of pinion (gear), mean circular $t\,(T)$ is the length of arc on the pitch cone between the two sides of the tooth at the mean cone distance.

Thickness of pinion (gear), mean normal chordal $t_{nc}\ (T_{nc})$ is the chordal thickness of the pinion tooth at the mean cone distance in a plane normal to the tooth trace.

11.2.3 Calculation Methods

Four methods of blank design are commonly used in the design of bevel and hypoid gears:

1. Standard taper
2. Duplex taper
3. Uniform taper
4. Tilted root-line taper

The taper you select depends in some instances on the manufacturing equipment available for producing the gear set. Therefore, before starting calculations, you should familiarize yourself with the equipment and method used by the gear manufacturer.

11.3 GEAR MANUFACTURING

11.3.1 Methods of Generation

Generation is the basic process in the manufacture of bevel and hypoid gears in that at least one member of every set must be generated. The theory of generation as applied to these gears involves an imaginary generating gear, which can be a crown gear, a mating gear, or some other bevel or hypoid gear. The gear blank or workpiece is positioned so that when it is rolled with the generating gear, the teeth of the workpiece are enveloped by the teeth of the generating gear.

In the actual production of the gear teeth, at least one tooth of the generating gear is described by the motion of the cutting tool or grinding wheel. The tool and its motion are carried on a rotatable machine member called a cradle, the axis of which is identical with the axis of the generating gear. The cradle and the workpiece roll together on their respective axes exactly as would the workpiece and the generating gear.

The lengthwise tooth curve of the generating gear is selected so that it is easily followed with a practical cutting tool and mechanical motion. Figure 11.8 illustrates the representation of a generating gear by a face-mill cutter. Figure 11.9 shows the basic machine elements of a bevel-gear face-mill generator.

Most generating gears are based on one of two fundamental concepts. The first is complementary crown gears, where two gears with 90° pitch angles fit together like mold castings. Each of the crown gears is the generating gear for one member of the mating set. Gears generated in this manner have line contact and are said to be *conjugate* to each other. With the second concept, the teeth of one member are form-cut without generation. This member becomes the generating gear for producing the mating member. Again, gears generated in this manner are conjugate to each other.

11.3.2 Localization of Contact

Any displacement in the nominal running position of either member of a mating conjugate gear set shifts the contact to the edges of the tooth. The result is concentrated loading and irregular motion. To accommodate assembly tolerances and deflections resulting from load, tooth surfaces are relieved in both the lengthwise and profile directions. The resulting localization of the contact pattern is achieved by using a generating setup which is deliberately modified from the conjugate generating gear.

11.3.3 Testing

The smoothness and quietness of operation, the tooth contact pattern, the tooth size, the surface finish, and appreciable runout can be checked in a running test. This is a subjective test. The machine consists of two spindles that can be set at the correct shaft angle, mounting distances, and offset. The gear to be inspected is mounted on

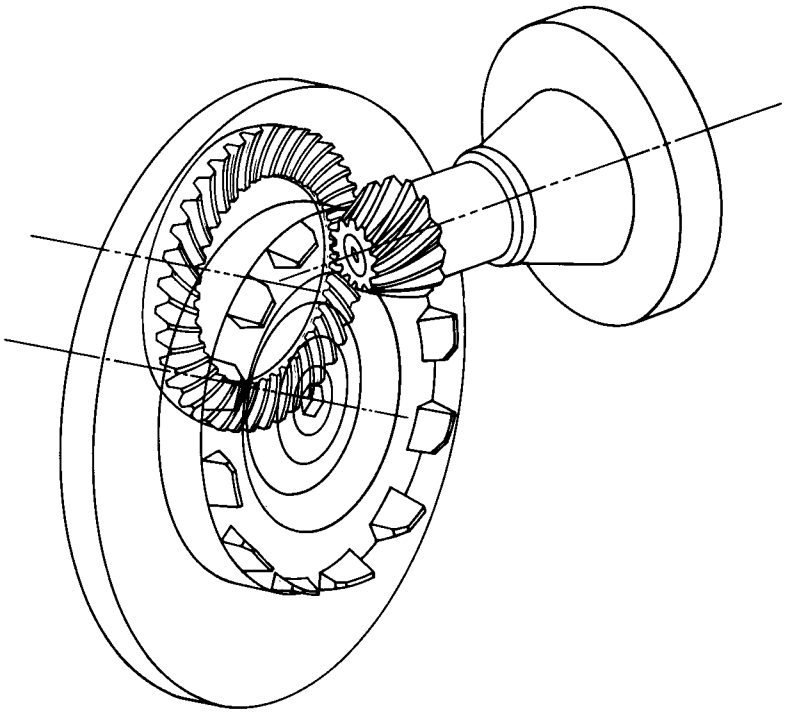

FIGURE 11.8 Imaginary generating gear.

one spindle, and the mating gear or a control gear is mounted on the other spindle. Tooth contact is evaluated by coating the teeth with a gear-marking compound and running the set under light load for a short time. At the same time, the smoothness of operation is observed. Spacing errors and runout are evaluated by noting variations in the contact pattern on the teeth around the blank. Poor surface finish shows up as variations within the marked contact pattern. Tooth size is measured by locking one member and rotating a tooth of the mating member within the slot to determine the backlash.

The contact pattern is shifted lengthwise along the tooth to the inside and outside of the blank by displacing one member along its axis and in the offset direction. The amount of displacement is used as a measure of the set's adjustability.

It is normal practice for tooth spacing and runout to be measured with an additional operation on inspection equipment designed specifically for that purpose. AGMA publication 2011-A98 specifies allowable tolerances for spacing and runout based on diametral pitch and pitch diameter.

Double- and single-flank test equipment can be used to measure tooth-profile errors, tooth spacing, and runout. The test equipment has transducers on the work spindles, and the output data are in chart form. The output data not only provide a record of the quality of the gear set, but can also be related to gear noise.

Three-dimensional coordinate-measuring machines can be used to compare the actual gear-tooth geometry with theoretical data.

BEVEL AND HYPOID GEARS

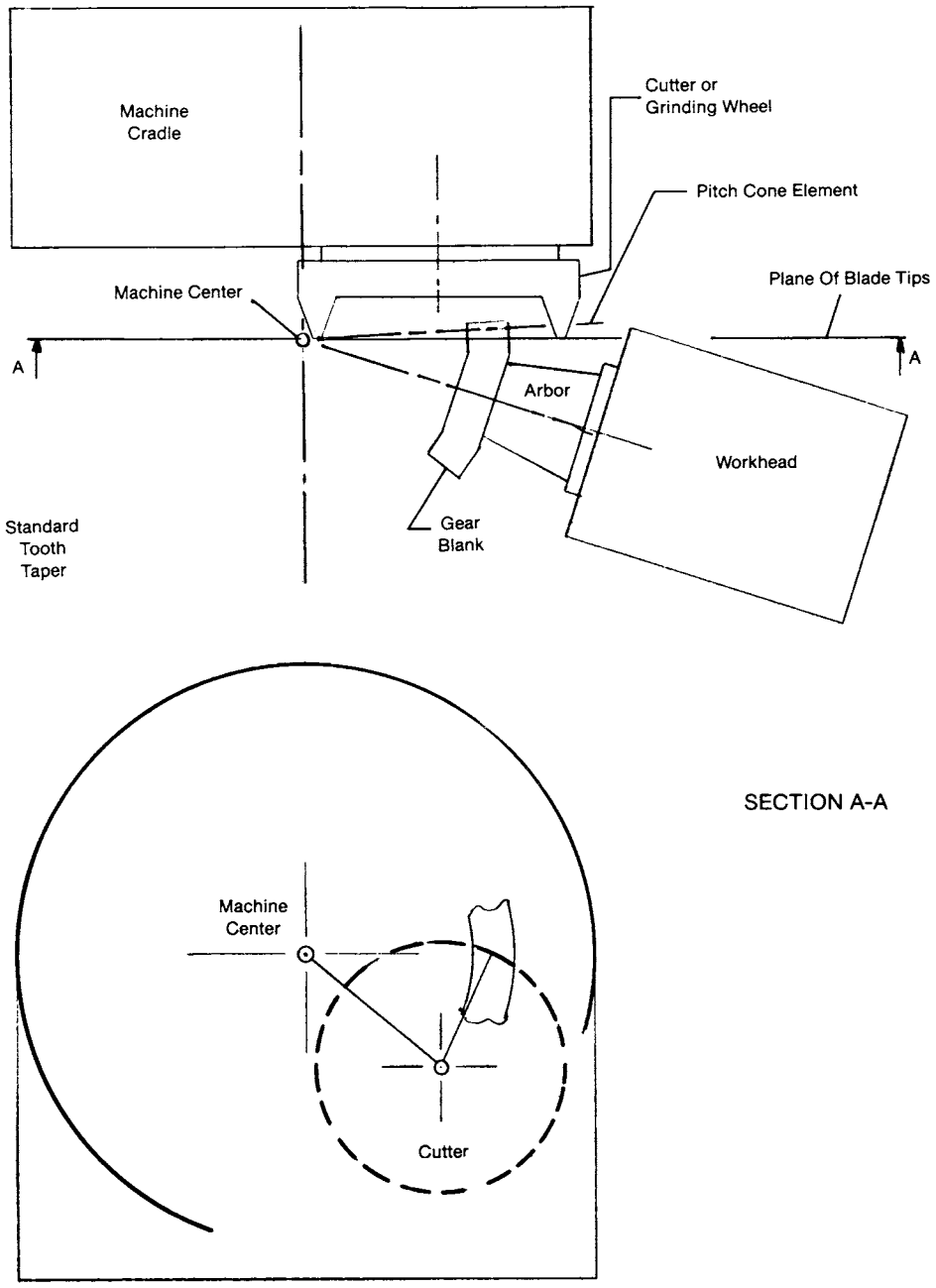

FIGURE 11.9 Basic machine setup of spiral-bevel face-mill generator.

11.4 GEAR DESIGN CONSIDERATIONS

11.4.1 Application Requirements

Bevel and hypoid gears are suitable for transmitting power between shafts at practically any angle and speed. The load, speed, and special operating conditions must be defined as the first step in designing a gear set for a specific application.

A basic load and a suitable factor encompassing protection from intermittent overloads, desired life, and safety are determined from

1. The power rating of the prime mover, its overload potential, and the uniformity of its output torque
2. The normal output loading, peak loads and their duration, and the possibility of stalling or severe loading at infrequent intervals
3. Inertia loads arising from acceleration or deceleration

The speed or speeds at which a gear set will operate must be known to determine inertia loads, velocity factor, type of gear required, accuracy requirements, design of mountings, and the type of lubrication.

Special operating conditions include

1. Noise-level limitations
2. High ambient temperature
3. Presence of corrosive elements
4. Abnormal dust or abrasive atmosphere
5. Extreme, repetitive shock loading or reversing
6. Operating under variable alignment
7. Gearing exposed to weather
8. Other conditions that may affect the operation of the set

11.4.2 Selection of Type of Gear

Straight-bevel gears are recommended for peripheral speeds up to 1000 feet per minute (ft/min) where maximum smoothness and quietness are not of prime importance. However, ground straight bevels have been successfully used at speeds up to 15 000 ft/min. Plain bearings may be used for radial and axial loads and usually result in a more compact and less expensive design. Since straight-bevel gears are the simplest to calculate, set up, and develop, they are ideal for small lots.

Spiral-bevel gears are recommended where peripheral speeds are in excess of 1000 ft/min or 1000 revolutions per minute (r/min). Motion is transmitted more smoothly and quietly than with straight-bevel gears. So spiral-bevel gears are preferred also for some lower-speed applications. Spiral bevels have greater load sharing, resulting from more than one tooth being in contact.

Zerol bevel gears have little axial thrust as compared to spiral-bevel gears and can be used in place of straight-bevel gears. The same qualities as defined under straight bevels apply to Zerol bevels. Because Zerol bevel gears are manufactured on the same equipment as spiral-bevel gears, Zerol bevel gears are preferred by some manufacturers. They are more easily ground because of the availability of bevel grinding equipment.

BEVEL AND HYPOID GEARS

Hypoid gears are recommended where peripheral speeds are in excess of 1000 ft/min and the ultimate in smoothness and quietness is required. They are somewhat stronger than spiral bevels. Hypoids have lengthwise sliding action, which enhances the lapping operation but makes them slightly less efficient than spiral-bevel gears.

11.4.3 Estimated Gear Size

Figures 11.10 and 11.11 relate size of bevel and hypoid gears to gear torque, which should be taken at a value corresponding to maximum sustained peak or one-half peak, as outlined below.

If the total duration of the peak load exceeds 10 000 000 cycles during the expected life of the gear, use the value of this peak load for estimating gear size. If, however, the total duration of the peak load is less than 10 000 000 cycles, use one-half the peak load or the value of the highest sustained load, whichever is greater.

Given gear torque and the desired gear ratio, the charts give gear pitch diameter. The charts are based on case-hardened steel and should be used as follows:

1. For other materials, multiply the gear pitch diameter by the material factor from Table 11.1.
2. For general industrial gearing, the preliminary gear size is based on surface durability.
3. For straight-bevel gears, multiply the gear pitch diameter by 1.2; for Zerol bevel gears, multiply the gear pitch diameter by 1.3.
4. For high-capacity spiral-bevel and hypoid gears, the preliminary gear size is based on both surface capacity and bending strength. Choose the larger of the gear diameters, based on the durability chart and the strength chart.

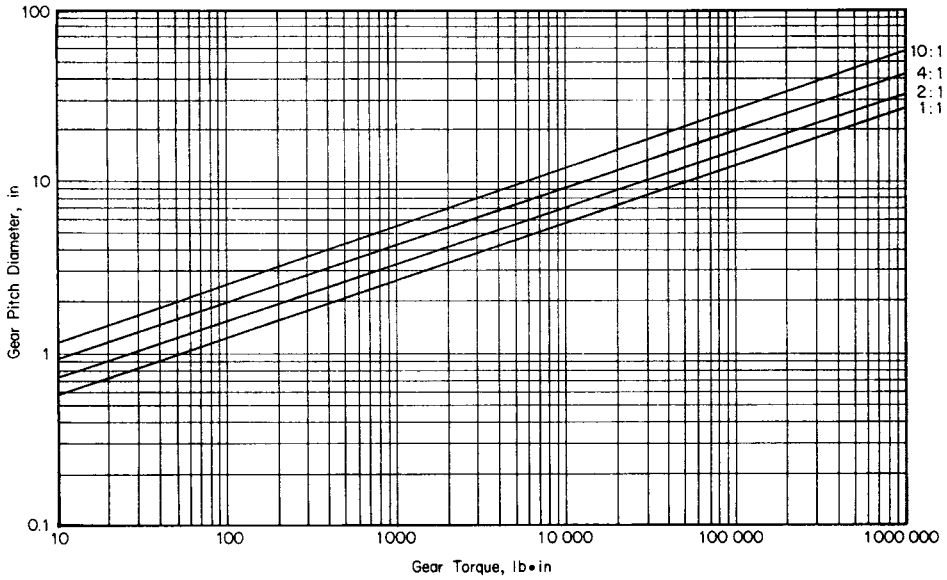

FIGURE 11.10 Gear pitch diameter based on surface durability.

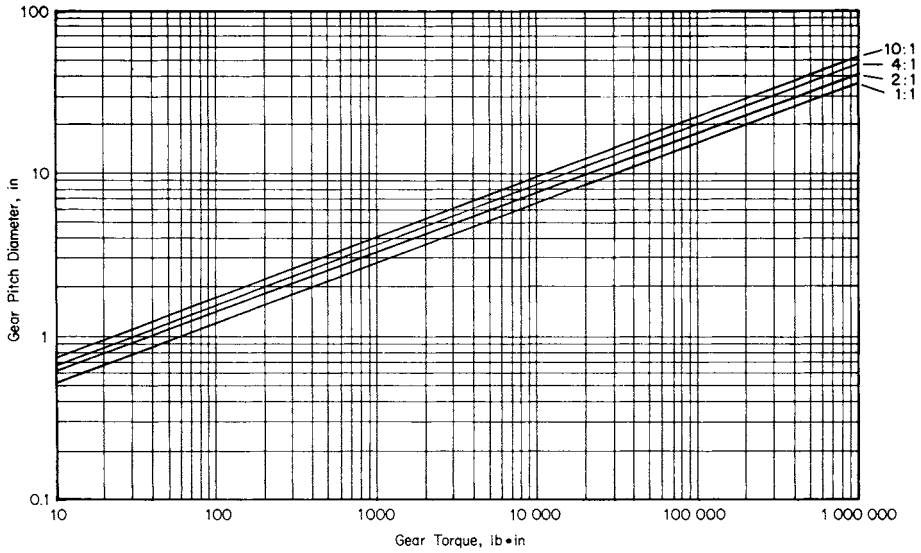

FIGURE 11.11 Gear pitch diameter based on bending strength.

5. For high-capacity ground spiral-bevel and hypoid gears, the gear diameter from the durability chart should be multiplied by 0.80.
6. For hypoid gears, multiply the gear pitch diameter by $D/(D + E)$.
7. Statically loaded gears should be designed for bending strength rather than surface durability. For statically loaded gears subject to vibration, multiply the gear diameter from the strength chart by 0.70. For statically loaded gears not subject to vibration, multiply the gear diameter from the strength chart by 0.60.
8. Estimated pinion diameter is $d = Dn/N$.

11.4.4 Number of Teeth

Figure 11.12 gives the recommended tooth numbers for spiral-bevel and hypoid gears. Figure 11.13 gives the recommended tooth numbers for straight-bevel and Zerol bevel gears. However, within limits, the selection of tooth numbers can be made in an arbitrary manner.

More uniform gears can be obtained in the lapping process if a common factor between gear and pinion teeth is avoided. Automotive gears are generally designed with fewer pinion teeth. Table 11.2 indicates recommended tooth numbers for automotive spiral-bevel and hypoid drives.

11.4.5 Face Width

The face width should not exceed 30 percent of the cone distance for straight-bevel, spiral-bevel, and hypoid gears and should not exceed 25 percent of the cone distance for Zerol bevel gears. In addition, it is recommended that the face width F be limited to

TABLE 11.1 Material Factors C_M

Gear		Pinion		Material factor C_M
Material	Hardness	Material	Hardness	
Case-hardened steel	58 R_C†	Case-hardened steel	60 R_C†	0.85‡
Case-hardened steel	55 R_C†	Case-hardened steel	55 R_C†	1.00
Flame-hardened steel	50 R_C†	Case-hardened steel	55 R_C†	1.05
Flame-hardened steel	50 R_C†	Flame-hardened steel	50 R_C†	1.05
Oil-hardened steel	375–425 H_B	Oil-hardened steel	375–425 H_B	1.20
Heat-treated steel	250–300 H_B	Case-hardened steel	55 R_C†	1.45
Heat-treated steel	210–245 H_B	Heat-treated steel	245–280 H_B	1.65
Cast iron		Case-hardened steel	55 R_C†	1.95
Cast iron		Flame-hardened steel	50 R_C†	2.00
Cast iron		Annealed steel	160–200 H_B	2.10
Cast iron		Cast iron		3.10

†Minimum values.
‡Gears must be file-hard.

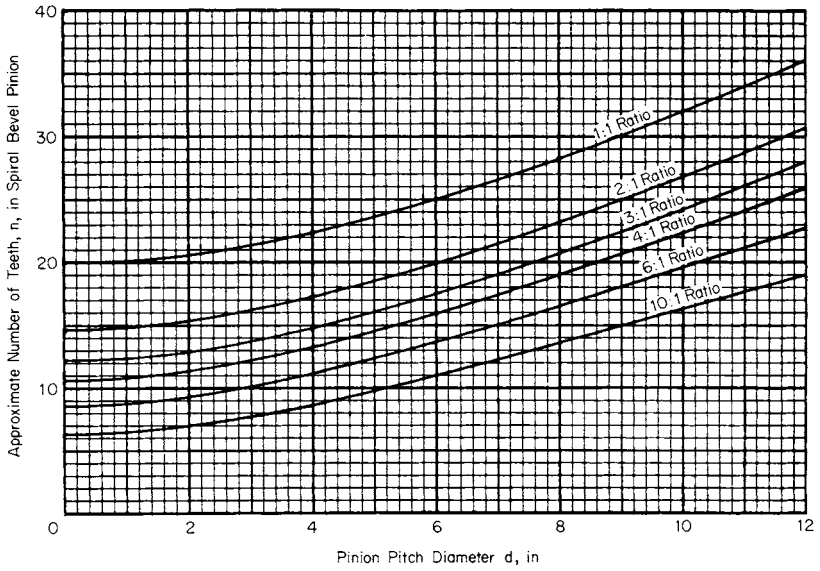

FIGURE 11.12 Recommended tooth numbers for spiral-bevel and hypoid gears.

$$F \leq \frac{10}{P_d}$$

The design chart in Fig. 11.14 gives the approximate face width for straight-bevel, spiral-bevel, and hypoid gears. For Zerol bevel gears, the face width given by this chart should be multiplied by 0.83.

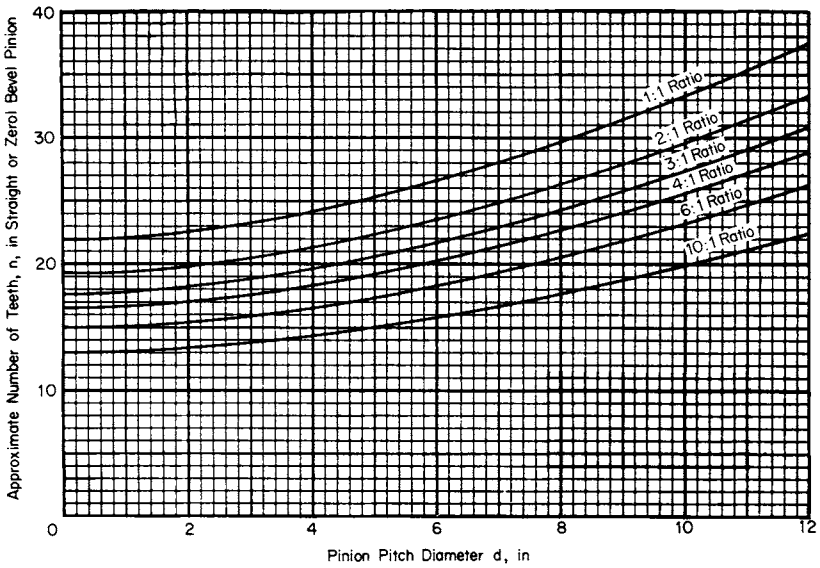

FIGURE 11.13 Recommended tooth numbers for straight- and Zerol-bevel gears.

11.4.6 Diametral Pitch

The diametral pitch is now calculated by dividing the number of teeth in the gear by the gear pitch diameter. Because tooling for bevel gears is not standardized according to pitch, it is not necessary that the diametral pitch be an integer.

TABLE 11.2 Recommended Tooth Numbers for Automotive Applications

Approximate ratio	Preferred no. pinion teeth	Allowable range
1.50/1.75	14	12 to 16
1.75/2.00	13	11 to 15
2.0/2.5	11	10 to 13
2.5/3.0	10	9 to 11
3.0/3.5	10	9 to 11
3.5/4.0	10	9 to 11
4.0/4.5	9	8 to 10
4.5/5.0	8	7 to 9
5.0/6.0	7	6 to 8
6.0/7.5	6	5 to 7
7.5/10.0	5	5 to 6

BEVEL AND HYPOID GEARS

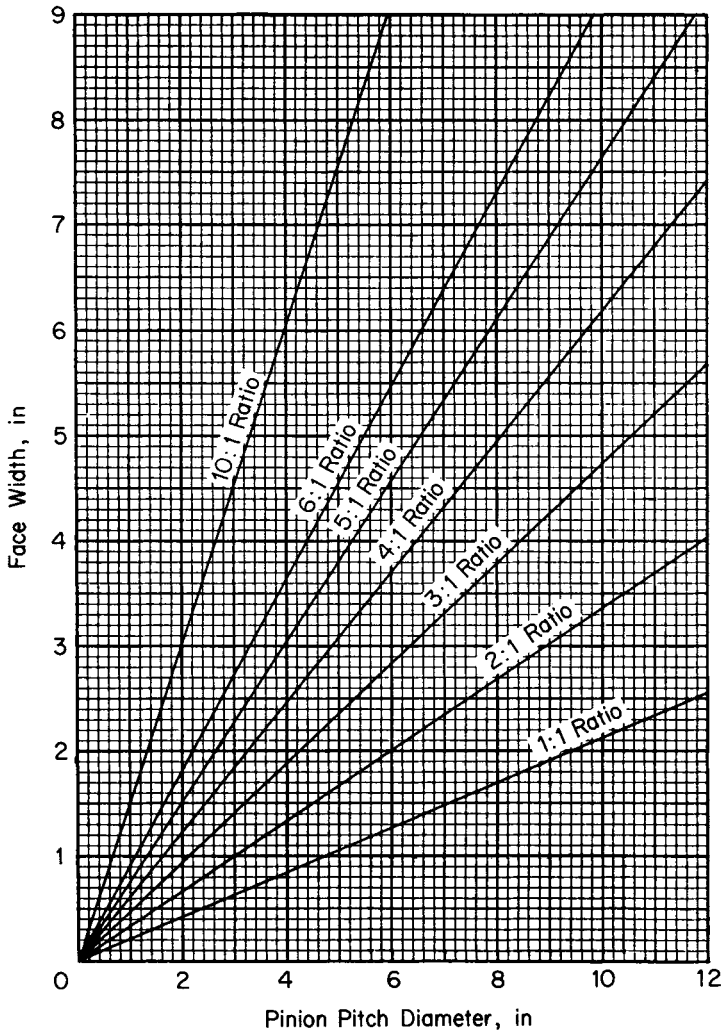

FIGURE 11.14 Face width of spiral-bevel and hypoid gears.

11.4.7 Hypoid Offset

In the design of hypoid gears, the offset is designated as being above or below center. Figure 11.15*a* and *b* illustrates the below-center position, and Fig. 11.15*c* and *d* illustrates the above-center position. In general, the shaft offset for power drives should not exceed 25 percent of the gear pitch diameter, and on very heavily loaded gears, the offset should be limited to 12.5 percent of the gear pitch diameter.

Hypoid pinions are larger in diameter than the corresponding spiral-bevel pinion. This increase in diameter may be as great as 30 percent, depending on the offset, spiral angle, and gear ratio.

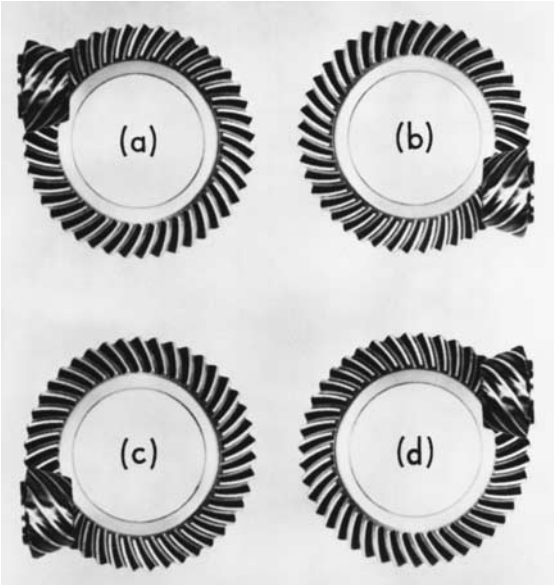

FIGURE 11.15 Hypoid offset. To determine the direction of offset, always look at the gear with the pinion at the right. Thus the gear sets of (*a*) and (*b*) are both offset *below* center; similar reasoning shows that (*c*) and (*d*) are offset *above* center. *(Gleason Machine Division.)*

11.4.8 Spiral Angle

In designing spiral-bevel gears, the spiral angle should be sufficient to give a face-contact ratio of at least 1.25. For maximum smoothness and quietness, the face-contact ratio should be between 1.50 and 2.00. High-speed applications should be designed with a face-contact ratio of 2.00 or higher for best results. Figure 11.16 may be used to assist in the selection of the spiral angle.

For hypoid gears, the desired pinion spiral angle can be calculated by

$$\psi_P = 25 + 5\sqrt{\frac{N}{n}} + 90\frac{E}{D}$$

where ψ_P is in degrees.

11.4.9 Pressure Angle

The commonly used pressure angle for bevel gears is 20°, although pressure angles of 22.5° and 25° are used for heavy-duty drives.

In the case of hypoids, the pressure angle is unbalanced on opposite sides of the gear teeth in order to produce equal contact ratios on the two sides. For this reason, the average pressure angle is specified for hypoids. For automotive drives, use 18° or 20°, and for heavy-duty drives, use 22.5° or 25°.

BEVEL AND HYPOID GEARS

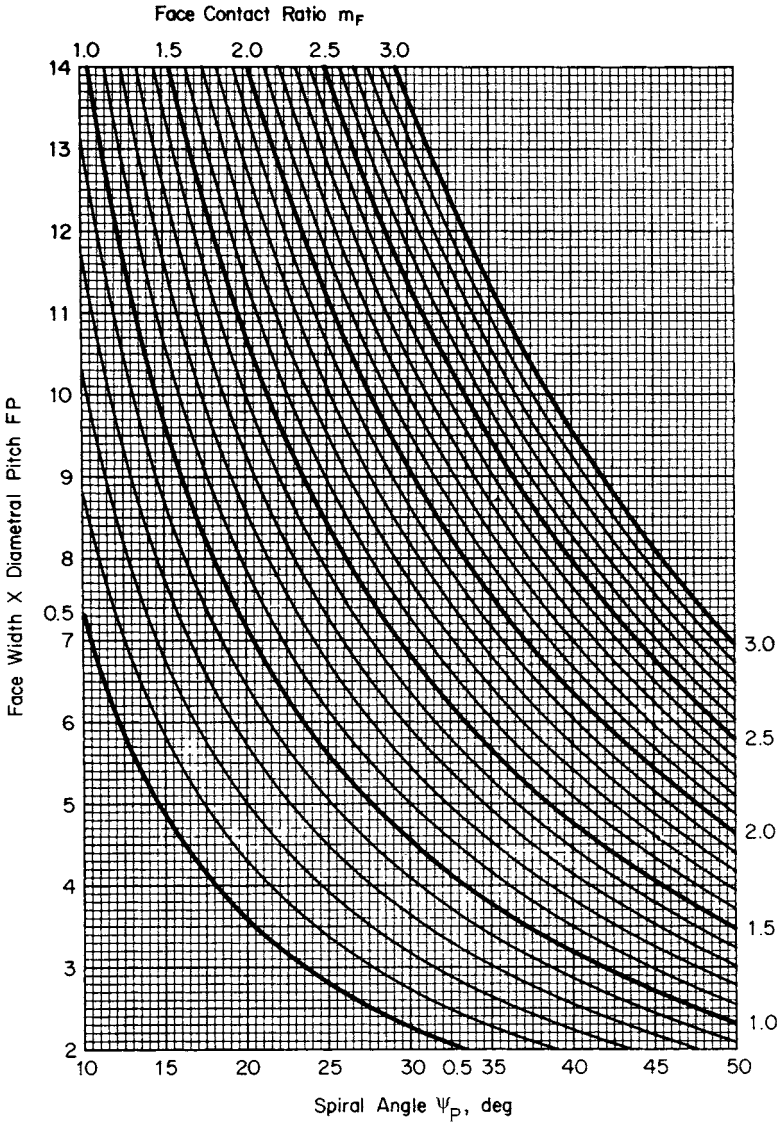

FIGURE 11.16 Selection of spiral angle.

11.4.10 Cutter Diameter

A cutter diameter must be selected for spiral-bevel, Zerol bevel, and hypoid gears. The usual practice is to use a cutter diameter approximately equal to the gear diameter. To increase adjustability of the gear set and obtain maximum strength, a smaller cutter should be used. Cutter diameters are standardized. Therefore, Table 11.3 is included to aid in cutter selection.

TABLE 11.3 Standard Cutter Radii Corresponding to Various Gear Pitch Diameters for Spiral-Bevel, Zerol Bevel, and Hypoid Gears

Pitch diameter D of gear, in	Cutter radius r_c, in (mm)
3.000–5.250	1.750
3.875–6.750	2.250
4.250–7.500	2.500
5.125–9.000	3.000
6.500–11.250	3.750
7.750–13.500	4.500
9.000–15.750	5.250
10.250–18.000	6.000
12.000–21.000	7.000
13.750–24.000	8.000
15.500–27.000	9.000
18.000–31.500	10.500
21.750–60.000	(320)
27.250–75.000	(400)
34.250–100.000	(500)

11.4.11 Materials and Heat Treatment

Through-hardening steels are used when medium wear resistance and medium load-carrying capacity are desired. The following steels are some of those used and listed, beginning with the steel of lowest hardenability: AISI 1045, 1144, 4640, 4150, and 4340. When greater hardenability is required for larger gears, it is sometimes necessary to increase the carbon content of these steels or to select a different steel.

Carburized gears are used when high wear resistance and high load-carrying capacity are required. Carburizing steels used in gears normally have a carbon content of 0.10 to 0.25 percent and should have sufficient alloy content to allow hardening in the section sizes in which they are used. For low-heat-treat distortion, 4620 or 8620 might be used; if high core hardness is desired, 9310 might be used. The following steels have been commonly used and are listed, beginning with the steel of lowest core hardenability: AISI 4620, 8620, 9310, and 4820.

Carburized gears should be specified as follows:

1. Total depth of carburized case after finishing operations
2. Surface hardness
3. Core hardness
4. Maximum case carbon content (optional)

Gears should be quenched from a temperature which will ensure a minimum amount of retained austenite.

Nitriding steels are used in applications which require high wear resistance with minimum distortion in heat treating. The commonly used steels are AISI 4140, 4150, and 4340. If extreme hardness and wear resistance are required, the nitralloy steels can be used. To achieve the desired results in the nitriding operation, all material

should be hardened and tempered above the nitriding temperature prior to finish machining. Sharp corners should be avoided on external surfaces.

Nitrided gears should be specified as follows:

1. Total depth of nitrided case after finishing operations
2. Surface hardness
3. Core hardness

Cast iron is used in place of non-heat-treated steel where good wear resistance plus excellent machineability is required. Complicated shapes can be cast more easily from iron than they can be produced by machining from bars or forgings.

11.5 GEAR-TOOTH DIMENSIONS

11.5.1 Calculation of Basic Bevel-Gear-Tooth Dimensions

All bevel-gear-tooth dimensions are calculated in a similar manner. Therefore, straight-bevel, spiral-bevel, and Zerol bevel gears are considered as a group. In Sec. 11.4 we selected

1. Number of pinion teeth n
2. Number of gear teeth N
3. Diametral pitch P_d
4. Shaft angle Σ
5. Face width F
6. Pressure angle ϕ
7. Spiral angle ψ
8. Hand of spiral (pinion), left-hand/right-hand (LH/RH)
9. Cutter radius r_c

The formulas in Table 11.4 are now used to calculate the blank and tooth dimensions.

11.5.2 Tooth Taper

Spiral-bevel- and hypoid-gear blanks are designed by one of four methods—standard taper, duplex taper, tilted root line, or uniform depth.

Standard taper is the case where the root lines of mating members, if extended, would intersect the pitch-cone apex. The tooth depth changes in proportion to the cone distance.

Duplex taper is the case where the root lines are tilted so that the slot width is constant. This condition permits each member of a pair to be finished in one operation, using circular cutters which cut in one slot.

Tilted root-line taper is a compromise between duplex and standard taper. The blanks are designed with duplex taper except when the taper becomes excessive. When the taper is 1.3 times standard taper or greater, 1.3 times standard taper is used.

Uniform-depth taper is the case where the root lines are not tilted. The tooth depth is uniform from the inside to the outside of the blank.

TABLE 11.4 Formulas for Computing Blank and Tooth Dimensions

Item	Item no.	Member	Formula
Pitch diameter	1	Pinion	$d = \frac{n}{P_d}$
		Gear	$D = \frac{N}{P_d}$
Pitch angle	2	Pinion	$\gamma = \tan^{-1} \frac{\sin \Sigma}{N/n + \cos \Sigma}$
		Gear	$\Gamma = \Sigma - \gamma$
Outer cone distance	3	Both	$A_o = \frac{0.50D}{\sin \Gamma}$
Mean cone distance	4	Both	$A_m = A_o - 0.5F$
Depth factor k_1	5	Both	Table 11.5
Mean working depth	6	Both	$h = \frac{k_1 A_m}{P_d A_o} \cos \psi$
Clearance factor k_2	7	Both	Table 11.6
Clearance	8	Both	$c = k_2 h$
Mean whole depth	9	Both	$h_m = h + c$
Equivalent 90° ratio	10	Both	$m_{90} = \sqrt{\frac{N \cos \gamma}{n \cos \Gamma}}$
Mean addendum factor C_1	11	Both	Table 11.7
Mean circular pitch	12	Both	$P_m = \frac{\pi A_m}{P_d A_o}$
Mean addendum	13	Pinion	$a_P = h - a_G$
		Gear	$a_G = C_1 h$
Mean dedendum	14	Pinion	$b_P = h_m - a_P$
		Gear	$b_G = h_m - a_G$
Sum of dedendum angles	15	Both	$\Sigma\delta$ (see Sec. 11.5.2)

BEVEL AND HYPOID GEARS

TABLE 11.4 Formulas for Computing Blank and Tooth Dimensions (*Continued*)

Item	Item no.	Member	Formula
Dedendum angle	16	Pinion	δ_P (see Sec. 11.5.2)
		Gear	δ_G (see Sec. 11.5.2)
Face angle of blank	17	Pinion	$\gamma_o = \gamma + \delta_G$
		Gear	$\Gamma_o = \Gamma + \delta_P$
Root angle of blank	18	Pinion	$\gamma_R = \gamma - \delta_P$
		Gear	$\Gamma_R = \Gamma - \delta_G$
Outer addendum	19	Pinion	$a_{oP} = a_P + 0.5F \tan \delta_G$
		Gear	$a_{oG} = a_G + 0.5F \tan \delta_P$
Outer dedendum	20	Pinion	$b_{oP} = b_P + 0.5F \tan \delta_P$
		Gear	$b_{oG} = b_G + 0.5F \tan \delta_G$
Outer working depth	21	Both	$h_k = a_{oP} + a_{oG}$
Outer whole depth	22	Both	$h_t = a_{oP} + b_{oP}$
Outside diameter	23	Pinion	$d_o = d + 2a_{oP} \cos \gamma$
		Gear	$D_o = D + 2a_{oG} \cos \Gamma$
Pitch apex to crown	24	Pinion	$x_o = A_o \cos \gamma - a_{oP} \sin \gamma$
		Gear	$X_o = A_o \cos \Gamma - a_{oG} \sin \Gamma$
Mean diametral pitch	25	Both	$P_{dm} = P_d \dfrac{A_o}{A_m}$
Mean pitch diameter	26	Pinion	$d_m = \dfrac{n}{P_{dm}}$
		Gear	$D_m = \dfrac{N}{P_{dm}}$
Thickness factor K	27	Both	Fig. 11.17
Mean normal circular thickness	28	Pinion	$t_n = P_m \cos \psi - T_n$
		Gear	$T_n = \dfrac{P_m}{2 \cos \psi} - (a_P - a_G) \tan \phi + \dfrac{K \cos \psi}{P_{dm} \tan \phi}$

TABLE 11.4 Formulas for Computing Blank and Tooth Dimensions (*Concluded*)

Item	Item no.	Member	Formula
Outer normal backlash allowance	29	Both	B (Table 11.8)
Mean normal chordal thickness	30	Pinion	$t_{nc} = t_n - \frac{t_n^3}{6d_m^2} - 0.5B\frac{A_m}{A_o}\sec\phi$
		Gear	$T_{nc} = T_n - \frac{T_n}{6D_m^2} - 0.5B\left(\frac{A_m}{A_o}\right)\sec\phi$
Mean chordal addendum	31	Pinion	$a_{cP} = a_P + \frac{t_n^2\cos\gamma}{4d_m}$
		Gear	$a_{cG} = a_G + \frac{T_n^2\cos\Gamma}{4D_m}$

TABLE 11.5 Depth Factor

Type of gear	No. pinion teeth	Depth factor k_1
Straight bevel	12 and higher	2.000
Spiral bevel	12 and higher	2.000
	11	1.995
	10	1.975
	9	1.940
	8	1.895
	7	1.835
	6	1.765
Zerol bevel	13 and higher	2.000
Hypoid	11 and higher	4.000
	10	3.900
	9	3.8
	8	3.7
	7	3.6
	6	3.5

TABLE 11.6 Clearance Factors

Type of gear	Clearance factor k_2
Straight bevel	0.140
Spiral bevel	0.125
Zerol bevel	0.110
Hypoid	0.150

BEVEL AND HYPOID GEARS

TABLE 11.7 Mean Addendum Factor

Type of gear	No. pinion teeth	Mean addendum factor C_1
Straight bevel	12 and higher	C_1†
Spiral bevel	12 and higher	C_1†
	11	0.490
	10	0.435
	9	0.380
	8	0.325
	7	0.270
	6	0.215
Zerol bevel	13 and higher	C_1†
Hypoid	21 and higher	C_1†
	9 to 20	0.170
	8	0.150
	7	0.130
	6	0.110

†Use $C_1 = 0.270 + 0.230/(m_{90})^2$.

TABLE 11.8 Minimum Normal Backlash Allowance†

Range of diametral pitch, teeth/in	Allowance, in (for AGMA quality number range)	
	4 to 9	10 to 13
1.00–1.25	0.032	0.024
1.25–1.50	0.027	0.020
1.50–2.00	0.020	0.015
2.00–2.50	0.016	0.012
2.50–3.00	0.013	0.010
3.00–4.00	0.010	0.008
4.00–5.00	0.008	0.006
5.00–6.00	0.006	0.005
6.00–8.00	0.005	0.004
8.00–10.00	0.004	0.003
10.00–12.00	0.003	0.002
12.00–16.00	0.003	0.002
16.00–20.00	0.002	0.001
20.00–25.00	0.002	0.001

†Measured at outer cone in inches.

In many cases, the type of taper depends on the manufacturing method. Before selecting a tooth taper, you should consult with the manufacturer to ensure compatibility between the design and the cutting method.

Straight-bevel gears are usually designed with standard taper. Zerol bevel gears are usually designed with duplex taper.

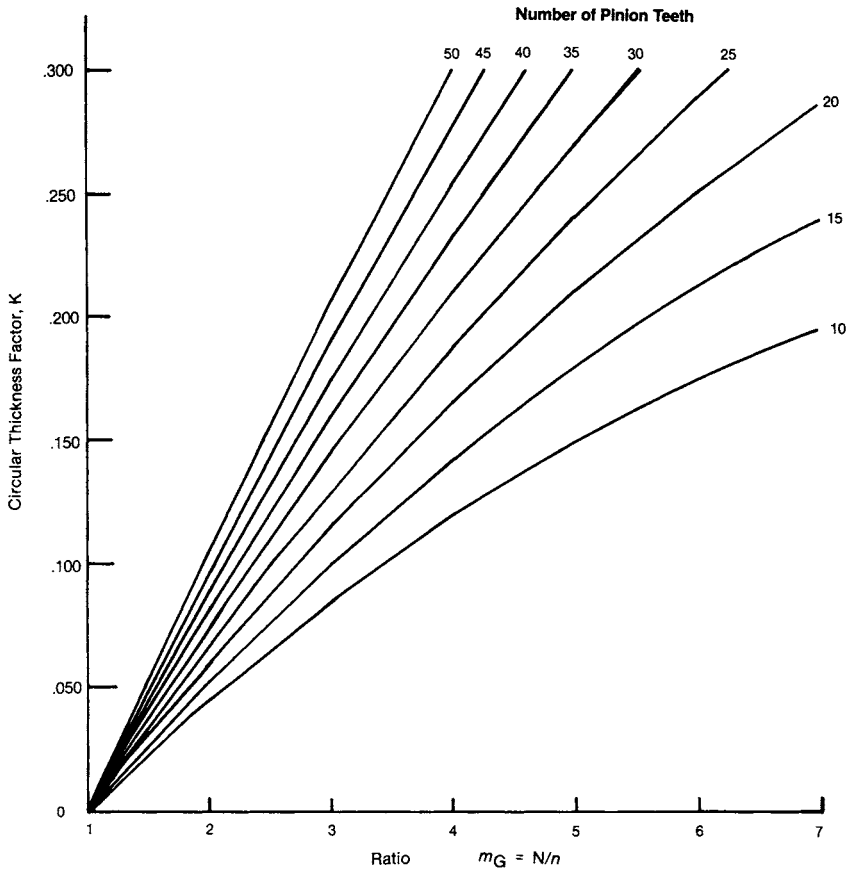

FIGURE 11.17 Circular thickness factor. These curves are plotted from the equation $K = -0.088 + 0.092m_G - 0.004m_G^2 + 0.0016\,(n - 30)\,(m_G - 1)$.

The formulas used to calculate the sum of dedendum angles and the dedendum angles are shown in Table 11.9.

11.5.3 Hypoid Dimensions

The geometry of hypoid gears is complicated by the offset between the axes of the mating members. Therefore a separate set of calculation formulas is needed.

The starting data are the same as for bevel gears with the following exceptions:

1. Hypoid offset E is required.
2. Pinion spiral angle ψ_P is specified.

The formulas in Table 11.10 are now used to calculate the blank and tooth dimensions.

TABLE 11.9 Formulas for Computing Dedendum Angles and Their Sum

Type of taper	Formula
Standard	$\Sigma\delta = \tan^{-1}\frac{b_P}{A_m} + \tan^{-1}\frac{b_G}{A_m}$ $\delta_P = \tan^{-1}\frac{b_P}{A_m} \qquad \delta_G = \Sigma\delta - \delta_P$
Duplex	$\Sigma\delta = \frac{90[1 - (A_m/r_c)\sin\psi]}{(P_d A_o \tan\phi\cos\psi)}$ $\delta_P = \frac{a_G}{h}\Sigma\delta \qquad \delta_G = \Sigma\delta - \delta_P$
Tilted root line	Use $\Sigma\delta = \frac{90[1 - (A_m/r_c)\sin\psi]}{(P_d A_o \tan\phi\cos\psi)}$ or $= 1.3\tan^{-1}\frac{b_P}{A_m} + 1.3\tan^{-1}\frac{b_G}{A_m}$ whichever is smaller. $\delta_P = \frac{a_G}{h} \qquad \delta_G = \Sigma\delta - \delta_P$
Uniform depth	$\Sigma\delta = 0$ $\delta_P = \delta_G = 0$

11.5.4 AGMA References†

The following AGMA standards are helpful in designing bevel and hypoid gears:

AGMA Design Manual for Bevel Gears, 2005
AGMA Rating Standard for Bevel Gears, 2003

These are available through American Gear Manufacturer's Association, Alexandria, Virginia.

11.6 GEAR STRENGTH

Under ideal conditions of operation, bevel and hypoid gears have a tooth contact which utilizes the full working profile of the tooth without load concentration in any

† The notation and units used in this chapter are the same as those used in the AGMA standards. These may differ in some respects from those used in other chapters of this Handbook.

TABLE 11.10 Formulas for Computing Blank and Tooth Dimensions of Hypoid Gears

Item	No.	Formula
Pitch diameter of gear	1	$D = \dfrac{N}{P_d}$
	2	$m = \dfrac{n}{N}$
	3	$\psi_{Po} = \psi_P$
	4	$\Delta\Sigma = 90 - \Sigma$
	5	$\tan \Gamma_i = \dfrac{\cos \Delta\Sigma}{1.2(m - \sin \Delta\Sigma)}$
	6	$R = 0.5(D - F \sin \Gamma_i)$
	7	$\sin \varepsilon_i' = \dfrac{E}{R} \sin \Gamma_i$
	8	$K_1 = \tan \psi_{Po} \sin \varepsilon_i' + \cos \varepsilon_i'$
	9	$R_{P2} = mRK_1$
	10	$\tan \eta = \dfrac{E}{R(\tan \Gamma_i \cos \Delta\Sigma - \sin \Delta\Sigma) + R_{P2}}$ first trial
	11	$\sin \varepsilon_2 = \dfrac{E - R_{P2} \sin \eta}{R}$
	12	$\tan \gamma_2 = \dfrac{\sin \eta}{\tan \varepsilon_2 \cos \Delta\Sigma} + \tan \Delta\Sigma \cos \eta$
	13	$\sin \varepsilon_2' = \dfrac{\sin \varepsilon_2 \cos \Delta\Sigma}{\cos \gamma_2}$
	14	$\tan \psi_{P2} = \dfrac{K_1 - \cos \varepsilon_2'}{\sin \varepsilon_2'}$
	15	$\Delta K = \sin \varepsilon_2' (\tan \psi_{Po} - \tan \psi_{P2})$
	16	$\dfrac{\Delta R_P}{R} = m(\Delta K)$
	17	$\sin \varepsilon_1 = \sin \varepsilon_2 - \dfrac{\Delta R_P}{R} \sin \eta$
Pinion pitch angle	18	$\tan \gamma = \dfrac{\sin \eta}{\tan \varepsilon_1 \cos \Delta\Sigma} + \tan \Delta\Sigma \cos \eta$
	19	$\sin \varepsilon_1' = \dfrac{\sin \varepsilon_1 \cos \Delta\Sigma}{\cos \gamma_1}$
Pinion spiral angle	20	$\tan \psi_P = \dfrac{K_1 + \Delta K - \cos \varepsilon_1'}{\sin \varepsilon_1'}$

TABLE 11.10 Formulas for Computing Blank and Tooth Dimensions of Hypoid Gears (*Continued*)

Item	No.	Formula
Gear spiral angle	21	$\psi_G = \psi_P - \varepsilon_1'$
Gear pitch angle	22	$\tan \Gamma = \dfrac{\sin \varepsilon_1}{\tan \eta \cos \Delta\Sigma} + \cos \varepsilon_1 \tan \Delta\Sigma$
Gear mean cone distance	23	$A_{mG} = \dfrac{R}{\sin \Gamma}$
Pinion mean cone distance	24	$\Delta R_P = R\left(\dfrac{\Delta R_P}{R}\right)$
	25	$A_{mP} = \dfrac{R_{P2} + \Delta R_P}{\sin \gamma}$
	26	$R_P = A_{mP} \sin \gamma$
Limit pressure angle	27	$-\tan \phi_{01} = \dfrac{\tan \gamma \tan \Gamma}{\cos \varepsilon_1'} \times \dfrac{A_{mP} \sin \psi_P - A_{mG} \sin \psi_G}{A_{mP} \tan \gamma + A_{mG} \tan \Gamma}$
	28	$\text{Den} = -\tan \phi_{01}\left(\dfrac{\tan \psi_P}{A_{mP} \tan \gamma} + \dfrac{\tan \psi_G}{A_{mG} \tan \Gamma}\right) + \dfrac{1}{A_{mP} \cos \psi_P} - \dfrac{1}{A_{mG} \cos \psi_G}$
	29	$r_{c1} = \dfrac{\sec \phi_{01} (\tan \psi_P - \tan \phi_G)}{\text{Den}}$
	30	$\left\lvert \dfrac{r_c}{r_{c1}} - 1 \right\rvert \le 0.01$ Loop back to no. 10 and change η until satisfied.
Gear pitch apex beyond crossing point	31	$Z_P = A_{mP} \tan \gamma \sin \Gamma - \dfrac{E \tan \Delta\Sigma}{\tan \varepsilon_1}$
	32	$Z = \dfrac{R}{\tan \Gamma} - Z_P$
Gear outer cone distance	33	$A_o = \dfrac{0.5D}{\sin \Gamma}$
	34	$\Delta F_o = A_o - A_{mG}$
Depth factor	35	k_1 (see Table 11.5)
Addendum factor	36	C_1 (see Table 11.7)
Mean working depth	37	$h = \dfrac{k_1 R \cos \psi_G}{N}$
Mean addendum	38	$a_P = h - a_G \qquad a_G = C_1 h$

TABLE 11.10 Formulas for Computing Blank and Tooth Dimensions of Hypoid Gears (*Continued*)

Item	No.	Formula
Clearance factor	39	k_2 (see Table 11.6)
Mean dedendum	40	$b_P = b_G + a_G - a_P \qquad b_G = h(1 + k_2 - C_1)$
Clearance	41	$c = k_2 h$
Mean whole depth	42	$h_m = a_G + b_G$
Sum of dedendum angle	43	$\Sigma\delta$ (see Sec. 11.5.2)
Gear dedendum angle	44	δ_G (see Sec. 11.5.2)
Gear addendum angle	45	$\alpha_G = \Sigma\delta - \delta_G$
Gear outer addendum	46	$a_{oG} = a_G + \Delta F_o \sin \alpha_G$
Gear outer dedendum	47	$b_{oG} = b_G + \Delta F_o \sin \delta_G$
Gear whole depth	48	$h_t = a_{oG} + b_{oG}$
Gear working depth	49	$h_k = h_{tG} - c$
Gear root angle	50	$\Gamma_R = \Gamma - \delta_G$
Gear face angle	51	$\Gamma_o = \Gamma + \alpha_G$
Gear outside diameter	52	$D_o = 2a_{oG} \cos \Gamma + D_G$
Gear crown to crossing point	53	$X_o = Z_P + \Delta F_o \cos \Gamma - a_{oG} \sin \Gamma$
Gear root apex beyond crossing point	54	$Z_R = Z + \dfrac{A_{mG} \sin \delta_G - b_G}{\sin \Gamma_R}$
Gear face apex beyond crossing point	55	$Z_o = Z + \dfrac{A_{mG} \sin \alpha_G - a_G}{\sin \Gamma_o}$
	56	$Q_R = \dfrac{A_{mG} \cos \delta_G}{\cos \Gamma_R} - Z$
	57	$Q_o = \dfrac{A_{mG} \cos \alpha_G}{\cos \Gamma_o} - Z$
	58	$\tan \xi_R = \dfrac{E \tan \Delta\Sigma}{Q_R}$

TABLE 11.10 Formulas for Computing Blank and Tooth Dimensions of Hypoid Gears (*Continued*)

Item	No.	Formula
Gear face apex beyond crossing point (*continued*)	59	$\tan \xi_o = \dfrac{E \tan \Delta\Sigma}{Q_o}$
	60	$\sin (\varepsilon_R + \xi_R) = \dfrac{E \cos \xi_R \tan \Gamma_R}{Q_R}$
	61	$\sin(\varepsilon_o + \xi_o) = \dfrac{E \cos \xi_o \tan \Gamma_o}{Q_o}$
Pinion face angle	62	$\sin \gamma_o = \sin \Delta\Sigma \sin \Gamma_R + \cos \Delta\Sigma \cos \Gamma_R \cos \varepsilon_R$
Pinion root angle	63	$\sin \gamma_R = \sin \Delta\Sigma \sin \Gamma_o + \cos \Delta\Sigma \cos \Gamma_o \cos \varepsilon_o$
Pinion face apex beyond crossing point	64	$G_o = \dfrac{E \sin \varepsilon_R \cos \Gamma_R - Z_R \sin \Gamma_R - c}{\sin \gamma_o}$
Pinion root apex beyond crossing point	65	$G_R = \dfrac{E \sin \varepsilon_o \cos \Gamma_o - Z_o \sin \Gamma_o - c}{\sin \gamma_R}$
	66	$\tan \lambda' = \dfrac{m \sin \varepsilon_i' \cos \Gamma}{\cos \gamma + m \cos \Gamma \cos \varepsilon_i'}$
Pinion addendum angle	67	$\alpha_P = \gamma_o - \gamma$
Pinion dedendum angle	68	$\delta_P = \gamma - \gamma_R$
Pinion whole depth	69	$h_{tP} = \dfrac{(x_o + G_o) \sin \delta_P}{\cos \gamma_o} - \sin \gamma_R (G_R - G_o)$
	70	$\Delta F_i = F - \Delta F_o$
	71	$\Delta F_{oP} = h \sin \varepsilon_R (1 - m)$
	72	$F_{oP} = \dfrac{\Delta F_o \cos \lambda'}{\cos (\varepsilon_i' - \lambda')}$
	73	$F_{iP} = \dfrac{\Delta F_i \cos \lambda'}{\cos (\varepsilon_i' - \lambda')}$
	74	$\Delta B_o = \dfrac{F_o \cos \gamma_o}{\cos \alpha_P} + \Delta F_{oP} - (b_G - c) \sin \gamma$
	75	$\Delta B_i = \dfrac{F \cos \gamma_o}{\cos \alpha_P} + \Delta F_{oP} - (b_G - c) \sin \gamma$
Pinion crown to crossing point	76	$x_o = \dfrac{E}{\tan \varepsilon_1 \cos \Delta\Sigma} - R_P \tan \gamma + \Delta B_o$

TABLE 11.10 Formulas for Computing Blank and Tooth Dimensions of Hypoid Gears (*Concluded*)

Item	No.	Formula
Pinion front crown to crossing point	77	$x_i = \dfrac{E}{\tan \varepsilon_1 \cos \Delta\Sigma} - R_P \tan \gamma - \Delta B_i$
Pinion outside diameter	78	$d_o = 2 \tan \gamma_o (x_o + G_o)$
Pinion face width	79	$F_P = \dfrac{x_o - x_i}{\cos \gamma_o}$
Mean circular pitch	80	$p_m = \dfrac{\pi A_{mG}}{P_d A_o}$
Mean diametral pitch	81	$P_{dm} = P_d \dfrac{A_o}{A_{mG}}$
Thickness factor	82	K (see Fig. 11-17)
Mean pitch diameter	83	$d_m = 2A_{mP} \sin \gamma$
	84	$D_m = 2A_{mG} \sin \Gamma$
Mean normal circular thickness	85	$t_n = p_m \cos \psi_G - T_n$
	86	$T_n = 0.5p_m \cos \psi_G - (a_P - a_G) \tan \phi + \dfrac{K \cos \psi}{P_{dm} \tan \phi}$
Outer normal backlash allowance	87	B (see Table 11-8)
Mean normal chordal thickness	88	$t_{nc} = t_n - \dfrac{t_n^3}{6d_m^2} - 0.5B \sec \phi \left(\dfrac{A_{mg}}{A_o}\right)$
	89	$T_{nc} = T_n - \dfrac{T_n^3}{6D_m^2} - 0.5B \sec \phi \left(\dfrac{A_{mG}}{A_o}\right)$
Mean chordal addendum	90	$a_{cP} = a_P + \dfrac{0.25t_n^2 \cos \gamma}{d_m}$
	91	$a_{cG} = a_G + \dfrac{0.25T_N^2 \cos \Gamma}{D_m}$

area. The recommendations and rating formulas which follow are designed for a tooth contact developed to give the correct pattern in the final mountings under full load.

11.6.1 Formulas for Contact and Bending Stress

The basic equation for contact stress in bevel and hypoid gears is

$$S_c = C_p \sqrt{\frac{2T_p C_o}{C_v} \frac{1}{FD^2} \frac{N}{n} \frac{1.2C_m C_f}{I}} \tag{11.1}$$

and the basic equation for bending stress is

$$S_t = \frac{2T_G K_o}{K_v} \frac{P_d}{FD} \frac{1.2K_m}{J} \tag{11.2}$$

where S_t = calculated tensile bending stress at root of gear tooth, pounds per square inch (lb/in^2)
S_c = calculated contact stress at point on tooth where its value will be maximum, lb/in^2
C_p = elastic coefficient of the gear-and-pinion materials combination, (lb)$^{1/2}$/in
T_P, T_G = transmitted torques of pinion and gear, respectively, pound-inches (lb · in)
K_o, C_o = overload factors for strength and durability, respectively
K_v, C_v = dynamic factors for strength and durability, respectively
K_m, C_m = load-distribution factors for strength and durability, respectively
C_f = surface-condition factor for durability
I = geometry factor for durability
J = geometry factor for strength

11.6.2 Explanation of Strength Formulas and Terms

The elastic coefficient for bevel and hypoid gears with localized tooth contact pattern is given by

$$C_p = \sqrt{\frac{3}{2\pi} \frac{1}{(1-\mu_P^2)/E_P + (1-\mu_G^2)/E_G}} \tag{11.3}$$

where μ_P, μ_G = Poisson's ratio for materials of pinion and gear, respectively (use 0.30 for ferrous materials)
E_P, E_G = Young's modulus of elasticity for materials of pinion and gear, respectively (use 30.0×10^6 lb/in^2 for steel)

The overload factor makes allowance for the roughness or smoothness of operation of both the driving and driven units. Use Table 11.11 as a guide in selecting the overload factor.

The dynamic factor reflects the effect of inaccuracies in tooth profile, tooth spacing, and runout on instantaneous tooth loading. For gears manufactured to AGMA class 11 tolerances or higher, a value of 1.0 may be used for dynamic factor. Curve 2 in Fig. 11.18 gives the values of C_v for spiral bevels and hypoids of lower accuracy or for large, planed spiral-bevel gears. Curve 3 gives the values of C_v for bevels of lower accuracy or for large, planed straight-bevel gears.

TABLE 11.11 Overload Factors K_o, C_o†

Prime mover	Character of load on driven member		
	Uniform	Medium shock	Heavy shock
Uniform	1.00	1.25	1.75
Medium shock	1.25	1.50	2.00
Heavy shock	1.50	1.75	2.25

†This table is for speed-decreasing drive; for speed-increasing drives add $0.01(N/n)^2$ to the above factors.

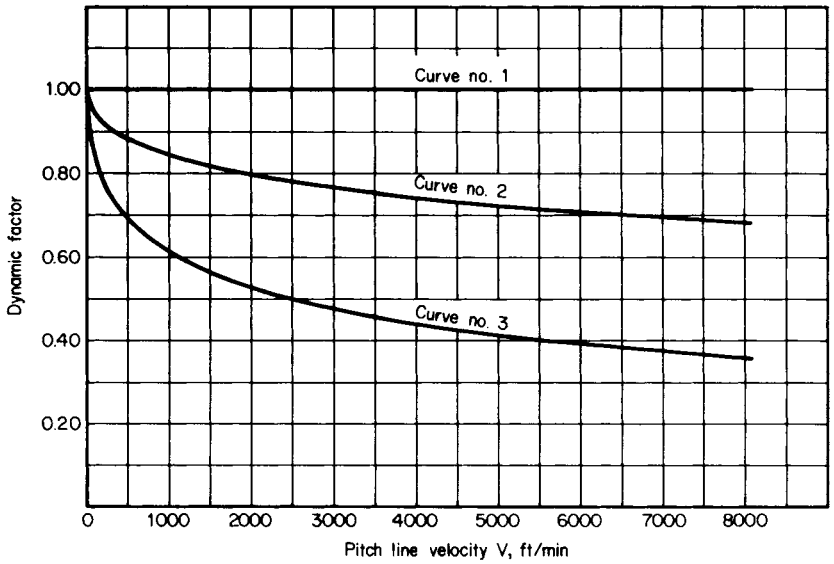

FIGURE 11.18 Dynamic factors K_v and C_v.

The load-distribution factor allows for misalignment of the gear set under operating conditions. This factor is based on the magnitude of the displacements of the gear and pinion from their theoretical correct locations. Use Table 11.12 as a guide in selecting the load-distribution factor.

The surface-condition factor depends on surface finish as affected by cutting, lapping, and grinding. It also depends on surface treatment such as lubrizing. And C_f can be taken as 1.0 provided good gear manufacturing practices are followed.

Use Table 11.13 to locate the charts for the two geometry factors I and J.

The geometry factor for durability I takes into consideration the relative radius of curvature between mating tooth surfaces, load location, load sharing, effective face width, and inertia factor.

The geometry factor for strength J takes into consideration the tooth form factor, load location, load distribution, effective face width, stress correction factor, and inertia factor.

TABLE 11.12 Load-Distribution Factors K_m, C_m

Application	Both members straddle-mounted	One member straddle-mounted	Neither member straddle-mounted
General industrial	1.00–1.10	1.10–1.25	1.25–1.40
Automotive	1.00–1.10	1.10–1.25	
Aircraft	1.00–1.25	1.10–1.40	1.25–1.50

TABLE 11.13 Location of Geometry Factors

				Figure no.	
Gear type	Pressure angle, ϕ	Shaft angle, Σ	Helix angle, ψ	*I* Factor	*J* Factor
Straight bevel	20°	90°	0°	11.19	11.20
	25°	90°	0°	11.21	11.22
Spiral bevel	20°	90°	35°	11.23	11.24
	20°	90°	25°	11.25	11.26
	20°	90°	15°	11.27	11.28
	25°	90°	35°	11.29	11.30
	20°	60°	35°	11.31	11.32
	20°	120°	35°	11.33	11.34
	20°†	90°	35°	11.35	11.36
Hypoid	19°	$E/D = 0.10$		11.37	11.38
	19°	$E/D = 0.15$		11.39	11.40
	19°	$E/D = 0.20$		11.41	11.42
	22½°	$E/D = 0.10$		11.43	11.44
	22½°	$E/D = 0.15$		11.45	11.46
	22½°	$E/D = 0.20$		11.47	11.48

† Automotive applications.

Interpolation between charts may be necessary for both the *I* and *J* factors.

11.6.3 Allowable Stresses

The maximum allowable stresses are based on the properties of the material. They vary with the material, heat treatment, and surface treatment. Table 11.14 gives nominal values for allowable contact stress on gear teeth for commonly used gear materials and heat treatments. Table 11.15 gives nominal values for allowable bending stress in gear teeth for commonly used gear materials and heat treatments.

Carburized case-hardened gears require a core hardness in the range of 260 to 350 H_B (26 to 37 R_C) and a total case depth in the range shown by Fig. 11.49.

The calculated contact stress S_c times a safety factor should be less than the allowable contact stress S_{ac}. The calculated bending stress S_t times a safety factor should be less than the allowable bending stress S_{at}.

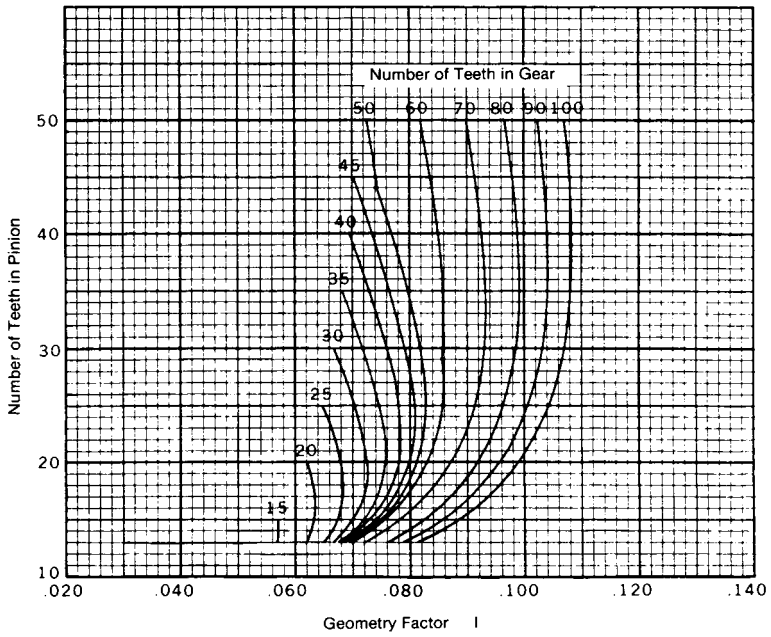

FIGURE 11.19 Geometry factor *I* for durability of straight-bevel gears with 20° pressure angle and 90° shaft angle.

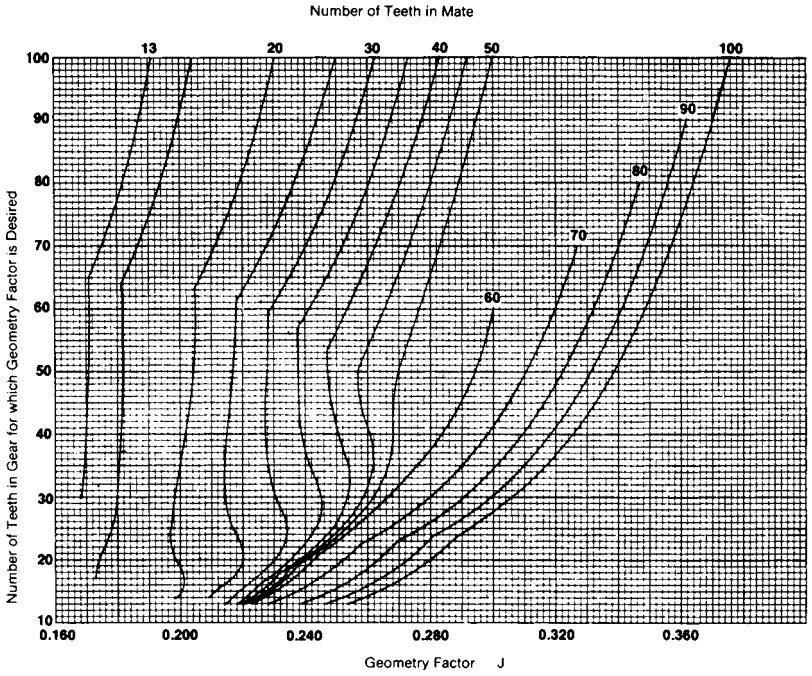

FIGURE 11.20 Geometry factor *J* for strength of straight-bevel gears with 20° pressure angle and 90° shaft angle.

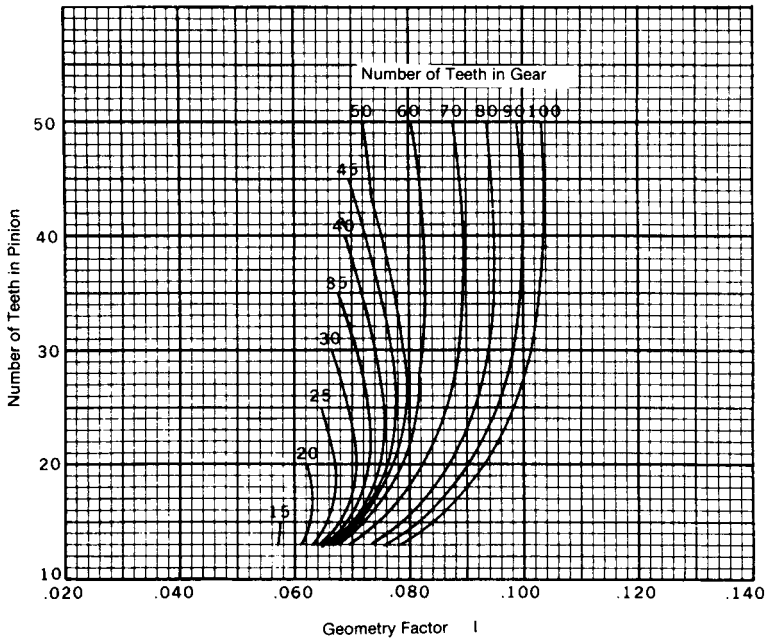

FIGURE 11.21 Geometry factor *I* for durability of straight-bevel gears with 25° pressure angle and 90° shaft angle.

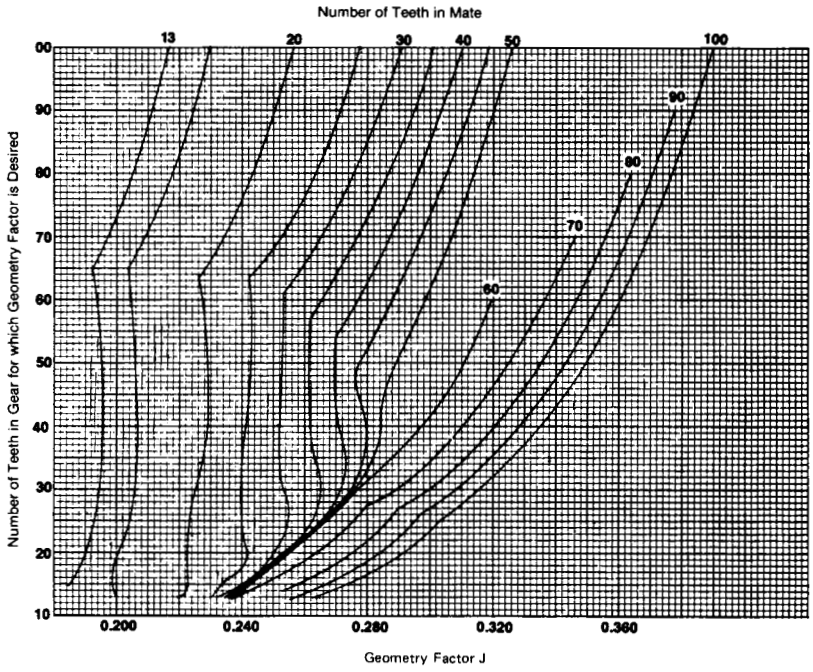

FIGURE 11.22 Geometry factor *J* for strength of straight-bevel gears with 25° pressure angle and 90° shaft angle.

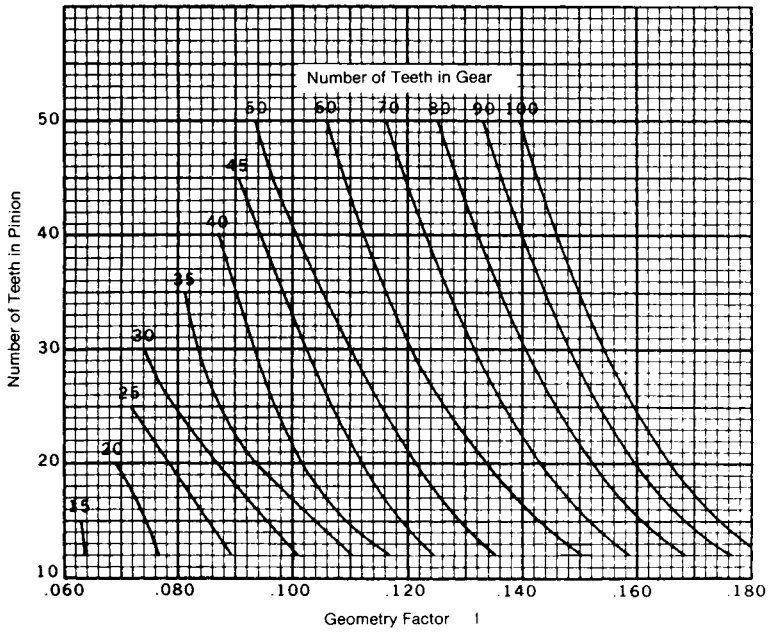

FIGURE 11.23 Geometry factor *I* for durability of spiral-bevel gears with 20° pressure angle, 35° spiral angle, and 90° shaft angle.

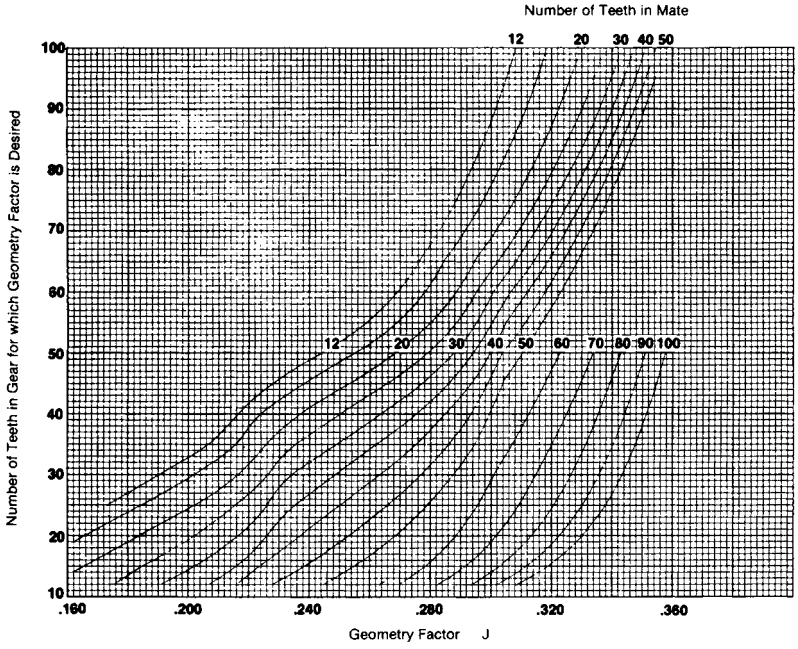

FIGURE 11.24 Geometry factor *J* for strength of spiral-bevel gears with 20° pressure angle, 35° spiral angle, and 90° shaft angle.

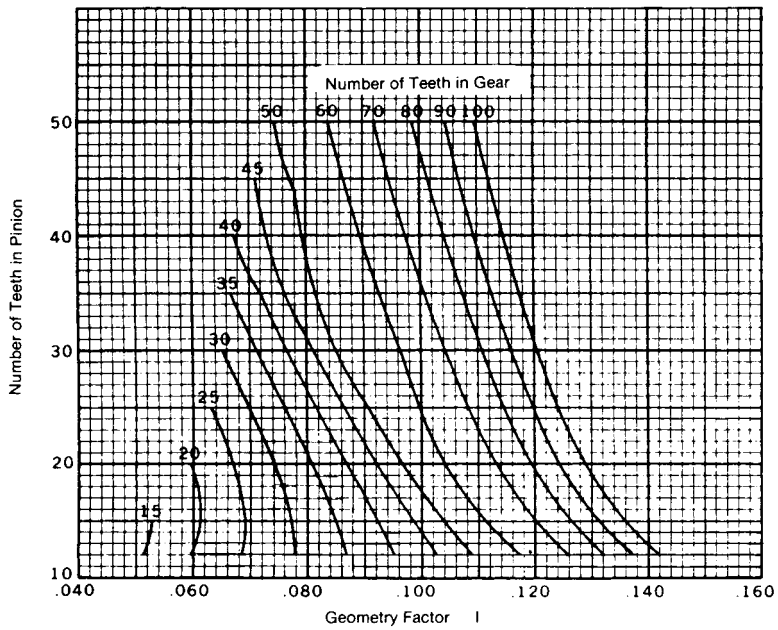

FIGURE 11.25 Geometry factor *I* for durability of spiral-bevel gears with 20° pressure angle, 25° spiral angle, and 90° shaft angle.

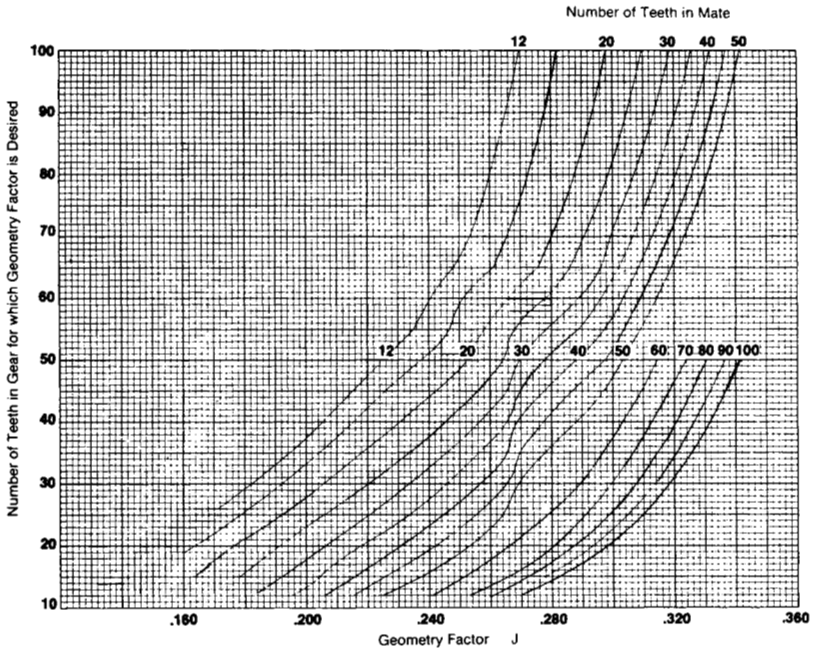

FIGURE 11.26 Geometry factor *J* for strength of spiral-bevel gears with 20° pressure angle, 25° spiral angle, and 90° shaft angle.

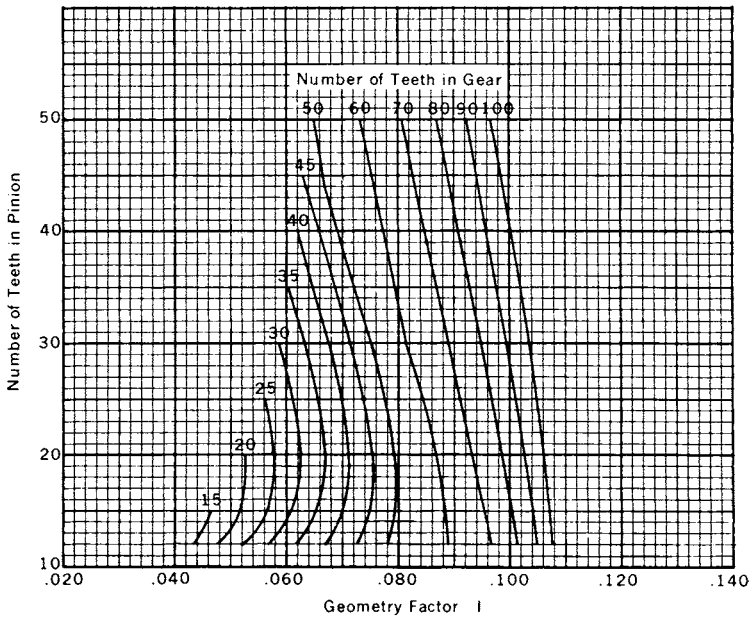

FIGURE 11.27 Geometry factor *I* for durability of spiral-bevel gears with 20° pressure angle, 15° spiral angle, and 90° shaft angle.

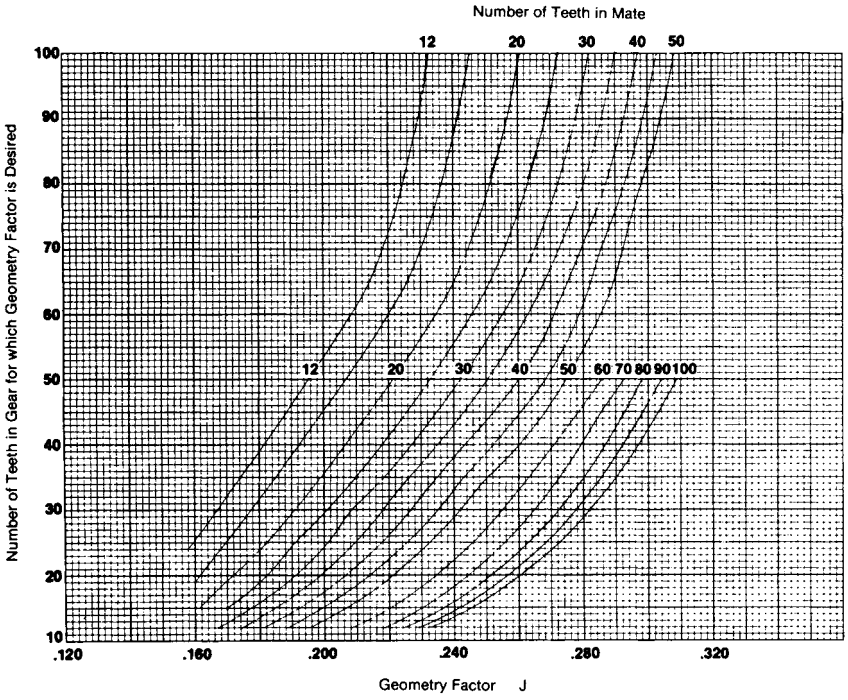

FIGURE 11.28 Geometry factor *J* for strength of spiral-bevel gears with 20° pressure angle, 15° spiral angle, and 90° shaft angle.

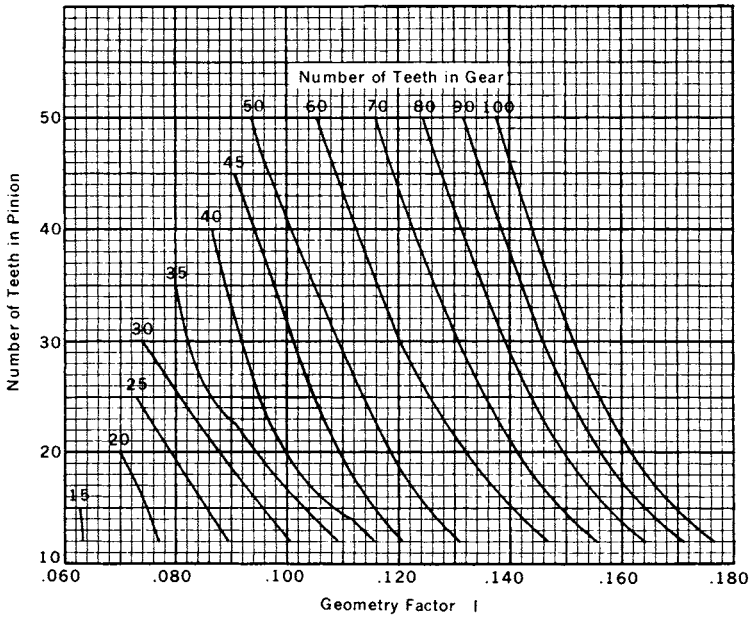

FIGURE 11.29 Geometry factor *I* for durability of spiral-bevel gears with 25° pressure angle, 35° spiral angle, and 90° shaft angle.

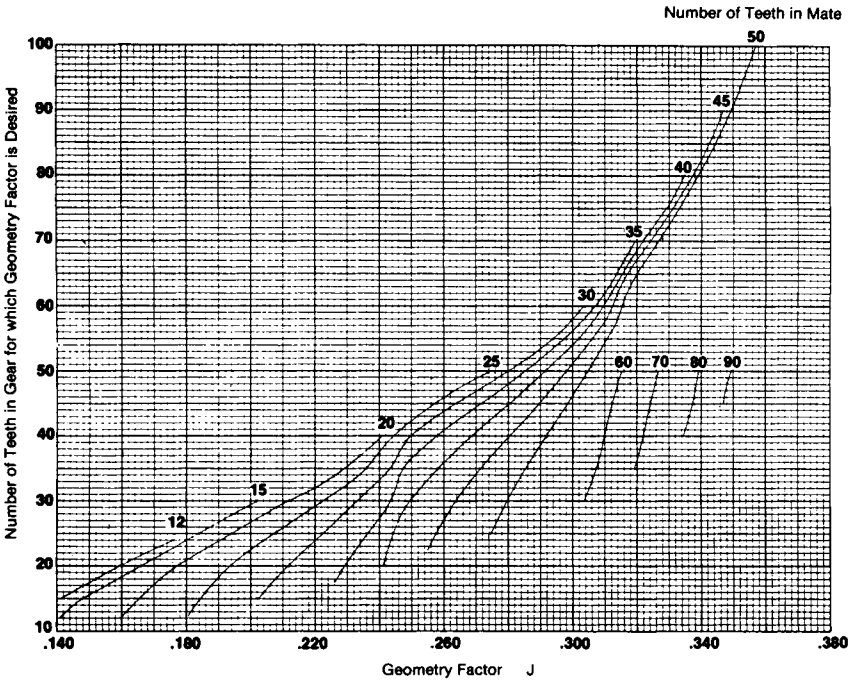

FIGURE 11.30 Geometry factor *J* for strength of spiral-bevel gears with 25° pressure angle, 35° spiral angle, and 90° shaft angle.

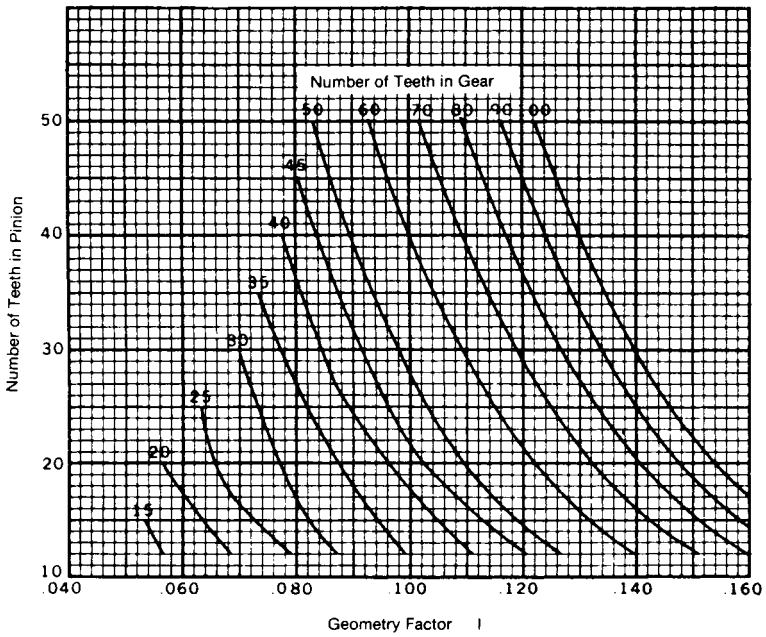

FIGURE 11.31 Geometry factor *I* for durability of spiral-bevel gears with 20° pressure angle, 35° spiral angle, and 60° shaft angle.

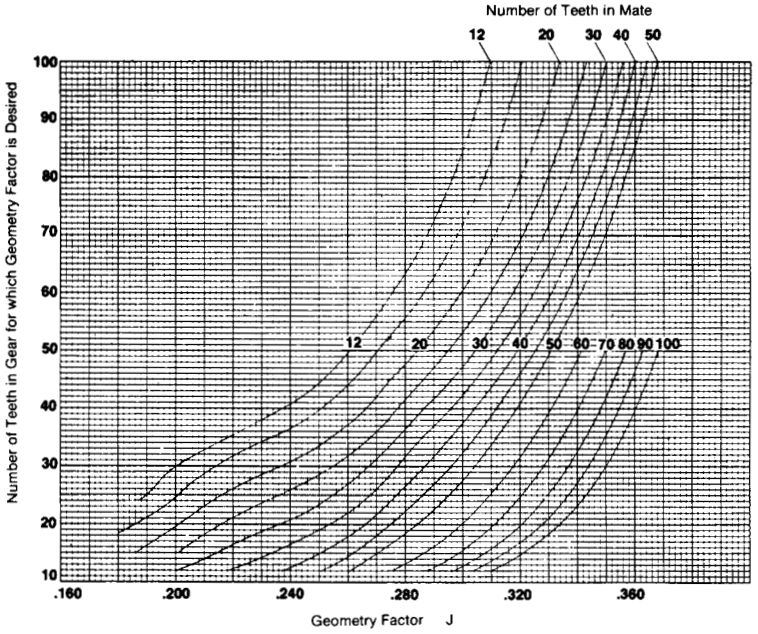

FIGURE 11.32 Geometry factor *J* for strength of spiral-bevel gears with 20° pressure angle, 35° spiral angle, and 60° shaft angle.

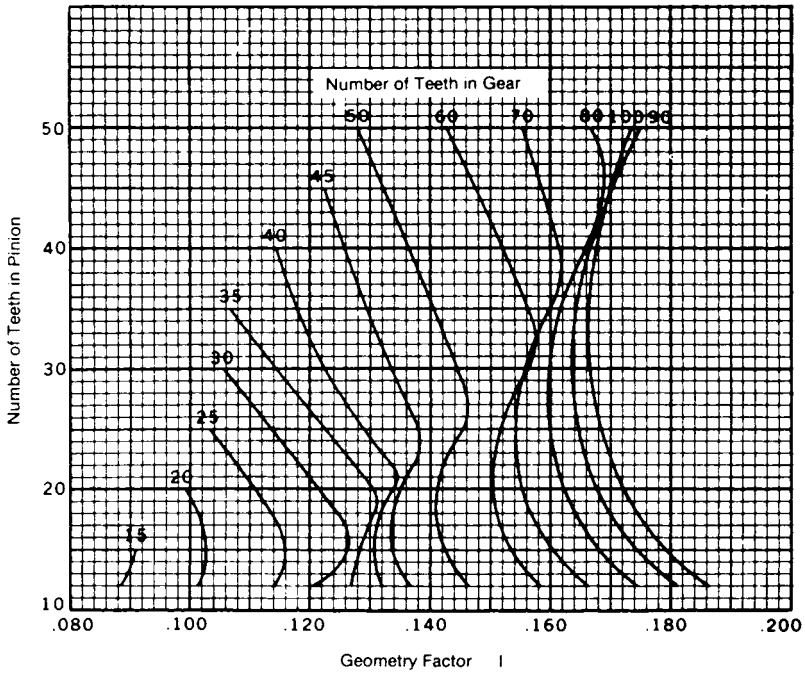

FIGURE 11.33 Geometry factor *I* for durability of spiral-bevel gears with 20° pressure angle, 35° spiral angle, and 120° shaft angle.

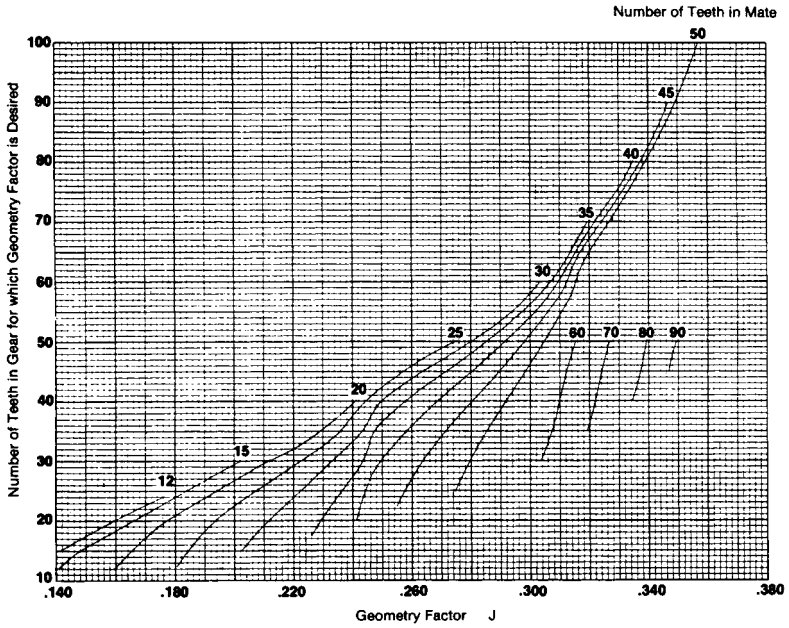

FIGURE 11.34 Geometry factor *J* for strength of spiral-bevel gears with 20° pressure angle, 35° spiral angle, and 120° shaft angle.

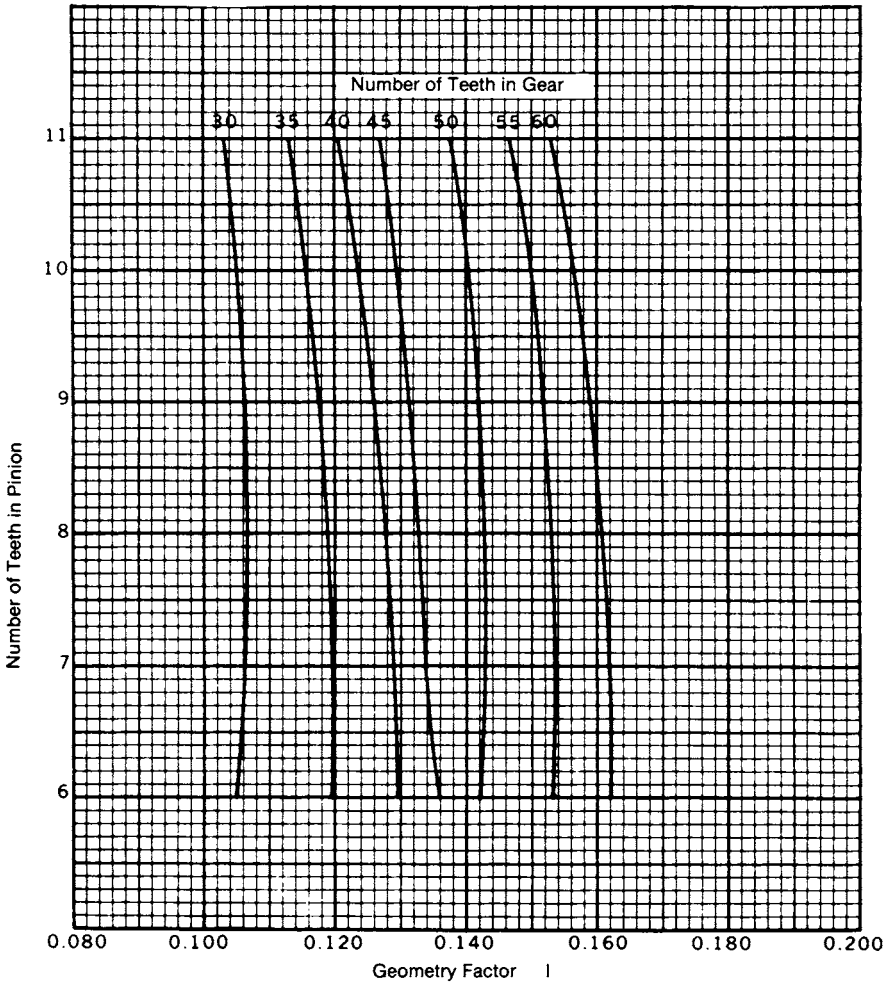

FIGURE 11.35 Geometry factor *I* for durability of automotive spiral-bevel gears with 20° pressure angle, 35° spiral angle, and 90° shaft angle.

11.6.4 Scoring Resistance

Scoring is a temperature-related process in which the surfaces actually tend to weld together. The oil film breaks down, and the tooth surfaces roll and slide on one another, metal against metal. Friction between the surfaces causes heat which reaches the melting point of the tooth material, and scoring results. The factors which could cause scoring are the sliding velocity, surface finish, and load concentrations along with the lubricant temperature, viscosity, and application. But see also Chap. 34. If you follow the recommendations under Sec. 11.7.6 on lubrication and the manufacturer uses acceptable practices in processing the gears, then scoring should not be a problem.

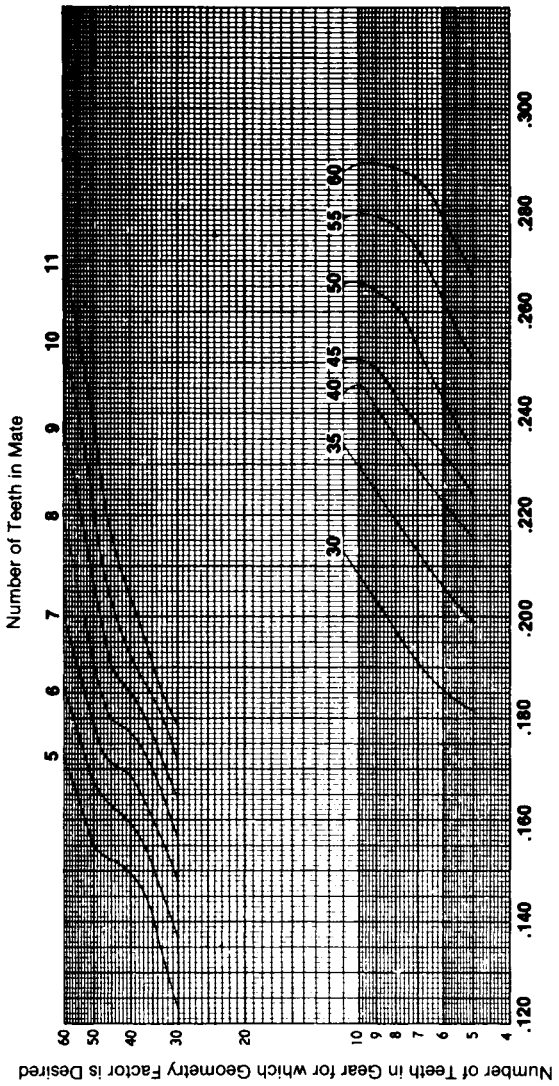

FIGURE 11.36 Geometry factor J for strength of automotive spiral-bevel gears with 20° pressure angle, 35° spiral angle, and 90° shaft angle.

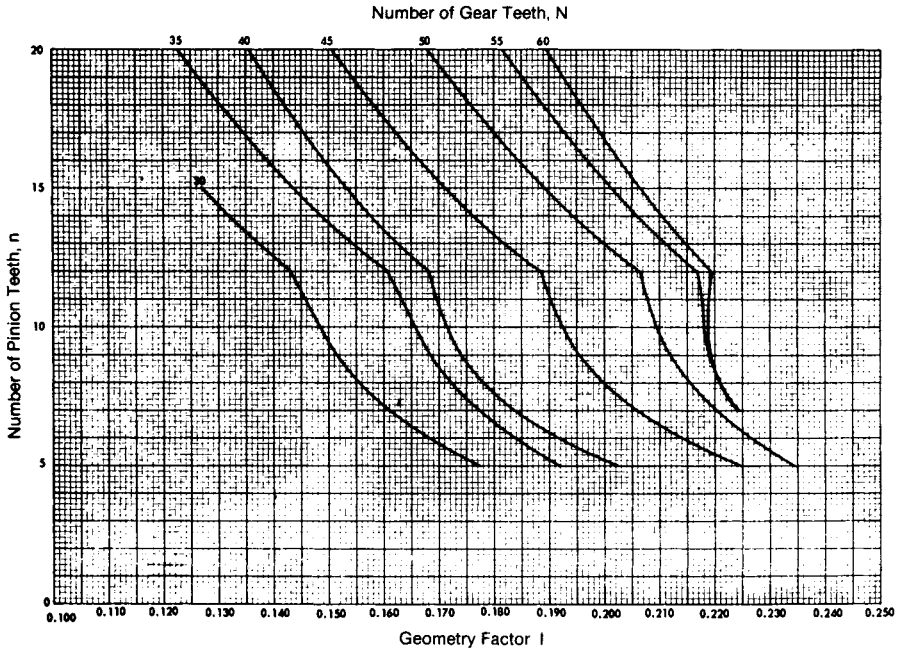

FIGURE 11.37 Geometry factor *I* for hypoid gears with 19° average pressure angle and *E*/*D* ratio of 0.10.

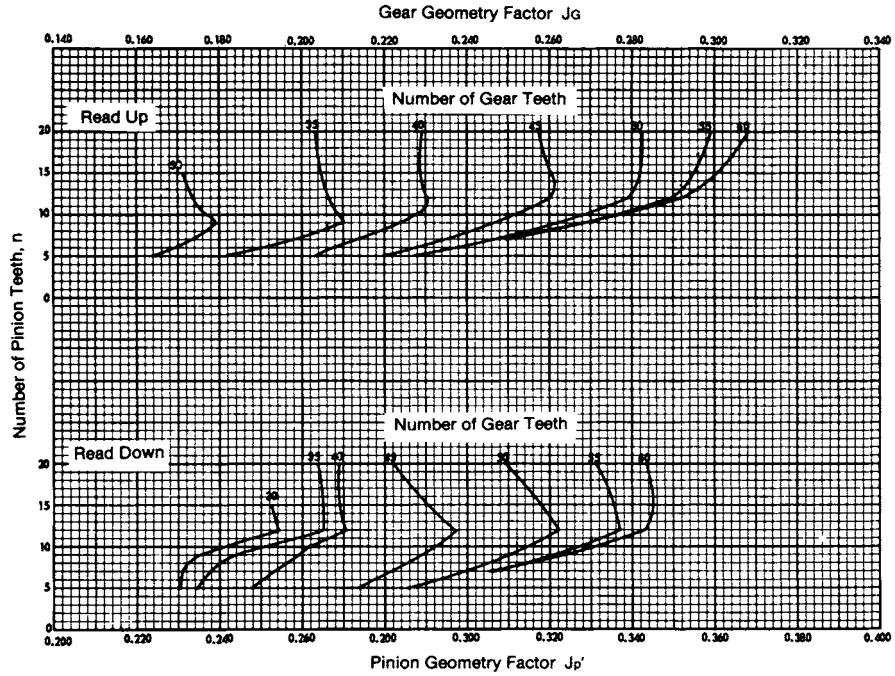

FIGURE 11.38 Geometry factor *J* for strength of hypoid gears with 19° average pressure angle and *E*/*D* ratio of 0.10.

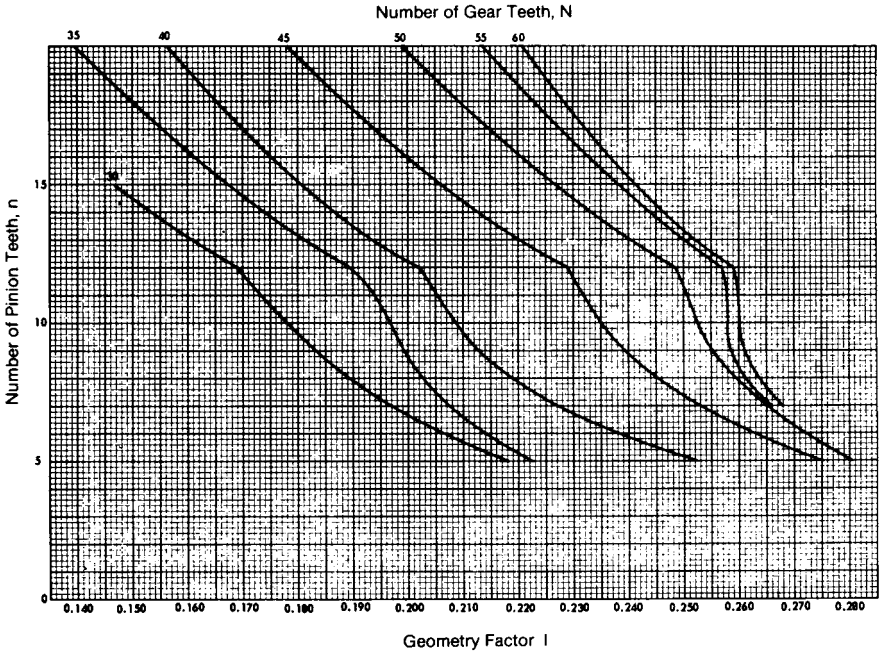

FIGURE 11.39 Geometry factor *I* for durability of hypoid gears with 19° average pressure angle and *E*/*D* ratio of 0.15.

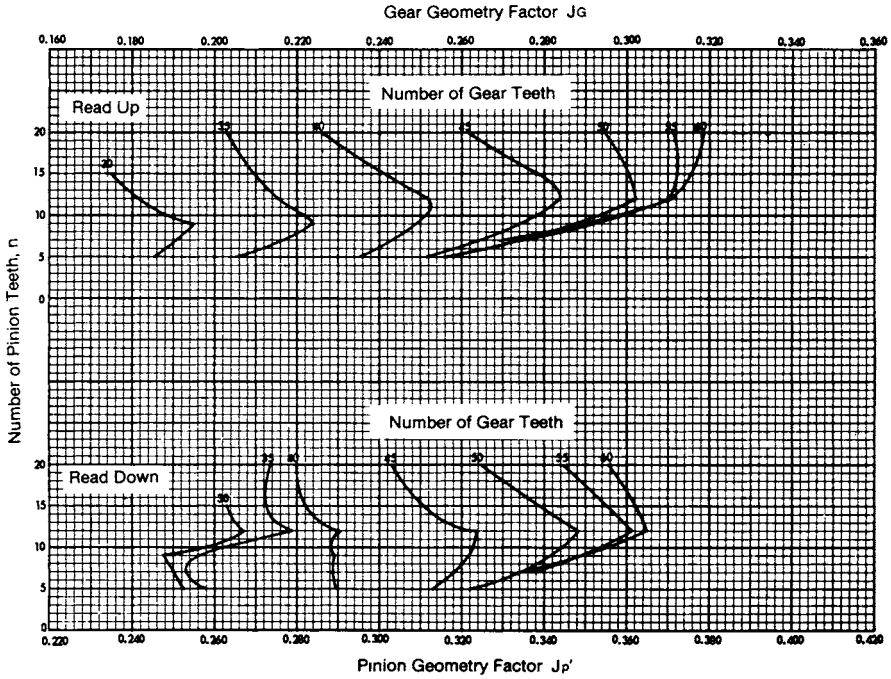

FIGURE 11.40 Geometry factor *J* for strength of hypoid gears with 19° average pressure angle and *E*/*D* ratio of 0.15.

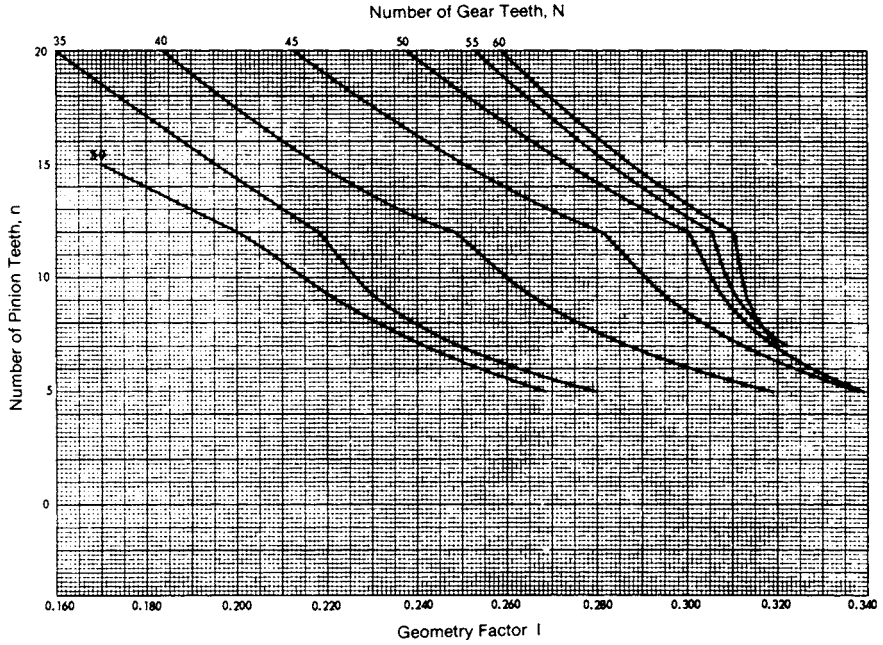

FIGURE 11.41 Geometry factor *I* for durability of hypoid gears with 19° average pressure angle and *E*/*D* ratio of 0.20.

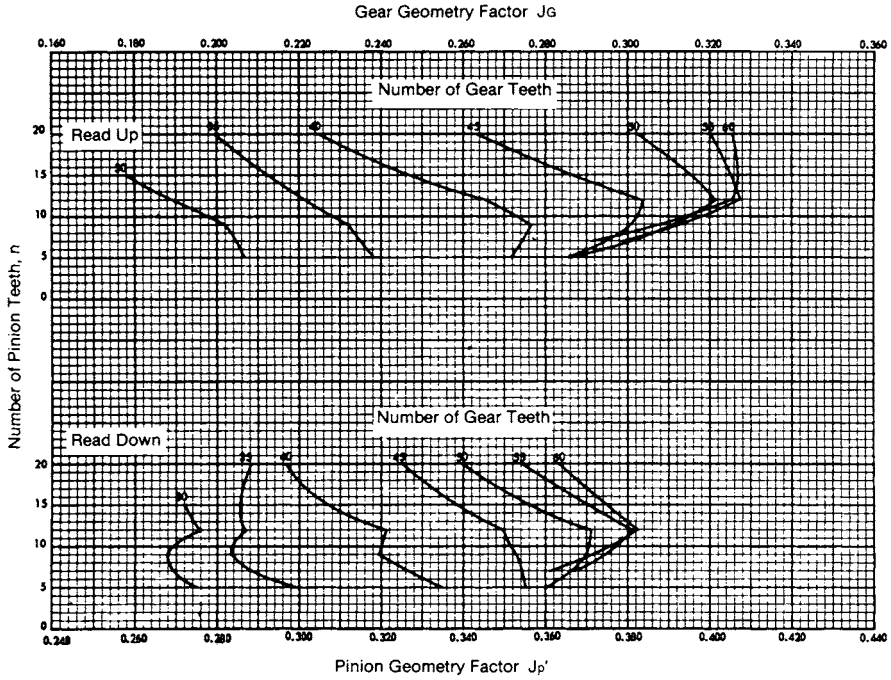

FIGURE 11.42 Geometry factor *J* for strength of hypoid gears with 19° average pressure angle and *E*/*D* ratio of 0.20.

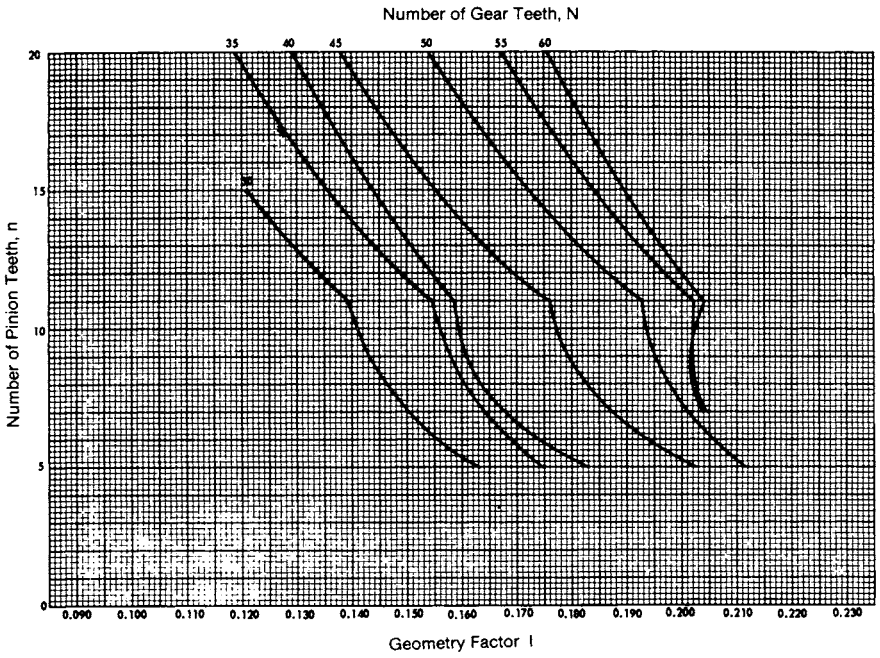

FIGURE 11.43 Geometry factor *I* for durability of hypoid gears with 22½° average pressure angle and *E*/*D* ratio of 0.10.

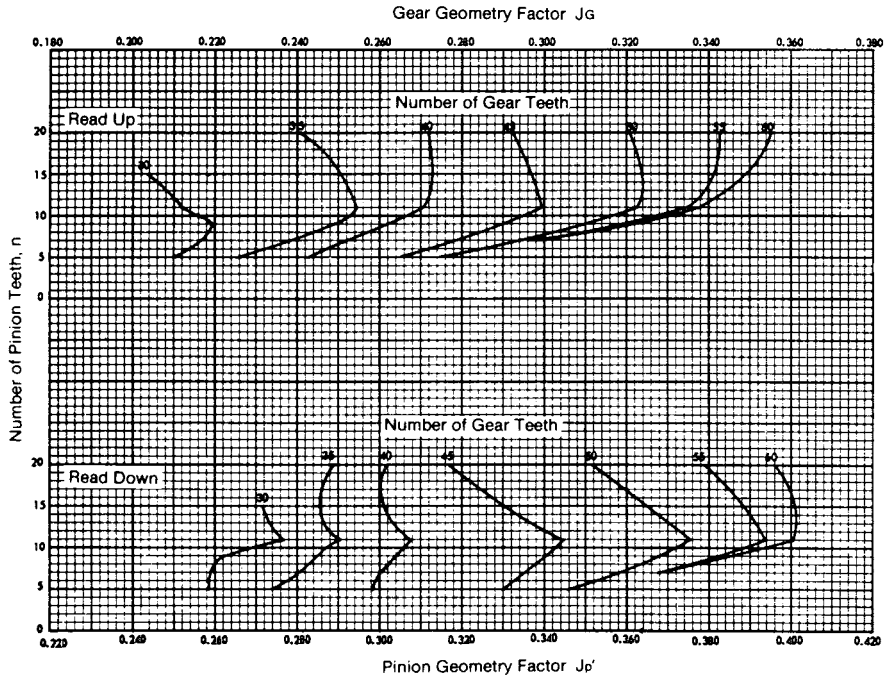

FIGURE 11.44 Geometry factor *J* for strength of hypoid gears with 22½° average pressure angle and *E*/*D* ratio of 0.10.

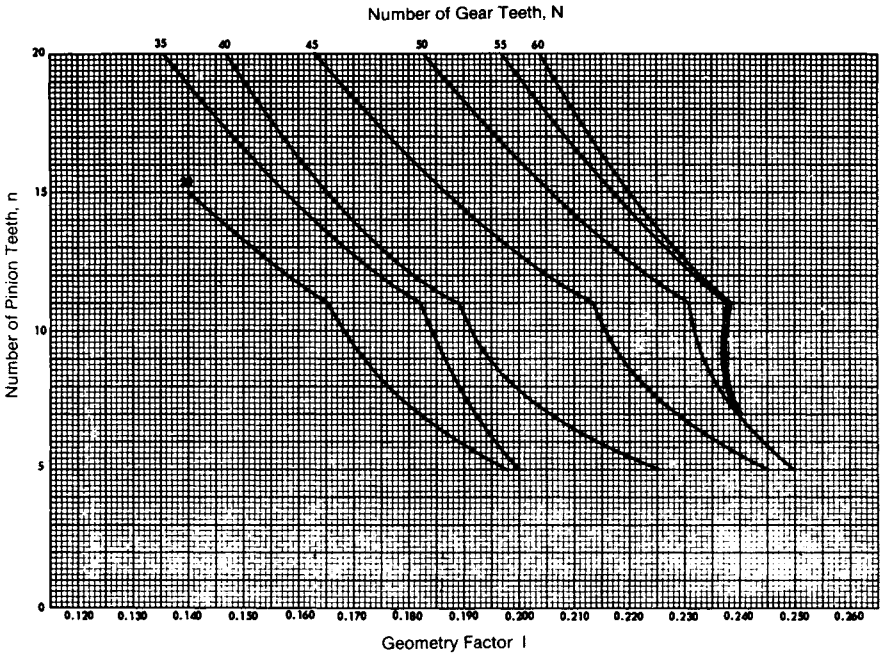

FIGURE 11.45 Geometry factor I for durability of hypoid gears with 22½° average pressure angle and E/D ratio of 0.15.

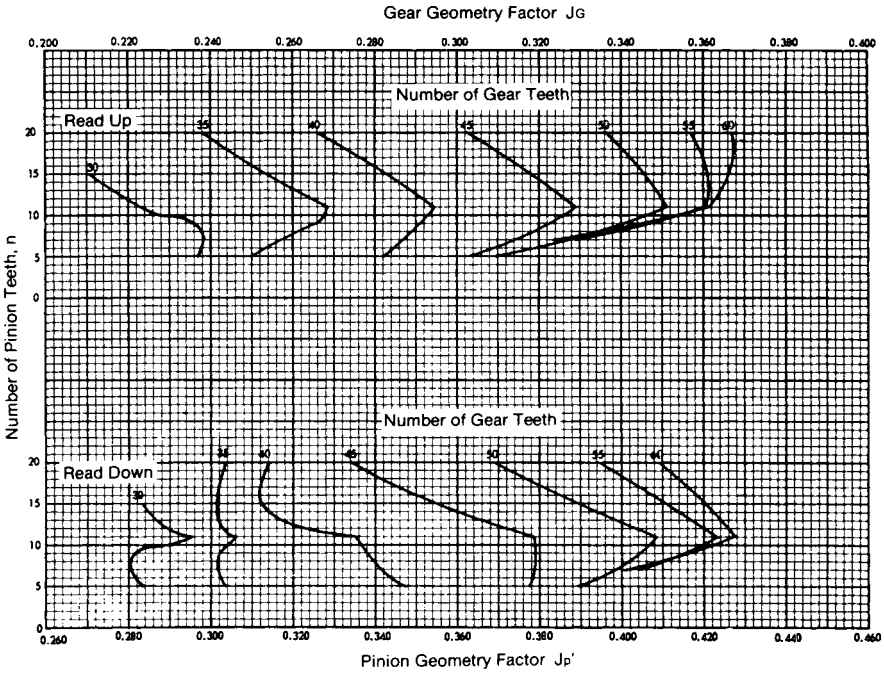

FIGURE 11.46 Geometry factor J for strength of hypoid gears with 22½° average pressure angle and E/D ratio of 0.15.

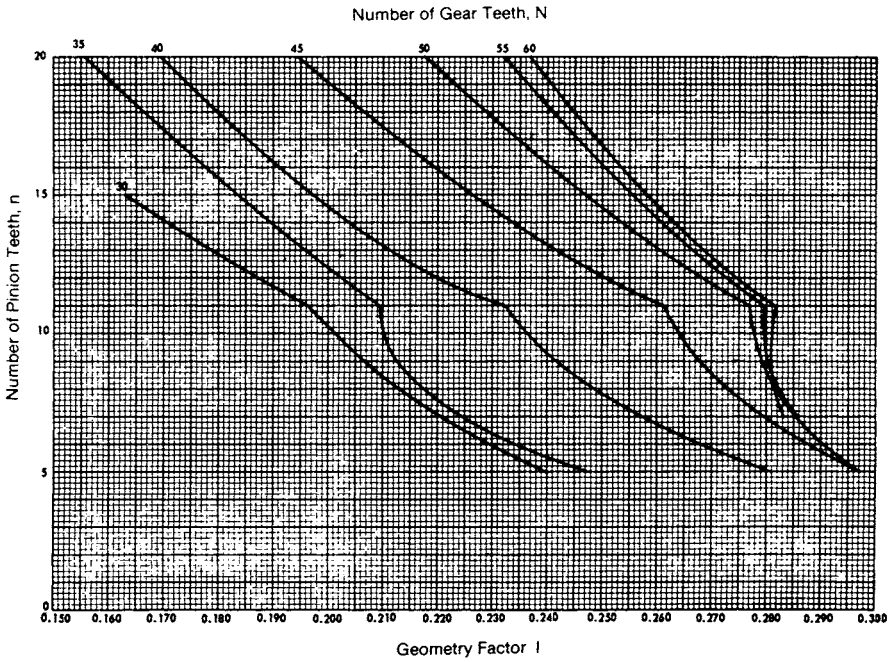

FIGURE 11.47 Geometry factor *I* for durability of hypoid gears with 22½° average pressure angle and *E*/*D* ratio of 0.20.

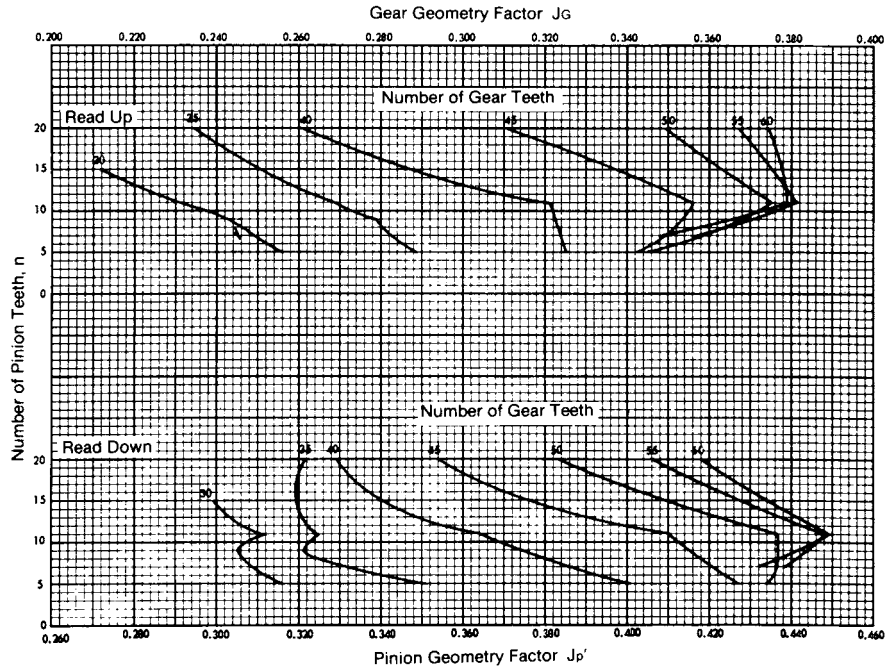

FIGURE 11.48 Geometry factor *J* for strength of hypoid gears with 22½° average pressure angle and *E*/*D* ratio of 0.20.

TABLE 11.14 Allowable Contact Stress S_{ac}

Material	Heat treatment	Minimum hardness		Contact stress S_{ac}, lb/in^2
		Brinell	Rockwell C	
Steel	Carburized (case-hardened)		60	250 000
Steel	Carburized (case-hardened)		55	210 000
Steel	Flame- or induction-hardened	500	50	200 000
Steel and nodular iron	Hardened and tempered	400		180 000
Steel	Nitrided		60	180 000
Steel and nodular iron	Hardened and tempered	300		140 000
Steel and nodular iron	Hardened and tempered	180		100 000
Cast iron	As cast	200		80 000
Cast iron	As cast	175		70 000
Cast iron	As cast			60 000

11.7 DESIGN OF MOUNTINGS

The normal load on the tooth surfaces of bevel and hypoid gears may be resolved into two components: one in the direction along the axis of the gear and the other perpendicular to the axis. The direction and magnitude of the normal load depend on the ratio, pressure angle, spiral angle, hand of spiral, and direction of rotation as well as on whether the gear is the driving or driven member.

11.7.1 Hand of Spiral

In general, a left-hand pinion driving clockwise (viewed from the back) tends to move axially away from the cone center; a right-hand pinion tends to move toward the center because of the oblique direction of the curved teeth. If possible, the hand of spiral should be selected so that both the pinion and the gear tend to move out of mesh, which prevents the possibility of tooth wedging because of reduced backlash. Otherwise, the hand of spiral should be selected to give an axial thrust that tends to move the pinion out of mesh. In a reversible drive, there is no choice unless the pair performs a heavier duty in one direction for a greater part of the time.

BEVEL AND HYPOID GEARS

TABLE 11.15 Allowable Bending Stress S_{at}

Material	Heat treatment	Surface hardness		Bending stress S_{at}, lb/in^2
		Brinell	Rockwell C	
Steel	Carburized (case-hardened)	575–625	55 min.	60 000
Steel	Flame- or induction-hardened (unhardened root fillet)	450–500	50 min.	27 000
Steel	Hardened and tempered	450 min.		50 000
Steel	Hardened and tempered	300 min.		42 000
Steel	Hardened and tempered	180 min.		28 000
Steel	Normalized	140 min.		22 000
Cast iron	As cast	200 min.		13 000
Cast iron	As cast	175 min.		8 500
Cast iron	As cast			5 000

On hypoids when the pinion is below center and to the right (when you are facing the front of the gear), the pinion hand of spiral should always be left-hand. With the pinion above center and to the right, the pinion hand should always be right-hand. See Fig. 11.15.

11.7.2 Tangential Force

The tangential force on a bevel or hypoid gear is given by

$$W_{tG} = \frac{2T_G}{D_m} = \frac{126\,000P}{D_m N} \tag{11.4}$$

where T_G = gear torque, lb · in
P = power, horsepower (hp)
N = speed of gear, r/min

The tangential force on the mating pinion is given by the equation

$$W_{tP} = \frac{W_{tG} \cos \psi_P}{\cos \psi_G} = \frac{2T_P}{d_m} \tag{11.5}$$

where T_P = pinion torque in pound-inches.

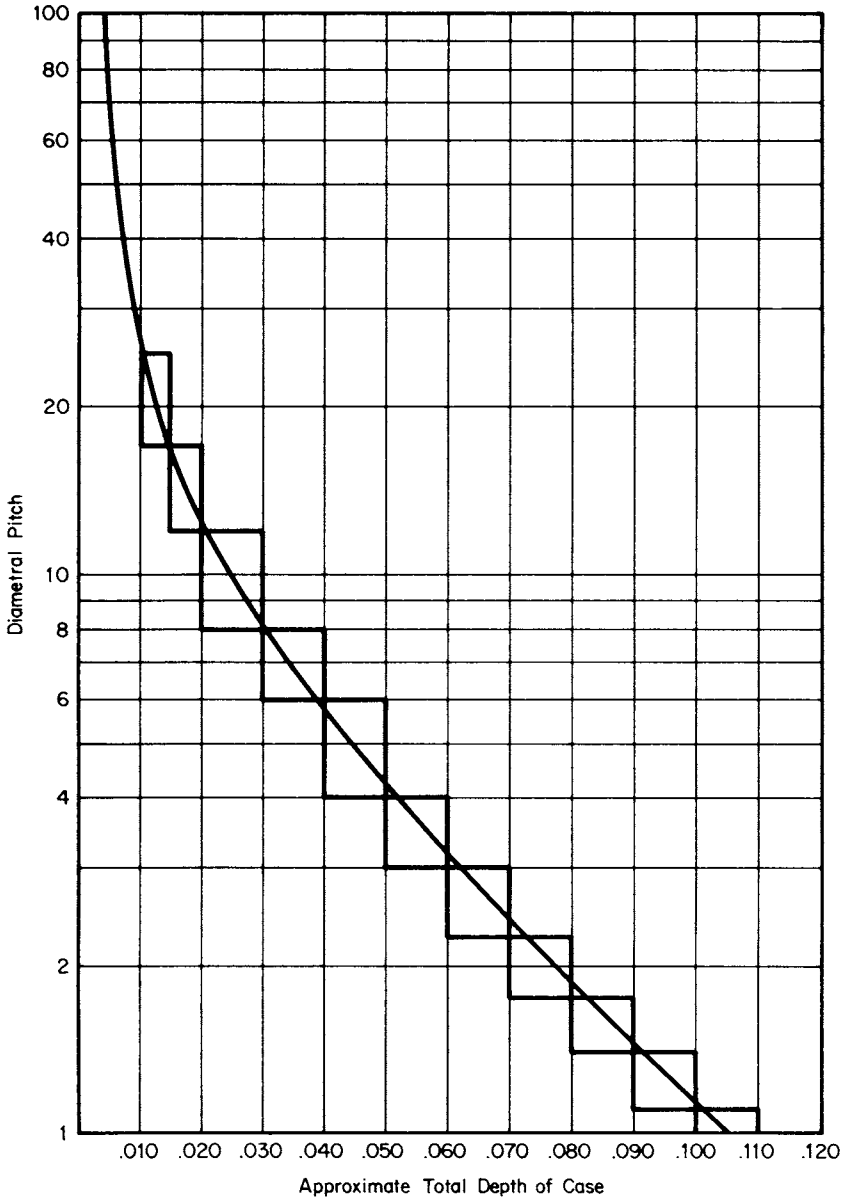

FIGURE 11.49 Diametral pitch versus total case depth. If in doubt, use the greater case depth on ground gears or on short face widths.

11.7.3 Axial Thrust and Radial Separating Forces

The formulas that follow are used to calculate the *axial thrust force* W_x and the *radial separating force* W_R for bevel and hypoid gears. The direction of the pinion (driver) rotation should be viewed from the pinion back.

For a pinion (driver) with a *right-hand* (*RH*) *spiral with clockwise* (*cw*) *rotation* or a *left-hand* (*LH*) *spiral with counterclockwise* (*ccw*) *rotation,* the axial and separating force components *acting on the pinion* are, respectively,

$$W_{xP} = W_{tP} \sec \psi_P (\tan \phi \sin \gamma - \sin \psi_P \cos \gamma) \tag{11.6}$$

$$W_{RP} = W_{tP} \sec \psi_P (\tan \phi \cos \gamma + \sin \psi_P \sin \gamma) \tag{11.7}$$

For a pinion (driver) with an *LH spiral with cw rotation* or an *RH spiral with ccw rotation,* the force components *acting on the pinion* are, respectively,

$$W_{xP} = W_{tP} \sec \psi_P (\tan \phi \sin \gamma + \sin \psi_P \cos \gamma) \tag{11.8}$$

$$W_{RP} = W_{tP} \sec \psi_P (\tan \phi \cos \gamma - \sin \psi_P \sin \gamma) \tag{11.9}$$

For a pinion (driver) with an *RH spiral with cw rotation* or an *LH spiral with ccw rotation,* the force components *acting on the gear* (driven) are, respectively,

$$W_{xG} = W_{tG} \sec \psi_G (\tan \phi \sin \Gamma + \sin \psi_G \cos \Gamma) \tag{11.10}$$

$$W_{RG} = W_{tG} \sec \psi_G (\tan \phi \cos \Gamma - \sin \psi_G \sin \Gamma) \tag{11.11}$$

For a pinion (driver) with an *LH spiral and cw rotation* or an *RH spiral with ccw rotation,* the force components *acting on the gear* are, respectively,

$$W_{xG} = W_{tG} \sec \psi_G (\tan \phi \sin \Gamma - \sin \psi_G \cos \Gamma) \tag{11.12}$$

$$W_{RG} = W_{tG} \sec \psi_G (\tan \phi \cos \Gamma + \sin \psi_G \sin \Gamma) \tag{11.13}$$

These equations apply to straight-bevel, Zerol bevel, spiral-bevel, and hypoid gears. When you use them for hypoid gears, be sure that the pressure angle corresponds to the driving face of the pinion tooth.

A plus sign for Eqs. (11.6), (11.8), (11.10), and (11.12) indicates that the direction of the axial thrust is *outward,* or away from the cone center. Thus a minus sign indicates that the direction of the axial thrust is *inward,* or toward the cone center.

A plus sign for Eqs. (11.7), (11.9), (11.11), and (11.13) indicates that the direction of the *separating* force is *away* from the mating gear. So a minus sign indicates an *attracting* force *toward* the mating member.

Example. A hypoid-gear set consists of an 11-tooth pinion with LH spiral and ccw rotation driving a 45-tooth gear. Data for the gear are as follows: 4.286 diametral pitch, 8.965-inch (in) mean diameter, 70.03° pitch angle, 31.48° spiral angle, and 30×10^3 lb · in torque. Pinion data are these: 1.500-in offset, 2.905-in mean diameter, concave pressure angle 18.13°, convex pressure angle 21.87°, pitch angle 19.02°, and spiral angle 50°. Determine the force components and their directions for each member of the set.

Solution. From Eq. (11.4) we find the tangential load on the gear to be

$$W_{tG} = \frac{2T_G}{D_m} = \frac{2(30 \times 10^3)}{8.965} = 6693 \text{ lb}$$

Since the pinion has LH spiral angle and rotates ccw, Eqs. (11.10) and (11.11) apply for the gear. Thus

$$W_{xG} = W_{tG} \sec \psi_G (\tan \phi \sin \Gamma + \sin \psi_G \cos \Gamma)$$

$$= 6693 \sec 31.48 (\tan 18.13° \sin 70.03° + \sin 31.48° \cos 70.03°)$$

$$= 3814 \text{ lb}$$

Substituting the same values and angles into Eq. (11.11) gives $W_{RG} = -2974$ lb. Thus the thrust is outward, and the separating force is toward the mating member.

Next we find the tangential load on the pinion from Eq. (11.5):

$$W_{tP} = \frac{W_{tG} \cos \psi_P}{\cos \psi_G} = \frac{6693 \cos 50°}{\cos 31.48°} = 5045 \text{ lb}$$

Equations (11.6) and (11.7) apply to the pinion:

$$W_{xP} = W_{tP} \sec \psi_P (\tan \phi \sin \gamma - \sin \psi_P \cos \gamma)$$

$$= 5045 \sec 50° (\tan 18.13° \sin 19.02° - \sin 50° \cos 19.02°)$$

$$= -4846 \text{ lb}$$

In a similar manner, Eq. (11.7) gives $W_{RP} = 4389$ lb. Thus the axial thrust is inward, and the separating force is away from the gear.

11.7.4 Bearing Loads

The bearings selected must be adequate to support the axial forces W_x for both directions of rotation and for the load conditions on both sides of the teeth.

Radial forces are transmitted indirectly through moment arms to the bearings. The radial bearing loads are derived from the gear separating force, the gear tangential force, and the gear thrust couple, along with the type of mounting and the bearing position.

11.7.5 Types of Mountings

Two types of mountings are generally used: *overhung,* where both bearings are located on the shaft behind the gear, and *straddle,* where one bearing is on either side of the gear. Because of the stiffer configuration, straddle mountings are generally used for highly loaded gears.

11.7.6 Lubrication

The lubrication system for a bevel- or hypoid-gear drive should sufficiently lubricate and adequately cool the gears and bearings. Splash lubrication is generally satisfactory for applications up to peripheral speeds of 2000 ft/min. The oil level should cover the full face of the lowest gear, and the quantity of oil should be sufficient to maintain the oil temperature within recommended limits.

Pressure lubrication is recommended for velocities above 2000 ft/min. The jets should be located to direct the stream to cover the full length of the teeth of both members, preferably close to the mesh point on the leaning side.

Experience has shown that an oil flow of 0.07 to 1.0 gallons per minute (gal/min) per 100 hp will result in an oil temperature rise of approximately 10°F.

Extreme-pressure (EP) lubricants are recommended for hypoid gears and for spiral-bevel gears which are subject to extreme conditions of shock, severe starting conditions, or heavy loads. The lubrication system should be fully protected against contamination by moisture or dirt. For continuous operation at temperatures above 160°F, the lubricants should be approved by the lubricant manufacturer.

In general, for a splash lubrication, an SAE 80 or 90 gear oil should be satisfactory. For a circulating system with an oil spray lubrication, SAE 20 or 30 should be satisfactory. AGMA "Specifications on Lubrication of Enclosed and Open Gearing" is a recommended guide to the type and grade of oil for various operating conditions.

11.7.7 Loaded Contact Check

With highly stressed bevel- and hypoid-gear applications such as aircraft and automotive, it is normal practice to perform a loaded contact check with the gear set assembled in its mountings. A brake load is applied to the output shafts, and the pinion member is rotated slowly at approximately 15 r/min. A marking compound is applied to the pinion and gear teeth to permit observation of the tooth contact pattern at the desired load conditions. The purpose of this test is to evaluate the rigidity of the mountings and ensure that the contact pattern remains within the tooth boundaries under all load conditions. Indicators can be mounted at various positions under load. An analysis of these data can result in modifications of the mounting design or contact pattern to ensure that the contact pattern does not reach the tooth boundaries at operating loads. This will eliminate an edge contact condition which can cause noise or premature failure of the gear teeth.

CHAPTER 12
WORM GEARING

K. S. Edwards, Ph.D.
Professor of Mechanical Engineering
University of Texas at El Paso
El Paso, Texas

GLOSSARY OF SYMBOLS

b_G	Dedendum of gear teeth
C	Center distance
d	Worm pitch diameter
d_o	Outside diameter of worm
d_R	Root diameter of worm
D	Pitch diameter of gear in central plane
D_b	Base circle diameter
D_o	Outside diameter of gear
D_t	Throat diameter of gear
f	Length of flat on outside diameter of worm
h_k	Working depth of tooth
h_t	Whole depth of tooth
L	Lead of worm
m_G	Gear ratio = N_G/N_W
m_o	Module, millimeters of pitch diameter per tooth (SI use)
m_p	Number of teeth in contact
n_w	Rotational speed of worm, r/min
n_G	Rotational speed of gear, r/min

N_G Number of teeth in gear
N_W Number of threads in worm
p_n Normal circular pitch
p_x Axial circular pitch of worm
P Transverse diametral pitch of gear, teeth per inch of diameter
W Force between worm and gear (various components are derived in the text)
λ Lead angle at center of worm, deg
ϕ_n Normal pressure angle, deg
ϕ_x Axial pressure angle at center of worm, deg

12.1 INTRODUCTION

Worm gears are used for large speed reduction with concomitant increase in torque. They are limiting cases of helical gears, treated in Chap. 10. The shafts are normally perpendicular, though it is possible to accommodate other angles. Consider the helical-gear pair in Fig. 12.1*a* with shafts at 90°.

The lead angles of the two gears are described by λ (lead angle is 90° less the helix angle). Since the shafts are perpendicular, $\lambda_1 + \lambda_2 = 90°$. If the lead angle of gear 1 is made small enough, the teeth eventually wrap completely around it, giving the appearance of a screw, as seen in Fig. 12.1*b.* Evidently this was at some stage taken to resemble a *worm,* and the term has remained. The mating member is called simply the *gear,* sometimes the *wheel.* The helix angle of the gear is equal to the lead angle of the worm (for shafts at 90°).

The worm is always the driver in speed reducers, but occasionally the units are used in reverse fashion for speed increasing. Worm-gear sets are self-locking when the gear cannot drive the worm. This occurs when the tangent of the lead angle is less than the coefficient of friction. The use of this feature in lieu of a brake is not rec-

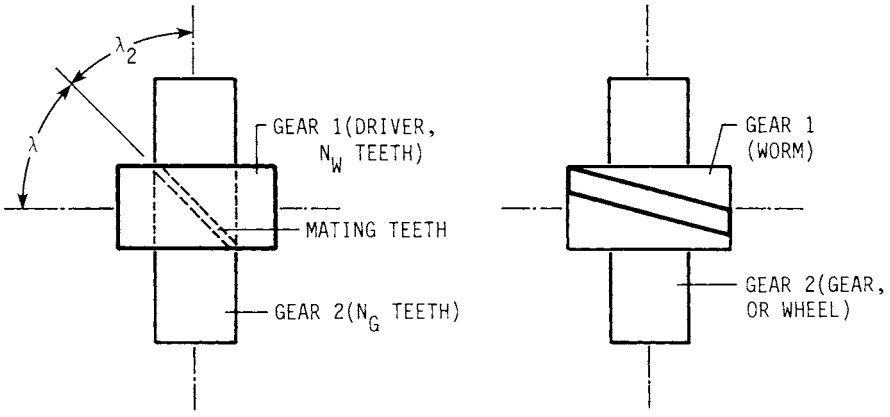

FIGURE 12.1 (*a*) Helical gear pair; (*b*) a small lead angle causes gear one to become a worm.

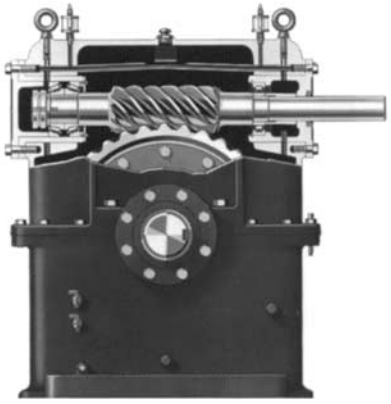

FIGURE 12.2 Photograph of a worm-gear speed reducer. Notice that the gear partially wraps, or envelopes, the worm. *(Cleveland Worm and Gear Company.)*

ommended, since under running conditions a gear set may not be self-locking at lead angles as small as 2°.

There is only point contact between helical gears as described above. Line contact is obtained in worm gearing by making the gear envelop the worm as in Fig. 12.2; this is termed a *single-enveloping gear set,* and the worm is cylindrical. If the worm and gear envelop each other, the line contact increases as well as the torque that can be transmitted. The result is termed a *double-enveloping gear set.*

The minimum number of teeth in the gear and the reduction ratio determine the number of threads (teeth) for the worm. Generally, 1 to 10 threads are used. In special cases a larger number may be required.

12.2 KINEMATICS

In specifying the pitch of worm-gear sets, it is customary to state the axial pitch p_x of the worm. For 90° shafts this is equal to the transverse circular pitch of the gear. The advance per revolution of the worm, termed the lead L, is

$$L = p_x N_W$$

This and other useful relations result from consideration of the developed pitch cylinder of the worm, seen in Fig. 12.3. From the geometry, the following relations can be found:

$$d = \frac{N_W p_n}{\pi \sin \lambda} \tag{12.1}$$

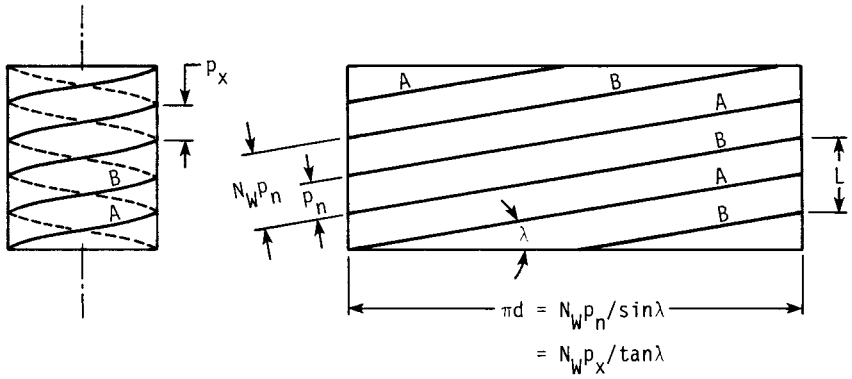

FIGURE 12.3 Developed pitch cylinder of worm.

$$d = \frac{N_W p_x}{\pi \tan \lambda} \tag{12.2}$$

$$\tan \lambda = \frac{L}{\pi d} = \frac{N_W p_x}{\pi d} \tag{12.3}$$

$$p_x = \frac{p_n}{\cos \lambda} \tag{12.4}$$

$$D = \frac{p_x N_G}{\pi} = \frac{N_G p_n}{\pi \cos \lambda} \tag{12.5}$$

From Eqs. (12.1) and (12.5), we find

$$\tan \lambda = \frac{N_W D}{N_G d} = \frac{1}{m_G} \frac{D}{d} \tag{12.6}$$

The center distance C can be derived from the diameters

$$C = \frac{p_n N_W}{2\pi} \left(\frac{m_G}{\cos \lambda} + \frac{1}{\sin \lambda} \right) \tag{12.7}$$

which is sometimes more useful in the form

$$\frac{m_G}{\cos \lambda} + \frac{1}{\sin \lambda} = \begin{cases} \dfrac{2\pi C}{p_n N_W} & \text{U.S. customary units} \\ \dfrac{2C}{m_o N_W \cos \lambda} & \text{SI units} \\ \dfrac{2C}{d \sin \lambda} & \text{either} \end{cases} \tag{12.8}$$

For use in the International System (SI), recognize that

$$\text{Diameter} = N m_o = \frac{N p_x}{\pi}$$

so that the substitution

$$p_x = \pi m_o$$

will convert any of the equations above to SI units.

The pitch diameter of the gear is measured in the plane containing the worm axis and is, as for spur gears,

$$D = \frac{N_G p_x}{\pi} \tag{12.9}$$

The worm pitch diameter is unrelated to the number of teeth. It should, however, be the same as that of the hob used to cut the worm-gear tooth.

12.3 VELOCITY AND FRICTION

Figure 12.4 shows the pitch line velocities of worm and gear. The coefficient of friction between the teeth μ is dependent on the sliding velocity. Representative values of μ are charted in Fig. 12.5. The friction has importance in computing the gear set efficiency, as will be shown.

12.4 FORCE ANALYSIS

If friction is neglected, then the only force exerted by the gear on the worm will be W, perpendicular to the mating tooth surface, shown in Fig. 12.6, and having the three components W^x, W^y, and W^z. From the geometry of the figure,

$$\begin{aligned} W^x &= W \cos \phi_n \sin \lambda \\ W^y &= W \sin \phi_n \\ W^z &= W \cos \phi_n \cos \lambda \end{aligned} \tag{12.10}$$

In what follows, the subscripts W and G refer to forces *on* the worm and the gear. The component W^y is the separating, or radial, force for both worm and gear (opposite in direction for the gear). The tangential force is W^x on the worm and W^z on the gear. The axial force is W^z on the worm and W^x on the gear. The gear forces are opposite to the worm forces:

$$\begin{aligned} W_{W_t} &= -W_{G_a} = W^x \\ W_{W_r} &= -W_{G_r} = W^y \\ W_{W_a} &= -W_{G_t} = W^z \end{aligned} \tag{12.11}$$

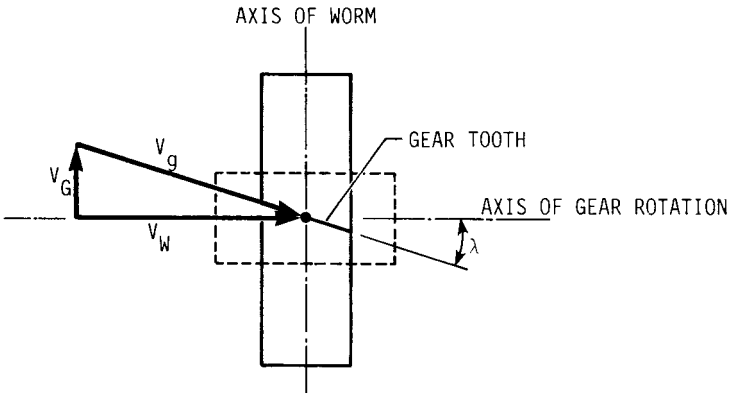

FIGURE 12.4 Velocity components in a worm-gear set. The sliding velocity is $V_S = (V_W^2 + V_G^2)^{1/2} = \dfrac{V_W}{\cos \lambda}$.

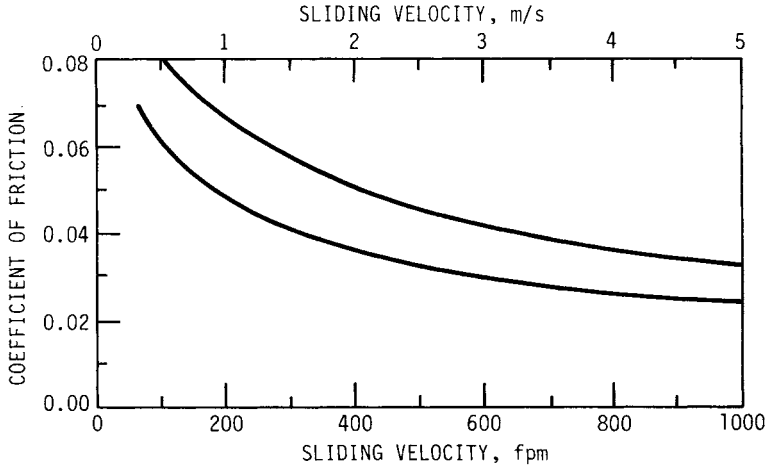

FIGURE 12.5 Approximate coefficients of sliding friction between the worm and gear teeth as a function of the sliding velocity. All values are based on adequate lubrication. The lower curve represents the limit for the very best materials, such as a hardened worm meshing with a bronze gear. Use the upper curve if moderate friction is expected.

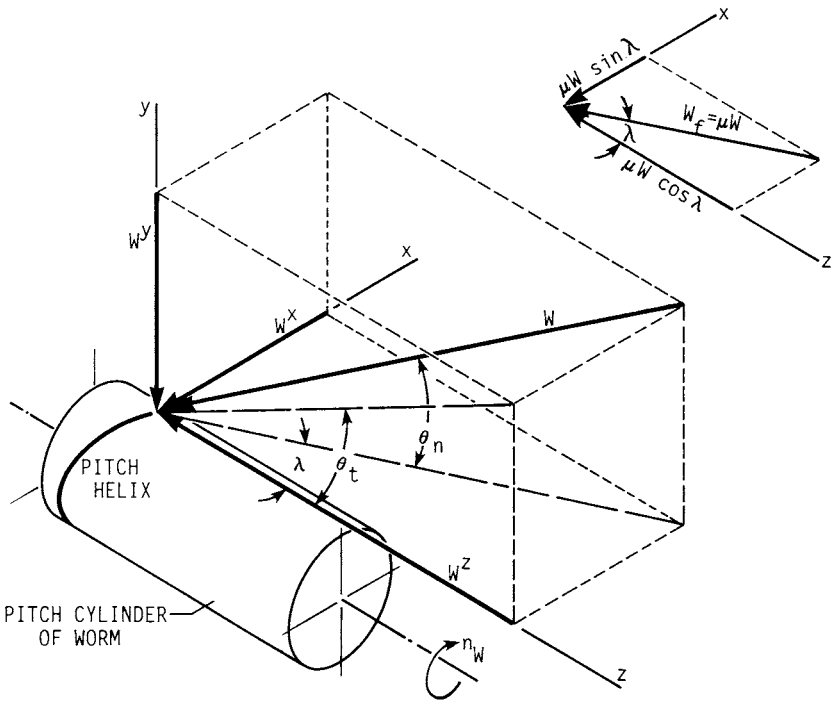

FIGURE 12.6 Forces exerted on worm.

where the subscripts are t for the tangential direction, r for the radial direction, and a for the axial direction. It is worth noting in the above equations that the gear axis is parallel to the x axis and the worm axis is parallel to the z axis. The coordinate system is right-handed.

The force W, which is normal to the profile of the mating teeth, produces a frictional force $W_f = \mu W$, shown in Fig. 12.6, along with its components $\mu W \cos \lambda$ in the negative x direction and $\mu W \sin \lambda$ in the positive z direction. Adding these to the force components developed in Eqs. (12.10) yields

$$\begin{aligned} W^x &= W(\cos \phi_n \sin \lambda + \mu \cos \lambda) \\ W^y &= W \sin \phi_n \\ W^z &= W(\cos \phi_n \cos \lambda - \mu \sin \lambda) \end{aligned} \tag{12.12}$$

Equations (12.11) still apply. Substituting W^z from Eq. (12.12) into the third of Eqs. (12.11) and multiplying by μ, we find the frictional force to be

$$W_f = \mu W = \frac{\mu W_{G_t}}{\mu \sin \lambda - \cos \phi_n \cos \lambda} \tag{12.13}$$

A relation between the two tangential forces is obtained from the first and third of Eqs. (12.11) with appropriate substitutions from Eqs. (12.12):

$$W_{W_t} = W_{G_t} \frac{\cos \phi_n \sin \lambda + \mu \cos \lambda}{\mu \sin \lambda - \cos \phi_n \cos \lambda} \tag{12.14}$$

The efficiency can be defined as

$$\eta = \frac{W_{W_t} \text{ (without friction)}}{W_{W_t} \text{ (with friction)}} \tag{12.15}$$

Since the numerator of this equation is the same as Eq. (12.14) with $\mu = 0$, we have

$$\eta = \frac{\cos \phi_n - \mu \tan \lambda}{\cos \phi_n + \mu \cot \lambda} \tag{12.16}$$

Table 12.1 shows how η varies with λ, based on a typical value of friction $\mu = 0.05$ and the pressure angles usually used for the ranges of λ indicated. It is clear that small λ should be avoided.

Example 1. A 2-tooth right-hand worm transmits 1 horsepower (hp) at 1200 revolutions per minute (r/min) to a 30-tooth gear. The gear has a transverse diametral pitch of 6 teeth per inch. The worm has a pitch diameter of 2 inches (in). The normal pressure angle is 14½°. The materials and workmanship correspond to the lower of the curves in Fig. 12.5. Required are the axial pitch, center distance, lead, lead angle, and tooth forces.

Solution. The axial pitch is the same as the transverse circular pitch of the gear. Thus

$$p_x = \frac{\pi}{P} = \frac{\pi}{6} = 0.5236 \text{ in}$$

TABLE 12.1 Efficiency of Worm-Gear Sets for $\mu = 0.05$

Normal pressure angle ϕ_n, deg	Lead angle λ, deg	Efficiency η, percent
$14\frac{1}{2}$	1	25.2
	2.5	46.8
	5	62.6
	7.5	71.2
	10	76.8
	15	82.7
20	20	86.0
	25	88.0
	30	89.2

The pitch diameter of the gear is $D = N_G/P = 30/6 = 5$ in. The center distance is thus

$$C = \frac{D + d}{2} = \frac{2 + 5}{2} = 3.5 \text{ in}$$

The lead is

$$L = p_x N_W = 0.5236(2) = 1.0472 \text{ in}$$

From Eq. (12.3),

$$\lambda = \tan^{-1} \frac{L}{\pi d} = \tan^{-1} \frac{1.0472}{2\pi} = 9.46°$$

The pitch line velocity of the worm, in inches per minute, is

$$V_W = \pi d n_W = \pi(2)(1200) = 7540 \text{ in/min}$$

The speed of the gear is $n_G = 1200(2)/30 = 80$ r/min. The gear pitch line velocity is thus

$$V_G = \pi D n_G = \pi(5)(80) = 1257 \text{ in/min}$$

The sliding velocity is the square root of the sum of the squares of V_W and V_G, or

$$V_S = \frac{V_W}{\cos \lambda} = \frac{7540}{\cos 9.46} = 7644 \text{ in/min}$$

This result is the same as 637 feet per minute (ft/min); we enter Fig. 12.5 and find $\mu = 0.03$.

Proceeding now to the force analysis, we use the horsepower formula to find

$$W_W = \frac{(33\,000)(12)(\text{hp})}{V_W} = \frac{(33\,000)(12)(1)}{7540} = 52.5 \text{ lb}$$

This force is the negative x direction. Using this value in the first of Eqs. (12.12) gives

$$W = \frac{W^x}{\cos \phi_n \sin \lambda + \mu \cos \lambda}$$

$$= \frac{52.5}{\cos 14.5° \sin 9.46° + 0.03 \cos 9.46°} = 278 \text{ lb}$$

From Eqs. (12.12) we find the other components of W to be

$$W^y = W \sin \phi_n = 278 \sin 14.5° = 69.6 \text{ lb}$$

$$W^z = W(\cos \phi_n \cos \lambda - \mu \sin \lambda)$$

$$= 278(\cos 14.5° \cos 9.46° - 0.03 \sin 9.46°)$$

$$= 265 \text{ lb}$$

The components acting on the gear become

$$W_{G_a} = -W^x = 52.5 \text{ lb}$$

$$W_{G_r} = -W^y = 69.6 \text{ lb}$$

$$W_{G_t} = -W^z = -265 \text{ lb}$$

The torque can be obtained by summing moments about the x axis. This gives, in inch-pounds,

$$T = 265(2.5) = 662.5 \text{ in} \cdot \text{lb}$$

It is because of the frictional loss that this output torque is less than the product of the gear ratio and the input torque (778 lb · in).

12.5 STRENGTH AND POWER RATING

Because of the friction between the worm and the gear, power is consumed by the gear set, causing the input and output horsepower to differ by that amount and resulting in a necessity to provide for heat dissipation from the unit. Thus

$$\text{hp(in)} = \text{hp(out)} + \text{hp(friction loss)}$$

This expression can be translated to the gear parameters, resulting in

$$\text{hp(in)} = \frac{W_{G_t} D n_W}{126\,000 m_G} + \frac{V_S W_f}{396\,000} \tag{12.17}$$

The force which can be transmitted W_{G_t} depends on tooth strength and is based on the gear, it being nearly always weaker than the worm (worm tooth strength can be computed by the methods used with screw threads, as in Chap. 13). Based on material strengths, an empirical relation is used. The equation is

$$W_{G_t} = K_s D^{0.8} F_e K_m K_v \tag{12.18}$$

TABLE 12.2 Materials Factor K_s for Cylindrical Worm Gearing†

Face width of gear F_G, in	Sand-cast bronze	Static-chill-cast bronze	Centrifugal-cast bronze
Up to 3	700	800	1000
4	665	780	975
5	640	760	940
6	600	720	900
7	570	680	850
8	530	640	800
9	500	600	750

†For copper-tin and copper-tin-nickel bronze gears operating with steel worms case-hardened to 58 R_C minimum.

SOURCE: Darle W. Dudley (ed.), *Gear Handbook,* McGraw-Hill, New York, 1962, p. 13–38.

where K_s = materials and size correction factor, values for which are shown in Table 12.2
F_e = effective face width of gear; this is actual face width or two-thirds of worm pitch diameter, whichever is less
K_m = ratio correction factor; values in Table 12.3
K_v = velocity factor (Table 12.4)

Example 2. A gear catalog lists a 4-pitch, 14½° pressure angle, single-thread hardened steel worm to mate with a 24-tooth sand-cast bronze gear. The gear has a 1½-in face width. The worm has a 0.7854-in lead, 4.767° lead angle, 4½-in face width, and a 3-in pitch diameter. Find the safe input horsepower.

From Table 12.2, $K_s = 700$. The pitch diameter of the gear is

$$D = \frac{N_G}{P} = \frac{24}{4} = 6 \text{ in}$$

The pitch diameter of the worm is given as 3 in; two-thirds of this is 2 in. Since the face width of the gear is smaller (1.5 in), $F_e = 1.5$ in. Since $m_G = N_G/N_W = 24/1 =$

TABLE 12.3 Ratio Correction Factor K_m

m_G	K_m	m_G	K_m	m_G	K_m
3.0	0.500	8.0	0.724	30.0	0.825
3.5	0.554	9.0	0.744	40.0	0.815
4.0	0.593	10.0	0.760	50.0	0.785
4.5	0.620	12.0	0.783	60.0	0.745
5.0	0.645	14.0	0.799	70.0	0.687
6.0	0.679	16.0	0.809	80.0	0.622
7.0	0.706	20.0	0.820	100.0	0.490

SOURCE: Darle W. Dudley (ed.), *Gear Handbook,* McGraw-Hill, New York, 1962, p. 13–38.

TABLE 12.4 Velocity Factor K_v

Velocity V_S, fpm	K_v	Velocity V_S, fpm	K_v
1	0.649	600	0.340
1.5	0.647	700	0.310
10	0.644	800	0.289
20	0.638	900	0.269
30	0.631	1000	0.258
40	0.625	1200	0.235
60	0.613	1400	0.216
80	0.600	1600	0.200
100	0.588	1800	0.187
150	0.558	2000	0.175
200	0.528	2200	0.165
250	0.500	2400	0.156
300	0.472	2600	0.148
350	0.446	2800	0.140
400	0.421	3000	0.134
450	0.398	4000	0.106
500	0.378	5000	0.089
550	0.358	6000	0.079

SOURCE: Darle W. Dudley (ed.), *Gear Handbook,* McGraw-Hill, New York, 1962, p. 13–39.

24, from Table 12.3, $K_m = 0.823$ by interpolation. The pitch line velocity of the worm is

$$V_W = \pi d n_W = \pi(3)(1800) = 16\,965 \text{ in/min}$$

The sliding velocity is

$$V_S = \frac{V_W}{\cos \lambda} = \frac{16\,965}{\cos 4.767°} = 17\,024 \text{ in/min}$$

Therefore, from Table 12.4, $K_v = 0.215$. The transmitted load is obtained from Eq. (12.18) and is

$$W_{G_t} = K_s d^{0.8} F_e K_m K_v = 700(6^{0.8})(1.5)(0.823)(0.215)$$
$$= 779 \text{ lb}$$

To find the friction load, the coefficient of friction is needed. Converting V_S to feet per minute and using Fig. 12.5, we find $\mu = 0.023$. From Eq. (12.13) we find

$$W_f = \frac{\mu W_{G_t}}{\mu \sin \lambda - \cos \phi_n \cos \lambda}$$
$$= \frac{0.023(779)}{0.023 \sin 4.767° - \cos 14.5° \cos 4.767°}$$
$$= 18.6 \text{ lb}$$

Next, using Eq. (12.17), we find the input horsepower to be

$$\text{hp(in)} = \frac{W_{G_t} D n_W}{126\,000 m_G} + \frac{W_f V_S}{396\,000}$$

$$= \frac{779(6)(1800)}{126\,000(24)} + \frac{18.6(17\,024)}{396\,000}$$

$$= 2.78 + 0.80 = 3.58$$

12.6 HEAT DISSIPATION

In the last section we noted that the input and output horsepowers differ by the amount of power resulting from friction between the gear teeth. This difference represents energy input to the gear set unit, which will result in a temperature rise. The capacity of the gear reducer will thus be limited by its heat-dissipating capacity.

The cooling rate for rectangular housings can be estimated from

$$C_1 = \begin{cases} \dfrac{n}{84\,200} + 0.01 & \text{without fan} \\ \dfrac{n}{51\,600} + 0.01 & \text{with fan} \end{cases} \tag{12.19}$$

where C_1 is the heat dissipated in Btu/(h)(in^2)(°F), British thermal units per hour–inch squared–degrees Fahrenheit, and n is the speed of the worm shaft in rotations per minute. Note that the rates depend on whether there is a fan on the worm shaft. The rates are based on the area of the casing surface, which can be estimated from

$$A_c = 43.2C^{1.7} \tag{12.20}$$

where A_c is in square inches.

The temperature rise can be computed by equating the friction horsepower to the heat-dissipation rate. Thus

$$\text{hp(friction)} = \frac{778 C_1 A_c \Delta T}{60(33\,000)} \tag{12.21}$$

or

$$\Delta T(°\text{F}) = \frac{\text{hp(friction)}(60)(33\,000)}{778 C_1 A_c} \tag{12.22}$$

The oil temperature should not exceed 180°F. Clearly the horsepower rating of a gear set may be limited by temperature rather than by gear strength. Both must be checked. Of course, means other than natural radiation and convection can be employed to solve the heat problem.

12.7 DESIGN STANDARDS

The American Gear Manufacturer's Association† has issued certain standards relating to worm-gear design. The purpose of these publications, which are the work of broad committees, is to share the experience of the industry and thus to arrive at good standard design practice. The following relate to industrial worm-gear design and are extracted from [12.1] with the permission of the publisher.

Gear sets with axial pitches of 3/16 in and larger are termed *coarse-pitch.* Another standard deals with fine-pitch worm gearing, but we do not include these details here. It is not recommended that gear and worm be obtained from separate sources. Utilizing a worm design for which a comparable hob exists will reduce tooling costs.

12.7.1 Number of Teeth of Gear

Center distance influences to a large extent the minimum number of teeth for the gear. Recommended minimums are shown in Table 12.5. The maximum number of teeth selected is governed by high ratios of reduction and considerations of strength and load-carrying capacity.

12.7.2 Number of Threads in Worm

The minimum number of teeth in the gear and the reduction ratio determine the number of threads for the worm. Generally, 1 to 10 threads are used. In special cases, a larger number may be required.

12.7.3 Gear Ratio

Either prime or even gear ratios may be used. However, if the gear teeth are to be generated by a single-tooth "fly cutter," the use of a prime ratio will eliminate the need for indexing the cutter.

† American Gear Manufacturer's Association (AGMA), Alexandria, Virginia.

TABLE 12.5 Recommended Minimum Number of Gear Teeth

Center distance, in	Minimum number of teeth†
2	20
3	25
5	25
10	29
15	35
20	40
24	45

†Lower numbers are permissible for specific applications.

12.7.4 Pitch

It is recommended that pitch be specified in the axial plane of the worm and that it be a simple fraction, to permit accurate factoring for change-gear ratios.

12.7.5 Worm Pitch Diameter

The pitch diameter of the worm for calculation purposes is assumed to be at the mean of the working depth. A worm does not have a true pitch diameter until it is mated with a gear at a specified center distance. If the actual addendum and dedendum of the worm are equal, respectively, to the addendum and dedendum of the gear, then the nominal and actual pitch diameters of the worm are the same. However, it is not essential that this condition exist for satisfactory operation of the gearing.

Although a relatively large variation in worm pitch diameter is permissible, it should be held within certain limits if the power capacity is not to be adversely affected. Therefore, when a worm pitch diameter is selected, the following factors should be considered:

1. Smaller pitch diameters provide higher efficiency and reduce the magnitude of tooth loading.
2. The root diameter which results from selection of a pitch diameter must be sufficiently large to prevent undue deflection and stress under load.
3. Larger worm pitch diameters permit utilization of larger gear face widths, providing higher strength for the gear set.
4. For low ratios, the minimum pitch diameter is governed, to some degree, by the desirability of avoiding too high a lead angle. Generally, the lead is limited to a maximum of 45°. However, lead angles up to 50° are practical.

12.7.6 Gear Pitch Diameter

The selection of an approximate worm pitch diameter permits the determination of a corresponding approximate gear pitch diameter. In the normal case where the addendum and dedendum of the worm are to be equal, respectively, to the addendum and dedendum of the gear, a trial value of gear pitch diameter may be found by subtracting the approximate worm pitch diameter from twice the center distance of the worm and gear. Once the number of teeth for the gear has been selected, it is desirable to arrive at an exact gear pitch diameter by selecting for the gear circular pitch a fraction, which can be conveniently factored into a gear train for processing purposes, and calculating gear pitch diameter from the formula in Table 12.6. Should the actual value of gear pitch diameter differ from the trial value, the worm pitch diameter must be adjusted accordingly through the use of the formula in Table 12.7.

It is not essential that the pitch circle of the gear be at the mean of the working depth. Where there are sufficient teeth in the gear and the pressure angle is high enough to prevent undercutting, the pitch line can be anywhere between the mean of the depth and the throat diameter of the gear, or even outside the throat. This results in a short addendum for the gear teeth and lengthens the angle of recess. It is

TABLE 12.6 Dimensions of the Gear

Quantity	Symbol	Formula
Pitch diameter	D	$\frac{N_G p_x}{\pi}$
Throat diameter	D_t	$D + 2a$
Effective face width	F_e	$\sqrt{(d + h_k)^2 - d^2}$

also practical for the gear pitch diameter to be located somewhat below the mean of the working depth.

12.7.7 Worm Thread and Gear-Tooth Proportions

Pressure Angle. Several factors deserve consideration in the selection of the pressure angle. Smaller values of pressure angle decrease the separating forces, extend the line of action, and result in less backlash change with change in center distance. Larger values of pressure angle provide stronger teeth and assist in preventing undercutting of the teeth where lead angles are larger. The recommended pressure angles are listed in Table 12.8. These, used with the system for stubbing teeth (Table 12.9), will avoid undercutting.

TABLE 12.7 Dimensions of the Worm

Quantity	Symbol	Formula
Lead	l	$N_W P_x$
Pitch diameter†	d	$2C - D$
Outside diameter	d_o	$d + 2a$
Minimum face width	f	$2\sqrt{\left(\frac{D_t}{2}\right)^2 - \left(\frac{D}{2} - a\right)}$
Lead angle	λ	$\tan^{-1}\frac{l}{\pi d}$
Normal pitch	p_n	$p_x \cos \lambda$
Normal pressure angle	ϕ_n	See Table 12.8

†Use only where addenda and dedenda of worm and gear are equal.

TABLE 12.8 Recommended Values for the Normal Pressure Angle

Normal pressure angle ϕ_n, deg	Lead angle λ, deg
20	Less than 30
25	30–45

Although its use is discouraged, a 14° normal pressure angle may be used for lead angles up to 17°. A detailed study of gear-tooth action is employed by some designers to utilize pressure angles less than 25° where worm lead angles are above 30°.

Tooth Depth Proportions. The choice of tooth depth proportions is governed, to a great extent, by the need to avoid undercutting of the gear teeth. Commonly used tooth depth proportions for lead angles to, but not including, 30° are listed in Table 12.10. However, other acceptable practices are used by several manufacturers.

TABLE 12.9 System for Stubbing Teeth†

Depth, percent	Lead angle λ, deg
90	30–34.99
80	35–39.99
70	40–45

†Other systems for stubbing gear teeth such as reducing the depth by 2 percent per degree of lead angle over 30° are also in common use.

TABLE 12.10 Dimensions Common to Both Worm and Gear†

Quantity	Symbol	Formula
Addendum	a	$0.3183p_x$
Whole depth	h_t	$0.6866p_x$
Working depth	h_k	$0.6366p_x$
Center distance‡	C	$\frac{D+d}{2}$

†Recommended for lead angles less than 30°. See Table 12.9 for others.

‡Nominal, where addenda and dedenda of worm and gear are equal.

Table 12.9 presents a system for stubbing teeth to be used in conjunction with the pressure angles in Table 12.8 for lead angles 30° and above.

Tooth Thickness. The gear-tooth normal thickness preferably should be not less than half the normal pitch at the mean of the working depth. In view of the lower-strength material normally used for the gear, it is the practice of some manufacturers to make the gear tooth appreciably thicker than the worm thread. The extent to which this procedure can be followed is limited by the necessity for providing adequate land thickness at the thread peaks.

Tooth or Thread Forms. The most important detail of the worm thread form is that it must be conjugate to that of the gear tooth. The thread form varies with individual manufacturers' practices and may be anything between the extremes of a straight side and the normal section of an involute helicoid.

12.7.8 Gear Blank Dimensions

Face Width. The effective face width of a worm gear varies with the nominal pitch diameter of the worm and the depth of the thread. The formula for gear face width given in Table 12.6 is based on the maximum effective face width of a worm gear (the length of a tangent to the mean worm diameter) between the points where it is intersected by the outside diameter of the worm. Any additional face width is of very little value and is wasteful of material.

Diameter Increment. This is the amount that is added to the throat diameter of the gear to obtain the outside diameter. The magnitude of this increment is not critical and may vary with manufacturers' practice. Normal practice is to use approximately one addendum. It is general practice to round the outside diameter to the nearest fraction of an inch.

The sharp corners at the point where gear face and outside diameter intersect should be removed by the use of either a chamfer or a radius, as shown in Fig. 12.7.

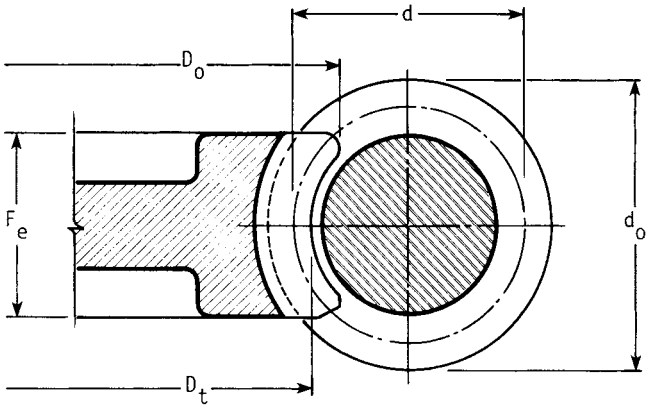

FIGURE 12.7 Section of worm and gear. Note that corners of gear teeth are usually rounded, as shown above the gear centerline; they may, however, be chamfered, as shown below.

Rim thicknesses are generally equal to or slightly greater than the whole depth of the teeth.

12.7.9 Worm Face

The face or length of the worm should be such that it extends beyond the point where contact between its threads and the teeth of the gear begins. Unlike with spur and helical gears, the pressure angle of a worm gear varies along the length of the tooth and becomes quite low on the leaving, or recess, side. This causes contact to occur on the worm almost to the point where the outside diameter of the worm intersects the throat diameter of the gear.

The formula in Table 12.7 provides a conservative value of the worm face width and is based on intersection of worm outside diameter with gear throat diameter.

More exact worm face widths may be determined by detailed calculations or layouts which take into consideration the face width of the gear and fix more definitely the extent of contact along the worm threads.

Good practice includes the breaking or rounding of the sharp edge of the worm threads at the end of the worm face. This procedure is particularly important where the worm face is less than provided for in the formula in Table 12.7.

12.7.10 Bored Worm Blanks

Where it is necessary to use a bored worm, the blank is normally designed with a key seat for driving purposes. The thickness of material between the worm root and the key seat should be at least $0.5h_t$. This is a general recommendation which is governed to some extent by whether the blank is hardened or unhardened. An increase in this amount may be necessary if the blank is hardened, particularly if a case-hardening process is used.

12.8 DOUBLE-ENVELOPING GEAR SETS[†]

12.8.1 Number of Teeth in Gear

The number of teeth for the gear is influenced to a large extent by center distance. The recommended number of teeth for various center distances is listed in Table 12.11. Should special considerations indicate a requirement for fewer teeth, it is advisable to consult a manufacturer of this type of gearing before you complete the design. For multiple-thread worms, the number of teeth in the gear should be within the limits listed in Table 12.11. The maximum number of teeth for single-threaded worms is limited only by the machines available for cutting gear sets and manufacturing tooling.

12.8.2 Number of Threads in Worm

The minimum number of teeth in the gear and the ratio determine the number of threads for the worm. Generally, one to nine threads are used. In special cases, a larger number of threads may be required.

[†] See Ref. [12.2].

TABLE 12.11 Range of Recommended Gear-Tooth Numbers

Center distance, in	No. teeth
2	24–40
3	24–50
4	30–50
8	40–60
15	50–60
20	50–70
24	60–80

12.8.3 Gear Ratio

The gear ratio is the quotient of the number of teeth in the gear and the number of threads in the worm. Either prime or even ratios may be used; however, hob life is improved with even ratios.

12.8.4 Pitch

It is recommended that pitch be specified in the axial section. Pitch is the result of design proportions.

12.8.5 Worm Root Diameter

The recommended root diameter for the worm is

$$d_R = \frac{C^{0.875}}{3} \tag{12.23}$$

It is desirable that the root diameter be not less than that indicated by this formula, even where the worm threads are cut integral with the shaft. For ratios less than 8/1, the worm root diameter may be increased. This increase may vary from zero for an 8/1 ratio to plus 15 percent for a 3/1 ratio.

12.8.6 Worm Pitch Diameter

The pitch diameter of the worm is assumed to be at the mean of the working depth at the center of the worm and is so considered for all calculations. The approximate worm pitch diameter is

$$d = \frac{C^{0.875}}{2.2}$$

and the corresponding root diameter is

$$d_R = d - 2b_G$$

where b_G is the dedendum of gear teeth in inches. Compare this root diameter with that given by Eq. (12.23). If it does not agree, alter the pitch diameter until the root diameter is within the desired limits.

Where horsepower rating is not a factor, there is no limitation regarding pitch diameter of the worm. Where efficiency is not as important as strength or load-carrying capacity, increasing the worm root diameter and gear face width will result in greater capacity.

12.8.7 Base Circle

The base circle may be secured from a layout in the following way. The normal pressure angle is always 20°. The axial pressure angle may be obtained from

$$\phi_x = \tan^{-1} \frac{\tan \phi_n}{\cos \lambda} \tag{12.24}$$

Once the centerline of the worm and gear, the vertical centerline, and the gear pitch circle are laid out, measure along the common worm and gear pitch circle to the right or left of the vertical centerline an amount equal to one-fourth the axial circular pitch p_x. Through the point thus established and at an angle to the vertical centerline equal to the axial pressure angle ϕ_x, extend a line upward. A circle tangent to this line and concentric to the gear axis is the base circle. Adjust this diameter to the nearest 0.01 in. The formula for figuring the base circle diameter is

$$D_b = D \sin \left(\phi_x + \frac{90°}{N_G} \right) \tag{12.25}$$

12.8.8 Tooth Depth Proportions

Formulas for figuring the whole depth, working depth, and dedendum of gear teeth are found in Table 12.12. Note that the working depth is based on the normal circular pitch and so varies for a given axial pitch.

It is common practice in double-enveloping worm gears to proportion the gear tooth and worm thread thickness as follows: The gear tooth thickness is 55 percent of the circular pitch, and the worm thread thickness is 45 percent of the circular pitch. The backlash in the gear set is subtracted from the worm thread thickness. This practice has been followed to secure greater tooth strength in the gear, which is the weaker member.

12.8.9 Tooth or Thread Forms

The thread form is usually straight in the axial section, but any other form may be used. Since there is no rolling action up or down the flanks, the form is unimportant, except that it must be the same on the worm and the hob. The straight-sided tooth in the axial section provides the greatest ease of manufacture and checking of both the gear sets and the cutting tools.

TABLE 12.12 Recommended Worm Tooth Dimensions

Quantity	Formula
Length of flat on outside diameter of worm, in	$f = \frac{p_x}{5.5}$
Whole depth of tooth	$h_t = \frac{p_n}{2}$
Working depth of tooth	$h_k = 0.9h_t$
Dedendum	$b_G = 0.611h_k$
Normal pressure angle	$\phi_n = 20°$
Axial pressure angle at center of worm	$\phi_x = \tan^{-1}\frac{\tan\phi_n}{\cos\lambda_c}$
Lead angle at center of worm	$\lambda_c = \tan^{-1}\frac{D}{m_G d}$

12.8.10 Worm Length

The effective length of the worm thread should be the base circle diameter minus $0.10C$ for lead angles up to and including 20° and minus $0.20C$ to $0.30C$ for lead angles from 20 to 45°. The principal reason for altering this length is to secure the proper amount of worm thread overlap. The overlap should be a distance along the worm thread greater than the face width of the gear. The worm thread extending beyond the effective length must be relieved to prevent interference.

The outside diameter of the worm equals the diameter at the tip of the worm thread at the effective length.

A formula for computing the flat on the outside diameter of the worm at the effective length is given in Table 12.12; the worm face equals the effective length plus twice the flat. The worm face angle is generally 45°.

12.8.11 Gear Blank Dimensions

The face width of the gear should be equal to the root diameter of the worm. Additional face width will not add proportional capacity and is wasteful of material. Where gear sets are to be used at less than their rated horsepower, the face width may be reduced in proportion.

The gear outside diameter may be the point at which the gear face angle intersects the gear throat radius or any desired amount less, except not less than the throat diameter. The gear throat diameter equals the gear pitch diameter plus one working depth.

There are generally three types of gear blanks in use: those having the hub integral, those flanged and counterbored for a bolted spider, and those having a through bore and fastened by setscrews (or bolts) inserted in drilled and tapped holes

located half in the joint between the blank and spider. In all designs, the thickness of metal beneath the teeth should be 1¼ to 1½ times the whole depth of the tooth.

12.8.12 Materials†

Most of the rating standards are based on the use of worms made from a through-hardened, high-carbon steel heat-treated to 32 to 38 R_C. Where case-hardened worms are employed, somewhat higher ratings may be used.

Many high-strength gear materials (such as aluminum, heat-treated aluminum, and nickel bronzes) are used for slow speeds and heavy loads at higher ratings than shown in [12.2].

REFERENCES

12.1 ANSI/AGMA 6022-C93 (R2000), "Design Manual for Cylindrical Wormgearing."

12.2 ANSI/AGMA 6035-A02, "Design, Rating and Application of Industrial Globoidal Wormgearing."

ADDITIONAL REFERENCE

ANSI/AGMA 6034-B92 (R1999), "Practice for Enclosed Cylindrical Wormgear Speed Reducers and Gearmotors."

† See Ref. [12.2].

CHAPTER 13
POWER SCREWS

Rudolph J. Eggert, Ph.D., P.E.
Associate Professor of Mechanical Engineering
University of Idaho
Boise, Idaho

LIST OF SYMBOLS

A	Area
$A(t)$	Screw translation acceleration
C	End condition constant
d	Major diameter
d_c	Collar diameter
d_m	Mean diameter
d_r	Root or minor diameter
E	Modulus of elasticity
F	Load force
F_c	Critical load force
G	Shear modulus
h	Height of engaged threads
I	Second moment of area
J	Polar second moment of area
k	Radius of gyration
L	Thread lead
L_c	Column length
n	Angular speed, r/min
n_s	Number of thread starts

N_e	Number of engaged threads
P_i	Basic load rating
p	Thread pitch
S_y	Yield strength
T_c	Collar friction torque
T_i	Basic static thrust capacity
T_R	Raising torque
T_L	Lowering torque
t	Time
$V(t)$	Screw translation speed
w	Thread width at root
W_i	Input work
W_o	Output work
α	Flank angle
α_n	Normalized flank angle
β	Thread geometry parameter
Δx	Screw translation
$\Delta\theta$	Screw rotation
η	Efficiency
λ	Lead angle
μ_t	Coefficient of thread friction
μ_c	Coefficient of collar friction
σ	Normal stress
σ'	von Mises stress
τ	Shear stress
Ψ	Helix angle

13.1 INTRODUCTION

Power screws convert the input rotation of an applied torque to the output translation of an axial force. They find use in machines such as universal tensile testing machines, machine tools, automotive jacks, vises, aircraft flap extenders, trench braces, linear actuators, adjustable floor posts, micrometers, and C-clamps. The mechanical advantage inherent in the screw is exploited to produce large axial forces in response to small torques. Typical design considerations, discussed in the following sections, include kinematics, mechanics, buckling and deflection, and stresses.

Two principal categories of power screws are machine screws and recirculating-ball screws. An example of a machine screw is shown in Fig. 13.1. The screw threads are typically formed by thread rolling, which results in high surface hardness, high strength, and superior surface finish. Since high thread friction can cause self-locking when the applied torque is removed, protective brakes or stops to hold the load are usually not required.

FIGURE 13.1 Power screw assembly using rolled thread load screw driven by worm shaft and gear nut. *(Simplex Uni-Lift catalog UC-101, Templeton, Kenly & Co., Inc., Broadview, Ill., with permission.)*

Three thread forms that are often used are the *Acme thread,* the *square thread,* and the *buttress thread.* As shown in Fig. 13.2, the Acme thread and the square thread exhibit symmetric leading and trailing flank angles, and consequently equal strength in raising and lowering. The Acme thread is inherently stronger than the square thread because of the larger thread width at the root or minor diameter. The general-purpose Acme thread has a 14½-degree flank angle and is manufactured in a number of standard diameter sizes and thread spacings, given in Table 13.1. The buttress thread is proportionately wider at the root than the Acme thread and is typically loaded on the 7-degree flank rather than the 45-degree flank. See Refs. [13.1], [13.2], [13.3], and [13.4] for complete details of each thread form.

Ball screws recirculate ball bearings between the screw rod and the nut, as shown in Fig. 13.3. The resulting rolling friction is significantly less than the sliding friction of the machine screw type. Therefore less input torque and power are needed. However, motor brakes or screw stops are usually required to prevent ball screws from *self-lowering* or *overhauling.*

13.2 KINEMATICS

The primary function or design requirement of a power screw is to move an axial load F through a *specified* linear distance, called the *travel.* As a single-degree-of-freedom mechanism, screw travel is constrained between the fully *extended* position x_{max} and the closed or *retracted* position x_{min}. The output *range of motion,* therefore, is $x_{max} - x_{min}$. As the input torque T is applied through an angle of rotation $\Delta\theta$, the screw travels Δx in proportion to the screw lead L or total number of screw turns N_t as follows:

$$\Delta x = L\frac{\Delta\theta}{2\pi} = LN_t \tag{13.1}$$

In addition to range of motion specifications, other kinematic requirements may be prescribed, such as velocity or acceleration. The linear screw speed V, in/min, is obtained for a constant angular speed of n, r/min, as

$$V = nL \tag{13.2}$$

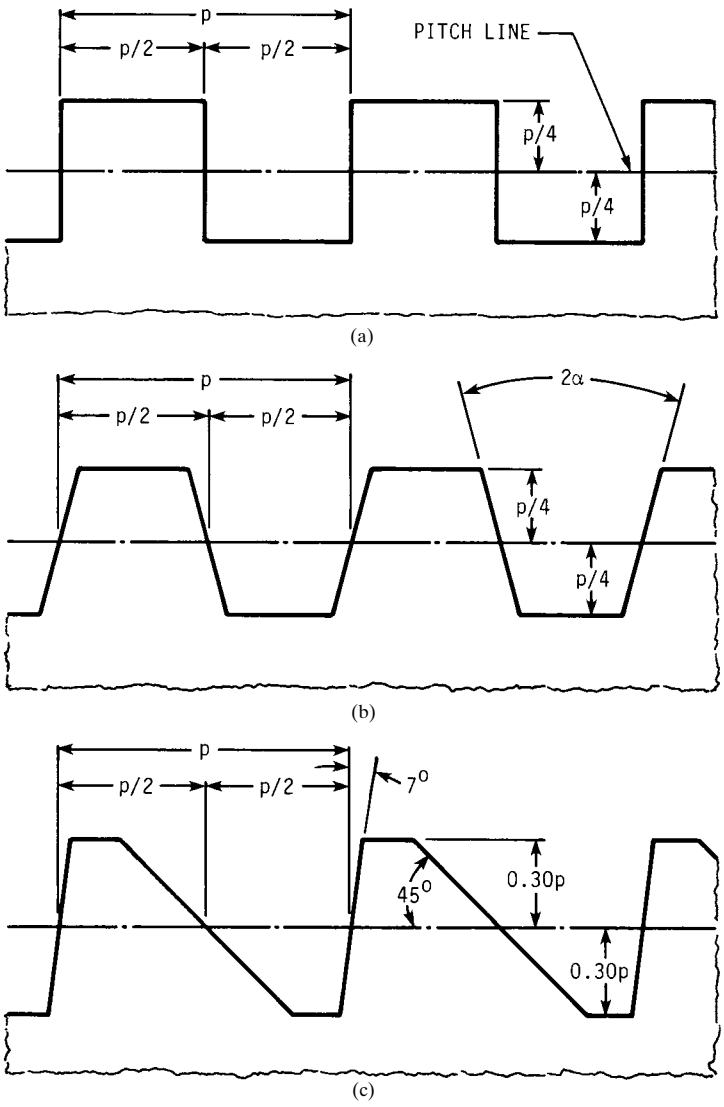

FIGURE 13.2 Basic thread forms. (*a*) Square; (*b*) general-purpose Acme; (*c*) buttress. The stub Acme thread height is 0.3*p*.

TABLE 13.1 Standard Thread Sizes for Acme Thread Form†

Size *D*, in	Threads per inch *n*
¼	**16**
5/16	16, **14**
⅜	16, 14, **12**, **10**
7/16	16, 14, **12**, **10**
½	16, 14, 12, **10**, 8
⅝	16, 14, 12, 10, **8**
¾	16, 14, 12, 10, 8, **6**
⅞	14, 12, 10, 8, **6**, 5
1	14, 12, 10, 8, 6, **5**
1⅛	12, 10, 8, 6, **5**, 4
1¼	12, 10, 8, 6, **5**, 4
1⅜	10, 8, 6, 5, **4**
1½	10, 8, 6, 5, **4**, 3
1¾	10, 8, 6, 4, **4**, 3, 2½
2	8, 6, 5, **4**, 3, 2½, 2
2¼	6, 5, 4, **3**, 2½, 2
2½	5, 4, **3**, 2½, 2
2¾	4, **3**, 2½, 2
3	4, 3, 2½, **2**, 1½, 1⅓
3½	4, 3, 2½, **2**, 1½, 1⅓, 1
4	4, 3, 2½, **2**, 1½, 1⅓, 1
4½	3, 2½, **2**, 1½, 1⅓, 1
5	3, 2½, **2**, 1½, 1⅓, 1

† The preferred size is shown in boldface.

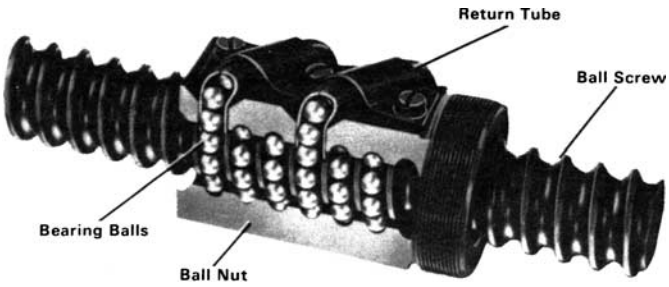

FIGURE 13.3 Ball screw assembly. *(Saginaw Steering Gear Division, General Motors Corporation.)*

The input speed may vary with respect to time *t,* resulting in a proportional change in output speed according to

$$V(t) = \dot{x}(t) = \frac{L}{2\pi}\dot{\theta}(t) \tag{13.3}$$

Similarly, the linear and angular accelerations of the load screw are related as follows:

$$A(t) = \ddot{x}(t) = \frac{L}{2\pi}\ddot{\theta}(t) \tag{13.4}$$

Inertia forces and *torques* are often neglected for screw systems which have small accelerations or masses. If the screw accelerates a large mass, however, or if a nominal mass is accelerated quickly, then inertia forces and torques should be analyzed. The total required input torque is obtained by *superposing* the static equilibrium torque, the torque required to accelerate the load, and the inertia torque of the screw rod itself. The inertia torque of the screw is sometimes significant for high-speed linear actuators. And lastly, impacts resulting from jerks can be analyzed using strain-energy methods or finite-element methods.

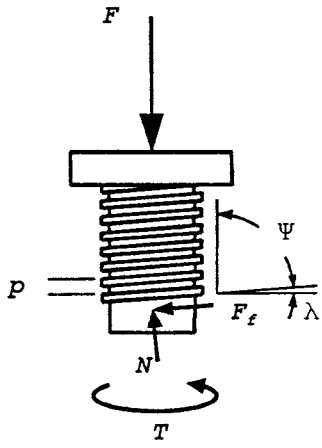

FIGURE 13.4 Free-body diagram of load screw.

13.3 MECHANICS

Under static equilibrium conditions, the screw rotates at a constant speed in response to the input torque T shown in the free-body diagram of Fig. 13.4. In addition, the load force F, normal force N, and sliding friction force F_f act on the screw. The friction force opposes relative motion. Therefore, the direction of the friction force F_f will reverse when the screw translates in the direction of the load rather than against it. The torques required to raise the load T_R (i.e., move the screw in the direction opposing the load) and to lower the load T_L are

$$T_R = \frac{Fd_m}{2}\left(\frac{\pi\mu_t d_m + L\beta}{\pi d_m\beta - \mu_t L}\right) \tag{13.5}$$

$$T_L = \frac{Fd_m}{2}\left(\frac{\pi\mu_t d_m - L\beta}{\pi d_m\beta + \mu_t L}\right) \tag{13.6}$$

where
$$d_m = d - p/2$$
$$L = pn_s$$
$$\tan\lambda = \frac{L}{\pi d_m}$$
$$\tan\alpha_n = \tan\alpha\cos\lambda$$
$$\beta = \cos\alpha_n \qquad (\beta = 1 \text{ for square threads})$$

The thread geometry parameter β includes the effect of the flank angle α as it is projected normal to the thread and as a function of the lead angle. For general-purpose single-start Acme threads, α is 14.5 degrees and β is approximately 0.968, varying less than 1 percent for diameters ranging from ¼ in to 5 in and thread spacing ranging from 2 to 16 threads per inch. For square threads, $\beta = 1$.

In many applications, the load slides relative to a collar, thereby requiring an additional input torque T_c:

$$T_c = \frac{F\mu_c d_c}{2} \tag{13.7}$$

Ball and tapered-roller thrust bearings can be used to reduce the collar torque.

The *starting torque* is obtained by substituting the *static* coefficients of friction into the above equations. Since the sliding coefficient of friction is roughly 25 percent less than the static coefficient, the *running torque* is somewhat less than the starting torque. For precise values of friction coefficients, specific data should be obtained from the published technical literature and verified by experiment.

Power screws can be *self-locking* when the coefficient of friction is high or the lead is small, so that $\pi\mu_t d_m > L$ or, equivalently, $\mu_t > \tan\lambda$. When this condition is not met, the screw will *self-lower* or *overhaul* unless an opposing torque is applied.

A measure of screw efficiency η can be formulated to compare the work output W_o with the work input W_i:

$$\eta = \frac{W_o}{W_i} = \frac{F\,\Delta x}{T\,\Delta\theta} \tag{13.8}$$

where T is the total screw and collar torque. Similarly, for one revolution or 2π radians and screw translation L,

$$\eta = \frac{FL}{2\pi T} \tag{13.9}$$

Screw manufacturers often list output travel speed V, in in/min, as a function of required motor torque T in lbf·in, operating at n r/min, to lift the rated capacity F, in lbf. The actual efficiency for these data is therefore

$$\eta = \frac{FV}{2\pi nT} \tag{13.10}$$

Efficiency of a square-threaded power screw with respect to lead angle λ, as shown in Fig. 13.5, is obtained from

$$\eta = \frac{1 - \mu\tan\lambda}{1 + \mu\cot\lambda} \tag{13.11}$$

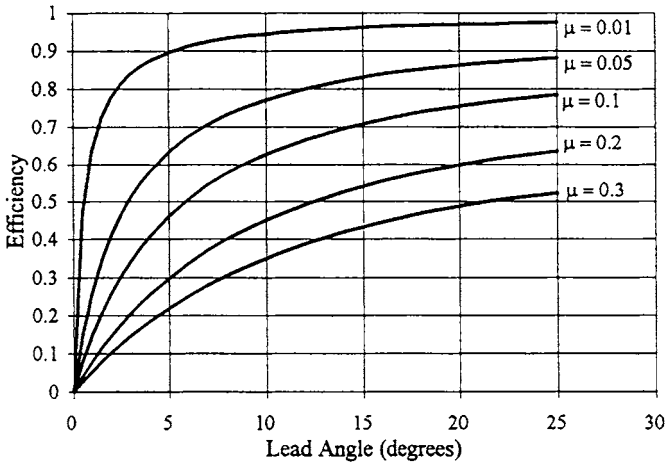

FIGURE 13.5 Screw efficiency η versus thread lead angle λ.

Note the importance of proper lubrication. For example, for $\lambda = 10$ degrees and $\mu = 0.05$, η is over 75 percent. However, as the lubricant becomes contaminated with dirt and dust or chemically breaks down over time, the friction coefficient can increase to $\mu = 0.30$, resulting in an efficiency $\eta = 35$ percent, thereby doubling the torque, horsepower, and electricity requirements.

13.4 BUCKLING AND DEFLECTION

Power screws subjected to compressive loads may buckle. The Euler formula can be used to estimate the critical load F_c at which buckling will occur for relatively long screws of column length L_c and second moment of area $I = \pi d_r^4/64$ as

$$F_c = \frac{C\pi^2 E}{L_c^2}\left(\frac{\pi d_r^4}{64}\right) \tag{13.12}$$

where C is the theoretical end-condition constant for various cases given in Table 13.2. Note that the critical buckling load F_c should be reduced by an appropriate load factor of safety as conditions warrant. See Chap. 30 for an illustration of various end conditions and effective length factor K, which is directly related to the end-condition constant by $C = 1/K^2$.

A column of length L_c and radius of gyration k is considered long when its slenderness ratio L_c/k is larger than the critical slenderness ratio:

$$\frac{L_c}{k} > \left(\frac{L_c}{k}\right)_{\text{critical}} \tag{13.13}$$

$$\frac{L_c}{k} > \left(\frac{2\pi^2 CE}{S_y}\right)^{1/2} \tag{13.14}$$

The radius of gyration k, cross-sectional area A, and second moment of area I are related by $I = Ak^2$, simplifying the above expression to

$$\frac{L_c}{d_r} > \frac{1}{4}\left(\frac{2\pi^2 CE}{S_y}\right)^{1/2} \tag{13.15}$$

For a steel screw whose yield strength is 60 000 psi and whose end-condition constant is 1.0, the critical slenderness ratio is about 100, and L_c/d_r is about 25. For steels whose slenderness ratio is less than critical, the Johnson parabolic relation can be used:

$$\frac{F_c}{A} = S_y - \frac{1}{CE}\left(\frac{S_y L_c}{2\pi k}\right)^2 \tag{13.16}$$

TABLE 13.2 Buckling End-Condition Constants

End condition	C
Fixed-free	¼
Rounded-rounded	1
Fixed-rounded	2
Fixed-fixed	4

which can be solved for a circular cross section of minor diameter d_r as

$$d_r = \sqrt{\frac{F_c}{\pi S_y} + \frac{S_y L_c^2}{\pi^2 CE}} \tag{13.17}$$

The load should be externally guided for long travels to prevent eccentric loading.

Axial compression or extension δ can be approximated by

$$\delta = \frac{FL_c}{AE} = \frac{4FL_c}{\pi d_r^2 E} \tag{13.18}$$

And similarly, angle of twist ϕ, in radians, can be approximated by

$$\phi = \frac{TL_c}{JG} = \frac{32TL_c}{\pi d_r^4 G} \tag{13.19}$$

13.5 STRESSES

Using St. Venants' principle, the nominal *shear* and *normal stresses* for cross sections of the screw rod away from the immediate vicinity of the load application may be approximated by

$$\tau = \frac{Tr}{J} = \frac{16T}{\pi d_r^4} \tag{13.20}$$

$$\sigma_x = \frac{F}{A} = \frac{4F}{\pi d_r^2} \tag{13.21}$$

Failure due to yielding can be estimated by the ratio of S_y to an equivalent, von Mises stress σ' obtained from

$$\sigma' = \sqrt{\left(\frac{4F}{\pi d_r^2}\right)^2 + 3\left(\frac{16T}{\pi d_r^3}\right)^2} = \frac{4}{\pi}\sqrt{\left(\frac{F}{d_r^2}\right)^2 + 48\left(\frac{T}{d_r^3}\right)^2} \tag{13.22}$$

The nominal *bearing* stress σ_b on a nut or screw depends on the number of engaged threads $N_e = h/p$ of pitch p and engaged thickness h and is obtained from

$$\sigma_b = \frac{F}{A_{\text{projected}}} = \frac{4F}{\pi\,(d^2 - d_r^2)}\left(\frac{p}{h}\right) \tag{13.23}$$

Threads may also shear or strip off the screw or nut because of the load force, which is approximately parabolically distributed over the cylindrical surface area A_{cyl}. The area depends on the width w of the thread at the root and the number of engaged threads N_e according to $A_{\text{cyl}} = \pi d w N_e$. The maximum shear stress is estimated by

$$\tau = \frac{3}{2}\frac{F}{A_{\text{cyl}}} \tag{13.24}$$

For square threads such that $w = p/2$, the maximum shear stress for the nut thread is

$$\tau = \frac{3F}{\pi dh} \tag{13.25}$$

To obtain the shear stress for the screw thread, substitute d_r for d. Since d_r is slightly less than d, the stripping shear stress for the screw is somewhat larger.

Note that the load flows from the point of load application through the thread geometry to the screw rod. Because of the nonlinear strains induced in the threads at the point of load application, each thread carries a *disproportionate* share of the load. A detailed analytical approach such as finite-element methods, backed up by experiments, is recommended for more accurate estimates of the above stresses and of other stresses, such as a thread bending stress and hoop stress induced in the nut.

13.6 BALL SCREWS

The design of ball screw assemblies is similar to that of machine screw systems. Kinematic considerations such as screw or nut travel, velocity, and acceleration can be estimated following Sec. 13.2. Similarly input torque, power, and efficiency can be approximated using formulas from Sec. 13.3. Critical buckling loads can be estimated using Eq. (13.12) or (13.16). Also, nominal shear and normal stresses of the ball screw shaft (or rod) can be estimated using Eqs. (13.20) and (13.21).

Design for strength, however, is typically completed using a catalog selection procedure rather than analytical stress-versus-strength analysis. Ball screw manufacturers usually list static and dynamic load capacities for a variety of screw shaft (rod) diameters, ball diameters, and screw leads; an example is shown in Table 13.3. The static capacity for *basic static thrust capacity* T_i, lbf, is the load which will produce a ball track deformation of 0.0001 times the ball diameter. The dynamic capacity or *basic load rating* P_i, lbf, is the constant axial load that a group of ball screw assemblies can endure for a rated life of 1 million inches of screw travel. The *rated life* is the length of travel that 90 percent of a group of assemblies will complete or exceed before any signs of fatigue failure appear. The catalog ratings, developed from laboratory test results, therefore involve the effects of hertzian contact stresses, manufacturing processes, and surface fatigue failure.

The catalog selection process requires choosing the appropriate combination of screw diameter, ball diameter, and lead, so that the axial load F will be sufficiently less than the basic static thrust capacity or the basic load rating for the rated axial travel life. For a different operating travel life of X inches, the modified basic load rating P_{iX}, lbf, is obtained from

$$P_{iX} = P_i \left(\frac{10^6}{X} \right)^{1/3} \tag{13.26}$$

An equivalent load rating P can be obtained for applications involving loads $P_1, P_2, P_3, \ldots, P_n$ that occur for $C_1, C_2, C_3, \ldots, C_n$ percent of the life, respectively:

$$P = \sqrt{\frac{C_1 P_1^3 + C_2 P_2^3 + \cdots + C_n P_n^3}{100}} \tag{13.27}$$

For the custom design of a ball screw assembly, see Ref. [13.5], which provides a number of useful relations.

TABLE 13.3 Sizes and Capacities of Ball Screws†

Major diameter, in	Lead, in, **mm**	Ball diameter, in	Dynamic capacity, lb	Static capacity, lb
0.750	0.200	0.125	1 242	4 595
	0.250	0.125	1 242	4 495
0.875	0.200	0.125	1 336	5 234
	0.250	0.125	1 336	5 234
1.000	0.200	0.125	1 418	5 973
	0.200†	0.156	1 909	7 469
	0.250	0.125	1 418	5 973
	0.250	0.156	1 909	7 469
	0.250	0.187	—	—
	0.400	0.125	1 418	5 973
	0.400	0.187	—	—
1.250	0.200	0.125	1 904	9 936
	0.200†	0.156	2 583	12 420
	0.250	0.125	1 904	9 936
	0.250	0.156	2 583	12 420
	0.250	0.187	3 304	15 886
1.500	0.200	0.125	2 046	11 908
	0.200†	0.156	2 786	14 881
	0.250	0.156	2 786	14 881
	0.250	0.187	3 583	18 748
	0.500	0.156	2 786	14 881
	0.500	0.250	5 290	24 762
1.500	**5**†	0.125	2 046	11 908
	5	0.156	2 787	14 881
	10	0.156	2 786	14 881
	10	0.250	5 290	24 762
	10	0.312	7 050	29 324
1.750	0.200	0.125	2 179	13 879
	0.200†	0.156	2 968	17 341
	0.250	0.156	2 968	17 341
	0.250	0.187	3 829	20 822
	0.500	0.187	3 829	20 882
	0.500	0.250	5 664	27 917
	0.500	0.312	7 633	33 232
2.000	0.200	0.125	2 311	15 851
	0.200†	0.156	3 169	19 801
	0.250	0.156	3 169	19 801
	0.250	0.187	4 033	23 172
	0.400	0.250	6 043	31 850
	0.500	0.312	8 135	39 854
	5	0.125	2 311	15 851
	5†	0.156	3 169	19 801
	6	0.156	3 169	19 801
	6	0.187	4 033	23 172
	10	0.250	6 043	31 850
	10	0.312	8 135	39 854

TABLE 13.3 Sizes and Capacities of Ball Screws† *(Continued)*

Major diameter, in	Lead, in, **mm**	Ball diameter, in	Dynamic capacity, lb	Static capacity, lb
2.250	0.250	0.156	3 306	22 262
	0.250	0.187	4 266	26 684
	0.500	0.312	8 593	44 780
	0.500	0.375	10 862	53 660
2.500	0.200	0.125	2 511	19 794
	0.200	0.156	3 134	24 436
	0.250	0.187	4 410	29 671
	0.400	0.250	6 633	39 746
	0.500	0.312	9 015	49 701
	0.500	0.375	10 367	59 308
	5	0.125	2 511	19 794
	5†	0.156	3 134	24 436
	10	0.250	6 633	39 746
	10	0.312	9 015	49 701
3.000	0.250	0.187	4 810	35 570
	0.400	0.250	7 125	47 632
	0.500	0.375	12 560	71 685
	0.660	0.375	12 560	71 685
	10	0.250	7 125	47 632
	10	0.312	9 744	58 648
3.500	0.500	0.312	10 360	69 287
	0.500	0.375	13 377	83 514
	1.000	0.500	19 812	111 510
	1.000	0.625	26 752	139 585
4.000	0.500	0.375	14 088	95 343
	1.000	0.500	21 066	127 282

† These values are not recommended; consult manufacturer.
Source: 20th Century Machine Company, Sterling Heights, Mich., by permission.

13.7 OTHER CONSIDERATIONS

A number of other important design factors should also be considered. Principal among these is lubrication. Greases using lithium thickeners with antioxidants and EP additives are effective in providing acceptable coefficients of sliding friction and corrosion protection. For operating environments which expose the screw threads to dust, dirt, or water, a protective boot, made of a compatible material, is recommended. Maintenance procedures should ensure that the screw threads are free of contaminants and have a protective film of grease. Operation at ambient temperatures in excess of 200°F requires special lubricants and boot materials as recommended by the manufacturer.

Screw and nut threads will wear with use, especially in heavy-duty-cycle applications, increasing the backlash from the as-manufactured allowance. Use of adjustable split nuts and routine inspection of thread thickness is recommended.

Power screws employing electric motors are often supplied with integral limit switches to control extension and retraction. To prevent ejection of the screw in case of a limit switch failure, a stop nut can be added. In addition, a torque-limiting clutch can be integrated at the motor to prevent equipment damage.

REFERENCES

13.1 ANSI B1.7M-1984 (R2001), "Screw Threads, Nomenclature, Definitions, and Letter Symbols," American Society of Mechanical Engineers, New York, 1992.

13.2 ANSI B1.5-1999, "Acme Screw Threads," American Society of Mechanical Engineers, New York, 1977.

13.3 ANSI B1.8-1977, "Stub Acme Screw Threads," American Society of Mechanical Engineers, New York, 1988.

13.4 ANSI B1.9-1973 (R1979), "Buttress Screw Threads," American Society of Mechanical Engineers, New York, 1973.

13.5 ANSI B5.48-1977 (R1988), "Ball Screws," American Society of Mechanical Engineers, New York, 1977.

POWER SCREWS

P · A · R · T · 4

POWER TRANSMISSION

POWER TRANSMISSION

CHAPTER 14
BELT DRIVES

Wolfram Funk, Prof. Dr.-Ing.
Fachbereich Maschinenbau
Fachgebiet Maschinenelemente und Getriebetechnik
Universität der Bundeswehr Hamburg
Hamburg, Germany

NOMENCLATURE

A	Cross section
b	Width
c_β	Angular factor
c_B	Service factor
d_1	Diameter of driving pulley
d_2	Diameter of driven pulley
e	Center distance
E	Modulus of elasticity
F	Force
f_b	Bending frequency
l	Datum length of flexible connector
M	Torque
n	Speed
P	Power
q	Mass per length
r	Radius
s	Belt thickness
t	Pitch
v	Velocity
z	Number

α	Included angle
β	Angle of wrap
ε	Elongation (strain)
μ	Coefficient of friction
η	Efficiency
ψ	Slip
ρ	Specific mass
σ	Stress

Indices

1	Driving
2	Driven
b	Bending
f	Centrifugal
max	Maximum
w	Effective
zul	Allowable
N	Nominal

14.1 GENERAL

Flexible-connector drives are simple devices used to transmit torques and rotational motions from one to another or to several other shafts, which would usually be parallel. Power is transmitted by a flexible element (flexible connector) placed on pulleys, which are mounted on these shafts to reduce peripheral forces. The transmission ratios of torques and speeds at the driving and driven pulleys are determined by the ratio of pulley diameters. Peripheral forces may be transmitted by either frictional (nonpositive) or positive locking of the flexible connector on the pulleys.

Because of their special characteristics, flexible-connector drives have the following advantages and disadvantages as compared with other connector drives:

Advantages:

- Small amount of installation work
- Small amount of maintenance
- High reliability
- High peripheral velocities
- Good adaptability to the individual application
- In some cases, shock- and sound-absorbing
- In some cases, with continuously variable speed (variable-speed belt drive)

Disadvantages:

- Limited power transmission capacity
- Limited transmission ratio per pulley step
- In some cases, synchronous power transmission impossible (slip)
- In some cases, large axle and contact forces required

14.1.1 Classification According to Function

According to function, flexible-connector drives are classified as (1) nonpositive and (2) positive.

Nonpositive flexible-connector drives transmit the peripheral force by means of friction (mechanical force transmission) from the driving pulley to the flexible connector and from there to the driven pulley(s). The transmissible torque depends on the friction coefficient of the flexible connector and the pulleys as well as on the surface pressure on the pulley circumference. The power transmission capacity limit of the drive is reached when the flexible connector starts to slip. By use of wedge-shaped flexible connectors, the surface pressure can be increased, with shaft loads remaining constant, so that greater torques are transmitted. Since nonpositive flexible-connector drives tend to slip, synchronous power transmission is impracticable.

The positive flexible-connector drive transmits the peripheral force by positive locking of transverse elements (teeth) on the connector and the pulleys. The surface pressure required is small. The transmissible torque is limited by the distribution of the total peripheral force to the individual teeth in engagement and by their functional limits. The power transmission capacity limit of the drive is reached when the flexible connector slips. Power transmission is slip-free and synchronous.

14.1.2 Geometry

The dimensions of the different components [pulley diameter, center distance, datum length (pitch length) of the flexible connector] and the operational characteristics (speed ratio, angle of wrap, included angle) are directly interrelated.

Two-Pulley Drives. For the standard two-pulley drive, the geometry is simple (Fig. 14.1). In general, this drive is designed with the center distance and the speed ratio as parameters. The individual characteristics are related as follows: Speed ratio:

$$i = \frac{n_1}{n_2} = \frac{d_2}{d_1} \tag{14.1}$$

Included angle:

$$\sin \alpha = \frac{d_2 - d_1}{2e} = \frac{d_1}{2e}\,(i - 1) \tag{14.2}$$

Angles of wrap:

$$\begin{aligned} \beta_1 &= 180° - 2\alpha = 180° - 2 \arcsin \frac{d_1}{2e}\,(i - 1) \\ \beta_2 &= 180° + 2\alpha = 180° + 2 \arcsin \frac{d_1}{2e}\,(i - 1) \end{aligned} \tag{14.3}$$

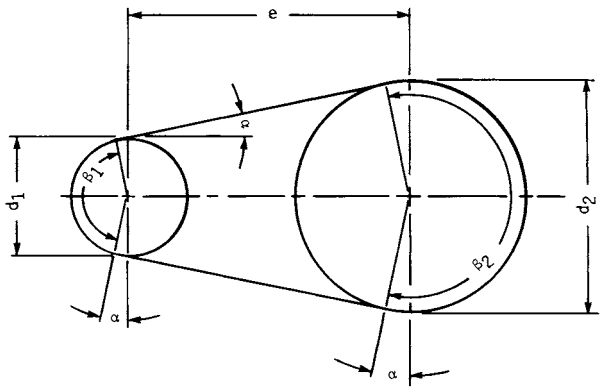

FIGURE 14.1 Two-pulley drive.

Datum length of flexible connector:

$$l = 2e\cos\alpha + \pi\left(d_1\frac{\beta_1}{360^\circ} + d_2\frac{\beta_2}{360^\circ}\right)$$
$$= 2e\cos\alpha + \frac{\pi d_1}{360^\circ}\,[180^\circ - 2\alpha + i(180^\circ + 2\alpha)] \tag{14.4}$$

Approximate equation:

$$l \approx 2e + 1.57(d_1 + d_2) + \frac{(d_2 - d_1)^2}{4e}$$
$$= 2e + 1.57d_1(i+1) + \frac{d_1^2}{4e}\,(i-1)^2 \tag{14.5}$$

The minimum diameter allowable for the flexible connector selected is often substituted for the unknown parameter d_1 (driving-pulley diameter) required for the design.

Multiple-Pulley Drives. For the multiple-pulley drive (one driving pulley, two or more driven pulleys), the geometry is dependent on the arrangement of the pulleys (Fig. 14.2). These drives have the following characteristics: Speed ratios:

$$i_{12} = \frac{n_1}{n_2} = \frac{d_2}{d_1} \qquad i_{13} = \frac{n_1}{n_3} = \frac{d_3}{d_1} \qquad i_{1m} = \frac{n_1}{n_m} = \frac{d_m}{d_1}$$

Included angles:

$$\sin\alpha_{12} = \frac{d_1}{2e_{12}}\,(i_{12} - 1) \tag{14.6}$$

$$\sin\alpha_{13} = \frac{d_1}{2e_{13}}\,(i_{13} - 1) \tag{14.7}$$

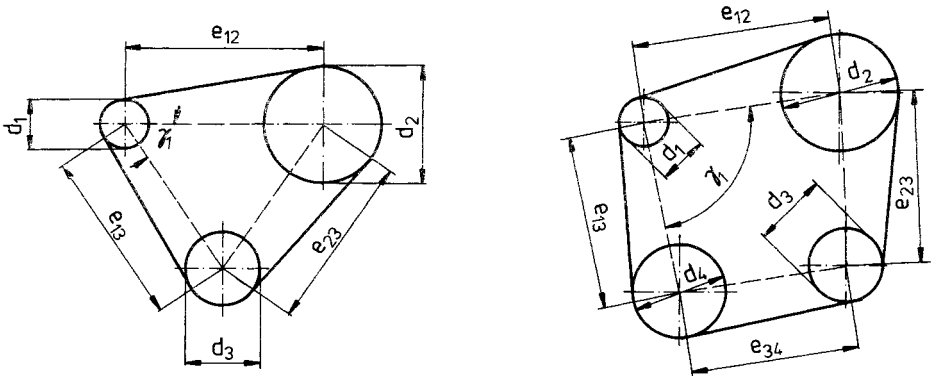

FIGURE 14.2 Multiple-pulley drives.

$$\sin \alpha_{1m} = \frac{d_1}{2e_{1m}} \ (i_{1m} - 1) \tag{14.8}$$

$$\sin \alpha_{km} = \frac{d_k}{2e_{km}} \ (i_{km} - 1) \tag{14.9}$$

Angles of wrap:

$$\beta_j = 180° - \alpha_{j,j-1} - \alpha_{j,j+1} - \gamma_j \tag{14.10}$$

where $_j$ = index of pulley
γ_j = angle between center distances

$$l = \frac{\beta_1 \pi d_1}{360} + e_{12} \cos \alpha_{12} + \frac{\beta_2 \pi d_2}{360} + e_{23} \cos \alpha_{23} + \cdots + \frac{\beta_k \pi d_k}{360} + e_{km} \cos \alpha_{km} + \frac{\beta_m \pi d_m}{360} + e_{1m} \cos \alpha_{1m} \tag{14.11}$$

14.1.3 Forces in Moving Belt

Friction is employed in transmitting the peripheral forces between the belt and the pulley. The relation of the friction coefficient μ, the arc of contact β, and the belt forces is expressed by Eytelwein's equation. For the extreme case, i.e., slippage along the entire arc of contact, this equation is

$$\frac{F_1'}{F_2'} = \exp \frac{\mu \beta \pi}{180} \tag{14.12}$$

For normal operation of the drive without belt slip, the peripheral force is transmitted only along the active arc of contact $\beta_w < \beta$ (according to Grashof), resulting in a force ratio between the belt sides of

$$\frac{F_1'}{F_2'} = \exp\frac{\mu\beta_w\pi}{180} \tag{14.13}$$

The transmission of the peripheral force between the belt and the pulley then occurs only within the active arc of contact β_w with belt creep at the driven pulley and the corresponding contraction slip at the driving pulley. During operation, the belt moves slip-free along the inactive arc of contact, then with creep along the active arc of contact. If the inactive arc of contact equals zero, the belt slips and may run off the pulley.

Along the inactive arc of contact, the angular velocity in the neutral plane equals that of the pulley. Along the active arc of contact, the velocity is higher in the tight side of the belt owing to higher tension in that side than in the slack side. Since this velocity difference has to be offset, slip results. This slip leads to a speed difference between the engagement point and the delivery point on each pulley, which amounts up to 2 percent depending on the belt material (modulus of elasticity), and load:

$$\psi = \frac{v_1 - v_2}{v_1} = \frac{(l_2 + \Delta l) - l_2}{l_2 + \Delta l} \approx \Delta\varepsilon = \frac{\sigma_1 - \sigma_2}{E} = \frac{\sigma_n}{E} \tag{14.14}$$

For practical design purposes, the calculations for a belt drive are usually based on the entire arc of contact β of the smaller pulley (full load), since the active arc of contact is not known, and the belt slips at the smaller pulley first.

$$\frac{F_1'}{F_2'} = m = \exp\frac{\mu\beta\pi}{180} \tag{14.15}$$

Centrifugal forces acting along the arcs of contact reduce the surface pressure there. As these forces are supported by the free belt sides, they act uniformly along the entire belt:

$$F_f = \rho v^2 A = qv^2 \tag{14.16}$$

With increasing belt velocity v, constant center distance e, and constant torques, the forces F_1 and F_2 acting along the belt sides as well as the peripheral force (usable force) F_u remain constant, whereas the surface pressure and the usable forces F_1' and F_2' in the belt sides are reduced. Usable forces in belt sides:

$$\begin{aligned} F_1' &= F_1 - F_f = mF_2' \\ F_2' &= F_2 - F_f = \frac{F_1'}{m} \end{aligned} \tag{14.17}$$

Peripheral force:

$$\begin{aligned} F_u = F_1' - F_2' = F_1 - F_2 &= F_1'\left(1 - \frac{1}{m}\right) \\ &= F_2'(m - 1) \end{aligned} \tag{14.18}$$

Because

$$F_u = F'_2(m-1) \qquad m = \exp\frac{\mu\beta_w\pi}{180} \tag{14.19}$$

β_w becomes greater, until the belt slips on the pulley with the smaller arc of contact when $\beta_w = \beta$. When $F_f = F_2$, there are no usable forces; that is, $F'_2 = F'_1 = F_u = 0$. In this case, no torque can be transmitted. If belt velocity v is increased further, the belt runs off the pulley.

The maximum force in the belt sides is given by

$$F_{\max} = F_1 = F'_2 + F_u + F_f \tag{14.20}$$

With only the centrifugal forces acting, the belt is in equilibrium. They do not act on the pulleys at all. Hence, the shaft load F_w of a belt drive results from only the usable forces F'_1 and F'_2 in the belt sides (Fig. 14.3):

$$Fw = \sqrt{F'^2_1 + F'^2_2 - 2F'_1F'_2\cos\beta} \tag{14.21}$$

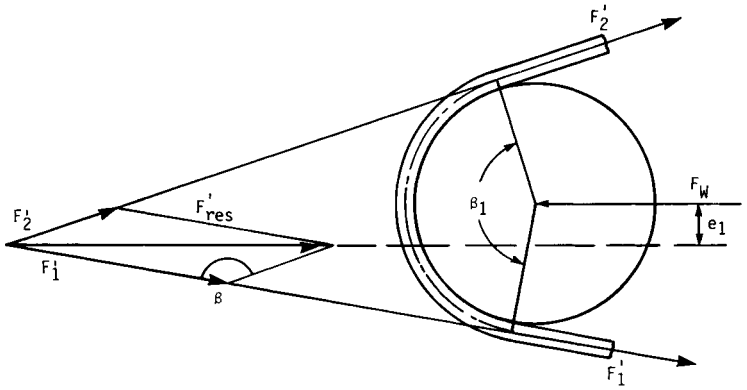

FIGURE 14.3 Equilibrium of forces.

The force rating

$$\Phi = \frac{F_u}{F_w} = (m-1)\sqrt{m2 + 1 - 2m\cos ß}$$

defines the minimum shaft tensioning force required for peripheral force production as a function of the friction coefficient μ and the arc of contact β.

The rated output $K = F_u/F'_1 = 1 - 1/m$ defines the peripheral force F_u which can be produced by the permissible force F'_1 as a function of the friction coefficient μ and the arc of contact β. The reduction in rated output with decreasing arc of contact is defined by an angular factor c_β, based on $\beta = 180°$, that is, a speed ratio of $i = 1$.

The tensions in a homogeneous belt result from the forces acting in the belt and the belt cross section, $A = bs$. For multiple-ply belts, these tensions can be used only as theoretical mean values.

Bending of the belt around the pulley produces the bending stress σ_b. This stress can be calculated from the elongation of the belt fibers with respect to the neutral axis:

$$\Delta l = \beta(r+s) - \beta\left(r+\frac{s}{2}\right) = \beta\,\frac{s}{2}$$

$$\varepsilon = \frac{\Delta l}{l} = \frac{\beta s/2}{\beta(r+s/2)} = \frac{s}{2r+s} \approx \frac{s}{d} \tag{14.22}$$

$$\sigma_b = \varepsilon E_b \approx \frac{s}{d}\,E_b \tag{14.23}$$

The strain ε increases with decreasing pulley diameter d. For practical design purposes, σ_b is not taken into consideration, since belt life depends much less on σ_b than on the bending frequency.

The maximum stress is in the tight side of the belt at the beginning and end of the arc of contact, i.e., the points where it passes onto or off the smaller pulley (Fig. 14.4):

$$\sigma_{\max} = \sigma_1' + \sigma_f + \sigma_b = \frac{F_1'}{A} + \rho v^2 + E_b\frac{s}{d} \tag{14.24}$$

The safety stress depends on the bending frequency and the smallest pulley diameter as well as on the material and the construction of the belt as indicated by the manufacturer. With z = number of pulleys, the bending frequency is given by

$$f_b = \frac{vz}{l} \tag{14.25}$$

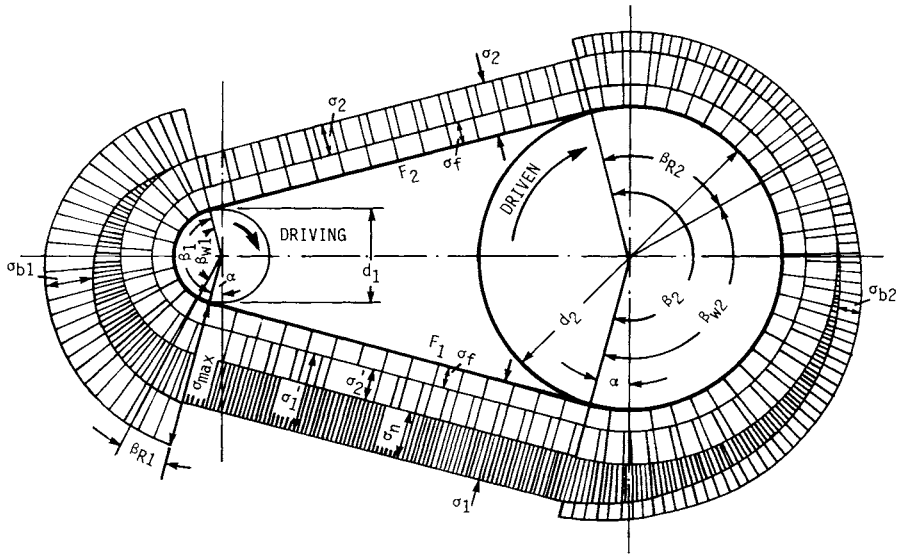

FIGURE 14.4 Stress distribution.

The maximum power transmission capacity of a belt drive can be determined as follows: The power transmission capacity

$$P = F_u v = \sigma_n A v$$

equals zero if the belt velocity v either equals zero or reaches a maximum at which the belt safety stress limit is approached by the centrifugal and bending stresses alone, so that

$$\sigma'_1 = \sigma'_2 = \sigma_n = 0$$

Then

$$\sigma_{zul} = \sigma_f + \sigma_b = \rho v_{max}^2 + \sigma_b \tag{14.26}$$

from which the maximum belt velocity can be calculated as follows:

$$v_{max} = \sqrt{\frac{\sigma_{zul} - \sigma_b}{\rho}} \tag{14.27}$$

Optimum power transmission is possible only at the optimum belt velocity v_{opt} within the range of $v = 0$ and $v = v_{max}$. It depends on the belt safety stress and is given by

$$v_{opt} = \frac{\sigma_{zul} - \sigma_b}{3\rho} = \frac{v_{max}}{\sqrt{3}} \tag{14.28}$$

In theory, this equation applies to all flexible connectors, under the assumption of σ_{zul} (belt safety stress) [or F_{zul} (allowable load)] being independent of belt velocity. Since σ_{zul} decreases with increasing belt velocity, though, the stress and power transmission capacity diagrams are as shown in Fig. 14.5.

14.1.4 Arrangement and Tensioning Devices

Because of their good twistability, flexible connectors are suited for drives with pulleys in different planes and nonparallel shafts of equal or opposite directions of rotation. Since the outer fibers of a twisted flat belt or synchronous belt are strained more than the center fibers, stress is higher there, resulting in the reduction of the belt power transmission capacity.

Figures 14.6 and 14.7 show several belt drives with pulleys in different planes. Note that for drives with crossed belts (Fig. 14.6), endless belts have to be used, in order to avoid damage. For half- or quarter-turn belt drives (Fig. 14.7), the side of delivery must lie in the plane of the mating pulley. By the use of step (cone) pulleys, different speed ratios may be obtained (Fig. 14.8). Pulley diameters have to be selected to ensure equal belt lengths on all steps.

The belt rim running onto the larger diameter of a cone pulley (Fig. 14.9) has a higher velocity than the opposite rim. Thus, the following belt portion is skewed and then runs onto a larger diameter. The drive is balanced when the bending moment due to the bending deformation of the belt is compensated by the skew of the belt side running off (Fig. 14.10).

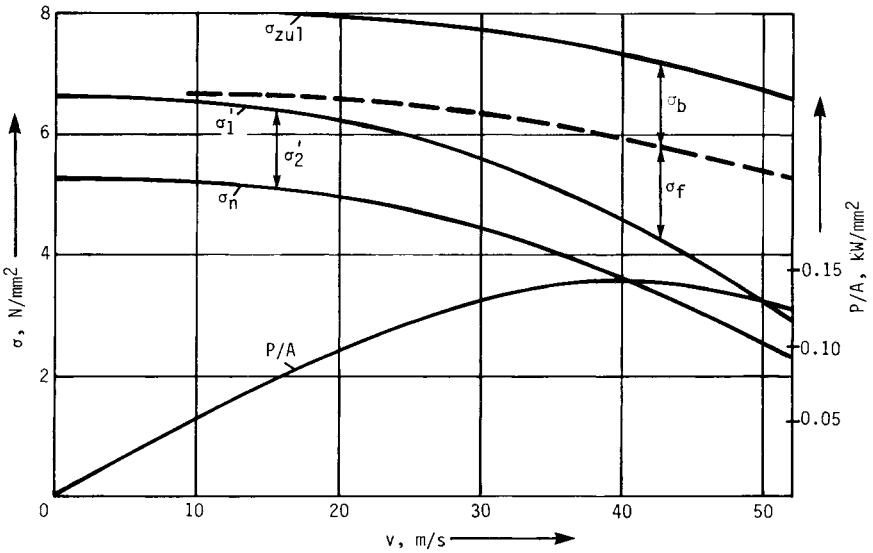

FIGURE 14.5 Stress and power transmission capacity.

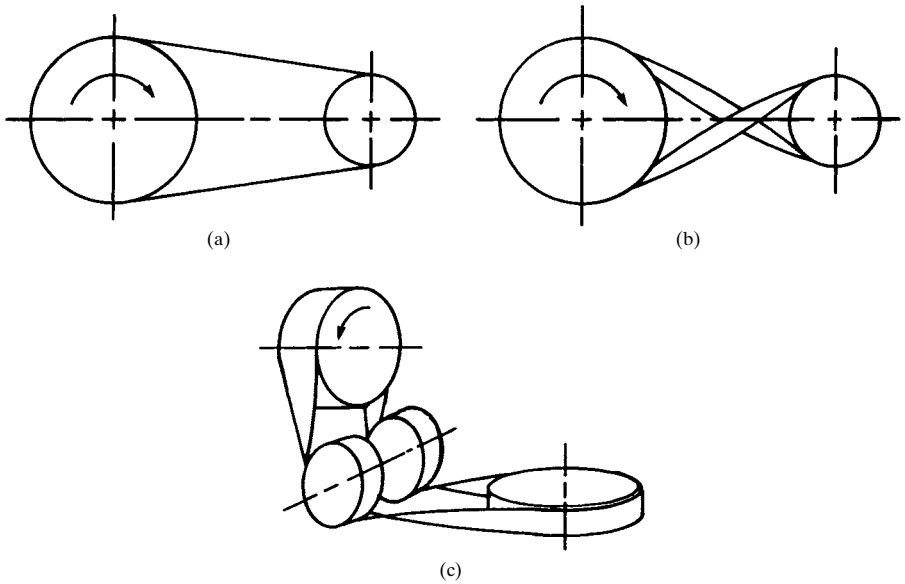

FIGURE 14.6 Examples of crossed belt drives.

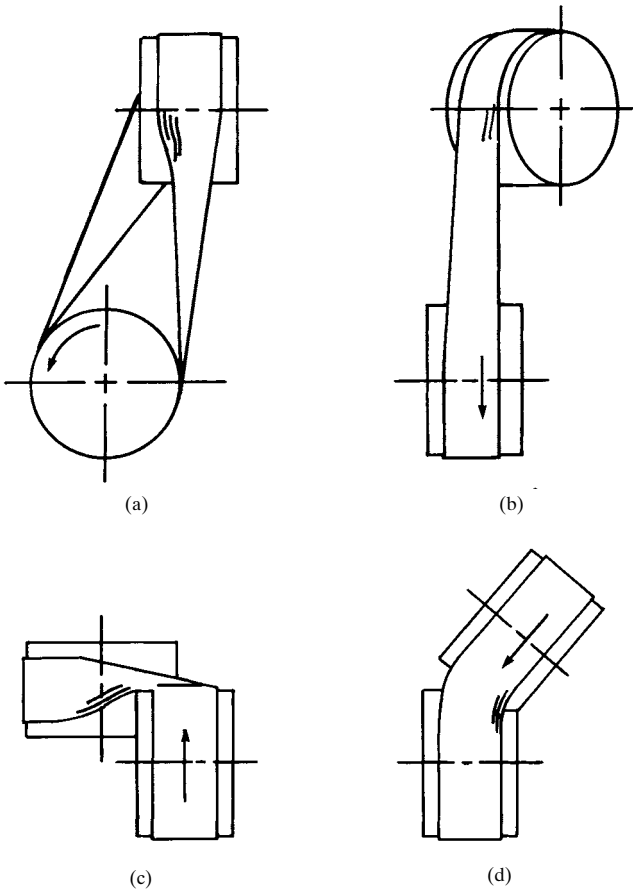

FIGURE 14.7 Belt drives with pulleys in different planes.

The minimum shaft tensioning force F_w required for nonpositive-type force transmission can be produced as shown in Figs. 14.11 to 14.14.

1. *Pretensioning by belt strain:* The belt is cut to such a length that it is elastically preloaded when it is placed on the pulleys. Since both the forces F' in the belt sides and the shaft initial tensioning force are reduced by the action of centrifugal forces, σ_f has to be added to the initial tension of the belt to ensure proper transmission of peripheral forces by friction.

2. *Pretensioning by adjustment of center distance:* The shaft tensioning force F_w is produced by shifting the driving motor on a slide. The belt drive may be preloaded either by adjustment of a threaded spindle or by spring action or weighting.

3. *Pretensioning by means of a belt tightener acting on the slack side:* The slack side of the belt is provided with a pulley to tighten it—with its own weight or by means of counterweights or by spring action—and increase the arcs of contact on

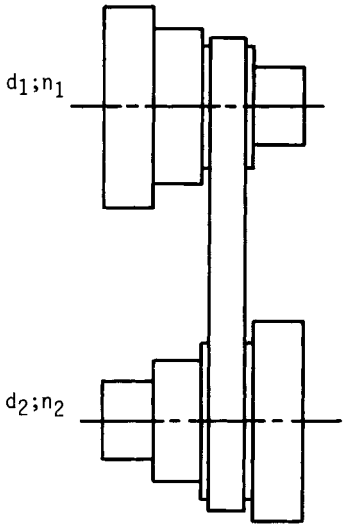

FIGURE 14.8 Step pulleys.

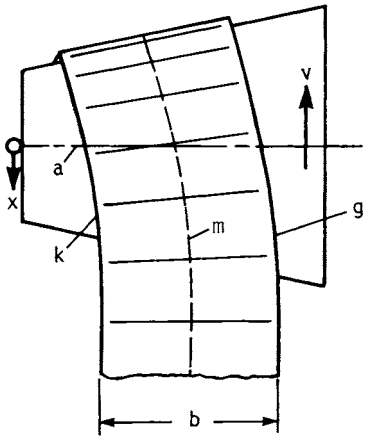

FIGURE 14.9 Cone pulley.

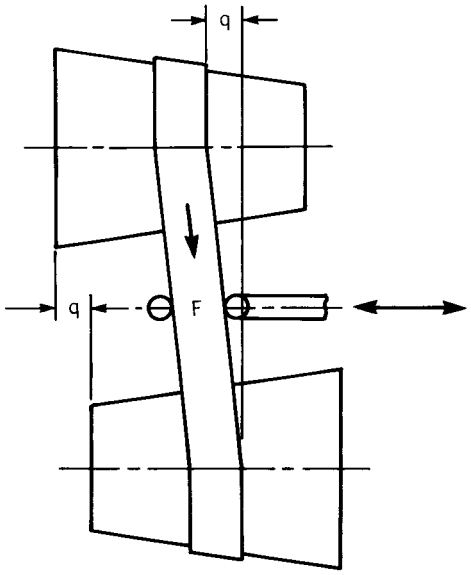

FIGURE 14.10 Cone-pulley drive.

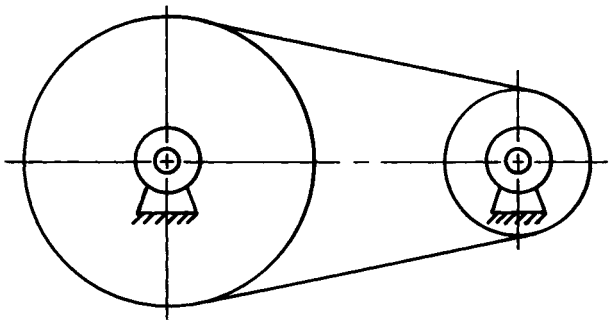

FIGURE 14.11 Pretensioning by belt strain.

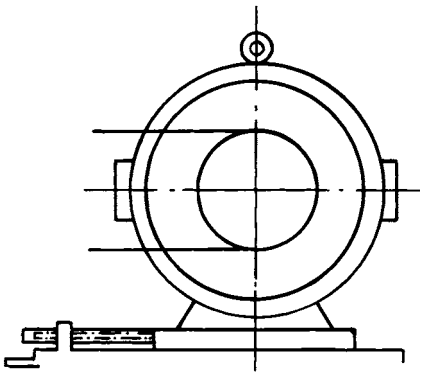

FIGURE 14.12 Pretensioning by adjustment of center distance.

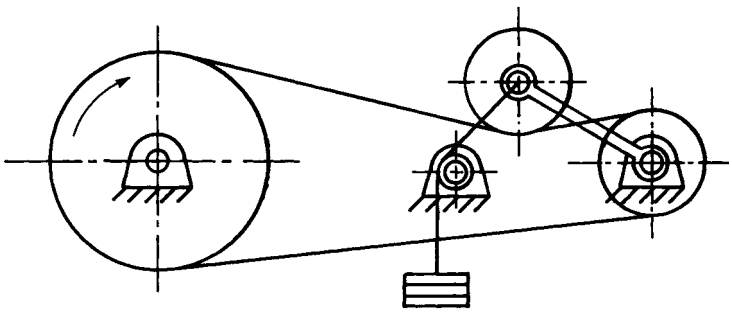

FIGURE 14.13 Pretensioning with a belt tightener.

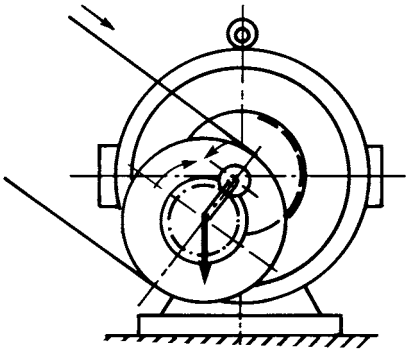

FIGURE 14.14 Pretensioning by torque.

both the driving and the driven pulleys. The belt tightener produces a constant force F_2' for all operating conditions but increases the bending frequency f_b, thus reducing the safety stress of the belt. Taking this into consideration, we see that the belt tightener used should have a minimum diameter equaling that of the smaller pulley, if possible.

4. *Pretensioning by torque making use of a rocker or pivoting pulley:* Figure 14.14 shows an arrangement with an eccentric pulley shaft pivoting the motor pulley shaft. The pulley is driven by a gear assembly. The shaft tensioning force F_w increases almost in proportion to the tooth force F_Z, and with the correct ratio of h_2/h_1, adapts automatically to the specific torque to be transmitted. Belt slipping is impossible with this method of pretensioning.

For all belt pretensioning methods using tensioning devices which can be adjusted during operation of the drive (e.g., methods 2 to 4 described above), the shaft tensioning force F_w and the usable forces F_1' and F_2' in the belt sides are not influenced by centrifugal force. Centrifugal force increases the belt stress by σ_f, though.

14.2 FLAT-BELT DRIVE

Calculations for flat-belt drives are based on Eytelwein's fundamental equation of belt friction:

$$\frac{F_1'}{F_2'} = \exp\frac{\mu\beta\pi}{180} \tag{14.29}$$

For calculations for a belt drive, the arc of contact of the smaller pulley is substituted for the arc of contact β, since the belt slips at the smaller pulley first, and the active arc of contact β_w is not known.

The transmissible power P is calculated from the peripheral forces

$$F_u = F_1' - F_2' = F_2'\left[\exp\left(\frac{\mu\beta\pi}{180}\right) - 1\right] \tag{14.30}$$

and the belt velocity v and is expressed by

$$P_1 = v_1 F_u P_2 = v_2 F_u \tag{14.31}$$

The belt velocities are

$$v_1 = \pi n_1 d_1 \qquad v_2 = \pi n_2 d_2 \tag{14.32}$$

Taking into consideration a service correction factor c_B (Table 14.1) for peak overloads due to heavy duty, we can calculate the power rating of the drive from P_1 by

$$P = c_B P_1 \tag{14.33}$$

The speed ratio, which is slightly dependent on the load because of slip, is

$$i = \frac{n_1}{n_2} = \frac{d_2 v_1}{d_1 v_2} = \frac{d_2}{d_1(1 - \sigma_n E)} = \frac{d_2}{d_1(1 - \psi)} \tag{14.34}$$

In calculations, the approximation

$$i \approx \frac{d_2}{d_1} \tag{14.35}$$

may be used.

The efficiency depends on the belt slip only, with the bearing friction and windage being neglected, since the pull of either belt side at both pulleys must be assumed to be equal:

$$\eta = \frac{P_2}{P_1} = \frac{M_2}{iM_1} = 1 - \frac{\sigma_n}{E} = 1 - \psi \tag{14.36}$$

where

$$M_1 = F_u \frac{d_1}{2} \qquad M_2 = F_u \frac{d_2}{2} \tag{14.37}$$

The bending frequency, which is of particular importance for belt life, is calculated by

$$f_b = \frac{vz}{l} \tag{14.38}$$

It should not exceed the limit specified for the particular belt material.

Modern high-performance flat belts are designed as multiple-ply belts. They consist of two or three plies, each serving a special purpose. Leather belts made from hide and balata belts are no longer used. In some cases, the improvements in power transmission capacity brought about by the development of modern high-performance flat belts are not fully utilized in standard belt-drive applications. The utilization of a drive unit is influenced by the design characteristics on which a flat-belt drive is based. Thus, it is advisable to always consider the whole flat-belt drive unit instead of just the flat belt.

The major components of a multiple-ply belt are the tension ply and the friction ply. The purpose of the tension ply is to absorb the forces resulting from the deformation of the belt by tensioning. The energy stored by tensioning of the belt at minimum elongation is the basis of the power transmission. In addition, the tension ply has to absorb the centrifugal forces acting on the belt during operation.

Since the materials used for the tension ply do not have the required frictional characteristics, a separate, laminated friction ply is used as the second layer. This friction ply, which is adapted to the operating conditions with regard to material and surface finish, transmits the friction forces from the pulley surface finish to the tension ply and vice versa (Fig. 14.15). The tension ply is usually made of highly drawn

TABLE 14.1 Service Factor c_B

Application		Prime movers		
Operating conditions	Examples	Alternating-current and three-phase motors with a low starting torque (up to 1.5 times nominal torque); dc shunt motors; internal combustion engines with eight or more cylinders	Alternating-current and three-phase motors with moderate starting torque (1.5 to 2.5 times nominal torque); internal combustion engines with six cylinders	Alternating-current and three-phase motors with high starting torque (above 2.5 times nominal torque); internal combustion engines with four cylinders or fewer
Continuous service, small accelerated masses	Liquid-stirring apparatus, agitators, calenders and drying equipment for paper manufacture, setters, slitters and folders, centrifugal pumps and compressors, fans up to 7.5 kW, light-duty woodworking machinery, sifting plants	1.2	1.4	1.6
Interrupted service without bumps, medium-sized accelerated masses	Agitators and mixers for semifluid media, machine tools (such as grinding, turning, drilling and milling machines), punches, embossing machines, presses, textile machinery, laundry machinery, fans above 7.5 kW, generators and exciters, rotary presses, vibrating screens	1.3	1.5	1.7
Interrupted service with bumps, medium-sized accelerated masses	Elevators and worm conveyors, centrifuges, paper manufacturing machinery such as grinding gear, pumps, shredders, beaters, piston pumps and compressors, blowers, high-power fans	1.5	1.7	1.8
Service with severe bumps, large accelerated masses	Crushers and rolling mills, ball mills, tile-molding machines, compressors and high-capacity pumps, hoists	1.6	1.8	1.9

The service factor c_B takes into account the type of prime movers and driven machines. Special operating conditions are not taken into account in these values. The factors stated are guide values.

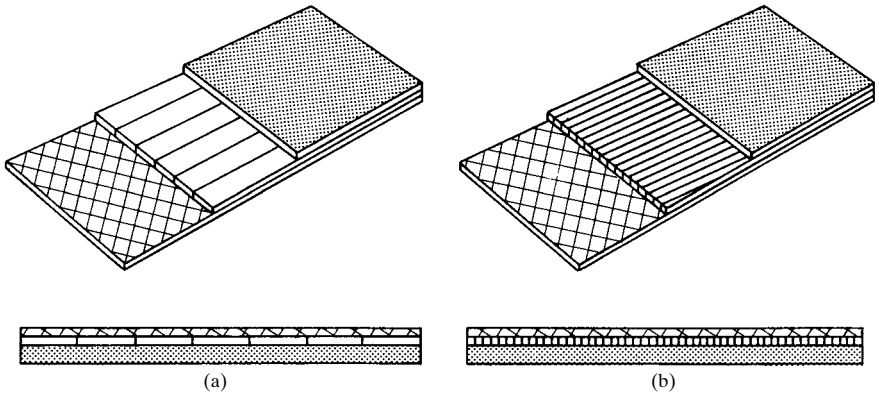

FIGURE 14.15 Multiple-ply belt.

polyamide strips or polyester cord. The friction ply, firmly attached to the tension ply, is made of either synthetic rubber or polyurethane or chrome leather. Table 14.2 shows the most important physical data for high-performance flat belts of the most commonly used tension ply materials, polyamide and polyester. The belts are manufactured in endless form according to the user length requirements or are made endless by heat-cementing the two beveled, feather-edged ends. Table 14.3 shows sizes of pulleys for flat belt drives and tolerances.

Calculations for a high-performance belt drive are usually based on data supplied by the belt manufacturer. Since the latest developments are always taken into consideration in this information, use of the latest manufacturers' data for the calculation is mandatory.

TABLE 14.2 Physical Data of High-Performance Flat Belts

Notion	Unit	Tension ply	
		Polyamid	Polyestercord
Tensile strength	N/mm^2	450–600	700–900
	N/cm	1300–18 000	1300–6600
Elongation at rupture	%	~22	~12–15
Stress at 1% elongation	N/cm	30–400	100–400
Service elongation	%	1.5–3.0	1.0–1.5
Specific nominal peripherical force	N/cm	40–800	100–400
Specific nominal power P_N	kW/cm	≤45	≤60
Maximum belt velocity	m/s	60–80	80–150
Maximum tolerable bending frequency	1/s	80–100	100–250
Elongation slip at nominal peripherical force	%	~0.8–1.0	~0.4–0.6
Attenuation (logarithmic decrement) ϑ		~0.28	~0.25
Efficiency η		0.98–0.99	0.985–0.99
Total thickness a	mm	1.0–8.0	0.8–4.0
Belt width	mm	Max. 1000	Max. 450
Belt length	mm	Unlimited	Max. 12 000

TABLE 14.3 Size of Pulleys for Flat-Belt Drives

Diameter d_1 nominal size	40	50	63	71	80	90	100	112	125
Allowable off size	0.5	0.6	0.8	1	1	1.2	1.2	1.2	1.6
Height of convexity	0.3	0.3	0.3	0.3	0.3	0.3	0.3	0.3	0.4
Tolerance of concentricity	0.2	0.2	0.2	0.2	0.2	0.2	0.2	0.3	0.3
Diameter d_1 nominal size	140	160	180	200	224	250	280	315	355
Allowable off size	1.6	2	2	2	2.5	2.5	3.2	3.2	3.2
Height of convexity	0.4	0.5	0.5	0.6	0.6	0.8	0.8	1	1
Tolerance of concentricity	0.3	0.3	0.4	0.4	0.4	0.4	0.5	0.5	0.5

In addition to the applicable ratings of the various high-performance flat belts, their types, and their configurations, the following data are necessary for the calculations for a single-step flat-belt drive:

1. Type of prime mover (driving assembly), e.g., electric motor, combustion engine, water turbine, etc.; this is important for the determination of the corresponding service-correction factors.
2. Type of machine (driven assembly); this determines corresponding load factors, dependent on acceleration, forces of gravity, changing loads, etc.
3. Power to be transmitted P, in kilowatts.
4. Speed of driving pulley n_1, in revolutions per minute.
5. Diameter of the driving pulley d_1, in millimeters.
6. Speed of the driven pulley n_2, in revolutions per minute.
7. Diameter of the driven pulley d_2, in millimeters.
8. Center distance e, in millimeters.
9. Adjustment range available (of tensioning device).
10. Allowable radial shaft loads of prime mover and driven assembly, loads on which the maximum shaft tensioning force F_w depends.

With the use of the above data and the manufacturer's data, calculations for the flat-belt drive can be made, giving the designer the type of belt, belt width, dynamic and static shaft stresses, and the required elongation, expressed as the percentage of belt strain.

Because of the special characteristics of flat-belt drives with high-performance belts, the determination of the drive data should be based on the following:

1. The belt velocity should be as high as possible (v_{opt}). The higher the belt speed, the smaller the belt width and thus the shaft load.
2. In calculating drives with changing loads or cyclic variations, you should determine to what extent the damping properties of the tension ply materials can be utilized.
3. You have to examine whether the initial tension of the belt or the shaft load can be accurately calculated from belt strain data.

4. The manufacturer can supply belts of all widths and lengths; you should examine, however, whether there are restrictions from the design point of view.
5. Finally, you must examine whether the belt can be manufactured in endless form or has to be assembled open-ended, with the ends being closed by welding after assembly.

The following general guidelines apply to pulley design:

1. The pulleys for open and crossed flat-belt drives are crowned in accordance with ISO R 100 (Table 14.3) in order to align the belt, which tends to move toward the larger pulley diameter.
2. For speed ratios higher than 1/3 ($i > 3$), the smaller pulley may be cylindrical. Spatial belt drives are equipped with cylindrical pulleys.
3. The requirements for smooth running of the belt are as follows: Parallelism of both shafts, smooth pulley faces, static balancing up to belt velocities v of 25 meters per second (m/s), and dynamic balancing for velocities above 25 m/s. When certain aluminum alloys are used, abrasion may occur, reducing friction between belt and pulley to such a degree as to make power transmission impossible.

Flat-belt drives are nonpositive flexible-connector drives used for the transmission of forces and motions between two or more shafts, particularly at greater center distances. This type of drive is superior because of its elasticity, enabling it to absorb shock loads, and its low-noise running. Its disadvantages are the greater forces acting on the shafts and bearings, resulting from the required initial tension, and the unavoidable belt slip.

These properties are decisive for the preferred applications of flat-belt drives, e.g., in machine tools, textile machinery, mixers and grinders, paper machines, gang saws, wire-drawing machines, presses, punches, and compressors. Flat belts with suitable contours may also be used as conveyor belts.

Figure 14.16 shows the drive of a hobbing machine. A high-performance flat belt was used in this case not because of its efficiency or damping properties, but because of the uniformity of rotational transmission from one pulley to the other. Preliminary studies have shown that even slight transmission deviations affect the dimensional accuracy of the tools manufactured on such machines. Belts for this application are subjected to a transmission accuracy test on a special test stand before delivery.

Figure 14.17 shows the tangential belt drive of a textile machine. This drive of a ring spinning frame is typical of a so-called multipoint drive or, in particular, a tangential belt drive. In this machine, a high-performance flat belt of 35-mm width and approximately 82-m length drives a total of 500 spindles on each side of the machine. The total power of 25 to 30 kW per machine side is thus distributed to 500 separate work positions. Depending on the spindle speed, the belt velocity ranges from 25 to 45 m/s. The absolute constancy of the belt operating tension throughout the life of the drive is a necessary prerequisite for this type of application.

14.3 V-BELT DRIVE

V-belt drives are nonpositive drives. The peripheral force F_u is transmitted by frictional forces acting on the flanks of the pulley-and-belt combination (Fig. 14.18). Bottoming of the belt in the groove leads to a reduction of the transmissible peripheral force, to belt slip, and to damages owing to overheating.

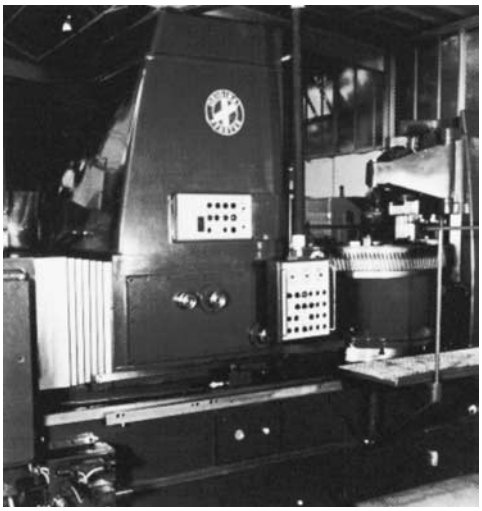

FIGURE 14.16 Drive of a hobbing machine. *(Siegling.)*

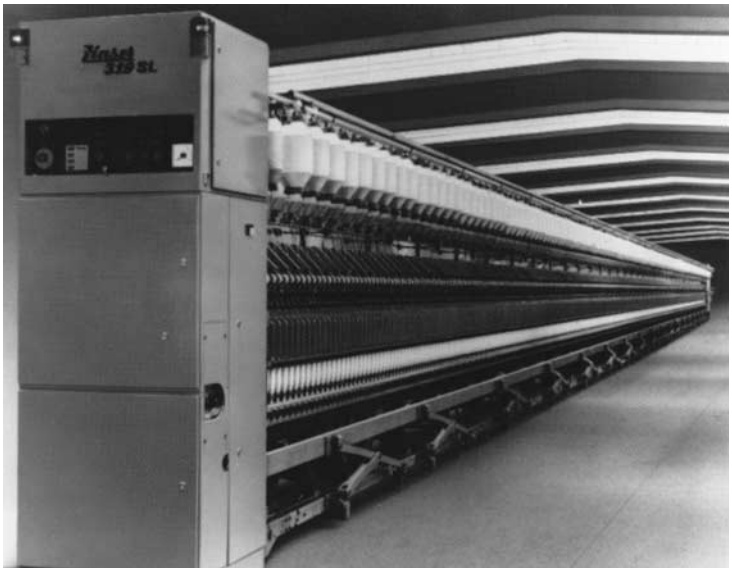

FIGURE 14.17 Tangential belt drive of a textile machine. *(Siegling.)*

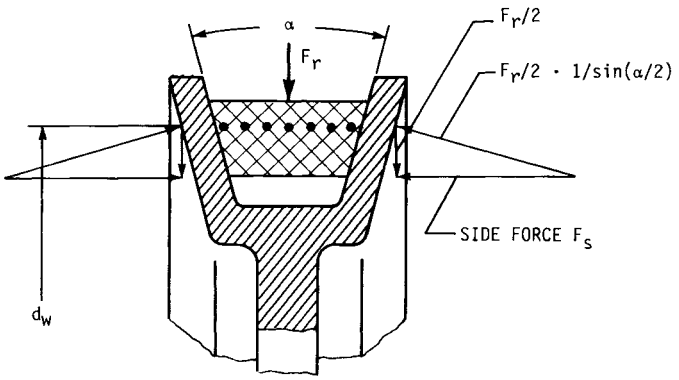

FIGURE 14.18 Section of a V-belt and sheave.

The known form of Eytelwein's equation cannot be used for the calculations for V-belt drives, since the belt creeps in the direction of travel and is simultaneously pulled radially into the groove by the radial component of the belt side force, with friction being reduced by this. Hence

$$\frac{F_1'}{F_2'} > \exp\left[\frac{\mu\beta\pi}{(\sin\alpha/2)180}\right] \tag{14.39}$$

The arc of contact β of the smaller pulley has to be used in the calculation of a V-belt drive.

In general, a belt angle α on the order of 36° is selected, since $\alpha < 20°$ would cause self-locking. Such a belt would operate with a lot of jerking and little efficiency. By bending around the pulley during operation, the belt is stretched on the outside and compressed on the inside, the belt angle thus being reduced compared to that of the straight belt. The smaller the pulley diameter, the larger the reduction of the belt angle. Since snug fit between belt and groove sides has to be ensured, the groove angle must be adjusted accordingly. Incorrect groove angles will reduce power transmission capacity and belt life.

The calculations for V-belt drives are internationally standardized (ISO R 155). In general, manufacturers' supply data for the calculations for V-belts and other belt types, too, are as follows:

Speed ratio:

$$i = \frac{n_1}{n_2} = \frac{d_{w2}}{d_{w1}} \tag{14.40}$$

For pulley diameters, standard series have been specified. When these pulley diameters are used, standardized speed ratios will result. Pulley diameters below the minimum values recommended for the belt section in question should not be used because the higher bending stress materially reduces belt life.

Distance between shaft centers:

$$\begin{aligned} &\text{Recommended lower limit: } e \geq 0.7(d_2 + d_1) \quad \text{mm} \\ &\text{Recommended upper limit: } e \leq 2(d_2 + d_1) \quad \text{mm} \end{aligned} \tag{14.41}$$

Shaft center distances that are too short (short belts) result in high bending frequencies, causing excessive heating and thus premature failure of the belt. Shaft center distances that are too long (long belts) may result in belt vibrations, especially of the slack side, also causing higher belt stress.

Adjustment of shaft center distance (Fig. 14.19):

$$X \geq 0.03L_w \quad \text{mm}$$
$$X \geq 0.015L_w \quad \text{mm} \tag{14.42}$$

The importance of the adjustability of the shaft center distance for tensioning and retensioning of the belt (X) as well as for easy application of the belt (Y) is often underestimated. The quantity Y in particular is often neglected, resulting in application problems, and the use of tools may cause belt damage when the belt is first applied.

The transmissible power of the belt is given by

$$P = 2\pi nM \tag{14.43}$$

where M = known torque and n = speed of the corresponding pulley.

Taking into consideration a service-correction factor c_B (Table 14.1), we can calculate the power rating of the drive from P by

$$P = c_B P_1 \tag{14.44}$$

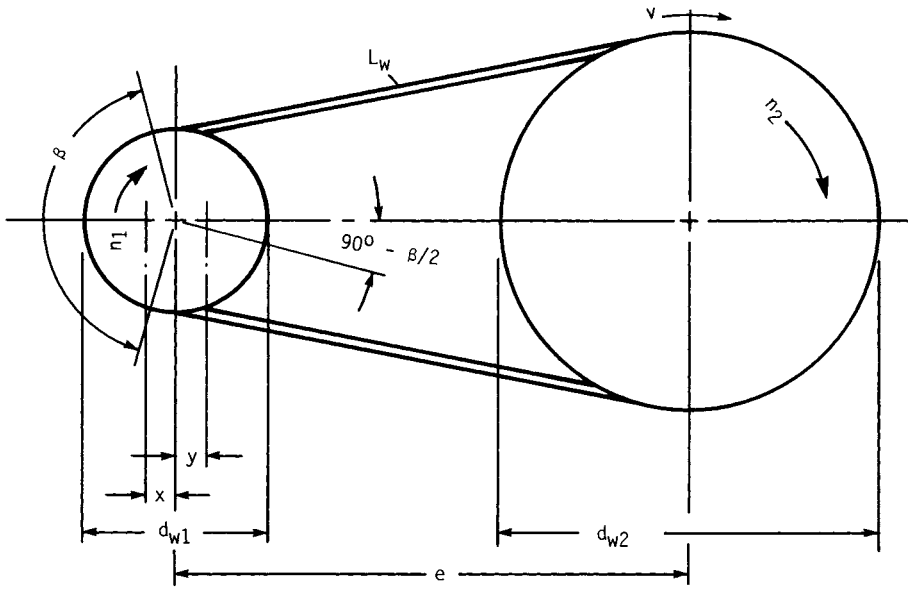

FIGURE 14.19 Adjustment of shaft center distance.

The calculation of belt velocity (peripheral velocity) is not really necessary, as the power rating tables are based on pulley diameter and speed:

$$v = \pi d_1 n_k \approx \pi d_2 n_g \tag{14.45}$$

For multiple drives, the number of V-belts required is calculated from

$$z = \frac{P c_B}{P_N c_1 c_3} \tag{14.46}$$

The arc of contact factor c_1, the service factor c_B, and the belt length correction factor c_3 can be found in the manuals of the manufacturers. The power rating P_N of each belt—based on the selected pitch diameter d_{w1} of the smaller pulley, the corresponding speed n_1, and the speed ratio—can be derived from tables. These tables also contain the nominal values of the service-correction factors to be used. When the guidelines mentioned in the design of a V-belt are observed, the belt life to be expected is 24 000 hours (h) of operation.

As for flat belts, the bending frequency is

$$f_b = \frac{vz}{l} \tag{14.47}$$

Normal bending frequencies are

$f_b < 30$ per second for endless standard V-belts

$f_b < 60$ per second for endless narrow-V-belts

The belts have to be pretensioned to limit belt slip to 1 percent. Improperly pretensioned belts have a life substantially shorter than the 24 000 h mentioned. The necessary initial tension will lead to equivalent shaft or bearing loads.

The approximate equation for the calculation of the required average shaft tension force is

$$F_w \cong \frac{aP}{v} \qquad 1.5 \le a \le 2 \tag{14.48}$$

where P = power to be transmitted and v = belt velocity. More accurate methods may be found in the manufacturers' publications containing a description of the correct initial tension adjustment by force and deflection measurements at the center of the belt side.

The different belt types are distinguished by section dimensions; the configurations, however, are distinguished by belt construction. Figure 14.20 shows the most widely used V-belt configurations.

V-belts consist of the following firmly vulcanized elements:

1. Intermediate ply of high-strength cord (cotton, polyester) for transmission of the rope-pull force
2. Highly elastic belt body (rubber, plastic) for transmission of the peripheral forces between the belt flanks and the cord ply

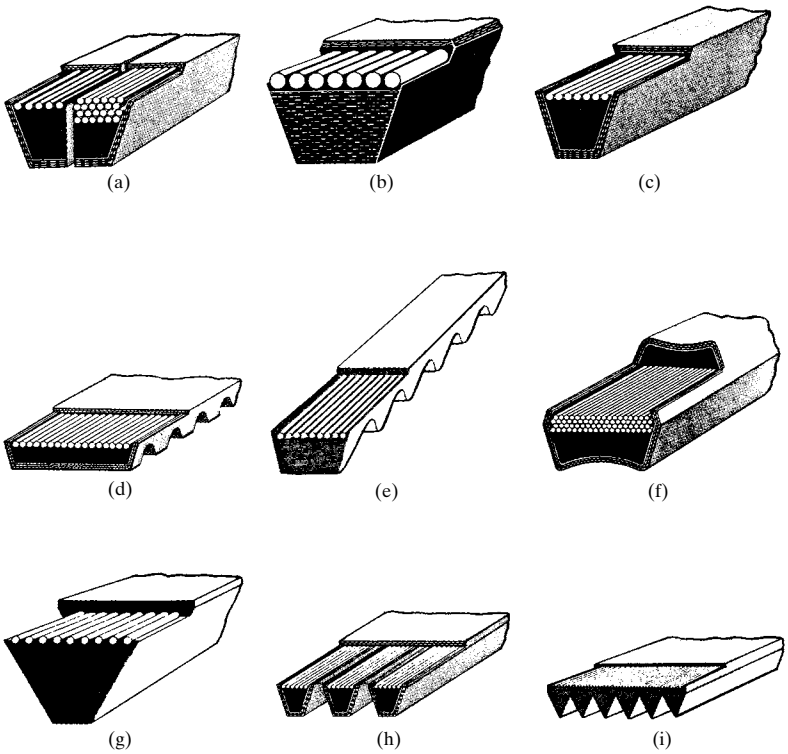

FIGURE 14.20 V-belt configurations.

3. Impregnated wear-resisting fabric coat (textile fibers) for transmission of the friction forces between the belt flanks and the V-belt pulley

Because of its higher modulus of elasticity, the cord ply forms both the neutral axis and the pitch diameter d_w of the V-belt in the groove, i.e., that diameter which is relevant for the transmission of peripheral velocity.

The endless standard V-belts (Fig. 14.20*a*) in accordance with ISO R606 are supplied in specified lengths and cannot be shortened.

Endless narrow-V-belts (Fig. 14.20*c*) in accordance with ISO R 459 and R 460 are most widely used today. Their power transmission capacity is higher than that of standard V-belts of the same pitch width.

FO-type V-belts (Fig. 14.20*b*), made by the Continental Gummi-Werke AG, are distinguished by their basically different construction. They are a promising new development superior to others for the unusually small change of length their tension members undergo when loaded. Transverse short fibers in the rubber filler lead to high lateral stiffness with high flexibility in the direction of belt travel. By grinding the flanks, the traveling accuracy of the FO-type V-belt can be improved systematically. The Continental belts of this type are manufactured as endless standard V-belts of small section dimensions and as endless narrow-V-belts.

The flexibility of the V-belts mentioned thus far may be increased by cross grooves worked into the inner surface of the profile (Fig. 14.20*e*). These grooved belts allow smaller pulley diameters and require less space at slightly reduced power transmission capacity than other belts; however, the grooves are the cause of periodic running in of shock loads and noise.

A V-belt assembly (Fig. 14.20*h*) is composed of up to five standard or narrow-V-belts connected by an elastic cover band which does not rest on the pulleys. The cover band prevents twisting or excessive vibration of individual belts.

The grooves of the V-belt pulleys are standardized (ISO standards). The pulleys are castings or weldings or steel-plate parts. In general, pulley diameters below the minimum specified should not be used. The groove flanks must be smooth and clean to ensure a sufficiently long belt life.

Applications of V-belts are practically unlimited. Because of the variety of sections available, the V-belt may be used for fractional-horsepower drives with minimum power transmission capacity in precision machines, phonographic equipment, and domestic appliances; for light drives, e.g., of centrifugal pumps and fans; and for all sizes of drives for general mechanical engineering purposes up to heavy-duty drives, such as rolling mill, rock crusher, excavator, and crane drives.

In general, the power transmission capacity is approximately 700 kW maximum; it may be increased to 1000 kW and in very rare cases to approximately 5000 kW.

Because of the extreme variety of applications in mechanical engineering, general belt-life data cannot be given. Another explanation is that belt life largely depends on the conditions of use. Assembly and operating conditions affect belt life, as do environmental conditions such as oil, dust, and climatic conditions.

The power transmission capacities specified in the relevant standards are based on the very high empiric belt life of 24 000 h, which can be reached only under optimum operating conditions, i.e., no misalignment of the pulleys, no overload, correct belt tension, normal ambient conditions, etc.

One of the particularly important areas of V-belt application is the automotive industry with its large primary equipment production series and substantial spare-part need. The V-belt as a drive unit connects the crankshaft and different accessory units, e.g., generator, cooling-water circulating pump, and fan. The V-belt may also be used for driving air-conditioning equipment or turbosuperchargers. The life of car V-belts is calculated for a total distance of 50 000 to 80 000 kilometers (km).

If higher power transmission capacities are required in mechanical engineering, multiple drives (Fig. 14.21) are used. When used as main drives in situations involving high cost in case of failure, such as mine fan drives and drives used in the metallurgical, glass, and cement industries, multiple drives also meet the demand for safety, since the probability of sudden failure of a complete belt set is very small. The uniformity of initial tensions and speed ratios of all belts of multiple drives is a prerequisite for smooth running and equal distribution of total power to all belts. Differences in speed ratios and initial tensions will lead to a reduction in belt life. Thus the complete set of belts should be replaced, if necessary, not just a single endless belt.

14.4 SYNCHRONOUS-BELT DRIVE

The synchronous belt is a relatively new machine element combining the advantages of positive and nonpositive flexible connectors. In contrast to the nonpositive belt drives, the pulleys and belts of synchronous-belt drives have meshing teeth, allowing synchronous power transmission with angular accuracy (Fig. 14.22). To prevent rid-

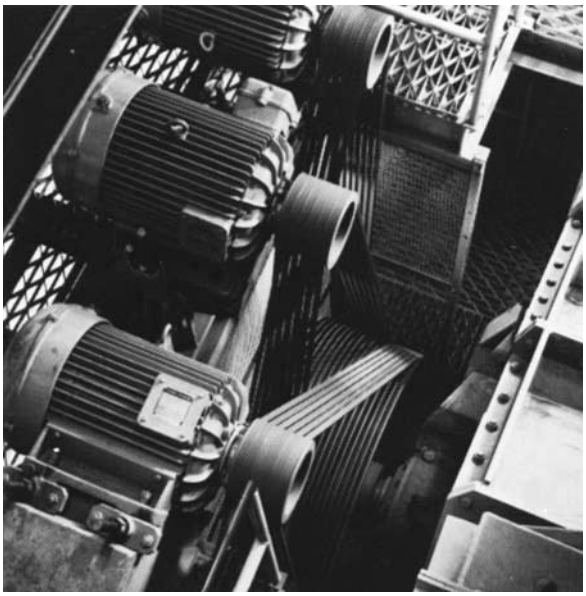

FIGURE 14.21 Multiple-V-belt drive of a crusher in mining. *(Arntz-Optibelt-KG.)*

ing off of the belt, at least one of the pulleys has flanges which are slightly beveled to reduce lateral friction.

Because of their special properties, synchronous belts are used wherever synchronous power transmission is asked for and the safety and freedom-from-maintenance requirements are strict.

As for all positive drives, the conformity of belt and pulley pitches is of utmost importance. The advancing belt tooth must correctly mesh with the corresponding pulley groove and remain there until leaving it. To achieve this, the pitch of the deflected belt must correspond exactly with that of the pulley. Hence, the belt must be made of high-strength material experiencing little length change under load; thus, the neutral axis may be assumed to be in the center. The pitch line is situated outside the pulley-tip-circle radius at a distance equaling that of the neutral axis (u value). This value is a largely invariable quantity which depends on the belt construction and must be taken into consideration in the design of the pulleys. Figure 14.22 shows the geometric relations between belt and pulley.

Despite the use of materials with little change of length under load for the tension member (fiber glass, steel cord), the belt pitch is a variable dependent on the strain properties of the belt and the applicable belt pull. Along the arcs of contact there is a step-by-step change in the belt pull with a corresponding change in local belt pitch, so that, in compensating belt and pulley pitch deviation, the teeth are deformed differently and the load differs accordingly. In addition, there is a minor pitch difference between belt and pulley, which is attributable to the production process and has to be compensated by deformation of the belt teeth, too.

The load distribution along the arc of contact as a measure of peripheral force distribution to the individual teeth is thus mainly dependent on the pitch deviation. The pitch deviation within the pretensioned belt (idling) is of particular importance:

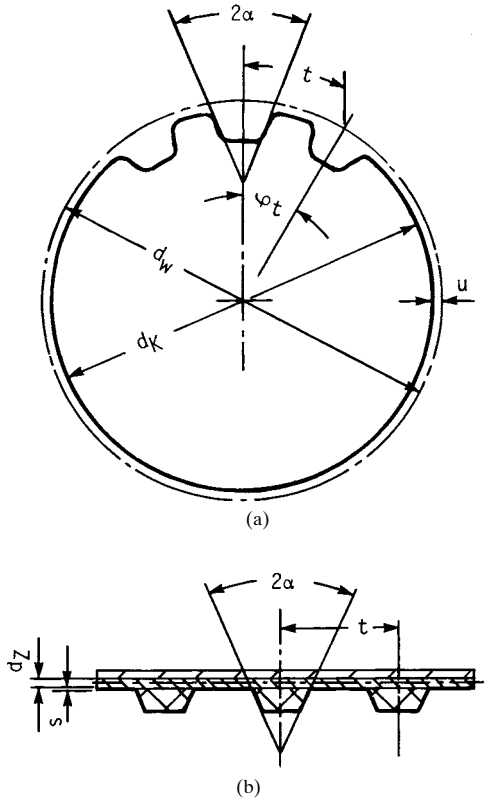

FIGURE 14.22 Synchronous-belt drive. (*a*) Pulley dimensions are d_w = working diameter, d_k = peripheral diameter, t = pitch, φ_t = pitch angle, u = theoretical distance to working diameter, and 2α = angle of tooth; (*b*) belt dimensions are d_z = diameter of tensile member and s = thickness of cover.

- Pitches of the pretensioned belt and the pulleys are exactly the same ($\Delta t = 0$). Load distribution is symmetric. The teeth at the beginning and at the end of the arc of contact carry a higher load than those along the center of the arc.
- The pitch of the pretensioned belt is smaller than the pulley pitch ($\Delta t < 0$). Load distribution is unsymmetric. Power is mainly transmitted at the beginning of the arc of contact (driven pulley) or the end of the arc of contact (driving pulley).
- The pitch of the pretensioned belt is larger than the pulley pitch ($\Delta t > 0$). Load distribution is unsymmetric. Power is mainly transmitted at the end of the arc of contact (driven pulley) or the beginning of the arc of contact (driving pulley).

For the driven pulley Fig. 14.23 shows the pull varying as a function of load-distribution deviations from the beginning of the arc of contact ($n/z = 0$) to the end of the arc of contact ($n/z = 1$).

Synchronous belts are available in different dimensions (pitch, belt width, and tooth geometry) according to the required application and range of capacity. The

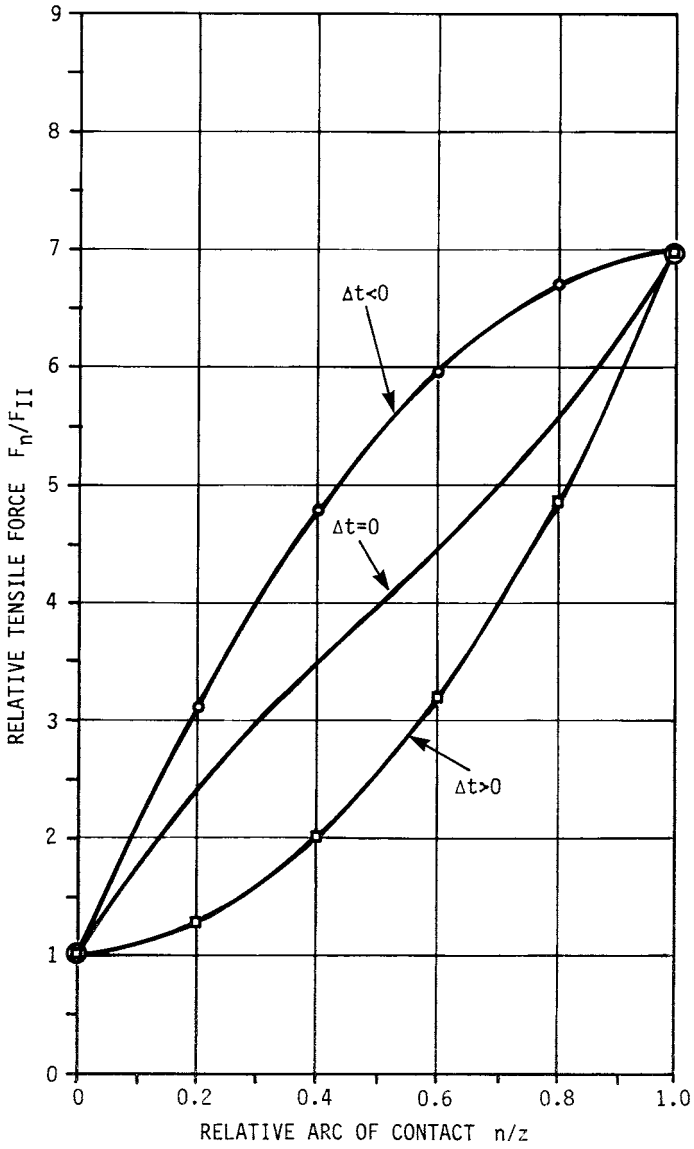

FIGURE 14.23 Theoretical tensile force diagram for the driven pulley.

transmissible power P is determined by the standard capacity P_N of the selected belt and by the operating conditions, expressed by the service-correction factor c_B:

$$P = \frac{P_N}{c_B} \tag{14.49}$$

The service-correction factors range from 1.0 to 2.10. The accurate value is determined by the type of drive and the type of application as well as the daily period of operation. For special applications, further restrictions may be required; details (meshing factor, acceleration factor, etc.) are contained in the manufacturers' catalogs.

The ranges of power transmission capacity are fixed in accordance with belt pitch. According to ISO 5296, standard belts have the standard pitch values shown in Table 14.4.

The capacities listed in Table 14.4 are nominal values for medium belt velocities; they may vary considerably to the positive or negative depending on the operating conditions. Accurate calculation has to be based on manufacturers' data.

When making calculations for a synchronous-belt drive, you must take into account that the pitch may be changed only in integral numbers, in contrast to non-positive belt drives. The individual design characteristics are as follows:

Speed ratio:

$$i = \frac{z_1}{z_2} = \frac{d_2}{d_1} \tag{14.50}$$

where z_2 = number of teeth of larger pulley
z_1 = number of teeth of smaller pulley
d_2 = pitch diameter of larger pulley
d_1 = pitch diameter of smaller pulley

Datum length:

$$l = 2e \sin \frac{d}{2} + \frac{t}{2} \left[z_1 + z_2 + \frac{\beta}{90^\circ} (z_2 - z_1) \right] \tag{14.51}$$

Approximation:

$$l \approx 2e + \frac{t}{2} (z_1 + z_2) + \left(\frac{t}{2\pi} \right)^2 \frac{(z_2 - z_1)^2}{l} \tag{14.52}$$

where z_1 = number of teeth of smaller pulley
z_2 = number of teeth of larger pulley
t = pitch, in
l = belt datum length = $z_R t$
z_R = number of belt teeth

TABLE 14.4 Standard Pitch Values

	Extra light (XL)	Light (L)	Heavy (H)	Extra heavy (XH)	Double extra heavy (XXH)
Belt pitch, in	$\frac{1}{4}$	$\frac{3}{8}$	$\frac{1}{2}$	$\frac{7}{8}$	$1\frac{1}{4}$
Nominal power, kW	0.15	1.0	10	40	100

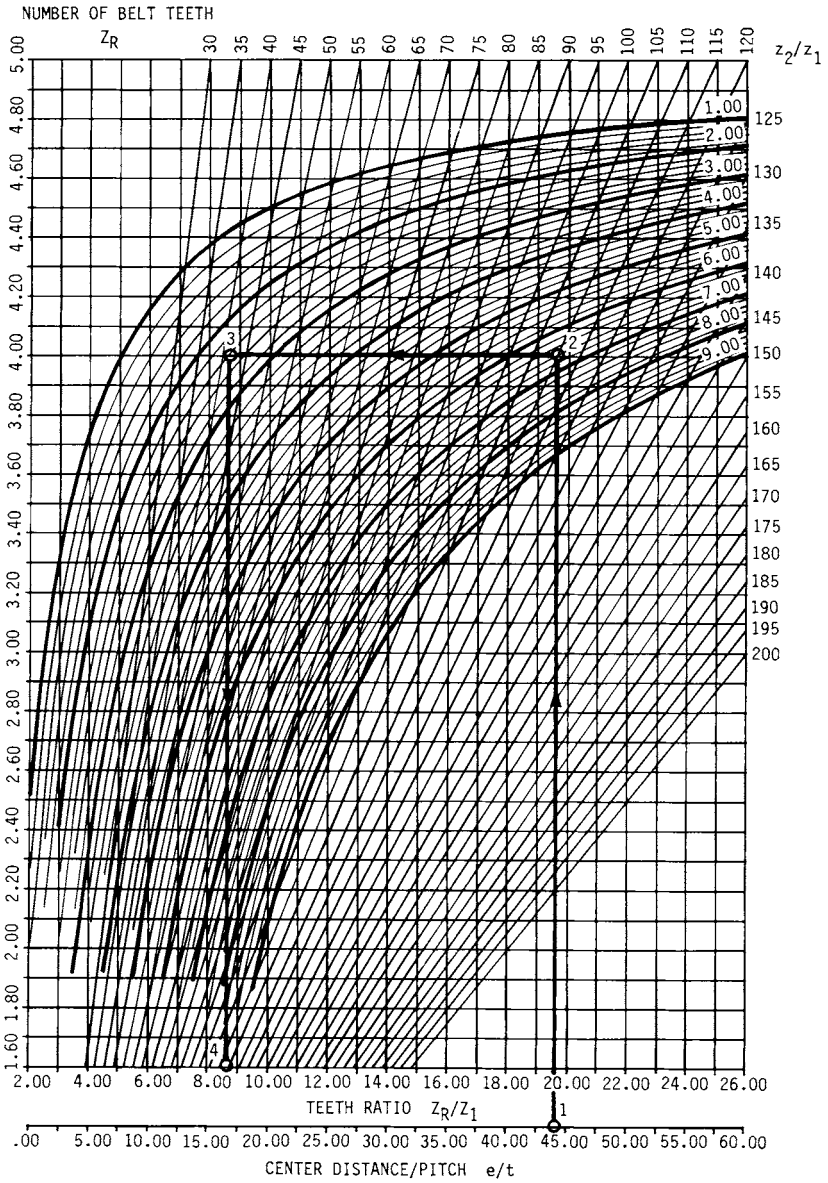

FIGURE 14.24 Determination of center distance of synchronous belts.

The accurate number of pulley and belt teeth for a given center distance may be found from detailed tables included in the manufacturers' catalogs. Guideline values may also be determined by using the nomogram in Fig. 14.24. Enter the nomogram at the ratio of given center distance to pitch (point 1), and proceed vertically to intersection 2 with the straight line indicating the number of teeth of the belt intended for use; then proceed horizontally from this point to intersection 3 with the curve of the given speed ratio. The number of teeth of the smaller pulley can be calculated from the applicable value on the axis of the tooth ratio of the belt and the smaller pulley (point 4), and the number of teeth of the larger pulley from the speed ratio; the results are rounded to the next higher whole numbers.

When calculating the number of teeth or the geometric design data, the designer has to ensure that the number of meshing teeth is at least six to eight. For the transmission of larger peripheral forces, the minimum number of meshing teeth has to be increased in accordance with manufacturers' data.

The transmissible peripheral force F_u is closely related to the effective shaft tensioning force F_w, which is dependent on the initial tensioning force F_A and the operating conditions. As in chain drives, the effective shaft tensioning force F_w increases with increasing load moment. As a guideline, assume the initial tensioning force F_A to be in the range

$$F_u \le F_A \le 1.5F_u \tag{14.53}$$

and the belt side-force ratio to be $F_{\mathrm{I}}/F_{\mathrm{II}} \cong 5$, where F_{I} is the tight-side force and F_{II} is the slack-side force.

The permissible initial tensioning force F_A is determined by the construction and the dimensions of the selected belt. Particular attention has to be paid to the fact that the belt should not be strained to such a degree as to prevent proper functioning of the belt-and-pulley combination because of the resultant pitch deviation.

In addition to the standard synchronous belts, according to ISO 5296, other types of synchronous belts with metric pitch but changed tooth configuration or shape are used for special applications. Figure 14.25 shows the different constructions of common synchronous belts.

The teeth of the standard synchronous belt (Fig. 14.25*a*) are trapezoidal. The belt is made of highly elastic synthetic rubber (polychloroprene) with an intermediate ply (tension member) of high-strength fiber-glass cord with little change of length under load. The pulley side of the belt is made of abrasion-resistant polyamide fabric. The back of the belt is ground to ensure nonpositive driving of belt tighteners or additional pulleys.

The polyurethane synchronous belt, shown in Fig. 14.25*b,* has a similar tooth shape. This belt is made of a highly elastic and abrasion-resistant plastic (polyurethane) and needs no pulley-side fabric cover to reduce wear. The intermediate ply taking the tension consists of steel cord, and so the belt strain is reduced to a minimum. The belt pitch is metric. Common pitch values are 5 mm for belt type T5, 10 mm for T10, and 20 mm for T20.

Heavy-duty belts are innovations with a tooth shape designed to ensure optimum distribution of the flank pressure over the entire tooth surface. The belt teeth have an enlarged cross-sectional area for the reduction of transverse (shear) stress, their edges being chamfered. Trade names differ among manufacturers (HTD, Super-Torque, etc.). Neither the tooth shape nor the pitch is standardized and both may vary with the product, although the pitch is usually metric. Belt materials and construction are similar to those of standard belts. Common pitch values are 8, 14, and 22 mm.

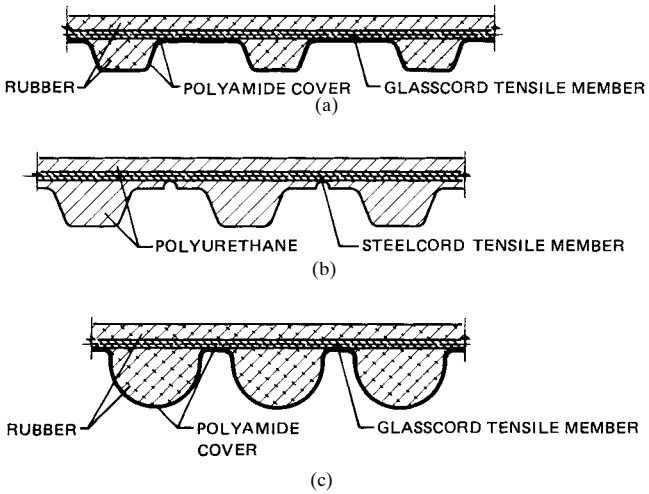

FIGURE 14.25 Construction and differences of timing belts. (*a*) Polychloroprene (rubber); (*b*) polyurethane; (*c*) heavy-duty.

In addition to the belt types mentioned above, there are special belts with pitches or tooth shapes adapted to particular applications. There exist also synchronous belts with teeth on the back to provide for a two-side running capability and others with special back configurations, e.g., for transportation purposes. Geometric data for these special belts may be found in the catalogs of the respective manufacturers. Figure 14.26 shows an assortment.

Because of their ability to transmit power synchronously with the required angular accuracy, synchronous belts are used to an ever-increasing extent, with new modes of application being added constantly. Classic applications are as follows:

- Light-duty conveyors (office machinery, food industry)
- Positioning drives (peripheral equipment of electronic data processing systems, machine tools, screening machinery)
- Synchronizing gears [camshaft drives (OHC), textile machinery, paper machinery]

Figures 14.27 to 14.29 show some typical synchronous-belt applications.

To ensure trouble-free operation and a long life of the drive, the following recommendations should be observed:

- The belt should be pretensioned only to the degree necessary to prevent skipping of the belt on starting or braking. Excessive initial tension leads to reduced belt life and in some cases to extreme noise levels.
- To prevent tension member damage (e.g., kinking or breaking), the belt has to be placed on the pulleys without tilting them. To facilitate this, an axial-shifting device should be provided on one of the pulleys.
- To prevent excessive wear of belt sides and noise from lateral contact of belt and pulley flanges, shafts and pulleys have to be aligned with extreme care. Slight lateral contact of belt and pulley flanges is attributable to the manufacturing process

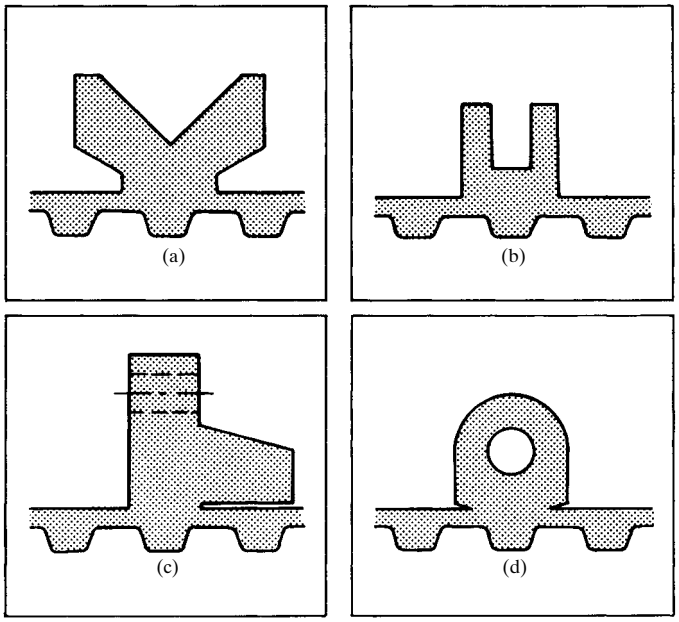

FIGURE 14.26 Synchronous belts with special back configuration.

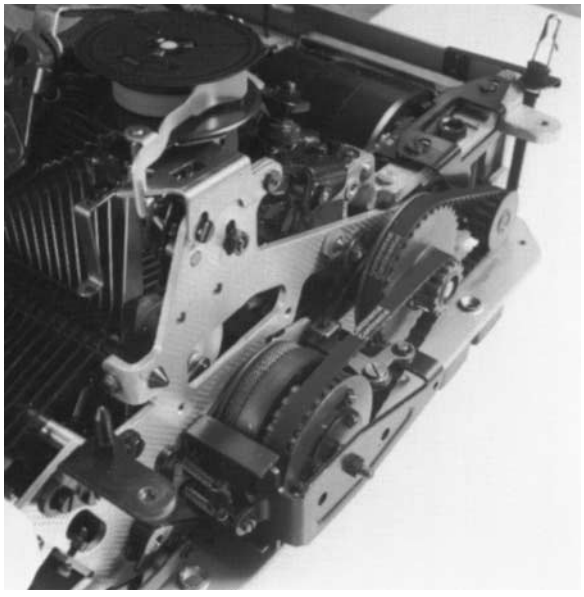

FIGURE 14.27 Synchrobelt timing belts for sophisticated typewriter drive mechanism. *(Continental Gummi-Werke Aktiengesellschaft.)*

FIGURE 14.28 Planer machine drive with Synchrobelt timing belt; the driving speed is 30 000 min^{-1}. *(Continental Gummi-Werke Aktiengesellschaft.)*

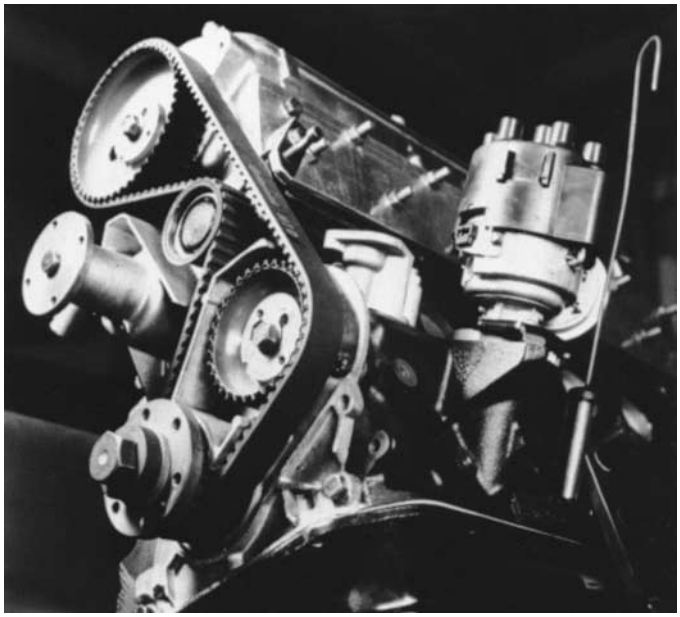

FIGURE 14.29 Camshaft control with Synchrobelt HTD timing belt. *(Continental Gummi-Werke Aktiengesellschaft.)*

(twisting of tension member and its slight inclination) and does not affect the running characteristics or the life of the belt.

- If feasible, belt tighteners should be arranged to act on the inner surface of the slack side of the belt; they should be toothed, too. The arc of contact should be as small as possible.

14.5 OTHER BELT DRIVES

14.5.1 Special Types

Poly-V-belts are similar to V-belt assemblies; however, their cover band rests on the pulleys, contains the cord, and takes the tension, whereas the individual V-sections, called *ribs,* solely transmit the peripheral force between pulley and cover band. The ribs have no cords (Fig. 14.20*i*) and fill up the pulley grooves almost to the bottom. Thus they are susceptible to foreign matter entering between the belt and the pulley. Because of the relatively rigid cover band resting on the face of the pulley, particularly accurate alignment of the pulleys is required, as it is with flat-belt drives. The belts are remarkably quiet.

V-belts with a belt-groove angle of 60° are cast belts (Fig. 14.20*g*) made of polyurethane with polyester tension members. Because of the higher friction coefficient of polyurethane on steel, the large included angle of 60° is required to prevent self-locking. Because of the manufacturing process, these belts show a substantially greater dimensional accuracy, resulting in particularly quiet operation. They are designed for maximum velocities of up to 50 m/s and are used mainly in machine tools.

Hexagonal (double-V) belts (Fig. 14.20*f*) have a symmetric special profile. The ratio of the maximum width to the height of the section is approximately 1.25. Double-V-belts may be operated in one plane on counterrotating pulleys. The power transmission capacity is approximately equal to that of conventional V-belts of equal width with small pulley diameters. Minimum pulley diameters are also about equal to those of conventional V-belts. Double-V-belts are suited for multiple-shaft drives operated in one plane with counterrotating pulleys. They are especially suited for coupled operation, with a tensioning or coupling shaft riding on the back of the belt and being able to transmit power, too.

Double-V-belts are used for medium-duty drives (combine harvester) as well as for light-duty tools (gardening equipment, rotary sweepers).

Toothed V-belts, which must not be confused with synchronous belts, are available as standard, narrow-, and wide-V-belts with punched or preformed teeth in the belt carcass to increase flexibility. Thus, with only a slight reduction in power transmission capacity, the minimum permissible diameter of the smaller pulley may almost be halved, so that the space requirement of such a belt drive with equal ratio or speed range is reduced substantially. These toothed V-belts are subject to the effects produced by their polygonal shape; i.e., the teeth cause running in of shock loads (which may result in irregular transmission of motion), additional dynamic stress of bearings, and even (in the case of high peripheral velocities) noise.

Round belts are versatile, simple, and reliable connectors for the transmission of small torques and medium velocities. Their main advantage is polydirectional flexibility. There are two different types: homogeneous round belts made of one material (rubber, plastic) and round belts with tension member (Fig. 14.30).

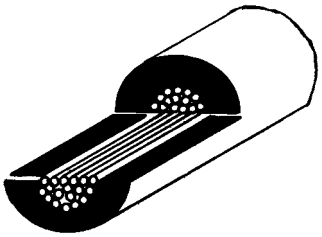

FIGURE 14.30 Continental round section belt.

14.5.2 Variable-Speed Belt Drives

For variable-speed belt drives (with a continuously variable speed ratio), especially wide V-belts have been developed in toothed and nontoothed configurations. The construction corresponds to that of endless standard V-belts with the exception of the substantially greater belt width. This great belt width (the ratio of the upper width of the belt to the section height $b/h = 2/5$) is required for radial shifting on pulleys, the halves of which can be moved in an axial direction (Fig. 14.20*d*). These variable-speed belt drives allow for a continuously variable speed ratio within the range of $i_{max}/i_{min} = 4/10$. With larger ratios of belt width to section height, greater speed ranges are possible in general.

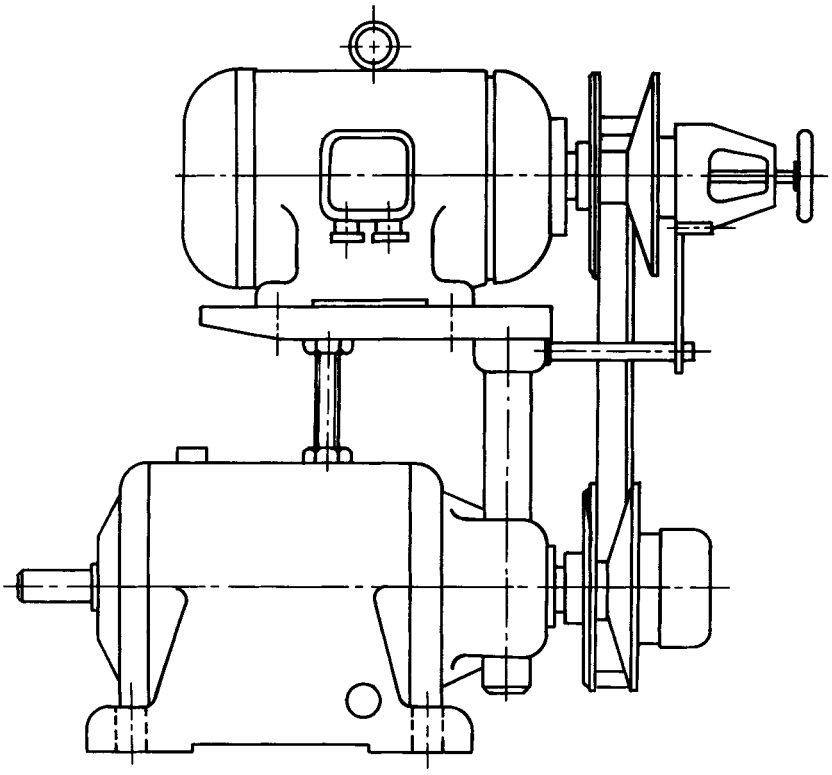

FIGURE 14.31 Variable-speed wide-belt drive.

The power transmission capacity of variable-speed belts is approximately equal to that of standard V-belts of equal section height; with increasing b/h ratio, however, it decreases by up to 20 percent. Depending on the speed range and the design of the variable-speed pulleys, the included angles range from 22° to 34° (ISO recommendation is 26°), with the smaller angles resulting in greater speed ranges but, because of the approach to the self-locking limit, reduced rated outputs.

A variable-speed wide-belt drive combined with an electric motor and a gear train is shown in Fig. 14.31. The top right half of the pulley may be shifted by turning the handwheel. The bottom pulley is an adjusting pulley (Fig. 14.32) which adapts itself automatically to the respective speed ratio.

14.6 COMPARISON OF BELT DRIVES

A flexible connector for a particular application should be selected on the basis of the following considerations:

- *Performance:* The flexible-connector drive has to perform reliably for an adequate period under the given operating conditions (speeds, moments, space

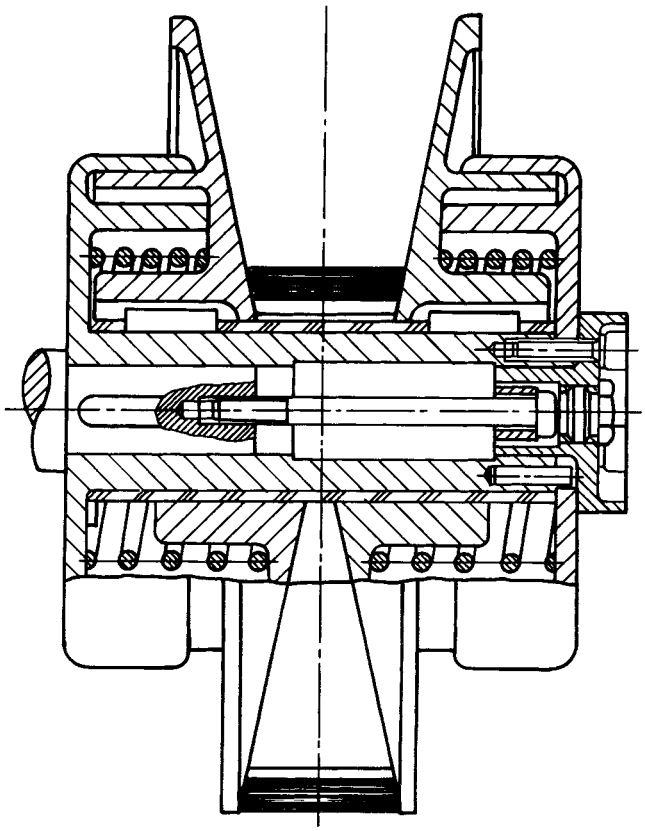

FIGURE 14.32 Adjusting pulley.

requirement, overloads, shaft dislocations, temperatures, and other environmental conditions).

- *Economy:* Those flexible-connector drives suitable under performance criteria are further investigated with respect to their applicability from the economic point of view. The economy of flexible drives is influenced by the following factors:

  1. Production cost of the flexible connector
  2. Subsequent design expenses required because of the selection made (e.g., pulley costs, costs of larger bearings to take up the required initial tensioning force, costs of lubrication facilities and seals required, of special installation arrangements, and of tensioning devices)
  3. Transportation and installation costs, mainly dependent on the space requirement and the weight of the drive
  4. Operation and maintenance costs
  5. Failure risk as well as costs of repair and subsequent costs

The relative importance of these factors varies with the machines used, and the costs of the flexible connector as the drive element are the least important. A drive unit will prevail wherever its special technical properties ensure the most economical drive.

To facilitate the selection of suitable flexible connectors, Table 14.5 compares the most important operating characteristics of flexible connectors and remarks on investment costs as well as maintenance and installation.

Figure 14.33 shows the results of a comparison of costs, when different flexible connectors are used, for a system consisting of two pulleys, the flexible connector, and the driven shaft, including the required roller bearings. The costs were determined following calculations for the drive with the power transmission capacity, the center distance, and the speed of the driving pulley given.

Figure 14.34 shows the specific power transmission capacity of different flexible-connector drives as a function of velocity. This specific power transmission capacity indicates the rating of the flexible connector and thus the space required. The higher the specific power transmission capacity of the flexible connector, the smaller the space required for the installation of the drive.

TABLE 14.5 Properties of Belt Drives

	Flat belts	Toothed belts†	Poly-V belts	Standard V belts	Narrow-V belts	Connected V belts†	Round belts†
Installation cost index	1.1	1.4	1.2	1.4	1.0	ND	ND
Maintenance	Yes	No	Yes	Yes	Yes	Yes	Yes
Power per volume, kW/cm^3	0.8	1.9	1.7	0.7	1.8	ND	ND
Maximum bending frequency, Hz	200	200	100	40	80	40	40
Shaft load	$2F_u$–$3F_u$	F_u	$2F_u$–$2.5F_u$	$2F_u$–$2.5F_u$	$2F_u$–$2.5F_u$	$2F_u$–$2.5F_u$	$2F_u$–$3F_u$
Efficiency, %	98	98	97	95	96	94	95
Diameter transmission	Constant	Constant	Constant		Variable		Constant
Bending rate d/s, dimensionless	15	15–30	5–11	8–14	8–12	8–14	8–10
Girder rate F_u/F_w, dimensionless	0.3–0.4	1	0.4–0.5	0.5–0.6	0.5–0.6	0.4–0.5	0.4
Admissible temperature, °C	−40 to +80	−50 to +120	−50 to +100	−55 to +70	−55 to +70	−55 to +70	−40 to +100
Adjustment of shaft center distance X, mm	$0.02L_w$	NA	$0.014L_w$	$0.02L_w$	$0.02L_w$	$0.02L_w$	$0.03L_w$
Mounting adjustment Y, mm	$0.01L_w$	$0.01L_w$	$0.02L_w$	$0.015L_w$	$0.015L_w$	$0.015L_w$	$0.01L_w$

†NA, not applicable; ND, no data.

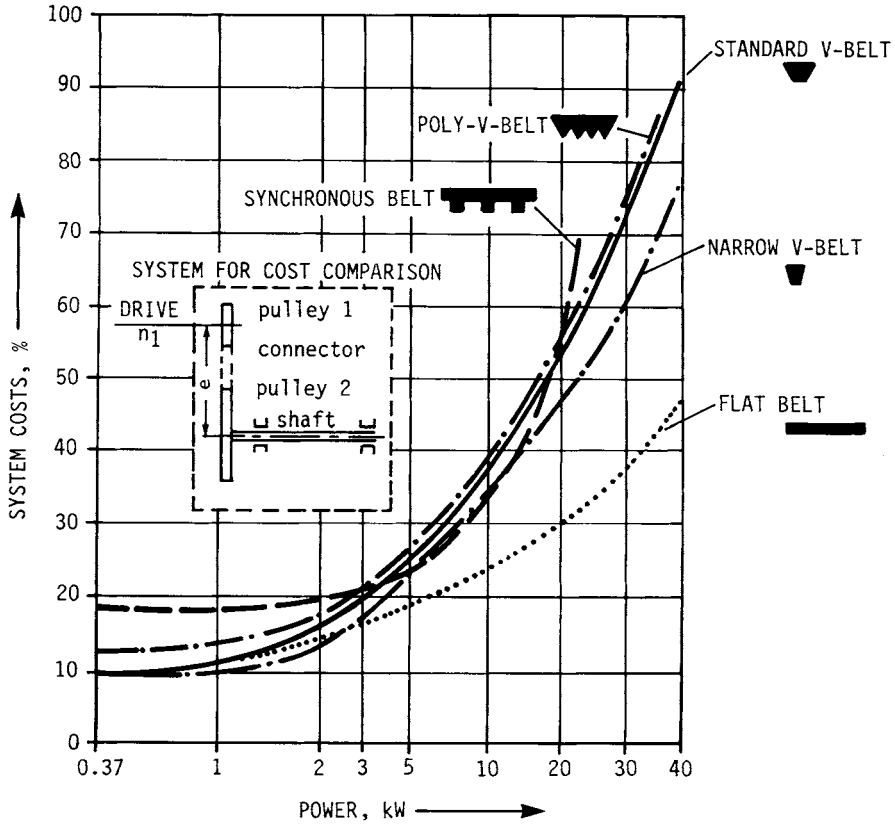

FIGURE 14.33 Comparison of system costs.

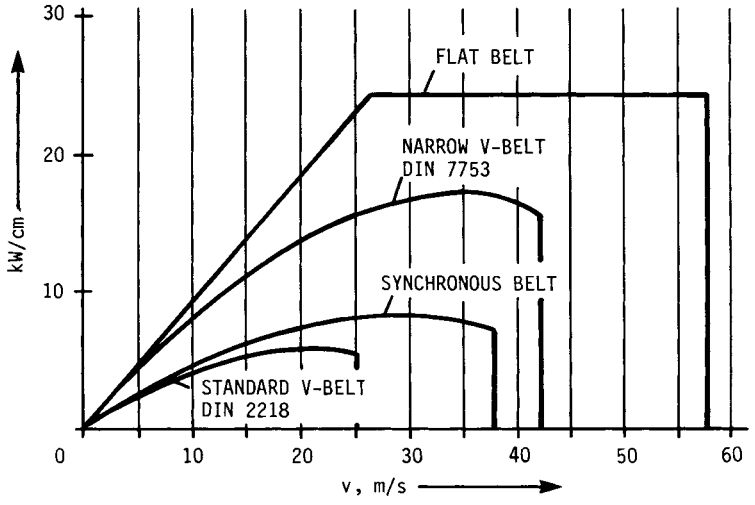

FIGURE 14.34 Specific power transmission capacity.

The figure also shows the range of applications of various flexible connectors and their maximum peripheral velocities. Belt drives reach their maximum specific power transmission capacity only at higher peripheral velocities.

It is not the maximum velocities, though, that determine the transmission of high specific powers, but the optimum velocities. The latter vary for the different flexible connectors because of the differing ratio of average density to the permissible tensile strain, as shown in Fig. 14.35. Accordingly, flat belts are particularly suited for maximum speeds and V-belts for most of the medium speeds of common electric motor and piston engines.

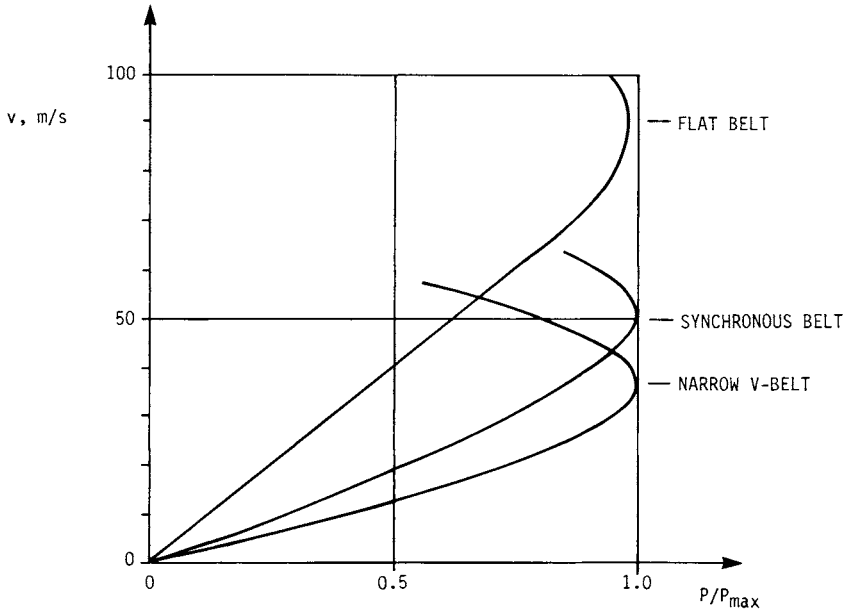

FIGURE 14.35 Optimum velocities.

CHAPTER 15
CHAIN DRIVES

John L. Wright
General Product Manager
Diamond Chain Company
Indianapolis, Indiana

NOTATION

BD	Bottom diameter, in
C	Center distance, in chain pitches
CD	Caliper diameter, in
CCD	Chain clearance diameter, in
D	Roller outside diameter, in
D_p	Gauge pin diameter, in
G	Maximum guide groove diameter, in
H	Maximum chain height, in
HP	Horsepower
K_f	Constant for link plate fatigue
K_r	Constant for roller and bushing impact
L	Chain length, in chain pitches
MHD	Maximum hub or groove diameter, in
MUTS	Minimum ultimate tensile strength, lb
n	Number of chain strands
N	Number of sprocket teeth
N_1	Number of teeth on small sprocket
N_2	Number of teeth on large sprocket

OD	Sprocket outside diameter, in
OGD	Over-gauge diameter, in
P	Chain pitch, in
PD	Sprocket pitch diameter, in
R	Sprocket speed, r/min
T	Thickness of link plate or sidebar, in
W	Chain (roller) width, in

15.1 TYPES, USES, AND CHARACTERISTICS

15.1.1 Chain Drives Compared

Three major types of chain are used for power transmission: roller, engineering steel, and silent. Roller chains are probably the most common and are used in a wide variety of low-speed to high-speed drives. Engineering steel chains are used in many low-speed, high-load drives. Silent chains are mostly used in high-speed drives. Other types of standard chains, and many types of special chains for unique applications, may be found in manufacturers' catalogs.

Chains can span long center distances like belts, and positively transmit speed and torque like gears. For a given ratio and power capacity, chain drives are more compact than belt drives, but less compact than gear drives. Mounting and alignment of chain drives does not need to be as precise as for gear drives. Chain drives can operate at 98 to 99 percent efficiency under ideal conditions. Chain drives are usually less expensive than gear drives and quite competitive with belt drives.

Chain drives can be dangerous. Provide proper guarding to prevent personnel from coming in contact with, or being caught in, a running drive. Any chain can break from unexpected operating conditions. If a chain breaks at speed, it can be thrown off the drive with great force and cause personal injury and property damage. Provide adequate guarding to contain a broken chain or to prevent personnel from entering an area where they might be struck by a broken chain. A broken chain can sometimes release a load and cause personal injury and property damage. Provide an adequate brake or restraint to stop and hold the load in case of a chain breakage.

15.1.2 Roller Chains

Standard Roller Chains. A portion of a typical roller-chain drive is shown in Fig. 15.1. The American National Standards Institute (ANSI) has standardized limiting dimensions, tolerances, and minimum ultimate tensile strength for chains and sprockets of 0.25 to 3.0 in pitch [15.1]. The chain pitch is the distance between successive roller, or bushing, centers, and is the basic dimension for designating roller chains. The standard includes both standard and heavy series chains.

Multiple-Strand Roller Chains. Multiple-strand roller chains consist of two or more parallel strands of chain assembled on common pins. They also are standardized [15.1].

Double-Pitch Roller Chains. Double-pitch roller chains are standardized in Ref. [15.2]. Double-pitch chains have the same pin, bushing, and roller dimensions as cor-

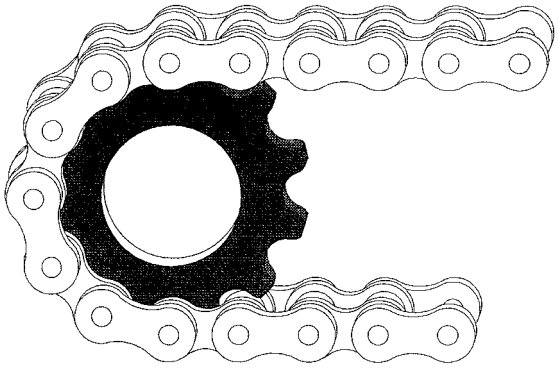

FIGURE 15.1 Typical roller chain on sprocket. *(Diamond Chain Company.)*

responding chains in Ref. [15.1], but the pitch of the link plates is twice as long. The standard [15.2] covers chains of 1.0 to 4.0 in pitch.

Nonstandard Roller Chains. Many manufacturers offer high-strength, extra-clearance, sintered metal bushing, sealed-joint, and corrosion-resistant chains for special applications or adverse environments. These chains are not covered by any standard, but most are designed to run on standard sprockets.

Sprockets. Roller-chain sprockets have precisely designed, radiused pockets which smoothly engage the rollers on the chain and positively transmit torque and motion. Driver sprockets receive power from the prime mover and transfer it to the chain. Driven sprockets take power from the chain and transfer it to the selected machinery. Idler sprockets transmit no power; they are used to take up slack chain, increase the amount of chain wrap on another sprocket, guide the chain around other machine members, and reverse the normal direction of rotation of another sprocket.

15.1.3 Engineering Steel Chains

Standard Engineering Steel Chains. The engineering steel chains designated for power transmission are heavy-duty offset sidebar chains. Limiting dimensions, tolerances, and minimum ultimate tensile strength for chains and sprockets of 2.5 to 7.0 in pitch are standardized in Ref. [15.3].

Nonstandard Chains. Some manufacturers offer engineering steel chains in straight-sidebar and multiple-strand versions, and in pitches that are not included in Ref. [15.3]. Although these chains are not standardized, they are listed in manufacturers' catalogs because they are used extensively in special applications.

Sprockets. Machine-cut engineering-steel-chain sprockets look much like roller-chain sprockets, but they have pitch line clearance and undercut bottom diameters to accommodate the dirt and debris in which engineering-class chain drives often operate.

15.1.4 Silent Chain

Standard Silent Chains. Silent (inverted-tooth) chains are standardized in Ref. [15.3] for pitches of 0.375 to 2.0 in. Silent chain is an assembly of toothed link plates interlaced on common pins. The sprocket engagement side of silent chain looks much like a gear rack. Silent chains are designed to transmit high power at high speeds smoothly and relatively quietly. Silent chains are a good alternative to gear trains where the center distance is too long for one set of gears. The capacity of a given pitch of silent chain varies with its width. Standard widths of silent chain range from 0.5 to 6.0 in for 0.375-in pitch, and from 4.0 to 30.0 in for 2.0-in pitch.

Nonstandard Silent Chains. Some manufacturers offer silent chains with special rocker-type joints. These chains generally transmit higher horsepower more smoothly and quietly than the standard joint designs. However, they generally require sprockets with special tooth forms.

Sprockets. Silent-chain sprockets have straight-sided teeth. They are designed to engage the toothed link plates of the chain with mostly rolling and little sliding action.

15.2 ROLLER CHAINS: NOMENCLATURE AND DIMENSIONS

15.2.1 Standard Roller-Chain Nomenclature

Roller Chain. Roller chain is an assembly of alternating roller links and pin links in which the pins pivot inside the bushings, and the rollers, or bushings, engage the sprocket teeth to positively transmit power, as shown in Fig. 15.1 and the illustration with Table 15.1.

Roller Links. Roller links are assemblies of two bushings press-fitted into two roller link plates with two rollers free to rotate on the outside of each of the bushings.

Pin Links. Pin links are assemblies of two pins press-fitted into two pin link plates.

Connecting Links. Connecting links are pin links in which one of the pin link plates is detachable and is secured either by a spring clip that fits in grooves on the ends of the pins or by cotters that fit in cross-drilled holes through the ends of the pins. Illustrations of connecting links may be found in Ref. [15.1] or [15.4] or in manufacturers' catalogs.

Offset Links. Offset links are links in which the link plates are bent to accept a bushing in one end and a pin in the other end. The pin may be a press fit in the link plates, or it may be a slip fit in the link plates and be secured by cotters. Illustrations of offset links may be found in Ref. [15.1] or [15.4] or in manufacturers' catalogs.

15.2.2 Roller-Chain Dimensions and Numbering

Standard Chain Dimensions. The three key dimensions for describing roller chain are pitch, roller diameter, and roller width. The pitch is the distance between adjacent bushing centers. The roller diameter is the outside diameter of the chain rollers.

TABLE 15.1 Roller-Chain Dimensions

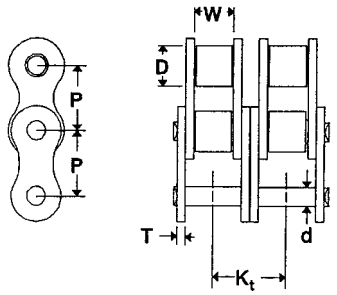

(Dimensions in inches; MUTS in lbf)

ANSI chain no.	Chain pitch, P	Roller diameter, D	Roller width, W	Pin diameter, d	Link plate thickness, T		Transverse pitch, K_t	
					Std.	Heavy	Std.	Heavy
25	0.250	0.130*	0.125	0.0905	0.030	—	0.252	—
35	0.375	0.200*	0.188	0.141	0.050	—	0.399	—
41**	0.500	0.306	0.250	0.141	0.050	—	—	—
40	0.500	0.312	0.312	0.156	0.060	—	0.566	—
50	0.625	0.400	0.375	0.200	0.080	—	0.713	—
60	0.750	0.469	0.500	0.234	0.094	0.125	0.897	1.028
80	1.000	0.625	0.625	0.312	0.125	0.156	1.153	1.283
100	1.250	0.750	0.750	0.375	0.156	0.187	1.408	1.539
120	1.500	0.875	1.000	0.437	0.187	0.219	1.789	1.924
140	1.750	1.000	1.000	0.500	0.219	0.250	1.924	2.055
160	2.000	1.125	1.250	0.562	0.250	0.281	2.305	2.437
180	2.250	1.406	1.406	0.687	0.281	0.312	2.592	2.723
200	2.500	1.562	1.500	0.781	0.312	0.375	2.817	3.083
240	3.000	1.875	1.875	0.937	0.375	0.500	3.458	3.985

* Bushing diameter. Chain is rollerless.
** Lightweight chain
Illustration courtesy of Diamond Chain Company.

The roller width actually is the inside distance between roller link plates. These and other selected dimensions are shown in Table 15.1.

Ultimate Tensile Strength. The minimum ultimate tensile strength (MUTS) for standard chains is given in Ref. [15.1]. The value is estimated from the equation

$$\text{MUTS} = 12\,500P^2n$$

Chain Numbering. A standard numbering system is described in Ref. [15.1]. The right digit indicates the type of chain: 0 for a standard roller chain, 5 for a rollerless bushing chain, and 1 for a light-duty roller chain. The left one or two digits designate the chain pitch in eighths of an inch; for example, 6 indicates ⅝, or ¾-in pitch. An H immediately following the right digit designates heavy series chain. Multiple-strand chain is designated by a hyphen and one or two digits following the right digit or letter. In Ref. [15.2], 2000 added to the chain number designates a double-pitch chain.

15.2.3 Roller-Chain Sprockets

Definitions and Types. Four styles of sprockets are standardized in Ref. [15.1]. Style A is a flat plate with no hub extensions. Style B has a hub extension on one side of the plate (flange). Style C has hub extensions on both sides of the flange. The extensions do not have to be equal. Style D has a detachable hub. The style D hub is normally attached to the flange with bolts. Most sprockets have a central bore with a keyway and setscrew to mount them on a shaft. Many other configurations of sprocket hubs and bores may be found in manufacturers' catalogs.

Tooth Form. The tooth form and profile dimensions for single- and multiple-strand roller-chain sprockets are defined in Ref. [15.1].

Sprocket Diameters. There are five important sprocket diameters defined in Ref. [15.1]. They are pitch, outside, bottom, caliper, and maximum hub diameters. The equations for those diameters, shown in Fig. 15.2, are

$$\text{PD} = P/\sin(180/N) \qquad \text{OD} = P[0.6 \cot(180°/N)]$$

$$\text{BD} = \text{PD} - D \qquad \text{CD} = \text{PD} \cos(90°/N) - D$$

$$\text{MHD} = P[\cot(180°/N) - 1] - 0.030$$

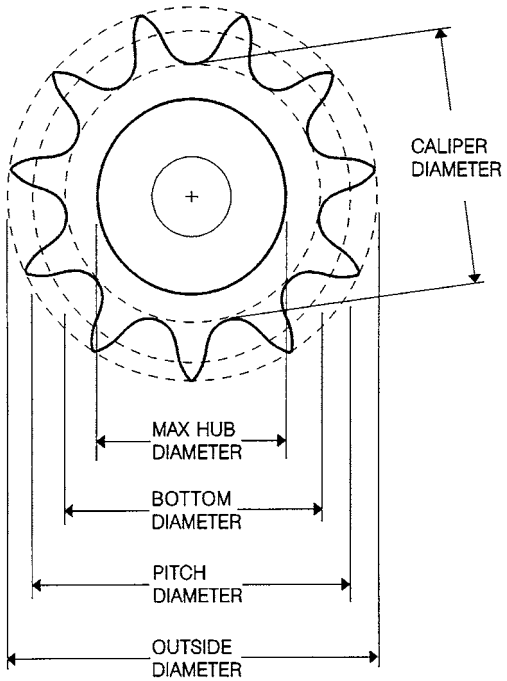

FIGURE 15.2 Roller-chain sprocket diameters. *(Diamond Chain Company.)*

15.3 SELECTION OF ROLLER-CHAIN DRIVES

15.3.1 General Design Recommendations

The following are only the more important considerations in roller-chain drive design. For more detailed information, consult Ref. [15.5] or manufacturers' catalogs.

Chain Pitch. The most economical drive normally employs the smallest-pitch single-strand chain that will transmit the required power. Small-pitch chains generally are best for lighter loads and higher speeds, whereas large-pitch chains are better for higher loads and lower speeds. The smaller the pitch, the higher the allowable operating speed.

Number of Sprocket Teeth

Small Sprocket. The small sprocket usually is the driver. The minimum number of teeth on the small sprocket is limited by the effects of chordal action (speed variation), as shown in Fig. 15.3. Lower speeds will tolerate more chordal action than higher speeds. The minimum recommended number of teeth on the small sprocket is

Slow speed	12 teeth
Medium speed	17 teeth
High speed	25 teeth

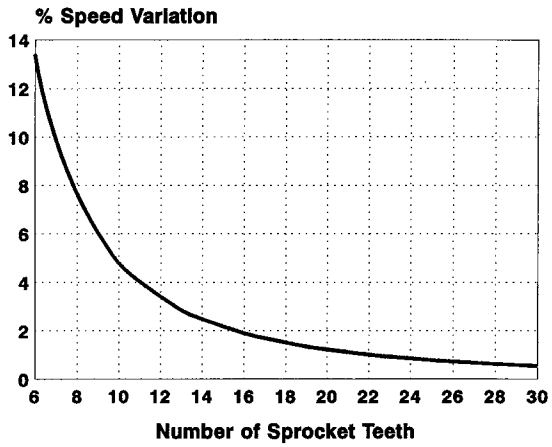

FIGURE 15.3 RC velocity variation versus number of teeth.

Large Sprocket. The number of teeth on the large sprocket normally should be limited to 120. Larger numbers of teeth are very difficult (expensive) to manufacture. The number of teeth on the large sprocket also limits maximum allowable chain wear elongation. The maximum allowable chain wear elongation, in percent, is $200/N_2$.

Hardened Teeth. The fewer the number of teeth on the sprocket, the higher the tooth loading. Sprocket teeth should be hardened when the number of teeth is less than 25 and any of the following conditions exist:

1. The drive is heavily loaded.
2. The drive runs at high speeds.
3. The drive runs in abrasive conditions.
4. The drive requires extremely long life.

Angle of Wrap. The minimum recommended angle of wrap on the small sprocket is 120°.

Speed Ratio. The maximum recommended speed ratio for a single-reduction roller-chain drive is 7:1. Speed ratios up to 10:1 are possible with proper design, but a double reduction is preferred.

Center Distance. The preferred center distance for a roller-chain drive is 30 to 50 times the chain pitch. At an absolute minimum, the center distance must be at least one-half the sum of the two sprocket outside diameters. A recommended minimum center distance is the pitch diameter of the large sprocket plus one-half the pitch diameter of the small sprocket. The recommended maximum center distance is 80 times the chain pitch.

The center distance should be adjustable to take up chain slack caused by wear. Adjustment of at least 2 pitches is recommended. If a fixed center distance must be used, consult a chain manufacturer.

Chain Length. Required chain length may be estimated from the following approximate equation:

$$L \doteq 2C + \frac{N_1 + N_2}{2} + \frac{N_2 - N_1}{4\pi^2 C} \tag{15.1}$$

Equation (15.1) will give chain length accurate to within ±½ pitch. If a more precise chain length is required, an equation for the exact chain length may be found in Ref. [15.5] or in manufacturers' literature.

The chain length must be an integral number of pitches. An even number of pitches is preferred. An odd number of pitches requires an offset link, and offset links reduce the chain's capacity.

Wear and Chain Sag. As a chain wears, it elongates. Roller-chain sprocket teeth are designed to allow the chain to ride higher on the teeth as it wears, to compensate for the elongation. Maximum allowable wear elongation normally is 3 percent. Where timing or smoothness is critical, maximum allowable elongation may be only 1.5 percent. The size of the large sprocket may also limit allowable elongation, as noted earlier.

As a chain elongates from wear, the excess length accumulates as sag in the slack span. In long spans, the sag can become substantial. It is important to design sufficient clearance into the drive to accommodate the expected amount of chain sag. For a drive with an approximately horizontal slack span, the required sag allowance for a particular amount of elongation is shown in Fig. 15.4. The drive centers should be adjusted periodically to maintain sag at 2 to 3 percent of the center distance.

Idlers. When the center distance is long, the drive centers are near vertical, the center distance is fixed, or machine members obstruct the normal chain path, idler

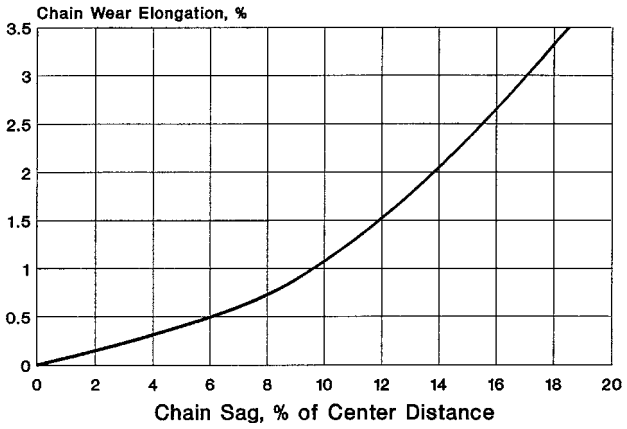

FIGURE 15.4 Chain sag versus center distance.

sprockets may be required. Idler sprockets should engage the chain in the slack span and should not be smaller than the small sprocket. At least 3 teeth on the idler should engage the chain, and there should be at least 3 free pitches of chain between sprocket engagement points.

Multiple-Strand Chain. Multiple-strand chain may be required when the load and speed are too great for a single-strand chain, or when space restrictions prevent the use of large enough single-strand sprockets.

Drive Arrangements. A number of recommended, acceptable, and not recommended drive arrangements are shown in Fig. 15.5.

15.3.2 Selection Procedure

Obtain Required Information. It is very important to obtain all the listed information before making a selection.

1. Source of input power
2. Type of driven equipment
3. Power to be transmitted
4. Speed and size of driver shaft
5. Speed and size of driven shaft
6. Desired center distance and drive arrangement
7. Means of center distance adjustment, if any
8. Available lubrication type
9. Space limitations
10. Adverse environmental conditions

Check for any unusual drive conditions, such as

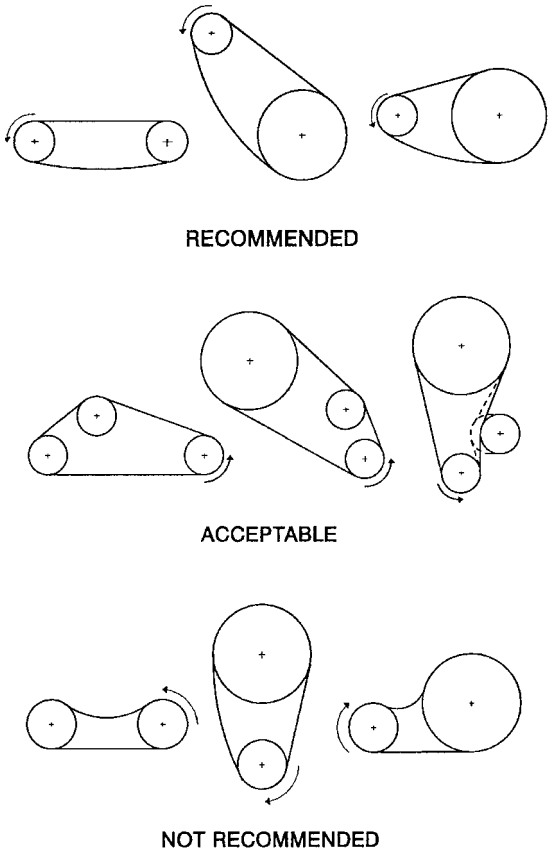

FIGURE 15.5 Drive arrangements.

- Frequent stops and starts
- High starting or inertial loads
- Temperatures above 150°F or below 0°F
- Large cyclic load variations in a single revolution
- Multiple driven shafts

If any of these, or any other unusual drive condition, is found, consult a chain manufacturer for help with the selection.

Determine Service Factor. The average required power for a drive usually is given. The peak power may be much greater than the average, depending on the power source and the driven equipment. A service factor, obtained from Table 15.2, accounts for the peak loads. The load classification for various types of driven equipment may be found in Ref. [15.1] or [15.5] or in manufacturers' catalogs.

Calculate Design Power. Obtain the design power by multiplying the average power times the service factor from Table 15.2.

TABLE 15.2 Service Factors for Roller Chain Drives

Type of driven load	Type of input power		
	Internal combustion engine with hydraulic drive	Electric motor or turbine	Internal combustion engine with mechanical drive
Smooth	1.0	1.0	1.2
Moderate shock	1.2	1.3	1.4
Heavy shock	1.4	1.5	1.7

Make Preliminary Chain Selection. Enter the chart, Fig. 15.6, with the design power and the speed of the small sprocket to select a preliminary chain. If no single-strand chain will transmit the design power at the required speed, or if space is restricted, multiple-strand chain may be required. If multiple-strand chain is to be selected, divide the design power by the multiple-strand factor, from Table 15.3, before entering the selection chart. Note that optimally the drive will operate near the peak of the rating curve. If the speed and power are low to moderate and the center distance is long, double-pitch chain may be acceptable. A selection procedure for double-pitch chains is given in Ref. [15.2].

TABLE 15.3 Roller Chain Multiple Strand Factors

Number of strands	Multiple strand factor
2	1.7
3	2.5
4	3.3

Select Small Sprocket. Refer to the horsepower tables in Ref. [15.1], [15.2], or [15.5] or in manufacturers' catalogs to select the small sprocket. Again, if multiple-strand chain is being considered, the design power must be divided by the proper multiple-strand factor from Table 15.3. Several different combinations of chain and sprocket sizes may be satisfactory for a given drive. Study the tables to see if increasing the number of teeth on the small sprocket might allow use of a smaller-pitch chain, or if decreasing the number of teeth on the small sprocket might allow use of a larger-pitch single-strand chain instead of a multiple-strand chain.

Consult sprocket manufacturers' catalogs to ensure that the sprocket bore capacity is adequate for the shaft. If it is not, select a larger sprocket.

Select Large Sprocket. Determine the number of teeth required on the large sprocket by multiplying the number of teeth on the small sprocket by the speed ratio. Ensure that the selected large sprocket will fit within any space restrictions and clear all obstructions. If there is an interference, a smaller-pitch, multiple-strand chain might be needed.

Make Final Chain Selection. Choose the most suitable drive from the alternatives selected earlier. The final choice may be based on economics, performance, effi-

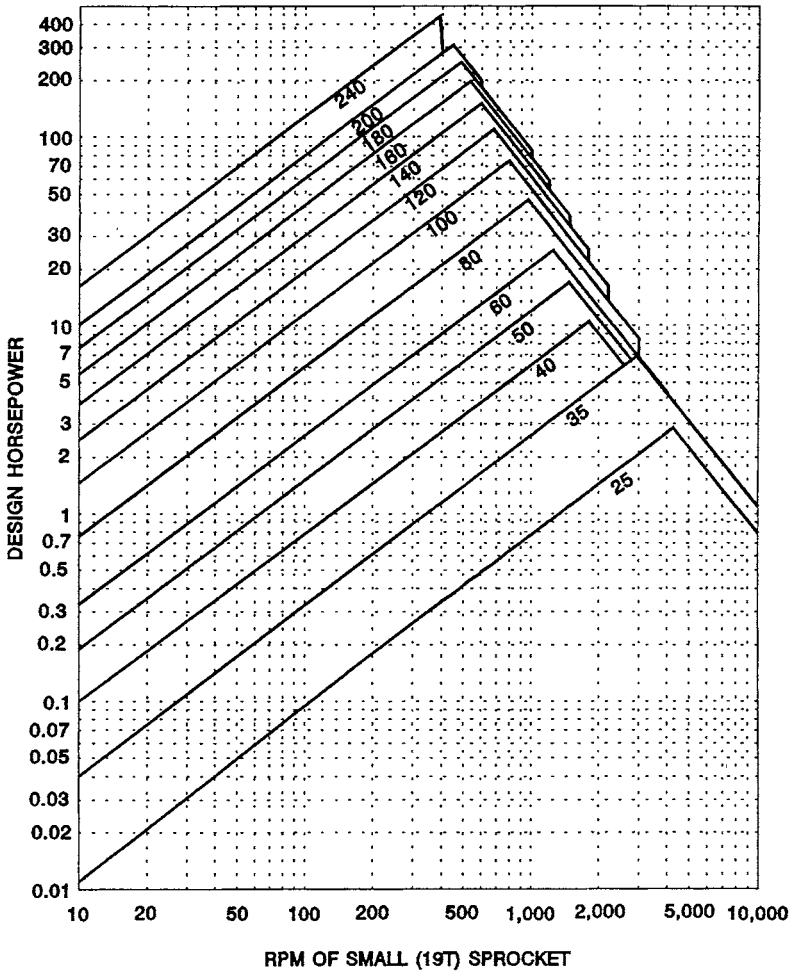

FIGURE 15.6 Roller chain selection chart.

ciency, space utilization, or a number of other considerations. Computer programs are available that automate the preliminary selection process and analyze the alternatives based on parameters provided by the designer.

Calculate Chain Length. For a two-sprocket drive, the approximate chain length may be estimated by Eq. (15.1). A more accurate chain length may be calculated by equations found in Ref. [15.5] or in manufacturers' catalogs. For three or more sprocket drives, the chain length may be estimated by graphic techniques, geometric layouts, computer programs, or certain CAD packages.

Determine Lubrication Type. The type of lubrication required may be obtained from the horsepower tables in Refs. [15.1] or [15.5], manufacturers' catalogs, or Sec. 15.4. It is very important to provide adequate lubrication to a roller-chain drive. Selecting an inferior type of lubrication can drastically reduce the life of the drive.

15.3.3 Power Ratings of Roller-Chain Drives

Conditions for Ratings. The roller-chain horsepower ratings presented in this section are based on the following conditions:

1. Standard or heavy series chain listed in Ref. [15.1]
2. Service factor of 1
3. Chain length of 100 pitches
4. Use of the recommended lubrication method
5. A two-sprocket drive, driver and driven
6. Sprockets properly aligned on parallel, horizontal shafts and chains
7. A clean, nonabrasive environment
8. Approximately 15 000 hours service life

Horsepower Rating Equations. When operating under the above conditions, the maximum horsepower capacity of standard roller chains is defined by the equations shown. Depending on speed and the number of teeth on the smaller sprocket, the power capacity may be limited by link plate fatigue, roller and bushing impact fatigue, or galling between the pin and the bushing. The power capacity of the chain is the lowest value obtained from the following three equations at the given conditions.

1. Power limited by link plate fatigue:

$$\mathrm{HP}_f = K_f N_1^{1.08} R^{0.9} P^{(3.0\,-\,0.07P)} \tag{15.2}$$

   where $K_f = 0.0022$ for no. 41 chain, and 0.004 for all other numbers.

2. Power limited by roller and bushing impact fatigue:

$$\mathrm{HP}_r = (K_r N_1^{1.5} P^{0.8})/R^{1.5} \tag{15.3}$$

   where $K_r = 29\,000$ for nos. 25 and 35 chain, 3400 for no. 41 chain, and 17 000 for nos. 40 through 240 chain.

3. Power limited by galling:

$$\mathrm{HP}_g = (\mathrm{RPN}_1/110.84)(4.413 - 2.073P - 0.0274N_2) - [\ln (R/1000)](1.59 \log P + 1.873) \tag{15.4}$$

The loci of these equations are presented in Fig. 15.6.

15.4 LUBRICATION AND WEAR

In all roller and engineering steel chains, and in many silent chains, each pin and bushing joint essentially is a traveling journal bearing. So, it is vital that they receive adequate lubrication to attain full potential wear life. Even silent chains with rocking-type joints are subject to some sliding and fretting, and so they also need good lubrication to obtain optimum wear life.

15.4.1 Purpose of Chain Lubrication

Effective lubrication aids chain performance and life in several ways:

1. By resisting wear between the pin and bushing surfaces
2. By flushing away wear debris and foreign materials
3. By lubricating the chain-sprocket contact surfaces
4. By dissipating heat
5. By cushioning impact loads
6. By retarding rust and corrosion

15.4.2 Lubricant Properties

General Lubricant Characteristics. Chain lubrication is usually best achieved by a good grade of nondetergent petroleum-base oil with the following properties:

- Low enough viscosity to penetrate to critical surfaces
- High enough viscosity to maintain an effective lubricating film at prevailing bearing pressures
- Free of contaminants and corrosive substances
- Able to maintain lubricating properties in the full range of operating conditions

Additives that improve film strength, resist foaming, and resist oxidation usually are beneficial, but detergents or additives to improve viscosity index normally are not needed.

Recommended Viscosities. The oil must be able to flow into small internal clearances in the chain, and so greases and very high-viscosity oils should not be used. The recommended viscosity for various ambient temperature ranges is shown in Table 15.4.

15.4.3 Application of Lubricant to Chain

Application Location and Flow Direction. It is vital to adequately lubricate the pin and bushing surfaces that articulate under load. It also is important to lubricate the surfaces between the roller and the bushing in roller and engineering steel chains. Oil should be applied to the upper link plate edges in the lower chain span just before the chain engages a sprocket. This places the oil where it can pass between the link plate faces and enter the critical bearing area. It also permits

TABLE 15.4 Recommended Oil Viscosity for Various Temperatures

Recommended grade	Temperature, °F
SAE 5	–50 to +50
SAE 10	–20 to +80
SAE 20	+10 to +110
SAE 30	+20 to +130
SAE 40	+30 to +140
SAE 50	+40 to +150

Source: Adapted from Ref. [15.6], p. 8, by courtesy of American Chain Association.

gravity and centrifugal force to aid the flow of oil in the desired direction. The extra oil that spills over the edges of the link plates should be adequate to lubricate the bearing surfaces between the rollers and the bushings in roller and engineering steel chain. It is important to supply oil uniformly across the entire width of silent and multiple-strand roller chains. For more information, see Refs. [15.5] and [15.6].

Flow Rates. When chain drives are transmitting large amounts of power at high speeds, oil-stream lubrication generally is required. The oil stream must cool the chain and carry away wear debris as well as lubricate the drive. A substantial oil flow rate is needed to accomplish all of that. The minimum flow rate for the amount of horsepower transmitted is shown in Table 15.5.

TABLE 15.5 Oil Flow Rates vs. Horsepower

Transmitted horsepower	Minimum flow rate, gal/min
50	0.25
100	0.50
150	0.75
200	1.00
250	1.25
300	1.50
400	2.00
500	2.25
600	3.00
700	3.25
800	3.75
900	4.25
1 000	4.75
1 500	7.00
2 000	10.0

Source: Adapted from Ref. [15.6], p. 12, by courtesy of American Chain Association.

15.4.4 Types of Chain Lubrication

All three types of chain drives—roller, engineering steel, and silent—will work with three types of lubrication system. The type of lubrication system used is dependent on the speed and the amount of power transmitted. The three types of chain drive lubrication systems are

Type 1. Manual or drip
Type 2. Oil bath or slinger disk
Type 3. Oil stream

A description of each type of lubrication follows.

Manual. Oil is manually applied periodically with a brush or spout can. The time period between applications is often 8 hours, but it may be longer if this is proven adequate for the particular conditions.

Drip. Oil is dripped between the link plate edges from a lubricator with a reservoir. Rates range from 4 to 20 drops per minute; 10 drops per minute is equal to about one ounce per hour. A distribution pipe is needed to direct oil to all the rows of link plates in multiple-strand chain, and a wick packing in the pipe will ensure uniform distribution of oil to all the holes in the pipe. Windage may misdirect the oil droplets. If that occurs, the lubricator must be relocated.

Oil Bath. A short section of chain runs through the oil in the sump of a chain casing. The oil level should not be higher than the pitch line of the chain at its lowest point in operation. Long sections of chain running through the oil bath can cause foaming and overheating. If that occurs, slinger disk–type lubrication should be considered.

Slinger Disk. The chain runs above the oil level while a disk on one shaft picks up oil from the sump and slings it against a collector plate. The oil is then directed into a trough which applies it to the upper edges of the chain link plates in the lower span of the chain. The disk diameter should be sized so that the disk runs at a rim speed of 600 to 8000 ft/min. Slower speeds will not effectively pick up the oil. Higher speeds can cause foaming and overheating.

Oil Stream. A pump sends a stream or spray of oil under pressure onto the chain. The oil must be applied evenly across the entire width of the chain, and it must be directed onto the lower span from the inside of the chain loop. Excess oil is collected in the sump and returned to the pump reservoir. The oil stream both lubricates and cools the chain when high power is transmitted at high speeds (Table 15.5). The oil may be cooled by radiation from the external surfaces of the reservoir or, if power is very high, by a separate heat exchanger.

15.4.5 Chain Casings

Chain casings provide a reservoir for the oil, contain excess oil slung off the drive, and prevent contaminants from contacting the drive. Chain casings usually are made of sheet metal, and are stiffened by embossed ribs or metal angles. Chain casings generally have doors or panels to allow access to the drive for inspection and maintenance.

Oil-retaining casings have single lap joints and single oil seals at each shaft opening. They are adequate for drip or oil bath types of lubrication. They are relatively

inexpensive, but they will allow some oil to escape and some dust and dirt to enter the casing. Oil- and dustproof casings have double lap joints and double oil seals at the shafts. They are strongly recommended for slinger disc and pressure stream types of lubrication. They are more expensive, but they virtually eliminate oil leakage and prevent contaminants from reaching the drive.

Sizing for Clearance. Sufficient clearance between the chain and the casing is essential if maximum potential wear life from the chain is to be obtained. At least 3 in clearance is needed around the periphery of the chain and ¾ in on each side of the chain. Additional clearance must be provided in the bottom of the casing to accommodate chain sag from wear elongation. The required allowance for chain sag may be obtained from Fig. 15.4.

Sizing for Heat Dissipation. A chain casing also may need sufficient surface area for heat dissipation. The oil temperature should not exceed 180°F (total of ambient temperature and temperature rise). The temperature rise for a given chain casing may be estimated from Eq. (15.5), which presumes 98 percent chain drive mechanical efficiency.

$$\Delta T_h = \frac{50.9 \text{ HP}}{AK_h} \tag{15.5}$$

where ΔT_h = temperature rise, °F
HP = transmitted horsepower
A = exposed casing area, ft^2
K_h = overall film coefficient of heat transfer, BTU/(h · ft^2 · °F)
K_h = 2.0 for still air, 2.7 for normal circulation, and 4.5 for rapid circulation

The equation may be rearranged to obtain the required surface area of the casing:

$$A = \frac{50.9 \text{ HP}}{\Delta T_h K_h} \tag{15.6}$$

If a casing with the required surface area is too large for the available space, a separate oil cooler may be needed.

This short section gives only the rudiments of designing a chain casing. More information may be found in Refs. [15.5] and [15.6], machine design textbooks, or manufacturers' literature.

15.4.6 Specific Lubrication Recommendations

Roller Chain. The required type of lubrication is directly related to the speed of a roller-chain drive. The limiting speeds for standard sizes of roller chain are shown in Table 15.6. More detailed information may be found in Refs. [15.5] and [15.6] or in manufacturers' literature.

Engineering Steel Chains. The required type of lubrication for an engineering steel drive is related to speed, but the relationship is more complex than for a roller-chain drive. The approximate limiting speeds for standard sizes of engineering steel chain, on 12-tooth sprockets only, are shown in Table 15.7. The values in the table are for general guidance only. When designing a drive, consult Ref. [15.5] or manufacturers' literature.

TABLE 15.6 Roller Chain Speed Limits by Lubrication Type

	Limiting speed, fpm												
ANSI No.	25	35	40	50	60	80	100	120	140	160	180	200	240
Type 1	480	350	300	250	215	165	145	125	110	100	90	80	75
Type 2	3250	2650	2200	1900	1750	1475	1250	1170	1050	1000	935	865	790
Type 3	At all speeds higher than for Type 2												

TABLE 15.7 Offset Sidebar Chain Speed Limits by Lubrication Type

	Limiting speed, rpm of 12-tooth sprocket only							
ANSI No.	2010	2512	2814	3315	3618	4020	4824	5628
Type 1	33	33	33	32	29	30	35	38
Type 2	300	200	160	115	100	85	65	N/A
Type 3	At all speeds higher than for Type 2							

Silent Chains. The required type of lubrication is related to speed for silent-chain drives also, but again, the relationship is more complex than for roller-chain drives. The approximate limiting speeds for standard sizes of silent chain are shown in Table 15.8. The values in the table are for general guidance only. When designing a drive, consult Refs. [15.4] and [15.5] or manufacturers' literature.

15.5 ENGINEERING STEEL CHAINS: NOMENCLATURE AND DIMENSIONS

The engineering steel chains that are specifically designated for power transmission are heavy-duty offset sidebar chains, standardized in Ref. [15.3].

15.5.1 Offset Sidebar Chain Nomenclature

In offset sidebar chain, each link is the same. Each link consists of a pair of offset-bent sidebars with a bushing assembled in one end of the pair of sidebars and a pin assembled in the other end. A roller that is free to rotate is assembled on each bushing. The pin is assembled into, and is free to pivot inside of, the bushing of the adjacent link, as shown in the illustration with Table 15.9.

TABLE 15.8 Silent Chain Speed Limits by Lubrication Type

	Limiting speed, FPM					
	Number of teeth on small sprocket					
	21	25	29	35	42	50
Type 1	1220	1250	1270	1290	1320	1350
Type 2	2400	2500	2650	2800	3000	3200
Type 3	At all speeds higher than for Oil Bath					

TABLE 15.9 Offset Sidebar Chain Dimensions

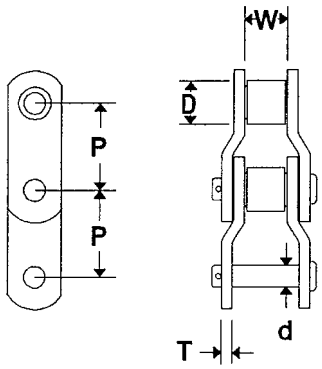

(Dimensions in inches, MUTS and F_w in lbf)

ANSI chain no.	Chain pitch, P	Roller width, W	Roller diameter, D	Pin diameter, d	Sidebar thickness, T	Minimum ultimate tensile strength, MUTS	Maximum allowable working load, F_w
2010	2.500	1.50	1.25	0.625	0.31	57 000	4 650
2512	3.067	1.56	1.62	0.750	0.38	77 000	6 000
2814	3.500	1.50	1.75	0.875	0.50	106 000	7 600
3315	4.073	1.94	1.78	0.938	0.56	124 000	10 000
3618	4.500	2.06	2.25	1.100	0.56	171 000	12 000
4020	5.000	2.75	2.50	1.250	0.62	222 500	17 500
4824	6.000	3.00	3.00	1.500	0.75	287 500	23 600
5628	7.000	3.25	3.25	1.750	0.88	385 000	60 500

Illustration courtesy of Diamond Chain Company.

15.5.2 Offset Sidebar Chain Dimensions and Data

Offset Sidebar Chain Dimensions. Just as for roller chain, the three key dimensions for describing offset sidebar chain are pitch, roller diameter, and roller width. These, other selected dimensions, minimum ultimate tensile strengths, and maximum working loads for standard offset sidebar chains are shown in Table 15.9.

Offset Sidebar Chain Numbering. A four-digit numbering system for designating standard offset sidebar chains is given in Ref. [15.3]. The left two digits denote the number of ⅛-in increments in the pitch. The right two digits denote the number of 1/16-in increments in the pin diameter. For example, chain no. 2814 designates a standard offset sidebar chain with 3.5-in pitch and ⅞-in pin diameter.

15.5.3 Sprockets

Machine-cut sprockets for offset sidebar chain look much like sprockets for roller chain. The standard (Ref. [15.3]) defines only tooth form, profile section, and important diameters. It does not define styles of sprockets because a great variety of styles

and materials are offered by manufacturers. When designing a drive, consult manufacturers' literature to select sprockets that will be appropriate for the application.

Tooth Form. The tooth form and profile dimensions for offset-sidebar-chain sprockets are defined in Ref. [15.3].

Sprocket Diameters. There are four important sprocket diameters defined in Ref. [15.3]. They are pitch, root, bottom, caliper, and chain clearance diameters. The equations for those diameters, shown in Fig. 15.7, are

$$\text{PD} = P/\sin(180/N) \qquad \text{RD} = \text{PD} - D \qquad \text{BD} = \text{RD} - C_b$$

$$\text{CD} = \text{BD}[\cos(90/N)] \qquad \text{CCD} = P[\cot(180/N) - 0.05] - H$$

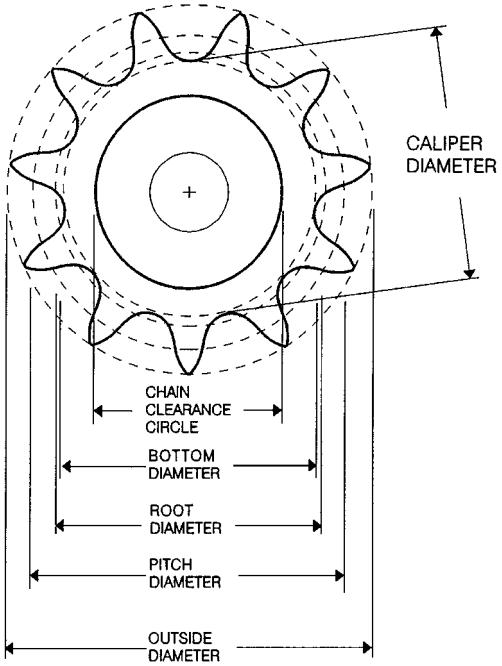

FIGURE 15.7 Engineering steel chain sprocket diameters. *(Diamond Chain Company).*

15.6 SELECTION OF OFFSET-SIDEBAR-CHAIN DRIVES

15.6.1 General Design Recommendations

Some of the general guidelines for offset-sidebar-chain selection are similar to those for roller-chain selection, but many are different. The selection of offset-sidebar-chain drives will be covered fully, even though there may be some repetition.

Chain Pitch. Generally, the smallest-pitch chain that will transmit the required power at the required speed provides the most economical drive.

Number of Sprocket Teeth

Small Sprocket. A small sprocket with 12 teeth is normally recommended. If the speed ratio is high or space is restricted, a small sprocket with 9 teeth is acceptable. If the speed ratio is low, center distance is long, and space is not limiting, a small sprocket with 15 teeth is suggested.

Large Sprocket. The size of the large sprocket is limited by available space, maximum allowable chain wear elongation, and manufacturing feasibility. Large sprockets with more than 66 teeth are not desirable because they limit maximum allowable chain wear elongation to less than 3 percent. Some manufacturers list their maximum-size stock sprockets at 50 teeth or less.

Angle of Wrap. The minimum recommended angle of wrap on the small sprocket is 135°, or three teeth engaging the chain.

Speed Ratio. The maximum recommended speed ratio for a single-reduction drive is 6:1. That is done so as to keep sprocket sizes within reasonable bounds and to obtain reasonably good chain wear life.

Center Distance. The preferred center distance is from 30 to 50 times the chain pitch. The center distance should be adjustable to compensate for chain wear elongation. The minimum adjustment should be equal to at least one chain pitch.

Chain Length. The required chain length may be estimated from Eq. (15.1). This will give chain length accurate to within ±½ chain pitch. If a more precise length is required, consult Ref. [15.5] or manufacturers' literature.

Wear and Chain Sag. Maximum allowable wear elongation for offset sidebar chains is determined by component size and hardness. Most offset sidebar chains are designed to provide 5 to 6 percent wear elongation. Wear elongation may be limited by the number of teeth on the large sprocket. For that case, the maximum allowable chain elongation, in percent, is $200/N_2$.

In a drive on approximately horizontal centers, chain wear elongation accumulates as sag in the slack span. The expected amount of sag for various amounts of wear elongation is shown in Fig. 15.4. The drive centers should be adjusted periodically to maintain sag at 2 to 3 percent of horizontal center distance.

Idlers. When the center distance is long, the drive centers are more than 45° from horizontal, or machine members obstruct the normal chain path, an idler sprocket may be required. Idler sprockets should engage the chain in the slack span and should not be smaller than the small sprocket in the drive. At least 3 teeth on the idler should engage the chain, and there should be at least 3 pitches of free chain between engagement points.

Drive Arrangements. A number of recommended, acceptable, and not recommended drive arrangements are shown in Fig. 15.5.

15.6.2 Selection Procedure

Obtain Required Information. Before an offset-sidebar-chain drive is selected, it is essential to obtain all the listed items of information. Note that the first 10 items are the same as for roller chain.

1. Source of input power
2. Type of driven equipment
3. Power to be transmitted
4. Speed and size of driver shaft
5. Speed and size of driven shaft
6. Desired center distance and drive arrangement
7. Means of center distance adjustment, if any
8. Available lubrication type
9. Space limitations
10. Adverse environmental conditions
11. Operating hours per day

In addition, check for any unusual drive conditions, such as

- Higher than listed speeds
- Inadequate lubrication
- Very heavy shock loads
- Corrosive or very abrasive conditions
- More than one driven shaft
- Other than precision-cut sprockets

When any of these, or any other unusual drive condition, is present, consult a chain manufacturer for assistance with the drive selection.

Determine Service Factor. The combined service factor SF is calculated by multiplying the three individual factors from Tables 15.10, 15.11, and 15.12:

$$SF = (SF_1)\ (SF_2)\ (SF_3)$$

The load classification for various types of driven equipment may be found in Ref. [15.5] or in manufacturers' literature.

TABLE 15.10 Service Factors for Offset-Sidebar-Chain Drives; Load Type, SF_1

	Type of input power		
Type of driven load	Internal combustion engine with hydraulic drive	Electric motor or turbine	Internal combustion engine with mechanical drive
Smooth	1.0	1.0	1.2
Moderate shock	1.2	1.3	1.4
Heavy shock	1.4	1.5	1.7

TABLE 15.11 Service Factors for Offset-Sidebar-Chain Drives; Environment, SF_2

Environmental conditions	Factor
Relatively clean, moderate temperature	1.0
Moderately dirty, moderate temperature	1.2
Very dirty, abrasive, exposed to weather, mildly corrosive, relatively high temperature	1.4

TABLE 15.12 Service Factors for Offset-Sidebar-Chain Drives; Operating Time, SF_3

Daily operating hours	Factor
8 to 10 hr/day	1.0
10 to 24 hr/day	1.4

Calculate Design Power. Obtain the design power by multiplying the average power times the combined service factor.

Make Preliminary Chain Selection. Enter the chart, Fig. 15.8, with the design power and the speed of the small sprocket to make a preliminary chain selection.

Select Small Sprocket. Refer to the horsepower tables in Ref. [15.5] or manufacturers' catalogs to select the small sprocket. Check the tables to see if increasing the number of teeth on the small sprocket might allow use of a smaller-pitch, more economical chain.

Consult sprocket manufacturers' catalogs to ensure that the sprocket bore capacity will accommodate the shaft. If it will not, a larger sprocket must be selected.

Select Large Sprocket. Determine the number of teeth required on the large sprocket by multiplying the number of teeth on the small sprocket by the speed ratio. Ensure that the selected large sprocket will fit within the available space and clear all obstructions. If there is an interference, a different chain and sprocket combination may have to be selected.

Make Final Chain Selection. Choose the most suitable drive from the alternatives selected earlier. The final choice may be based on economics, performance, efficiency, space utilization, or a number of other considerations. Computer programs are available that automate the preliminary selection process and analyze the alternatives based on parameters provided by the designer.

Calculate Chain Length. Calculate the chain length from Eq. (15.1). More accurate chain length may be calculated using equations in Ref. [15.5] or manufacturers' literature. For drives with more than two sprockets, the chain length may be obtained using graphical techniques, geometric layouts, computer programs, and certain CAD packages.

Determine Lubrication Type. The required lubrication type may be obtained from horsepower tables in Ref. [15.5], manufacturers' literature, or Sec. 15.4. It is very

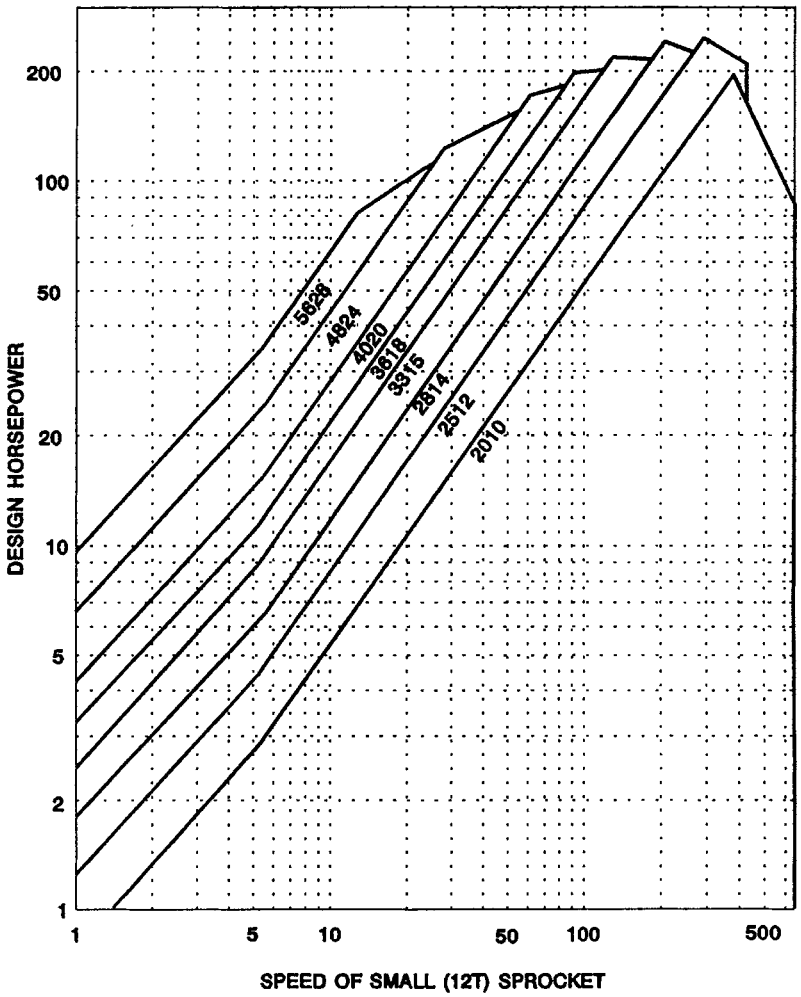

FIGURE 15.8 Engineering steel chain selection chart.

important to provide adequate lubrication to a chain drive. Selecting an inferior type of lubrication can drastically reduce the life of the drive.

Direction of Chain Travel. The wear life of an offset sidebar chain can be affected by its direction of travel. To obtain greater wear life, in a drive with other than a one-to-one ratio, the narrow or roller end of the links in the taut span should face the smaller sprocket. It may be helpful in many cases for the drive designer to specify the direction in which the chain is to be installed. A complete explanation of this phenomenon may be found in Ref. [15.5].

15.6.3 Horsepower Ratings of Offset Sidebar Chains

Conditions for Ratings. The offset sidebar chain ratings presented here and in Ref. [15.5] are based on the following conditions:

1. Standard chain listed in Ref. [15.3]
2. Service factor of 1
3. Chain length of 100 pitches
4. Use of the recommended lubrication method
5. A two-sprocket drive, driver and driven
6. Sprockets well aligned on parallel, horizontal shafts
7. Precision-machined tooth sprockets
8. A clean, nonabrasive environment
9. Approximately 15 000 hours service life

Horsepower Ratings. The ratings for offset sidebar chains on 12-tooth sprockets are shown on the chart in Fig. 15.8. The rating equations for offset sidebar chains are much more complex than those for roller chains, and they are not generally published.

15.7 SILENT CHAINS: NOMENCLATURE AND DIMENSIONS

15.7.1 Silent-Chain Nomenclature

Silent chain is a series of toothed links alternately interlaced on joint components so that the joint between each pitch articulates essentially as shown in the illustration with Table 15.13. The joint components may be any combination of pins, bushings, or specially configured components that cause the toothed links to engage a standard sprocket so that the joint centers lie on the pitch circle. In addition to the toothed links and joint components, silent chain has guide links (not toothed) that run either on the sides of the sprocket or in circumferential grooves in the sprocket to control the chain laterally.

Silent chains do not have discrete strands as roller and engineering steel chains do. Silent chain may be assembled in an almost infinite number of "strands" because of the way the toothed links are alternately interlaced on the joint components, as shown in Fig. 15.9. Silent chain is produced in standard widths, in inches, designated in Ref. [15.4].

15.7.2 Silent-Chain Dimensions and Data

Silent-Chain Dimensions. The standard for silent chain (Ref. [15.4]) defines the sprockets in more detail than the chains. A silent chain is a standard silent chain if it functions properly on a standard sprocket. The only standardized chain dimensions are those shown in Table 15.13.

TABLE 15.13 Silent Chain Dimensions

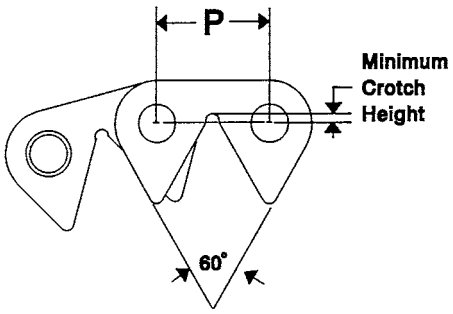

Dimensions in inches			
ANSI chain no.	Chain pitch	Min. crotch height	Standard chain widths
SC3	0.375	0.0232	.5, .75, 1, 1.25, 1.5, 1.75, 2, 2.25, 2.5, 3, 4, 5, 6
SC4	0.500	0.0310	.5, .75, 1, 1.25, 1.5, 1.75, 2, 2.25, 2.5, 2.75, 3, 4, 5, 6, 8
SC5	0.625	0.0388	1, 1.25, 1.5, 1.75, 2, 2.5, 3, 4, 5, 6, 7, 8, 10
SC6	0.750	0.0465	1, 1.25, 1.5, 2, 2.5, 3, 3.5, 4, 5, 6, 7, 8, 9, 10, 12
SC8	1.00	0.0620	2, 2.5, 3, 4, 5, 6, 7, 8, 9, 10, 12, 14, 16
SC10	1.25	0.0775	2.5, 3, 4, 5, 6, 7, 8, 9, 10, 12, 14, 16, 18, 20
SC12	1.50	0.0930	3, 4, 5, 6, 7, 8, 9, 10, 12, 14, 16, 18, 20, 22, 24
SC16	2.00	0.1240	4, 5, 6, 7, 8, 10, 12, 14, 16, 18, 20, 22, 24, 30

Illustration courtesy of Diamond Chain Company.

Silent-Chain Numbering. A standard numbering system is described in Ref. [15.4]. Chain numbers begin with the two letters SC. They are followed by one or two digits that designate the chain pitch in increments of ⅛ in. The pitch designators are then followed by two or three digits that designate the chain width in increments of ¼ in. For example, chain number SC836 is a standard silent chain with a pitch of 1 in and a width of 9 in.

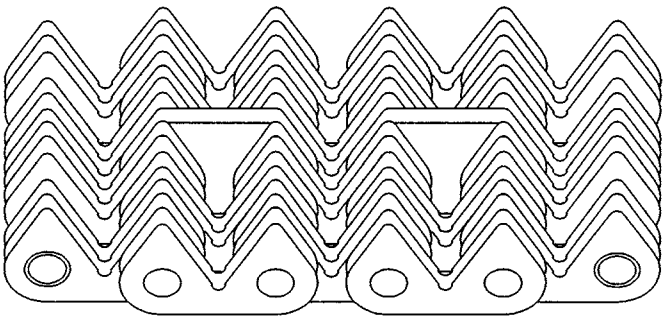

FIGURE 15.9 Typical silent chain. *(Diamond Chain Company).*

15.7.3 Silent-Chain Sprockets

Tooth Form. The tooth form, profile, and guide groove width and profile dimensions are defined in Ref. [15.4].

Sprocket Diameters. There are five important sprocket diameters defined in Ref. [15.4]. They are pitch, outside, over-gauge, maximum guide groove, and maximum hub diameters. The equations for those diameters, shown in Fig. 15.10, are

$$\text{PD} = P/\sin(180/N) \qquad D_p = 0.625P$$

$$\text{OD (for rounded teeth)} = P[\cot(180/N) + 0.08]$$

$$\text{OGD (for even number of teeth)} = \text{PD} - 0.125P \csc[30 - (180/N)] + D_p$$

$$\text{OGD (for odd number of teeth)} = [\cos(90/N)]\{\text{PD} - 0.125P \csc[30 - (180/N)]\} + D_p$$

$$G = P[\cot(180/N) - 1.16]$$

$$\text{MHD (for hobbed teeth)} = P[\cot(180/N) - 1.33]$$

$$\text{MHD (for straddle-cut teeth)} = P[\cot(180/N) - 1.25]$$

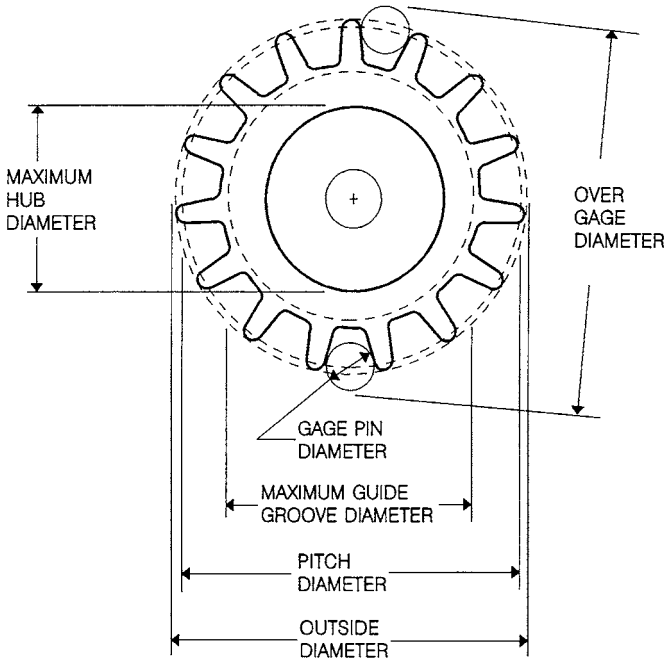

FIGURE 15.10 Silent chain sprocket diameters. *(Diamond Chain Company.)*

15.8 SELECTION OF SILENT-CHAIN DRIVES

15.8.1 General Design Recommendations

The following guidelines are only the more important considerations in designing silent-chain drives. For more detailed information, consult Ref. [15.5] or manufacturers' literature.

Chain Pitch. It is very important to match the silent-chain pitch to the desired shaft speeds. Generally, the smaller the pitch, the greater the allowable speed.

Number of Sprocket Teeth

Small Sprocket. The absolute minimum number of teeth that a silent-chain sprocket can have is 12. However, the minimum recommended number of teeth on the small sprocket is much more than that:

Normal operation	21 teeth
Speed increasing (step-up)	23 teeth
High speed (over 1500 ft/min)	25 teeth

Large Sprocket. The number of teeth on the large sprocket normally should not exceed 120. The number of teeth on the large sprocket also limits maximum allowable chain wear elongation. The maximum allowable chain wear elongation, in percent, is $200/N_2$.

Hardened Teeth. The teeth on the small sprocket should be hardened when they are running at moderate to high speeds or transmitting nearly maximum rated power.

Angle of Wrap. The minimum recommended angle of wrap on the small sprocket is 120°.

Speed Ratio. The maximum recommended speed ratio is 8:1 for a single-reduction drive. Speed ratios of up to 12:1 are possible with proper design, but in such situations double-reduction drives are preferred.

Center Distance. The preferred center distance for a silent-chain drive is 30 to 50 times the pitch. The center distance should be adjustable to take up slack chain caused by wear. The center distance adjustment should be at least 2 pitches. If a fixed center distance must be used, consult a chain manufacturer.

Chain Length. The required chain length may be calculated from Eq. (15.1). It will give chain length accurate to within ±½ pitch. If a more precise chain length is needed, equations for exact chain length may be found in Ref. [15.5] or in manufacturers' literature.

Chain length must be an integral number of pitches. An even number of pitches is preferred. An odd number of pitches requires the use of an offset link, and offset links reduce the capacity of the chain.

Wear and Chain Sag. Silent chain elongates with wear just as other types of chain do. Silent-chain sprocket teeth are designed to allow the chain to run higher on the teeth as it wears, thus compensating for the elongation. The maximum allowable chain wear is limited by the number of teeth on the large sprocket, as noted earlier.

In a drive where the shaft centers are nearly horizontal, chain wear accumulates as sag in the slack span. The amount of sag for various amounts of wear elongation is shown in Fig. 15.4. The drive centers should be adjusted periodically to maintain chain sag at 2 to 3 percent of the center distance.

Idlers. In drives where the center distance is long, the shaft centers are near vertical, or if the center distance is not adjustable, idler sprockets or guide shoes may be needed. Idler sprockets may be used when they engage the inside of the chain loop, but guide shoes with a large radius are advised for contact on the back of the chain. Idlers should have at least 17 teeth. They should have at least 3 teeth engaging the chain, and allow at least 3 pitches of free chain between engagement points. Guide shoes may be of wood, metal, or polymeric material. They should contact the back of the slack span near the small sprocket to increase the angle of wrap on the small sprocket.

Drive Arrangements. A number of recommended, acceptable, and not recommended drive arrangements are shown in Fig. 15.5. These apply to silent chain as well as roller chain, except that a radiused guide shoe should be used where idler sprockets contact the back side of the chain.

15.8.2 Selection Procedure

Obtain Required Information. Before a silent-chain drive is selected, it is essential to obtain all the listed items of information. Note that the first 10 items are the same as for roller chain.

1. Source of input power
2. Type of driven equipment
3. Power to be transmitted
4. Speed and size of driver shaft
5. Speed and size of driven shaft
6. Desired center distance and drive arrangement
7. Means of center distance adjustment, if any
8. Available lubrication type
9. Space limitations
10. Adverse environmental conditions
11. Operating hours per day

In addition, check for any unusual drive conditions, such as

- Frequent stops and starts
- High starting or inertial loads
- Multiple driven shafts
- Inferior lubrication type
- Corrosive or abrasive environment

If these or any other unusual drive conditions are present, consult a chain manufacturer for advice on the selection.

Determine Service Factor. Determine the service factor from Table 15.14. Load classifications may be obtained from Refs. [15.4] and [15.5] or from manufacturers'

TABLE 15.14 Silent Chain Service Factors

Load classification	IC engine with fluid coupling or electric motor		IC engine with mechanical drive		IC engine with torque converter	
	10 hr/day	24 hr/day	10 hr/day	24 hr/day	10 hr/day	24 hr/day
Very smooth	1.0	1.3	1.2	1.5	1.4	1.7
Mild shock	1.2	1.5	1.4	1.7	1.6	1.9
Moderate shock	1.4	1.7	1.6	1.9	1.8	2.1
Heavy shock	1.6	1.9	1.8	2.1	2.0	2.3

literature.

Calculate Design Power. Obtain the design power by multiplying the average power times the service factor from Table 15.14.

Make Preliminary Chain Selection. Enter the chart, Fig. 15.11, with design power and the speed of the small sprocket to make a preliminary chain selection. The solid lines on the chart represent the maximum horsepower per inch of width for each

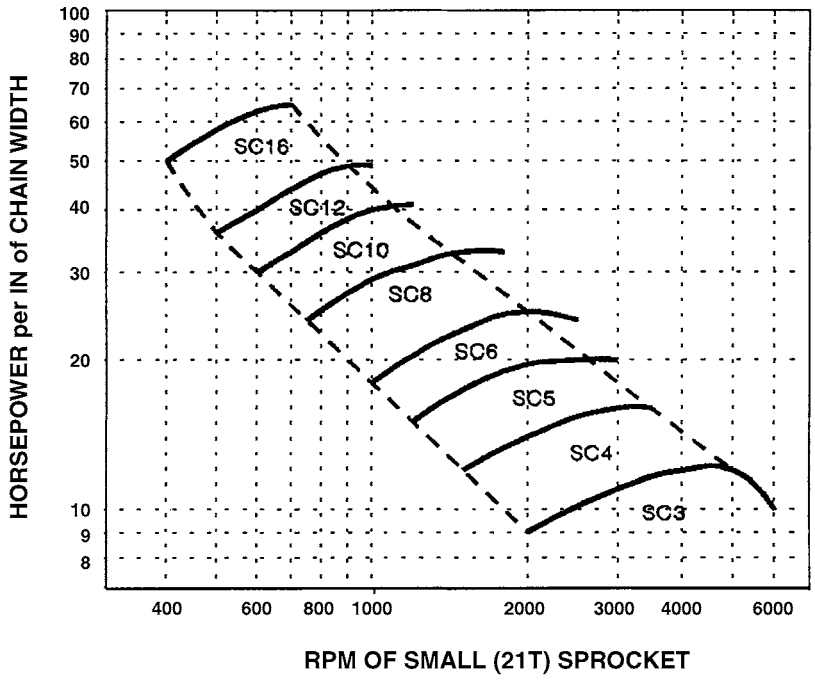

FIGURE 15.11 Silent chain selection chart.

silent-chain size when operating on a 21-tooth small sprocket. The dashed lines represent the minimum and maximum recommended speeds for each silent-chain size.

Select Small Sprocket. Refer to the horsepower tables in Ref. [15.4] or [15.5] or in manufacturers' catalogs to select the small sprocket. Use an odd number of teeth in the small sprocket whenever possible. More than one selection will work well in most situations, so check the tables to see if changing the number of teeth might yield a more economical or more convenient selection.

Consult sprocket manufacturers' catalogs to ensure that the bore in the small sprocket will accommodate the shaft. If it will not, a larger sprocket must be selected.

Select Large Sprocket. Determine the number of teeth required on the large sprocket by multiplying the number of teeth on the small sprocket by the speed ratio. Ensure that the selected large sprocket will fit within the available space and clear any obstructions. If there is an interference, a different chain and sprocket combination may be necessary.

Make Final Chain Selection. Choose the most suitable drive from the alternatives selected earlier. The final choice may be based on economics, performance, efficiency, space utilization, or a number of other considerations. Computer programs are available that automate the preliminary selection process and analyze the alternatives based on parameters provided by the designer.

Calculate Chain Length. Calculate the chain length from Eq. (15.1). More accurate chain lengths may be obtained from equations in Ref. [15.5] or in manufacturers' literature. For drives with three or more sprockets, chain length may be obtained using graphical techniques, geometric layouts, computer programs, and certain CAD packages.

Determine Lubrication Type. Select the proper type of lubrication from the tables in Ref. [15.4] or [15.5], manufacturers' literature, or Sec. 15.4. It is extremely important to provide adequate lubrication to a silent-chain drive. Selecting an inferior type of lubrication can drastically reduce the life of the drive. In addition, because silent-chain drives generally operate at higher speeds than roller- or engineering steel–chain drives, inadequate lubrication can cause serious damage to the drive or to the machine in which it is used.

15.8.3 Horsepower Ratings of Silent-Chain Drives

Conditions for Ratings. The silent-chain power ratings presented here are based on the following conditions:

1. Standard chain listed in Ref. [15.4]
2. Service factor of 1
3. Chain length of 100 pitches
4. Use of recommended lubrication type
5. A two-sprocket drive, driver and driven
6. Sprockets properly aligned on parallel, horizontal shafts and chains

7. A clean, nonabrasive environment
8. Approximately 15 000 hours service life

Horsepower Ratings. Silent-chain power capacity ratings are stated in terms of horsepower per inch of chain width, and they vary with the chain pitch, number of teeth on the small sprocket, and speed of the small sprocket. The ratings consider fatigue strength of the chains, wear resistance of drive components, adequacy of lubrication, and effects of speed and chordal action. The equations for silent-chain ratings are not published, as those for roller-chain ratings are, but complete tables of power ratings for standard silent chains are shown in Ref. [15.4]. Figure 15.11 is a silent-chain quick-selection chart, using an abridged version of the ratings.

REFERENCES

15.1 ANSI B29.1M-1993, "Precision Power Transmission Roller Chains, Attachments, and Sprockets," American Society of Mechanical Engineers, New York, 1993.

15.2 ANSI B29.3M-1994, "Double-Pitch Power Transmission Roller Chains and Sprockets," American Society of Mechanical Engineers, New York, 1994.

15.3 ANSI B29.10M-1997(R1997), "Heavy Duty Offset Sidebar Power Transmission Roller Chains and Sprocket Teeth," American Society of Mechanical Engineers, New York, 1997.

15.4 ANSI B29.2M-1982(1987), "Inverted Tooth (Silent) Chains and Sprockets," American Society of Mechanical Engineers, New York, 1982.

15.5 American Chain Association, *Chains for Power Transmission and Material Handling,* Marcel Dekker, New York, 1982.

15.6 American Chain Association, *Identification, Installation, Lubrication, and Maintenance of Power Transmission Chains,* American Chain Association, Naples, Fl., 1993.

CHAPTER 16
COUPLINGS

Howard B. Schwerdlin
Engineering Manager
Lovejoy, Inc.
Downers Grove, Illinois

GLOSSARY OF SYMBOLS

A	Area or parallel misalignment
b	Bearing spacing
d	Diameter
D	Diameter or distance between equipment
e	Eccentricity
E	Young's modulus or shape factor for maximum allowable stress, psi
F	Force
g	Acceleration due to gravity
h	Height of keyway
I	Second moment of area
J	Polar second moment of area
K_a	U-joint angle correction factor
K_L	U-joint life correction factor
K_s	U-joint speed correction factor
L	Life or length of engagement
ℓ	Length
m	Mass

n	Speed, r/min
N	Number of active elements or bellows convolutions
P	Pressure
PV	Pressure times velocity
r	Radius
R	Operating radius
R_c	Centroidal radius or distance
s	Maximum permissible stroke per convolution for bellows
S	Link length, shape factor, or maximum permissible total bellows stroke
t	Thickness
T	Torque
V	Velocity
w	Width
X	Angular misalignment
Y	Parallel misalignment
α	Rotational position
β	Torsional amplitude
γ	U-joint angle
δ	Deflection or U-joint angle
Δ	Deflection
ζ	Damping ratio
θ	Shaft or joint angle
θ_{eff}	Torsional equivalent angle
τ	Shear stress
ω	Angular velocity

16.1 GENERAL

16.1.1 System Requirements

When selecting a coupling, you have to consider all the system's requirements. It is not enough to know what the driver and load are and how big the shaft is. You must also know how the two halves are assembled and whether there is misalignment, as well as the system's operating range and the operating temperature.

Before you select a coupling, determine the following about the system:

1. *Driver* Type; electric motor, internal-combustion engine, number of cylinders, etc.
2. *Load* Fan, pump, rockcrusher, etc., to determine the inertias.
3. *Nominal torque* T_{kn} Continuous operating torque.
4. *Maximum torque* $T_{\max}$ Peak expected on startup, shutdown, overload, etc.
5. *Vibratory torque* T_{kw} Oscillating torque about the nominal $T_{kn} \pm T_{kw}$.
6. *Number of startups per hour.*

7. *Misalignment* Amount and type of misalignment between the driver and the load: parallel, angular, and/or axial.
8. *Type of mounting* Shaft to shaft, shaft to flywheel, blind fit, etc.
9. *Shaft size* Diameter of the shafts for both the driver and the load.
10. *Operating temperature* General operating temperature and whether the drive is enclosed (unventilated).
11. *Operating speed range* The upper and lower limits of the operating range.
12. *Service factor* A "fudge factor" designed to combine many of the above operating conditions and lump them into one multiplier to oversize the coupling in order to accommodate these parameters. Typical service factors are shown in Table 16.1.

16.1.2 Coupling Characteristics

Once the system requirements have been determined, check the characteristics of the coupling chosen to verify the selection. You should be able to check the following characteristics:

1. *Torque capacity*
2. *Bore size* Minimum and maximum bore
3. *Type of mounting* Mounting configurations available for any given coupling
4. *Maximum speed range*
5. *Misalignment* Degree of misalignment that can be accepted in mounting
6. *Flexible material* Capability of material to withstand heat or oil contamination; torsional stiffness

16.1.3 Selecting the Coupling

The first step is to make a preliminary selection based on the torque transmitted and the shaft dimensions. Then verify that the selection will satisfy the requirements for type of mount, degree of misalignment, operating speed, and operating temperature. Don't forget to check for the possibility of resonance.

Not all systems require all these steps. Smooth operating systems, such as electric motors driving small loads, are seldom subject to severe vibration. The natural frequency probably does not have to be checked.

As a simple guideline for determining system requirements for smooth systems, coupling manufacturers have developed the service factor. The service factor is a rough approximation of the temperature requirements, maximum torque, and natural frequency. It is stated as a multiplier, such as 1.5. To be sure the coupling you have selected is adequate, multiply the nominal torque required for the system by the service factor and select a coupling with that torque rating or better.

The service factor is adequate for some systems. Its drawbacks are that it is imprecise and, in severe applications, does not evaluate all the variables. Also, when you are selecting according to the service factor, be careful not to overspecify, getting more coupling than needed. This is not cost-effective.

Perhaps the most important thing to remember in selecting a coupling is that the coupling manufacturer can make a recommendation for you only based on the

TABLE 16.1 Service Factors and Load Classification for Flexible Couplings†

Agitators	
Pure liquids	1.0
Liquids, variable density	1.0
Barge puller	2.0
Beaters	1.5
Blowers	
Centrifugal	1.0
Lobe	1.25
Vane	1.25
Can-filling machinery	1.0
Car dumpers	2.5
Car pullers	1.5
Compressors	
Centrifugal	1.0
Lobe	1.25
Reciprocating	‡
Conveyors, uniformly loaded or fed	
Assembly	1.0
Belt	1.0
Screw	1.0
Bucket	1.25
Live roll, shaker and reciprocating	3.0
Conveyors (heavy-duty), not uniformly fed	
Assembly	1.2
Belt	1.2
Oven	1.2
Reciprocating	2.5
Screw	1.2
Shaker	3.0
Cranes and hoists	
Main hoists	2.0
Reversing	2.0
Skip	2.0
Trolley drive	2.0
Bridge drive	2.0
Slope	2.0
Crushers	
Ore	3.0
Stone	3.0
Dredges	
Cable reels	2.0
Conveyors	1.5
Cutter head drives	2.5
Maneuvering winches	1.5
Pumps	1.5
Elevators	
Bucket	1.5
Escalators	1.0
Freight and passenger	2.0
Evaporators	1.0
Fans	
Centrifugal	1.0
Fans (*cont.*)	
Cooling towers	2.0
Forced draft	1.5
Induced draft w/o damper control	2.0
Propellor	1.5
Induced draft w/damper control	1.25
Feeders	
Belt	1.0
Screw	1.0
Reciprocating	2.5
Generators	
Not welding	1.0
Welding	2.0
Hoist	1.5
Hammer mills	2.0
Kilns	1.5
Laundry washers, reversing	2.0
Line shafting any processing mach.	1.5
Lumber machinery	
Barkers	2.0
Edger feed	2.0
Live rolls	2.0
Planer	2.0
Slab conveyor	2.0
Machine tools	
Bending roll	2.0
Plate planer	2.0
Punch press gear driven	2.0
Tapping machinery	2.0
Other	
Main drive	1.5
Aux. drives	1.0
Metal-forming machines	
Draw bench carriage	2.0
Draw bench main drive	2.0
Extruder	2.0
Forming machinery	2.0
Slitters	1.5
Table conveyors	
Nonreversing	2.5
Reversing	2.5
Wire drawing	2.0
Wire winding	1.5
Coilers	1.5
Mills, rotary type	
Ball	2.0
Cement kilns	2.0
Dryers, coolers	2.0
Kilns	2.0
Pebble	2.0
Rolling	2.0
Tube	2.0
Tumbling	1.5

TABLE 16.1 Service Factors and Load Classification for Flexible Couplings† (*Continued*)

Mixers		Pumps (*cont.*)	
Concrete, cont.	1.75	1 cyl., single- or double-acting	2.0
Muller	1.5	2 cyl. single-acting	2.0
Papermills		2 cyl. double-acting	1.75
Agitators (mixers)	1.2	3 or more cyl.	1.5
Barker mech.	2.0	Rubber machinery	
"Barking" drum spur gear	2.5	Mixer	2.5
Beater and pulper	2.0	Rubber calender	2.0
Calenders	1.5	Screens	
Calenders, super	1.5	Air washing	1.0
Converting machines	1.2	Rotary stone or gravel	1.5
Conveyors	1.2	Vibrating	2.5
Dryers	1.5	Water	1.0
Jordans	2.0	Grizzly	2.0
Log haul	2.0	Shredders	1.5
Dresses	2.0	Steering gear	1.0
Reel	1.2	Stokers	1.0
Winder	1.2	Textile machinery	
Printing presses	1.5	Dryers	1.2
Pug mill	1.75	Dyeing mach.	1.2
Pumps		Tumbling barrel	1.75
Centrifugal	1.0	Windlass	2.0
Gear, rotary or vane	1.25	Woodworking machinery	1.0
Reciprocating			

†The values of the service factors listed are intended only as a general guide. For systems which frequently use the peak torque capacity of the power source, check that this peak torque does not exceed the normal torque capacity of the coupling.

The values of the service factors given are to be used with prime movers such as electric motors, steam turbines, or internal combustion engines having four or more cylinders. For drives involving internal combustion engines of two cylinders, add 0.3 to values; and for a single-cylinder engine add 0.70.

‡Consult the manufacturer.

SOURCE: Ref. [16.1].

information you provide. A little time spent selecting the right coupling can save a lot of time and money later.

Selecting a flexible coupling involves more than meeting torque and shaft size requirements. It is also important to understand the functions of a flexible coupling in the system, the operating requirements of the system, and the characteristics of the coupling selected. Flexible couplings serve four main functions in a drive system:

1. They transmit torque and rotation from the drive to the load.
2. They dampen vibration.
3. They accommodate misalignment.
4. They influence the natural frequency of the system.

The torque-handling capacity of a given coupling design defines the basic size of a coupling. The nominal torque T_{kn} is the coupling's continuous load rating under conditions set by the manufacturer. The maximum torque rating $T_{\max}$ is the peak torque the coupling can handle on startup, shutdown, running through resonance, and momentary overloads. As defined in the German standards for elastomeric couplings, Ref. [16.2], a coupling should be able to withstand 10^5 cycles of maximum

torque at a frequency of not more than 60 per hour. Vibratory torque ($\pm T_{kw}$) is the coupling vibratory rating at 10 hertz (Hz) for elastomeric couplings. The rotary output of the coupling may be uniform (constant velocity) or cyclic (e.g., Hooke's joint).

All drive systems experience some vibration. Vibration can exceed the limits of design, which can cause system failure. Flexible couplings are one method of dampening the amount of vibration from either the driver or the driven equipment.

When a flexible coupling is used, the vibration is transferred to a material which is designed to absorb it rather than transmit it through the entire drive. Soft materials, such as natural rubber, can absorb greater amounts of vibration than stiffer materials, such as Hytrel† or steel. As a comparison, the relative vibration damping capabilities of Buna N rubber, Hytrel, and steel are shown in the transmissibility chart of Fig. 16.1.

If a system has misalignment, there are two factors to consider. First, you must use a coupling that can operate between two misaligned shafts. Second, you must be sure that the coupling does not exert excessive forces on the equipment because of misalignment. Perfect alignment between the driver and the load is difficult to obtain and maintain over the life of the system. A cost-effective alternative to precise alignment is a coupling that can accommodate misalignment between two shafts. The amount of misalignment a coupling can accept varies. Steel drive plates, for example, can accept only misalignment equal to their machining tolerances, frequently as little as 0.005 inch (in) parallel. Other couplings can accommodate mis-

† Hytrel is a trademark of E.I. du Pont de Nemours.

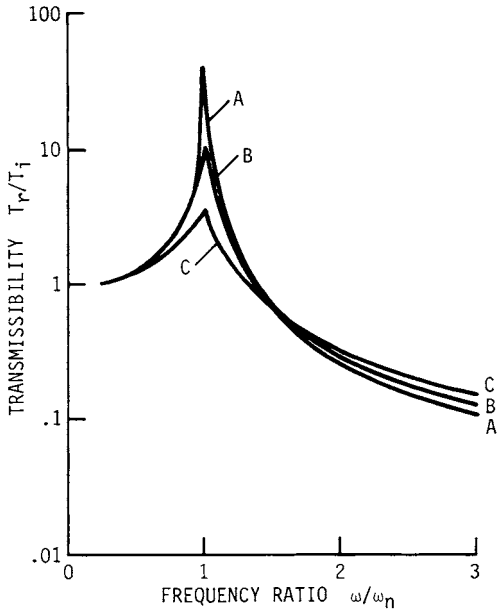

FIGURE 16.1 Effect of damping ratio on torque transmission. A, steel, $\xi = 0.01$; B, Hytrel, $\xi = 0.03$; C, Buna N rubber, $\xi = 0.13$, where T_r is the transmitted torque and T_i the input torque.

alignment up to 45°. The maximum allowable misalignment is a function of the percentage of torque capacity being utilized and the amount of vibratory torque the system is transmitting under perfect alignment.

If there is system misalignment, the material used in the coupling is important. Misalignment may cause radial forces to be exerted on the system. If the radial forces are too great, components such as bearings, seals, and shafts can experience undue stresses and fail prematurely. Different materials exert different radial forces; softer materials typically exert less radial force than stiff materials.

The natural frequency of a system can be altered by changing either the inertia of any of the components or the stiffness of the coupling used. See Chap. 31. Generally, after a system is designed, it is difficult and costly to change the inertia of the components. Therefore, coupling selection is frequently used to alter the natural frequency.

16.2 RIGID COUPLINGS

The solid coupling does not allow for misalignment, except perhaps axial, but enables the addition of one piece of equipment to another. In its simplest form, the rigid coupling is nothing more than a piece of bar stock bored to receive two shafts, as shown in Fig. 16.2. Its torque-handling capacity is limited only by the strength of the material used to make the connection. The coupling is installed on one shaft before the equipment is lined up, and the mating equipment is brought into position without much chance of accurate alignment when the equipment is bolted into position.

The maximum shear stress occurs at the outer radius of the coupling and at the interface of the two bores. This stress can be derived from the torsion formula (see Chap. 36) and is

$$\tau_{\max} = \frac{TD_o}{2J} \tag{16.1}$$

where J, the polar second moment of the area, is

$$J = \frac{\pi}{32}(D_o^4 - D_i^4) \tag{16.2}$$

The coupling must be sized so that, typically, the stress given by Eq. (16.1) does not exceed 10 percent of the ultimate tensile strength of the material, as shown in Table 16.2; but see Chap. 28.

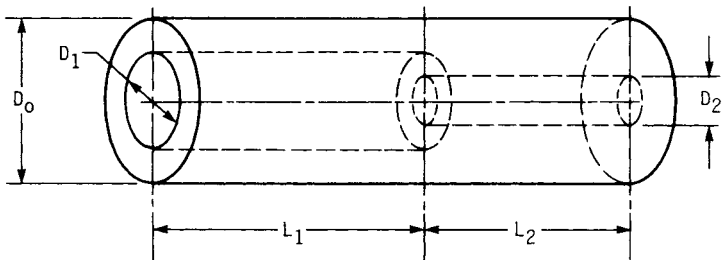

FIGURE 16.2 Schematic view of a rigid coupling.

TABLE 16.2 Maximum Allowable Shear Stress for Some Typical Materials

Material	Stress, psi	Material	Stress, psi
Steel	8000	Powdered iron (Fe-Cu)	4000
Ductile iron (60-45-12)	6000	Aluminum (SAE 380)	4000
Cast iron (Class 40)	4500	Tobin brass	3500

Other factors to consider are the length of engagement into the coupling. The shear stress over the keyway must not exceed the allowable shear stress as given above. Based on Fig. 16.3, the centroidal radius is

$$R_c = \frac{1}{2}\left(\frac{D_o}{2} + \frac{D_i}{2} + h\right) \tag{16.3}$$

The centroid of the bearing area is at radius $(D_i + h)/2$. If the transmitted torque is T, then the compressive force F is $2T/(D_i + h)$. The bearing stress σ_b is

$$\sigma_b = \frac{F}{A} = \frac{4T}{wL(D_i + h)} \tag{16.4}$$

The allowable compressive stress from distortion energy theory of failure is $\sigma_{all} = \tau_{all}/0.577$. Combining this with Eq. (16.4) gives

$$\tau_{all} = \frac{0.577(4)T}{wL(D_i + h)} \tag{16.5}$$

with τ_{all} coming from Table 16.2.

Next, the length of key stock, for keyed shafts, must be examined to keep its shear loading from exceeding the allowable shear stress. Referring to Fig. 16.4, we note that the shear force is $F = T/(D_i/2) = 2T/D_i$. Therefore the average shear stress is

$$\tau = \frac{F}{A} = \frac{2T}{wLD_i} \tag{16.6}$$

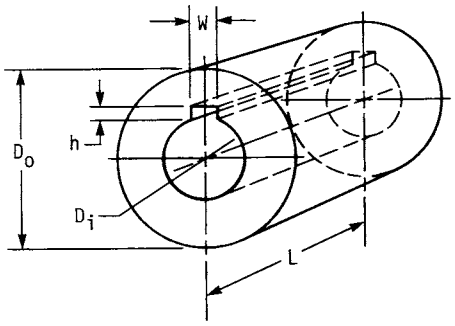

FIGURE 16.3 Portion of coupling showing keyway.

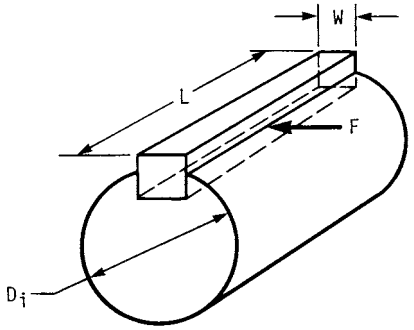

FIGURE 16.4 Portion of shaft showing key.

Both keys must be checked, although experience has shown that small-diameter shafts are more prone to failure of the key and keyway when these precautions are not followed because of their normally smaller key width and length of engagement. As a rule of thumb, the maximum allowable shear stress for some typical materials is shown in Table 16.2.

The *ribbed, hinged,* and *flanged* couplings are shown in Figs. 16.5, 16.6, and 16.7, respectively. These can be analyzed using the same approach as described above.

16.3 FLEXIBLE METALLIC COUPLINGS

16.3.1 Flexible Disk and Link Couplings

In this coupling (Fig. 16.8), misalignment is accommodated by the flexing of steel laminations. Parallel misalignment capacity is virtually zero unless two separated disk packs are used, in which case parallel misalignment is seen in the form of angular misalignment of each pack. This type of coupling can support large imposed radial loads, such as in rolling mills or long, floating shafts. The disk packs can be made from any material and are frequently manufactured from stainless steel for severe service. This coupling requires no lubrication.

The large radial loads imposed by long sections of tubing connecting to widely separated disk packs [up to 20 feet (ft)] are due to the heavy wall section necessary to give the tubing (or shafting) the necessary rigidity to resist whirling due to the

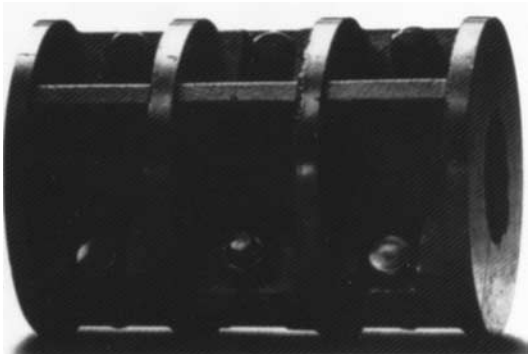

FIGURE 16.5 This ribbed coupling is made of two identical halves, split axially, and bolted together after the shafts have been aligned.

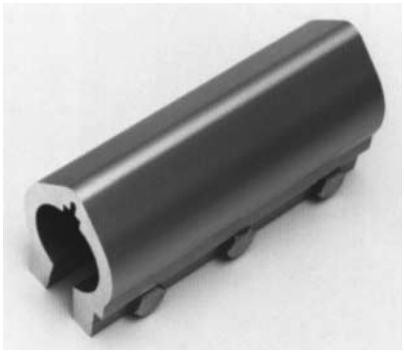

FIGURE 16.6 This hinged coupling is used mostly for light-duty applications. *(CraneVeyor Corp.)*

weight of the tubing (shafting). Specifically, the whirling speed of a uniform tube due to its weight is

$$n_c = \frac{60}{2\pi}\sqrt{\frac{\Delta}{g}} \qquad (16.7)$$

where Δ = static deflection of the tube due to its own weight. See Chap. 37 for deflection formulas, and Chap. 17 for method.

The standard rule of thumb is to keep the critical whirling speed at least 50 percent above the operating speed for subcritical running, or 40 percent below the operating speed for supercritical speeds. This forbidden range of

$$0.6n_c < n_c < 1.4n_c$$

corresponds to the amplification region of a lightly damped resonance curve, as shown in Fig. 16.9. Thus, for a whirling speed of 1800 revolutions per minute (r/min), the operating speed must not be in the range of 1280 to 2700 r/min.

The link coupling in Fig. 16.10 is similar to the metallic disk coupling except that the disk is replaced by links connecting the two shaft hubs. This coupling can be misaligned laterally, considerably more than the disk type. Both the disk and the link type carry torque in tension and compression in alternating arms. Proper bolt torque of the axial bolts holding the links or disks to the hubs is important. Insufficient torque may cause fretting from relative motion between the links or disks. Too much bolt clamping weakens the links or disks at their connecting points as a result of excessive compressive stress.

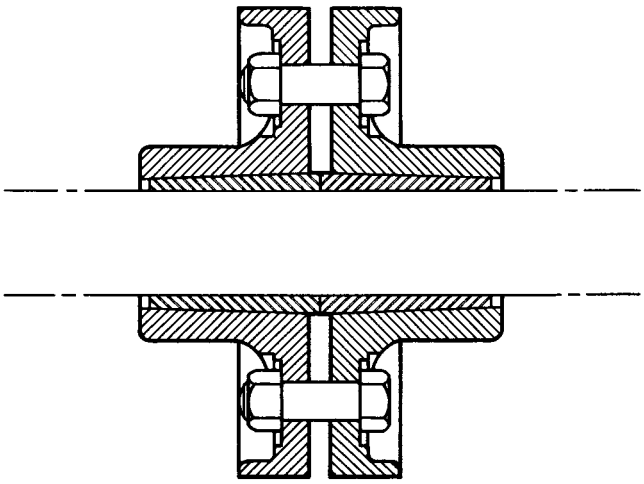

FIGURE 16.7 Schematic view of a flanged sleeve coupling.

(a)

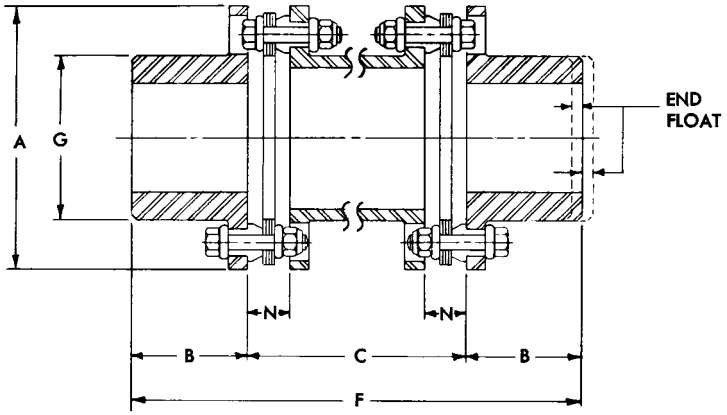

(b)

FIGURE 16.8 (*a*) Flexible-disk coupling; (*b*) cross section. *(Rexnord, Inc., Coupling Division.)*

16.3.2 Chain, Grid, and Beam Couplings

The chain coupling of Fig. 16.11 consists of two sprockets joined by an endless double-roller chain or inverted-tooth silent chain. This type of coupling will accommodate small amounts of angular, axial, and radial misalignment, which is provided by clearances between interfacing surfaces of the component parts.

For maximum service life, chain coupling sprockets should have hardened teeth. The coupling should be lubricated and enclosed in a greasetight case. Chain couplings can be assembled by using unhardened sprockets and operated without lubrication or a cover. This can be hazardous and can result in injury to personnel as well as a short coupling service life. This author has seen many such worn-out couplings. The availability of chain couplings is very good worldwide. Most manufacturers publish horsepower ratings to aid in proper coupling selection.

In the grid coupling (Fig. 16.12) the gears are separated by a specific minimum distance that allows for misalignment (Fig. 16.13). Large axial misalignment is

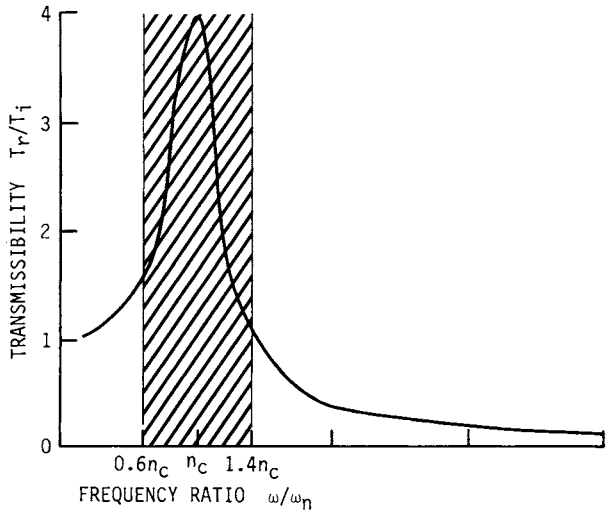

FIGURE 16.9 Lightly damped resonance curve showing forbidden speed range $0.6n_c < n_c < 1.4n_c$.

accomplished by sliding of the gear teeth in the rather long grid area. This coupling requires a guard (which is supplied) and lubrication.

The beam coupling is a single bar of metal cut as shown in Fig. 16.14 so that a continuous helical coil is produced. This coupling is torsionally rigid and free from backlash and provides constant velocity. Two designs exist for this type of coupling, one for maximum misalignment, the other for maximum torque (for the package size where axial movement is not a requirement). This coupling requires no lubrication. Speeds to 25 000 rev/min are possible depending on the coupling size.

FIGURE 16.10 Link coupling. *(Eaton Corp., Industrial Drives Operation.)*

16.3.3 Diaphragm and Hydraulic Couplings

As the name suggests, diaphragm couplings are made of a thin diaphragm or multiple thin diaphragms (see Fig. 16.15). Normally the diaphragms are made of metal. The diaphragms may be straight-sided, contoured, tapered, or convoluted; they may have various cutouts in them or take on many other forms. This coupling is connected to one shaft at the periphery [outer diameter (OD)] while the inner diameter (ID) is connected to the shaft or to a spacer piece, which may connect to another

(a) (b)

FIGURE 16.11 (*a*) Silent-chain coupling; (*b*) roller-chain coupling. *(Morse Industrial Products, Borg-Warner Corp.)*

diaphragm(s). This coupling is most often used in pairs (two flex elements), which converts parallel misalignment to angular misalignment between two flex elements. Misalignment is accommodated by stretching (straight, contoured, or tapered diaphragms or unrolling convoluted diaphragms) the diaphragm material. This type of coupling requires no lubrication and is considered torsionally rigid.

The hydraulic coupling consists of two sleeves, one with a tapered OD and one with a tapered ID, which slide over one another, as shown in Fig. 16.16. Oil is forced, under pressure, between the two sleeves to allow the outer sleeve to be positioned at a predetermined position on the inner sleeve. The pressure is released, and the outer sleeve firmly compresses the inner sleeve and shafting. In larger couplings, oil is also forced into a piston chamber to force the outer sleeve into position. To remove the coupling, the area between the sleeves is repressurized, and the outer sleeve can be slid away, releasing the coupling.

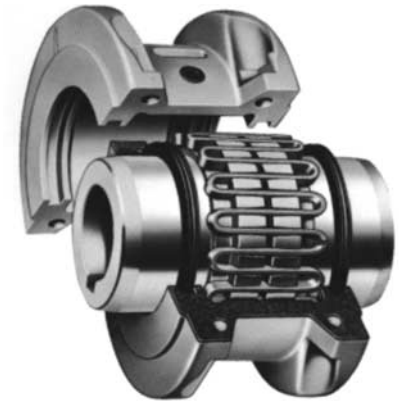

FIGURE 16.12 Metallic grid coupling with cover removed to show grid detail. *(Falk Corp.)*

16.3.4 Gear Couplings

Double-engagement gear couplings, as shown in Fig. 16.17, transmit more power per unit volume and unit weight than any other flexible coupling design, because of their relatively small OD (compared with other types of similar horsepower). The basic design consists of two gear-type hubs (similar to spur gears) loosely connected by an internal-spline sleeve, which could be one piece or two internal-spline mating flanges bolted together.

Clearance between the mating teeth in the hub and the sleeve allows this type of coupling to absorb angular, parallel,

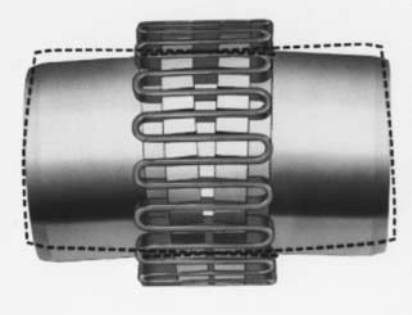

FIGURE 16.13 How the grid coupling accommodates misalignment. *(Falk Corp.)*

FIGURE 16.14 Beam coupling. *(Helical Products Corp.)*

and axial misalignment, as shown in Fig. 16.18. There is no relative rotation between the gear teeth, as in a normal gear set. Various tooth profiles (including crowned and/or barrel-shaped teeth) or changes in pressure angle allow for different misalignment, life, and load capacities. Straight-tooth couplings allow misalignment of 1° per gear mesh; with barrel-shaped teeth on the hub and straight teeth on the sleeve, 6° per mesh can be allowed.

With perfect alignment, all the teeth in the coupling are in contact, and the load is evenly distributed among them. Misalignment concentrates the load on just a few teeth; the number of teeth under load is a function of misalignment and load. The greater the misalignment (angular and parallel), the fewer the number of teeth in contact and the higher the load per tooth. Barrel-shaped teeth distribute the load over a larger area per tooth and may allow a greater number of teeth to be in contact under misaligned conditions, as shown in Fig. 16.19.

The two gear meshes can be separated by large distances, as shown in Fig. 16.20. In this case, two single-engagement couplings are connected by a floating shaft. For

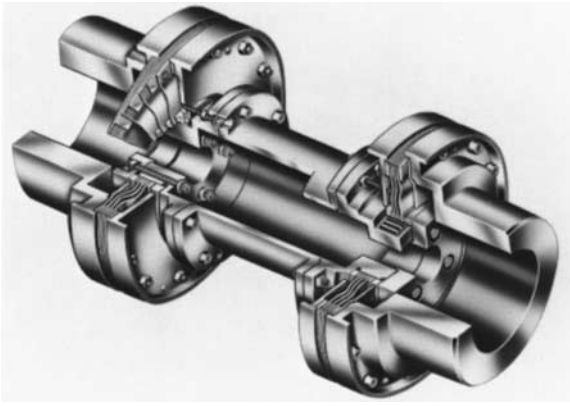

FIGURE 16.15 Cutaway view of diaphragm coupling assembly showing multiple convoluted diaphragms. *(Zurn Industries, Inc., Mechanical Drives Div.)*

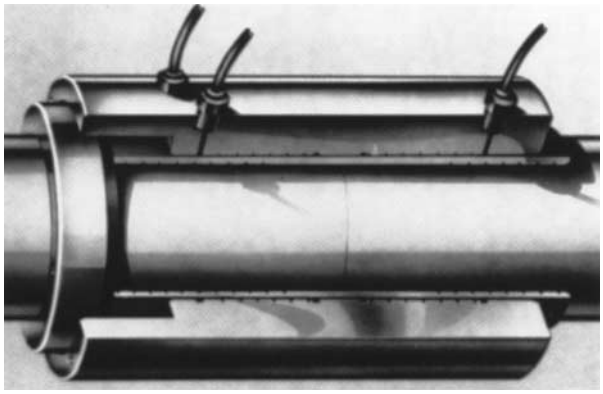

FIGURE 16.16 Hydraulic coupling; cutaway shows oil forced between inner and outer tapered sleeves. Note the oil piston chamber at left. *(SKF Industries.)*

this style coupling, large amounts of parallel misalignment are made possible by converting the angular misalignment capacity per mesh to parallel misalignment.

Parallel misalignment capacity for one single-engagement coupling is virtually nonexistent, however, and these couplings must be used in pairs, as shown in Fig. 16.20, to handle parallel misalignment.

Gear couplings must be lubricated for proper operation. Because of the high contact pressures obtained under misaligned conditions, only extreme-pressure (EP) greases should be used with gear couplings operating at maximum load. At high speeds (over 25 000 rpm), centrifugal effects separate the filler (soap) from the oil in most greases; the filler then collects between the teeth, preventing the oil from lubricating this highly loaded area. To overcome this problem, most high-speed gear couplings use a circulating oil system. The centrifugal effect still separates the fine particles from the oil, even in finely filtered systems. This sludge buildup necessitates cleaning of the teeth at regular intervals to prevent premature coupling failure.

FIGURE 16.17 Cutaway of flange-type gear coupling. *(Dodge Division, Reliance Electric.)*

Gear couplings, while inherently balanced, being machined all over and self-centering, may still require balancing to remove any residual unbalance due to bore runout. The magnitude F of this unbalanced or centrifugal force is

$$F = me\omega^2 \qquad (16.8)$$

where m = mass of the coupling, e = eccentricity, and ω = angular velocity in radians per second. See also Chaps. 17 and 31.

16.3.5 Spring and Flexible Shaft

Flexible shafts are constructed from a casing and a core, which is a series of

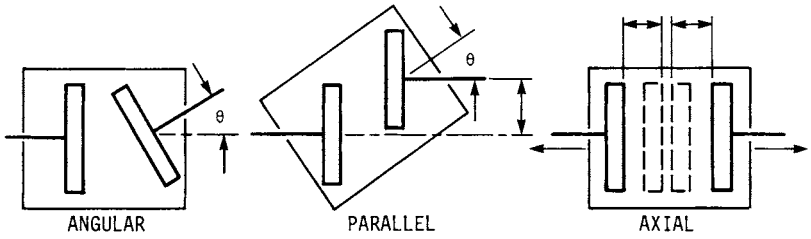

FIGURE 16.18 How double-engagement gear couplings accommodate angular, parallel, and axial misalignment.

multistranded layers of wire successively wrapped about a single central wire. Each wire layer is wound opposite to and at right angles to the layer beneath it to transmit maximum power and retain the greater flexibility.

The casing protects the rotating core from dust and moisture, but does not rotate itself. It is also reinforced to support the core and prevent helixing under torque load. *Helixing* is the tendency for a rope, or wire, to bend back on itself when subjected to torsional stress (Fig. 16.21). The casing also provides a cavity for grease to lubricate the rotating core. The core is attached to the hub on either end and then connected to the equipment.

The power transmission capacity of flexible shafting is limited only by the core construction, minimum radius of curvature of the shafting, and maximum unsupported length.

Flexible shafts are commercially available with ratings up to 1500 pound-inches (lb·in) at 440 r/min. Such a shaft is 1½ in [38 millimeters (mm)] in diameter and has a minimum operating radius R of 24 in (600 mm). In Fig. 16.22, let R be the required

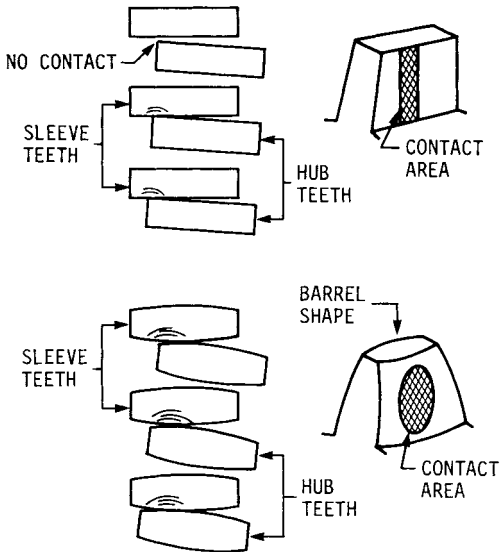

FIGURE 16.19 How change in tooth shape affects load distribution on the teeth of the gear coupling.

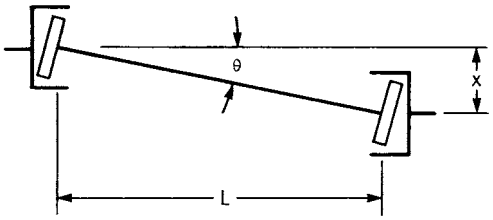

FIGURE 16.20 Diagram shows how parallel misalignment is converted to angular misalignment in each gear coupling mesh. For example, for an extended floating shaft with $L = 12$ in and $\theta = 1°$, the misalignment is $x = L \tan \theta = 0.20$ in. For a standard double-engagement coupling with $L = 2$ in and $\theta = 1°$, $x = 0.03$, which is significantly less.

operating radius corresponding to a misalignment A and a spacing D between equipment. Then the following relations can be derived from Fig. 16.22:

$$R = \frac{D^2 + A^2}{4A} \tag{16.9}$$

$$A = 2R - (4R^2 - D^2)^{1/2} \tag{16.10}$$

$$D = [A(4R - A)]^{1/2} \tag{16.11}$$

$$C_L = \frac{\pi R}{90} \sin^{-1} \frac{D}{2R} \tag{16.12}$$

where C_L = flexible length between the equipment.

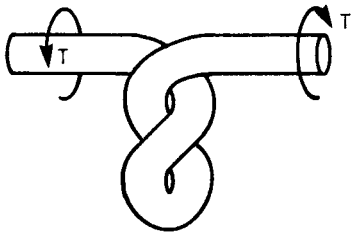

FIGURE 16.21 "Helixed" flexible shaft made of wire or rope.

If the casing is eliminated from the flexible shaft, a flexible coupling is created with much shorter maximum length (owing to lack of support and antihelixing without the casing). Typical commercial availability of this type of coupling is limited to 50 lb·in and 16-in lengths with an 8-in minimum operating radius.

Another similar coupling, the Uniflex,† consists of three layers of springs, each with three rectangular wires wound around an open-air core. This coupling (Fig. 16.23) also runs without a casing and has maximum speeds of up to 20 000 rpm, depending on size. It is relatively free from backlash and winds up about 1° at rated torque. This design uses spring elements up to 3 in long with rated torque up to 2000 lb·in at up to 4.5° misalignment.

16.3.6 Bellows Coupling

This type of coupling, shown in Fig. 16.24, consists of an all-metal circular bellows attached to two hubs. The design exhibits zero backlash and constant-velocity operation and is torsionally rigid. However, commercial couplings are typically rated to a maximum of 30 lb·in.

† Uniflex is a trademark of Lovejoy, Inc.

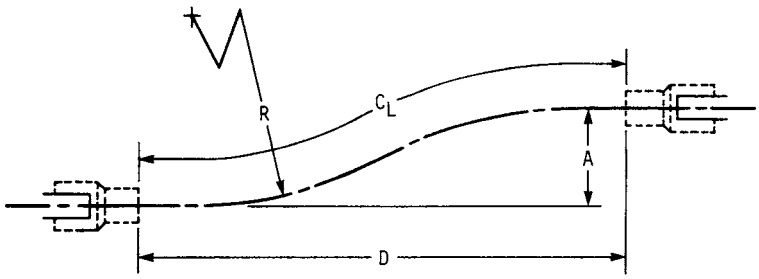

FIGURE 16.22 Maximum parallel misalignment of flexible shafting. *(Stow Manufacturing Company.)*

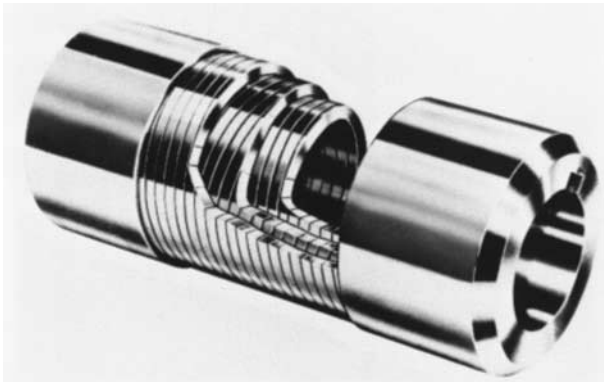

FIGURE 16.23 Uniflex flexible-spring coupling. *(Lovejoy, Inc.)*

The torque rating is obtained from

$$T = \frac{8pkD_o^2}{\ell} \tag{16.13}$$

where T = torque, in·oz
p = pitch, in
k = spring rate per convolution, oz/in
D_o = outside diameter, in
ℓ = length of a single convolution

The windup of the coupling (angular deflection) is measured in seconds of arc per inch-ounce of torque and is

$$u = \frac{0.08\ell}{(D_o + D_i)^3 t} \tag{16.14}$$

where u = windup, seconds/(in·oz)
D_i = inside diameter, in
t = thickness of bellows, in

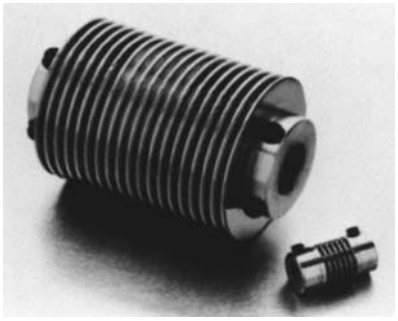

FIGURE 16.24 A bellows coupling. *(Servometer Corp.)*

Equations (16.15) and (16.16), which follow, apply to the determination of the life of this type of coupling. This life is dependent on the flexing motion due to angular and parallel misalignment, as shown in Fig. 16.25. The formula gives the operating misalignment corresponding to 10^5 flexing cycles (5×10^4 r). For 10^8 cycles, derate by 24 percent. Now,

$$X = \frac{71.6NS}{D_o} \tag{16.15}$$

$$Y = \frac{N^2 nS}{D_o} \tag{16.16}$$

where X = angular misalignment in degrees, Y = parallel misalignment, N = number of bellows convolutions, S = maximum total permissible bellows stroke, D_o = outside bellows diameter, and n = r/min.

16.4 FLEXIBLE ELASTOMERIC COUPLINGS

In this type of coupling, it is an elastomeric cushioning material—rather than only a metal part, as in the rigid, flexible metallic, or universal-joint (U-joint) couplings—that is subjected to the dynamic stresses of the operating system. These flexible elastomeric couplings need no lubrication and only periodic visual inspection for maintenance. They are available as compression, precompression, shear, and tension types.

The compression coupling is also known as the jaw, or block, coupling (Fig. 16.26). In this type of coupling, elastomeric cushioning blocks, rollers, or "spiders" are compressed between alternating pairs of fingers on the two hubs of the coupling.

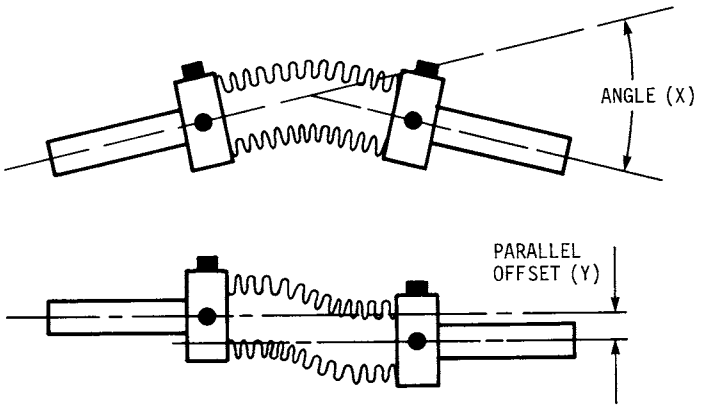

FIGURE 16.25 Bellows coupling with angular misalignment X and parallel misalignment Y. *(Servometer Corp.)*

FIGURE 16.26 Exploded view of jaw-type compression coupling showing the two hubs and the flexible spider insert. *(Lovejoy Inc.)*

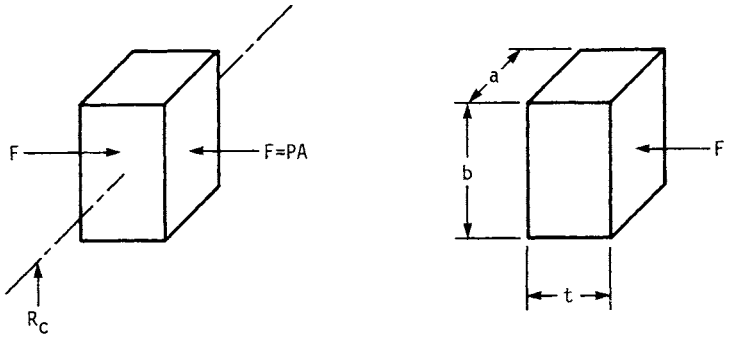

FIGURE 16.27 (*a*) Loading of one cushion at distance R_c from the center of a compression block coupling; (*b*) parameters used to calculate shape factor S for materials such as rubber where load area is ab and force F compresses the material at a thickness t.

The elastomeric elements can be of varying degrees of hardness or different materials to suit load-carrying capacities and temperature and chemical resistance requirements, in addition to torsional stiffness. Overall major dimensions may be altered by changing the number of active elements, element size, and radius on which the load is applied. The loading on one cushion is shown in Fig. 16.27*a,* and the torque rating of the coupling is

$$T = NPAR_c \tag{16.17}$$

where T = torque, N = number of cushions, P = pressure, and R_c = centroidal radius.

From Eq. (16.17) we can see that large couplings with many active elements are capable of handling very large loads. Typically, the design limit for rubber in com-

pression is 300 pounds per square inch (psi), while a plastic like Hytrel is capable of 1100 psi. The recommended load capacity of some elastomers is dependent on the *shape factor S,* which is the ratio of one load area to the total free area of the cushion. See Fig. 16.27*b.* Thus

$$S = \frac{ab}{2t(a+b)} \tag{16.18}$$

As this ratio changes from a thin plate (high S) to a fat block (low S), the maximum allowable stress E decreases, and the deformation of the block (compression) increases, as shown in Fig. 16.28.

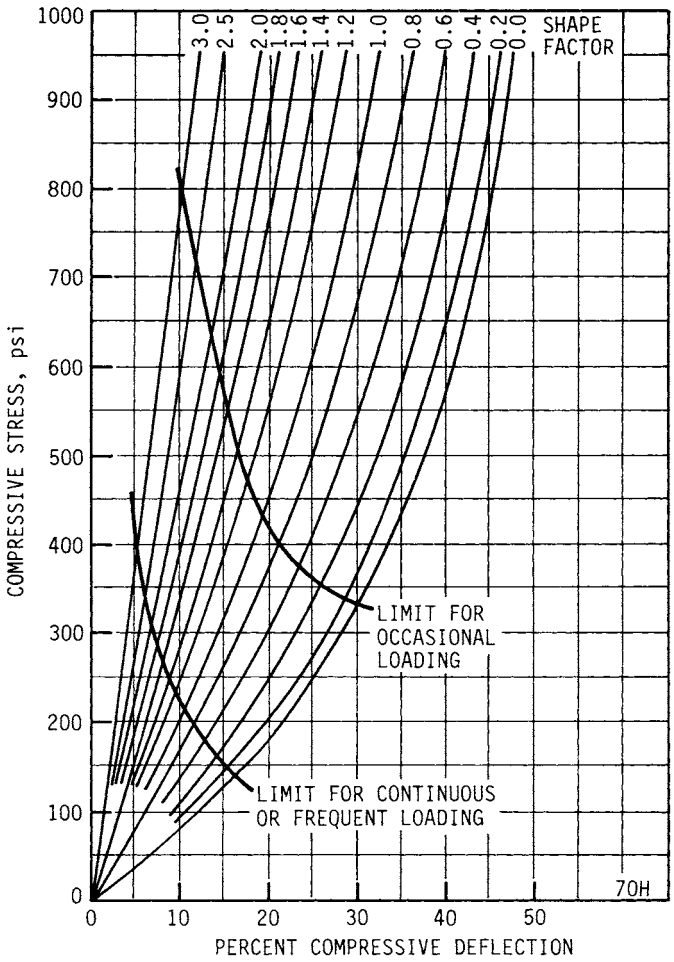

FIGURE 16.28 How the shape factor changes the maximum allowable stress in 70 durometer (Shore A) rubber. *(From Ref. [16.5], p. 77.)*

The basic misalignment capacity of these couplings is determined by the mating tolerances of the two hubs, the elastomeric element, and the particular jaw design. The larger the difference between the cushion and the jaw dimensions, the greater the misalignment that can be accommodated without exerting undue reaction forces on the system. However, this arrangement also leads to noisy operation, pulsating power transmission, and the transmission of shock through the system. A tradeoff between these effects is made in the final design. Alternatively, thick blocks of material can be used and deformed under misalignment. This may cause high restoring forces but decrease noise and pulsation of power owing to loading and unloading of the flexible elements. These couplings exert some axial thrust with increasing torque unless special jaws are used.

The shear unclamped coupling shown in Fig. 16.29 transmits power through shear in the elastomer, which can be rubber or a suitable plastic. Since rubber in shear can be loaded to only 20 percent of the load permitted on rubber in compression (70 versus 350 psi), the shear coupling is correspondingly larger in diameter and has a thicker element cross section than a corresponding compression coupling. The basic rating for this coupling type is

$$T = \frac{\pi t_{\max}(r_0^4 - r_i^4)}{2r_0} \tag{16.19}$$

These couplings may have both internal and external teeth in the hubs which mate to teeth in the flexible element, or the element may be bonded to the internal hubs and friction-fit into the outer hub (Fig. 16.30). For proper operation of the toothed-type coupling, the element must be twisted because of torque; this causes the gear teeth to rest properly. If the coupling is too large for a particular application (high service factor), the teeth will not load properly and the coupling will wear out prematurely. The toothed type of coupling is the double-engagement type and may allow more parallel and angular misalignment than a corresponding compression coupling.

The bonded type is designed to slip when torque exceeds the maximum rating; however, the heat generated by prolonged overload will destroy the coupling. The

FIGURE 16.29 Shear unclamped coupling. *(T. B. Wood's Sons, Inc.)*

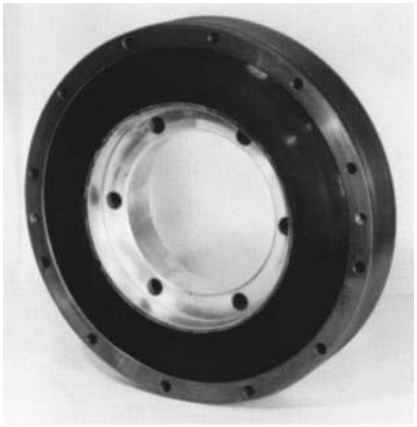

FIGURE 16.30 Bonded type of a shear unclamped coupling. *(Lord Corp., Industrial Products Div.)*

bonded type is torsionally softer than the corresponding toothed type, with windup of 15° to 20° versus 5° to 6° for the toothed type. This coupling is not fail-safe; when the flexible element fails, the driver and driven equipment are no longer connected.

The shear clamped or tire (torus) coupling is designed around a tire-shaped element, as shown in Figs. 16.31 and 16.32. The tire beads are clamped to a hub on either side, and torque is transmitted by shear and tension in the tire body. These couplings may be reinforced or unreinforced (without cords); in either case, the geometry allows very short overall length for a given torque capacity at the expense of diameter, which becomes correspondingly larger. This large diameter can cause some problems resulting from axial pull from the coupling as it is rotated at high speed. Centrifugal forces on the tire cause the two hubs to collapse inward as the speed is increased. The tire shape allows lower restoring force to larger misalignments than the shear unclamped or compression coupling.

The tension coupling shown in Fig. 16.33 is very similar to the link coupling (see Sec. 16.3.1), in that alternate legs (links) are in compression or tension. The links may have reinforcing cords to increase their tensile rating. In this coupling the rating is

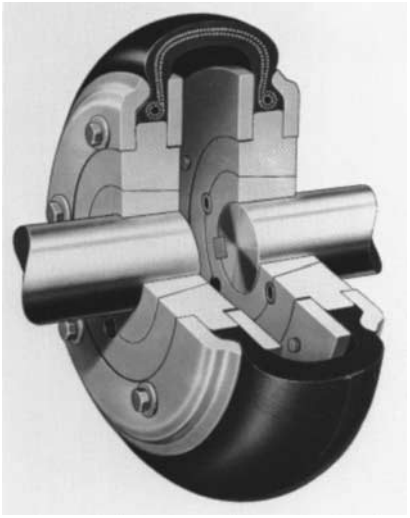

FIGURE 16.31 Tire coupling. *(Dodge Div., Reliance Electric.)*

FIGURE 16.32 Torus coupling. *(Falk Corp.)*

FIGURE 16.33 Tension coupling. *(Lovejoy Inc.)*

determined by the compression buckling of the leg pairs or the tensile strength of the other leg pairs, whichever is less. These couplings may be made of plastic, although rubber treated against ozone, when used with reinforcing cords, is also available.

To eliminate the effect of tension on rubber in a design similar to the one in Fig. 16.33, the rubber element is precompressed by assembling the element into a state smaller than the free state. This allows the "trailing leg" (formerly the tension leg) to stretch almost to neutral but never into tension, which would promote early failure.

In the radially restrained type, a tight metal band is slipped around the OD of the element while it is being held in a radially compressed state. After assembly to the mating hub, the band is snipped off, and the assembly bolts hold the element in precompression. Alternatively, radial bolts are used to draw the rubber element into compression. See Fig. 16.34.

Both these designs use fairly thick cross sections for their flexing elements and are quite compliant in all forms of misalignment. Rubber hardness and type can be changed to alter torque capacity, damping, and chemical-temperature resistance.

Alternatively, axial restraint can be used. In this design, the rubber element is installed between two hubs which are set a fixed distance apart, as shown in Fig. 16.35. The rubber element is then installed by means of bolts into this space, which is smaller than the free state of the rubber. This design is also very compliant, but generates an axial force because of the forced axial compression of the element.

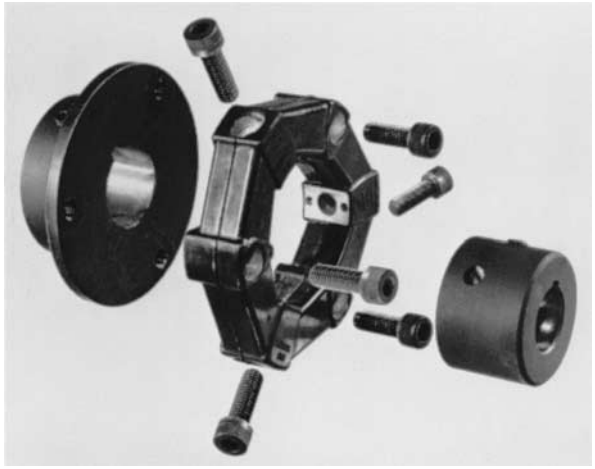

FIGURE 16.34 Precompressed radially restrained coupling. *(Lovejoy, Inc.)*

16.5 UNIVERSAL JOINTS AND ROTATING-LINK COUPLINGS

Another class of shaft connectors is composed of the linkage types, which include universal joints (U-joints) and rotating-link couplings. These couplings all rely on translating misalignment to relative rotation between parts of the coupling. The simplest universal joint is the one for a compass suspension universal joint described by Geronimo Cardano in the sixteenth century and explained mathematically by Robert Hooke in the seventeenth century. The universal joint basically consists of two shaft connections (yokes) which pivot about a pair of centrally located bearings. See Fig. 16.36.

FIGURE 16.35 Precompressed axially restrained coupling. *(Koppers Co. Inc., Power Transmission Div.)*

Shafts A and B are inclined to each other at angle θ (shaft centerlines must intersect); when shaft A is rotated, the center member (spider) causes shaft B to rotate by virtue of the connection. The output speed of shaft B is not constant when the shafts are at an angle. Specifically, the output velocity is

$$\omega_0 = \frac{\omega_i \cos \theta}{1 - \sin^2 \alpha \sin^2 \theta} \tag{16.20}$$

where α = rotation position angle and θ = joint or shaft angle. In addition, the change in velocity peaks twice during every revolution. This leads to a second-order harmonic excitation frequency for the drive system. Specifically, the torsional magnitude β of this excitation is

$$\beta = \tan^{-1} (\sec \theta)^{1/2} - \tan^{-1} (\cos \theta)^{1/2} \tag{16.21}$$

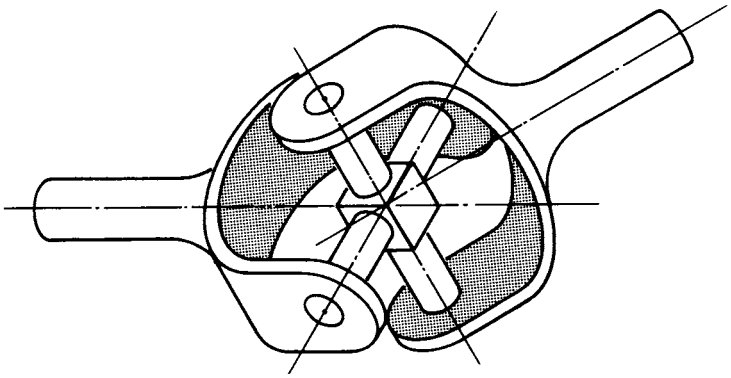

FIGURE 16.36 Basic Hooke's or Cardan universal joint.

The single Hooke's universal joint is not capable of accepting parallel misalignment (shaft centerlines do not meet at pivot member) except for very minor amounts resulting from manufacturing tolerances. Axial misalignment is usually compensated for by using a sliding connection on the input-output shafts or between the two universal joints.

When two universal joints are connected in series, parallel misalignment can be compensated for, because the parallel misalignment is converted to angular in each joint (see Fig. 16.37). By connecting two universal joints in this manner, it is possible to obtain approximately uniform output velocity between *A* and *C.* Basically, if joints *A* and *B* are aligned such that the pivot pins in their input and output yokes, respectively, are in the same plane, then the nonuniform output of joint *A* into shaft *B* is transformed to uniform output in joint *C.* However, if any angle exists between the joint *A* input yoke plane and the output yoke plane of joint *C,* then a nonuniform output will be generated. That nonuniform velocity and angle are, if we refer to Fig. 16.37*c,*

$$\omega_0 = \frac{\omega_i \cos \theta_{\text{eff}}}{1 - \sin^2 \alpha \sin^2 \theta} \tag{16.22}$$

where θ_{eff} = equivalent torsional angle given by

$$\theta_{\text{eff}} = (\delta^2 - \gamma^2)^{1/2} \tag{16.23}$$

Note that δ and γ are the U-joint angles as given in Fig. 16.37*c.*

16.5.1 Pin and Block

In its simplest form, the universal joint consists of two yokes and four pivot pins. The pivot pins ride in holes in the yoke and oscillate as the universal joint rotates. All the bearing takes place between the pins and the yoke, without the use of rolling-element bearings. In this type of joint, a thin film of lubricant or surface coating is all that prevents disaster from occurring, namely, the pin freezing in the journal (yoke) because of galling, corrosion, or adhesive transfer of metal. A first approximation to bearing pressure and velocity is as follows (shown in Fig. 16.38):

$$PV = \frac{Tn\theta}{6875 R_c t} \tag{16.24}$$

where T = operating torque, n = operating speed, θ = joint angle in degrees, t = yoke ear thickness, and R_c = the distance, as shown on Fig. 16.38. Since the velocity is actually nonuniform, the average speed of the pin-yoke oscillation has been used. We can see that the product $n\theta$, speed in revolutions per minute times angle in degrees, becomes a convenient unit to relate to the torque capacity. In fact, that is the typical unit used by most manufacturers for their ratings; see Fig. 16.39. These types of rating curves must be used with care, since a practical limit on angle limits the $n\theta$ parameter and the bearing area limits the PV parameter. A typical load-rating formula, given PV = 1000 psi·in/s, is

$$T = (0.6875 \times 10^7) \left(\frac{R_c t}{n\theta} \right) \tag{16.25}$$

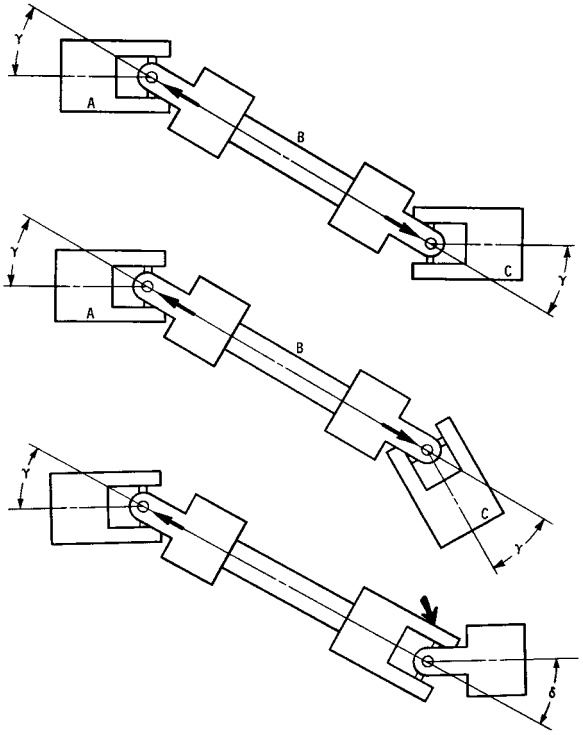

FIGURE 16.37 How two universal joints convert angular misalignment to parallel misalignment. (*a*), (*b*) Correct, yoke ears are aligned and angles are equal. (*c*) Incorrect, yoke ears are not in alignment and angles γ and δ are not equal. A residual angle θ_{eff} results from improper phasing of the two universal joints.

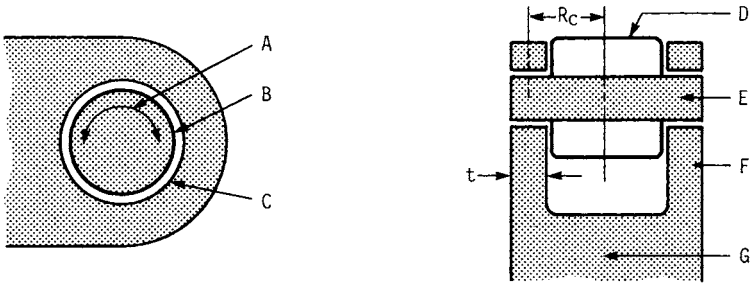

FIGURE 16.38 Plain bearing-type, pin-and-block, universal-joint geometry. A, oscillating pin; B, sliding at yoke interface; C, bore in yoke ear; D, center block; E, bearing pin; F, ear; G, yoke.

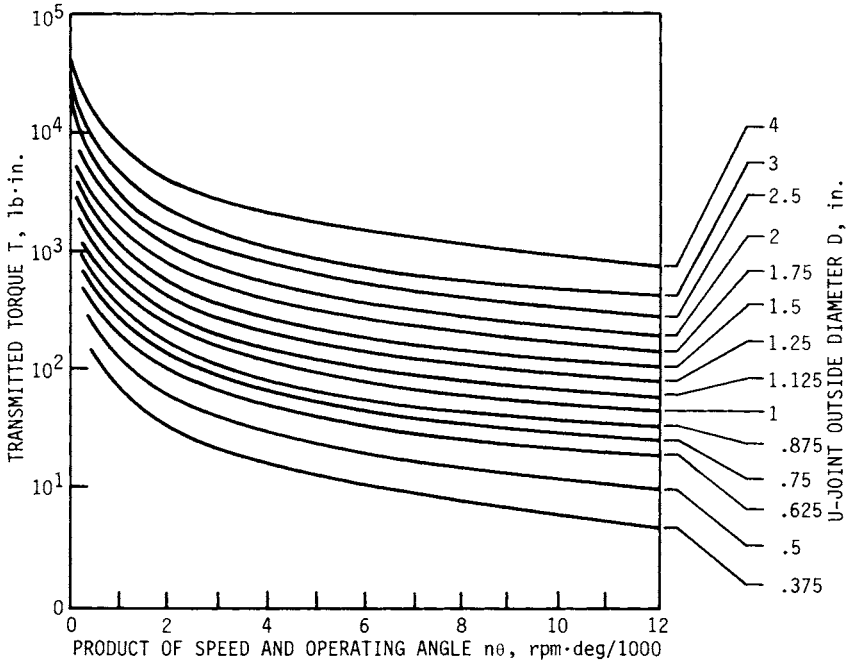

FIGURE 16.39 Torque ratings for pin-and-block universal joint. This chart shows the effect of the speed, operating angle, and OD parameters on the rated torque. These curves are based on a PV value of 1000 psi.in/s.

16.5.2 Needle Bearing

The pin-yoke interface is now changed to a pin and rolling-element bearing. This type of universal joint is also referred to as an automobile type, since it is found in most automobile drivelines. This universal joint also exhibits nonuniform rotational output velocity. A typical needle-bearing universal joint in cross section is shown in Fig. 16.40.

Corresponding to 3000 hours (h) of B_{10} life, the basic torque rating of a needle-bearing universal joint is given by

$$T_R = 4500 K_a K_s d \ell b \tag{16.26}$$

where T_R = basic torque rating, lb·in
K_a = joint angle correction factor
K_s = speed correction factor
d = bearing pin diameter, in
ℓ = length of needle rollers, in
b = bearing spacing, in

The dimensions d, ℓ, and b are shown in Fig. 16.40. The correction factor K_a in Eq. (16.26) is unity when the joint angle γ is 3°. For other angles, use the formula

$$K_a = \frac{1.432}{\gamma^{0.3269}} \tag{16.27}$$

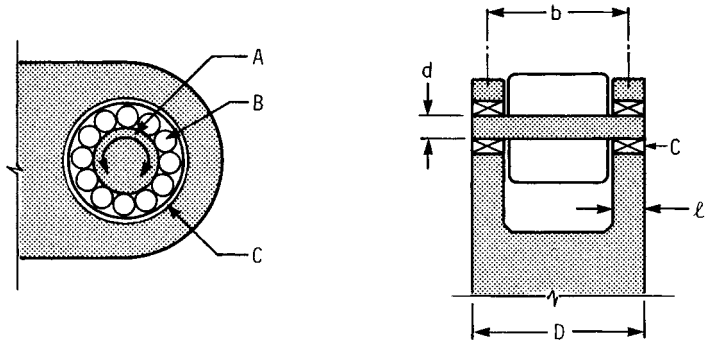

FIGURE 16.40 Geometry of the universal joint with needle bearings. A, oscillating pin; B, rolling motion occurs in the yoke-pin interface; C, needle bearing.

The correction factor K_s in Eq. (16.26) is unity when the speed n is 1000 r/min. For other speeds, use the equation

$$K_s = \frac{9.24}{n^{0.3219}} \tag{16.28}$$

We also define a life factor K_L as the ratio of the actual transmitted torque to the basic torque rating. Thus

$$K_L = \frac{T}{T_R} \tag{16.29}$$

For an expected life L of 3000 h, the life factor is unity. For other lives, use the equation

$$L = \left(\frac{15.5}{K_L}\right)^{2.921} \tag{16.30}$$

where L = expected B_{10} life (see Chap. 18) in hours.

Example 1. A universal joint has an outside diameter $D = 3$ in, an operating speed $n = 4000$ r/min, and a joint angle $\gamma = 5°$. The needle bearings have a needle length of 0.75 in and a bearing pin diameter $d = 0.875$ in. Find the expected B_{10} life if 2400 lb·in of torque is to be transmitted.

Solution. From Fig. 16.40 we find

$$b = D - \ell = 3 - 0.75 = 2.25 \text{ in}$$

Equation (16.27) gives the joint angle correction factor as

$$K_a = \frac{1.432}{\gamma^{0.3269}} = \frac{1.432}{5^{0.3269}} = 0.846$$

The speed correction factor is obtained from Eq. (16.28):

$$K_s = \frac{9.24}{n^{0.3219}} = \frac{9.24}{(4000)^{0.3219}} = 0.640$$

Thus, from Eq. (16.26), we find the basic torque rating to be

$$T_R = 4500K_aK_sd\ell b = 4500(0.846)(0.640)(0.875)(0.75)(2.25)$$

$$= 3598 \text{ lb} \cdot \text{in}$$

Since the actual torque to be transmitted is 2400 lb·in, the life factor is

$$K_L = \frac{T}{T_R} = \frac{2400}{3598} = 0.667$$

So, from Eq. (16.30), the expected life is

$$L = \left(\frac{15.5}{K_L}\right)^{2.921} = \left(\frac{15.5}{0.667}\right)^{2.921} = 9878 \text{ h}$$

16.5.3 Constant-Velocity Universal Joints

Double Cardan Joint. As mentioned previously, two simple Hooke's (Cardan) universal joints can be connected to give relatively constant output velocity (Fig. 16.37). However, if the universal joints are not exactly at the same angle, a small fluctuation in output velocity will occur. Specifically, the torsional equivalent angle $\theta_{eff} = \sqrt{\theta_1^2 + \theta_2^2}$ for a universal joint when the bearing planes are in the same plane. When the bearing planes are perpendicular, θ_{eff} becomes

$$\theta_{eff} = \sqrt{\theta_1^2 + \theta_2^2} \tag{16.31}$$

The torsional equivalent angle is used as if only one Cardan joint were in the system.

Tracta. The Tracta joint operates through the sliding action of two internally connected sliding couplings. This type of joint has a fairly high torque and angle capacity for its diameter; however, because of heat buildup from sliding friction, it cannot be used for any extended time at high loads. It can, however, be used satisfactorily at low angles with high loads.

The C-shaped input-output yokes generally have an opening of less than 180° so as to lock into two grooved couplings, which are, in turn, locked together in a tongue-and-groove fashion. See Fig. 16.41.

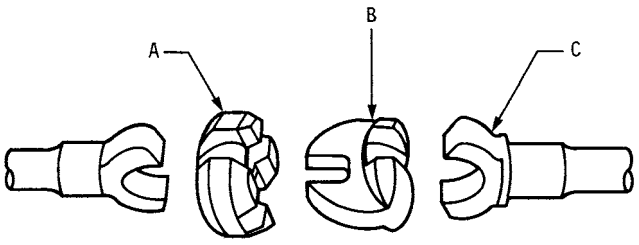

FIGURE 16.41 Exploded view of the Tracta universal joint. A, grooved coupling; B, tongue-and-groove coupling; C, fork yoke. *(From Ref. [16.6].)*

Rzeppa Universal Joint. This constant-velocity joint uses driving balls and curved axial-groove races; see Fig. 16.42. When the joint is at the same angle θ, the balls on one side of the joint will be farther from the joint centerline than the others. The off-center condition occurs because the groove generation point is displaced to provide camming action necessary for proper ball location and joint operation. Since the outer-race ball grooves act as cam surfaces, frictional locking can occur unless the cam surfaces have a divergent angle of 15° to 17° to prevent this. If the divergent angle were not present, the joint would lock going through zero angle.

Roller and Trunion. If the yoke ears in the simple pin-and-block or needle roller universal joints are elongated to form races, some axial movement is allowed, which decreases greatly the axial force developed by a single rotating universal joint. This joint is not a constant-velocity type. It is also called a *bipot* (see Fig. 16.43).

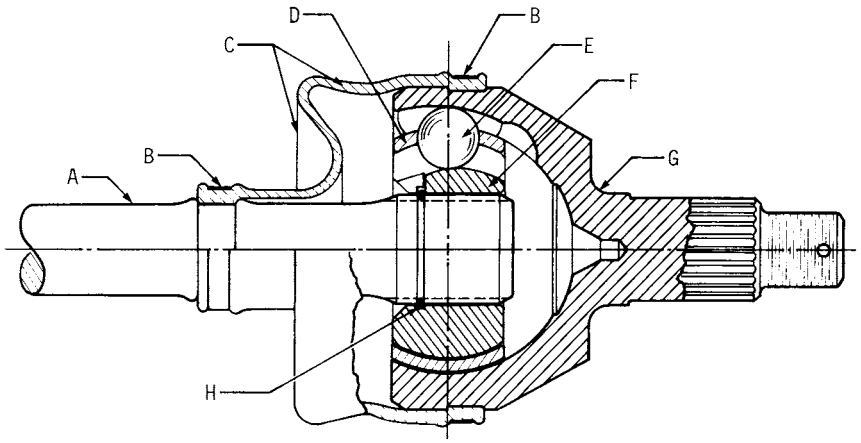

FIGURE 16.42 Rzeppa universal joint in cross section. A, shaft; B, clamp or band; C, boot seal; D, cage; E, ball; F, inner race; G, bell-type outer race; H, retaining ring. *(From Ref. [16.6].)*

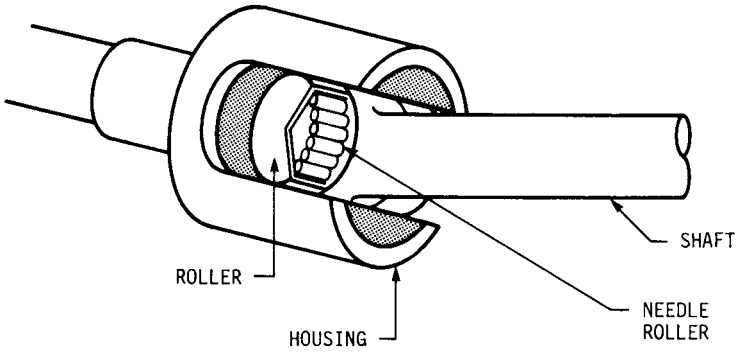

FIGURE 16.43 Roller trunion universal joint.

Tripot. If three equally spaced rollers are used, the joint will transmit constant velocity because of the cancellation of torque couples within the joint. The center of this joint may be free to float (end motion type), in which case the axial force generated by the joint is low and the joint is self-supporting. In the fixed-center type, the joint center is fixed, which causes the joint to orbit about its center; this limits it to low-speed use, because of inertial effects, and places where this orbital motion can be tolerated (such as in conjunction with self-aligning bearings or other universal joints). See Ref. [16.6].

16.5.4 Rotating-Link Coupling

This coupling consists of three disks connected by two sets of three links, as shown in Fig. 16.44. Typically, one set of links is attached to shafts on the driver and center disks, while the other set of links connects the center to the lower disk. All links are of equal length, and all the shafts are equally spaced on the same bolt circle on each hub. The maximum parallel displacement of the input and output shafts is determined by and equal to the link length S. With this arrangement, unless the input and output shafts were misaligned at least a small amount S_{min}, the center disk would be free to swing about the center of the shafts. This would cause an unbalance in the coupling and would result in high vibration and limited life. This effect gives the misalignment range of this coupling of S_{min} to S.

FIGURE 16.44 Rotating-link coupling. *(Schmidt Couplings, Inc.)*

The construction of this coupling causes the links to move parallel to one another and results in constant angular velocity. In addition, because three links are equally spaced about each hub and are of equal size and mass, the sum of all link forces is zero, resulting in smooth operation without imposing side loads.

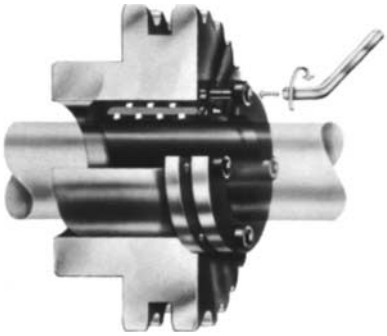

FIGURE 16.45 Pressure bushing. *(FFV Industrial Products.)*

16.6 METHODS OF ATTACHMENT

There are several methods of attaching the coupling hubs to the shafts on equipment. Among these are split-taper bushings, keys and splines, shrink-fit and spline profile distortion, and pressure bushings. The first two items are covered in Chap. 24; shrink fits are discussed in Chap. 27.

Spline profile distortion causes the entire bore area of the coupling hub to deform around the mating shaft. This

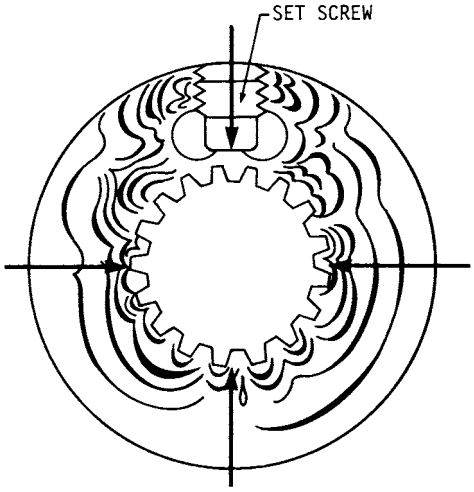

FIGURE 16.46 Drawing of a model of Centaloc spline profile distortion obtained by photoelastic methods showing lines of constant stress. *(Lovejoy, Inc.)*

method of attachment allows a much greater clamping force to be exerted than with a split-taper hub with internal spline. This clamping about the entire spline is important and eliminates fretting corrosion (caused by loose-fitting spline shafts and mating hubs) and point contact obtained with split bushing types, as shown in Fig. 16.46.

Pressure bushings (Fig. 16.45) are similar to the hydraulic coupling except that both the inner and outer surfaces are allowed to deform, compressing onto the shaft and expanding into the coupling hub. The pressure source for this type is usually applied through axial compression of the bladder with a clamping ring.

REFERENCES

16.1 AGMA Standard 922-A96 *Load Classification and Service Factors for Flexible Couplings.*

16.2 DIN 740, *Flexible (Shaft) Couplings; Dimensions, Nominal Torque.*

16.3 AGMA Standard 9000-C90, *Flexible Couplings—Potential Unbalance Classification.*

16.4 ISO 1940, *Balance Quality of Rotating Rigid Bodies.* 2003.

16.5 *Handbook of Molded and Extruded Rubber,* Goodyear Tire and Rubber Co., Akron, Ohio, 1969.

16.6 SAE, *Universal Joint and Drive Shaft Design Manual AE-7,* 1979.

16.7 AGMA Standard 9002-A86, *Bore and Keyway Sizes for Flexible Couplings.*

16.8 SAE J744c, *Hydraulic Power Pumps,* 1970.

16.9 ISO R773, *Rectangular or Square Parallel Keys and Their Corresponding Keyways,* 1969.

16.10 DIN 7154, *ISO-Close Tolerance Standard Bores.*

16.11 JISB 1301, *Bore and Keyway Tolerances.*

16.12 ANSI B92.1, *Involute Splines and Inspection.*

16.13 DIN 5482, *Internal and External Involute Spline Profiles.*

16.14 DIN 5480, *Serrated Shaft Connections with Involute Spline Profiles.*

16.15 SAE J499a, *Parallel Side Splines for Soft Broached Holes in Fittings,* 1975.

BIBLIOGRAPHY

Beercheck, Richard: "The Right Flexible Coupling," *Machine Design,* Aug. 24, 1978, pp. 101–104.

Bigden, J. V., and Ziegler, Carl: "Universal Joints," *Power Transmission Design Handbook 1983–84,* Penton IPC, 1983, pp. C189–192.

Calistrat, Michael: *Flexible Coupling Installation,* Koppers Co. Inc., Baltimore, Md. "Diaphragm Couplings Challenge Disk and Gear Types for High Torque," *Product Engineering,* June 1977, pp. 33–36.

Hitchcox, Alan: "High Performance Couplings Meet Heavy Demands," *Power Transmission Design,* October 1982, pp. 46–48.

McCormick, Doug: "Finding the Right Flexible Coupling," *Design Engineering,* October 1981, pp. 62–66.

Proceedings of the International Conference on Flexible Couplings for High Powers and Speeds, University of Sussex, Brighton, England, July 1972.

Schalitz, August: *Kupplungs-Atlas,* Druckhaus Korntal Fritz Pfitzer, 1975 (German).

Schmidt, Richard: *Unique Couplings for Large Offset Shafts,* Schmidt Couplings, Cincinnati.

Schwerdlin, Howard: "Combatting Heat in U-joints," *Machine Design,* July 23, 1981, pp. 83–86.

Schwerdlin, Howard: "Flexible Couplings," *Power Transmission Design Handbook 1983–84,* Penton IPC, 1983, pp. 123–126.

Wiedenroth, Wolfgang: "Fachgebiete in Jahresübersichten," *VDI-Z,* no. 17, September 1980 (German).

CHAPTER 17
SHAFTS

Charles R. Mischke, Ph.D., P.E.
Professor Emeritus of Mechanical Engineering
Iowa State University
Ames, Iowa

NOMENCLATURE

a	Distance
A	Area
b	Distance
c_0	Constant
C_1, C_2	Constants
d	Outside diameter of shaft
d_i	Inside diameter of hollow shaft
E	Modulus of elasticity
F	Load
g	Gravitation constant
i	index
I	Second moment of area
J	Polar second area moment
k	Torsional spring rate
K	Transverse shear stress magnification factor
K_f	Fatigue stress concentration factor
ℓ	Span

m	Mass per unit length
M	Bending moment
n	Design factor, factor of safety
p	Shrink-fit pressure
r	Load line slope
R	Bearing reaction
S_a	Strength amplitude ordinate to fatigue locus
S_e	Endurance strength
S_m	Strength steady coordinate to fatigue locus
S_y	Yield strength
S_{ut}	Ultimate tensile strength
T	Torsional or twisting moment
V	Transverse shear force
w_i	Weight of ith segment of shaft
W	Weight of shaft
x	Coordinate
x_a, x_b	Coordinates of bearings
y	Coordinate, deflection
y_0	Constant
z	Coordinate
γ	Weight density
θ	Angle
σ	Normal stress
σ'	Von Mises normal stress
τ	Shear stress
ω	First critical angular frequency

17.1 INTRODUCTION

A shaft is a rotating part used to transmit power, motion, or analogic information. It often carries rotating machine elements (gears, pulleys, cams, etc.) which assist in the transmission. A shaft is a member of a fundamental mechanical pair: the "wheel and axle." Traditional nomenclature includes

Axle A stationary member supporting rotating parts.
Shaft A rotating member supporting attached elements.
Spindle A short shaft or axle.
Head or stud shaft A shaft integral with a motor or prime mover.
Line shaft A shaft used to distribute power from one prime mover to many machines.
Jack shaft A short shaft used for power transmission as an auxiliary shaft between two other shafts (counter shaft, back shaft).

Geometric fidelity is important to many shaft functions. Distortion in a loaded body is unavoidable, and in a shaft design it is controlled so as to preserve function. There are elastic lateral displacements due to bending moment and transverse shear, and there are elastic displacements of an angular nature due to transmitted torque. Fracture due to fatigue and permanent distortion due to yielding destroy function. The tight constraint in shaft design is usually a distortion at a particular location. For example, shaft slope at a bearing centerline should typically be less than 0.001 rad for cylindrical and tapered roller bearings, 0.004 rad for deep-groove ball bearings, and 0.0087 rad for spherical ball bearings. At a gear mesh, the allowable relative slope of two gears with uncrowned teeth can be held to less than 0.0005 rad each. Deflection constraints for involute gears tolerate larger (but not smaller) than theoretical center-to-center distances, with a small increase in pressure angle but with observable increases in backlash. The typical upper bound on center-to-center distance in commercial-quality spur gearing is for diametral pitches up to 10, 0.010 in; for those 11 to 19, 0.005 in; and those for 20 to 50, 0.003 in.

A harsh reality is that a deflection or slope at a shaft section is a function of the geometry and loading *everywhere*. The stress at a shaft section is a function of the local geometry and local bending moment, a simpler problem. Shaft designers often size the shaft to meet the active distortion constraint, then check for strength adequacy. Young's modulus is about the same for most shaft steels, and so adjusting the material and its condition does not significantly undo the distortional adequacy.

Shafts are proportioned so that mounted elements are assembled from one or both ends, which accounts for the stepped cylinder, fat middle aspect. This also efficiently places the most material toward the center. Shaft geometric features may also include chamfers, shoulders, grooves, keyways, splines, tapers, threads, and holes for pins and lubricant access. Shafts may even be hollow, square, etc. The effect of each of these features must be considered when checking shaft performance adequacy.

17.2 DISTORTION DUE TO BENDING

Since the most likely active constraint is a slope or a deflection at some shaft section, it is useful to determine the *constant*-diameter shaft that meets the requirement. This establishes in the designer's mind the "heft" of the shaft. Then, as one changes the local diameters and their lengths to accommodate element mounting, the material removed near the bearings has to be replaced in part, but nearer the center. It is a matter of guiding perspective at the outset. Figure 17.1 depicts shafts with a single transverse load F_i or a single point couple M_i which could be applied in either the horizontal or the vertical plane. From [17.1], Tables A-9-6 and A-9-8, expressions for slopes at each bearing can be developed. It follows by superposition that for the left bearing,

$$d = \left(\frac{32n}{3\pi E \ell \Sigma\theta} \left\{ [\Sigma F_i b_i (b_i^2 - \ell^2) + \Sigma M_i (3a_i^2 - 6a_i \ell + 2\ell^2)\,]_H^2 + [\Sigma F_i b_i (b_i^2 - \ell^2) + \Sigma M_i (3a_i^2 - 6a_i \ell + 2\ell^2)]_V^2 \right\}^{1/2} \right)^{1/4} \quad (17.1)$$

and for the right bearing,

$$d = \left(\frac{32n}{3\pi E \ell \Sigma\theta} \left\{ [\Sigma F_i a_i (\ell^2 - a_i^2) + \Sigma M_i (3a_i^2 - \ell^2)]_H^2 + [\Sigma F_i a_i (\ell^2 - a_i^2) + \Sigma M_i (3a_i^2 - \ell^2)]_V^2 \right\}^{1/2} \right)^{1/4} \quad (17.2)$$

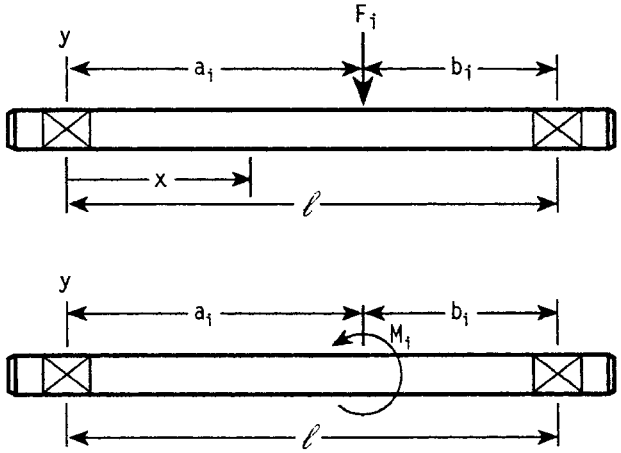

FIGURE 17.1 Simply supported shafts with force F_i and couple M_i applied.

where $\Sigma\theta$ is the absolute value of the allowable slope at the bearing. These equations are an ideal task for the computer, and once programmed interactively, are convenient to use.

Example 1. A shaft is to carry two spur gears between bearings and has loadings as depicted in Fig. 17.2. The bearing at A will be cylindrical roller. The spatial centerline slope is limited to 0.001 rad. Estimate the diameter of the uniform shaft which limits the slope at A with a design factor of 1.5.

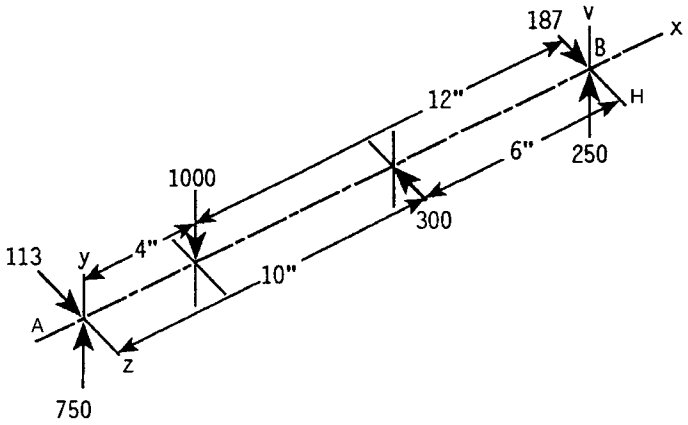

FIGURE 17.2 A shaft carries two spur gears between bearings A and B. The gear loads and reactions are shown.

Solution. Equation (17.1) is used.

$$d = \left(\frac{32n}{3\pi E \ell \Sigma \theta} \left\{ [F_1 b_1 (b_1^2 - \ell^2)]_H^2 + [F_2 b_2 (b_2^2 - \ell^2)]_V^2 \right\}^{1/2} \right)^{1/4}$$

$$= \left(\frac{32(1.5)}{3\pi 30(10)^6 \, 16(0.001)} \left\{ [300(6)(6^2 - 16^2)]^2 + [1000(12)(12^2 - 16^2)]^2 \right\}^{1/2} \right)^{1/4}$$

$$= 1.964 \text{ in}$$

Transverse bending due to forces and couples applied to a shaft produces slopes and displacements that the designer needs to control. Bending stresses account for most or all of such distortions. The effects of transverse shear forces will be addressed in Sec. 17.3.

Most bending moment diagrams for shafts are piecewise linear. By integrating once by the trapezoidal rule and a second time using Simpson's rule, one can obtain deflections and slopes that are *exact,* can be developed in tabular form, and are easily programmed for the digital computer. For bending moment diagrams that are piecewise polynomial, the degree of approximation can be made as close as desired by increasing the number of station points of interest. See [17.1], pp. 103–105, and [17.2]. The method is best understood by studying the tabular form used, as in Table 17.1.

The first column consists of station numbers, which correspond to cross sections along the shaft at which transverse deflection and slope will be evaluated. The minimum number of stations consists of those cross sections where M/EI changes in magnitude or slope, namely discontinuities in M (point couples), in E (change of material), and in I (diameter change, such as a shoulder). Optional stations include other locations of interest, including shaft ends. For integration purposes, midstation locations are chosen so that the second integration by Simpson's rule can be exact. The moment column M is dual-entry, displaying the moment as one approaches the station from the left and as one approaches from the right. The distance from the origin to a station x is single-entry. The diameter d column is dual-entry, with the entries differing at a shoulder. The modulus E column is also dual-entry. Usually the shaft is of a single material, and the column need not be filled beyond the first entry. The first integration column is single-entry and is completed by applying the trapezoidal rule to the M/EI column. The second integration column is also single-entry, using the midstation first integration data for the Simpson's rule integration.

TABLE 17.1 Form for Tabulation Method for Shaft Transverse Deflection Due to Bending Moment

	Moment M	Dist. x	Dia. d	Modulus E	$\frac{M}{EI}$	$\int_0^x \frac{M}{EI}\,dx$	$\int_0^x \left(\int_0^x \frac{M}{EI}\,dx \right) dx$	Defl. y	Slope $\frac{dy}{dx}$
1						0	0		
2									
3									

The deflection entry y is formed from the prediction equation

$$y = \int_0^x \int_0^x \frac{M}{EI}\, dx\, dx + C_1 x + C_2 \tag{17.3}$$

The slope dy/dx column is formed from the prediction equation

$$\frac{dy}{dx} = \int_0^x \frac{M}{EI}\, dx + C_1 \tag{17.4}$$

where the constants C_1 and C_2 are found from

$$C_1 = \frac{\int_0^{x_a} \int_0^{x_a} M/(EI)\, dx\, dx - \int_0^{x_b} \int_0^{x_b} M/(EI)\, dx\, dx}{x_a - x_b} \tag{17.5}$$

$$C_2 = \frac{x_b \int_0^{x_a} \int_0^{x_a} M/(EI)\, dx\, dx - x_a \int_0^{x_b} \int_0^{x_b} M/(EI)\, dx\, dx}{x_a - x_b} \tag{17.6}$$

where x_a and x_b are bearing locations.

This procedure can be repeated for the orthogonal plane if needed, a Pythagorean combination of slope, or deflections, giving the spatial values. This is a good time to plot the end view of the deflected shaft centerline locus in order to see the spatial lay of the loaded shaft.

Given the bending moment diagram and the shaft geometry, the deflection and slope can be found at the station points. If, in examining the deflection column, any entry is too large (in absolute magnitude), find a new diameter d_{new} from

$$d_{\text{new}} = d_{\text{old}} \left| \frac{n y_{\text{old}}}{y_{\text{all}}} \right|^{1/4} \tag{17.7}$$

where y_{all} is the allowable deflection and n is the design factor. If any slope is too large in absolute magnitude, find the new diameter from

$$d_{\text{new}} = d_{\text{old}} \left| \frac{n(dy/dx)_{\text{old}}}{(\text{slope})_{\text{all}}} \right|^{1/4} \tag{17.8}$$

where $(\text{slope})_{\text{all}}$ is the allowable slope. As a result of these calculations, find the largest $d_{\text{new}}/d_{\text{old}}$ ratio and multiply all diameters by this ratio. The tight constraint will be at its limit, and all others will be loose. Don't be concerned about end journal size, as its influence on deflection is negligible.

Example 2. A shaft with two loads of 600 and 1000 lbf in the same plane 2 inches (in) inboard of the bearings and 16 in apart is depicted in Fig. 17.3. The loads are from 8-pitch spur gears, and the bearings are cylindrical roller. Establish a geometry of a shaft which will meet distortion constraints, using a design factor of 1.5.

Solution. The designer begins with identification of a uniform-diameter shaft which will meet the likely constraints of bearing slope. Using Eq. (17.2), expecting the right bearing slope to be controlling,

$$d = \left[\frac{32(1.5)}{3\pi 30(10)^6 16(0.001)} \left| 600(2)(16^2 - 2^2) + 1000(14)(16^2 - 14^2) \right| \right]^{1/4}$$

$$= 1.866 \text{ in}$$

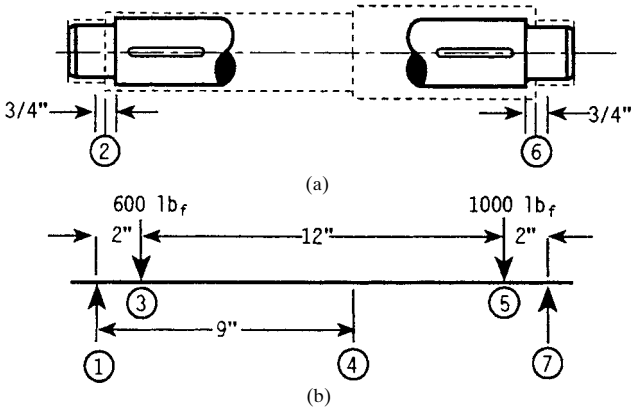

FIGURE 17.3 (*a*) The solid-line shaft detail is the designer's tentative geometry. The dashed lines show shaft sized to meet bending distortion constraints. (*b*) The loading diagram and station numbers.

Based on this, the designer sketches in some tentative shaft geometry as shown in Fig. 17.3*a*. The designer decides to estimate the bearing journal size as 1.5 in, the next diameter as 1.7 in, the diameter beyond a shoulder 9 in from the left bearing as 1.9 in, and the remaining journal as 1.5 in. The next move is to establish the moment diagram and use seven stations to carry out the tabular deflection method by completing Table 17.1. Partial results are shown below.

Station	x, in	Moment M, in · lbf	Diameter d, in	Deflection y, in	Slope dy/dx
1	0	0	1.5	0	–0.787E-03
2	0.75	487.5	1.5/1.7	–0.584E-03	–0.763E-03
3	2	1300	1.7	–0.149E-02	–0.672E-03
4	9	1650	1.7/1.9	–0.337E-02	0.168E-03
5	14	1900	1.9	–0.140E-02	0.630E-03
6	15.25	712.5	1.9/1.5	–0.554E-03	0.715E-03
7	16	0	1.5	0	0.751E-03

The gears are 8 pitch, allowing 0.010/2 = 0.005 in growth in center-to-center distance, and both y_3 and y_5 have absolute values less than 0.005/1.5 = 0.00333, so that constraint is loose. The slope constraints of 0.001/1.5 are violated at stations 1 and 7, so using Eq. (17.8),

$$(d_1)_{\text{new}} = 1.5\left|\frac{1.5(-0.000\,787)}{0.001}\right|^{1/4} = 1.5(1.042)\text{ in}$$

$$(d_7)_{\text{new}} = 1.5\left|\frac{1.5(0.000\,751)}{0.001}\right|^{1/4} = 1.5(1.030)\text{ in}$$

and the gear mesh slope constraints are violated at stations 3 and 5, so using Eq. (17.8),

$$(d_3)_{\text{new}} = 1.7\left|\frac{1.5(0.001\,49)}{0.0005}\right|^{1/4} = 1.7(1.454)\text{ in}$$

$$(d_5)_{\text{new}} = 1.9\left|\frac{1.5(0.001\,40)}{0.0005}\right|^{1/4} = 1.9(1.432)\text{ in}$$

The largest d_{new}/d_{old} ratio among the four violated constraints is 1.454, so *all* diameters are multiplied by 1.454, making $d_1 = 1.5(1.454) = 2.181$ in, $d_3 = 1.7(1.454) = 2.472$ in, $d_5 = 1.9(1.454) = 2.763$ in, and $d_7 = 1.5(1.454) = 2.181$ in. The diameters d_1 and d_7 can be left at 1.5 or adjusted to a bearing size without tangible influence on transverse deflection or slope. One also notes that the largest multiplier 1.454 is associated with the now tight constraint at station 3, all others being loose. Rounding d_3 and/or d_5 up will render all bending distortion constraints loose.

17.3 DISTORTION DUE TO TRANSVERSE SHEAR

Transverse deflection due to transverse shear forces associated with bending becomes important when the the shaft length-to-diameter ratio is less than 10. It is a short-shaft consideration. A method for estimating the shear deflection is presented in Ref. [17.2]. There are two concerns associated with shear deflection. The first is that it is often forgotten on short shafts. The second is that it is often neglected in formal education, and engineers tend to be uncomfortable with it. Ironically, it is simpler than bending stress deflection.

The loading influence is the familiar shear diagram. The transverse shear force V is piecewise linear, and the single integration required is performed in a tabular method suitable to computer implementation. Table 17.2 shows the form. The left-hand column consists of station numbers which identify cross sections along the shaft at which shear deflection and slope are to be estimated. The minimum number of stations consists of those cross sections where $KV/(AG)$ changes abruptly, namely at discontinuities in transverse shear force V (at loads), in cross-sectional area A (at shoulders), and in torsional modulus G (if the material changes). Optional stations include other locations of interest. There is no need for midstation locations, since the trapezoidal rule will be used for integration, maintaining exactness. The shear force column V is dual-entry, the location x is single-entry, and the diameter d column is dual-entry, as is the torsional modulus G column, if included. The $KV/(AG)$ column is dual-entry, as is the slope dy/dx column.

The single-entry integral column is generated using the trapezoidal rule. The single-entry deflection column y is generated from the prediction equation

$$y = \int_0^x \frac{KV}{AG}\,dx + c_0 x + y_0 \tag{17.9}$$

TABLE 17.2 Form for Tabulation Method for Shaft Transverse Deflection Due to Transverse Shear

	Shear V	Dist. x	Dia. d	Modulus G	$\frac{KV}{AG}$	$\int_0^x \frac{KV}{AG}\,dx$	Defl. y	Slope $\frac{dy}{dx}$	Avg. slope $(dy/dx)_{av}$
1						0			
2									
3									
4									

The dual-entry slope dy/dx column is generated from the other prediction equation,

$$\frac{dy}{dx} = -\frac{KV}{AG} + c_0 \tag{17.10}$$

where

$$c_0 = \frac{\int_0^{x_a} KV/(AG)\,dx - \int_0^{x_b} KV/(AG)\,dx}{x_a - x_b} \tag{17.11}$$

$$y_0 = \frac{x_a \int_0^{x_b} KV/(AG)\,dx - x_b \int_0^{x_a} KV/(AG)\,dx}{x_a - x_b} \tag{17.12}$$

where x_a and x_b are bearing locations and K is the factor 4/3 for a circular cross section (the peak stress at the centerline is 4/3 the average shear stress on the section). The slope column can have dual entries because Eq. (17.10) contains the discontinuous $KV/(AG)$ term.

Example 3. A uniform 1-in-diameter stainless steel [$G = 10(10)^6$ psi] shaft is loaded as shown in Fig. 17.4 by a 1000-lbf overhung load. Estimate the shear deflection and slope of the shaft centerline at the station locations.

Solution. Omitting the G column, construct Table 17.3. After the integral column is complete, c_0 and y_0 are given by Eqs. (17.11) and (17.12), respectively:

$$c_0 = \frac{0 - 339.5(10^{-6})}{1 - 11} = 33.95(10^{-6})$$

$$y_0 = \frac{1(339.5)10^{-6} - 11(0)}{1 - 11} = -33.95(10^{-6})$$

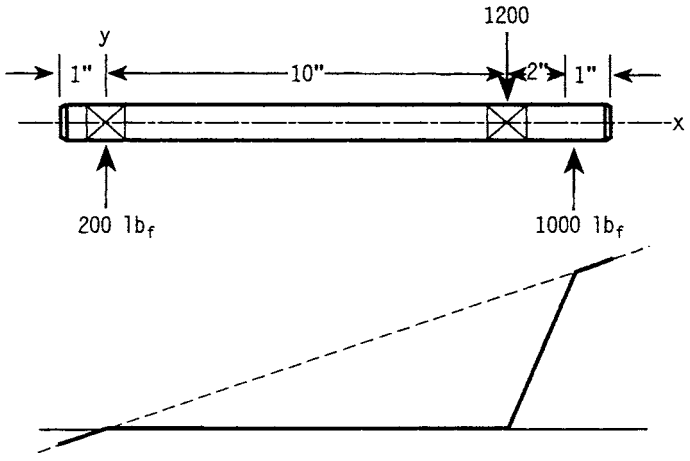

FIGURE 17.4 A short uniform shaft, its loading, and shear deflection.

TABLE 17.3 Transverse Shear Deflection in Shaft of Fig. 17.4

Station	V	x	d	$\frac{KV}{AG}$	$\int_0^x \frac{KV}{AG}\,dx$	y	dy/dx	$(dy/dx)_{av}$
1	0	0	0	0	0	−33.95E-06	33.95E-06	33.95E-06
	0		1	0			33.95E-06	
2	0	1	1	0	0	0	33.95E-06	16.98E-06
	200		1	33.95E-06			0	
3	200	11	1	33.95E-06	339.5E-06	0	0	101.9E-06
	−1000		1	−169.8E-06			203.75E-06	
4	−1000	13	1	−169.8E-06	0	407.4E-06	203.75E-06	118.9E-06
	0		1	0			33.95E-06	
5	0	14	1	0	0	441.4E-06	33.95E-06	33.95E-06
	0		0	0			33.95E-06	

The prediction Eqs. (17.9) and (17.10) are

$$y = -\int_0^x \frac{KV}{AG}\,dx + 33.95(10^{-6})x - 33.95(10^{-6})$$

$$\frac{dy}{dx} = 33.95(10^{-6}) - \frac{KV}{AG}$$

and the rest of the table is completed.

A plot of the shear deflection curve is shown under the shaft in Fig. 17.4. Note that it is piecewise linear. The droop of the unloaded overhang is a surprise when the between-the-bearings shaft is straight and undeflected. The discontinuous curve arises from discontinuities in loading V. In reality, V is not discontinuous, but varies rapidly with rounded corners. If a rolling contact bearing is mounted at station 2, the bearing inner race will adopt a compromise angularity between $dy/dx = 33.95(10^{-6})$ and $dy/dx = 0$. This is where the average (midrange) slope $(dy/dx)_{av}$ is useful in estimating the extant slope of the inner race with respect to the outer race of the bearing.

Figure 17.5 shows a short shaft loading in bending. Table 17.4 shows the deflection analysis of Sec. 17.2 for this shaft in columns 3 and 4, the shear deflection analysis of Sec. 17.3 in columns 5 and 6, and their superposition in columns 7 and 8. Figure 17.5 shows the shear deflection at station 7 to be about 28 percent of the bending deflection, and the shear slope at station 9 to be about 15 percent of the bending slope. Both of these locations could involve an active constraint. In the deflection analysis of shafts with length-to-diameter aspect ratios of less than 10, the transverse shear deflections should be included.

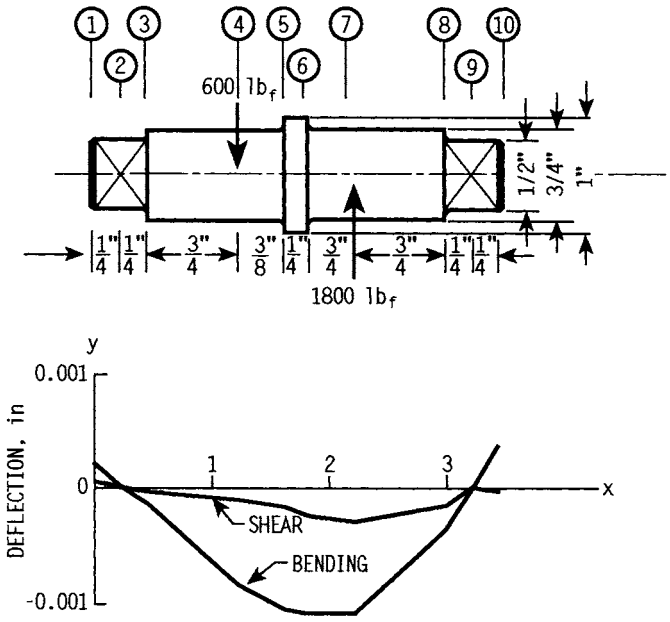

FIGURE 17.5 A short shaft of several diameters, its loading, and the consequential shear and bending deflections.

TABLE 17.4 Deflections of Shaft of Fig. 17.5

Station	x_i	Bending† y_i	Bending $(dy/dx)_i$	Shear‡ y_i	Shear $(dy/dx)_{avi}$	Combined y_i	Combined $(dy/dx)_i$
1		0.000 240	–0.000 959	0.738E-05	–0.295E-04	0.247E-03	–0.988E-03
2	0.250	0	–0.000 959	0	–0.886E-04	0	–0.105E-02
3	0.500	–0.000 234	–0.000 891	–0.369E-04	–0.115E-03	–0.271E-03	–0.101E-02
4	1.250	–0.000 842	–0.000 690	–0.984E-04	–0.116E-03	–0.940E-03	–0.850E-03
5	1.625	–0.001 05	–0.000 408	–0.188E-03	–0.194E-03	–0.124E-02	–0.601E-03
6	1.875	–0.001 14	–0.000 306	–0.225E-03	–0.194E-03	–0.137E-02	–0.500E-03
7	2.250	–0.001 14	0.000 378	–0.315E-03	–0.328E-05	–0.145E-02	0.375E-03
8	3.000	–0.000 403	0.001 38	–0.140E-03	0.397E-03	–0.543E-03	0.178E-02
9	3.250	0	0.001 72	0	0.266E-03	0	0.199E-02
10	3.500	0.000 431	0.001 72	–0.738E-05	–0.295E-04	0.424E-03	0.169E-02

† $C_1 = -0.959(10^{-3})$, $C_2 = 0.240(10^{-3})$, Eqs. (17.5) and (17.6).
‡ $c_0 = -0.295(10^{-4})$, $y_0 = 0.738(10^{-5})$, Eqs. (17.11) and (17.12).

17.4 DISTORTION DUE TO TORSION

Angular deflection in a right circular cylindrical shaft due to torque T is

$$\theta = \frac{T\ell}{GJ} \quad \text{rad} \tag{17.13}$$

For a stepped shaft of individual cylinder length ℓ_i with torques T_i, the angular deflection is

$$\theta = \Sigma\theta_i = \sum \frac{T_i \ell_i}{G_i J_i} \tag{17.14}$$

which becomes $\theta = (T/G)\Sigma(\ell_i/J_i)$ for constant torque through homogeneous material. The torsional stiffness can be defined as $k_i = T_i/\theta_i$, and since $\theta_i = T_i/k_i$ and $\theta = \Sigma\theta_i = \Sigma(T_i/k_i)$, one may write for constant torque $\theta = T\Sigma(1/k_i)$. It follows that

$$\frac{1}{k} = \sum \frac{1}{k_i} \tag{17.15}$$

The equation $\theta = (T/G)\Sigma\ell_i/J_i$ is not precise, since experimental evidence shows that θ is larger than given by this equation.

The material in a step (shoulder) has a surface free of shear. Some material loafs, so other material is more distressed and distorts more. The existence of keyways, splines, and tapered sections increases angular flexibility also. For quantitative treatment of these realities, see Ref. [17.3], pp. 93–99. When a coupling is keyed or splined to a shaft, that shaft can be considered to twist independently of the coupling for one-third of its hub length.

17.5 SHAFT MATERIALS

Most steels have similar moduli of elasticity, so that the rigidity requirement can be met by geometric decisions, independent of the material choice among steels. Strength to resist loading stresses affects the choice of material. ANSI 1020-1050 steels and 11XX free-machining steels are common choices. Heat treating 1340-50, 3140-50, 4140, 4340, 5140, and 8650 steels produces greater strength. Hardness is a function of size, and the methods of Grossman and Fields and of Crafts and Lamont in Chapter 33 are important to quantitatively relate strength to size and heat-treatment regimen. Carburizing grades 1020, 4320, 4820, and 8620 are chosen for surface-hardening purposes.

Cold-rolled sections are available up to about 3½ in in diameter. Hot-rolled rounds are available up to nearly 6 in. Above this size, forging precedes machining.

When a shaft geometry is created (prior to final machining) by a volume-conservative process (casting or hot or cold forming), then optimality can be pursued by minimizing the material amount if production volume permits. Constraints can be made nearly active at several locations. Many shafts are created for small production runs by machining round stock, and optimality may be achieved by minimizing the amount of material removed from the work piece, which minimizes the machining effort.

17.6 LOAD-INDUCED STRESSES

Shafts that transmit power are often loaded in such a way that the torsion which performs the work induces transverse bending forces at gears. If the torsion is stochastic, so is the induced bending due to pitch-line forces. Both the torsion and the bending moment have the same distribution and coefficient of variation. The same is true of a point couple induced at a helical gear.

For ductile shaft materials, distortion energy theory is used, and the array of stresses at a critical location element are combined to form the von Mises stress. If the normal stresses at a point are σ_x, σ_y, σ_z and the associated shear stresses are τ_{xy}, τ_{yz}, τ_{zx}, then the von Mises stress σ' is given by

$$\sigma' = \frac{1}{\sqrt{2}} [(\sigma_x - \sigma_y)^2 + (\sigma_y - \sigma_z)^2 + (\sigma_z - \sigma_x)^2 + 6(\tau_{xy}^2 + \tau_{yz}^2 + \tau_{zx}^2)]^{1/2} \quad (17.16)$$

In a shaft, the critical location is usually at a surface, and two normal stresses (say σ_y and σ_z) and two shear stresses (say τ_{xz} and τ_{zx}) are zero. Equation (17.16) simplifies to

$$\sigma' = (\sigma_x^2 + 3\tau_{xy}^2)^{1/2} \quad (17.17)$$

The bending stress σ_x is usually expressed as $32K_fM/(\pi d^3)$ and the shear stress τ_{xy} is expressed as $16K_f'T/(\pi d^3)$, or without the stress concentration K_f' if torsion is steady, and so Eq. (17.17) is written as

$$\sigma' = \left[\left(\frac{32K_fM}{d^3} \right)^2 + 3\left(\frac{16T}{d^3} \right)^2 \right]^{1/2} \quad (17.18)$$

As the shaft rotates and the stress field remains stationary, the bending moment induces a completely reversed stress σ_x on the rotating element in Fig. 17.6. The amplitude component of this stress σ_a' is

$$\sigma_a' = \left| \frac{32K_fM_a}{\pi d^3} \right| \quad (17.19)$$

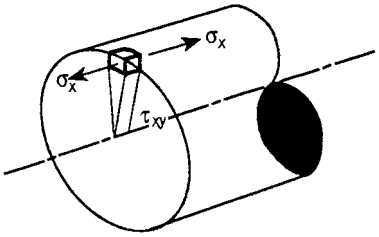

FIGURE 17.6 A stress element at a shaft surface.

The subscript on M_a is to designate the bending moment inducing a completely reversed normal stress on the element as the shaft turns. The bending moment itself may indeed be steady. The steady component of stress σ_m', from Eq. (17.18), is

$$\sigma_m' = \left| \frac{16\sqrt{3}\,T_m}{\pi d^3} \right| \quad (17.20)$$

The stochastic nature of $\mathbf{K}_f$, $\mathbf{M}_a$, and $\mathbf{d}$ controls the nature of $\boldsymbol{\sigma}_a'$. Usually the geometric variation in $\mathbf{d}$ involves coefficients of variation of 0.001 or less, and that of $\mathbf{K}_f$ and $\mathbf{M}_a$ is more than an order of magnitude higher, and so $\mathbf{d}$ is usually considered deterministic. The distribution of $\boldsymbol{\sigma}_a'$ depends on the distributions of $\mathbf{K}_f$ and $\mathbf{M}_a$. When $\mathbf{M}_a$ is lognormal (and since $\mathbf{K}_f$ is robustly lognormal), the distribution of $\boldsymbol{\sigma}_a'$ is lognormal. When $\mathbf{M}_a$ is not lognormal, then a computer simulation will give the stochastic information on $\boldsymbol{\sigma}_a'$.

A press fit induces a surface pressure p and a hoop normal stress of $-p$, so the three orthogonal normal stresses are σ_x, $-p$, and $-p$, and Eq. (17.16) becomes

$$\sigma' = \frac{1}{\sqrt{2}}\{[\sigma_x - (-p)]^2 + [-p - (-p)]^2 + (-p - \sigma_x)^2 + 6\tau_{xy}^2\}^{1/2}$$

$$\sigma' = [(\sigma_x + p)^2 + 3\tau_{xy}^2]^{1/2}$$

The amplitude and steady components of the von Mises stress at a surface element in a press fit are, respectively,

$$\sigma'_a = (\sigma_x^2)^{1/2} = \sigma_x \tag{17.21}$$

$$\sigma'_m = (p^2 + 3\,\tau_{xy}^2)^{1/2} \tag{17.22}$$

On the designer's fatigue diagram, the σ'_a, σ'_m coordinates don't necessarily define a point because certain geometric decisions may not yet have been made. In such cases, a locus of possible points which is called the *load line* is established. Often the load line includes the origin, and so the slope together with one point on the line defines the load line. Its slope r is the ratio σ'_a/σ'_m.

17.7 STRENGTH

For the first-quadrant fatigue locus on the designer's fatigue diagram, effective regression models include the 1874 Gerber parabola and the recent ASME-elliptic locus, both of which lie in and among the data. The Gerber parabola is written as

$$\frac{n\sigma_a}{S_e} + \left(\frac{n\sigma_m}{S_{ut}}\right)^2 = 1 \tag{17.23}$$

and the failure locus itself, substituting $n\sigma_a = S_a$ and $n\sigma_m = S_m$ in Eq. (17.23), is expressible as

$$\frac{S_a}{S_e} + \left(\frac{S_m}{S_{ut}}\right)^2 = 1 \tag{17.24}$$

Combining the damaging stress [distortion energy von Mises stress, Eqs. (17.19) and (17.20)] with the strengths in Eq. (17.23) leads to

$$d = \left\{\frac{16nK_fM_a}{\pi S_e}\left[1 + \sqrt{1 + 3\left(\frac{T_mS_e}{K_fM_aS_{ut}}\right)^2}\right]\right\}^{1/3} \tag{17.25}$$

$$\frac{1}{n} = \frac{16K_fM_a}{\pi d^3 S_e}\left[1 + \sqrt{1 + 3\left(\frac{T_mS_e}{K_fM_aS_{ut}}\right)^2}\right] \tag{17.26}$$

Equations (17.25) and (17.26) are called distortion energy–Gerber equations, or D.E.–Gerber equations.

The ASME-elliptic of Ref. [17.4] has a fatigue locus in the first quadrant expressed as

$$\left(\frac{n\sigma_a}{S_e}\right)^2 + \left(\frac{n\sigma_m}{S_y}\right)^2 = 1 \tag{17.27}$$

and the fatigue locus itself is expressed as

$$\left(\frac{S_a}{S_e}\right)^2 + \left(\frac{S_m}{S_y}\right)^2 = 1 \tag{17.28}$$

Combining Eqs. (17.19) and (17.20) with (17.28) gives

$$d = \left\{\frac{32n}{\pi}\left[\left(\frac{K_f M_a}{S_e}\right)^2 + \frac{3}{4}\left(\frac{T_m}{S_y}\right)^2\right]^{1/2}\right\}^{1/3} \tag{17.29}$$

$$\frac{1}{n} = \frac{32}{\pi d^3}\left[\left(\frac{K_f M_a}{S_e}\right)^2 + \frac{3}{4}\left(\frac{T_m}{S_y}\right)^2\right]^{1/2} \tag{17.30}$$

which are called D.E.–elliptic or ASME-elliptic equations.

On the designer's fatigue diagram, the slope of a radial load line r is given by

$$r = \frac{\sigma_a'}{\sigma_m'} = \frac{32K_f M_a}{\pi d^3} \cdot \frac{\pi d^3}{16\sqrt{3}T_m} = \frac{2}{\sqrt{3}}\frac{K_f M_a}{T_m} \tag{17.31}$$

The expressions for d and n in Eqs. (17.29) and (17.30) are for a threat from fatigue failure. It is also possible on the first revolution to cause local yielding, which changes straightness and strength and involves now-unpredictable loading. The Langer line, $S_a + S_m = S_y$, predicts yielding on the first cycle. The point where the elliptic locus and the Langer line intersect is described by

$$\frac{S_a}{S_e} = \frac{2S_e/S_y}{1 + (S_e/S_y)^2} \tag{17.32}$$

$$\frac{S_m}{S_y} = \frac{1 - (S_e/S_y)^2}{1 + (S_e/S_y)^2} \tag{17.33}$$

The *critical slope* contains this point:

$$r_{\text{crit}} = \frac{2(S_e/S_y)^2}{1 - (S_e/S_y)^2} \tag{17.34}$$

If the load line slope r is greater than r_{crit}, then the threat is from fatigue. If r is less than r_{crit}, the threat is from yielding.

For the Gerber fatigue locus, the intersection with the Langer line is described by

$$S_a = \frac{S_{ut}^2 - 2S_e S_y}{2S_e}\left[-1 + \sqrt{1 + \frac{4(S_{ut}^2 - S_y^2)}{(S_{ut}^2/S_e - 2S_y)^2}}\right] \tag{17.35}$$

$$S_m = \frac{S_{ut}^2}{2S_e}\left[1 - \sqrt{1 + \frac{4S_e^2(1 - S_y/S_e)}{S_{ut}^2}}\right] \tag{17.36}$$

and $r_{\text{crit}} = S_a/S_m$.

Example 4. At the critical location on a shaft, the bending moment M_a is 2520 in · lbf and the torque T_m is 6600 in · lbf. The ultimate strength S_{ut} is 80 kpsi, the yield strength S_y is 58 kpsi, and the endurance limit S_e is 31.1 kpsi. The stress concentration

factor corrected for notch sensitivity K_f is 1.54. Using an ASME-elliptic fatigue locus, ascertain if the threat is from fatigue or yielding.

Solution. From Eq. (17.31),

$$r = \frac{2(1.54)2520}{\sqrt{3}\,6600} = 0.679$$

From Eq. (17.34),

$$r_{\text{crit}} = \frac{2(31.1/58)^2}{1-(31.1/58)^2} = 0.807$$

Since $r_{\text{crit}} > r$, the primary threat is from fatigue. Using the Gerber fatigue locus, $r_{\text{crit}} = S_a/S_m = 26.18/31.8 = 0.823$.

For the distortion energy–Gerber failure locus, the relation for the strength amplitude S_a is given in Eq. (29.34) and C_{Sa} in Eq. (29.35); these quantities are given by Eqs. (29.37) and (29.38), respectively, for the ASME-elliptic failure locus.

17.8 CRITICAL SPEEDS

Critical speeds are associated with uncontrolled large deflections, which occur when inertial loading on a slightly deflected shaft exceeds the restorative ability of the shaft to resist. Shafts must operate well away from such speeds. Rayleigh's equation for the first critical speed of a shaft with transverse inertial loads w_i deflected y_i from the axis of rotation for simple support is given by Ref. [17.6] as

$$\omega = \sqrt{\frac{g\Sigma w_i y_i}{\Sigma w_i y_i^2}} \tag{17.37}$$

where w_i is the inertial load and y_i is the lateral deflection due to w_i and *all other loads.* For the shaft itself, w_i is the inertial load of a shaft section and y_i is the deflection of the center of the shaft section due to all loads. Inclusion of shaft mass when using Eq. (17.37) can be done.

Reference [17.7], p. 266, gives the first critical speed of a uniform simply supported shaft as

$$\omega = \frac{\pi^2}{\ell^2}\sqrt{\frac{EI}{m}} = \frac{\pi^2}{\ell^2}\sqrt{\frac{gEI}{A\gamma}} \tag{17.38}$$

Example 5. A steel thick-walled tube with 3-in OD and 2-in ID is used as a shaft, simply supported, with a 48-in span. Estimate the first critical speed (*a*) by Eq. (17.38) and (*b*) by Eq. (17.37).

Solution. (*a*) $A = \pi(3^2 - 2^2)/4 = 3.927$ in^2, $I = \pi(3^4 - 2^4)/64 = 3.19$ in^4, $w = A\gamma = 3.925(0.282) = 1.11$ lbf/in. From Eq. (17.38),

$$\omega = \frac{\pi^2}{48^2}\sqrt{\frac{386(30)(10^6)(3.19)}{3.927(0.282)}} = 782.4 \text{ rad/s} = 7471 \text{ r/min}$$

(*b*) Divide the shaft into six segments, each 8 in long, and from the equation for the deflection at x of a uniformly loaded, simply supported beam, develop an expression for the deflection at x.

$$y = \frac{wx}{24EI}(2\ell x^2 - x^3 - \ell^3) = \frac{1.11x}{24(30)(10^6)(3.19)}[2(48)x^2 - x^3 - 48^3]$$
$$= 0.483(10^{-9})(x)(96x^2 - x^3 - 48^3)$$

Prepare a table for x, y, and y^2 at the six stations.

x_i	y_i	y_i^2
4	0.000 210 8	$4.44(10^{-8})$
12	0.000 570 9	$32.6(10^{-8})$
20	0.000 774 7	$60.0(10^{-8})$
28	0.000 774 7	$60.0(10^{-8})$
36	0.000 570 9	$32.6(10^{-8})$
44	0.000 210 8	$4.44(10^{-8})$
Σ	0.003 112 8	$194(10^{-8})$

From Eq. (17.37),

$$\omega = \sqrt{\frac{g\Sigma y_i}{\Sigma y_i^2}} = \sqrt{\frac{386(0.003\ 112\ 8)}{194(10^{-8})}} = 787 \text{ rad/s} = 7515 \text{ r/min}$$

which agrees with the result of part (*a*), but is slightly higher, as expected, since the static deflection shape was used.

Since most shafts are of variable diameter, Eq. (17.37) will be more useful for estimating the first critical speed, treating simultaneously the contributions of concentrated masses (gears, pulleys, sprockets, cams, etc.) and the distributed shaft mass as well.

Example 6. Assume that the shaft of Example 2 has been established with its final geometry as shown in Fig. 17.7. The shaft is decomposed into 2-in segments. The weight of each segment is applied as a concentrated force w_i at the segment centroid. Additionally, the left-side gear weighs 30 lbf and the right-side gear weighs 40 lbf. Estimate the first critical speed of the assembly.

Solution. Bearing in mind the tabular deflection method of Sec. 17.2, 12 stations are established. Also, bending moment diagrams will be superposed.

For the distributed shaft mass load, the shaft weight is estimated as $W = 24.52$ lbf, and it follows that bearing reactions are $R_1' = 11.75$ lbf and $R_2' = 12.77$ lbf. Because each reaction is opposed by a bearing seat weight of 1.772 lbf, the net reactions are $R_1 = 11.75 - 1.722 = 9.98$ lbf and $R_2 = 12.77 - 1.772 = 11.0$ lbf. The bending moments M_i due to shaft segment weights are shown in column 3 of Table 17.5.

For the gears, $R_1 = 31.25$ lbf and $R_2 = 38.75$ lbf, and the resulting bending moments are shown in column 4. The superposition of the moment diagrams for these two sources of bending occurs in column 5. Column 6 displays the shaft segment weights at the station of application. Column 7 shows the concentrated gear weights and their station of application. Column 8 is the superposition of columns 6 and 7. Column 9 is obtained by using the tabular method of Sec. 17.2 and imposing the bending moment diagram of column 5. Columns 10 and 11 are extensions of columns 8 and 9. The sums of columns 10 and 11 are used in Eq. (17.37):

$$\omega = \sqrt{\frac{386(2.348)(10^{-3})}{6.91(10^{-8})}} = 3622 \text{ rad/s} = 34\ 588 \text{ r/min}$$

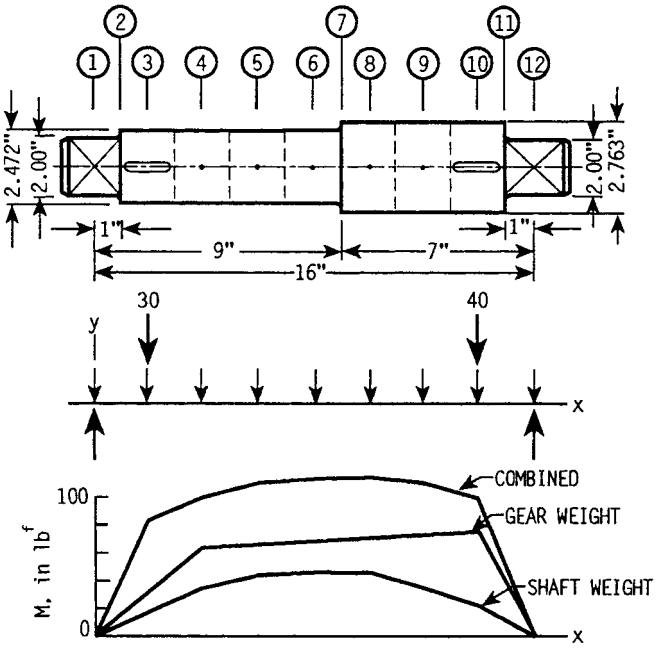

FIGURE 17.7 The final geometry of the shaft of Ex. 17.2. For critical speed estimation, weights of shaft segments and affixed gears generate separate and combined bending moments. The static deflection under such loading found by the tabulation method provides the deflections used in Rayleigh's critical speed equation. See Table 17.5 and Ex. 17.6.

The methods of Secs. 17.2 and 17.3 and this section can be programmed for the digital computer for rapid and convenient use.

17.9 HOLLOW SHAFTS

Advantages accruing to hollow shafting include weight reduction with minor increase in stress (for the same outside diameter), ability to circulate fluids for lubrication or cooling, and the use of thick-walled tubing as shaft stock. However, unbalance must be checked and corrected, and thick-walled tubing may not have enough material in its wall to accommodate the desired external geometry.

For a shaft section with outside diameter d, inside diameter d_i, and $K = d_i/d$, for torsional and bending loading, $d(1 - K^4)^{1/3}$ may be substituted for diameter d in equations such as (17.25), (17.26), (17.29), and (17.30). Equations (17.25) and (17.29) can no longer be solved explicitly for diameter d unless K is known. In cases where it is not known, iterative procedures must be used.

TABLE 17.5 Critical Speed Tabulation for Example 6

Station	x_i	Distributed load M_i	Gear M_i	Super-posed M_i	Shaft section w_i	Concentrated load P_i	Super -posed w_i	Tabulation† method y_i	$w_i y_i$	$w_i y_i^2$
1	0	0	0	0	1.772		1.772	0	0	0
2	1	9.98	31.25	41.23				–0.122E-04		
3	2	19.96	62.5	82.46	2.707	30	32.07	–0.233E-04	0.747E-03	1.741E-08
4	4	34.51	65.0	99.51	2.707		2.707	–0.411E-04	0.111E-03	0.457E-08
5	6	43.64	67.5	111.14	2.707		2.707	–0.517E-04	0.140E-03	0.724E-08
6	8	47.36	70.0	117.36	2.707		2.707	–0.543E-04	0.147E-03	0.798E-08
7	9	46.51	71.25	117.76				–0.524E-04		
8	10	45.66	72.5	118.16	3.382		3.382	–0.488E-04	0.165E-03	0.805E-08
9	12	37.20	75.0	112.2	3.382		3.382	–0.375E-04	0.127E-03	0.476E-08
10	14	21.98	77.5	99.48	3.382	40	43.382	–0.210E-04	0.911E-03	1.913E-08
11	15	10.99	38.75	49.74				–0.110E-04		
12	16	0	0	0	1.772		1.772	0	0	0
									2.348E-03	6.91E-08

† Column 9 obtained by tabular method of Sec. 17.2. The constants $C_1 = –0.1249E-04$ and $C_2 = 0$ of prediction Eqs. (17.5) and (17.6) were used.

REFERENCES

17.1 Joseph E. Shigley and Charles R. Mischke, *Mechanical Engineering Design,* 5th ed., McGraw-Hill, New York, 1989.

17.2 Charles R. Mischke, "An Exact Numerical Method for Determining the Bending Deflection and Slope of Stepped Shafts," *Advances in Reliability and Stress Analysis,* Proceedings of the Winter Annual Meeting of A.S.M.E., San Francisco, December 1978, pp. 105–115.

17.3 R. Bruce Hopkins, *Design Analysis of Shafts and Beams,* McGraw-Hill, New York, 1970, pp. 93–99.

17.4 ANSI/ASME B106.1-M-1985, "Design of Transmission Shafting," second printing, March 1986.

17.5 S. Timoshenko, D. H. Young, and W. Weaver, *Vibration Problems in Engineering,* 4th ed., John Wiley & Sons, New York, 1974.

17.6 S. Timoshenko and D. H. Young, *Advanced Dynamics,* McGraw-Hill, New York, 1948, p. 296.

17.7 Charles R. Mischke, *Elements of Mechanical Analysis,* Addison-Wesley, Reading, Mass., 1963.

RECOMMENDED READING

ANSI B17.1, 1967, "Keys and Keyseats."

Mischke, Charles R., "A Probabilistic Model of Size Effect in Fatigue Strength of Rounds in Bending and Torsion," *Transactions of A.S.M.E., Journal of Mechanical Design,* vol. 102, no. 1, January 1980, pp. 32–37.

Peterson, R. E., *Stress Concentration Factors,* John Wiley & Sons, New York, 1974.

Pollard, E. I., "Synchronous Motors . . . , Avoid Torsional Vibration Problems," *Hydrocarbons Processing,* February 1980, pp. 97–102.

Umasankar, G., and C. R. Mischke, "A Simple Numerical Method for Determining the Sensitivity of Bending Deflections of Stepped Shafts to Dimensional Changes," *Transactions of A.S.M.E., Journal of Vibration, Acoustics, Stress and Reliability in Design,* vol. 107, no. 1, January 1985, pp. 141–146.

Umasankar, G., and C. Mischke, "Computer-Aided Design of Power Transmission Shafts Subjected to Size, Strength and Deflection Constraints Using a Nonlinear Programming Technique," *Transactions of A.S.M.E., Journal of Vibration, Acoustics, Stress and Reliability in Design,* vol. 107, no. 1, January 1985, pp. 133–140.

SHAFTS

P · A · R · T · 5

BEARINGS AND LUBRICATION

CHAPTER 18
ROLLING-CONTACT BEARINGS

Charles R. Mischke, Ph.D., P.E.
Professor Emeritus of Mechanical Engineering
Iowa State University
Ames, Iowa

GLOSSARY OF SYMBOLS

a	Exponents; $a = 3$ for ball bearings; $a = 10/3$ for roller bearings
AF	Application factor
b	Weibull shape parameter
C_s	Static load rating
C_{10}	Basic load rating or basic dynamic load rating
f	Fraction
F	Load
F_a	Axial load
F_{eq}	Equivalent radial load
F_i	ith equivalent radial load
F_r	Radial load
I	Integral
L	Life measure, r or h
L_D	Desired or design life measure
L_R	Rating life measure
L_{10}	Life measure exceeded by 90 percent of bearings tested

n	Design factor
n_D	Desired or design rotative speed, r/min
n_i	Application or design factor at ith level
n_R	Rating rotative speed, r/min
R	Reliability
V	Rotation factor; inner ring rotations, $V = 1$; outer ring, $V = 1.20$
x	Life measure in Weibull survival equation
x_0	Weibull guaranteed life parameter
X	Radial factor for equivalent load prediction
Y	Thrust factor for equivalent load prediction
θ	Weibull characteristic life parameter, rotation angle
ϕ	Period of cyclic variation, rad

18.1 INTRODUCTION

Figures 18.1 to 18.12 illustrate something of the terminology and the wide variety of rolling-contact bearings available to the designer. Catalogs and engineering manuals can be obtained from bearing manufacturers, and these are very comprehensive and of excellent quality. In addition, most manufacturers are anxious to advise designers on specific applications. For this reason the material in this chapter is concerned mostly with providing the designer an independent viewpoint.

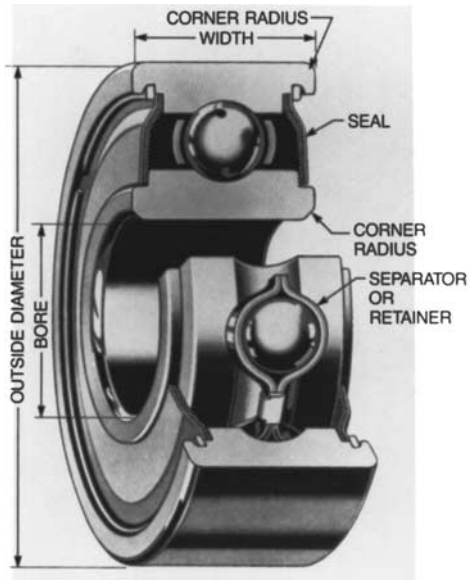

FIGURE 18.1 Photograph of a deep-groove precision ball bearing with metal two-piece cage and dual seals to illustrate rolling-bearing terminology. *(The Barden Corporation.)*

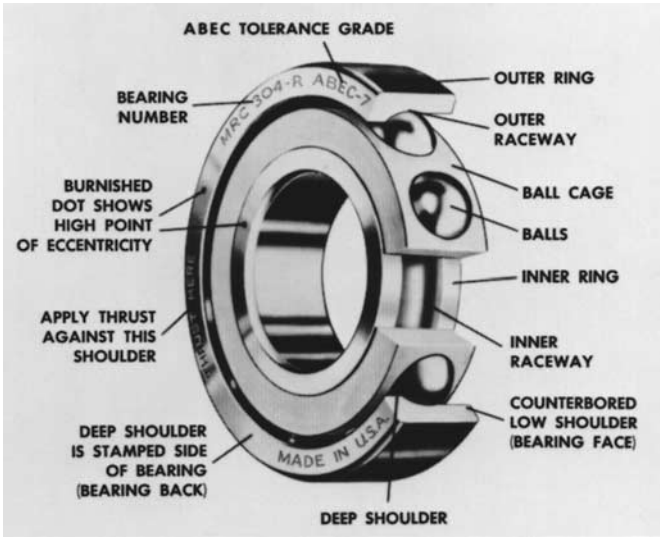

FIGURE 18.2 Photograph of a precision ball bearing of the type generally used in machine-tool applications to illustrate terminology. *(Bearings Division, TRW Industrial Products Group.)*

FIGURE 18.3 Rolling bearing with spherical rolling elements to permit misalignment up to ±3° with an unsealed design. The sealed bearing, shown above, permits misalignment to ±2°. *(McGill Manufacturing Company, Inc.)*

FIGURE 18.4 A heavy-duty cage-guided needle roller bearing with machined race. Note the absence of an inner ring, but standard inner rings can be obtained. *(McGill Manufacturing Company, Inc.)*

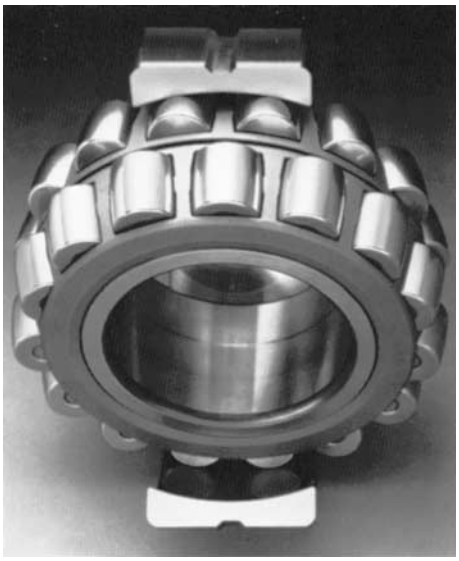

FIGURE 18.5 A spherical roller bearing with two rows of rollers running on a common sphered raceway. These bearings are self-aligning to permit misalignment resulting from either mounting or shaft deflection under load. *(SKF Industries, Inc.)*

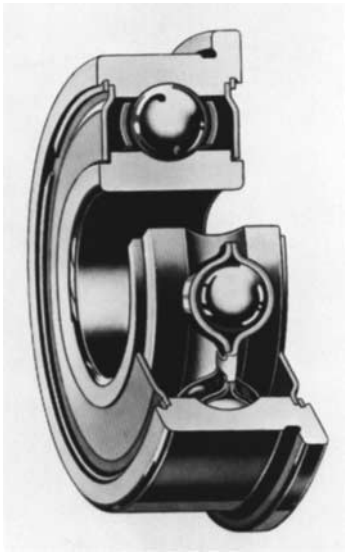

FIGURE 18.6 Shielded, flanged, deep-groove ball bearing. Shields serve as dirt barriers; flange facilitates mounting the bearing in a through-bored hole. *(The Barden Corporation.)*

FIGURE 18.7 Ball thrust bearing. *(The Torrington Company.)*

FIGURE 18.8 Spherical roller thrust bearing. *(The Torrington Company.)*

FIGURE 18.9 Tapered-roller thrust bearing. *(The Torrington Company.)*

FIGURE 18.10 Tapered-roller bearing; for axial loads, thrust loads, or combined axial and thrust loads. *(The Timken Company.)*

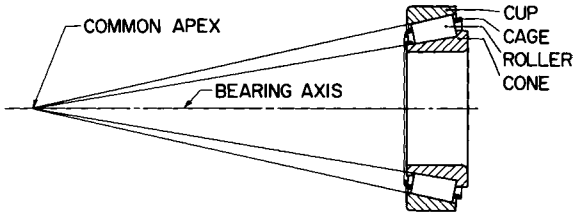

FIGURE 18.11 Basic principle of a tapered-roller bearing with nomenclature. *(The Timken Company.)*

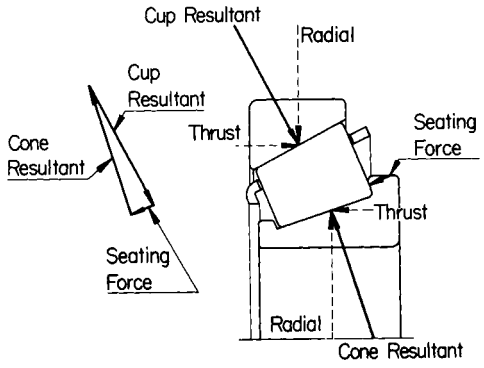

FIGURE 18.12 Force analysis of a Timken bearing. *(The Timken Company.)*

TABLE 18.1 Coefficients of Friction

Bearing type	Coefficient of friction μ
Self-aligning ball	0.0010
Cylindrical roller with flange-guided short rollers	0.0011
Ball thrust	0.0013
Single-row ball	0.0015
Spherical roller	0.0018
Tapered roller	0.0018

SOURCE: Ref. [18.1].

Rolling-contact bearings use balls and rollers to exploit the small coefficients of friction when hard bodies roll on each other. The balls and rollers are kept separated and equally spaced by a separator (cage, or retainer). This device, which is essential to proper bearing functioning, is responsible for additional friction. Table 18.1 gives friction coefficients for several types of bearings [18.1]. Consult a manufacturer's catalog for equations for estimating friction torque as a function of bearing mean diameter, load, basic load rating, and lubrication detail. See also Chap. 20.

Permissible speeds are influenced by bearing size, properties, lubrication detail, and operating temperatures. The speed varies inversely with mean bearing diameter. For additional details, consult any manufacturer's catalog.

Some of the guidelines for selecting bearings, which are valid more often than not, are as follows:

- Ball bearings are the less expensive choice in the smaller sizes and under lighter loads, whereas roller bearings are less expensive for larger sizes and heavier loads.
- Roller bearings are more satisfactory under shock or impact loading than ball bearings.
- Ball-thrust bearings are for pure thrust loading only. At high speeds a deep-groove or angular-contact ball bearing usually will be a better choice, even for pure thrust loads.
- Self-aligning ball bearings and cylindrical roller bearings have very low friction coefficients.
- Deep-groove ball bearings are available with seals built into the bearing so that the bearing can be prelubricated to operate for long periods without attention.
- Although rolling-contact bearings are "standardized" and easily selected from vendor catalogs, there are instances of cooperative development by customer and vendor involving special materials, hollow elements, distorted raceways, and novel applications. Consult your bearing specialist.

It is possible to obtain an estimate of the basic static load rating C_s. For ball bearings,

$$C_s = Mn_b d_b^2 \tag{18.1}$$

For roller bearings,

$$C_s = Mn_r l_e d \tag{18.2}$$

where C_s = basic static loading rating, pounds (lb) [kilonewtons (kN)]
n_b = number of balls
n_r = number of rollers
d_b = ball diameter, inches (in) [millimeters (mm)]
d = roller diameter, in (mm)
l_e = length of single-roller contact line, in (mm)

Values of the constant M are listed in Table 18.2.

TABLE 18.2 Value of Constant M for Use in Eqs. (18.1) and (18.2)

	Constant M	
Type of bearing	C_s, lb	C_s, kN
Radial ball	1.78×10^3	5.11×10^3
Ball thrust	7.10×10^3	20.4×10^3
Radial roller	3.13×10^3	8.99×10^3
Roller thrust	14.2×10^3	40.7×10^3

18.2 LOAD-LIFE RELATION FOR CONSTANT RELIABILITY

When proper attention is paid to a rolling-contact bearing so that fatigue of the material is the only cause of failure, then nominally identical bearings exhibit a reliability–life-measure curve, as depicted in Fig. 18.13. The *rating life* is defined as the life measure (revolutions, hours, etc.) which 90 percent of the bearings will equal or exceed. This is also called the L_{10} life or the B_{10} life. When the radial load is adjusted so that the L_{10} life is 1 000 000 revolutions (r), that load is called the *basic load rating* C (SKF Industries, Inc.). The Timken Company rates its bearings at 90 000 000. Whatever the rating basis, the life L can be normalized by dividing by the rating life L_{10}. The *median life* is the life measure equaled or exceeded by half of the bearings. Median life is roughly 5 times rating life.

For steady radial loading, the life at which the first tangible evidence of surface fatigue occurs can be predicted from

$$F^a L = \text{constant} \tag{18.3}$$

where $a = 3$ for ball bearings and $a = 10/3$ for cylindrical and tapered-roller bearings. At constant reliability, the load and life at condition 1 can be related to the load and life at condition 2 by Eq. (18.3). Thus

$$F_1^a L_1 = F_2^a L_2 \tag{18.4}$$

If F_1 is the basic load rating C_{10}, then L_1 is the rating life L_{10}, and so

$$C_{10} = \left(\frac{L}{L_{10}}\right)^{1/a} (F) \tag{18.5}$$

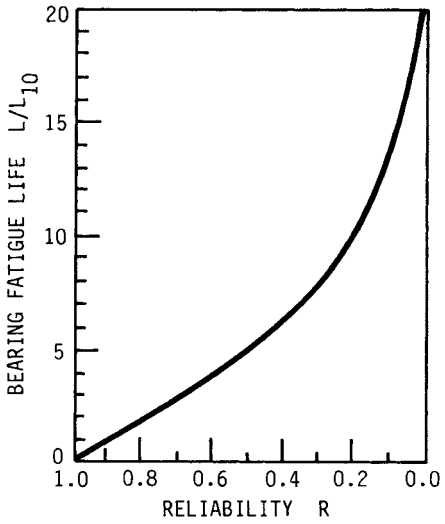

FIGURE 18.13 Survival function representing endurance tests on rolling-contact bearings from data accumulated by SKF Industries, Inc. *(From Ref. [18.2].)*

If L_R is in hours and n_R is in revolutions per minute, then $L_{10} = 60 L_R n_R$. It follows that

$$C_{10} = F_D \left(\frac{L_D n_D}{L_R n_R} \right)^{1/a} \tag{18.6}$$

where the subscript D refers to desired (or design) and the subscript R refers to rating conditions.

18.3 SURVIVAL RELATION AT STEADY LOAD

Figure 18.14 shows how reliability varies as the loading is modified [18.2]. Equation (18.5) allows the ordinate to be expressed as either F/C_{10} or L/L_{10}. Figure 18.14 is based on more than 2500 SKF bearings. If Figs. 18.13 and 18.14 are scaled for recovery of coordinates, then the reliability can be tabulated together with L/L_{10}. Machinery applications use reliabilities exceeding 0.94. An excellent curve fit can be realized by using the three-parameter Weibull distribution. For this distribution the reliability can be expressed as

$$R = \exp\left[-\left(\frac{x - x_0}{\theta - x_0} \right)^b \right] \tag{18.7}$$

where x = life measure, x_0 = Weibull guaranteed life measure, θ = Weibull characteristic life measure, and b = Weibull shape factor. Using the 18 points in Table 18.3 with $x_0 = 0.02$, $\theta = 4.459$, and $b = 1.483$, we see that Eq. (18.7) can be particularized as

$$R = \exp\left[-\left(\frac{L/L_{10} - 0.02}{4.439} \right)^{1.483} \right] \tag{18.8}$$

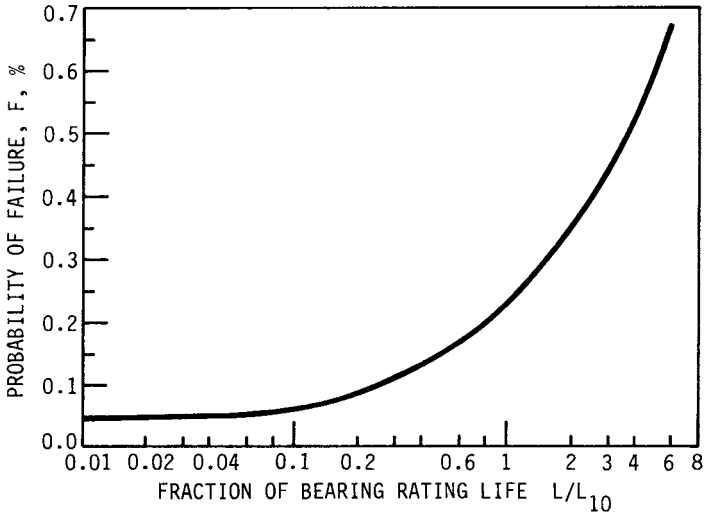

FIGURE 18.14 Survival function at higher reliabilities based on more than 2500 endurance tests by SKF Industries, Inc. *(From Ref. [18.2].)* The three-parameter Weibull constants are $\theta = 4.459$, $b = 1.483$, and $x_0 = 0.02$ when $x = L/L_{10} = Ln/(L_R n_R)$.

For example, for $L/L_{10} = 0.1$, Eq. (18.8) predicts $R = 0.9974$.

18.4 RELATING LOAD, LIFE, AND RELIABILITY GOAL

If Eq. (18.3) is plotted on log-log coordinates, Fig. 18.15 results. The FL loci are rectified, while the parallel loci exhibit different reliabilities. The coordinates of point A are the rating life and the basic load rating. Point D represents the desired (or design) life and the corresponding load. A common problem is to select a bearing which will provide a life L_D while carrying load F_D and exhibit a reliability R_D. Along line BD, constant reliability prevails, and Eq. (18.4) applies:

TABLE 18.3 Survival Equation Points at Higher Reliabilities†

Reliability R	Life measure L/L_{10}	Reliability R	Life measure L/L_{10}
0.94	0.67	0.994	0.17
0.95	0.60	0.995	0.15
0.96	0.52	0.996	0.13
0.97	0.435	0.997	0.11
0.975	0.395	0.9975	0.095
0.98	0.35	0.998	0.08
0.985	0.29	0.9985	0.07
0.99	0.23	0.999	0.06
0.992	0.20	0.9995	0.05

†Scaled from Ref. [18.2], Fig. 2.

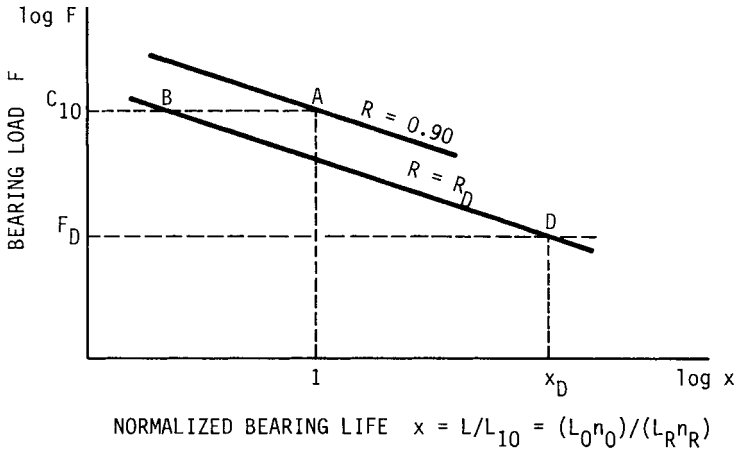

FIGURE 18.15 Reliability contours on a load-life plot useful for relating catalog entry, point *A*, to design goal, point *D*.

$$F_B = F_D\left(\frac{x_D}{x_B}\right)^{1/a} \tag{18.9}$$

Along line AB the reliability changes, but the load is constant and Eq. (18.7) applies. Thus

$$R = \exp\left[-\left(\frac{x - x_0}{\theta - x_0}\right)^b\right] \tag{18.10}$$

Now solve this equation for x and particularize it for point B, noting that $R_D = R_B$.

$$x_B = x_0 + (\theta - x_0)\left(\ln\frac{1}{R_D}\right)^{1/b} \tag{18.11}$$

Substituting Eq. (18.11) into Eq. (18.9) yields

$$F_B = C_{10} = F_D\left\{\frac{x_D}{x_0 + (\theta - x_0)[\ln\,(1/R_D)]^{1/b}}\right\}^{1/a} \tag{18.12}$$

For reliabilities greater than 0.90, which is the usual case, $\ln\,(1/R) \cong 1 - R$ and Eq. (18.12) simplifies as follows:

$$C_{10} = F_D\left[\frac{x_D}{x_0 + (\theta - x_0)(1 - R)^{1/b}}\right]^{1/a} \tag{18.13}$$

The desired life measure x_D can be expressed most conveniently in millions of revolutions (for SKF).

Example 1. If a ball bearing must carry a load of 800 lb for 50×10^6 and exhibit a reliability of 0.99, then the basic load rating should equal or exceed

$$C_{10} = 800\left[\frac{50}{0.02 + (4.439)(1 - 0.99)^{1/1.483}}\right]^{1/3}$$

$$= 4890 \text{ lb}$$

This is the same as 21.80 kN, which corresponds to the capability of a 02 series 35-mm-bore ball bearing. Since selected bearings have different basic load ratings from those required, a solution to Eq. (18.13) for reliability extant after specification is useful:

$$R = 1 - \left[\frac{x_D - x_0(C_{10}/F_D)^a}{(\theta - x_0)(C_{10}/F_D)^a}\right]^b \tag{18.14}$$

Example 2. If the bearing selected for Example 1, a 02 series 50-mm bore, has a basic load rating of 26.9 kN, what is the expected reliability? And $C_{10} = (26.9 \times 10^3)/445 = 6045$ lb. So

$$R = 1 - \left[\frac{50 - 0.02(6045/800)^3}{(4.439)(6045/800)^3}\right]^{1.483} = 0.9966$$

The previous equations can be adjusted to a two-parameter Weibull survival equation by setting x_0 to zero and using appropriate values of θ and b. For bearings rated at a particular speed and time, substitute $L_D n_D/(L_R n_R)$ for x_D.

The survival relationship for Timken tapered-roller bearings is shown graphically in Fig. 18.16, and points scaled from this curve form the basis for Table 18.4. The survival equation turns out to be the two-parameter Weibull relation:

$$R = \exp\left[-\left(\frac{x}{\theta}\right)^b\right] = \exp\left[-\left(\frac{L/L_{10}}{4.890}\right)^{1.4335}\right] \tag{18.15}$$

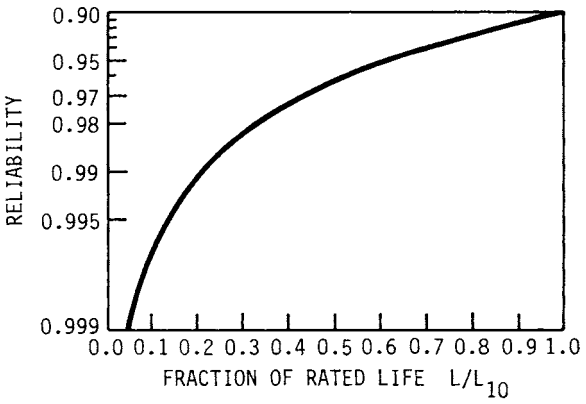

FIGURE 18.16 Survival function at higher reliabilities based on the Timken Company tapered-roller bearings. The curve fit is a two-parameter Weibull function with constants $\theta = 4.48$ and $b = \frac{1}{2}$ ($x_0 = 0$) when $x = Ln/(L_R n_R)$. *(From Ref. [18.3].)*

TABLE 18.4 Survival Equation Points for Tapered-Roller Bearings†

Reliability R	Life measure L/L_{10}	Reliability R	Life measure L/L_{10}
0.90	1.00	0.96	0.53
0.91	0.92	0.97	0.43
0.92	0.86	0.98	0.325
0.93	0.78	0.99	0.20
0.94	0.70	0.995	0.13
0.95	0.62	0.999	0.04

†Scaled from Fig. 4 of *Engineering Journal*, Sec. 1, The Timken Company, Canton, Ohio, rev. 1978.

The equation corresponding to Eq. (18.13) is

$$C_{10} = F_D\left[\frac{x_D}{\theta(1-R)^{1/b}}\right]^{1/a}$$

$$= F_D\left(\frac{x_D}{\theta}\right)^{1/a}(1-R)^{-1/ab} \tag{18.16}$$

And the equation corresponding to Eq. (18.14) is

$$R = 1 - \left(\frac{x_D}{\theta}\right)^b\left(\frac{C_{10}}{F_D}\right)^{-ab} \tag{18.17}$$

Example 3. A Timken tapered-roller bearing is to be selected to carry a radial load of 4 kN and have a reliability of 0.99 at 1200 hours (h) and a speed of 600 revolutions per minute (r/min). Thus

$$x_D = \frac{L_D n_D}{L_R n_R} = \frac{1200(600)}{3000(500)} = 0.480$$

and

$$C_{10} = 4\left[\frac{0.48}{4.48(1-0.99)^{1/1.5}}\right]^{3/10} = 5141 \text{ N}$$

Timken bearings are rated in U.S. Customary System (USCS) units or in newtons; therefore, a basic load rating of 5141 N or higher is to be sought.

For any bearings to be specified, check with the manufacturer's engineering manual for survival equation information. This is usually in the form of graphs, nomograms, or equations of available candidates. Check with the manufacturer on cost because production runs materially affect bearing cost.

18.5 COMBINED RADIAL AND THRUST LOADINGS

Ball bearings can resist some thrust loading simultaneously with a radial load. The equivalent radial load is the constant pure radial load which inflicts the same dam-

age on the bearing per revolution as the combination. A common form for weighting the radial load F_r and the axial load F_a is

$$F_e = VXF_r + YF_a \tag{18.18}$$

where F_e = equivalent radial load. The weighting factors X and Y are given for each bearing type in the manufacturer's engineering manual. The parameter V distinguishes between inner-ring rotation, $V = 1$, and outer-ring rotation, $V = 1.20$. A common form of Eq. (18.18) is

$$F_e = \max(VF_r, X_1VF_r + Y_1F_a, X_2VF_r + Y_2F_a, \ldots) \tag{18.19}$$

18.6 APPLICATION FACTORS

In machinery applications the peak radial loads on a bearing are different from the nominal or average load owing to a variation in torque or other influences. For a number of situations in which there is a body of measurement and experience, bearing manufacturers tabulate application factors that are used to multiply the average load to properly account for the additional fatigue damage resulting from the fluctuations. Such factors perform the same function as a design factor. In previous equations, F_D is replaced by nF_D or $\mathrm{AF}(F_D)$, where AF is the application factor.

18.7 VARIABLE LOADING

At constant reliability the current F^aL product measures progress toward failure. The area under the F^a versus L curve at failure is an index to total damage resulting in failure. The area under the F^aL locus at any time prior to failure is an index to damage so far. If the radial load or equivalent radial load varies during a revolution or several revolutions in a periodic fashion, then the equivalent radial load is related to the instantaneous radial load by

$$F_{\mathrm{eq}} = \left(\frac{1}{\phi} \int_0^{\phi} F^a \, d\theta \right)^{1/a} \tag{18.20}$$

where ϕ = period of the variation—2π for repetition every revolution, 4π for repetition every second revolution, etc. (see Fig. 18.17).

Example 4. A bearing load is given by $F(\theta) = 1000 \sin \theta$ in pounds force. Estimate the equivalent load by using Simpson's rule,

$$F_{\mathrm{eq}} = \left[\frac{1}{\pi} \int_0^{\pi} (1000 \sin \theta)^{10/3} \, d\theta \right]^{3/10} = 762 \text{ lb}$$

When equivalent loads are applied in a stepwise fashion, the equivalent radial load is expressible by

$$F_{\mathrm{eq}} = \left[\sum_{i=1}^{k} f_i (n_i F_i)^a \right]^{1/a} \tag{18.21}$$

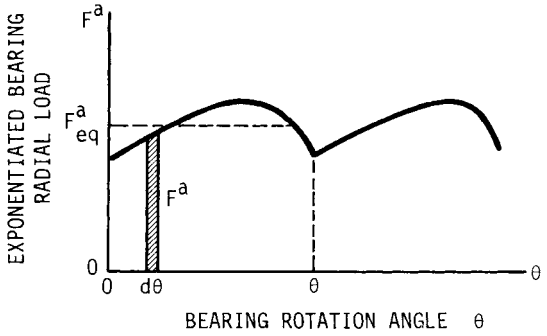

FIGURE 18.17 Equivalent radial load when load varies periodically with angular position.

where f_i = fraction of revolution at load F_i
n_i = application or design factor
F_i = ith equivalent radial load
a = applicable exponent—3 for ball bearings and 10/3 for roller bearings

Example 5. A four-step loading cycle is applied to a ball bearing. For one-tenth of the time, the speed is 1000 rpm, $F_r = 800$ lb, and $F_a = 400$ lb; for two-tenths of the time, the speed is 1200 rpm, $F_r = 1000$ lb, and $F_a = 500$ lb; for three-tenths of the time, the speed is 1500 rpm, $F_r = 1500$ lb, and $F_a = 700$ lb; for four-tenths of the time, the speed is 800 rpm, $F_r = 1100$ lb, and $F_a = 500$ lb. For this shallow-angle, angular-contact ball bearing, $X_1 = 1$, $Y_1 = 1.25$, $X_2 = 0.45$, $Y_2 = 1.2$, and $V = 1$. This loading cycle is also depicted in Fig. 18.18.

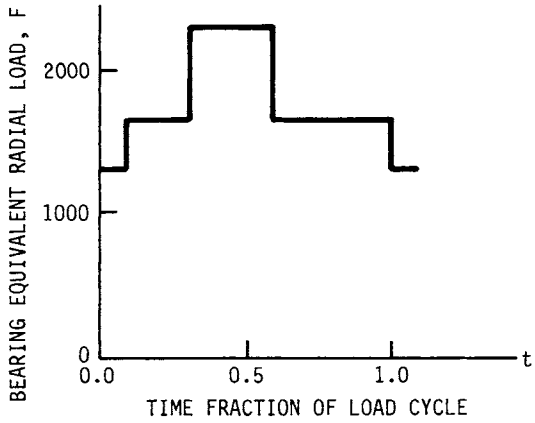

FIGURE 18.18 Loading cycle: one-tenth of time at 1000 rpm, $F_r = 800$, $F_a = 400$; two-tenths of time at 1200 rpm, $F_r = 1000$, $F_a = 500$; three-tenths of time at 1500 rpm, $F_r = 1500$, $F_a = 700$; four-tenths of time at 800 rpm, $F_r = 1100$, $F_a = 500$; $X_1 = 1$, $Y_1 = 1.25$, $X_2 = 0.45$, $Y_2 = 1.2$, $V = 1$.

TABLE 18.5 Tabulation for Example 5

Time fraction	Speed, rpm	Product	Revolution fraction f_i	Radial load F_r	Axial load F_a	Equivalent load F_e	Application factor AF	Product (AF)(F_e)
0.1	1000	100	0.090	800	400	1300	1.1	1430
0.2	1200	240	0.216	1000	500	1625	1.25	2031
0.3	1500	450	0.405	1500	700	2375	1.25	2969
0.4	800	320	0.288	1100	500	1725	1.50	2588
		1110						

The first step in the solution is to create Table 18.5. The equivalent radial load is

$$F_{eq} = [0.090(1430)^3 + 0.216(2031)^3 + 0.405(2969)^3 + 0.288(2588)^3]^{1/3} = 2604 \text{ lb}$$

Without the use of design factors, the equivalent radial load is

$$F_{eq} = [0.090(1300)^3 + 0.216(1625)^3 + 0.405(2375)^3 + 0.288(1725)^3]^{1/3} = 2002 \text{ lb}$$

The overall design factor is 2604/2002, or 1.30. If this sequence were common in a machinery application, a bearing manufacturer might recommend an application factor of 1.30 for this particular application.

18.8 MISALIGNMENT

The inner ring of a rolling-contact bearing is tightly fitted to the shaft, and the axis of rotation is oriented, as is the shaft centerline. The outer ring is held by some form of housing, and its axis is oriented as demanded by the housing. As the shaft deflects under load, these two axes lie at an angle to each other. This misalignment for very small angles is accommodated in "slack," and no adverse life consequences are exhibited. As soon as the slack is exhausted, the intended deflection is resisted and the bearing experiences unintended loading. Life is reduced below prediction levels. A shaft design which is too limber does not fail, but bearings are replaced with much greater frequency. It is too easy to be critical of bearings when the problem lies in the shaft design.

Figure 18.19 shows the dramatic fractional life reduction owing to misalignment in line-contact bearings [18.4].

If there is misalignment, it should not exceed 0.001 radian (rad) in cylindrical and tapered-roller bearings, 0.0087 rad for spherical ball bearings, or about 0.004 rad for

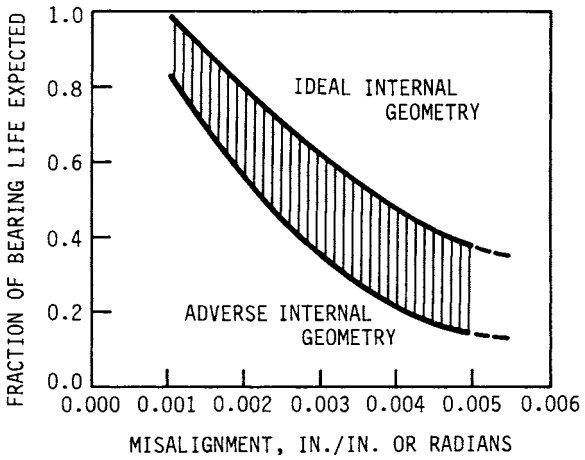

FIGURE 18.19 Fractional bearing life to be expected as a function of misalignment in line-contact bearings. *(From Ref. [18.4], Fig. 11.)*

ROLLING-CONTACT BEARINGS

deep-groove ball bearings. Self-aligning ball or spherical roller bearings are more tolerant of misalignment. The bibliography of Ref. [18.4] is extensive on this subject.

REFERENCES

18.1 *SKF Engineering Data,* SKF Industries, Inc., Philadelphia, 1979.

18.2 T. A. Harris, "Predicting Bearing Reliability," *Machine Design,* vol. 35, no. 1, Jan. 3, 1963, pp. 129–132.

18.3 *Bearing Selection Handbook,* rev. ed., The Timken Company, Canton, Ohio, 1986.

18.4 E. N. Bamberger, T. A. Harris, W. M. Kacmarsky, C. A. Moyer, R. J. Parker, J. J. Sherlock, and E. V. Zaretsky, *Life Adjustment Factors for Ball and Roller Bearings,* ASME, New York, 1971.

CHAPTER 19
JOURNAL BEARINGS

Theo G. Keith, Jr., Ph.D.
Professor and Chairman of Mechanical Engineering
University of Toledo
Toledo, Ohio

LIST OF SYMBOLS

a	Axial-flow land width
a_f	Pad load coefficient
A	Area
b	Circumferential-flow land width
C	Clearance
C^*	Specific heat
D	Diameter
e	Eccentricity
f	Coefficient of friction
F_j	Friction on journal
h	Film thickness
h_0	Minimum film thickness
H	Dimensionless film thickness
J	Mechanical equivalent of heat
k	Permeability
L	Bearing width
M	Rotor mass at bearing
M_j	Frictional torque on journal

n	Number of pads or recesses
N	Revolutions per unit time
p	Pressure
p_a	Ambient pressure
p_0	Short-bearing pressure
p_r	Recess pressure
p_s	Supply pressure
p_∞	Long-bearing pressure
$\bar{p}$	Dimensionless pressure
P	Unit loading
q	Volume flow rate per unit length
q_f	Flow factor
Q	Volume flow rate
Q_s	Side leakage flow rate
R	Radius of journal
R_b	Radius of bearing = $R + C$
s	Stiffness
S	Sommerfeld number = $(\mu N/P)(R/C)^2$
t	Time
t_p	Thickness of porous liner
T	Temperature
u, v, w	Velocity in x, y, z directions, respectively
U	Velocity of journal
W	Load
W_R	Load component directed along line of centers
W_T	Load component normal to line of centers
x, y, z	Rectangular coordinates
X	Dimensionless minimum-film-thickness parameter = $(h_0/R)[P/(2\pi N\mu)]^{1/2}$
Y	Dimensionless frictional torque parameter = $[M_j/(WR)][P/(2\pi N\mu)]^{1/2}$
α	Porous material slip coefficient
β	Included angle of partial bearing, porous bearing parameter
β_1	Angle from line of centers to leading edge of partial bearing
γ	Circumferential-flow parameter
ε	Eccentricity ratio e/c
ζ	Dimensionless axial dimension = $z/(L/2)$
θ	Angular position measured from line of centers
θ_1	Angular position to leading edge of film
θ_2	Angular position to zero pressure in film
θ_3	Angular position to trailing edge of film
θ_{cav}	Angular position to cavitation boundary

Λ	Bearing number = $(6\mu\omega/p_a)(R/C)^2$
λ	Ratio of heat conduction loss to heat generation rate, reduced bearing number = $\Lambda/6$
μ	Dynamic viscosity
ρ	Density
τ	Shear stress
ϕ	Attitude angle
ω	Angular velocity
Ω	Porous bearing parameter

19.1 INTRODUCTION

The design of journal bearings is of considerable importance to the development of rotating machinery. Journal bearings are essential machine components for compressors, pumps, turbines, internal-combustion engines, motors, generators, etc.

In its most basic form (Fig. 19.1), a *journal bearing* consists of a rotatable shaft (the journal) contained within a close-fitting cylindrical sleeve (the bearing). Generally, but not always, the bearing is fixed in a housing. The journal and bearing surfaces are separated by a film of lubricant (liquid or gas) that is supplied to the *clearance* space between the surfaces. The clearance space is generally quite small (on the order of one-thousandth of the journal radius) and has four major functions:

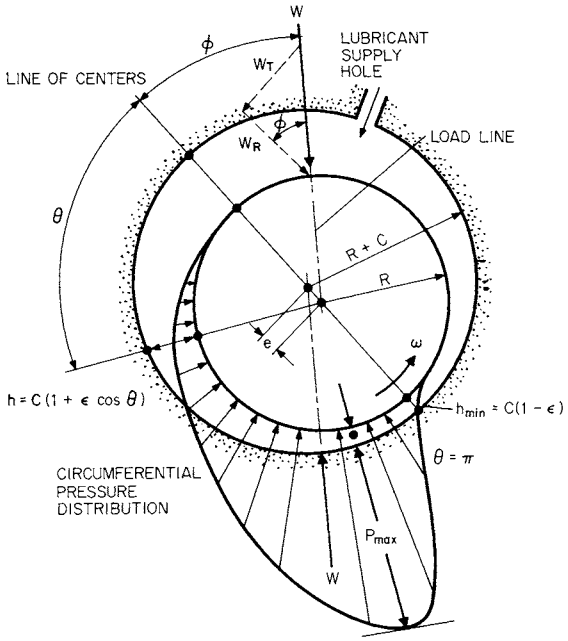

FIGURE 19.1 Journal and bearing notation.

to permit assembly of the journal and bearing, to provide space for the lubricant, to accommodate unavoidable thermal expansions, and to tolerate any shaft misalignment or deflection.

The fundamental purpose of a journal bearing is to provide radial support to a rotating shaft. Under load, the centers of the journal and the bearing are not coincident but are separated by a distance called the *eccentricity.* This eccentric arrangement establishes a converging-wedge geometry which, in conjunction with the relative motion of the journal and the bearing, permits a pressure to be developed by viscous effects within the thin film of lubricant and thus produces a load-carrying capability. However, if the load is too large or the shaft rotation too slow, the wedge-like geometry will not form and solid-to-solid contact can occur.

Journal bearings can operate in any of three lubrication regimes: *thick-film lubrication, thin-film lubrication,* or *boundary lubrication.* Generally, thick-film operation is preferred. Figure 19.2 is a diagram of the three lubrication regimes. Table 19.1 provides some of the characteristics of each regime.

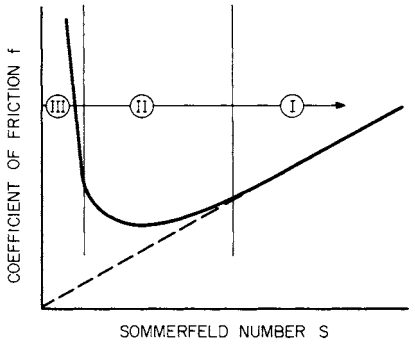

FIGURE 19.2 Three lubrication regimes: I, thick film; II, thin film; III, boundary.

Journal bearings may be classified according to the fluid mechanism that establishes the film load capacity: *Hydrodynamic* journal bearings, also called *self-acting* bearings, depend entirely on the relative motion of the journal and the bearing to produce film pressure for load support. *Hydrostatic* journal bearings, also called *externally pressurized* bearings, achieve load support by the supply of fluid from an external high-pressure source and require no relative motion between journal and bearing surfaces. *Hybrid* journal bearings are designed to use both hydrodynamic and hydrostatic principles to achieve load support between moving surfaces.

19.2 BEARING AND JOURNAL CONFIGURATIONS

19.2.1 Bearing Geometries

A wide range of bearing configurations are available to the journal bearing designer. Figure 19.3 depicts several of these bearings. The configurations range from the very simple plain journal bearing to the very complex tilting-pad bearing. The choice of bearing configuration depends on several factors. Among the more important are cost, load, power loss, dynamic properties, ease of construction, and difficulty of installation.

Journal bearings are termed *full bearings* (Fig. 19.3*a*) when the bearing surface completely surrounds the journal. Because they are easy to make and do not cost much, full bearings are the most commonly used bearing in rotating machinery. Full bearings become distorted during installation, and so they are generally not perfectly circular.

Journal bearings are called *partial bearings* when the bearing surface extends over only a segment of the circumference, generally 180° or less (Fig. 19.3*b*). Par-

TABLE 19.1 Characteristics of Lubrication Regimes

Lubrication regime	Contact of bearing surfaces	Range of film thickness, in	Coefficient of friction	Degree of wear	Comments
Thick film	Only during startup or stopping	10^{-3}–10^{-4}	0.01–0.005	None	1. Light-loading high-speed regime 2. Friction coefficient proportional to $\mu N/[W/(LD)]$
Thin film	Intermittent; dependent on surface roughness	10^{-4} to 0.5×10^{-4}	0.005–0.05	Mild	1. High operating temperatures
Boundary	Surface to surface	0.5×10^{-4} to molecular thicknesses	0.05– 0.15	Large	1. Heavy-loading (unit load > 3000 psi) low-speed (< 60 fpm) operating regime 2. Heat generation and friction not dependent on lubricant viscosity

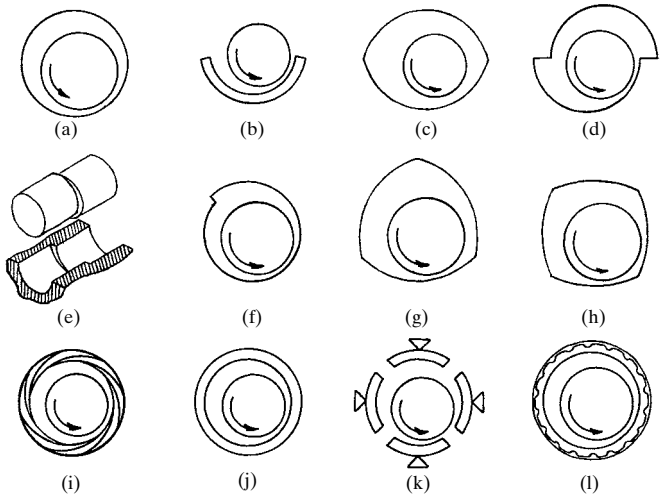

FIGURE 19.3 Journal bearing geometries. (*a*) Full bearing; (*b*) partial bearing; (*c*) elliptical, or lemon, bearing; (*d*) offset bearing; (*e*) rocking journal bearing; (*f*) pressure dam bearing; (*g*) three-lobe bearing; (*h*) four-lobe bearing; (*i*) multileaf bearing; (*j*) floating-ring bearing; (*k*) tilting- or pivoted-pad bearing; (*l*) foil bearing.

tial bearings are used in situations where the load is mainly unidirectional. Partial journal bearings have been found to reduce frictional torque on the journal and provide convenient accessibility, and they do not, in many instances, require strict manufacturing tolerance. Partial journal bearings in which the bearing radius exceeds the journal radius are called *clearance bearings,* whereas partial journal bearings in which the bearing and the journal radii are equal are termed *fitted bearings.*

Geometries in which two circular sectors are employed are called *elliptical,* or *lemon, bearings* (Fig. 19.3*c*). These bearings are really not elliptical at all but are fabricated by uniting two halves of a circular bearing which have had their mating faces machined so that the bearing has an approximately elliptical appearance. Lemon bearings are probably the most widely used bearings at low and moderate speeds. They are extensively used in turbine applications.

Elliptical bearings in which the two cylindrical halves are laterally displaced along the major axis are termed *offset bearings* (Fig. 19.3*d*). The relative displacement of the center of each half of the bearing is called the *preset.* When the upper half of the bearing is displaced horizontally in the direction of rotation, the bearing has negative preset. It is found that load capacity increases with preset. Offset bearings have relatively high horizontal stiffness, which helps prevent dynamic instability. Further, offset bearings allow greater lubricant flow and so run cooler.

Novel offset journal bearing designs for reducing power loss and wear in duty cycles which combine nonreversing loading with limited journal angular oscillation or in steady operation with counterrotation of journal and bearing under a constant load have been studied. In these applications, conventional journal bearings are found to develop extremely thin lubricant films, which in turn results in high friction and wear. Figure 19.3*e* depicts a journal bearing in which both the journal and the bearing are divided axially into segments with offset centerlines. This arrangement produces a dynamic rocking motion which promotes a thicker lubricating film. Accordingly the assembly has been called a *rocking journal bearing.*

When a step is milled from the surface of the bearing (Fig. 19.3*f*), the resulting bearing is called a *pressure dam,* or *step, bearing.* The purpose of the step is to create additional hydrodynamic pressure on the top of the journal as the lubricant is rotated into the step. In turn, this pressure buildup enhances the load on the journal and therefore diminishes its susceptibility to vibration problems. Pressure dam bearings are very popular in the petrochemical industry.

Bearing geometries consisting of three or more sectors (Fig. 19.3*g* and *h*) are termed *lobed,* or *multilobed, bearings.* Generally, bearings with more than three lobes are used only in gas bearing applications. Multilobed bearings act as a number of partial bearings in series. The cost of multilobed bearings is considered moderate.

The *multileaf journal bearing* (Fig. 19.3*i*) is a variant of a multilobed bearing. It consists of a number of identical circular arcs, or leaves, whose centers are equally spaced around the generating circle. The operating characteristics of a multileaf bearing are practically independent of the direction of loading for bearings with eight or more leaves.

In a *floating-ring journal bearing* (Fig. 19.3*j*), the lubricating film is divided in two by the addition of a "floating" ring between the journal and the bearing. Floating-ring bearings have lower frictional losses and reduced heat generation and provide better stability.

Hydrodynamic journal bearings may be distinguished by whether the bearing surface can pivot. The basic advantage of *pivoting,* or *tilting-pad, journal bearings* (Fig. 19.3*k*) over fixed-pad journal bearings is that they can accommodate, with little loss in performance, any shaft deflection or misalignment.

A *foil journal bearing* (Fig. 19.3*l*) consists of a very thin compliant bearing surface resting atop a series of corrugations. When it is compared to a conventional gas bearing, the foil bearing has a thicker film, higher load capacity, lower power loss, better stability, and superior endurance to high operating temperatures.

19.2.2 Journal Shapes

Although the journal is generally assumed to be perfectly circular, wear effects or poor manufacture can lead to journals with the shapes shown in Fig. 19.4*a, b,* and *c.* In addition, the possibility of developing pressure by grooving the surface of the journal has been investigated. Three grooved patterns that were found to yield good stability characteristics are shown in Fig. 19.4*c, d,* and *e.*

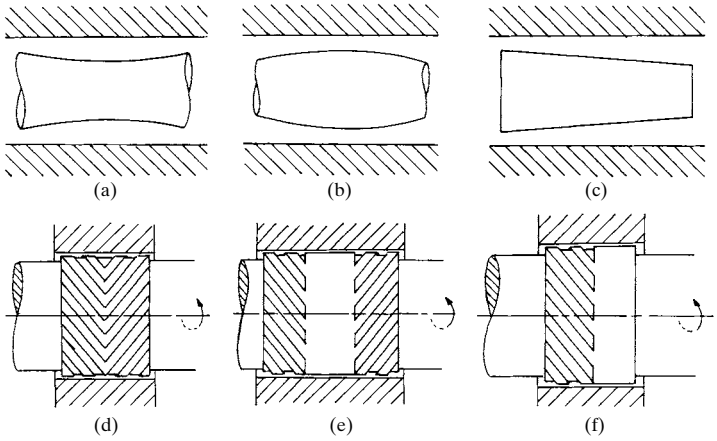

FIGURE 19.4 Journal shapes. (*a*) Hourglass; (*b*) barrel; (*c*) tapered; (*d*) herringbone; (*e*) partly grooved symmetrical pattern: (*f*) partly grooved asymmetrical pattern. *(Parts (d), (e), and (f) are from [19.1].)*

19.3 BEARING MATERIALS AND SELECTION CRITERIA

19.3.1 Bearing Materials

The ideal journal bearing material would have the following characteristics:

1. High compressive strength to withstand the applied radial loading
2. High fatigue strength to endure any cyclic changes in load direction and/or load intensity
3. Compatibility with the journal material to minimize surface scoring and bearing seizure whenever the journal and bearing surfaces come into contact (e.g., during startup)
4. Embedability to permit foreign particles in the lubricant to penetrate the bearing surface to avoid scoring and wear

5. Conformability of surface to tolerate journal misalignment, deflection, or manufacturing inaccuracies
6. High corrosion resistance to withstand chemical attack by the lubricant
7. High thermal conductivity to permit generated heat to be transported from the lubricant film
8. Appropriate coefficient of thermal expansion to avoid differences in thermal expansion of the journal and bearing
9. Low wear to prevent surface destruction, especially under boundary lubrication conditions (i.e., thin-film high-friction lubrication), and thereby lengthen the life of the bearing

Besides all these, the material should be inexpensive, highly available, and easily machined.

To be sure, no single material has been developed that satisfactorily combines all characteristics of the ideal bearing material. In fact, some of the characteristics are contradictory. For example, soft bearing materials generally do not have sufficient strength. To strengthen soft bearing materials, they are frequently bonded to stronger backing materials. Bearing linings or overlays may be cast, electrodeposited, sprayed, or chemically applied, and they have thicknesses which range from 0.01 to 0.5 inch (in).

Journal bearing materials may be broadly divided into two groups: metallics and nonmetallics. The metallic group includes aluminum alloys, babbitts (tin-, lead-, and aluminum-based), copper alloys (brass and bronze), zinc, and iron. The nonmetallic group includes plastics, carbon graphites, cemented carbides, and other proprietary materials. The nonmetallics have been widely used in self-lubrication applications because they can provide low friction and wear without the aid of a lubricant.

Because of the wide diversity of materials available for use in journal bearings, it is difficult to provide comprehensive tables of all relevant properties. Manufacturers and materials suppliers are the best sources for that information. Nevertheless, some physical properties of a variety of journal bearing materials are presented in Table 19.2 [19.2]. Typical applications and useful comments concerning a number of journal bearing alloys are displayed in Table 19.3, while Table 19.4 contains a numerical ranking of the performance characteristics of these alloys.

General information for a variety of self-lubricating materials is given in Table 19.5 [19.3]. Note that the table contains maximum values of the *PV* factor. This factor is the product of the bearing load per unit of projected area and the sliding velocity (i.e., speed in revolutions per minute times the bearing circumference). The *PV* parameter provides an indication of material wear and internal heat generation. Failure in self-lubricated bearings is frequently the direct result of internal overheating.

19.3.2 Bearing Material Selection Criteria

Selection of a bearing material invariably requires a compromise based on particular characteristics regarded by the designer to be of principal importance to the application at hand. DeGee [19.4] has developed a systematic approach for selecting a material for lubricated journal bearings. In this method, certain component criteria are identified within major property groups. Table 19.6 gives one such listing.

Not all the criteria presented in Table 19.6 need be considered. For example, in a particular application, environmental properties may be of no concern because the

TABLE 19.2 Physical Properties of Journal Bearing Materials

Material	Hardness H_B	Tensile strength, kpsi	Modulus of elasticity, Mpsi	Thermal conductivity, Btu/(h·ft·°F)	Coefficient of expansion, μin/(in·°F)	Density, lbm/ft^3
Metals						
Lead babbitt	21	10	4.2	14	14	630
Tin babbitt	25	11	7.6	32	13	462
Copper lead	25	8	7.6	170	11	562
Silver	25	23	11	238	10.9	655
Cadmium	35	....	8	53	16.6	537
Aluminum alloy	45	22	10.3	119	13.5	181
Lead bronze	60	34	14	27	9.9	555
Tin bronze	70	45	16	29	10	549
Steel	150	75	30	29	6.4	487
Cast iron	180	35	23	30	5.7	449
Porous metals						
Bronze	40	18	....	17	10.5	399
Iron	50	25	....	16	6.7	381
Aluminum	H55†	15	....	....	....	144
Plastics						
TFE	D60‡	3	0.06	0.10	55	137
Nylon	M79†	11	0.41	0.14	55	71
Phenolic	M100	10	0.5	0.21	12	85
Acetal	M94	10	0.41	0.13	45	89
Polycarbonate	M70	8.5	0.32	0.11	70	75
Filled polyimide	E99†	7.5	....	0.44	22	89
Other nonmetallics						
Rubber	....	....	....	0.09	43	75
Wood	....	1.1	1.8	0.11	2.7	42
Carbon graphite	75§	2	2	10	1.5	106
Cemented tungsten carbide	A91†	130	81	40	3.3	886
Fused aluminum oxide	A85	30	50	1.6	8.2	243

†Rockwell. ‡Shore durometer. §Shore scleroscope.

SOURCE: Ref. [19.2].

TABLE 19.3 Bearing Alloy Material Applications

Material	Nominal composition, % by weight	Applications and remarks
Aluminum, low tin	Al 92 Sn 8	Tin added to improve compatibility; too much tin lowers strength. Has thermal expansion problems in steel housings. Requires hard journals. Good at high temperatures. Used in diesel engines and compressors.
Aluminum, high tin	Al 80 Sn 20	Produced by special working and annealing process so tin content does not greatly reduce strength. Used in automotive engines (crankshafts) and in aircraft equipment.
Babbitt, tin-based	Sn 84 Cu 8 Sb 8	Fatigue strength decreases as thickness increases. Low load capacity, thus usually bonded to one (bimetal) or two (trimetal) backing materials. Good in dirty applications, motors.
Babbitt, lead-based	Pb 75 Sn 10 Sb 15	Antimony (Sb) greater than 15% can cause brittleness. Cheaper than tin-based babbitt. Used in crankshaft bearings, transmission bushings, and electric equipment.
Lead bronze	Cu 70 Pb 25 Sn 5	Good for high-load high-speed applications; can be used with soft journals. Used as bushings in pumps, many home appliances, railroad cars.
Phosphor bronze	Cu 80 Sn 10 Pb 10	General-duty popular bushing; tin added to improve strength. Has high hardness; should be used with harder journals (300 BHN). Good impact resistance; used in lathes, pumps, home appliances.
Copper lead (cast)	Cu 75 Pb 25	Lead in pockets in copper matrix. Lead improves bearing surface but has corrosion problems. Frequently used as lining material on steel-backed bearings. Used in heavy-duty applications.
Copper lead (sintered)	Cu 75 Pb 25	Frequently used with a babbitt overlay in a trimetal bearing. Widely used in heavy-duty (high-temperature high-load) applications.
Silver (oven-plated)		Frequently used with lead indium overlay.

bearing operates in a clean, moderate-temperature environment and is not part of an electric machine.

After the list of criteria has been established, each component criterion is compared with all other criteria, and a graduation mark is allocated from 0, if there is no difference in the criterion, to 3, if there are large differences. For example, compressive strength (A1 in Table 19.6) might receive a 0 when compared with fatigue strength (A2) but receive a 3 when compared to thermal conductivity (B1), and so forth. When all component criteria have been compared with one another and graduation marks assigned, the graduation marks of each criterion are totaled and the sum of all these totals is divided into each amount, to obtain the component criteria weighting factors. The sum of all the weighting factors obviously is unity.

TABLE 19.4 Performance Ratings from 5 (High) to 1 (Low) for Bearing Alloy Materials

Material	Nominal composition, % by weight	Fatigue strength	Corrosion resistance	Seizure resistance	Embedability	Compatibility	Thermal conductivity
Aluminum, low tin	Al 92 Sn 8	2	4	2	1	1	4
Aluminum, high tin	Al 80 Sn 20	2	4	2	2	2	4
Babbitt, tin-based	Sn 84 Cu 8 Sb 8	1	5	4	5	4	3
Babbitt, lead-based	Pb 75 Sn 10 Sb 15	1	3	4	5	4	2
Lead bronze	Cu 70 Pb 25 Sn 5	4	2	3	3	2	3
Phosphor bronze	Cu 80 Sn 10 Pb 10	4	2	3	1	2	3
Copper lead (cast)	Cu 75 Pb 25	3	1	3	3	3	4
Copper lead (sintered)	Cu 60 Pb 40	3	1	3	3	3	4
Silver (over-plated)		5	4	1	1	1	5

TABLE 19.5 General Information on Self-Lubricating Bearing Materials

Material	Maximum load,† kpsi	Maximum speed, fpm	Maximum *PV* factor,‡ kpsi·fpm	Friction coefficient	Critical temperature, °F	Resistance to humidity	Resistance to chemicals§
Nylon	1.5	200–400	1	0.1–0.4	400	Fair	Good
Acetal	1.5	200–500	1	0.1–0.4	300	Good	Good
Polyimide	10	1000	0.3	0.1–0.3	600	Good	Good
Phenolic	4	1000	0.1	0.9–1.1	300–400	Good	Good
Filled nylon	2	200–400	1	0.1–0.4	400	Fair	Good
Acetal PTFE filled	1.8	800	2.5	0.05–0.15	300	Good	Good
Filled polyimide	10	1000	6	0.1–0.3	600	Good	Good
Reinforced phenolic	4–5	200	4	0.1–0.4	300–400	Good	Good
Filled PTFE	1	500–1000	5–20	0.05–0.25	500	Excellent	Excellent
PTFE	100	50	1–10	0.05–0.25		Excellent	Excellent

†Load on projected area at zero speed.
‡For continuous service.
§At bearing surface.
SOURCE: Ref. [19.3].

TABLE 19.6 Journal Bearing Material Selection Criteria

Major property group	Component criteria
A. Mechanical	1. Compressive strength 2. Fatigue strength 3. Conformability (modulus of elasticity)
B. Thermal	1. Thermal conductivity 2. Thermal expansion
C. Chemical	1. Corrosion rate
D. Manufacturing	1. Cost 2. Machinability 3. Availability of material
E. Environmental	1. Behavior under abrasive conditions (embedability) 2. Resistance against electric-discharge pitting 3. Resistance to thermal degradation
F. Tribological	1. Wear rate 2. Coefficient of friction 3. Cavitation erosion resistance

Next the candidate materials are given quality marks for the various component criteria. These marks range from 5 (excellent, or high) to 1 (poor, or low). For instance, tin-based babbitts are known to have only fair (2) fatigue strength, whereas they have excellent (5) resistance to corrosion. The final ranking of the candidate materials is obtained by comparing the sums of the products of all component criteria weighting factors and quality marks.

19.4 PRESSURE EQUATION FOR A LUBRICATING FILM

19.4.1 Reynolds Equation

The differential equation which governs the pressure in a lubricating film is called the *Reynolds equation.* Bearing performance can be evaluated once the solution of this equation is in hand.

To develop the Reynolds equation, consider a portion of the fluid film of a journal bearing (Fig. 19.1). In general, there are three velocity components in the film: u, v, and w. There are three equations of motion (momentum equations), one for each coordinate direction. The collection is known as the *Navier-Stokes equations,* and each equation may be written in the following form:

$$\text{Inertial forces} = \text{pressure forces} + \text{body forces} + \text{viscous forces} \qquad (19.1)$$

The Navier-Stokes equations in their complete form are too involved for analytical solution. They can, however, be reduced, and subsequently solved, by making several simplifying yet plausible assumptions:

1. The flow is laminar.
2. The inertial and body forces are small compared to the pressure and viscous forces.
3. The curvature of the film is negligible; the bearing surfaces are, therefore, nearly parallel.
4. The variation of pressure across the film $\partial P/\partial y$ is negligibly small.
5. The transverse velocity component across the film, v, is small compared to the other velocity components.
6. The velocity gradients across the film dominate over all other velocity gradients.

Application of these assumptions to mathematical versions of Eq. (19.1), and to an integrated version of the conservation of mass (the continuity equation), yields the *Reynolds equation* for a liquid-lubricated bearing:

$$\frac{\partial}{\partial x}\left(\frac{h^3}{\mu}\frac{\partial p}{\partial x}\right)+\frac{\partial}{\partial z}\left(\frac{h^3}{\mu}\frac{\partial p}{\partial z}\right)=6(U_b+U_j)\frac{\partial h}{\partial x}+6h\frac{\partial(U_b+U_j)}{\partial x}+12\frac{\partial h}{\partial t} \tag{19.2}$$

The first grouping on the right-hand side of Eq. (19.2) is called the *wedge* term and must be negative to generate positive pressures. The third term on the right is called the *squeeze* term, and it will generate positive pressures when $\partial h/\partial t < 0$. The squeeze term vanishes for a steadily loaded bearing. Both the wedge and the squeeze terms vanish for a purely hydrostatic case. If the bearing surface is fixed ($U_b = 0$), if the shaft is rotating with a speed ω (that is, $U_j = U = R\omega$), and if the viscosity of the lubricant is constant, then Eq. (19.2) may be written as

$$\frac{\partial}{\partial x}\left(h^3\frac{\partial p}{\partial x}\right)+\frac{\partial}{\partial z}\left(h^3\frac{\partial p}{\partial z}\right)=6\mu R\omega\frac{\partial h}{\partial x}+6\mu h\frac{\partial U}{\partial x}+12\mu\frac{\partial h}{\partial t} \tag{19.3}$$

For comparative purposes, it is useful to cast the steady version of Eq. (19.3) into nondimensional form. This can be accomplished by defining the following nondimensional variables:

$$\theta\equiv\frac{x}{R}\qquad \zeta\equiv\frac{z}{L/2}\qquad H\equiv\frac{h}{C}$$

$$\bar{p}\equiv\frac{p}{6\mu(U/R)}\left(\frac{C}{R}\right)^2=\frac{p}{6\mu\omega}\left(\frac{C}{R}\right)^2$$

Also, since $\omega = 2\pi N$,

$$\bar{p}=\frac{p}{12\pi\mu N}\left(\frac{C}{R}\right)^2$$

Substituting these into Eq. (19.3) yields

$$\frac{\partial}{\partial\theta}\left(H^3\frac{\partial\bar{p}}{\partial\theta}\right)+\left(\frac{D}{L}\right)^2\frac{\partial}{\partial\zeta}\left(H^3\frac{\partial\bar{p}}{\partial\zeta}\right)=\frac{\partial H}{\partial\theta} \tag{19.4}$$

This equation can be interpreted as

Circumferential pressure flow + axial pressure flow = shear flow

The governing equation of a gas film differs from that of a liquid film by the appearance of the *density* ρ. The steady compressible version of the Reynolds equation for an isoviscous gas can be written

$$\frac{\partial}{\partial x}\left(h^3\rho\frac{\partial p}{\partial x}\right)+\frac{\partial}{\partial z}\left(h^3\rho\frac{\partial p}{\partial z}\right)=6\mu R\omega\frac{\partial(\rho h)}{\partial x} \tag{19.5}$$

Since the energy dissipated by frictional forces is very small in normal gas bearing operation, we may assume that the film has a constant temperature and $p = k\rho$; thus, Eq. (19.5) becomes

$$\frac{\partial}{\partial x}\left(h^3\frac{\partial p^2}{\partial x}\right)+\frac{\partial}{\partial z}\left(h^3\frac{\partial p^2}{\partial z}\right)=12\,\mu R\omega\frac{\partial(ph)}{\partial x} \tag{19.6}$$

This equation can be written in nondimensional form as

$$\frac{\partial}{\partial\theta}\left(H^3\frac{\partial\overline{p}^2}{\partial\theta}\right)+\left(\frac{D}{L}\right)^2\frac{\partial}{\partial\zeta}\left(H^3\frac{\partial\overline{p}^2}{\partial\zeta}\right)=2\Lambda\frac{\partial(\overline{p}H)}{\partial\theta} \tag{19.7}$$

where

$$\overline{p}\equiv\frac{p}{p_a}\qquad p_a=\text{ambient or supply pressure}$$

$$H\equiv\frac{h}{C}\qquad\zeta=\frac{z}{L/2}\qquad\Lambda\equiv\frac{6\mu\omega}{p_a}\left(\frac{R}{C}\right)^2$$

Here Λ is called the *bearing,* or *compressibility, number.*

To solve the Reynolds equation, we require an expression for the *film thickness h.* From the triangle *ABC* in Fig. 19.5, we may write

$$\overline{AC}=h+R=R_b\cos\xi+e\cos\theta$$

where θ is measured from the line of centers. And since $e \ll R_b$, $\cos\xi \sim 1$, and thus

$$h=R_b-R+e\cos\theta$$

The *radial clearance* is $C \equiv R_b - R$, and the *eccentricity ratio* is $\varepsilon \equiv e/C$; hence

$$h=C(1+\varepsilon\cos\theta) \tag{19.8}$$

19.4.2 Boundary Conditions

Three sets of circumferential boundary conditions are commonly applied to the solutions of the Reynolds equation. These boundary conditions have been given the

names *Sommerfeld, Gumbel,* and *Swift-Stieber.* Of the three, the Sommerfeld conditions are the easiest to apply, but they yield certain unrealistic results. For example, in a liquid-lubricated bearing, Sommerfeld conditions produce negative pressures in the film. This results in the shaft's being displaced at right angles to the load line as the load is increased. Gumbel conditions are similar to Sommerfeld conditions except that all negative pressures are disregarded. Although this approach leads to more realistic load results, it produces a violation of the conservation of mass. The Swift-Stieber conditions come closest to representing the actual conditions in a film, but they are more difficult to apply. They are widely used in numerical investigations. The three sets of boundary conditions are summarized in Table 19.7.

19.5 JOURNAL BEARING PERFORMANCE

Once the pressure distribution is established, the journal bearing performance may be determined. Performance is generally measured in terms of four quantities: bearing load capacity, frictional losses, lubricant flow requirement, and temperature rise.

19.5.1 Bearing Load Relations

Five parameters are associated with the load capacity of a journal bearing:

1. The radial load component W_R acts along the line of centers (Fig. 19.1) and is computed from

$$W_R = -R \int_{-L/2}^{L/2} \int_{\theta_1}^{\theta_3} p \cos \theta \, d\theta \, dz$$

TABLE 19.7 Typical Boundary Conditions on the Reynolds Equation

Names associated with boundary conditions	Pressure profile	Mathematical expression
Sommerfeld (full Sommerfeld)	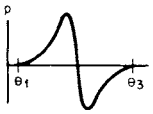	$p(\theta_1) = p(\theta_3) = 0$ (zero pressure means ambient or atmospheric pressure) For complete journal bearings: $\theta_1 = 0, \quad \theta_3 = 2\pi$ For partial journal bearings: $\theta_1 = \beta_1, \quad \theta_3 = \theta_1 + \beta$
Gumbel (half Sommerfeld)	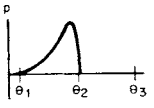	$p(\theta_1) = p(\theta_2) = 0$ $p(\theta_2 \leq \theta \leq \theta_3) = 0$ For complete journal bearings: $\theta_1 = 0, \quad \theta_2 = \pi, \quad \theta_3 = 2\pi$
Swift-Stieber (Reynolds)	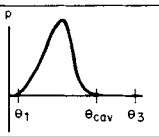	$p(\theta_2) = p_{cav}$ = atmospheric pressure $\frac{\partial p}{\partial \theta}(\theta_2) = 0$ $\theta_2 = \theta_{cav}$ which must be determined

where θ_1 and θ_3 are, respectively, the leading and trailing angular locations of the lubricating film.

2. The tangential load component W_T acts perpendicular to the line of centers:

$$W_T = R \int_{-L/2}^{L/2} \int_{\theta_1}^{\theta_3} p \sin \theta \, d\theta \, dz$$

3. The bearing load W must be supported by the pressure developed within the lubricating film. Generally the load is specified or enters the design via the *unit load P,* which is defined as the load per unit projected area, or

$$P = \frac{W}{LD}$$

Typical values of the unit load are given in Table 19.8.

TABLE 19.8 Range of Unit Loads for Various Applications

Application	Bearing	Unit load range, kpsi
Automotive engines	Main	0.6–0.8
	Crankpin	1.7–2.3
Diesel engines	Main	0.9–2.3
	Crankpin	1.1–2.3
	Wristpin	2.0–2.3
Steam turbines	Main	0.12–0.25
Air compressors	Main	0.14–0.28
	Crankpin	0.28–0.5
Centrifugal pumps	Shaft	0.1–0.18
Electric motors	Shaft	0.12–0.25

4. The *Sommerfeld number S* is a dimensionless parameter that characterizes bearing performance; large S (say, greater than 0.15) indicates a lightly loaded bearing operating at a small eccentricity. The Sommerfeld number may be calculated from

$$S = \frac{\mu UL}{\pi W}\left(\frac{R}{C}\right)^2 = \frac{\mu N}{P}\left(\frac{R}{C}\right)^2$$

5. The *attitude angle* ϕ is the angular distance between the load line and the line of centers (Fig. 19.1). It locates the minimum film thickness as measured from the load line. Because $W_R = W \cos \phi$ and $W_T = W \sin \phi$,

$$\phi = \tan^{-1} \frac{W_T}{W_R}$$

19.5.2 Bearing Friction Relations

Four parameters are involved with the frictional behavior of a journal bearing:

1. The *shear stress* τ, acting on either the shaft or the bearing surface, consists of two terms; one is due to motion of the shaft (pure shear), and the other is due to the circumferential pressure distribution (pressure-induced shear):

$$\tau = \frac{\mu U}{h} \pm \frac{h}{2R}\frac{\partial p}{\partial \theta}$$

   The plus sign corresponds to the shear stress on the journal surface; the minus sign, to the shear stress on the bearing surface.

2. The *frictional force* acting on the journal F_j is found by integrating the pure shear stress over the entire surface of the journal and the pressure-induced shear stress up to the trailing edge of the film. This yields

$$F_j = \left(\frac{2\pi}{1-\varepsilon^2}\right)(\mu UL)\left(\frac{R}{C}\right) + \frac{\varepsilon W_T}{2}\left(\frac{C}{R}\right)$$

3. The *friction coefficient* f is the ratio of the journal frictional force to the bearing load:

$$f = \frac{F_j}{W}$$

   The *friction variable* is the product $(R/C)(f)$ and so may be written

$$\left(\frac{R}{C}\right)(f) = \left(\frac{2\pi^2}{1-\varepsilon^2}\right)(S) + \frac{\varepsilon \sin \phi}{2}$$

4. The power that must be supplied to the journal to overcome friction is called the *frictional horsepower loss* HP, and it may be computed from

$$\text{HP} = C_1 F_j U = C_2 f W R N$$

   where C_1 and C_2 depend on the system of units. For F_j in pounds (lb) and U in inches per second (in/s), $C_1 = 1/6600$ for W (lb), R (in), and N in revolutions per second (r/s), $C_2 = 2\pi C_1 = 9.51998 \times 10^{-4}$.

The relevant geometry for the execution of these tasks is depicted in Fig. 19.5.

19.5.3 Lubricant Flow Relations

Lubricant flow rates are needed to estimate the capacity of the lubricant supply system and to determine the cooling requirements of the bearing. This involves evaluation of the lubricant flow within the clearance space, the lubricant flow that leaks out the sides of the bearing, and the lubricant flow that is supplied to the bearing.

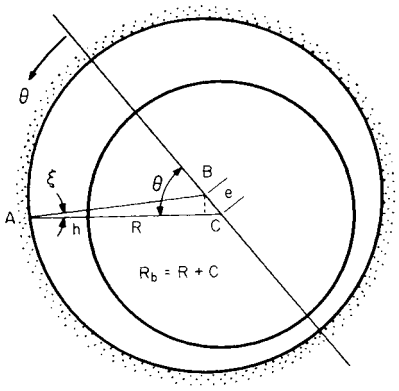

FIGURE 19.5 Film thickness geometry

In general, volume flow rate per unit length is composed of a term due to surface motion (shear flow) and another due to the pressure (pressure-induced flow). Journal bearing circumferential and axial flows per unit length are

$$q_\theta = \frac{Uh}{2} - \frac{h^3}{12\mu R}\frac{\partial p}{\partial \theta} \qquad q_z = -\frac{h^3}{12\mu}\frac{\partial p}{\partial z} \tag{19.9}$$

The total flow rates may be found by integrating Eq. (19.9) across the bearing length for the circumferential flow rate and around the bearing circumference for the axial flow rate.

Assuming that lubricant is supplied in the unloaded portion of the bearing (Fig.19.6), we see that the rate at which lubricant leaks out of the active portion of the film is

$$Q_{sa} = Q_1 - Q_2 \tag{19.10}$$

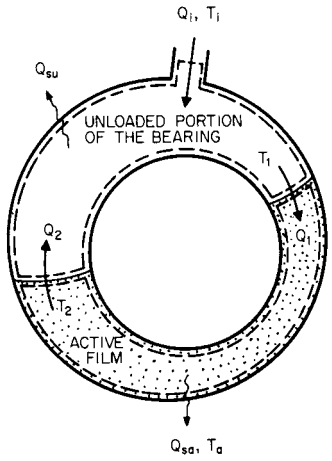

FIGURE 19.6 Control volumes for lubricant flow and heat balances.

where Q_1 = flow into the leading edge of the film and Q_2 = flow out of the trailing edge.

When the input flow rate equals the leakage flow rate, Q_1 is called the *classical rate.* For given values of *W, U,* and μ, the classical rate is the largest flow that can be carried into the active film by shaft rotation. However, in practice, Q_i, the input flow rate, may be greater (the *flooded condition*) or less (the *starved condition*) than the appropriate value to achieve the classical rate. For flooded conditions, side flow will also occur in the unloaded portion of the bearing, and we may write

$$Q_{su} = Q_2 + Q_i - Q_1 \tag{19.11}$$

Thus, $Q_{su} + Q_{sa} = Q_s = Q_i$

19.5.4 Bearing Thermal Relations

The steady energy balance equation can be simply expressed as

Energy inflow rate – energy outflow rate + energy generation rate = 0

An energy balance may be performed on the unloaded portion of the film (Fig. 19.6). Toward that end, it is assumed that there is complete mixing between the inlet

Q_i and the carryover Q_2 flows so that $T_u = T_1$. It is further assumed that there is no energy generation and negligible heat transfer. Hence, for the unloaded portion of the film,

$$Q_i T_i + Q_2 T_2 = (Q_2 + Q_i)(T_1) \tag{19.12}$$

Next an energy balance is performed on the active portion of the lubricating film (Fig. 19.6). The energy generation rate is taken to be $F_j U/J$, and the conduction heat losses to the shaft and bearing are taken to be a portion of the heat generation rate, or $\lambda F_j U/J$. Accordingly,

$$\rho Q_1 C^* T_1 - (\rho Q_{sa} C^* T_a + \rho Q_2 C^* T_2) + \frac{(1-\lambda) F_j U}{J} = 0 \tag{19.13}$$

Combining Eqs. (19.10) to (19.13) and assuming that the side-flow leakage occurs at the average film temperature $T_a = (T_1 + 2\ T_2)/2$, we find that

$$\frac{J\rho C^*(T_a - T_i)}{(1-\lambda)P} = \frac{1 + 2Q_2/Q_i}{2 - Q_{sa}/Q_1} \frac{4\pi(R/C)(f)}{Q_1/(RCNL)} \tag{19.14}$$

This shows that the lubricant temperature rise is $1 - \lambda$ times the rise when conduction is neglected.

19.6 LIQUID-LUBRICATED JOURNAL BEARINGS

In the hydrodynamic operation of a liquid-lubricated journal bearing, it is generally assumed that the lubricant behaves as a continuous incompressible fluid. However, unless the lubricant is admitted to the bearing under relatively high hydrostatic head, the liquid film can experience periodic vaporization which can cause the film to rupture and form unstable pockets, or cavities, within the film. This disruption of the film is called *cavitation,* and it occurs when the pressure within the bearing falls to the vapor pressure of the lubricant. Narrow liquid-lubricated bearings are especially susceptible to this problem. Figure 19.7 illustrates the general film condition in which lubricant is admitted through a lubricating groove at some angular position θ_0. Clearly incomplete films complicate the analysis, and therefore the design, of a liquid-lubricated journal bearing.

19.6.1 *L*/*D* Effects on Cylindrical Full Journal Bearings

Long-Length Bearings. When the length of a bearing is such that $L > 2D$, the axial pressure flow term in the Reynolds equation may be neglected and the bearing performs as if it were infinitely long. Under this condition, the reduced Reynolds equation can be directly integrated. Table 19.9 contains long-bearing results for both Sommerfeld and Gumbel boundary conditions.

Short-Length Bearings. When the length of a bearing is such that $L < D/4$, the axial pressure flow will dominate over the circumferential flow, and again the Reynolds equation can be readily integrated. Results of such a short-bearing integration with Gumbel boundary conditions are shown in Table 19.10.

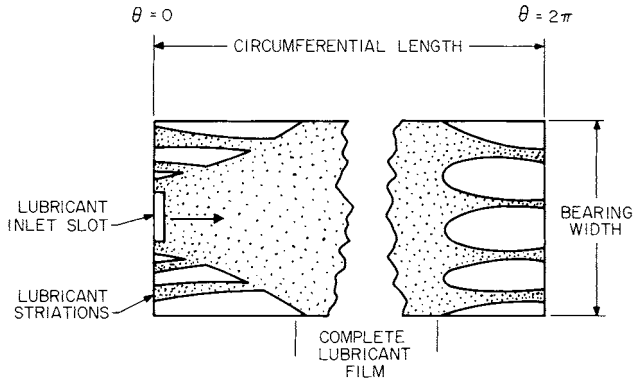

FIGURE 19.7 Diagram of an incomplete fluid film.

TABLE 19.9 Long-Bearing Pressure and Performance Parameters

Performance parameter	Sommerfeld conditions	Gumbel conditions
$\frac{p}{12\pi\mu N}\left(\frac{C}{R}\right)^2$	$\frac{(\varepsilon \sin\theta)(2+\varepsilon\cos\theta)}{(2+\varepsilon^2)(1+\varepsilon\cos\theta)^2}$	$\frac{(\varepsilon \sin\theta)(2+\varepsilon\cos\theta)}{(2+\varepsilon^2)(1+\varepsilon\cos\theta)^2}$ $0<\theta\ \pi$, $0,\ \pi<\theta<2\pi$
$\frac{W_R}{3\mu UL}\left(\frac{C}{R}\right)^2$	0	$\frac{4\varepsilon^2}{(2+\varepsilon^2)(1-\varepsilon^2)}$
$\frac{W_T}{3\mu UL}\left(\frac{C}{R}\right)^2$	$\frac{4\pi\varepsilon}{(2+\varepsilon^2)\sqrt{1-\varepsilon^2}}$	$\frac{2\pi\varepsilon}{(2+\varepsilon^2)\sqrt{1-\varepsilon^2}}$
ϕ	$\frac{\pi}{2}$	$\tan^{-1}\left(\frac{\pi}{2}\frac{\sqrt{1-\varepsilon^2}}{\varepsilon}\right)$
S	$\frac{(2+\varepsilon^2)\sqrt{1-\varepsilon^2}}{12\pi^2\varepsilon}$	$\frac{(2+\varepsilon^2)(1-\varepsilon^2)}{6\pi\varepsilon\sqrt{4\varepsilon^2+\pi^2(1-\varepsilon^2)}}$
$\frac{F_j}{\mu UL}\frac{C}{R}$	$\frac{4\pi(1+2\varepsilon^2)}{(2+\varepsilon^2)\sqrt{1-\varepsilon^2}}$	$\frac{\pi(4+5\varepsilon^2)}{(2+\varepsilon^2)\sqrt{1-\varepsilon^2}}$
$\left(\frac{R}{C}\right)(f)$	$\frac{1+2\varepsilon^2}{3\varepsilon}$	$\frac{4+5\varepsilon^2}{6\varepsilon}\sqrt{\frac{1-\varepsilon^2}{4\varepsilon^2+\pi(1-\varepsilon^2)}}$
$\frac{Q_s}{RCNL}$	0	0

TABLE 19.10 Short-Bearing Pressure and Performance Parameters

Performance parameter	Gumbel conditions
$\frac{p}{12\pi\mu N}\left(\frac{C}{R}\right)^2$	$-\frac{\varepsilon \sin\theta}{2(1+\varepsilon\cos\theta)^3}\left(\frac{L}{D}\right)^2(\zeta^2-1) \quad 0 \le \theta \le \pi,$ $0, \pi \le \theta \le 2\pi$
$\frac{W_R}{3\mu UL}\left(\frac{C}{R}\right)^2$	$\frac{4\varepsilon^2}{3(1-\varepsilon^2)^2}\left(\frac{L}{D}\right)^2$
$\frac{W_T}{3\mu UL}\left(\frac{C}{R}\right)^2$	$\frac{\pi\varepsilon^2}{3(1-\varepsilon^2)^3}\left(\frac{L}{D}\right)^2$
$\frac{W}{3\mu UL}\left(\frac{C}{R}\right)^2$	$\frac{\varepsilon\sqrt{\pi^2(1-\varepsilon^2)+16\varepsilon^2}}{3(1-\varepsilon^2)^2}\left(\frac{L}{D}\right)^2$
ϕ	$\tan^{-1}\frac{\pi(1-\varepsilon^2)^2}{4\varepsilon}$
S	$\frac{(1-\varepsilon^2)^2}{\pi\varepsilon\sqrt{\pi^2(1-\varepsilon^2)+16\varepsilon^2}}\left(\frac{D}{L}\right)^2$
$\frac{F_j}{\mu UL}\frac{C}{R}$	$\frac{2\pi}{\sqrt{1-\varepsilon^2}}$
$\left(\frac{R}{C}\right)(f)$	$\frac{(2\pi)(1-\varepsilon^2)^{3/2}}{\varepsilon\sqrt{\pi^2(1-\varepsilon^2)+16\varepsilon^2}}$
$\frac{Q_s}{RCNL}$	$2\pi\varepsilon$

Finite-Length Bearings. The *slenderness ratio L/D* for most practical designs ranges between 0.5 and 2.0. Thus, neither the short-bearing theory nor the long-bearing theory is appropriate. Numerous attempts have been made to develop methods which simultaneously account for both length and circumferential effects. Various analytical and numerical methods have been successfully employed. Although such techniques have produced important journal bearing design information, other simplified methods of analysis have been sought. These methods are useful because they do not require specialized analytical knowledge or the availability of large computing facilities. What is more, some of these simple, approximate methods yield results that have been found to be in good agreement with the more exact results. One method is described.

Reason and Narang [19.5] have developed an approximate technique that makes use of both long- and short-bearing theories. The method can be used to accurately design steadily loaded journal bearings on a hand-held calculator.

It was proposed that the film pressure p be written as a harmonic average of the short-bearing pressure p_0 and the long-bearing pressure p_∞, or

$$\frac{1}{p} = \frac{1}{p_0} + \frac{1}{p_\infty} \qquad \text{or} \qquad p = \frac{p_0}{1 + p_0/p_\infty}$$

The pressure and various performance parameters that can be obtained by this combined solution approximation are presented in Table 19.11. Note that several of these parameters are written in terms of two quantities, I_s and I_c. Accurate values of these quantities and the Sommerfeld number are displayed in Table 19.12. With the exception of the entrainment flow, which is increasingly overestimated at large ε and L/D, the predictions of this simple method have been found to be very good.

Example 1. Using the Reason and Narang combined solution approximation, determine the performance of a steadily loaded full journal bearing for the following conditions:

$\mu = 4 \times 10^{-6}$ reyn $\quad D = 1.5$ in

$N = 1800$ r/min $\quad L = 1.5$ in

$W = 500$ lbf $\quad C = 1.5 \times 10^{-3}$

Solution. The unit load is $P = W/(LD) = 222$ pounds per square inch (psi), and the Sommerfeld number is

$$S = \frac{\mu N}{P}\left(\frac{R}{C}\right)^2 = 0.135$$

Entering Table 19.12 at this Sommerfeld number and a slenderness ratio of 1, we find that $\varepsilon = 0.582$, $I_c = 0.2391$, and $I_s = 0.3119$. The bearing performance is computed by evaluating various parameters in Table 19.11. Results are compared in Table 19.13 to values obtained by Shigley and Mischke [19.6] by using design charts.

19.6.2 Design Charts

Design charts have been widely used for convenient presentation of bearing performance data. Separate design graphs are required for every bearing configuration or variation. Use of the charts invariably requires repeated interpolations and extrapolations. Thus, design of journal bearings from these charts is somewhat tedious.

Raimondi-Boyd Charts. The most famous set of design charts was constructed by Raimondi and Boyd [19.7]. They presented 45 charts and 6 tables of numerical information for the design of bearings with slenderness ratios of ¼, ½, and 1 for both partial (60°, 120°, and 180°) and full journal bearings. Consequently, space does not permit all those charts to be presented. Instead a sampling of the charts for bearings with an L/D ratio of 1 is given. Figures 19.8 to 19.13 present graphs of the *minimum-film-thickness variable* h_0/C (note that $h_0/C = 1 - \varepsilon$), the *attitude angle* ϕ (or location of the minimum thickness), the *friction variable* $(R/C)(f)$, the *flow variable* $Q/(RCNL)$, the *flow ratio* Q_s/Q, and the *temperature-rise variable* $J\rho C^* \Delta T/P$. Table 19.14 is a tabular presentation of these data.

TABLE 19.11 Pressure and Performance Parameters of the Combined Solution Approximation

Performance parameter	Equation
$\frac{p}{12\pi\mu N}\left(\frac{C}{R}\right)^2$	$\dfrac{\frac{1}{2}\left(\frac{L}{D}\right)^2(1-\zeta^2)\dfrac{\varepsilon\sin\theta}{(1+\varepsilon\cos\theta)^3}}{1+\left(\frac{L}{D}\right)^2\dfrac{(2+\varepsilon^2)(1-\zeta^2)}{2(1+\varepsilon\cos\theta)(2+\varepsilon\cos\theta)}}$
$\frac{W_R}{3\mu UL}\left(\frac{C}{R}\right)^2$	$-2I_c$
$\frac{W_T}{3\mu UL}\left(\frac{C}{R}\right)^2$	$2I_s$
ϕ	$\tan^{-1}\left(\frac{-I_s}{I_c}\right)$
S	$\dfrac{1}{6\pi\sqrt{I_s^2+I_c^2}}$
$\frac{F_j}{\mu UL}\frac{C}{R}$	$3\varepsilon I_s+\dfrac{2\pi}{\sqrt{1-\varepsilon^2}}$
$\left(\frac{R}{C}\right)(f)$	$6\pi S\left(\frac{\varepsilon I_S}{2}+\dfrac{\pi}{3\sqrt{1-\varepsilon^2}}\right)$
$\frac{Q_{0,\pi}}{RCNL}$ †	$\pi\left[1+\varepsilon\mp\varepsilon E\left(1-\dfrac{2E}{\sqrt{1+2E}}\tanh^{-1}\dfrac{1}{\sqrt{1+2E}}\right)\left(\frac{L}{D}\right)^2\right]$ where $E=\dfrac{(1\pm\varepsilon)(2\pm\varepsilon)}{(2+\varepsilon^2)}\left(\frac{D}{L}\right)^2$
$\frac{Q_s}{Q_0}$	$1-\dfrac{Q_\pi}{Q_0}$
$\frac{J\rho C^*\Delta T}{P}$	$\dfrac{1}{1-\frac{1}{2}Q_s/Q_0}\dfrac{4\pi(R/C)f}{Q_0/(RCNL)}$

†For Q_0 (flow through maximum film thickness at $\theta = 0$) use top signs; for Q_π (flow through minimum film thickness at $\theta = \pi$) use lower signs.

TABLE 19.12 Values of I_s, I_c, and Sommerfeld Number for Various Values of L/D and ε

ε \ L/D	0.25	0.5	0.75	1.0	1.5	2	∞
0.1	0.0032†	0.0120	0.0244	0:0380	0.0636	0.0839	0.1570
	−0.0004	−0.0014	−0.0028	−0.0041	−0.0063	−0.0076	−0.0100
	16.4506	4.3912	2.1601	1.3880	0.8301	0.6297	0.3372
0.2	0.0067	0.0251	0.0505	0.0783	0.1300	0.1705	0.3143
	−0.0017	−0.0062	−0.0118	−0.0174	−0.0259	−0.0312	−0.0408
	7.6750	2.0519	1.0230	0.6614	0.4002	0.3061	0.1674
0.3	0.0109	0.0404	0.0804	0.1236	0.2023	0.2628	0.4727
	−0.0043	−0.0153	−0.0289	−0.0419	−0.0615	−0.0733	−0.0946
	4.5276	1.2280	0.6209	0.4065	0.2509	0.1944	0.1100
0.4	0.0164	0.0597	0.1172	0.1776	0.2847	0.3649	0.6347
	−0.0089	−0.0312	−0.0579	−0.0825	−0.1183	−0.1391	−0.1763
	2.8432	0.7876	0.4058	0.2709	0.1721	0.1359	0.0805
0.5	0.0241	0.0862	0.1656	0.2462	0.3835	0.4831	0.8061
	−0.0174	−0.0591	−0.1065	−0.1484	−0.2065	−0.2391	−0.2962
	1.7848	0.5076	0.2694	0.1845	0.1218	0.0984	0.0618
0.6	0.0363	0.1259	0.2345	0.3306	0.5102	0.6291	0.9983
	−0.0338	−0.1105	−0.1917	−0.2590	−0.3474	−0.3949	−0.4766
	1.0696	0.3167	0.1752	0.1242	0.0859	0.0714	0.0480
0.7	0.0582	0.1927	0.3430	0.4793	0.6878	0.8266	1.2366
	−0.0703	−0.2161	−0.3549	−0.4612	−0.5916	−0.6586	−0.7717
	0.5813	0.1832	0.1075	0.0798	0.0585	0.0502	0.0364
0.8	0.1071	0.3264	0.5425	0.7220	0.9771	1.1380	1.5866
	−0.1732	−0.4797	−0.7283	−0.8987	−0.0941	−1.1891	−0.3467
	0.2605	0.0914	0.0584	0.0460	0.0362	0.0322	0.0255
0.9	0.2761	0.7079	1.0499	1.3002	1.6235	1.8137	2.3083
	−0.6644	−1.4990	−2.0172	−2.3269	−2.6461	−2.7932	−3.0339
	0.0737	0.0320	0.0233	0.0199	0.0171	0.0159	0.0139
0.95	0.6429	1.3712	1.8467	2.1632	2.5455	2.7600	3.2913
	−2.1625	−3.9787	−4.8773	−5.3621	−5.8315	−6.0396	−6.3776
	0.0235	0.0126	0.0102	0.0092	0.0083	0.0080	0.0074
0.99	3.3140	4.9224	5.6905	6.1373	6.6295	6.8881	8.7210
	−22.0703	−28.5960	−30.8608	−31.9219	−32.8642	−33.2602	−33.5520
	0.0024	0.0018	0.0017	0.0016	0.0016	0.0016	0.0015

†The three numbers associated with each ε and L/D pair are, in order from top to bottom, I_s, I_c, and S.

TABLE 19.13 Comparison of Predicted Performance between Two Methods for Example 1

Method \ Parameter	ε	ϕ	$\left(\frac{R}{C}\right)(f)$	$\frac{Q}{RCNL}$	$\frac{Q_s}{Q}$	ΔT
Combined solution approximation	0.582	52.5°	3.508	4.473	0.652	26.6°F
Design charts†	0.58	53.°	3.50	4.28	0.655	26.6°F

†SOURCE: Shigley and Mischke [19.6].

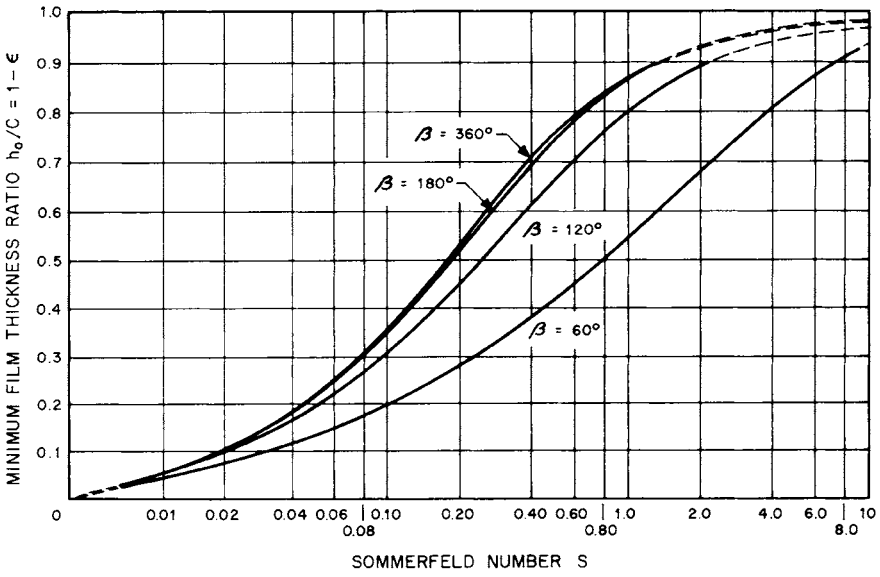

FIGURE 19.8 Minimum film thickness ratio versus Sommerfeld number for full and partial journal bearings, $L/D = 1$, Swift-Stieber boundary conditions. *(From Raimondi and Boyd [19.7].)*

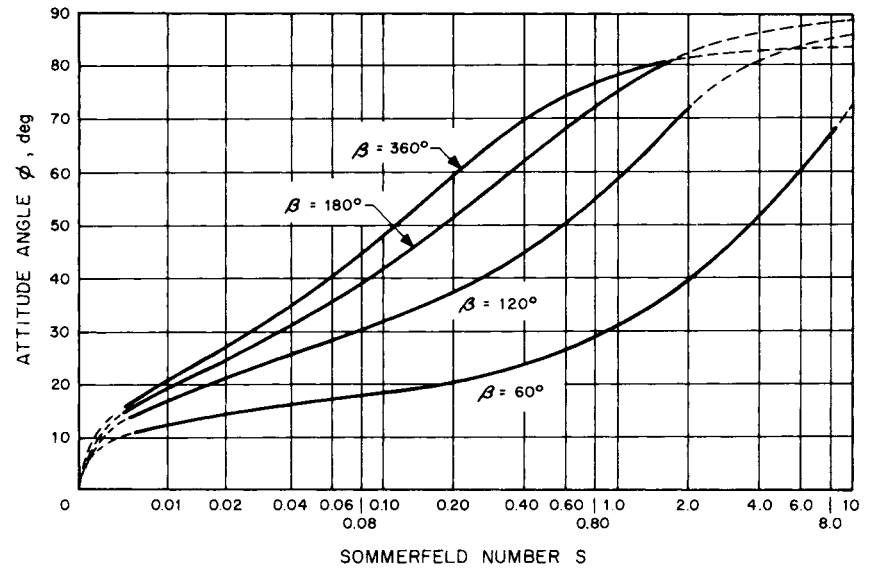

FIGURE 19.9 Attitude angle versus Sommerfeld number for full and partial journal bearings, $L/D = 1$, Swift-Stieber boundary conditions. *(From Raimondi and Boyd [19.7].)*

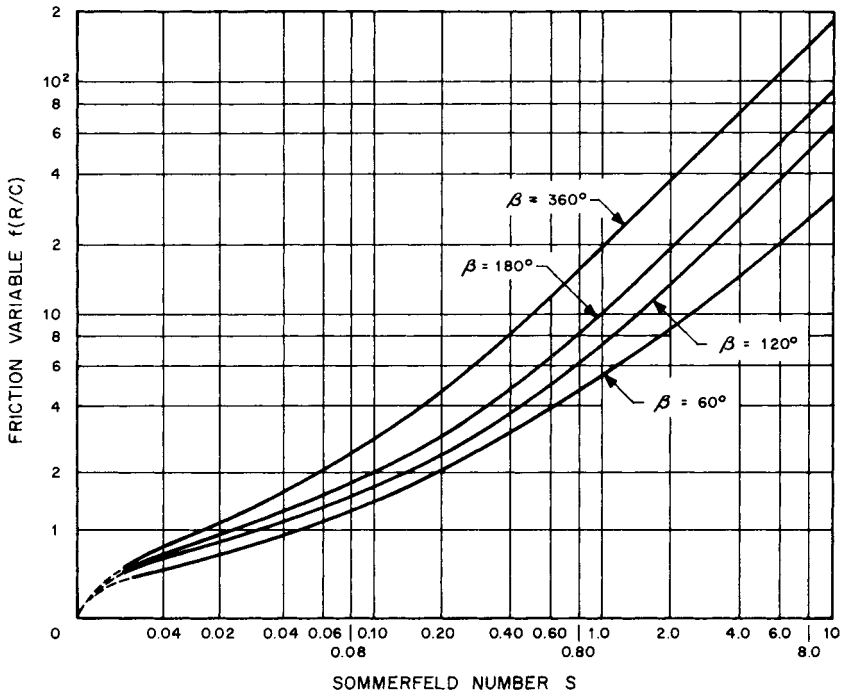

FIGURE 19.10 Friction variable versus Sommerfeld number for full and partial journal bearings, $L/D = 1$, Swift-Stieber boundary conditions. *(From Raimondi and Boyd [19.7].)*

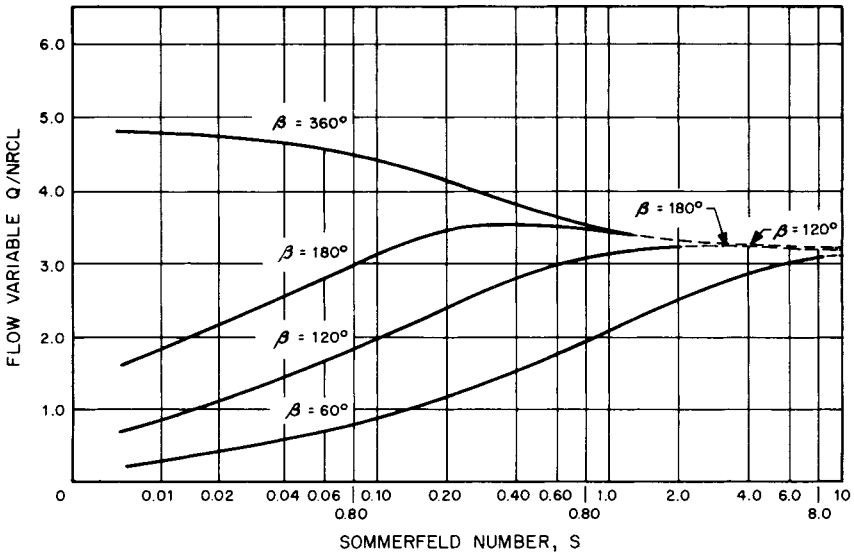

FIGURE 19.11 Flow variable versus Sommerfeld number for full and partial journal bearings, $L/D = 1$, Swift-Stieber boundary conditions. *(From Raimondi and Boyd [19.7].)*

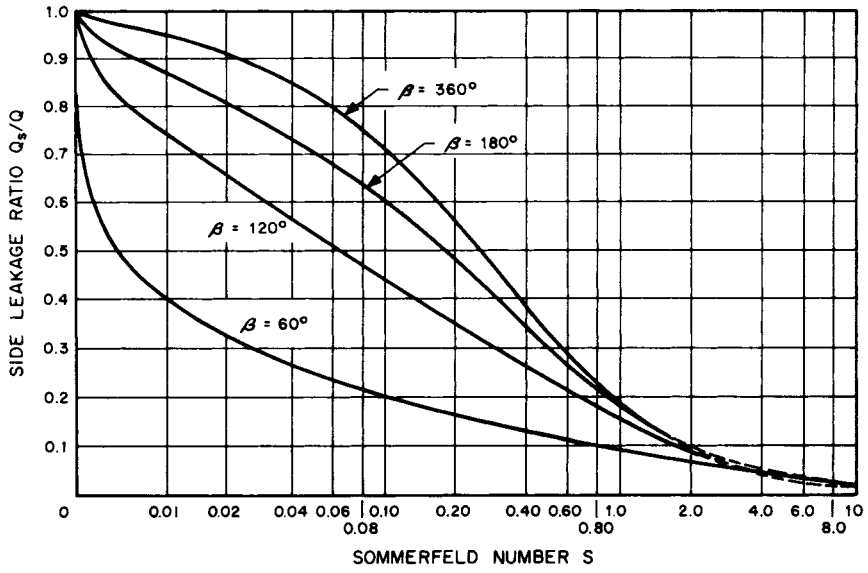

FIGURE 19.12 Side-leakage ratio versus Sommerfeld number for full and partial journal bearings, $L/D = 1$, Swift-Stieber boundary conditions. *(From Raimondi and Boyd [19.7].)*

For slenderness ratios other than the four displayed (∞, 1, ½, and ¼), Raimondi and Boyd suggest the use of the following interpolation formula:

$$y_{L/D} = \left(\frac{D}{L}\right)^3 \left[-\frac{1}{8}\left(1-\frac{L}{D}\right)\left(1-2\frac{L}{D}\right)\left(1-4\frac{L}{D}\right)y_\infty + \frac{1}{3}\left(1-2\frac{L}{D}\right)\left(1-4\frac{L}{D}\right)y_1 - \frac{1}{4}\left(1-\frac{L}{D}\right)\left(1-4\frac{L}{D}\right)y_{1/2} + \frac{1}{24}\left(1-\frac{L}{D}\right)\left(1-2\frac{L}{D}\right)y_{1/4}\right]$$

where y = any performance variable, that is, $(R/C)(f)$, h_0/C, etc., and the subscript of y is the L/D value at which the variable is being evaluated.

For partial bearings with bearing arc angles other than the three displayed (180°, 120°, and 60°), Raimondi and Boyd recommend using the following interpolation formula:

$$y_\beta = \frac{1}{7200}\left[(\beta-120)(\beta-60)y_{180} - 2(\beta-180)(\beta-60)y_{120} + (\beta-180)(\beta-120)y_{60}\right]$$

where y = any performance variable and the subscript of y is the β at which the variable is being evaluated.

Some of the tedium associated with use of charts can be removed by employing curve fits of the data. Seireg and Dandage [19.8] have developed approximate equations for the full journal bearing data of the Raimondi and Boyd charts. Table 19.15 gives the coefficients to be used in these curve-fitted equations.

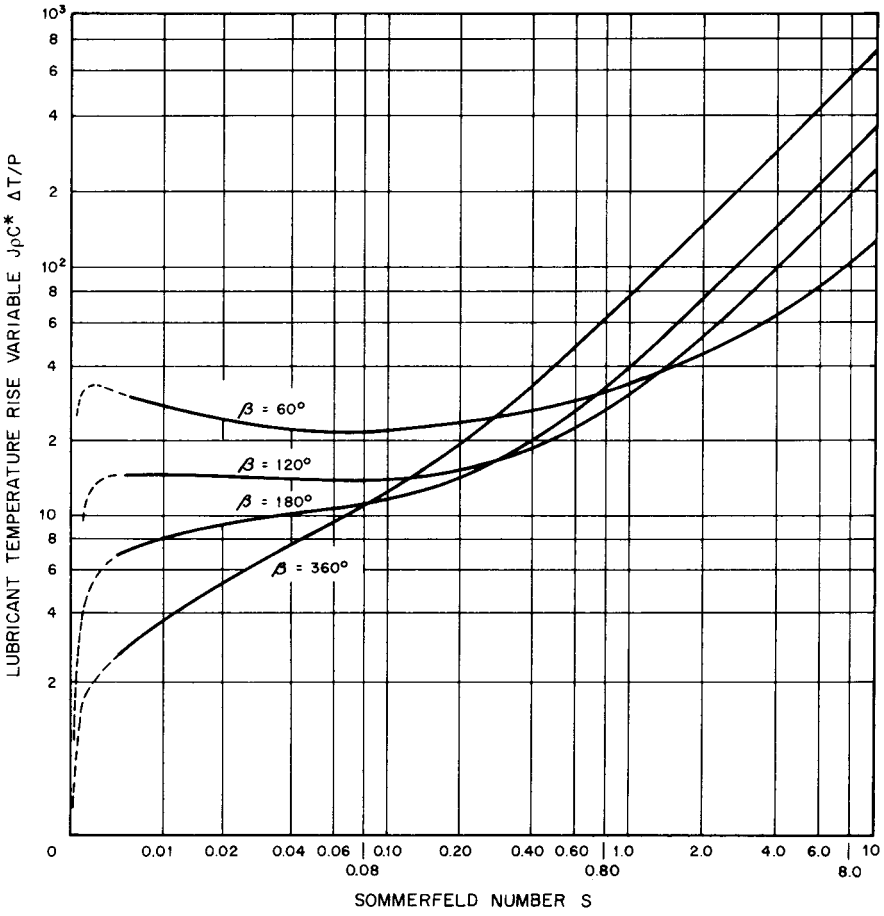

FIGURE 19.13 Lubricant temperature-rise variable versus Sommerfeld number for full and partial journal bearings, $L/D = 1$, Swift-Stieber boundary conditions. *(From Raimondi and Boyd [19.7].)*

Example 2. For the following data

$N = 3600$ r/min $L = 4$ in

$W = 7200$ lbf $C = 6.0 \times 10^{3}$ in

$D = 6$ in Lubricant: SAE 20 oil

Inlet temperature $T_i = 110°F$

determine the isoviscous performance of a centrally loaded full journal bearing. The viscosity-temperature relation is contained in Table 19.16.

Solution. Because the viscosity varies with temperature, an iterative procedure is required. By this procedure, a first-guess viscosity is used to determine the film temperature rise. From this an average film temperature is determined, which will permit a second film temperature rise to be determined, and so on, until a converged result is obtained.

TABLE 19.14 Performance Data for Full and Partial Journal Bearings, $L/D = 1$, Swift-Stieber Boundary Conditions

L/D	ε	θ_1	S	ϕ	$\left(\frac{R}{C}\right)(f)$	$\frac{Q}{RCNL}$	$\frac{Q_s}{Q}$	$\frac{J\rho C^* \Delta T}{P}$
				Full bearing				
∞	0.1	0	0.240	69.10	4.80	3.03	0	19.9
	0.2	0	0.123	67.26	2.57	2.83	0	11.4
	0.4	0	0.0626	61.94	1.52	2.26	0	8.47
	0.6	0	0.0389	54.31	1.20	1.56	0	9.73
	0.8	0	0.0210	42.22	0.961	0.760	0	15.9
	0.9	0	0.0115	31.62	0.756	0.411	0	
1	0.1	0	1.33	79.5	26.4	3.37	0.150	106
	0.2	0	0.631	74.02	12.8	3.59	0.280	52.1
	0.4	0	0.264	63.10	5.79	3.99	0.497	24.3
	0.6	0	0.121	50.58	3.22	4.33	0.680	14.2
	0.8	0	0.0446	36.24	1.70	4.62	0.842	8.00
	0.9	0	0.0188	26.45	1.05	4.74	0.919	5.16
	0.97	0	0.00474	15.47	0.514	4.82	0.973	2.61
1/2	0.1	0	4.31	81.62	85.6	3.43	0.173	343
	0.2	0	2.03	74.94	40.9	3.72	0.318	164
	0.4	0	0.779	61.45	17.0	4.29	0.552	68.6
	0.6	0	0.319	48.14	8.10	4.85	0.730	33.0
	0.8	0	0.0923	33.31	3.26	5.41	0.874	13.4
	0.9	0	0.0313	23.66	1.60	5.69	0.939	6.66
	0.97	0	0.00609	13.75	0.610	5.88	0.980	2.56
1/4	0.1	0	16.2	82.31	322	3.45	0.180	1287
	0.2	0	7.57	75.18	153	3.76	0.330	611
	0.4	0	2.83	60.86	61.1	4.37	0.567	245
	0.6	0	1.07	46.72	26.7	4.99	0.746	107
	0.8	0	0.261	31.04	8.80	5.60	0.884	35.4
	0.9	0	0.0736	21.85	3.50	5.91	0.945	14.1
	0.97	0	0.0101	12.22	0.922	6.12	0.984	3.73
				Partial bearing, $\beta = 60°$				
∞	0.1	84.00	5.75	65.91	19.7	3.01	0	82.3
	0.2	101.00	2.66	48.91	10.1	2.73	0	46.5
	0.4	118.00	0.931	31.96	4.67	2.07	0	28.4
	0.6	126.80	0.322	23.21	2.40	1.40	0	21.5
	0.8	132.60	0.0755	17.39	1.10	0.722	0	19.2
	0.9	135.06	0.0241	14.94	0.667	0.372	0	22.5
	0.97	139.14	0.00495	10.88	0.372	0.115	0	40.7
1	0.1	82.00	8.52	67.92	29.1	3.07	0.0267	121
	0.2	99.00	3.92	50.96	14.8	2.82	0.0481	67.4
	0.4	116.00	1.34	33.99	6.61	2.22	0.0849	39.1
	0.6	125.50	0.450	24.56	3.29	1.56	0.127	28.2
	0.8	131.60	0.101	18.33	1.42	0.883	0.200	22.5
	0.9	134.67	0.0309	15.33	0.822	0.519	0.287	23.2
	0.97	139.10	0.00584	10.88	0.422	0.226	0.465	30.5

TABLE 19.14 Performance Data for Full and Partial Journal Bearings, $L/D = 1$, Swift-Stieber Boundary Conditions (*Continued*)

L/D	ε	θ_1	S	ϕ	$\left(\frac{R}{C}\right)(f)$	$\frac{Q}{RCNL}$	$\frac{Q_s}{Q}$	$\frac{J\rho C^* \Delta T}{P}$
				Partial bearing, $\beta = 60°$ (*Continued*)				
1/2	0.1	81.00	14.2	69.00	48.6	3.11	0.0488	201
	0.2	97.50	6.47	52.60	24.2	2.91	0.0883	109
	0.4	113.00	2.14	37.00	10.3	2.38	0.160	59.4
	0.6	123.00	0.695	26.98	4.93	1.74	0.236	40.3
	0.8	130.40	0.149	19.57	2.02	1.05	0.350	29.4
	0.9	134.09	0.0422	15.91	1.08	0.664	0.464	26.5
	0.97	139.22	0.00704	10.85	0.490	0.329	0.650	27.8
1/4	0.1	78.50	35.8	71.55	121	3.16	0.0666	499
	0.2	91.50	16.0	58.51	58.7	3.04	0.131	260
	0.4	109.00	5.20	41.01	24.5	2.57	0.236	136
	0.6	119.80	1.65	30.14	11.2	1.98	0.346	86.1
	0.8	128.30	0.333	21.70	4.27	1.30	0.496	54.9
	0.9	133.10	0.0844	16.87	2.01	0.894	0.620	41.0
	0.97	139.20	0.0110	10.81	0.713	0.507	0.786	29.1
				Partial bearing, $\beta = 120°$				
∞	0.1	53.300	0.877	66.69	6.02	3.02	0	25.1
	0.2	67.400	0.431	52.60	3.26	2.75	0	14.9
	0.4	81.000	0.181	39.02	1.78	2.13	0	10.5
	0.6	87.300	0.0845	32.67	1.21	1.47	0	10.3
	0.8	93.200	0.0328	26.80	0.853	0.759	0	14.1
	0.9	98.500	0.0147	21.51	0.653	0.388	0	21.2
	0.97	106.15	0.00406	13.86	0.399	0.118	0	42.4
1	0.1	47.500	2.14	72.43	14.5	3.20	0.0876	59.5
	0.2	62.000	1.01	58.25	7.44	3.11	0.157	32.6
	0.4	76.000	0.385	43.98	3.60	2.75	0.272	19.0
	0.6	84.500	0.162	35.65	2.16	2.24	0.384	15.0
	0.8	92.600	0.0531	27.42	1.27	1.57	0.535	13.9
	0.9	98.667	0.0208	21.29	0.855	1.11	0.657	14.4
	0.97	106.50	0.00498	13.49	0.461	0.694	0.812	14.0
1/2	0.1	45.000	5.42	74.99	36.6	3.29	0.124	149
	0.2	56.650	2.51	63.38	18.1	3.32	0.225	77.2
	0.4	72.000	0.914	48.07	8.20	3.15	0.386	40.5
	0.6	81.500	0.354	38.50	4.43	2.80	0.530	27.0
	0.8	92.000	0.0973	28.02	2.17	2.18	0.684	19.0
	0.9	99.000	0.0324	21.02	1.24	1.70	0.787	15.1
	0.97	107.00	0.00631	13.00	0.550	1.19	0.899	10.6
1/4	0.1	43.000	18.4	76.97	124	3.34	0.143	502
	0.2	54.000	8.45	65.97	60.4	3.44	0.260	254
	0.4	68.833	3.04	51.23	26.6	3.42	0.442	125
	0.6	79.600	1.12	40.42	13.5	3.20	0.599	75.8
	0.8	91.560	0.268	28.38	5.65	2.67	0.753	42.7
	0.9	99.400	0.0743	20.55	2.63	2.21	0.846	25.9
	0.97	108.00	0.0105	12.11	0.832	1.69	0.931	11.6

TABLE 19.14 Performance Data for Full and Partial Journal Bearings, $L/D = 1$, Swift-Stieber Boundary Conditions (*Continued*)

L/D	ε	θ_1	S	ϕ	$\left(\frac{R}{C}\right)(f)$	$\frac{Q}{RCNL}$	$\frac{Q_s}{Q}$	$\frac{J\rho C^* \Delta T}{P}$
				Partial bearing, $\beta = 180°$				
∞	0.1	17.000	0.347	72.90	3.55	3.04	0	14.7
	0.2	28.600	0.179	61.32	2.01	2.80	0	8.99
	0.4	40.000	0.0898	49.99	1.29	2.20	0	7.34
	0.6	46.900	0.0523	43.15	1.06	1.52	0	8.71
	0.8	56.700	0.0253	33.35	0.859	0.767	0	14.1
	0.9	64.200	0.0128	25.57	0.681	0.380	0	22.5
	0.97	74.650	0.00384	15.43	0.416	0.119	0	44.0
1	0.1	11.500	1.40	78.50	14.1	3.34	0.139	57.0
	0.2	21.000	0.670	68.93	7.15	3.46	0.252	29.7
	0.4	34.167	0.278	58.86	3.61	3.49	0.425	16.5
	0.6	45.000	0.128	44.67	2.28	3.25	0.572	12.4
	0.8	58.000	0.0463	32.33	1.39	2.63	0.721	10.4
	0.9	66.000	0.0193	24.14	0.921	2.14	0.818	9.13
	0.97	75.584	0.00483	14.57	0.483	1.60	0.915	6.96
1/2	0.1	10.000	4.38	79.97	44.0	3.41	0.167	177
	0.2	17.800	2.06	72.14	21.6	3.64	0.302	87.8
	0.4	32.000	0.794	58.01	9.96	3.93	0.506	42.7
	0.6	45.000	0.321	45.01	5.41	3.93	0.665	25.9
	0.8	59.000	0.0921	31.29	2.54	3.56	0.806	15.0
	0.9	67.200	0.0314	22.80	1.38	3.17	0.886	9.80
	0.97	76.500	0.00625	13.63	0.581	2.62	0.951	5.30
1/4	0.1	9.000	16.3	81.40	163	3.44	0.176	653
	0.2	16.300	7.60	73.70	79.4	3.71	0.320	320
	0.4	31.000	2.84	58.99	35.1	4.11	0.534	146
	0.6	45.000	1.08	44.96	17.6	4.25	0.698	79.8
	0.8	59.300	0.263	30.43	6.88	4.07	0.837	36.5
	0.9	68.900	0.0736	21.43	2.99	3.72	0.905	18.4
	0.97	77.680	0.0104	12.28	0.877	3.29	0.961	6.46

SOURCE: Raimondi and Boyd [19.7].

Since $L/D = \frac{2}{3}$, the Raimondi and Boyd charts would require interpolation. Alternatively, the Seireg-Dandage curve-fitted equations are used. The unit load may be immediately computed:

$$P = \frac{W}{LD} = \frac{7200}{(6)(4)} = 300 \text{ psi}$$

The first guess of viscosity is based on the inlet temperature:

$$\mu_1 = 1.36 \times 10^{-8} \exp \frac{1271.6}{110 + 95} = 6.72 \times 10^{-6} \text{ reyn}$$

$$S_1 = \frac{\mu_1 N}{P}\left(\frac{R}{C}\right)^2 = 0.336$$

TABLE 19.15 Seireg-Dandage Curve Fits of Raimondi-Boyd Charts: Variable = $a\left(\frac{L}{D}\right)^{b_1} S^{(b_2 + b_3(L/D))}$

Variable		$S \le 0.15$						$S > 0.15$					
		a	b_1	b_2	b_3			a	b_1	b_2	b_3		
$\frac{h_0}{C} = 1 - \varepsilon$	$S \le 0.04$	2.7258	0.83621	0.75101	0.08113	$S \le 1$		0.91437	0.4538	0.6119	−0.2890		
	$S > 0.04$	1.7176	1.0478	0.4999	0.1868	$S > 1$		0.89574	0.3895	0.3076	−0.2537		
ϕ, rad	.....	110.9067	0.60907	0.28856	0.07485	.....		74.0225	0.2395	0.3131	−0.2172		
$\left(\frac{R}{C}\right)(f)$	.....	9.9533	−0.4758	0.6705	−0.1124	.....		3.5251	−0.2333	−0.1926	0.1149		
$\frac{Q}{RCNL}$	.....	4.1036	−0.306242	−0.024799	−0.009982	.....		20.4422	−0.1125	0.8551	0.1014		
$\frac{J\rho C^* \Delta T}{P}$	.....	42.0097	−0.4146	0.6869	−0.1600	.....		84.2989	−0.08167	0.85540	0.08787		
$\frac{p}{p_{\max}}$	.....	0.79567	0.59651	0.25659	0.04321	.....		0.52529	0.2486	0.2335	−0.1870		

$\frac{1}{4} \le L/D \le 1$

TABLE 19.15 Seireg-Dandage Curve Fits of Raimondi-Boyd Charts: Variable = $a\left(\frac{L}{D}\right)^{b_1} S^{b_2 + b_3(L/D)}$ (*Continued*)

Variable	$S \le 0.15$					$S > 0.15$				
		a	b_1	b_2	b_3		a	b_1	b_2	b_3
					$\frac{1}{4} \le L/D \le \frac{1}{2}$					
$\frac{h_0}{C} = 1 - \varepsilon$	$S \le 0.04$	9.2341	2.0673	0.4286	0.9247	$S \le 1$	1.1674	0.80824	0.48016	−0.02463
	$S > 0.04$	1.1545	0.4637	0.7851	−0.3788	$S > 1$	1.1263	0.7279	0.5117	−0.6581
ϕ, rad	.....	112.7756	0.6332	0.2592	0.1336	.....	93.6908	0.5313	0.3139	−0.2923
$\left(\frac{R}{C}\right)(f)$	.....	9.4896	−0.5446	0.7290	−0.2293	.....	17.1809	−0.3133	0.7993	0.2887
$\frac{Q}{RCNL}$	.....	4.5607	−0.153864	−0.005371	−0.48838	.....	3.4980	−0.23973	−0.11107	−0.04103
$\frac{J\rho C^* \Delta T}{P}$	.....	38.7604	−0.5307	0.7322	−0.2505	.....	69.4842	−0.3075	0.8003	0.2783
$\frac{p}{p_{max}}$	.....	0.78635	0.57952	0.23620	0.0840	.....	0.64927	0.5037	0.2783	−0.3534

SOURCE: Ref. [19.8].

TABLE 19.16 Constants for Use in Viscosity-Temperature Equation for Various Oils

Oil	μ_0†, reyn	b, °F
SAE 10	1.58×10^{-8}	1157.5
SAE 20	1.36×10^{-8}	1271.6
SAE 30	1.41×10^{-8}	1360.9
SAE 40	1.21×10^{-8}	1474.4
SAE 50	1.70×10^{-8}	1509.6
SAE 60	1.87×10^{-8}	1564.0

†$\mu = \mu_0 \exp [b/(T + 95)]$.
SOURCE: Ref. [19.8].

From Table 19.15, the appropriate curve-fitted equation for the temperature rise is

$$\Delta T = 84.2989 \frac{P}{J\rho C^*} \left(\frac{L}{D}\right)^{-0.08167} S^{0.8554 + 0.08787L/D}$$

Taking $\rho = 0.03$ pound mass per cubic inch (lbm/in^3) and $C^* = 0.40$ Btu/(lbm · °F) as representative values for lubricating oil, we obtain

$$\Delta T_1 = 233.33(0.336)^{0.914} = 86.1°\text{F}$$

And so the second estimate of the film mean temperature is

$$T_{a2} = 110 + \frac{86.1}{2} = 153.1°\text{F}$$

Repeated calculations (13 iterations) produce

$$S = 0.176 \qquad \mu = 3.5 \times 10^{-6} \text{ reyn} \qquad \Delta T = 47.7°\text{F}$$

With the Sommerfeld number, the remaining performance parameters are easily calculated.

Connors' Lubricant Supply Charts. The Raimondi-Boyd lubricant flow and temperature rise data are based on the notion that there is no carryover flow into the active film; that is, $Q_2 = 0$ in Eq. (19.14). From an analogous view, these results are applicable to the situation where $Q_i >> Q_2$. Accordingly, Raimondi-Boyd predictions represent fully flooded bearing conditions and yield the coolest running lubricant temperatures for a given set of operating conditions, not accounting for any heat conduction losses.

To remedy this and thus provide more realistic design information, Connors [19.9] developed design charts which incorporate the influence of lubricant supply rate on the performance of a full journal bearing for $L/D = 1$. Figures 19.14 to 19.16 are plots that can be used over the entire range of flows to determine minimum film thickness, friction, and temperature rise from given values of the Sommerfeld number and the inlet flow variable.

Example 3. Determine the lubricant temperature rise as a function of the inlet flow rate for the following design parameters:

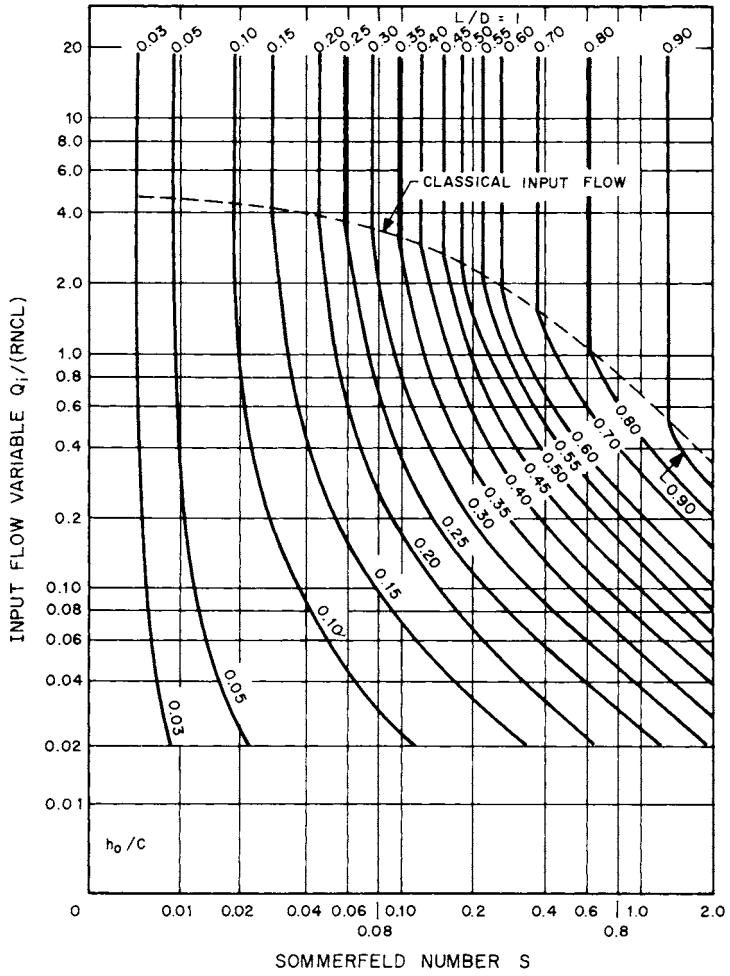

FIGURE 19.14 Inlet flow variable versus Sommerfeld number for parametric values of minimum film thickness ratio; $L/D = 1$, full journal bearing. *(From Connors [19.9].)*

$W = 1500$ lbf $\quad C = 4 \times 10^{-3}$ in

$N = 1800$ r/min $\quad$ SAE 30 oil

$D = 4$ in $\quad T_i = 100°\text{F}$

$L = 4$ in

Solution. To solve this type of problem, a plot or equation of lubricant viscosity as a function of temperature must be available. The calculation procedure is as follows: